U.S.NRC
United States Nuclear Regulatory Commission
Protecting People and the Environment

NUREG/CR-7203
ORNL/TM-2013/92

A Quantitative Impact Assessment of Hypothetical Spent Fuel Reconfiguration in Spent Fuel Storage Casks and Transportation Packages

Office of Nuclear Regulatory Research

AVAILABILITY OF REFERENCE MATERIALS IN NRC PUBLICATIONS

NRC Reference Material

As of November 1999, you may electronically access NUREG-series publications and other NRC records at NRC's Public Electronic Reading Room at http://www.nrc.gov/reading-rm.html. Publicly released records include, to name a few, NUREG-series publications; *Federal Register* notices; applicant, licensee, and vendor documents and correspondence; NRC correspondence and internal memoranda; bulletins and information notices; inspection and investigative reports; licensee event reports; and Commission papers and their attachments.

NRC publications in the NUREG series, NRC regulations, and *Title 10, Energy*, in the Code of *Federal Regulations* may also be purchased from one of these two sources:

1. The Superintendent of Documents
   U.S. Government Printing Office
   P.O. Box SSOP
   Washington, DC 20402–0001
   Internet: bookstore.gpo.gov
   Telephone: 202–512–1800
   Fax: 202-512-2250
2. The National Technical Information Service
   Springfield, VA 22161–0002
   www.ntis.gov
   1–800–553–6847 or, locally, 703–605–6000

A single copy of each NRC draft report for comment is available free, to the extent of supply, upon written request as follows:

Address: Office of the Chief Information Officer,
Reproduction and Distribution
Services Section
U.S. Nuclear Regulatory Commission
Washington, DC 20555–0001
E-mail: DISTRIBUTION@nrc.gov
Facsimile: 301–415–2289

Some publications in the NUREG series that are posted at NRC's Web site address http://www.nrc.gov/reading-rm/doc-collections/nuregs are updated periodically and may differ from the last printed version. Although references to material found on a Web site bear the date the material was accessed, the material available on the date cited may subsequently be removed from the site.

Non-NRC Reference Material

Documents available from public and special technical libraries include all open literature items, such as books, journal articles, and transactions, *Federal Register* notices, Federal and State legislation, and congressional reports. Such documents as theses, dissertations, foreign reports and translations, and non-NRC conference proceedings may be purchased from their sponsoring organization.

Copies of industry codes and standards used in a substantive manner in the NRC regulatory process are maintained at—

The NRC Technical Library
Two White Flint North
11545 Rockville Pike
Rockville, MD 20852–2738

These standards are available in the library for reference use by the public. Codes and standards are usually copyrighted and may be purchased from the originating organization or, if they are American National Standards, from—

American National Standards Institute
11 West 42nd Street
New York, NY 10036–8002
www.ansi.org
212–642–4900

Legally binding regulatory requirements are stated only in laws; NRC regulations; licenses, including technical specifications; or orders, not in NUREG-series publications. The views expressed in contractor-prepared publications in this series are not necessarily those of the NRC.

The NUREG series comprises (1) technical and administrative reports and books prepared by the staff (NUREG/XXXX) or agency contractors (NUREG/CR-XXXX), (2) proceedings of conferences (NUREG/CP-XXXX), (3) reports resulting from international agreements (NUREG/IA-XXXX), (4) brochures (NUREG/BR-XXXX), and (5) compilations of legal decisions and orders of the Commission and Atomic and Safety Licensing Boards and of Directors' decisions under Section 2.206 of NRC's regulations (NUREG-0750).

NUREG/CR-7203
ORNL/TM-2013/92

A Quantitative Impact Assessment of Hypothetical Spent Fuel Reconfiguration in Spent Fuel Storage Casks and Transportation Packages

Manuscript Completed: September 2013
Date Published: Month 2015

Prepared by

J. M. Scaglione, G. Radulescu, W. J. Marshall, and K. R. Robb
Oak Ridge National Laboratory
Managed by UT-Battelle, LLC
Oak Ridge, TN 37831-6170

Prepared for
Office of Nuclear Regulatory Research
U.S. Nuclear Regulatory Commission
Washington, DC 20555-0001
M. F. Bales, NRC Project Manager
NRC Job Code N6789/N6686

Office of Nuclear Regulatory Research

ABSTRACT

Based on the current knowledge, commercial spent nuclear fuel (SNF), including high burnup fuel (burnup > 45 GWd/MTU) in the United States can be stored and transported safely in accordance with the respective regulatory requirements. The NRC periodically conducts research activities to confirm the safety of operations and enhance the regulatory framework to address any changes in technology, science, and policies. This includes analyses of beyond design basis conditions to confirm that regulatory requirements continue to provide reasonable assurance for safe storage and transportation of spent nuclear fuel. The research documented in this report is an effort of such nature.

This report documents an evaluation of the impact of a wide range of extremely unlikely postulated fuel reconfigurations under non-mechanistic causes of fuel assembly geometry change with respect to four technical disciplines: criticality, shielding (dose rates), containment, and thermal. The term “fuel reconfiguration” refers to any change to the storage and transportation system nominal intact fuel assembly configuration used for the basis of cask certification. Many configurations were considered to be physically unlikely realizable scenarios.

Three fuel reconfiguration categories were considered: configurations characterized by (1) cladding failure, (2) rod/assembly deformation without cladding failure or (3) changes to assembly axial alignment without cladding failure. The analyses considered representative SNF designs and storage cask/ transportation packages, and a range of fuel initial enrichments, discharge burnup values, and decay times.

Overall, the safety impacts of fuel reconfiguration are system design, content type, and loading dependent. The areas and magnitude of the impact vary from cask/package design to cask/package design. It should also be noted that some of the scenarios are extreme and physically unlikely to occur; they represent bounding values. The spent fuel storage systems and transportation packages approved by the NRC to date provide reasonable assurance that they are safe under normal, off-normal, and hypothetical accident conditions as prescribed in 10 CFR Part 71 and 72 regulations.

FOREWORD

Part 72 and Part 71 of Title 10 of Code of Federal Regulations (10 CFR) govern the storage and transportation of spent nuclear fuel (SNF). Based on the current knowledge of material properties and mechanical performance of fuel cladding, the Nuclear Regulatory Commission (NRC) has reasonable assurance that spent nuclear fuel, including high burnup fuel (burnup > 45 GWd/MTU), is safe for storage and transport under normal, off-normal, and hypothetical accident conditions as prescribed in 10 CFR Part 72 and Part 71 for all the storage systems and transportation packages approved to date. The NRC periodically conducts research activities to confirm the safety of operations and enhance the regulatory framework to address any changes in technology, science, and policies. This includes analyses of beyond design basis conditions to confirm that regulatory requirements continue to provide reasonable assurance for safe storage and transportation of spent nuclear fuel. The research documented in this report is an effort of such nature.

This study performed a quantitative assessment of the impact of very unlikely beyond design basis hypothetical changes of fuel geometry on the safety of spent nuclear fuel storage casks and transportation packages. Specifically, this study examined the potential changes to criticality, shielding, confinement/containment, and thermal characteristics of the systems due to change of fuel geometry. The motivation of this study is, in part, to help understand the characteristics of the system's responses to fuel geometry changes.

TABLE OF CONTENTS

LIST OF FIGURES

Page

LIST OF FIGURES (continued)

LIST OF FIGURES (continued)

LIST OF FIGURES (continued)

LIST OF FIGURES (continued)

LIST OF FIGURES (continued)

LIST OF FIGURES (continued)

LIST OF FIGURES (continued)

LIST OF TABLES

Page

LIST OF TABLES (continued)

LIST OF TABLES (continued)

LIST OF TABLES (continued)

LIST OF TABLES (continued)

EXECUTIVE SUMMARY

This research performed a quantitative assessment of the safety impact of unlikely beyond-design-basis hypothetical geometric changes of the fuel in spent fuel storage casks and transportation packages. The motivation of this study is, in part, to help understand the characteristics of the system's responses to hypothetical fuel geometry changes. This study analyzed potential changes in system characteristics with respect to criticality, shielding, containment/confinement, and thermal safety parameters under a wide range of fuel reconfiguration scenarios. The following is a summary of the results of this study.

For criticality, it was postulated that the cask/package was fully flooded under normal and accident conditions, although it is very unlikely. NUREG-2125 indicates that if an accident were to occur, there is about a one-in-a-billion chance that the accident would result in loss of containment, which is a prerequisite for flooding cask internals. The actual probability of flooding is even lower when one factors in the probability of such an accident in presence of a sufficient depth of water to enable full flooding of the cask internals, as was postulated in this study for criticality. The assessment results showed that the majority of the evaluated pressurized water reactor (PWR) and channeled boiling water reactor (BWR) fuel reconfigurations result in increases in system reactivity, keff, less than 4 %Δkeff when the reconfigured fuel remains inside the neutron absorber panel envelope. For reconfigurations with fuel materials beyond the neutron absorber panel envelope and others involving unchanneled BWR fuel, the system reactivity varies widely, ranging from decreases to increases greater than 5 %Δkeff, depending on the water-to-fuel ratio and length of fuel outside the absorber envelope. However, the results are dependent on the modeling assumptions and canister characteristics, particularly the available volume above and below the neutron absorber panel envelope for the fuel rods and failed fuel fragments to accumulate. This indicates that using axial spacers to limit axial movement of fuel is an effective measure to maintain criticality safety under such conditions.

With respect to shielding design, the results showed that fuel redistribution within the central axial region of the fuel basket results in relatively small changes (up to ~10%) in the maximum dose rates at the transportation package external surfaces relative to the nominal intact fuel configuration. However, fuel redistribution toward the package internal cavity bottom and/or top regions would significantly increase (factor of 2.1 to 23.6) the dose rates at the transportation package external surfaces. For storage systems, fuel configuration changes can also cause a significant increase (factor of 1.2 to 9.6) in dose rates near the storage cask air vents. The results indicate that using axial spacers to limit axial movement of fuel is an effective measure to limit the impact on dose rates under such conditions. At locations away from storage cask air vents, the change in radiation dose rate is insignificant.

The allowable leakage rates for a storage cask and transportation package were analyzed for postulated reconfigurations under various assumptions of numbers of breached fuel rods and various release fractions. The results showed that the allowable leakage rate exhibits greatest sensitivity to changes in the fractions of fuel released as fuel fines due to cladding breaches. The results also show that the fractional contribution to radioactive material release from the pellet region increases as fuel burnup increases. Fuel released as fuel fines from the high-burnup rim structure (i.e., rim pellet region) yields a smaller allowable leakage rate than the fuel released as fuel fines from the non-rim pellet region. Because the allowable leakage rate is a function of decay-time, increases in fuel rod failure rates are offset by longer decay times. The results indicate that for the BWR fuel, the same allowable leakage rate can be obtained

for failed fuel fractions of 0.03, 0.4, and 0.7 at 5-, 40-, and 100-year decay times, respectively. The results indicate that for PWR fuel, the same allowable leakage rate can be obtained for failed fuel fractions of 0.03, 0.10, and 0.15 at 5-, 40-, and 100-year decay times, respectively.

With respect to thermal safety, the results show that postulated fuel reconfiguration resulting in relocation of the fuel pellets had the largest impact on the temperatures of the internal components of the cask. Cladding breach without fuel pellet relocation has a minor impact on component temperature for vertically oriented packages that rely on convective heat transfer because release of fission gases improves heat transfer. For bounding configurations in a vertical cask where the failed fuel was represented as a particle bed at the bottom of each basket cell, the maximum increase in component temperatures observed was 128˚C relative to the nominal intact fuel configuration. In horizontal casks that rely on conductive heat transfer, the release of the fission product gases from all assemblies would increase the internal component temperatures by about 42˚C, and for particle bed configurations, the maximum increase observed in component temperatures was 31˚C relative to the nominal intact fuel configuration. Depending on the timing, the thermal impacts of fuel failure may be offset by the decreased heat load of the fuel because the decay heat load is decreasing as a function of decay time. Results evaluated showed decreases in component temperatures by greater than 220˚C between 20 and 60 year decay times. Axial shifting of the assemblies and variations in the rod pitch has minimal impact on both internal component temperatures and the external surface temperature.

Overall, the safety impacts of fuel reconfiguration are system design, content type, and loading dependent. The areas and magnitude of the impact vary from cask/package design to cask/package design. It should also be noted that some of the scenarios are extreme and physically unlikely to occur; they represent bounding values. The spent fuel storage systems and transportation packages approved by the NRC to date provide reasonable assurance that they are safe under normal, off-normal, and hypothetical accident conditions as prescribed in 10 CFR Part 71 and 72 regulations.

ACKNOWLEDGMENTS

The authors wish to thank Michelle Flanagan, Project Manager, and Mourad Aissa of the U.S. Nuclear Regulatory Commission's Office of Regulatory Research; and Zhian Li and Meraj Rahimi of the NRC Office of Nuclear Materials Safety and Safeguards for their help in initiating, planning, and implementing this research effort. The authors also wish to thank John Wagner and Steve Bowman for their reviews, and Debbie Weaver, Katherine Ragle, and Wendy Hames for assistance in formatting and preparing the final document.

ACRONYMS

ANS	American Nuclear Society
ANSI	American National Standards Institute
BWR	boiling water reactor
CFR	Code of Federal Regulations
COBRA-SFS	Coolant Boiling in Rod Arrays—Spent Fuel Storage
CSAS	Criticality Safety Analysis Sequence
DBTT	ductile-to-brittle transition temperature
EALF	Energy of average lethargy of a neutron causing fission
ENDF/B	Evaluated Nuclear Data Files, Part B
F/I	failed to intact configuration dose rate ratio
GBC	generic burnup credit
GE	General Electric
HAC	hypothetical accident conditions
IGSCC	intergranular stress corrosion cracking
ISG	Interim Staff Guidance
k_{eff}	effective neutron multiplication factor
LWR	light water reactor
MAVRIC	Monaco with Automated Variance Reduction using Importance Calculations
MPC	multipurpose canister
NA	not applicable
NCT	normal conditions of transport
NRC	Nuclear Regulatory Commission
NUREG	NRC technical report designation (Nuclear Regulatory Commission)
OFA	optimized fuel assembly
ORIGEN-ARP	Oak Ridge Isotope Generation – Automatic Rapid Processing
ORIGEN-S	Oak Ridge Isotope Generation in Scale
ORNL	Oak Ridge National Laboratory
PWR	pressurized water reactor
SNF	spent nuclear fuel
STARBUCS	Standardized Analysis of Reactivity for Burnup Credit using Scale
TRITON	Transport Rigor Implemented with Time-Dependent Operation for Neutronic depletion

W	Westinghouse
wppm	parts per million by weight

DEFINITIONS

Assembly defect	Any change in the physical as-built condition of the assembly with the exception of normal in-reactor changes such as elongation from irradiation growth or assembly bow. Examples of assembly defects: (a) missing rods; (b) broken or missing grids or grid straps (spacers); and (c) missing or broken grid springs, etc. An assembly with a defect is damaged only if it can't meet its fuel-specific and system-related functions required by the applicable regulations. [1]
Breached spent fuel rod	Spent nuclear fuel (SNF) rod with cladding defects that permit the release of gas from the interior of the fuel rod. A breached spent fuel rod may also have cladding defects sufficient to permit the release of fuel particulate. A breach may be limited to a pinhole leak or hairline crack, or may be a gross breach. [1]
Damaged spent nuclear fuel	Any fuel rod or fuel assembly that cannot fulfill its fuel-specific or system-related functions. [1]
Grossly breached spent fuel rod	A subset of breached rods. A breach in spent fuel cladding that is larger than a pinhole leak or a hairline crack. An acceptable examination for a gross breach is a visual examination that has the capability to determine the fuel pellet surface may be seen through the breached portion of the cladding. [1]
Intact spent nuclear fuel	Any fuel that can fulfill all fuel-specific and system-related functions, and that is not breached. Note that all intact SNF is undamaged, but not all undamaged fuel is intact, since under most situations, breached spent fuel rods that are not grossly breached will be considered undamaged. [1]
Normal events and conditions	The maximum level of an event or condition expected to routinely occur. The cask system is expected to remain fully functional and to experience no temporary or permanent degradation from normal operations, events and conditions. [2]
Off-normal events and conditions	The maximum level of an event or condition that although not occurring regularly can be expected to occur with moderate frequency and for which there is a corresponding maximum specified resistance, limit of response, or requirement for a given level of continuing capability. “Off-Normal” events and conditions are similar to “Design Event II” of ANSI/ANS 57.9. An independent spent fuel storage installation structure, system, or component is expected to experience off-normal events and conditions without permanent deformation or degradation of capability to perform its full function (although operations may be suspended or curtailed during off-normal conditions) over the full license period. [2]
Ready retrieval	The ability to move a canister containing spent fuel to either a transportation package or to a location where the spent fuel can be removed. Ready retrieval also means maintaining the ability to handle individual or canned spent fuel assemblies by the use of normal means. [3]

Undamaged spent nuclear fuel	SNF that can meet all fuel-specific and system-related functions. Undamaged fuel may be breached. Fuel assembly classified as undamaged SNF may have “assembly defects.” [1]

1. INTRODUCTION

In the United States, spent nuclear fuel (SNF) is expected to remain in storage for an extended period of time. The spent fuel will then be transported to a final repository or interim storage facilitie(s). One of the possible concerns associated with spent fuel storage and transportation safety is cladding material hydride reorientation because an elevated amount of hydride reorientation in the cladding material could impair the mechanical performance of fuel assembly. This potential phenomenon is of particular concern with high burnup fuel (HBU, >45 GWd/MTU) because the potential of hydride reorientation increases as fuel burnup increases. To obtain material property data and assess the mechanical performance of high burnup cladding, Argonne National Laboratory examined the material property of some samples from high burnup fuel rods with static tests [Ref. 1, 2] and Oak Ridge National Laboratory conducted bending vibration tests [Ref. 3, 4] on high burnup fuel rods. The initial results of static and vibration tests of HBU Zircaloy-4 cladding have confirmed that HBU fuel is structurally robust. Based on results of these tests, it is determined that there is reasonable assurance that spent nuclear fuel, including high burnup (burnup > 45 GWd/MTU) fuel, is safe for storage and transport under normal, off-normal, and hypothetical accident conditions as prescribed in 10 CFR Part 71 and Part 72. Note that these confirmatory tests are not inclusive for all cladding materials. Also, the fuel assemblies will cool off over time and the external environment may change as well. Both factors may affect the mechanical performance of the fuel cladding and the fuel assembly as a whole after an extended period of storage.

This study performed a quantitative assessment of the impacts of fuel geometry changes on criticality, shielding, containment/confinement, and thermal safety of SNF storage casks and transportation packages under an unlikely hypothetical event of fuel reconfiguration. Specifically, this study examined the potential changes of these characteristics of the systems resulting from changes in fuel assembly geometry in comparison with the nominal intact fuel configuration values of these parameters.

This research has two objectives. The first one is to gain a better understanding of the safety performance characteristics of the storage casks and transportation package with respect to change in fuel geometry. The second one is to obtain insights regarding areas of the cask and package where design enhancements would result in maximum safety benefits.

Three fuel reconfiguration categories were considered and they were characterized by: (1) cladding failure, (2) rod/assembly deformation without cladding failure or (3) changes to assembly axial alignment without cladding failure. The analyses considered representative SNF designs and storage cask/ transportation packages, and a range of fuel initial enrichments, discharge burnup values, and decay times. The analyses encompass the impact from normal, off-normal, and accident conditions of storage and transportation on the fuel and fuel assembly structures. The impact on the storage cask/ transportation package system mechanical and structural components was beyond the scope of this analysis.

Under the above-mentioned three categories, a wide range of fuel reconfiguration scenarios were analyzed. The generic pressurized water reactor (PWR) and boiling water reactor (BWR) storage cask and transportation package models used in previous studies [4, 5] were adapted for use in the analyses. The PWR models contain thirty two (32) 17×17 PWR fuel assemblies representative of a Westinghouse (W) optimized fuel assembly (OFA) design and the BWR models contain sixty eight (68)10×10 BWR fuel assemblies representative of a General Electric-14 (GE14) design. Both the PWR and BWR models are representative of high-capacity-type casks/packages, and are referred to as generic burnup credit (GBC)-32 and GBC-68,

respectively. Different initial fuel enrichments (1.92 to 5.0 wt % ^{235}U), burnups (0 to 70 GWd/MTU), and decay times (5 to 300 years) were considered in the analyses. The impacts on system safety in each technical discipline with respect to fuel configuration changes were assessed relative to the corresponding nominal intact fuel configuration. However, there was no study or comparison of mechanical properties, finite element analysis stress distribution, or physical testing to evaluate the likelihood of each reconfiguration scenario. The likelihood of any particular fuel reconfiguration and the impact of that configuration on each technical discipline are dependent on many factors, and will need to be addressed on a specific basis for each storage and transportation system design. In certain instances, a reconfiguration scenario used in this study may be extreme (i.e. not physically likely). In those cases, the reconfiguration scenarios are used to represent a worst case scenario rather than a physical realization.

The baseline intact configuration consists of 0% failed fuel (i.e., intact fuel conditions). The fuel assemblies are assumed to be positioned in the center of the fuel cells of the baskets for criticality and thermal evaluations. The fuel and assembly materials are assumed to be homogenously distributed inside each fuel cell for shielding and containment analyses. Specific cases evaluated for each category were tailored with respect to each technical discipline to reflect the extent of mechanical considerations governed by the requirements of the separate nuclear safety analyses. For example, in the criticality evaluations, the cask/package is modeled as fully flooded under normal and accident conditions, although it is very unlikely (i.e., conditional probability of accident that results in loss of containment breach that could allow flooding is estimated to be 1.08×10^{-9} [6] which is consistent with other studies [i.e., 7.8×10^{-9}] [7]). The actual probability of flooding is even lower when one factors in the probability of such an accident in presence of a sufficient depth of water to enable full flooding of the cask internals.

Definitions of the various fuel reconfiguration categories selected and the basis for choosing them are provided in Sect.2. Pertinent results obtained from these analyses are provided in Sect.3; conclusions and recommendations are provided in Sect.4. Detailed descriptions of the cases developed to represent the different configurations for the technical disciplines criticality, shielding, containment, and thermal are provided in Appendixes A, B, C, and D, respectively.

2. FAILED FUEL ASSEMBLY CONFIGURATION CATEGORIES

To evaluate the potential safety implications of fuel configuration changes that can result from normal, off-normal, and accident conditions of spent fuel storage, and normal and accident conditions of transportation, three fuel reconfiguration categories were considered:

(Category 1) cladding failure
(Category 2) rod/assembly deformation without cladding failure
(Category 3) changes to assembly axial alignment without cladding failure

Within configuration categories 1 and 2, multiple scenarios were identified:

Cladding failure category

Scenario 1(a)—breached spent fuel rods
Scenario 1(b)—damaged spent fuel rods

Rod/assembly deformation category

Scenario 2(a)—configurations associated with side drop
Scenario 2(b)—configurations associated with end drop

The configuration category of assembly axial alignment changes was not broken into multiple scenarios; instead, Scenario 3 encompasses all changes to assembly axial alignment.

Each technical discipline has specific analyses that are used to demonstrate cask system performance under normal, off-normal, and accident conditions of spent fuel storage, and normal and accident conditions of transportation. Therefore, parameters were developed and analyzed for each scenario that would have the most significant implications in each technical discipline.

The following subsections will discuss each fuel reconfiguration category, including the safety-significant parameters important for the four technical disciplines, example initiating events that could result in the subject configurations, and the assumptions and conservatisms used in the analysis for the subject configurations.

2.1 CATEGORY 1: CLADDING FAILURE

The structural integrity of the cladding for high-burnup fuel may become challenged under a variety of cladding degradation mechanisms [8, 9, 10]. Several of the identified mechanisms that could lead to degradation of cladding structural integrity are driven by mechanical property changes because of hydrogen-related phenomena, including hydride embrittlement, delayed hydride cracking, and hydride reorientation. Hydrogen uptake by clad during reactor operation is a known phenomenon that affects the mechanical properties of the cladding. The hydrogen typically remains in solution at elevated temperatures and precipitates out during cooling as platelets primarily oriented in the circumferential direction [11, 12]. During spent fuel cask-drying operations, cladding temperatures become elevated because of decreased heat removal because of the removal of water. At elevated temperatures some of the hydrogen goes into solution while the rod-internal-pressure-induced stress increases relative to in-reactor operation (i.e., reactor primary coolant is pressurized). As the cladding cools under stress, some of the

dissolved hydrogen reprecipitates in the radial direction across the cladding wall if the hoop stress is high enough. This phenomenon is known as hydride reorientation. Radial hydrides can degrade the ductility of the cladding. After cooling to about 200°C, most of the dissolved hydrogen will have reprecipitated as hydrides, with further cooling during storage potentially resulting in radial-hydride-induced embrittlement. The temperature at which embrittlement occurs is referred to as the ductile-to-brittle transition temperature (DBTT) [11].

The cladding temperature of fuel that has been in storage for a long time may drop below DBTT. Once the cladding temperature goes below DBTT, the fuel rods are more susceptible to failure under load impacts. In addition, measured data are limited and typically are characterized by a relatively high level of uncertainty regarding mechanical performance of high-burnup fuel cladding. Given the uncertainty and variability of fuel rod material properties, different degrees of fuel rod cladding failure followed by release of material into the canister cavity during normal handling and transfer operations before and during transportation should be considered. Grossly breached spent fuel rods within the canister potentially may occur under the impacts of natural phenomena such as earthquakes or tornados, resulting in cask tip-over. Horizontal drops can induce pinch forces that can result in longitudinal tearing as described in Ref. [13] and illustrated in Figure 1 resulting in fuel particle relocation. During transportation, if the cladding temperature is below DBTT, failure of fuel rods within the package may occur under normal conditions of transport (NCT) as prescribed in 10 CFR 71.71, as well as a result of impacts from accident loads specified in 10 CFR 71.73, particularly the 30-ft drop and puncture testing in the orientations that cause the most damage to the package containment vessel.

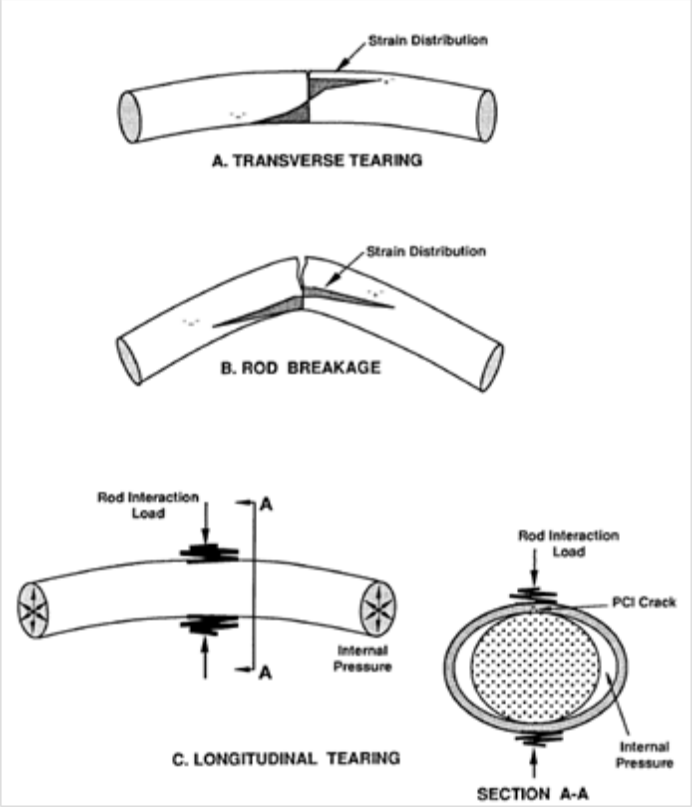

Figure 1 – Illustration of fuel rod failure mechanisms [13]

Analyses of the cladding failure category was designed to represent the effects of two scenarios: S1(a), breached spent fuel rods where the cladding has failed to the extent to allow for a loss of gas and fuel particles from single or multiple locations with the rod segment and fuel fragments collecting at different locations within the cask, and S1(b), damaged spent fuel rods where the cladding has failed to the extent to allow free movement of fuel particles and pellets within a basket cell. Damaged SNF is a bounding condition that represents the maximum degree of fuel configuration change that may occur under cladding failure scenarios.

Safety-significant parameters with respect to this category for each scenario in each technical discipline are provided in Table 1 and Table 2.

Table 1 – Case descriptions to evaluate the effects of breached spent fuel rods

Technical discipline	Configuration scenario	Parameter(s) evaluated	Rationale for parameter selection
Criticality	S1(a)	Lattice positions from where fuel particulate could be displaced	Commercial light water reactor (LWR) fuel assemblies are designed to be undermoderated. Fuel rods that suffer cladding failure can result in sections of fuel within the lattice being replaced with water, which increases moderation and potentially increases reactivity. The issue of concern is whether the reactivity increase exceeds the original licensed design basis subcritical limit.
Shielding	S1(a)	Fraction of spent fuel redistributed and canister basket cavity regions where particulate accumulates	Storage and transportation overpacks are designed to maintain dose rates within acceptable limits assuming known source distributions based on intact assemblies. Clad failure can result in relocation of the fuel mixture and associated radiation source terms, thereby potentially affecting the design basis external dose rates.
Containment	S1(a)	Fraction of breached spent fuel rods; in addition for high-burnup fuel, release fractions for the contributors to the releasable activity and pellet region from which the radioactive material originates	Evaluate impacts on allowable leakage rates of different spent fuel rod breach fractions for NCT and releasable source term distribution in high-burnup fuel caused by rim effect. A sensitivity analysis is performed for high-burnup fuel because the range of parameters important for the containment analysis (i.e., the release fractions and breached spent fuel rod fraction) has not been established yet for NCT.
Thermal	S1(a)	Fraction of spent fuel rods experiencing cladding failure that release fission product and rod backfill gases (varied from 0 to100%)	The release of fuel rod inert gas and fission product gases affects the thermophysical properties of the canister gas space. The change in gas properties can affect the efficiency of heat removal, and therefore component temperatures, to varying degrees depending on the cask/package design and orientation. The sensitivity analysis will investigate the impact on component temperatures.

Table 2 – Case descriptions to evaluate the effects of damaged fuel

Technical discipline	Configuration scenario	Parameter(s) evaluated	Rationale for parameter selection
Criticality	S1(b)	Geometry changes and modeling homogenous versus heterogeneous representations of fuel debris mixture	Geometry and neutron energy spectrum are fundamental parameters used to define a design basis configuration. Any changes in these parameters will affect the system k_{eff}. These cases evaluate the effects of having an uncontrolled geometry, and the effects of different modeling simplifications to represent regions and packing fractions where particulate could relocate.
Shielding	S1(b)	Regions where fuel particles could redistribute	Fuel particle relocation has a potential of increasing cask external dose rates at the top or bottom because of its proximity to those surfaces and as a result of intensifying the source term where the fuel has relocated. This can also affect the dose at the controlled area boundary. In addition, neutron streaming above or below the radial neutron shield in a transportation package may significantly increase the neutron dose rate on the package external radial surface.
Containment	S1(b)	For high-burnup fuel, varying release fractions for the contributors to the releasable activity and pellet region from which the radioactive material originates	Evaluate impacts on allowable leakage rates for hypothetical accident conditions (HAC) considering releasable source term distribution in high-burnup fuel caused by the rim-effect. A sensitivity analysis is performed for high-burnup fuel because the range of parameters important for the containment analysis (i.e., the release fractions) has not been established yet for HAC.
Thermal	S1(b)	The number of assemblies (1 or 32 [all]) and the packing fraction of the debris (0.612–0.313) to investigate the impact of fuel redistribution on component temperatures.	Changes to the internal canister gas properties as well as location and geometry of the heat source within the canister can alter the convective flow paths within the canister. These phenomena can affect the efficiency of heat removal from the cask/package and therefore the temperatures of components important to safety.

2.2 CATEGORY 2: ROD/ASSEMBLY DEFORMATION

Depending upon the fuel temperature and mechanical properties of the fuel assembly, a range of potential internal configurations are possible when a spent fuel package is involved in an impact event. The side, end, and corner drops may result in geometry changes depending on the orientation of the cask during the drop, the magnitude of the impact, and the mechanical properties of the fuel assembly components.

Packages used for storage and transportation have been certified via analysis or testing and, in many instances, by using a combination of analysis and testing. A number of studies and tests

have been performed over the years to investigate the impact of NCT and HAC on fuel assemblies that are contained within a transportation package [13, 14, 15, 16, 17, 18]. Additionally, in the early 2000s, TN International and International Nuclear Services started a joint program, the Fuel Integrity Project, to assess potential damage to fuel assemblies and confirm assumptions used in criticality-safety studies [15]. Overall, analyses and tests have indicated that during horizontal (side) drop, the fuel rods are primarily subjected to loads that can result in fuel rod bending or some degree of plastic deformation when the cladding is still ductile so that the lattice pitch of the fuel assemblies tends to reduce. In a vertical (end) drop orientation, the axial loading can lead to buckling of the fuel rods. Several pictures showing the resultant configurations of “dummy” fresh fuel assemblies after drop tests are presented in Figure 2 and Figure 3. The difference between actual fuel assemblies and the “dummy” fuel assemblies is that actual enriched UO_2 fuel pellets were substituted with depleted UO_2 pellets with similar mechanical properties [15]. Note that these drop tests are from fuel contained in a fresh fuel package, which experiences higher g-loads than a spent fuel package would receive, but they are illustrated here to show how fuel may deform after an impact event.

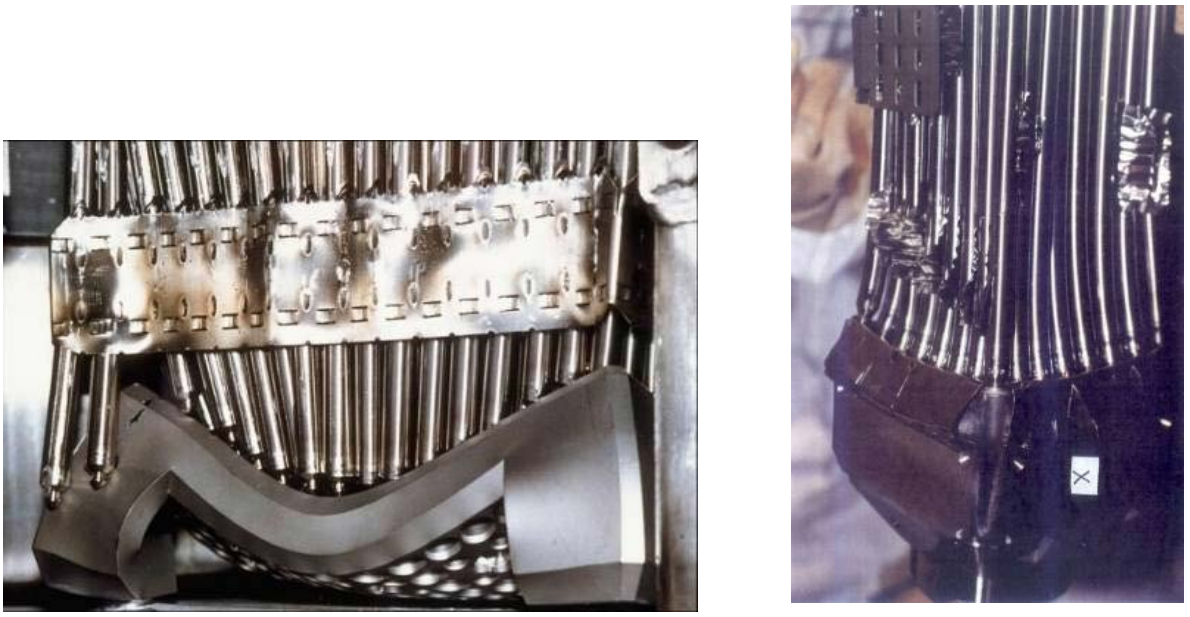

(a) PWR fuel assembly (b) BWR fuel assembly

Figure 2 – Photographs of dummy fuel assemblies after 9-m end drops [15]

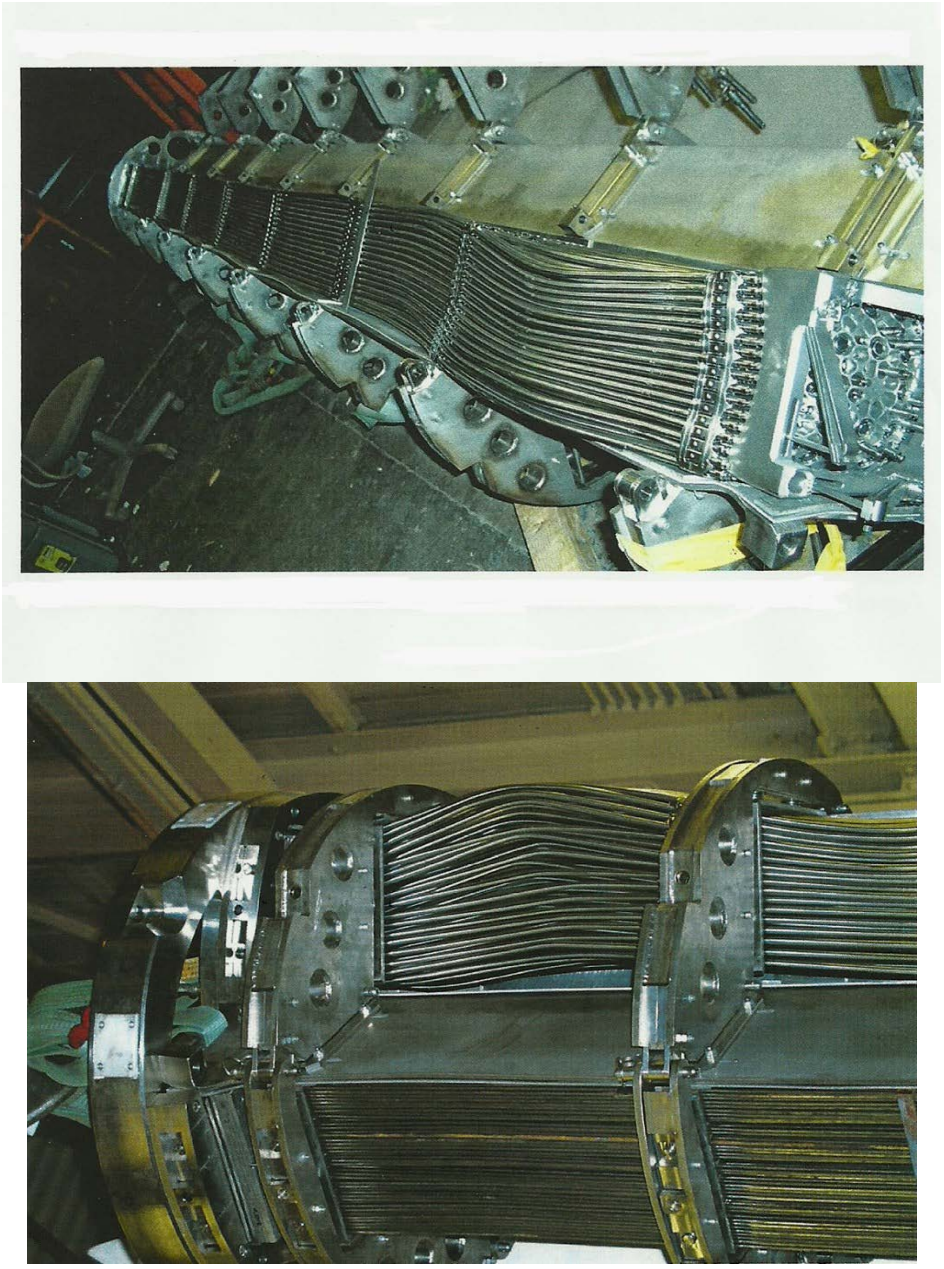

Figure 3 – Photographs illustrating assembly fuel rod buckling after a 9-m end drop test [19]

Effects that can influence material strength and structural integrity of the cladding and fuel assembly include neutron fluence (e.g., grid spring relaxation, irradiation hardening, growth, cladding creep down), corrosion (e.g., thinning, oxidation, hydrogen uptake), operating conditions (e.g., temperature), and drying conditions (e.g., temperature, residual moisture). Analytical methods for calculating load responses and characteristics of fuel rods during and after impact events require assumptions that are difficult to determine, such as percentage of fuel mass that is bonded to or participates with the cladding during the buckling process as discussed in Ref. [20]. Additionally, BWR and PWR fuel assemblies are designed differently, and some of these differences result in different mechanical responses on the fuel rods under

impact events. Representative BWR and PWR fuel assemblies are shown in Figure 4 to illustrate some of the design differences. Besides the BWR fuel assembly being channeled, the fuel rods are connected to upper and lower tie plates. In the PWR fuel assembly, the fuel rods are not directly connected to the upper and lower end fittings, leaving a small gap between the ends of the rods and the end fittings. Under horizontal drop events, this design difference does not result in noticeable differences on fuel rod response between a PWR and BWR fuel assembly; however, it can alter the response under vertical drop events [15]. This fuel reconfiguration category investigates the impact of pin pitch changes that could result as potential end states associated with side/horizontal and end/vertical drop events consistent with NCT as prescribed in 10 CFR 71.71, as well as a result of impacts from accident loads specified in 10 CFR 71.73.

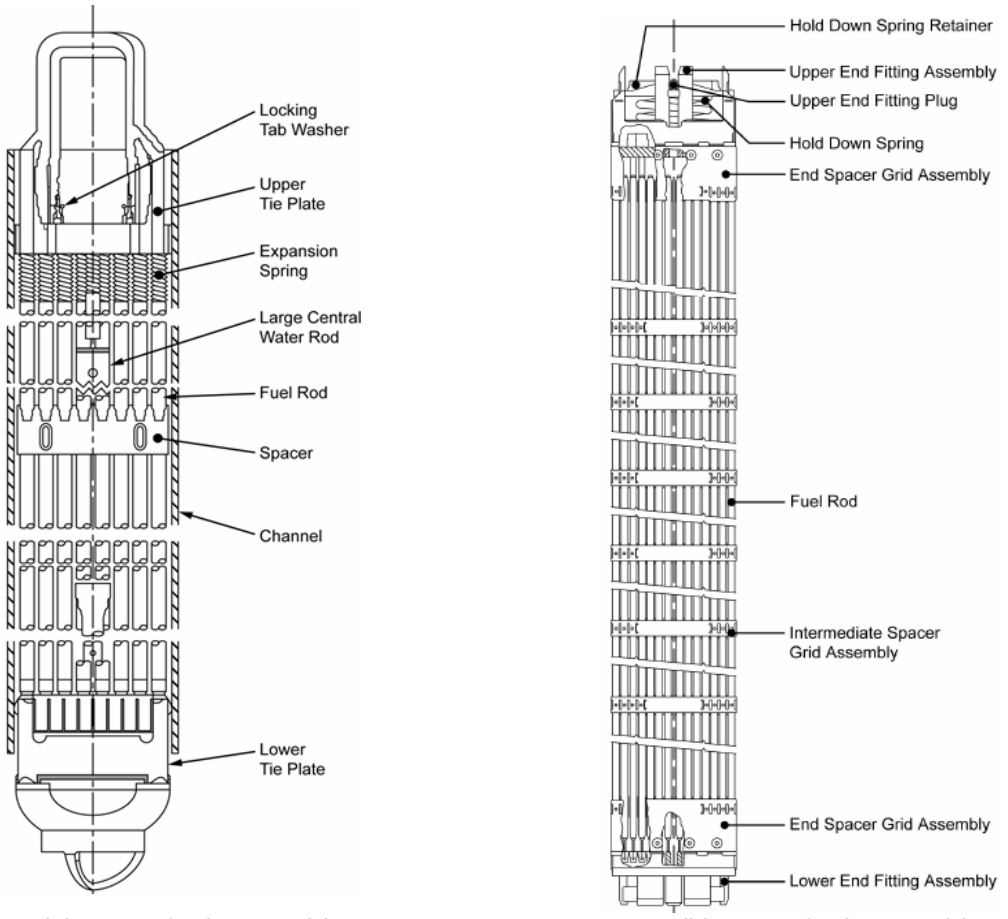

(a) BWR fuel assembly (b) PWR fuel assembly

Figure 4 – Representative BWR and PWR fuel assemblies [21]

Analyses in this fuel reconfiguration category evaluate the impact of fuel rod and assembly deformation when the fuel cladding is able to absorb the loads of the initial impact event and remain intact (i.e., cladding does not fail). All configurations that involve cladding failure are evaluated in the cladding failure category (see Sect. 2.1). Two fuel reconfiguration scenarios are considered: S2(a), configurations associated with side/horizontal drop; and S2(b), configurations associated with end/vertical drop.

Schematic illustrations of the resultant changes to the fuel assembly lattice geometry considered for a horizontal drop event are illustrated in Figure 5 and Figure 6 for a PWR and a BWR package, respectively. The parameters identified to represent the most significant implications of the horizontal drop event in each technical discipline are provided in Table 3.

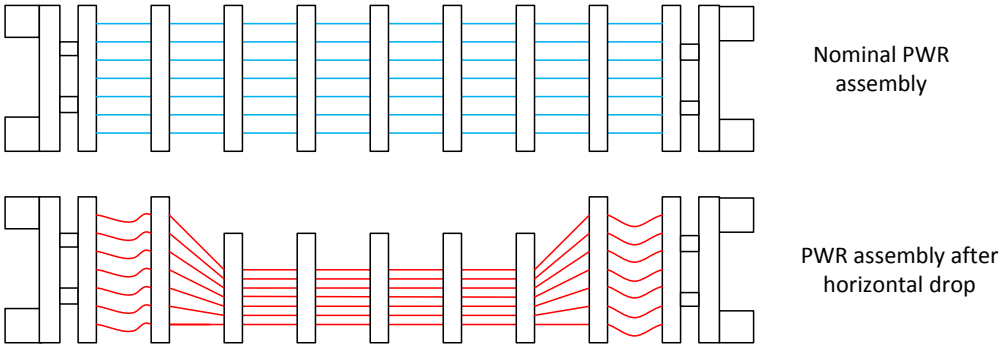

Figure 5 – Schematic representation of PWR fuel assembly before and after horizontal drop event (figure adapted from Ref. [15]**)**

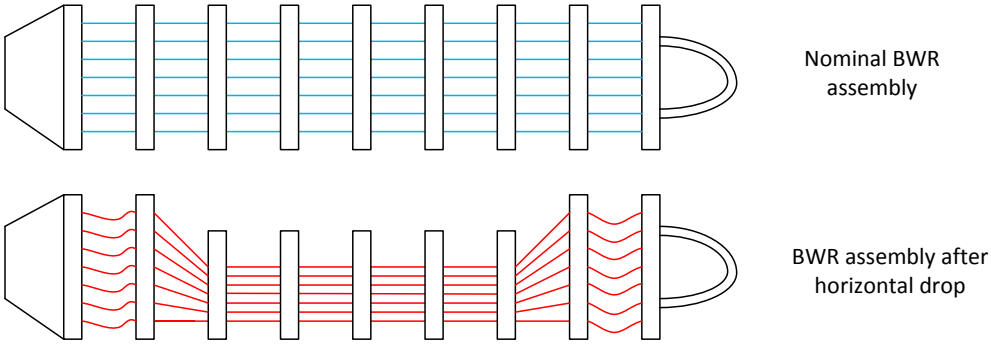

Figure 6 – Schematic representation of BWR fuel assembly before and after horizontal drop event (figure adapted from Ref. [15]**)**

Table 3 – Parameters to evaluate the effects of rod/assembly deformation resulting from side/horizontal drop events in each technical discipline

Technical discipline	Configuration scenario	Parameter(s) evaluated	Rationale for parameter selection
Criticality	S2(a)	Pin pitch contraction	Evaluate impacts of changes to design basis neutron energy spectrum
Shielding	S2(a)	Assembly lattice collapse	Localized source displacement toward cask radial surface can affect radial dose rate requirements as a result of reduced geometric attenuation
Containment	S2(a)	Fraction of crud that spalls off cladding (varied from 0.05 to 1.0)	Evaluate sensitivity to fraction of crud removed.
Thermal	S2(a)	Pin pitch contraction	The contraction of the fuel assembly lattice can affect the efficiency of heat removal from the fuel because of changes in flow area (convection), conduction lengths (conduction), and radiation view factors (thermal radiation).

Schematic illustrations of the resultant changes to the fuel assembly lattice geometry considered for a vertical drop event are illustrated in Figure 7 and Figure 8. Note that compaction is shown for the BWR assembly (also referred to as bottlenecking), and expansion is shown for the PWR assembly (also referred to as birdcaging), but a combination of the two along the axial length of the fuel assembly is also considered. The parameters identified to represent the most significant implications of the vertical drop event in each technical discipline are provided in Table 4.

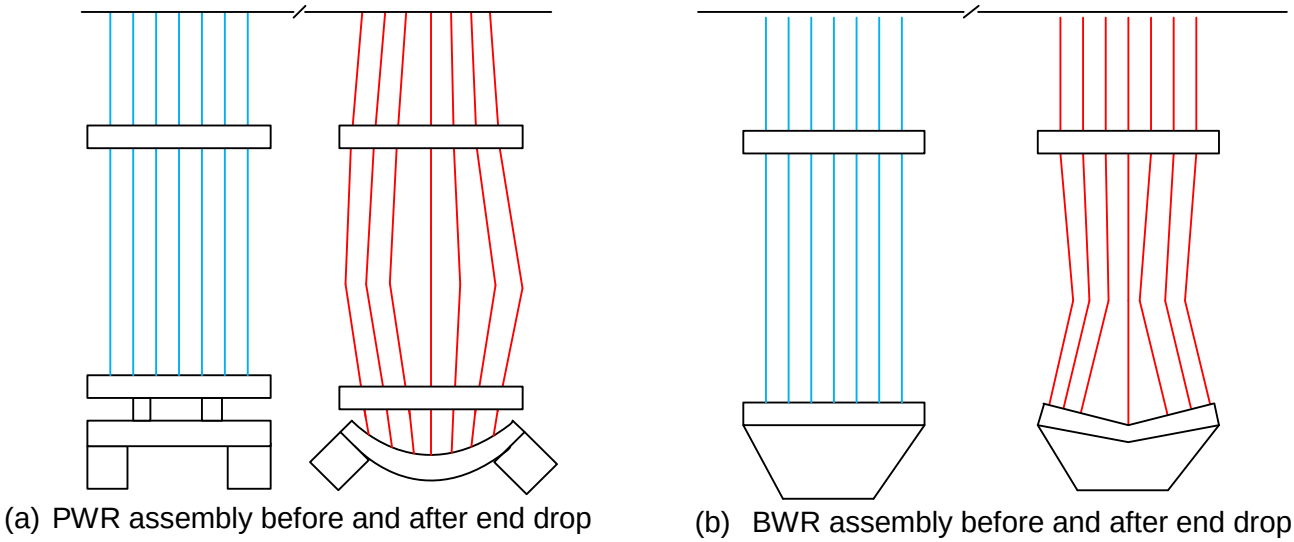

(a) PWR assembly before and after end drop (b) BWR assembly before and after end drop

Figure 7 – Schematic representation of PWR and BWR fuel assemblies before and after a vertical drop event (figure adapted from Ref. [15]**)**

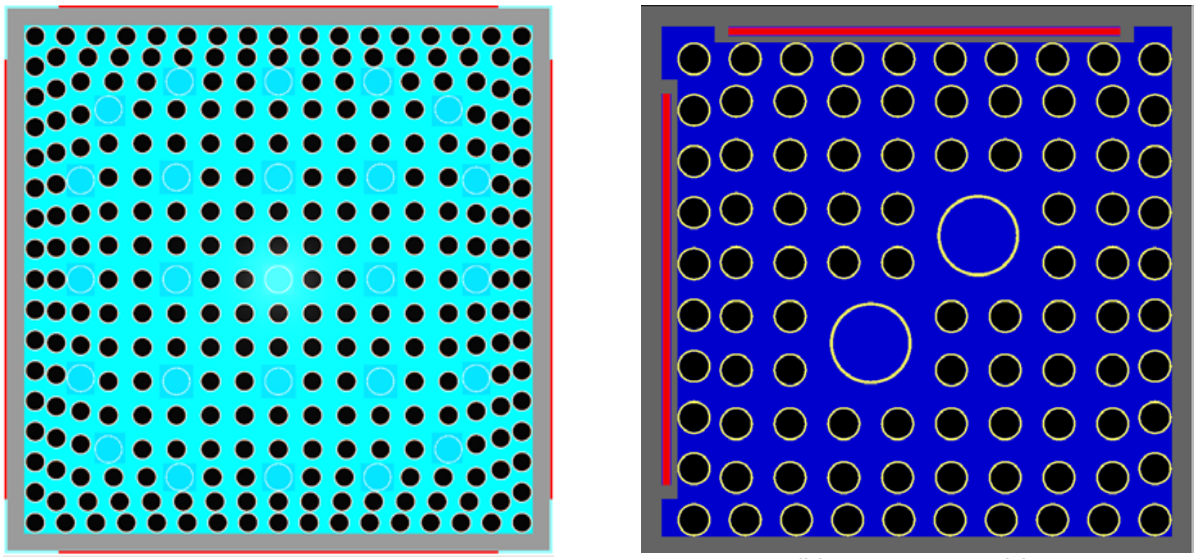

(a) PWR assembly (b) BWR assembly

Figure 8 – Example configuration for non-uniform pitch expansion

Table 4 – Parameters to evaluate the effects of rod/assembly deformation resulting from end/vertical drop events in each technical discipline

Technical discipline	Configuration scenario	Parameter(s) evaluated	Rationale for parameter selection
Criticality	S2(b)	Uniform and non-uniform radial and axial pin pitch changes (birdcaging and bottlenecking)	Evaluate impacts of changes to design basis geometry and neutron energy spectrum
Shielding	S2(b)	Not applicable	Bounding configuration for this category is scenario S3 (Table 5) where fuel assembly axial displacement toward the bottom lid is evaluated.
Containment	S2(b)	Fraction of crud that spalls off cladding (varied from 0.05 to 1.0)	Evaluate sensitivity to fraction of crud removed.
Thermal	S2(b)	Assembly pin pitch expansion	The expansion of the fuel assembly lattice can affect the efficiency of heat removal from the fuel because of changes in flow area (convection), conduction lengths (conduction), and radiation view factors (thermal radiation).

2.3 CATEGORY 3: CHANGES TO ASSEMBLY AXIAL ALIGNMENT

Fuel baskets used in typical storage and transportation packages contain neutron absorbers affixed to the basket cell walls. Most of the absorbers present in currently deployed spent fuel canisters are in plate form that does not extend the full length of the basket; they are held in place by a thin gauge stainless steel sheath. A schematic representation of a fuel assembly within a basket cell is illustrated in Figure 9. Some of the more recent basket designs made of metal matrix composites integrate the absorber into the basket material, in which case the absorber does extend the full length of the basket [22].

Different types of overpacks are used for storage and transportation. The storage system typically consists of a thick storage overpack made of steel, concrete, or a combination of the two that fully encompasses the spent fuel canister. Figure 10 illustrates a typical storage overpack configuration. For transportation, the overpack typically consists of a layered shell with several different materials to provide shielding for gamma rays and neutrons, as well as to provide a means for heat removal. The axial extent of the package radial neutron shielding does not always extend the full length of the containment vessel because the package needs an allowance for attaching the impact limiters on the ends. Hence, the cavity volume of the canister may not be fully covered with shielding material. Figure 11 illustrates a typical configuration for a rail spent fuel transportation package.

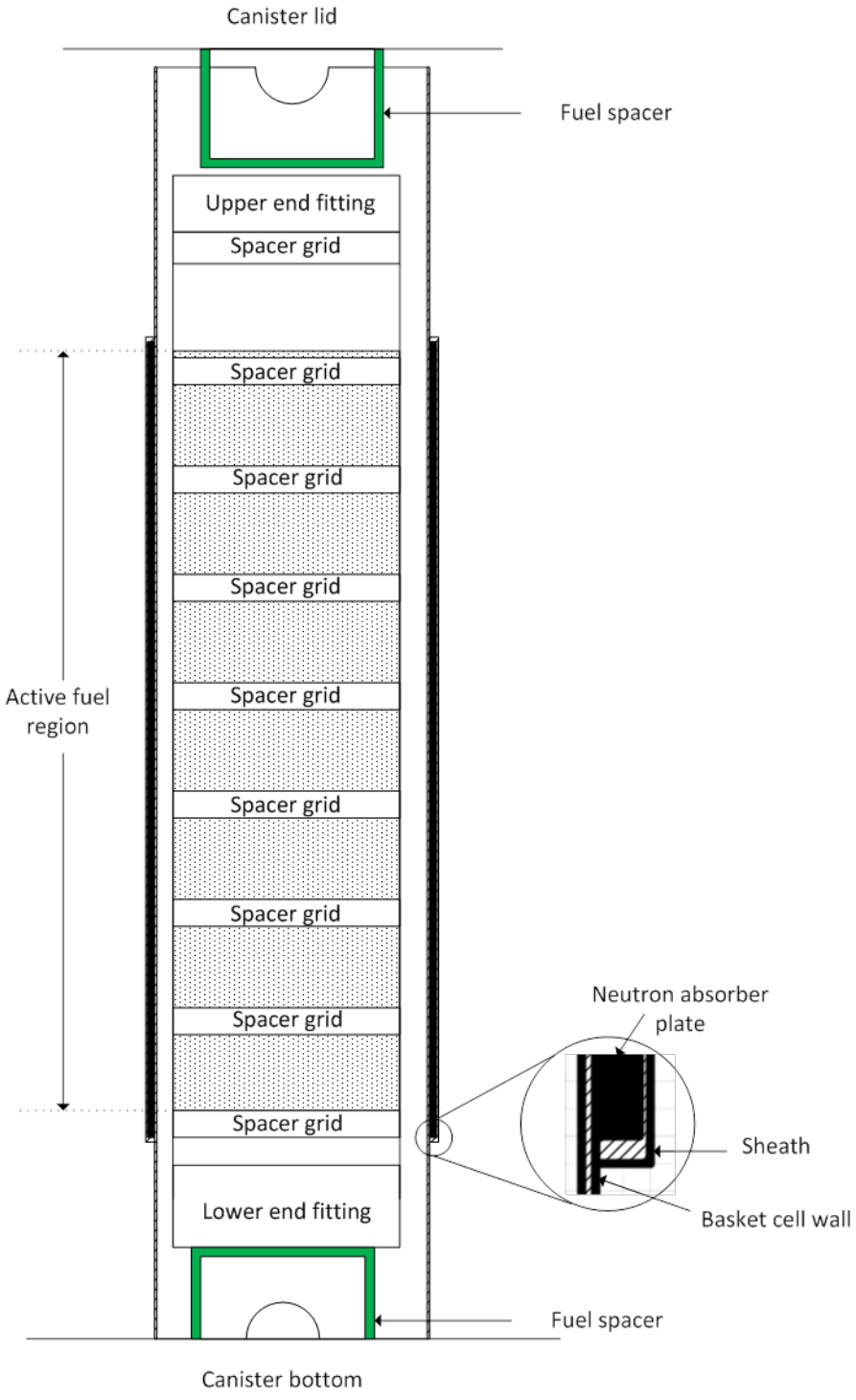

Figure 9 – Schematic representation of fuel assembly within a typical basket cell

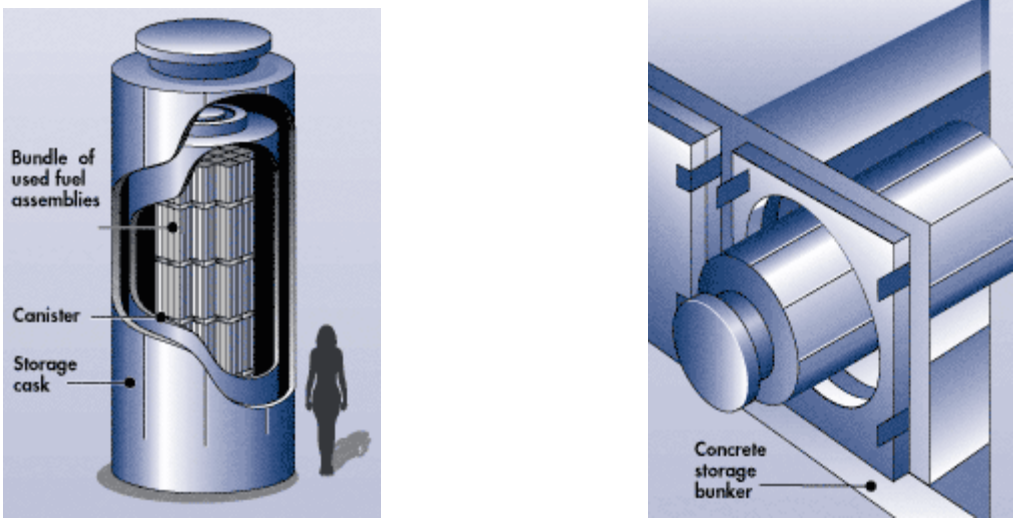

(a) Illustration of vertical aboveground concrete or steel structure.

(b) Illustration of horizontal aboveground concrete bunker.

Figure 10 – Example storage pack configuration for both vertical (a) and horizontal (b) storage modules [23]

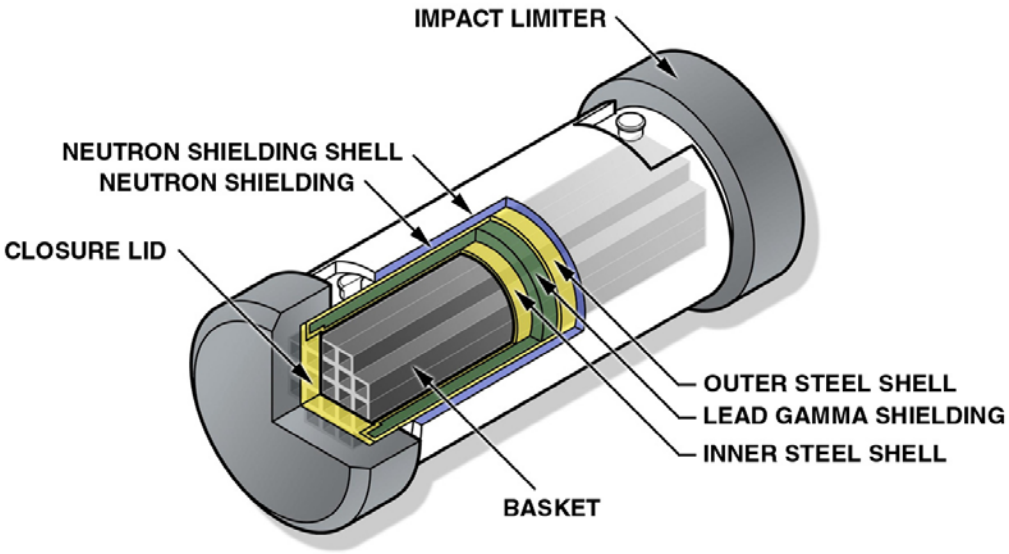

Figure 11 – Example rail spent fuel transportation package [24]

The safety features of the canister fuel basket and the transportation overpack (e.g., neutron absorber plates, gamma and neutron shield, and cooling fins) typically have been designed presuming that the fuel assembly remains in a fixed geometric location within the package under normal and accident conditions of transportation. Fuel spacers are designed to restrain the fuel assembly within the basket cell to ensure axial alignment of the active fuel region within the neutron absorber envelope, as well as to provide a fixed source location within the extent of the transportation overpack.

While the degree of axial movement should be limited, transportation package testing has shown that post-buckling bending deformations, regions of lattice expansion, and interaction with deformed nozzles, such as illustrated in Figure 2(a) above, can result in some fuel rods sliding past the end fitting, resulting in a loss of axial geometry control from the as-designed configurations. Other drop test results such as that shown in Figure 12 illustrate how the end region of an assembly can become crushed.

Figure 12 – Photo of BWR assembly after drop test [25]

Additionally, the presence of some residual moisture in the canister after drying is expected, and can promote corrosion and/or stress corrosion cracking of fuel assembly hardware components while the SNF is in dry storage. Intergranular stress-corrosion cracking (IGSCC) is a known failure mechanism that can result in dislocation of the top nozzle end fitting from the remainder of the assembly [26], leaving space for fuel rod axial shifting.

Finally, sequences that can lead to axial movements include handling operations while preparing a package for transportation, under NCT as prescribed in 10 CFR 71.71, and HAC loads as specified in 10 CFR 71.73. These phenomena (i.e., end fitting deformation, IGSCC, lattice expansion), individually or in combination indicate that changes to the axial alignment of the fuel within the cask should be considered and are being evaluated with regards to the potential effects on the safety functions.

Analyses in this fuel reconfiguration category evaluate the impact of changes to assembly axial alignment assuming the fuel cladding is able to absorb the loads of the initial impact event and remain intact (i.e., cladding did not fail). All configurations that involve cladding failure are evaluated in the cladding failure category (see Sect. 2.1). Safety-significant parameters with respect to this category for each technical discipline are provided in Table 5.

Table 5 – Parameters to evaluate the effects of fuel assembly components being axially displaced within the basket cavity of a transportation package in each technical discipline

Technical discipline	Configuration scenario	Parameter(s) evaluated	Rationale for parameter selection
Criticality	S3	Fuel assembly axial position	Evaluate effects of active fuel region being outside neutron absorber plate envelope in basket cell.
Shielding	S3	Fuel assembly axial position	This configuration has the potential to significantly increase dose rate at the cask top and bottom surfaces as well as at the radial surface above and below the neutron shield because the radiation sources are moved closer to these surfaces.
Containment	S3	Fraction of crud that spalls off cladding (varied from 0.05 to 1.0)	Evaluate sensitivity to fraction of crud removed.
Thermal	S3	Fuel assembly axial position	Axial shifting of the assembly changes the heat source location within the canister. This can affect the heat removal via convection within vertical casks/packages. Shifting of assemblies is likely to have a minor impact on component temperatures. However, cases were investigated where all the assemblies are fully shifted axially within their respective basket cells to investigate the impact on component temperatures.

3. CONSEQUENCE ANALYSIS

This section addresses the consequences of fuel configuration changes with respect to the different technical disciplines. Nominal intact fuel configuration cases were developed for each technical discipline against which the impacts of the fuel reconfiguration could be measured. The nominal intact fuel configuration models and corresponding analysis approach are described in Appendixes A, B, C, and D for the criticality, shielding, containment, and thermal analyses, respectively. The consequences are reported as relative changes between the fuel reconfiguration and the nominal intact configuration. Criticality consequences are associated with a change in k_{eff}, shielding consequences are associated with changes to external dose rates, containment consequences are associated with release rates, and thermal consequences are concerned with component (e.g., seals, cladding, basket, neutron absorber, and surface) temperature changes. For all analyses, it was assumed that the containment barrier had not been breached for a sufficient length of time to make oxidation of structures, systems, or components a consideration. The basis for this assumption is that this allows the effects of geometry changes to be evaluated individually for impact on system performance.

The following descriptions apply when referring to a canister, cask, or package: The spent fuel is emplaced within a canister (as shown in Figure 10) which is then either represented as being surrounded by a concrete storage cask (see Figure 10) or a multi-layered transportation cask (see Figure 11). The combined canister and transportation cask is referred to as a transportation package. The terms GBC-32 and GBC-68 identify whether the canister contains PWR or BWR fuel, respectively.

3.1 CATEGORY 1: CLADDING FAILURE

Cladding failure includes breached spent fuel rods, grossly breached spent fuel rods, and damaged fuel. This fuel reconfiguration category encompasses the greatest amount of variability for consideration when developing explicit models.

3.1.1 Criticality

The consequences of cladding failure with respect to criticality control require criticality calculations to investigate the changes associated with both grossly breached and damaged spent fuel geometries. To have an effect on system performance the SNF rods must be grossly breached such that the geometry and neutron energy spectrum present within the SNF canister are altered from the design basis configuration. The primary requirements for demonstrating subcriticality include 10 CFR 71.55(b), (d), and (e).

Because of the effects of geometry changes, the cladding failure category can result in a large number of potential configurations with a wide range of reactivity effects. Two configuration scenarios were developed to evaluate the effects of cladding failure: S1(a), breached spent fuel rods; and S1(b), damaged spent fuel rods.

Breached spent fuel rods. To evaluate the effects of breached spent fuel rods, including grossly breached spent fuel rods, cases were developed to model the effects of rod failure and changes in moderator-to-fuel ratios. Multiple rod removal patterns were evaluated by removing groups of rods in symmetric patterns until a peak k_{eff} value was identified. Figure 13 shows the results for the GBC-32 cases and Figure 14 shows the results for the GBC-68 cases. For these two sets of cases, the displaced fuel was omitted from the model, assuming that it would be

sufficiently dispersed away from the lattice in a thin, undermoderated heap resulting in a less reactive system than if incorporated into the model. The maximum Δk_{eff} value (i.e., a k_{eff} increase of 1.87% Δk_{eff}) for the GBC-32 cask representation occurs for the 5 wt % ^{235}U initial enriched fuel with a burnup of 44.25 GWd/MTU and 300-year decay time case when 44 rods have been removed from the lattice configuration. The maximum Δk_{eff} value (i.e., k_{eff} increase of 2.40% Δk_{eff}) for the GBC-68 cask occurs for the 5 wt % ^{235}U initial enriched fuel with a burnup of 35 GWd/MTU and 5-year decay time case when 18 rods have been removed from the lattice configuration with the channel present. The maximum Δk_{eff} value changes for this configuration scenario are provided in Table 6.

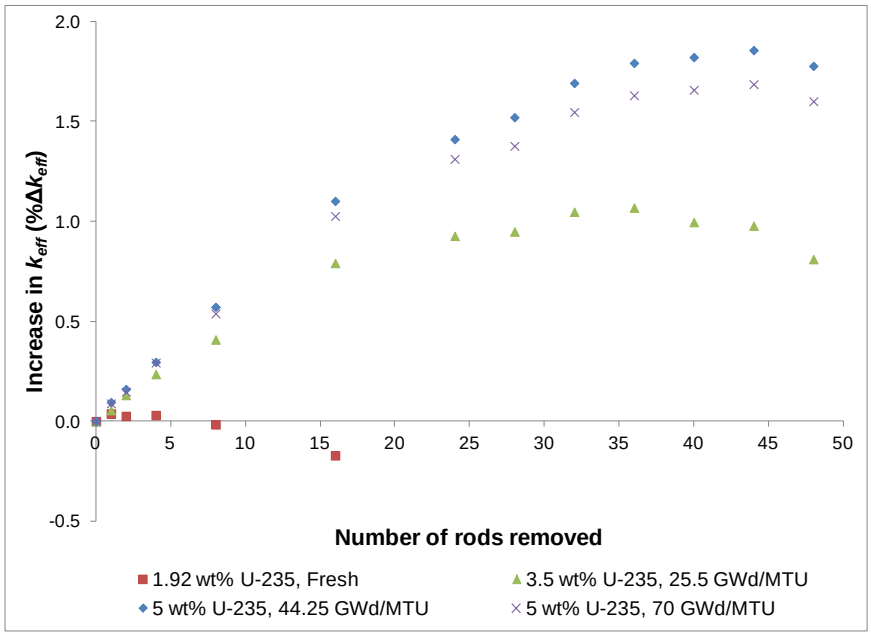

Figure 13 – Change in k_{eff} in GBC-32 as a function of number of rods removed

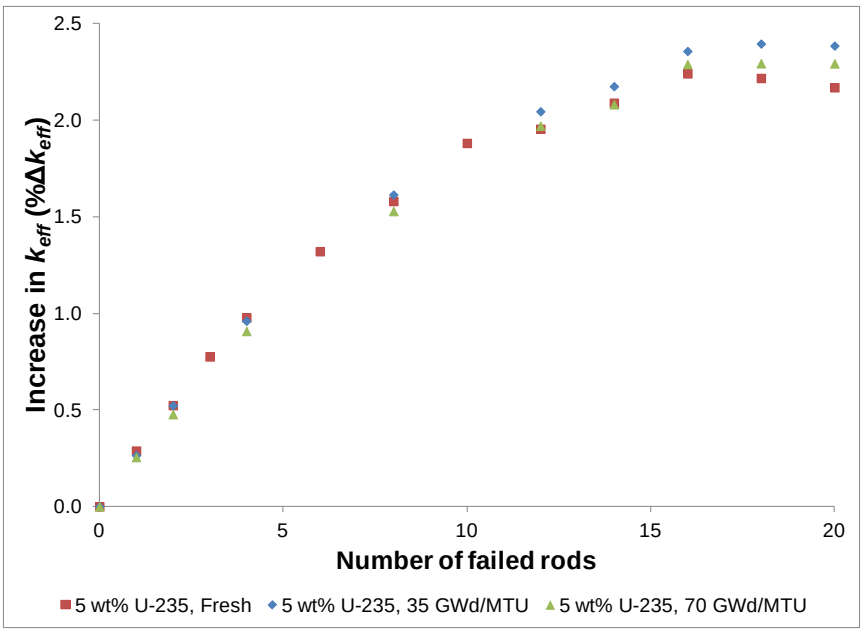

Figure 14 – Change in k_{eff} in GBC-68 as a function of number of rods removed

Table 6 – Criticality results for scenario S1(a)—breached spent fuel rods

Parameter				
PWR system				
Burnup (GWd/MTU)	0	25.5	44.25	70
Initial enrichments (wt % ^{235}U)	Maximum change in k_{eff} (%Δk_{eff})			
1.92	0.04	NC	NC	NC
3.5 with 5-year decay time	NC	1.07	NC	NC
5.0 with 5-year decay time	NC	NC	1.86	1.69
5.0 with 80-year decay time	NC	NC	1.86	1.62
5.0 with 300-year decay time	NC	NC	1.87	1.62
BWR system				
Burnup (GWd/MTU)	0	35	70	
Initial enrichment (wt % ^{235}U)	Maximum change in k_{eff} (%Δk_{eff}) channeled/unchanneled			
5.0 with 5-year decay time	2.24/2.11	2.40/2.30	2.30/2.20	
5.0 with 80-year decay time	NC	2.40/2.31	2.31/2.18	
5.0 with 300-year decay time	NC	2.42/2.29	2.32/2.20	

Note: NC = not calculated.

An additional subset of cases was developed to investigate the combined effects of rod removal and spent fuel displacement to regions outside the neutron absorber envelope. Only the PWR fuel was represented with 5.0 wt% ^{235}U initial enrichment at 44.25 GWd/MTU burnup and 5-year decay time. For these cases, the region above the active fuel zone and outside the neutron absorber plate envelope was modeled with fuel at different volume fractions simulating various sized particles with different bulk densities. The volume displacement of hardware components in this region was omitted from these models to maximize the reactivity effect. Note that this is a significant conservative assumption. Results provided in Table 7 show that combining the rod removal with displaced fuel distributed at ratios approaching optimum moderation conditions outside the absorber envelope yields higher changes in k_{eff} than the rod removal configurations alone. However, the magnitude of the effect is highly sensitive to the available void volume

outside the neutron absorber panel envelope, which is canister basket, fuel spacer, and assembly design dependent.

Table 7 – Combined rod removal and displaced fuel model results in GBC-32

Number of failed rods	Volume fraction of displaced fuel	Length of region above absorber filled (cm)	Change in k_{eff} (%Δk_{eff})	Change in k_{eff} (%Δk_{eff}) (Rod removal only)
40	0.524	30	3.89	1.82
28	0.341	30	4.91	1.52
8	0.146	20	3.55	0.57

Damaged fuel. To evaluate the consequences of extensive cladding failure, cases were developed to represent scenario S1(b), damaged spent fuel rods. Two subclasses of cases were used for this evaluation – one where the fuel is represented as a homogenous rubble mixture distributed throughout the basket cavity, and the other where the fuel is represented as a uniform pellet array to simulate a heterogeneous mixture. The fuel mixtures were allowed to be distributed throughout the entire basket cell cavity including outside the neutron absorber envelope. Fuel spacers were not included in the representations, and assembly hardware (i.e., cladding and guide tubes) were only included in the homogeneous rubble mixture representations. The results for this fuel reconfiguration scenario are provided in Table 8 and show that the modeling approximations based on homogenous representations are less conservative than the heterogeneous models. While models of 100% fuel rubblization are extreme and not physically likely under normal, off-normal, and accident conditions of storage, and under NCT as prescribed in 10 CFR 71.71, or as a result of impacts from accident loads specified in 10 CFR 71.73, they provide a simplified approach for estimating an upper bound on the potential reactivity increase. The consequences for this configuration scenario are very sensitive to the modeling approximations and resultant water to fuel ratio represented above or below the neutron absorber panel envelope.

Table 8 – Criticality results for scenario S1(b)—damaged spent fuel rods

Parameter				
PWR system				
Burnup (GWd/MTU)	0	25.5	44.25	70
Initial enrichments (wt % ^{235}U)	Maximum change in k_{eff} (%Δk_{eff}) limiting pellet array/homogeneous mixture			
1.92	11.09/6.66	NC	NC	NC
3.5 with 5-year decay time	NC	20.20/13.95	NC	NC
5.0 with 5-year decay time	NC	NC	21.37/14.30	21.43/14.20
5.0 with 80-year decay time	NC	NC	22.21/15.29	21.63/14.77
5.0 with 300-year decay time	NC	NC	22.21/15.34	21.77/14.90
BWR system				
Burnup (GWd/MTU)	0	35		70
Initial enrichment (wt % ^{235}U)	Maximum change in k_{eff} (%Δk_{eff}) limiting pellet array (homogeneous mixture channeled/unchanneled)			
5.0 with 5-year decay time	28.12 (21.68/22.90)	34.40 (28.58/29.36)		35.22 (29.31/29.93)
5.0 with 80-year decay time	NC	34.88 (29.12/29.87)		35.57 (29.74/30.33)
5.0 with 300-year decay time	NC	34.87 (29.13/29.83)		35.63 (29.81/30.40)

Note: NC = not calculated.

Overall, the most limiting configurations to evaluate the consequences of cladding failure on criticality safety are represented by models where displaced fuel is relocated to regions above or below the neutron absorber panel envelope. Configurations that only consider rod removal may be under-predicting the impact of cladding failure by not accounting for the displaced fuel. Configurations that represent the fuel as damaged and distributed throughout the basket cavity are bounding but may not be physically likely under normal, off-normal, or accident conditions of storage, or normal and accident conditions of transportation.

3.1.2 Shielding

Understanding the consequences of cladding failure on external radiation dose rates requires shielding analyses to investigate the changes associated with both breached and damaged fuel geometries. The primary transportation requirements that shielding analyses address are identified in 10 CFR 71.47 for NCT and 10 CFR 71.51 for HAC. The requirements describe package external dose rate limits for specific distances from the package or transportation vehicle. For storage of SNF, dose limits at the controlled area boundary are specified in 10 CFR 72.104 for normal and off-normal conditions and 10 CFR 72.106 for accident conditions. Regulatory guidance [2] indicates that a shielding analysis of a single cask and a generic array of casks at large distances may be used to demonstrate that the radiation shielding features of a proposed dry storage system are sufficient for it to meet the radiation dose requirements in 10 CFR 72.104 and 10 CFR 72.106(b). The minimum distance required between spent fuel and the controlled area boundary specified in 10 CFR 72.106 is 100 m. For storage, the effects of fuel configuration changes on dose rate were determined at 1 m from a generic storage cask and at 100 m from a 4×2 cask array (see Appendix B.3.2).

The consequences of fuel configuration changes were evaluated by comparing external dose rate values between the nominal intact and fuel reconfigurations. This approach helps identify the fuel reconfigurations that yield higher external dose rates than the nominal intact fuel configuration and thus have the potential to exceed the regulatory limits. Package/storage cask external gamma and neutron dose rate values were evaluated separately because fuel configuration changes have different effects on gamma and neutron radiation, and the overall impact of fuel configuration changes on the external dose rate depends on the individual gamma and neutron dose rate contributions to the total dose rate. Generic PWR and BWR SNF transportation package/storage cask models based on GBC-32 and GBC-68, respectively, were developed for the shielding analysis (see Appendix B). The transportation package models have general shielding characteristics (e.g., thick inner gamma shield and outer neutron shield) similar to real high-capacity SNF transportation packages. The storage cask model has a vertical concrete overpack.

The W 17×17 OFA and GE14 assemblies with 5 wt % ^{235}U initial enrichment, 65 GWd/MTU burnup, and typical axial burnup profiles were used in this analysis (see Appendix B). The effect of fuel configuration changes on external radiation dose rates was determined as a function of decay time (i.e., time after fuel discharge from the reactor). The fuel decay times of 5 and 40 years were analyzed because the contribution to cask external dose rates of ^{60}Co (half-life [$t_{1/2}$] = 5.271 years), which is an activation source in the assembly plenum and lower and upper hardware regions, is significant for a 5-year decay time and negligible for a 40-year decay time. Neutron and gamma spectra variations are relatively small for decay times relevant to this analysis (e.g., <120 years) beyond 5 and 40 years after fuel discharge, respectively.

For the 5-year decay time, the gamma dose rate at the package bottom and top surfaces is high primarily because of the proximity of the ^{60}Co activation source to those surfaces, the activation source strength, and energetic gamma rays of 1.25-MeV average energy. The ^{60}Co activation source has negligible contributions to gamma dose rates for the 40-year decay time and beyond. Therefore, the contribution of the ^{60}Co activation source to the gamma dose rates at the package bottom and top surfaces varies as a function of decay time. A large contribution of the ^{60}Co activation source to the gamma dose rate, as in the case of a 5-year decay time, equates to a relatively small increase of the gamma dose rate because of fuel relocation to the assembly hardware regions. A small or negligible contribution of the ^{60}Co activation source to the gamma dose rate, as in the case of a 40-year decay time, equates to a relatively large increase of the gamma dose rate because of fuel relocation to assembly hardware regions. That is, the effects on the gamma dose rates at the package bottom and top surfaces from fuel relocation into assembly hardware regions are significantly smaller for the 5-year decay time than those for the 40-year decay time.

Breached spent fuel rods. The effects of breached spent fuel rods (i.e., source term redistribution) on package external dose rates was analyzed by considering different percentages of failed fuel rods per assembly (i.e., 10% and 25% for the PWR fuel and 11% for the BWR fuel) and fuel redistribution to different assembly axial regions, including the active fuel region, and the lower and upper hardware regions. Important parameters used in the calculation models:

(1) Relocation of fuel fragments and particulates from a failed assembly is confined within the space delimited by the fuel assembly basket plates and by the assembly top and bottom spacers.
(2) One hundred percent of the fuel in the failed fuel rods is displaced to a different assembly region.
(3) Fuel fragments and particulates from failed fuel rods form a closely packed mixture with a mass packing fraction of 0.58 based on powder mechanics for particles similar to sand [27].

Because the packing fraction, or particle density, is dependent upon the particle size distribution a second higher mass packing fraction value of 0.67 was also used for sensitivity calculations. The specific fuel rod failure percentage values were selected arbitrarily because actual data on the expected fuel rod failure rate is not available. However, the whole range of fuel failure with respect to the amount of fuel mixture (0 – 100%) that may be displaced to canister cavity regions is analyzed in this report under the different fuel reconfiguration categories. The 25% fuel rod failure value for the PWR SNF was analyzed to determine whether there is a direct proportionality between the amount of redistributed fuel mixture and the external dose rate (i.e., whether an increase in the displaced fuel mixture quantity from 10% to 25% equates to an increase in external dose rate by a factor of 2.5).

Damaged fuel. To evaluate the consequences of extensive cladding failure representative of scenario S1(b)—damaged spent fuel rods, two cases were analyzed: (1) fuel mixture assumed to form closely packed powder in the canister cavity bottom; and (2) fuel mixture homogeneously distributed within the canister cavity volume. These configurations are bounding for cladding failure scenarios resulting in fuel fragments and particulates being collected into the inner cavity regions below or above the fuel spacers or between the canister basket outer plates and radial canister wall. The latter modeling approach is often used to generate conservative dose rate estimates because the model is characterized by reduced gamma self-shielding (i.e., reduced gamma radiation absorption within the fuel mixture with lower particle density) as well

as reduced gamma and neutron geometric attenuation (i.e., radiation source is closer to inner cavity walls) compared to the nominal intact fuel configuration. From all cases analyzed in this study, the damaged fuel configurations produced the greatest changes in the maximum dose rate on the cask external surfaces relative to the nominal intact fuel configuration.

The ratio of the maximum surface dose rate value for a fuel reconfiguration to the maximum surface dose rate for the nominal intact fuel configuration, which is identified as the failed to intact (F/I) configuration dose rate ratio, is summarized in Table 9 (cases 1 to 8 for the breached spent fuel rod cases, and cases 9 and 10 for the damaged fuel cases) for the evaluated PWR fuel reconfigurations and in Table 10 (cases 1 to 4 for the breached spent fuel rod cases, and cases 5 and 6 for the damaged fuel cases) for the evaluated BWR fuel reconfigurations, under NCT. For the analysis considering NCT, the F/I dose rate values are provided at the package external surfaces and at the 2 m locations. For the analysis considering HAC, the outer neutron shield considered in the package models for NCT was replaced with air and the dose rates were calculated at 1 m from the package external surfaces. The F/I dose rate ratio values for HAC are provided in Table 11 and Table 12 for PWR and BWR package models, respectively.

For the breached spent fuel rod cases analyzed:

- the change in maximum gamma and neutron dose rates on the external surfaces of the casks was insignificant (~10% for both PWR and BWR fuel) for fuel collected into the middle portion of the active fuel (i.e., away from the upper and lower ends of the active fuel);

- a significant increase of the maximum neutron dose rate (e.g., ~6.2, 3.5, and 2.8 times as large as the reference maximum top, radial, and bottom dose rate values, respectively, for the analyzed PWR cases) was determined for fuel mixture collected into either assembly bottom or top regions;

- the impact on dose rates from fuel redistribution to the assembly top and bottom regions was more pronounced for BWR fuel than for PWR fuel (e.g., ~22 versus 5 times as large as the nominal intact configuration maximum top neutron dose rate values, respectively);

- for shorter decay times (e.g., 5-years), fuel configuration changes had a greater impact on the neutron dose rate than on the gamma dose rate at the external surfaces of the packages (e.g., maximum dose rate on the radial surface from all analyzed cases increased by ~30% for the gamma radiation and by a factor of 3.5 for the neutron radiation);

- for longer decay times (e.g., 40-years), fuel configuration changes had a greater impact on the gamma dose rate than on the neutron dose rate at the external surfaces of the packages (e.g., maximum dose rate on the top surface from all analyzed cases increased by a factor of ~85 for the gamma radiation and by a factor of ~24 for the neutron radiation); and

- a larger percentage (i.e., 25% versus 10% analyzed for PWR fuel) of fuel mixture distributed to the assembly axial regions did not increase the dose rates at the package axial surfaces proportionally to the source strength increase (e.g., the F/I ratio values for the neutron dose rate at the top external surface were ~6.2 and 5 for the 25% and 10%

quantities, respectively) because of an increased geometric attenuation associated with the larger percentage value.

For the damaged fuel cases analyzed:

- the maximum top, radial, and bottom neutron dose rate values were ~6.7, 3.9, and 4.2 times as large as the corresponding nominal intact configuration dose rate values for the PWR package model; the maximum top, radial, and bottom neutron dose rate values were ~23.5, 3.3, and 6 times as large as the corresponding nominal intact configuration dose rate values for the BWR package model;

- for the 40-year decay time, the maximum top and bottom PWR gamma dose rates were ~14 and 7 times, respectively, as large as the corresponding PWR nominal intact configuration dose rate values; the maximum top and bottom BWR gamma dose rates were ~84 and 27 times, respectively, as large as the corresponding BWR nominal intact configuration dose rate values; and

- the gamma dose rate increase for shorter decay times (e.g.5-years) is significantly smaller than that for longer decay times (e.g., 40-years).

Table 9 – PWR package maximum dose rate change for NCT

Package external surfaces				Top			Side			Bottom		
Case #	Scenario	Fuel relocation region[b]	Decay time (years)	F/I dose rate ratio[a]								
				n	γ	Total	n	γ	Total	n	γ	Total
1	10% fuel rod failure	Assembly active fuel	5	1.09	1.01	1.07	1.01	1.02	1.01	1.04	1.00	1.02
			40	1.09	1.00	1.09	1.01	1.01	1.00	1.03	1.00	1.03
2	10% fuel rod failure	Assembly lower end fitting	5	1.06	1.00	1.05	1.62	0.99	0.99	2.52	1.34	2.10
			40	1.06	1.00	1.06	1.59	0.98	1.32	2.53	5.17	2.67
3	10% fuel rod failure	Assembly plenum	5	3.96	0.98	3.43	2.37	0.99	1.48	1.03	1.01	1.02
			40	3.96	3.35	3.96	2.38	0.99	1.96	1.02	0.99	1.02
4	10% fuel rod failure	Assembly upper end fitting	5	4.98	0.93	4.27	2.75	0.99	1.66	1.05	1.01	1.01
			40	4.99	11.55	5.00	2.77	0.99	2.34	1.02	1.00	1.02
5	25% fuel rod failure	Assembly active fuel	5	1.12	1.00	1.10	1.06	1.12	1.09	1.00	1.00	1.00
			40	1.13	1.00	1.13	1.06	1.10	1.07	1.00	0.96	0.99
6	25% fuel rod failure	Assembly lower end fitting	5	1.05	1.00	1.04	1.76	0.98	0.96	2.76	1.33	2.25
			40	1.05	1.00	1.05	1.76	0.97	1.45	2.76	5.16	2.88
7	25% fuel rod failure	Assembly plenum	5	4.59	0.97	3.95	2.79	0.95	1.69	1.00	0.99	0.99
			40	4.58	3.34	4.57	2.80	0.96	2.30	0.99	0.96	0.99
8	25% fuel rod failure	Assembly upper end fitting	5	6.16	0.93	5.23	3.50	0.95	2.03	1.00	1.00	1.00
			40	6.13	11.59	6.14	3.51	0.96	2.94	0.99	0.95	0.99
9	Damaged	Canister cavity bottom	5	0.32	0.001	0.26	2.57	1.19	1.47	4.18	1.72	3.30
			40	0.32	0.02	0.32	2.59	1.21	2.18	4.13	8.37	4.34
10	Damaged	Entire canister cavity	5	6.69	0.84	5.56	3.89	1.10	2.48	3.04	1.43	2.47
			40	6.67	14.10	6.68	3.89	1.24	3.40	3.05	7.30	3.21

Table 9 – continued

2 m from the package surfaces				Top			Side			Bottom		
Case #	Scenario	Fuel relocation region[b]	Decay time (years)	F/I dose rate ratio[a]								
				n	γ	Total	n	γ	Total	n	γ	Total
1	10% fuel rod failure	Assembly active fuel	5	1.07	1.01	1.05	1.02	1.00	1.01	1.02	1.00	1.01
			40	1.08	1.00	1.08	1.02	1.00	1.01	1.02	0.99	1.02
2	10% fuel rod failure	Assembly lower end fitting	5	1.04	1.01	1.03	1.02	0.99	1.00	2.29	1.33	1.92
			40	1.06	1.02	1.06	1.06	1.01	1.05	2.23	4.82	2.40
3	10% fuel rod failure	Assembly plenum	5	3.48	0.99	2.93	1.02	0.98	1.00	1.04	1.01	1.03
			40	3.36	1.26	3.36	1.07	1.01	1.05	1.00	0.98	1.00
4	10% fuel rod failure	Assembly upper end fitting	5	4.27	0.94	3.54	1.01	0.99	1.00	1.04	1.01	1.00
			40	4.19	2.85	4.21	1.08	1.01	1.07	1.00	0.98	1.00
5	25% fuel rod failure	Assembly active fuel	5	1.11	1.00	1.09	1.04	1.04	1.04	0.99	0.99	0.99
			40	1.11	0.99	1.11	1.02	1.00	1.02	0.98	0.96	0.98
6	25% fuel rod failure	Assembly lower end fitting	5	1.04	1.00	1.03	0.99	0.96	0.98	2.51	1.34	2.06
			40	1.05	0.96	1.05	1.03	1.00	1.02	2.39	4.76	2.54
7	25% fuel rod failure	Assembly plenum	5	4.08	0.98	3.40	1.06	0.95	0.97	0.99	0.99	1.00
			40	4.00	1.28	3.99	1.09	1.01	1.07	0.96	0.96	0.96
8	25% fuel rod failure	Assembly upper end fitting	5	5.27	0.95	4.32	1.25	0.95	0.96	0.99	0.99	0.99
			40	5.13	2.88	5.14	1.15	1.01	1.10	0.97	0.95	0.97
9	Damaged	Canister cavity bottom	5	0.30	0.03	0.23	1.02	1.07	1.02	4.01	2.17	3.30
			40	0.29	0.26	0.29	0.94	0.94	0.92	3.95	10.56	4.38
10	Damaged	Entire canister cavity	5	5.94	1.04	4.86	1.28	1.11	1.08	2.90	1.78	2.47
			40	5.79	5.02	5.83	1.24	1.32	1.19	2.80	9.11	3.21

[a]Relative error (95% confidence level) less than 7% for all values except for the gamma F/I value for the case #9, top surface, the relative error is 15%.
[b]Farthest region for fuel relocation identified. Fuel mixture may extend into adjacent assembly axial regions; axial location is described in Sect. B.5.1

Table 10 – BWR package maximum dose rate change for NCT

Package external surfaces				Top			Side			Bottom		
Case #	Scenario	Fuel relocation region[b]	Decay time (years)	F/I dose rate ratio[a]								
				n	γ	Total	n	γ	Total	n	γ	Total
1	11% fuel rod failure	Assembly active fuel	5	1.13	0.98	1.11	1.02	1.02	1.02	1.06	0.99	1.02
			40	1.14	1.01	1.14	1.03	1.01	1.02	1.07	0.97	1.07
2	11% fuel rod failure	Assembly lower tie plate and nosepiece	5	1.14	1.02	1.12	1.43	0.97	0.99	4.37	1.21	2.88
			40	1.14	1.00	1.13	1.42	0.97	1.22	4.44	24.39	4.58
3	11% fuel rod failure	Assembly plenum	5	12.74	1.40	11.05	1.78	0.96	1.11	1.05	0.99	1.02
			40	12.98	13.67	12.98	1.75	0.98	1.48	1.08	0.97	1.08
4	11% fuel rod failure	Assembly upper tie plate and handle	5	21.78	3.22	19.02	2.42	0.96	1.65	1.06	1.01	1.04
			40	21.77	84.60	21.83	2.41	0.99	2.12	1.07	0.98	1.07
5	Damaged	Canister cavity bottom	5	0.60	0.003	0.51	1.84	1.35	1.63	5.99	1.17	3.72
			40	0.61	0.15	0.61	1.81	1.40	2.12	6.04	32.19	6.22
6	Damaged	Entire canister cavity	5	23.48	2.90	20.41	3.27	0.98	2.25	4.31	0.94	2.72
			40	23.52	84.18	23.58	3.26	1.11	2.90	4.37	26.71	4.53
2 m from the package surfaces				**Top**			**Side**			**Bottom**		
Case #	**Scenario**	**Fuel relocation region[b]**	**Decay time (years)**	**F/I dose rate ratio[a]**								
				n	**γ**	**Total**	**n**	**γ**	**Total**	**n**	**γ**	**Total**
1	11% fuel rod failure	Assembly active fuel	5	1.11	0.99	1.08	1.04	0.98	1.02	1.04	0.99	1.01
			40	1.11	0.98	1.11	0.98	1.00	0.97	1.03	0.99	1.03
2	11% fuel rod failure	Assembly lower tie plate and nosepiece	5	1.12	1.00	1.09	1.04	0.96	1.01	3.78	1.19	2.43
			40	1.09	1.01	1.09	1.05	1.00	1.04	3.79	19.79	3.97
3	11% fuel rod failure	Assembly plenum	5	10.62	1.44	8.70	1.03	0.96	1.11	1.04	0.99	1.01
			40	10.15	1.37	10.15	1.07	0.99	1.06	1.05	1.00	1.05
4	11% fuel rod failure	Assembly upper tie plate and handle	5	17.12	3.21	14.21	1.02	0.97	1.00	1.02	1.00	1.01
			40	16.24	4.94	16.33	1.04	0.99	1.03	1.05	1.01	1.05
5	Damaged	Canister cavity bottom	5	0.53	0.12	0.42	2.19	1.29	1.76	5.62	1.34	3.38
			40	0.52	0.46	0.52	2.01	1.24	1.90	5.57	32.09	5.86
6	Damaged	Entire canister cavity	5	25.23	3.28	7.77	1.23	0.98	0.98	3.93	1.07	2.44
			40	18.88	6.07	18.99	1.11	1.18	1.08	3.89	26.50	4.14

[a] Relative error (at the 95% confidence level) less than 7% for all values except for the gamma F/I value for case #5, top surface, the relative error is 20%.

[b] Farthest region for fuel relocation identified. Fuel mixture may extend into adjacent assembly axial regions; axial location is described in Sect. B.5.3.

Table 11 – PWR package maximum dose rate change for HAC

1 m from the package surfaces				Top			Side			Bottom		
Case #	Scenario	Fuel relocation region[b]	Decay time (years)	F/I dose rate ratio[a]								
				n	γ	Total	n	γ	Total	n	γ	Total
1	10% fuel rod failure	Assembly active fuel	5	1.07	1.00	1.06	1.01	1.00	1.01	1.02	1.00	1.01
			40	1.07	0.98	1.08	1.02	0.97	1.02	1.02	0.96	1.02
2	10% fuel rod failure	Assembly lower end fitting	5	1.04	0.99	1.02	1.02	1.00	1.02	2.14	1.33	1.96
			40	1.05	1.00	1.05	1.02	0.97	1.02	2.19	4.89	2.27
3	10% fuel rod failure	Assembly plenum	5	3.35	0.98	2.79	1.02	1.00	1.02	1.03	1.01	1.02
			40	3.36	1.28	3.44	1.00	0.97	1.00	1.02	0.95	1.02
4	10% fuel rod failure	Assembly upper end fitting	5	4.12	0.93	3.37	0.99	0.97	1.01	1.13	1.01	1.10
			40	4.17	3.31	4.19	1.01	0.96	1.01	1.09	0.95	1.01
5	25% fuel rod failure	Assembly active fuel	5	1.10	0.99	1.07	1.01	1.02	1.01	0.99	0.98	0.99
			40	1.10	1.04	1.11	1.01	0.99	1.01	1.16	0.94	1.16
6	25% fuel rod failure	Assembly lower end fitting	5	1.03	1.00	1.02	1.00	0.96	0.99	2.42	1.35	2.18
			40	1.03	1.01	1.03	0.99	0.94	0.99	2.37	4.88	2.37
7	25% fuel rod failure	Assembly plenum	5	3.92	0.98	3.23	0.99	0.97	0.99	0.99	0.99	0.99
			40	3.99	2.02	3.99	0.98	1.08	0.98	0.98	1.05	0.98
8	25% fuel rod failure	Assembly upper end fitting	5	5.05	0.93	4.08	0.99	0.96	0.99	1.00	0.99	1.00
			40	5.12	4.74	5.21	0.98	1.09	0.98	0.98	1.05	0.98
9	Damaged	Canister cavity bottom	5	0.29	0.02	0.22	0.78	0.99	0.81	3.79	2.23	3.44
			40	0.29	0.26	0.21	0.80	1.05	0.81	3.82	10.19	4.01
10	Damaged	Entire canister cavity	5	5.80	1.06	4.69	0.96	1.14	0.99	2.73	1.83	2.53
			40	5.90	5.43	5.93	0.93	1.17	0.93	2.69	8.66	2.89

[a]Relative error (at the 95% confidence level) less than 5% for all values except for the gamma F/I value for case #9, top surface, the relative error is 20%.
[b]Farthest region for fuel relocation identified. Fuel mixture may extend into adjacent assembly axial regions, as described in Sect. B.5.1.

Table 12 – BWR package maximum dose rate change for HAC

1 m from the package surfaces				Top			Side			Bottom		
Case #	Scenario	Fuel relocation region[b]	Decay time (year)	F/I dose rate ratio[a]								
				n	γ	Total	n	γ	Total	n	γ	Total
1	11% fuel rod failure	Assembly active fuel	5	1.04	1.01	1.08	1.04	0.98	1.03	1.08	0.99	1.05
			40	0.99	0.99	0.99	1.02	0.98	1.02	1.06	0.96	1.06
2	11% fuel rod failure	Assembly lower end fitting	5	1.04	1.00	1.10	1.01	0.96	1.00	3.57	1.21	2.79
			40	1.01	1.01	1.00	1.00	0.97	1.01	3.65	16.99	3.72
3	11% fuel rod failure	Assembly plenum	5	6.86	1.42	6.65	1.04	0.97	1.03	1.04	1.00	1.03
			40	6.72	1.58	6.65	1.01	0.98	1.01	1.07	0.98	1.07
4	10% fuel rod failure	Assembly upper end fitting	5	11.36	3.18	11.15	1.00	0.97	1.00	1.06	1.00	1.04
			40	11.06	6.49	11.00	1.00	0.97	1.00	1.05	0.94	1.05
5	Damaged	Canister cavity bottom	5	0.43	0.06	0.45	0.77	1.02	0.80	5.26	1.37	3.98
			40	0.44	0.33	0.43	0.77	1.03	0.78	5.33	26.24	5.45
6	Damaged	Entire canister cavity	5	12.84	3.28	12.56	0.83	0.99	0.85	3.69	1.09	2.83
			40	12.74	7.39	12.90	0.83	1.05	0.84	3.68	21.69	3.78

[a]Relative error (at the 95% confidence level) less than 5% for all values except for the gamma F/I value for case #5, top surface, the relative error is 20%.
[b]Farthest region for fuel relocation identified. Fuel mixture may extend into adjacent assembly axial regions, as described in Sect. B.5.3.

Graphs illustrating comparisons of the neutron and gamma dose rate profiles between the nominal intact fuel configuration and the fuel reconfigurations analyzed are provided in Appendix B for the 40-year decay time. The effects on the total dose rate profiles at the PWR package external surfaces and at the 2 m locations are illustrated in Figure 15 and Figure 16, respectively, for the fuel reconfiguration with 25% fuel mixture collected into the assembly bottom region. The relative errors (at the 95% confidence level) are 3% and 5% for the total dose rates at the package external surfaces and at the 2 m locations, respectively. Note the total dose rate profiles illustrated in the figures are specific to the package model used in this analysis, which is described in Sect. B.3.1, and are not applicable to different package designs.

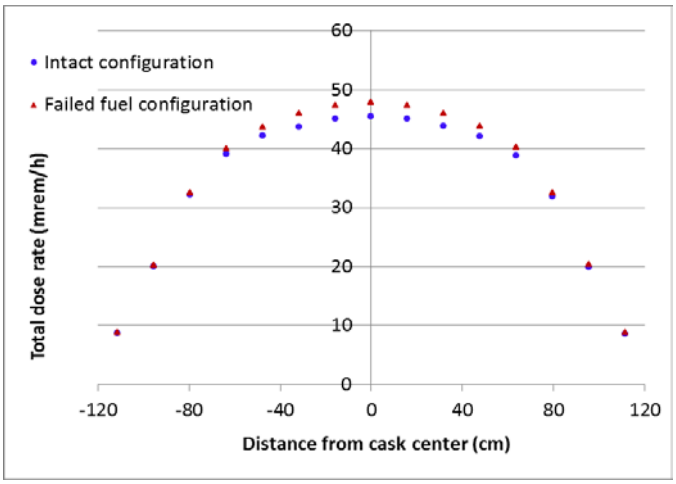

(a)

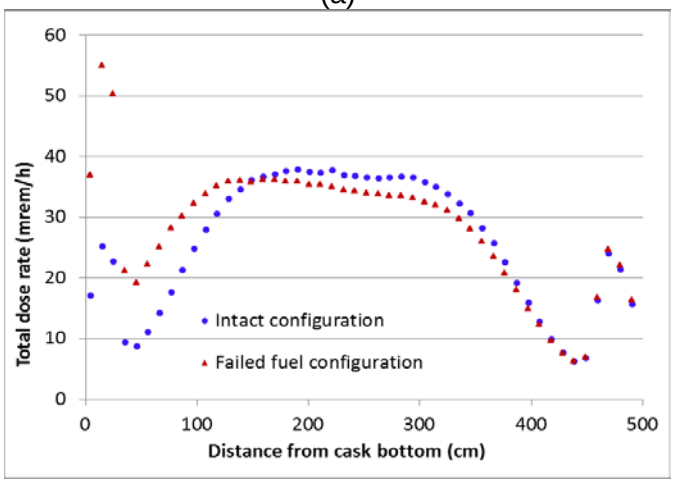

(b)

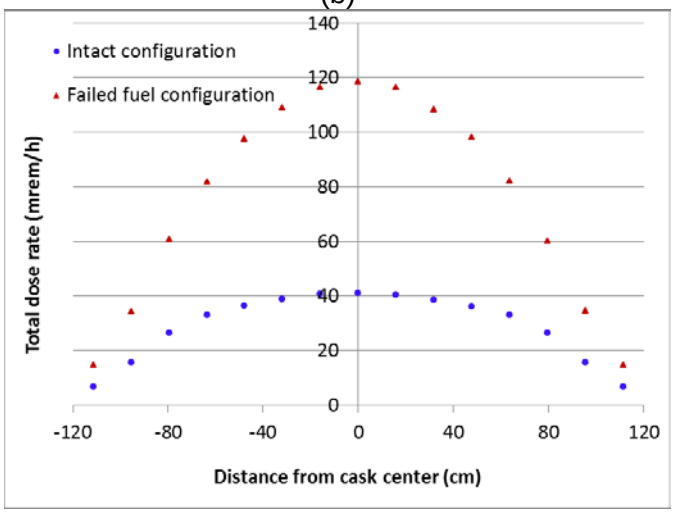

(c)

Figure 15 – Total dose rate profiles along the PWR transport package external top surface (a), radial surface (b), and bottom surface (c) for the intact fuel configuration and the fuel reconfiguration with 25% fuel mixture collected into the assembly bottom region, NCT

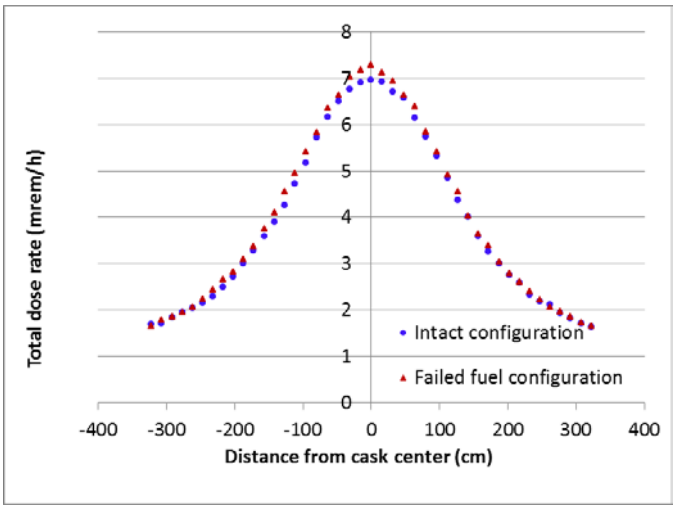

(a)

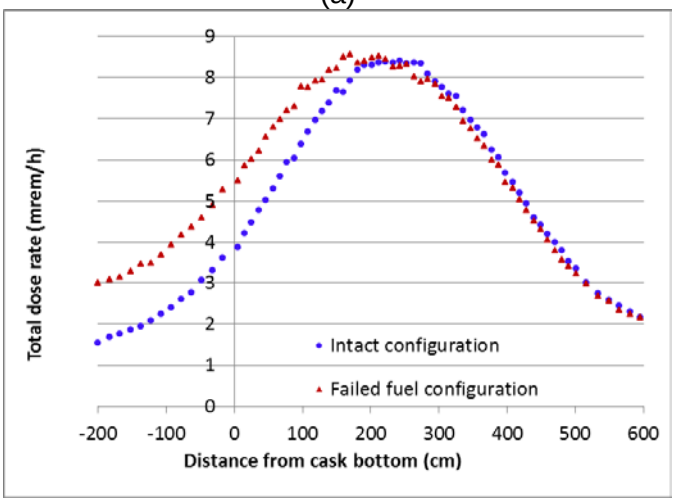

(b)

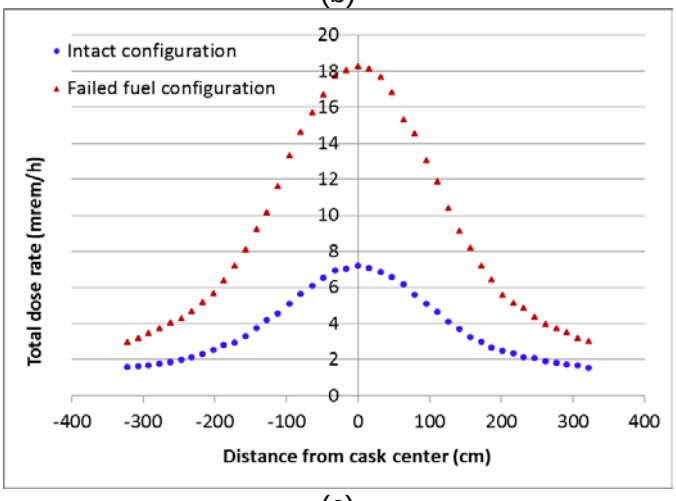

(c)

Figure 16 – Total dose rate profiles at 2 m from the PWR transport package external top surface (a), radial surface (b), and bottom surface (c) for the intact fuel configuration and the fuel reconfiguration with 25% fuel mixture collected into the assembly top region, NCT

The dose rates were calculated at 1 m from either a PWR or BWR storage cask (see Sect. B.3.2 for a description of the models) for fuel configuration changes in casks with a vertical orientation. The changes (F/I dose rate ratio) relative to the nominal intact configuration of the maximum neutron, gamma, and total dose rates at 1 m from the storage cask are summarized in Table 13. Fuel configuration changes cause significant dose rate changes relative to the nominal intact configuration in the cask outer regions that face air vent locations, (i.e., receive radiation directly from streaming through the air vents). At locations away from air vents, the change in radiation dose rate is either small (e.g., ~30% for damaged fuel configurations) or negligible.

Table 13 – Maximum dose rate change at 1 m from a storage cask

1 m from the PWR storage cask surfaces				Top[a]			Side[a]			Side[b]		
Case #	Scenario	Fuel relocation region[c]	Decay time (years)	F/I dose rate ratio								
				n	γ	Total	n	γ	Total	n	γ	Total
2	10% fuel rod failure	Assembly lower end fitting	5	1.09	0.70	0.70	1.68	1.87	1.87	1.05	1.00	1.00
			40	1.09	0.90	0.90	1.68	2.91	2.86	1.05	1.04	1.03
9	Damaged	Canister cavity bottom	5	0.22	0.07	0.08	2.73	4.17	4.05	0.97	1.20	1.20
			40	0.22	0.18	0.18	2.73	4.09	4.02	0.97	0.77	0.85
1 m from the BWR storage cask surfaces				**Top[a]**			**Side[a]**			**Side[b]**		
Case #	**Scenario**	**Fuel relocation region[c]**	**Decay time (years)**	**F/I dose rate ratio**								
				n	**γ**	**Total**	**n**	**γ**	**Total**	**n**	**γ**	**Total**
2	11% fuel rod failure	Assembly lower tie plate and nosepiece	5	1.02	0.56	0.56	2.16	1.78	1.79	1.05	0.97	0.97
			40	1.02	0.82	0.79	2.16	2.73	2.70	1.05	1.00	1.01
5	Damaged	Canister cavity bottom	5	0.22	0.15	0.15	3.23	5.58	5.51	0.92	1.09	1.08
			40	0.22	0.40	0.39	3.23	9.58	9.23	0.92	1.31	1.24

[a]Facing air vent locations; relative error (at the 95% confidence level) is 10% for the radial surface and 20% for the top surface.
[b]Away from air vent locations; relative error (at the 95% confidence level) is 6%.
[c]Farthest region for fuel relocation identified. Fuel mixture may extend into adjacent assembly axial regions, as described in Sect. B.5.1.

Neutron and gamma dose rates at the controlled area boundary from a generic 4×2 storage cask array were calculated at 100 m from the array and are shown in Table 14. The results show that, relative to the nominal intact fuel configuration, the closely packed fuel mixture model reduces site boundary dose rates by ~70% for gamma radiation and ~30% for neutron radiation, whereas the models with the fuel mixture homogeneously distributed within the entire canister cavity increase the site boundary dose rates by a factor of ~2.4 for gamma radiation and by a factor of ~2.7 for neutron radiation. The dose rate changes are caused by source geometry changes and gamma self-shielding effects associated with the different fuel configurations.

Table 14 – Site boundary dose rate change

Case description	F/I dose rate ratio[a]		
	n	γ	Total
PWR fuel mixture collected into canister cavity bottom	0.58 ± 0.07	0.22 ± 0.03	0.21 ± 0.03
BWR fuel mixture collected into canister cavity bottom	0.65 ± 0.01	0.30 ± 0.01	0.30 ± 0.01
PWR fuel mixture homogeneously distributed within canister cavity	2.20 ± 0.08	1.75 ± 0.12	1.76 ± 0.13
BWR fuel mixture homogeneously distributed within canister cavity	2.74 ± 0.04	2.41 ± 0.05	2.38 ± 0.03

[a]F/I dose rate ratio ± 2 sigma statistical error.

3.1.3 Containment

Understanding the consequences of cladding failure on containment performance requires analyses to investigate the changes associated with varying the fraction of rods that develop cladding breach under NCT, from 0.01 to 1 (all rods breached), and specifically for high-burnup fuel analyses, varying the release fractions for the contributors to the releasable source terms in addition to the fraction of breached spent fuel rods. This technical approach was used because the range of parameters for the containment analysis of high-burnup fuel (i.e., the release fractions and breached spent fuel rod fraction) has not been established yet for high-burnup fuel. The release fractions for gases, volatiles, and fuel fines provided in NUREG-1617, Table 4-1 [28], were used in the containment analysis of low-burnup fuel (i.e., 40 GWd/MTU). However, the applicability of the release fractions described in NUREG-1617 to long-term storage should also be confirmed in future evaluations. For the high-burnup fuel analysis, the fraction of fuel rods that develop breaches was varied from 0.01 to 1, the fraction of crud that spalls off the cladding varied from 0.15 to 1, the fraction of gases varied from 0.1 to 0.4, the fraction of volatiles varied from 2×10^{-4} to 2×10^{-3}, and the mass fraction of fuel fines was varied from 3×10^{-5} to 3×10^{-4}. Total releasable activity, effective A_2 value, allowable radionuclide release rate, and allowable leakage rate were calculated for the generic PWR and BWR transportation packages referred to as GBC-32 and GBC-68, respectively (see Appendix B for model specifications). Representative fuel assemblies selected for analysis are the PWR W 17×17 OFA and BWR GE14 10×10 lattice with 40- and 65 GWd/MTU burnup values. The impact on the releasable activity of the discharged radioactive material original location (i.e., non-rim region of the fuel pellet or the peripheral rim structure) was evaluated for the 65 GWd/MTU burnup value. The results of the containment analysis are provided in Appendixes C.4 and C.5 for the fuel assemblies with low-burnup (i.e., 40 GWd/MTU) and high-burnup (i.e., 65 GWd/MTU), respectively.

Figure 17 and Figure 18 illustrate the allowable leakage rate variation as a function of the fraction of spent fuel rods with cladding breaches for the GBC-32 and GBC-68 containing fuel assemblies, respectively, with 40 GWd/MTU burnup. With a more restrictive allowable leakage rate, GBC-68 can accommodate greater fuel rod failure rates than GBC-32. For GBC-68 with low-burnup fuel, an allowable leakage rate of ~2.4×10^{-5} cm^3/s was obtained for the 0.03, 0.4, 0.7, and 1.0 breached spent fuel rod fractions at the 5-, 40-, 100-, and 300-year decay times, respectively. For GBC-32 with low-burnup fuel, an allowable leakage rate of ~1×10^{-4} cm^3/s was obtained for the 0.03, 0.10, 0.15, and 0.25 breached spent fuel rod fractions at the 5-, 40-, 100-, and 300-year decay times, respectively.

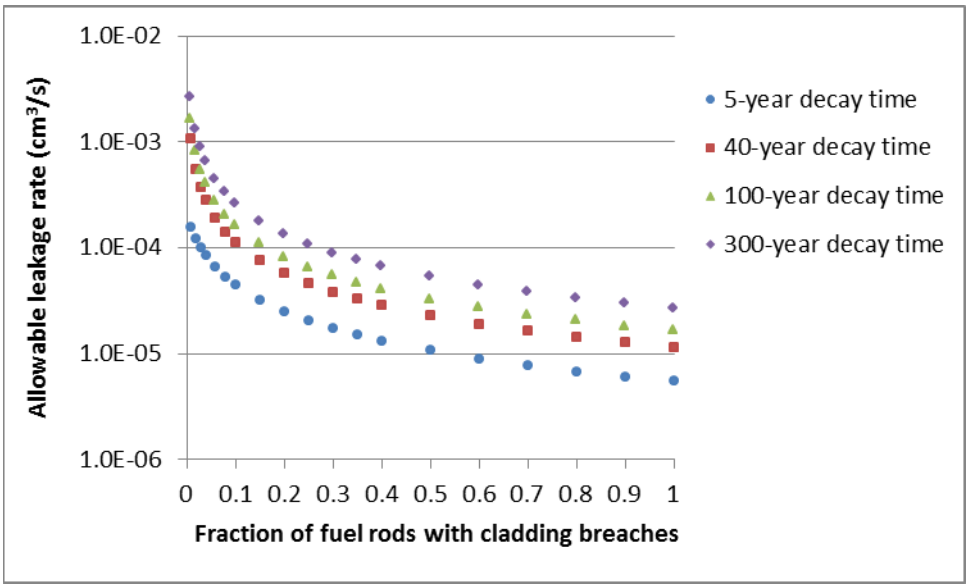

Figure 17 – Allowable leakage rate variation as a function of spent fuel rod cladding breaches for the GBC-32 cask and 40 GWd/MTU burnup at different decay times

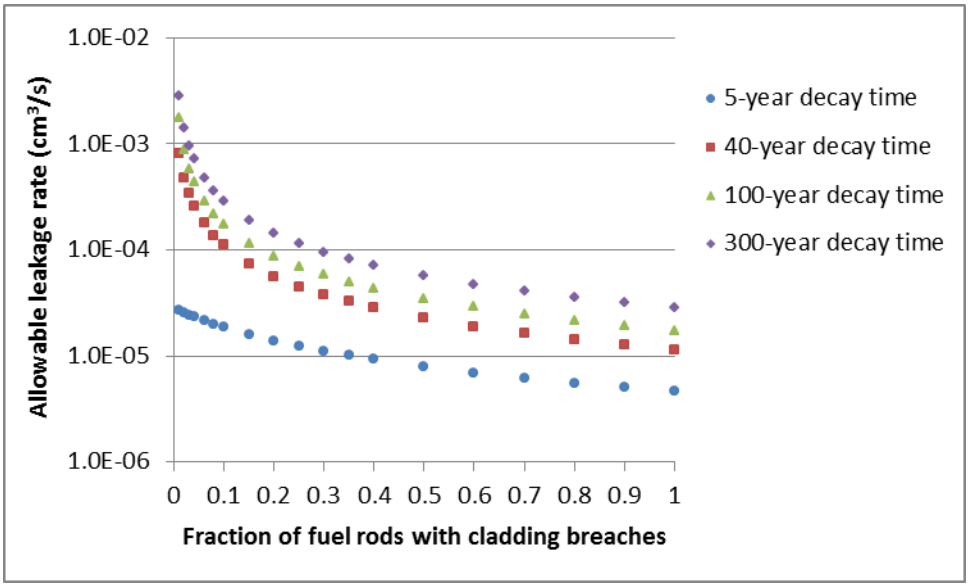

Figure 18 – Allowable leakage rate variation as a function of spent fuel rod cladding breaches for the GBC-68 cask and 40 GWd/MTU burnup at different decay times

The containment analysis for high-burnup fuel under NCT evaluated the impact on the allowable leakage rate of varying the fraction of spent fuel rods that develop breaches (0.01 to 1), fraction of crud (0.15 to 1) that spalls off cladding, fraction of gases (0.1 to 0.4), volatiles (2×10^{-4} to 2×10^{-3}), fuel fines (3×10^{-5} to 3×10^{-4}) released due to cladding breach, and the fuel pellet radial region from which the releasable activity originates. For each fuel type, decay time, and fraction of fuel rods that develop breaches, 15 different cases were analyzed, each case using a combination of the values previously described for the parameters important to containment

analysis. The calculated allowable leakage rates are provided in the tables and graphs in Appendix C.5.4 with a summary of the results provided as follows.

Decay time. Decay time has a significant impact on the releasable activity and allowable leakage rate primarily because of the decay of ^{60}Co ($t_{1/2}$ = 5.271 years), which is the source of radioactivity in crud, and ^{85}Kr ($t_{1/2}$ = 10.76 years), which dominates the gaseous species. The allowable leakage rate increases with increasing decay time.

Fraction of fuel rods that develop cladding breaches. The allowable leakage rate decreases with increasing fraction of breached spent fuel rods. The decrease is relatively small for short decay times when crud has a large contribution to the total releasable activity (e.g., a 15% decrease because of an increase in spent fuel rod breach fraction from 0.01 to 0.03 for the BWR fuel with 5-year decay time) and is fairly large when the fuel fines dominate the total releasable activity (e.g. a decrease by a factor of 2.5 because of an increased failed fuel rod fraction from 0.01 to 0.03 for the BWR fuel with 40-year decay time).

Fraction of crud that spalls off cladding. Crud is an important factor in the calculation of the allowable leakage rate for the time interval 5 to 40 years after fuel discharge from the reactor because of its relatively high contribution to the total releasable activity. Crud has a more pronounced effect on the BWR packages than on the PWR packages because of the larger ^{60}Co activity per fuel rod surface area associated with the BWR fuel. As a result, the BWR package allowable leakage rates are smaller (i.e., more restrictive) than the PWR package allowable leakage rates. For GBC-68 and the 5-year decay time, an increase in the fraction of crud that spalls off the cladding by a factor of two would cause a decrease in the allowable leakage rate by a factor of approximately two.

Fraction of gases released due to cladding breach. For each decay time and fraction of breached spent fuel rods, an increase in the fraction of gaseous species from 0.1 to 0.4 would cause a relatively small decrease (up to ~30%) in the allowable release rate.

Fraction of volatiles released due to cladding breach. The volatile source term is dominated by ^{137}Cs ($t_{1/2}$ = 30.07 years) and ^{90}Sr ($t_{1/2}$ = 28.78 years). An increase in the fraction of volatile source term by one order of magnitude would cause a maximum decrease in the allowable leakage rate by a factor of approximately two.

Fraction of fuel fines released due to cladding breach. Allowable leakage rate exhibits the greatest sensitivity to changes in the mass fraction of fuel released as fuel fines due to cladding breach. Depending on the crud contribution to the total releasable activity, an increase in the fraction of fuel fines by a factor of 10 would cause a decrease in the allowable leakage rate by a factor of ~1.5 to 10.

Fuel pellet radial region. Allowable radionuclide release rate and leakage rate for high-burnup fuel vary as a function of the pellet regions from which the radioactive material is released. Radioactive material released from the pellet peripheral region produced smaller allowable leakage rates than the radioactive material released from the non-rim region of the fuel pellet. The extent to which the pellet radial region from which the radioactive material is released affects the allowable leakage rate depends on the contribution of crud to the total releasable activity. Small effects are observed for GBC-32 with 5-year decay time and a small fraction of breached spent fuel rods (e.g., 0.01), as well as for GBC-68 with 5-year decay time and any fraction of breached spent fuel rods, as crud has a significant contribution to the total releasable activity for these cases. For the cases where crud has a small or insignificant contribution to the

total releasable activity (e.g., failed fuel fraction of 0.1 and decay time of 40 years), the allowable leakage rate based on radioactive material from the outer rim structure is approximately half the allowable leakage rate based on radioactive material from the non-rim region. The importance of the pellet region from which the radioactive material is released increases with increasing decay time and breached spent fuel rod fraction for NCT. This is illustrated in Figure 19, which shows the effects of the pellet location from which the releasable activity may originate (i.e., either from the non-rim region of the fuel pellet or only from the rim structure) on the allowable leakage rate for the GBC-32 cask with decay times of 5 and 40 years, and varying the fraction of fuel rods with cladding breaches. The release fractions for gases, volatiles, fuel fines, and crud that were used to calculate the allowable leakage rates illustrated in Figure 19 are those typically used for low-burnup fuel as provided in NUREG-1617 [29].

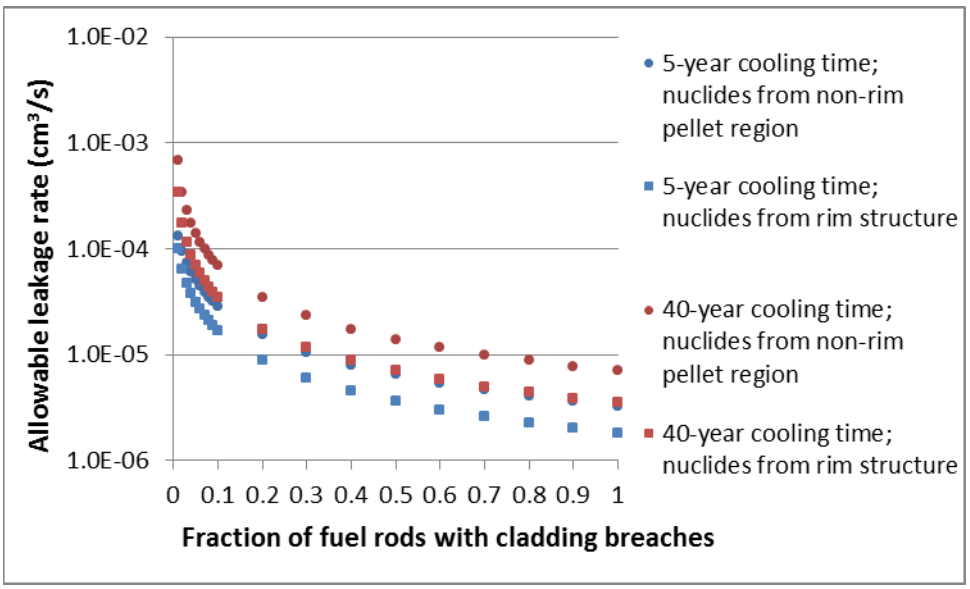

Figure 19 – Effects of the location from which the fuel fines may originate on allowable leakage rate for the GBC-32 cask at 65 GWd/MTU burnup

The containment analysis for high-burnup fuel under HAC evaluated the impact on the allowable leakage rate of fraction of gases (0.3 and 0.4), volatiles (2×10^{-4} and 2×10^{-3}), and fuel fines (3×10^{-5} and 3×10^{-4}) released due to cladding breach, as well as the fuel pellet radial region from which the releasable activity originates. The fraction of fuel rods that have cladding breaches was 1, and the fraction of crud that spalls off the cladding was 1. For each fuel type and decay time, five different cases were analyzed, with each case using a combination of the values previously described for the parameters important to containment analysis. The calculated allowable leakage rates are provided in the tables and graphs in Appendix C.5.4. Similar to the NCT cases, the HAC allowable leakage rate has the largest sensitivity to the mass fraction of fuel released as fines. Depending on the decay time, an increase in the mass fraction of fuel released as fuel fines by a factor of 10 can cause a decrease in the allowable leakage rate by a factor of ~5 to 10 for the GBC-32 package and by a factor of ~3.5 to 10 for the GBC-68 package.

3.1.4 Thermal

The consequences of cladding failure require thermal calculations to investigate the changes associated with both breached and damaged fuel geometries. The thermal evaluations are limited to a representative GBC-32 transportation package with representative W 17×17 OFA SNF as described in Appendix D. It is anticipated that the thermal response of a similarly designed BWR transportation package would follow similar trends as the analyzed PWR system. Both the vertical and horizontal configurations were considered. The primary parameters of interest are the component and cladding temperatures, and the peak surface temperature (with respect to 10 CFR 71.43).

For the thermal analysis results presented, the case identifier (ID) nomenclature is as follows: The first letter indicates whether the package is in the vertical, "V," or horizontal, "H," orientation. The next number indicates the number of years of fuel decay time (i.e., "40" is 40-year decay time). The nominal intact configuration case is 40 years. The next set of numbers preceding the "pr" indicates the percentage of rods assumed to be ruptured (i.e., "3.125pr" indicates 3.125% of the rods have been breached). A number followed by "pf" indicates the fuel is assumed to be in a particle bed geometry, and the number indicates the packing fraction of the debris (i.e., ".313pf" is a packing fraction of 0.313). A number followed by "pdr" indicates the assembly fuel rod pitch has been altered, and the number indicates the pitch to diameter ratio (i.e., "116pdr" is a pitch to diameter ratio of 1.16).

This fuel failure configuration category considered two sets of cases. The first set is representative of breached spent fuel rod configurations where a fraction of the fuel rod cladding is assumed to fail, releasing the gaseous contents, but otherwise remaining in their nominal geometry. The second case set represents damaged fuel and evaluates either one assembly or all assemblies damaged within their respective basket cells.

Breached spent fuel rods. Depending on the package orientation (i.e., horizontal or vertical) release of fission product gases into the canister gas space can cause either a significant increase or a significant decrease to component peak temperatures as illustrated in Table 15.

Table 15 – Thermal results for scenario S1(a)—breached spent fuel rods

Case ID	Fraction of rods failed	Change in temperature (Δ°C)						
		Max. clad	Min. clad	Max. outer surface	Min. outer surface	Max. neutron absorber	Max. basket SS[b]	Max. neutron shield
V.40[a]	0.0	0	0	0	0	0	0	0
V.40.3.125pr	0.3125	-14	+2	0	+1	-13	-13	0
V.40.10pr	0.10	-29	+8	-1	+2	-27	-27	0
V.40.50pr	0.50	-59	+19	-2	+5	-56	-56	-2
V.40.100pr	1.00	-74	+24	-2	+6	-71	-71	-2
H.40	0.0	0	0	0	0	0	0	0
H.40.3.125pr	0.3125	+4	0	0	0	+3	+3	0
H.40.10pr	0.10	+11	+1	0	0	+10	+10	0
H.40.50pr	0.50	+33	+2	0	0	+30	+31	-1
H.40.100pr	1.00	+45	+3	0	0	+42	+42	-1

[a]Nominal intact configuration.
[b]SS = stainless steel.

For packages in a vertical orientation, the release of fission product gases leads to an overall decrease in peak component temperatures, while resulting in an increase in minimum temperatures. The recirculating mass flow rate for 100% rod break is 22.78 kg/min compared to 0.57 kg/min for the 0% rod break nominal intact configuration case. This is primarily because of the increase in gas density with fission product gas release but, it is also because of higher predicted recirculation velocities (e.g., 0.055 m^3/s for 100% rod break vs. 0.030 m^3/s for 0% rod break at 204˚C). The specific heat capacity of the gas phase decreases with increasing fission product gases. However, the net effect of increased density and decreased heat capacity is a higher volumetric heat capacity of the flow. Thus, the convective flow is able to transport more heat with increasing Xe and Kr gas content. In other words, the convective flow can transport the same amount of heat at lower temperature differentials (e.g., the convective flow can transport approximately 175 W/K at 100% rod failure vs 50 W/K at 0% rod failure). This results in a flattening of the temperature profiles within the package (compare Figure D.17 to Figure 20).

For the horizontal package, the release of fission gas products leads to an overall increase in peak and minimum component temperatures. In the horizontal package orientation, there is minimal convective heat transport within the canister. Therefore, the heat removal relies upon thermal radiation and conduction. The release of the fission products has a negligible impact on thermal radiation heat transfer; however, it reduces the thermal conductivity of the canister gas. The reduced thermal conductivity of the gas results in poorer heat transfer through the gas space and higher internal component temperatures. The change in gas properties has a negligible impact on the axial temperature profile of components within the package (compare Figure D.18 to Figure 21).

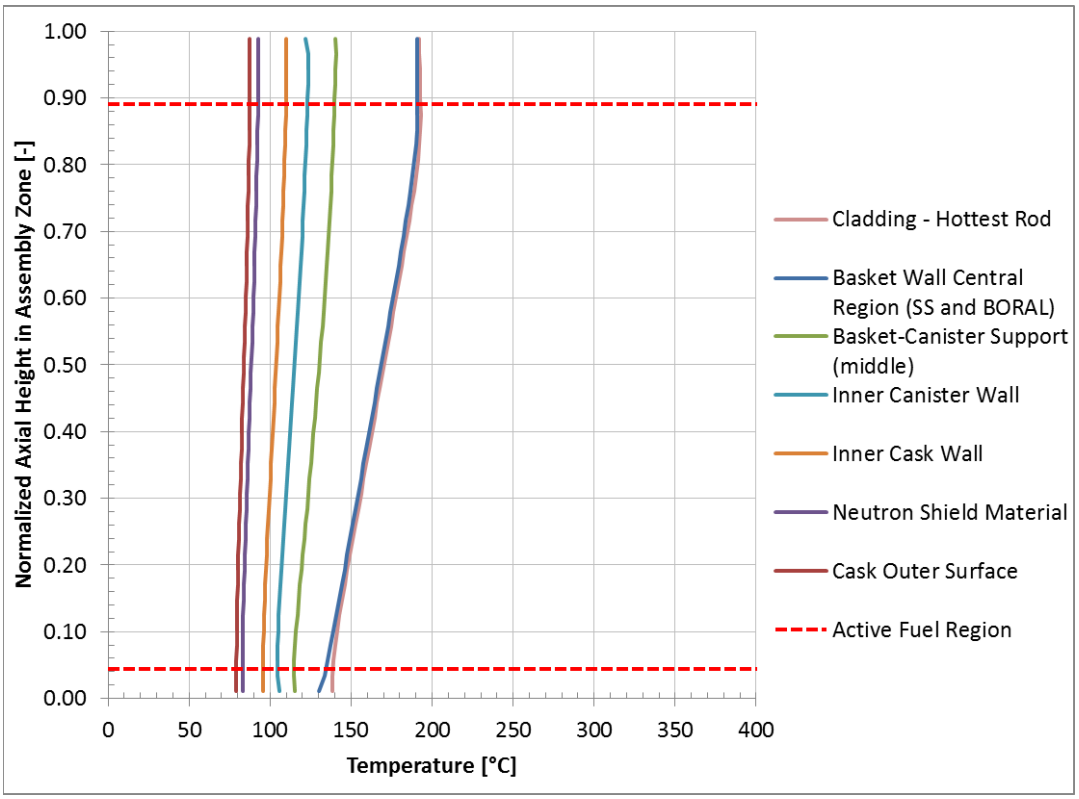

Figure 20 – Structural temperatures with 100% rod breach—vertical orientation

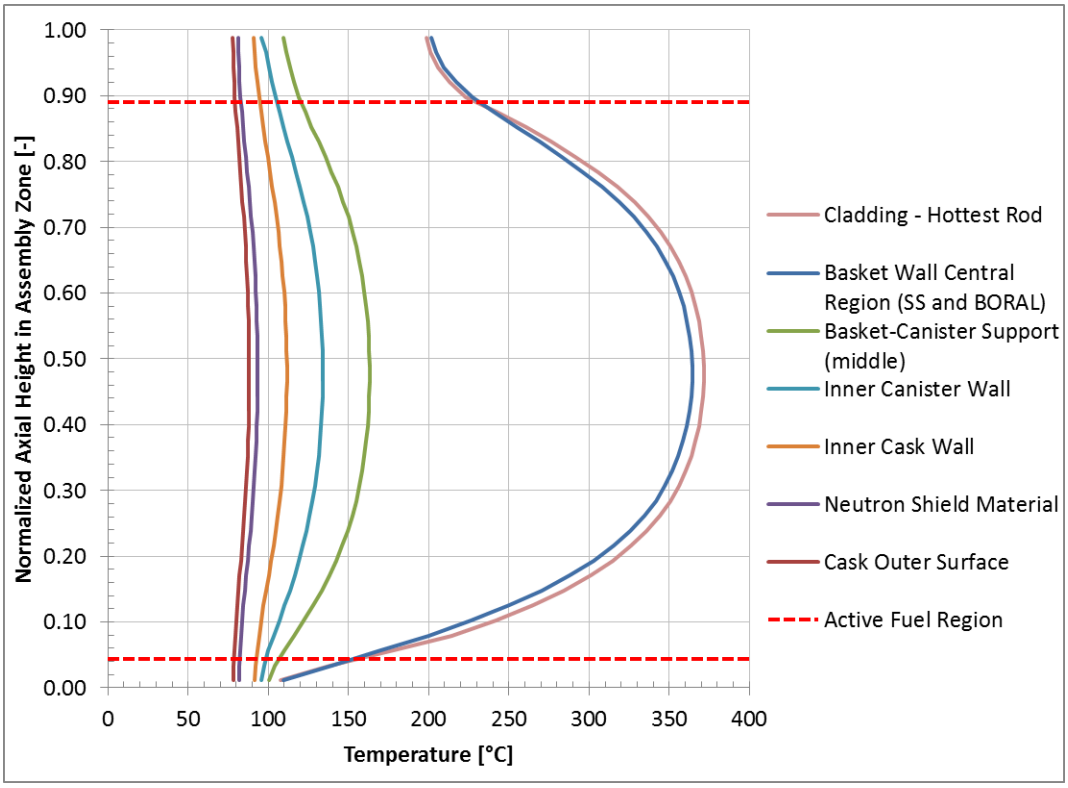

Figure 21 – Structural temperatures with 100% rod breach—horizontal orientation.

Damaged fuel. The fuel reconfiguration where a single, central, assembly was represented as a debris pile that inside its basket cell had a minor impact on the component temperatures (see Table 16). The single assembly fuel reconfiguration had a larger impact on the component temperatures for the vertical orientation than for the horizontal orientation. Most of the impact is because of the release of the fission product gases into the canister space as opposed to the formation of the particle bed (Figure 22 and Figure 23). This can be seen by comparing the case where 3.125% of the rods are breached (equal to one assembly) but stay in their nominal geometry (cases V.40.3.125pr and H.40.3.125pr in Table 16) to the cases where the same amount of gas is released, but the assembly forms a debris bed (Table 16). The packing fraction of the debris bed had a minor impact on the predicted temperatures.

Table 16 – Single assembly failure results summary

Case ID	Packing fraction	Change in temperature (Δ°C)						
		Max. intact clad	Min. intact clad	Max. outer surface	Min. outer surface	Max. neutron absorber	Max. basket SS[b]	Max. neutron shield
V.40[a]	NA	0	0	0	0	0	0	0
V.40.3.125pr	NA	-14	+2	0	+1	-13	-13	0
V.40.3.125pr.313pf	0.313	-11	+2	0	+1	-9	-8	0
V.40.3.125pr.320pf	0.320	-11	+2	0	+1	-8	-8	0
V.40.3.125pr.417pf	0.417	-12	+3	0	+1	-11	-11	0
V.40.3.125pr.574pf	0.574	-13	+3	0	+1	-13	-13	0
V.40.3.125pr.626pf	0.626	-14	+3	0	+1	-14	-14	0
H.40	NA	0	0	0	0	0	0	0
H.40.3.125pr	NA	+4	0	0	0	+3	+3	0
H.40.3.125pr.313pf	0.313	+3	0	0	0	+2	+2	0
H.40.3.125pr.417pf	0.417	+2	0	0	0	+1	+1	0
H.40.3.125pr.626pf	0.626	+1	+1	0	0	0	0	0

Note: NA = not applicable.
[a]Nominal intact fuel configuration.
[b]SS = stainless steel.

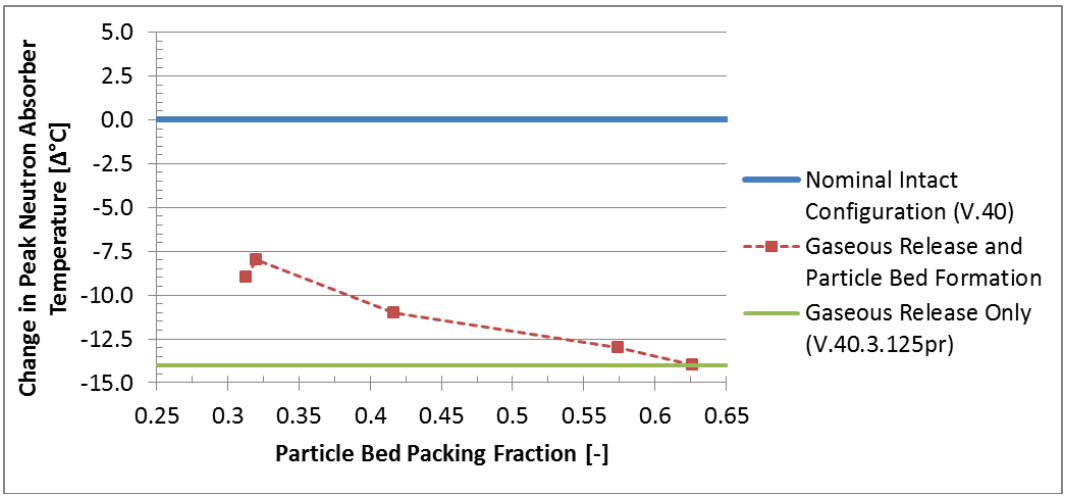

Figure 22 – Change in peak neutron absorber temperature with failure of one assembly—vertical cask

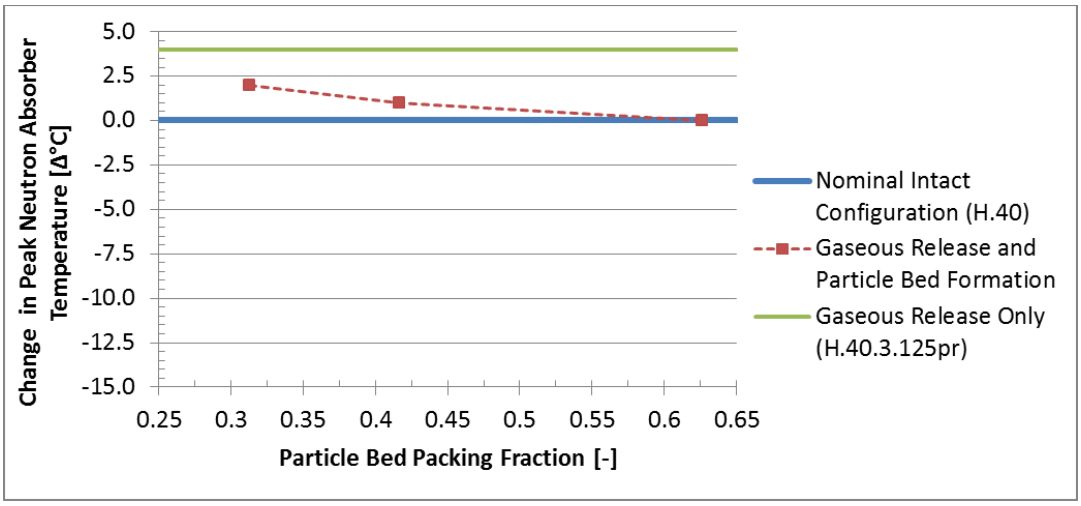

Figure 23 – Change in peak neutron absorber temperature with failure of one assembly—horizontal cask

For configurations where all of the assemblies are represented as debris piles, which remain inside their respective basket cells, large impacts on the predicted internal cask temperatures were observed as shown in Table 17. Significant increases in package component temperatures could result in the package not meeting the thermal requirements for such systems. For the vertical orientation, the maximum temperature of the basket stainless steel walls and neutron absorber material increased by over 79°C compared to the nominal intact configuration case as shown in Figure 24. The assembly debris is assumed to block the basket cell channels causing a reduction in the convective heat transfer within the canister. In addition, the release of the fission product gases results in a decrease in gas thermal conductivity, resulting in lower heat conduction and heat transfer through the gas space. Both effects—lower convection and lower gas thermal conductivity—result in the large increase in internal temperatures. Increasing the packing fraction of the debris caused a greater increase in the maximum basket wall temperature. This is expected as the debris, generating the same amount of heat, has less

debris-to-wall contact area for heat removal as the packing fraction is increased. Axial conduction reduces the thermal impact to structures toward the outer surfaces of the cask.

Table 17 – Failure of all assemblies results summary

Case ID	Debris packing fraction	Change in temperature (Δ°C)						
		Max. intact clad	Min. intact clad	Max. outer surface	Min. outer surface	Max. neutron absorber	Max. basket SS[b]	Max. neutron shield
V.40[a]	NA	0	0	0	0	0	0	0
V.40.100pr	NA	-74	+24	-2	+6	-71	-71	-2
V.40.100pr.313pf	0.313	NA	NA	-5	+10	+79	+79	-6
V.40.100pr.417pf	0.417	NA	NA	-5	+8	+102	+102	-5
V.40.100pr.626pf	0.626	NA	NA	-3	+7	+127	+128	-2
H.40[a]	NA	0	0	0	0	0	0	0
H.40.100pr	NA	+45	+3	0	0	+42	+42	-1
H.40.100pr.313pf	0.313	NA	NA	-4	-1	+30	+31	-5
H.40.100pr.417pf	0.417	NA	NA	-2	-2	+31	+31	-3
H.40.100pr.626pf	0.626	NA	NA	-1	-2	+21	+21	-2

Note: NA = not applicable.
[a]Nominal intact fuel configuration.
[b]*SS* = stainless steel.

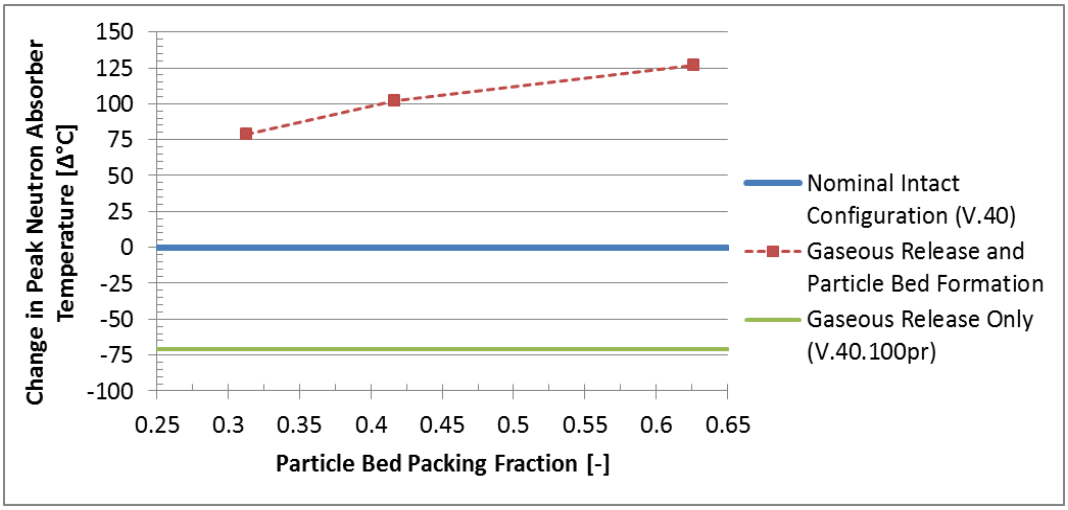

Figure 24 – Change in peak neutron absorber temperature with failure of all assemblies in vertical cask

For the horizontal orientation, the fuel reconfiguration (i.e., all assemblies represented as debris piles within their respective basket cells) also increased the maximum temperature of the basket stainless steel walls and neutron absorber material. The internal heat transport for the horizontal case relies on heat conduction and thermal radiation as there is limited internal convection both in the nominal geometry and in the fuel reconfiguration geometry. The debris was represented as being evenly distributed along the length of the basket cell with a uniform decay heat profile. By spreading out the energy source term and putting the debris in direct contact with the basket cell walls, the maximum basket temperatures are increased by an amount less than the

increase predicted for the case where 100% of the rods break, but the nominal geometry of the fuel latice is retained (case H.40.100pr). At a packing fraction of 0.313, the debris fully fills the basket cell and comes in contact with the top wall of the basket cell. The increased debris-wall contact area, for the 0.313 packing fraction case, causes the non-linearity in the trend in Figure 25.

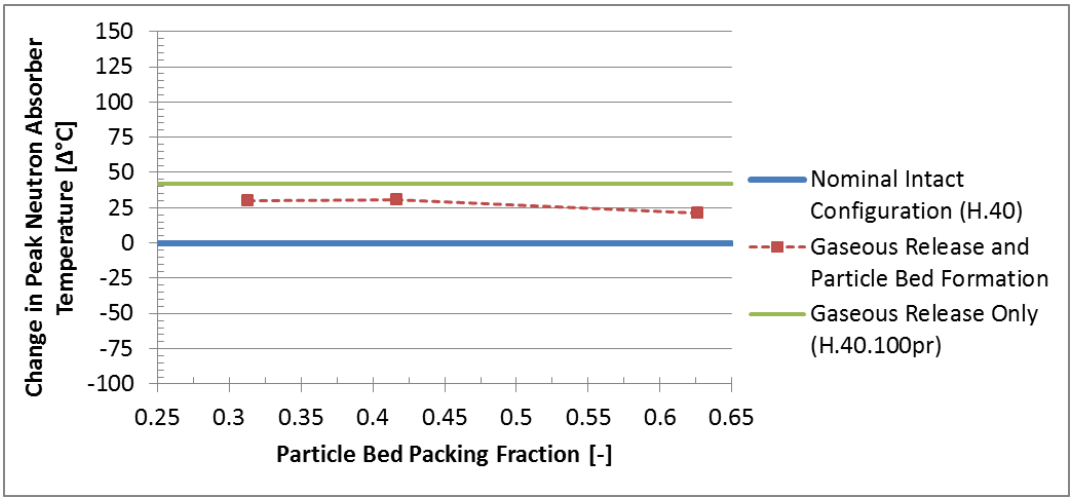

Figure 25 – Change in peak neutron absorber temperature with failure of all assemblies in horizontal cask

3.2 CATEGORY 2: ROD/ASSEMBLY DEFORMATION

Fuel reconfigurations associated with rod/assembly deformation investigate the impact of pin pitch changes that could result as potential end states associated with spacer grid failure, and side and end drop events consistent with normal, off-normal, and accident conditions of storage as well as under normal and accident conditions of transportation.

3.2.1 Criticality

Because of the effects of geometry changes on criticality calculations, changes in pin pitch can result in a wide range of reactivity effects. Both uniform and non-uniform pin pitch variations were considered to investigate the effects of axial and radial rod/assembly deformation on criticality calculations. To investigate the effects associated with side impact/drop events, cases were evaluated to represent configuration scenario S2(a)—configurations associated with side drop, as depicted in Figure 5 and Figure 6 for the PWR and BWR assembly, respectively. Because LWR assemblies are under-moderated, configurations that result in pin pitch contraction will result in decreases in k_{eff}.

Assembly deformation from end drop events is more significant for criticality safety implications. Axial effects to represent the phenomenon referred to as “birdcaging” and/or “bottlenecking” were evaluated by expanding pitches in one region and contracting pitches in another region. Results for configuration scenario S2(b)—configurations associated with end drop— are illustrated in Figure 26 for PWR assemblies, and in Figure 27 and Figure 28 for BWR assemblies with and without channels, respectively. Maximum changes to k_{eff} occurred when

radial nonuniform pin pitch variations were modeled. A cross-sectional view of a PWR and BWR assembly with this configuration was illustrated in Figure 8.

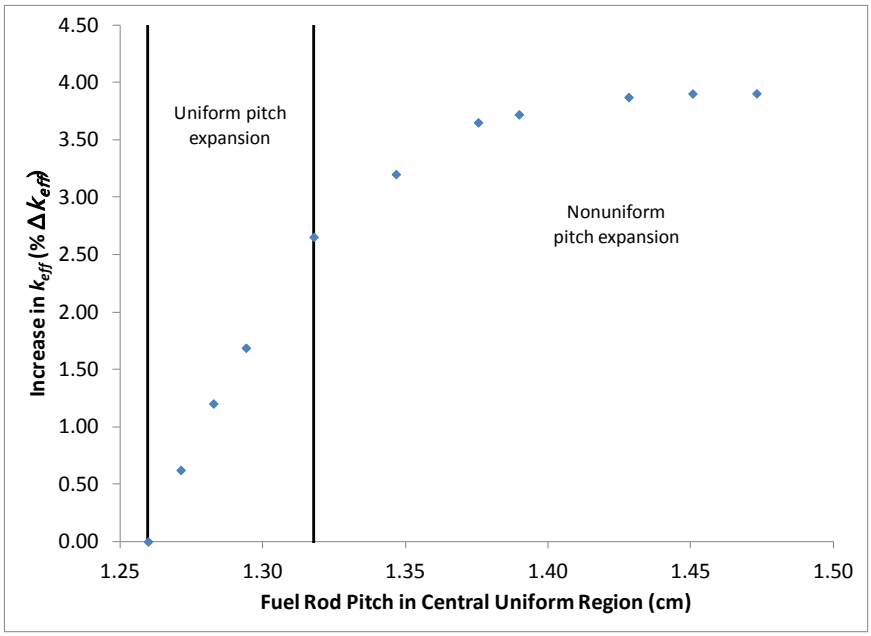

Figure 26 – GBC-32 criticality analysis results from pin pitch variation

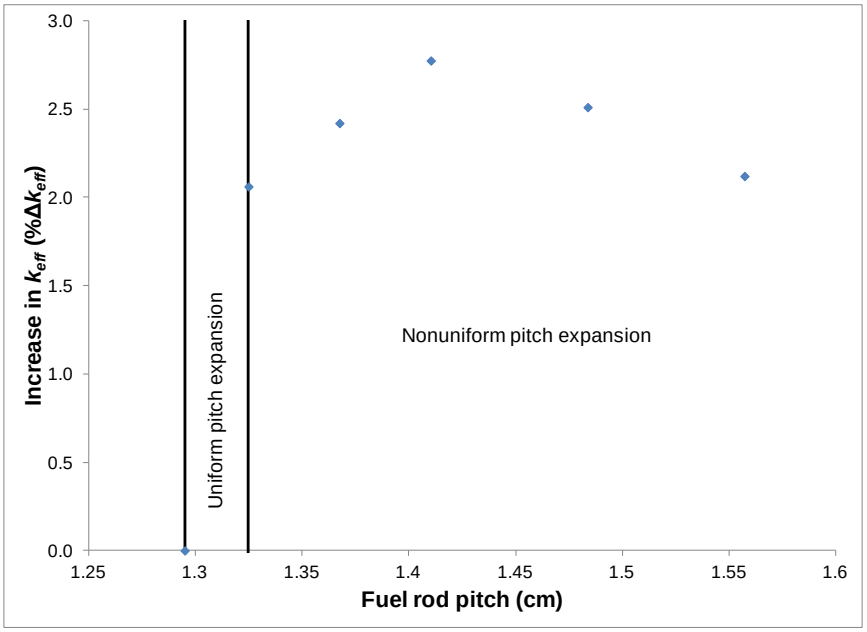

Figure 27 – GBC-68 criticality analysis results from pin pitch variation for channeled fuel

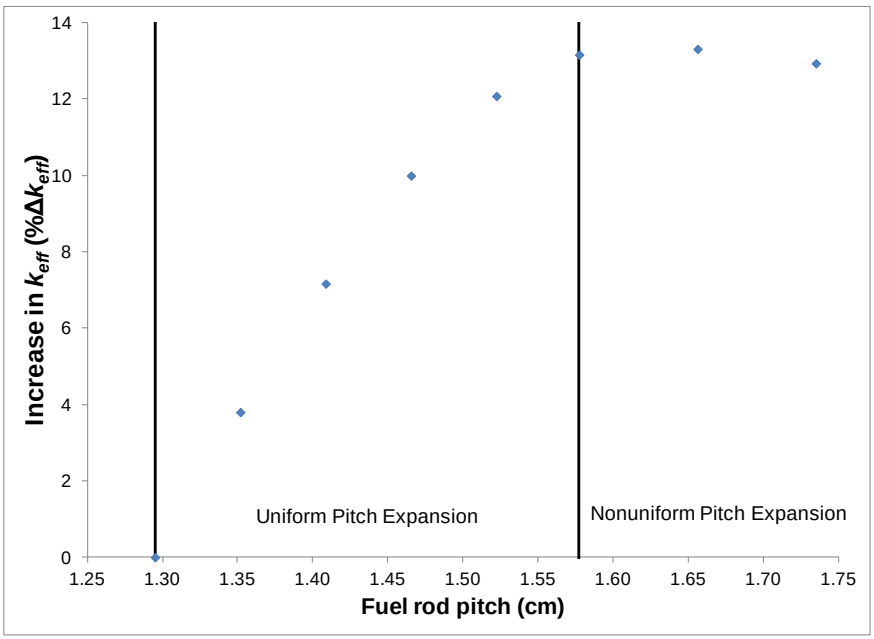

Figure 28 – GBC-68 criticality analysis results from pin pitch variation for unchanneled fuel

The effects of axial varying pitch were bounded by the nonuniform radial pin pitch variations. Investigation of the combined effect of at least one pin pitch contracted region with the other regions in the bounding radial nonuniform expansion cases showed essentially no change in results when compared with the bounding radial nonuniform expansion (i.e., 3.89 %Δk_{eff} versus 3.90 %Δk_{eff}).

3.2.2 Shielding

Fuel rod lattice collapse against the fuel basket plates within a transportation package was analyzed for the rod/assembly deformation category (see Appendix B, Figure B.8 for model illustration). The assembly axial location for this fuel reconfiguration is identical to that of the nominal intact configuration. The calculation results indicate that fuel rod lattice collapse causes a small increase in the radial dose rates relative to intact fuel for both PWR and BWR SNF assemblies. For the specific models used in this study, the maximum radial dose rate increase was ~20%. Collapsed fuel rod lattices also cause an increase in neutron dose rates at the package bottom and top surfaces because of neutron streaming. For the specific models used in this study, the maximum axial neutron dose rate increase was ~50%. The change in gamma dose rate at the package top and bottom surfaces was negligible (i.e., within statistical error). The fuel reconfiguration analyzed is considered to be bounding for assembly deformation involving fuel rod lattice collapse with respect to package radial and axial dose rates because it provides the greatest neutron streaming and radiation source density near the package radial surface.

The ratio of the maximum surface dose rate value for a fuel reconfiguration to the maximum surface dose rate value for the nominal intact fuel configuration, identified as the F/I dose rate ratio, is summarized in Table 18 and Table 19 for the evaluated PWR and BWR fuel reconfigurations, respectively.

Table 18 – PWR package maximum dose rate change for NCT

Package external surfaces				Top			Side			Bottom		
Case #	Scenario	Fuel relocation region	Decay time (years)	F/I dose rate ratio[a]								
				n	γ	Total	n	γ	Total	n	γ	Total
11	Assembly lattice collapse	See Figure B.8 (a)	5	1.36	0.96	1.29	1.13	1.11	1.12	1.22	0.93	1.10
			40	1.36	0.87	1.36	1.14	1.10	1.13	1.19	0.64	1.16
12	Assembly lattice collapse	See Figure B.8 (b)	5	1.27	0.99	1.22	1.03	0.93	0.98	1.17	0.96	1.10
			40	1.16	0.89	1.16	1.04	0.96	1.03	1.16	0.80	1.14
Two meters from package external surfaces				**Top**			**Side**			**Bottom**		
Case #	**Scenario**	**Fuel relocation region**	**Decay time (years)**	**F/I dose rate ratio[a]**								
				n	**γ**	**Total**	**n**	**γ**	**Total**	**n**	**γ**	**Total**
11	Assembly lattice collapse	See Figure B.8 (a)	5	1.31	0.98	1.24	1.15	1.10	1.12	1.19	0.93	1.09
			40	1.32	1.04	1.31	1.17	1.09	1.15	1.17	0.73	1.14
12	Assembly lattice collapse	See Figure B.8 (b)	5	1.22	1.00	1.17	1.04	0.94	0.99	1.15	0.95	1.07
			40	1.12	0.96	1.12	1.04	0.96	1.02	1.11	0.77	1.09

[a]Relative error (95% confidence level) less than 5%.

Table 19 – BWR package maximum dose rate change for NCT

Package external surfaces				Top			Side			Bottom		
Case #	Scenario	Fuel relocation region	Decay time (years)	F/I dose rate ratio[a]								
				n	γ	Total	n	γ	Total	n	γ	Total
7	Assembly lattice collapse	See Figure B.8 (a)	5	1.48	1.01	1.41	1.07	1.08	1.07	1.26	1.00	1.14
			40	1.49	1.01	1.49	1.06	1.07	1.06	1.27	0.89	1.27
Two meters from package external surfaces				**Top**			**Side**			**Bottom**		
Case #	**Scenario**	**Fuel relocation region**	**Decay time (years)**	**F/I dose rate ratio[a]**								
				n	**γ**	**Total**	**n**	**γ**	**Total**	**n**	**γ**	**Total**
7	Assembly lattice collapse	See Figure B.8 (a)	5	1.41	1.00	1.32	1.06	1.05	1.06	1.20	1.00	1.09
			40	1.37	0.96	1.37	1.04	1.05	1.04	1.19	0.89	1.19

[a]Relative error (95% confidence level) less than 5%.

For the analysis under HAC, the dose rate at 1 m from the package external surfaces was calculated with a model using air in place of the outer neutron shield considered in the package models for NCT. The ratio of the maximum surface dose rate value for the fuel reconfiguration analyzed to the maximum surface dose rate value for the nominal intact configuration (as the F/I dose rate ratio), is summarized in Table 20 for the PWR and BWR package models. The maximum radial neutron and gamma dose rate values increased by ~15%; the maximum neutron dose rates on the package top and bottom surfaces increased by ~30% and 20%, respectively.

Table 20 – Package maximum dose rate change for HAC

1 m from the PWR package external surfaces				Top			Side			Bottom		
Case #	Scenario	Fuel relocation region	Decay time (years)	F/I dose rate ratio[a]								
				n	γ	Total	n	γ	Total	n	γ	Total
11	Assembly lattice collapse	See Figure B.8 (a)	5	1.31	0.99	1.24	1.12	1.09	1.12	1.19	0.93	1.13
			40	1.30	1.04	1.30	1.13	1.06	1.13	1.17	0.66	1.15
12	Assembly lattice collapse	See Figure B.8 (b)	5	1.13	1.00	1.10	1.04	0.94	1.03	1.13	0.95	1.09
			40	1.13	0.91	1.13	0.95	0.90	0.94	1.14	0.74	1.13
1 m from the BWR package external surfaces				**Top**			**Side**			**Bottom**		
Case #	**Scenario**	**Fuel relocation region**	**Decay time (years)**	**F/I dose rate ratio[a]**								
				n	**γ**	**Total**	**n**	**γ**	**Total**	**n**	**γ**	**Total**
7	Assembly lattice collapse	See Figure B.8 (a)	5	1.07	1.00	1.04	1.03	1.06	1.04	1.20	1.00	1.13
			40	1.03	1.00	1.03	1.03	1.04	1.03	1.21	1.02	1.21

[a]Relative error (95% confidence level) less than 5% for all values.

3.2.3 Containment

The rod/assembly deformation category does not include cladding failure. All cladding failure scenarios are evaluated under Category 1 (Sect. 3.1). Normal, off-normal, and accident conditions of spent fuel storage and normal and accident conditions of transportation that can cause rod/assembly deformation can affect the amount of crud that spalls off the cladding. Hence, the allowable leakage rate was calculated as a function of the fraction of crud that spalls off the cladding to evaluate the effect of varying crud releasable activity (see Appendix C.6). The allowable leakage rate is inversely proportional to the fraction of crud assumed to spall off the cladding. For the 5-year decay time, an increase in the fraction of crud from 0.05 to 1 would cause a decrease in the allowable leakage rate from 6.58×10^{-4} cm^3/s to 3.29×10^{-5} cm^3/s for GBC-32 and from 7.54×10^{-5} cm^3/s to 3.77×10^{-6} cm^3/s for GBC-68. For the 40-year decay time, an increase in the fraction of crud from 0.05 to 1 would cause a decrease in the allowable leakage rate from 6.56×10^{-2} cm^3/s to 3.28×10^{-3} cm^3/s for GBC-32 and from 7.52×10^{-3} cm^3/s to 3.76×10^{-4} cm^3/s for GBC-68.

3.2.4 Thermal

Depending on the initial assembly geometry and whether the package relies on convection for heat transfer, changes to the lattice pitch could cause either an increase or decrease in the package component temperatures as shown in Figure 29 and Table 21. For the thermal analysis results presented, the case ID naming convention is as described in Sect. 3.1.4.

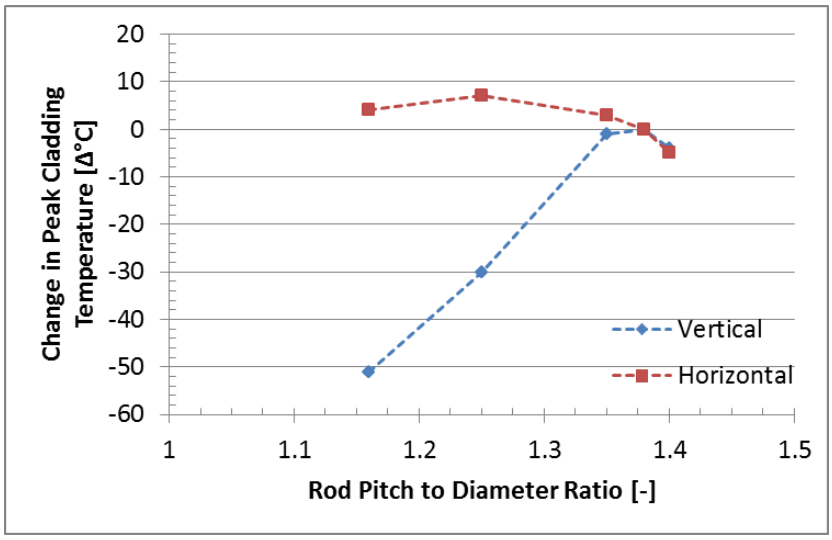

Figure 29 – Change in peak cladding temperature vs. rod pitch to diameter ratio

Table 21 – Rod/assembly deformation results summary

Case ID	Pitch to diameter ratio	Change in Temperature (Δ°C)						
		Max. clad	Min. clad	Max. outer surface	Min. outer surface	Max. neutron absorber	Max. basket SS[b]	Max. neutron shield
V.40.116pdr	1.16	-51	+11	-2	+3	-51	-51	-1
V.40.125pdr	1.25	-30	+5	-1	+2	-30	-30	0
V.40.135pdr	1.35	-1	0	0	0	0	0	0
V.40[a]	1.38	0	0	0	0	0	0	0
V.40.140pdr	1.40	-4	0	-1	+1	-3	-3	0
H.40.116pdr	1.16	+4	0	0	0	+4	+4	0
H.40.125pdr	1.25	+7	0	0	0	+6	+6	0
H.40.135pdr	1.35	+3	0	0	0	+3	+3	0
H.40[a]	1.38	0	0	0	0	0	0	0
H.40.140pdr	1.40	-5	0	0	0	-5	-5	0

[a]Nominal intact fuel configuration.
[b]SS = stainless steel.

For the vertical orientation, both increasing and decreasing the fuel lattice pitch caused a decrease in the maximum cladding, basket wall, and neutron absorber temperature as shown in Table 21. The heat transport within the canister relies on complex parallel and intersecting paths of conduction, convection and thermal radiation. Decreasing the lattice pitch resulted in a higher predicted recirculating mass flow rate within the canister as shown in Figure 30, thereby increasing convective heat transport. However, the flow loss coefficients for spacer grids and entrance/exit losses were not modified between cases. Depending on how the assembly was deformed, the spacer grids and/or the entrance/exit flow losses may be impacted. Increasing the lattice pitch increases the cladding-to-basket wall view factors, thereby increasing thermal radiation heat transport. Of the cases analyzed, the nominal intact configuration case resulted in the highest temperatures.

For the horizontal orientation, changes to the fuel lattice pitch had only a minor impact on the package temperatures as shown in Table 21. Of the cases analyzed, the case with a rod pitch-to-diameter ratio of 1.25 resulted in the highest temperatures.

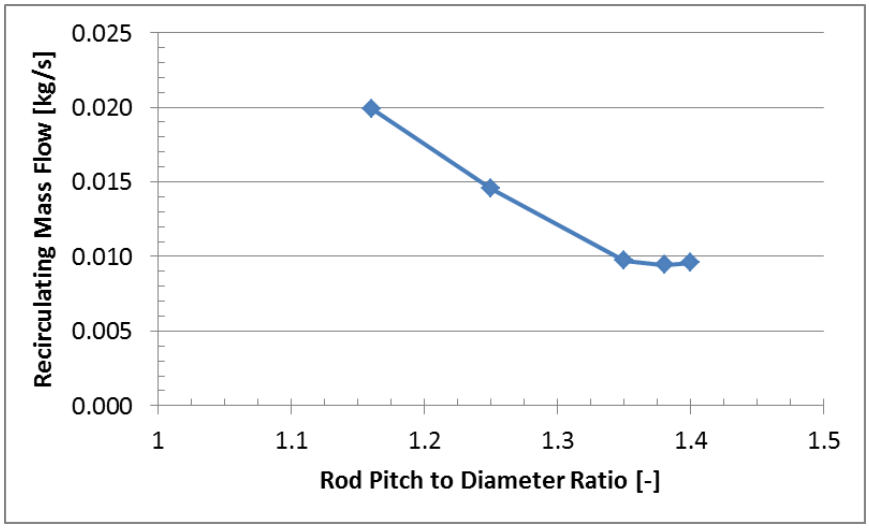

Figure 30 – Recirculating mass flow rate vs. rod pitch to diameter ratio for vertical package

3.3 CATEGORY 3: CHANGES TO INTACT ASSEMBLY AXIAL ALIGNMENT

Changes to the nominal intact axial alignment of the spent fuel within the canister basket can impact the design basis safety analyses that are based on a fixed geometry.

3.3.1 Criticality

The consequences of changes to intact assembly axial alignment require criticality calculations to investigate the changes in k_{eff} associated with active fuel exposure above and below the absorber plate envelope within a basket cell. The upward (toward the lid) misalignment is of higher importance for SNF criticality evaluations because the reactivity of the assembly is driven by the burnup gradient near the top of the assembly. Because of differences in canister design, fuel spacers, and assembly designs, the amount of space available for the active fuel to potentially be outside the absorber envelope will vary, which affects the extent of the range of possible movement. As such, representative ranges of active fuel exposure were evaluated.

The PWR and BWR fuel axial displacement models were developed such that all the fuel assemblies within a canister are moved uniformly up or down relative to their original position. Exposed fuel ranges were varied to a maximum of 30 cm above the absorber. The reactivity increase is calculated at several points over the range to map the response; the maximum misalignments considered are intended to be larger than realistic misalignments to remove any design-specific constraints. The variation of the k_{eff} change as a function of axial position is shown in Figure 31 for several PWR fuel initial enrichment and burnup combinations and in Figure 32 for the BWR fuel initial enrichment and burnup combinations. Maximum changes in

k_{eff} for 30 cm versus 20 cm for PWR fuel, and for 31.78 cm versus 13.65 cm for BWR fuel are provided in Table 22 for comparative purposes.

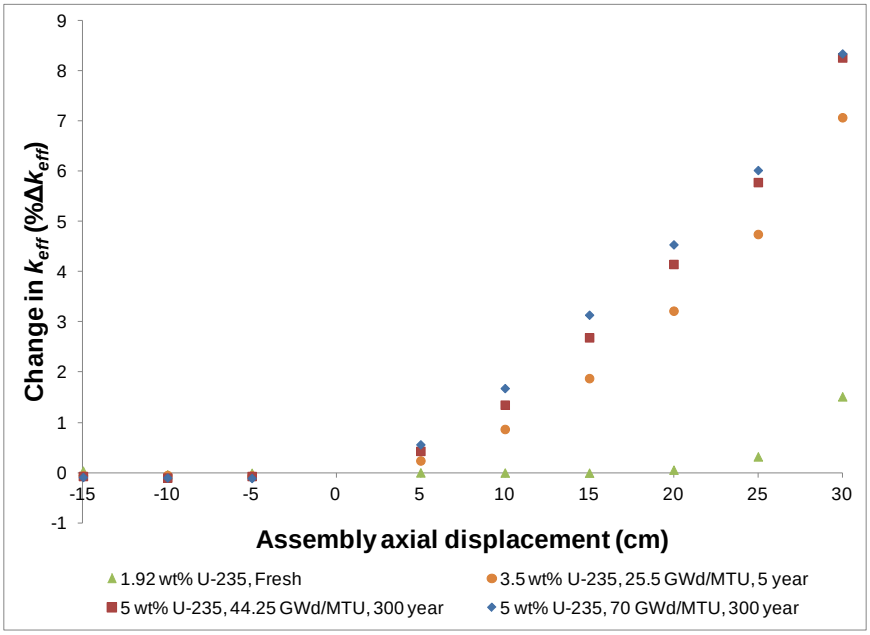

Figure 31 – GBC-32 criticality analysis results from axial misalignment

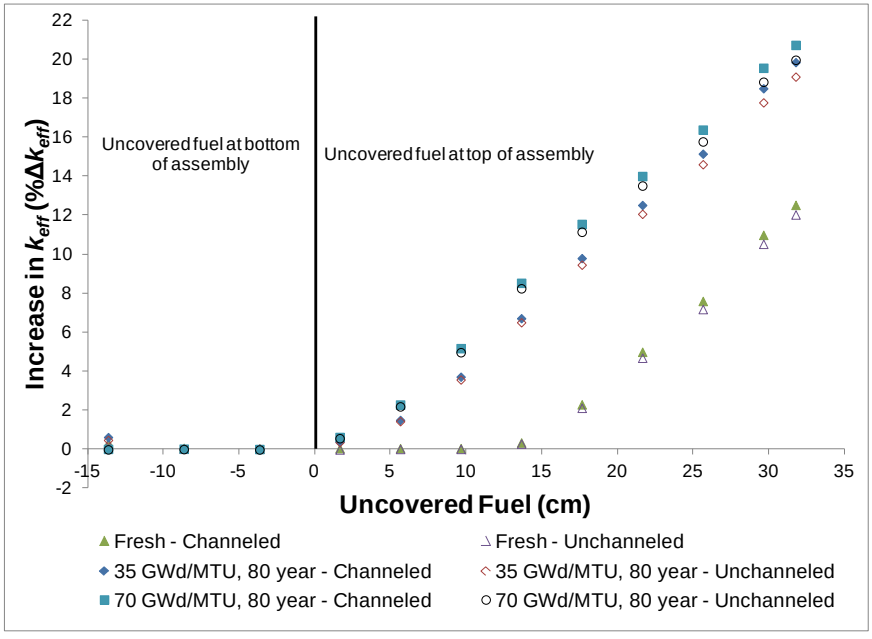

Figure 32 – GBC-68 criticality analysis results from axial misalignment

Table 22 – Criticality results for axial displacement of intact fuel

Parameter				
PWR system				
Burnup (GWd/MTU)	0	25.5	44.25	70
Initial enrichments (wt % ^{235}U)	Maximum change in k_{eff} (%Δk_{eff}) (30 cm/20 cm exposed fuel)			
1.92	1.52/0.06	NC	NC	NC
3.5 with 5-year decay time	NC	7.07/3.22	NC	NC
5.0 with 5-year decay time	NC	NC	7.69/3.64	8.06/4.13
5.0 with 80-year decay time	NC	NC	8.28/4.18	8.28/4.51
5.0 with 300-year decay time	NC	NC	8.26/4.15	8.34/4.54
BWR system				
Burnup (GWd/MTU)	0	35	70	
Initial enrichment (wt % ^{235}U)	Maximum change in k_{eff} (%Δk_{eff}) channeled (31.78 cm exposed fuel/13.65 cm exposed fuel)			
5.0 with 5-year decay time	12.52/0.33	19.40/6.29	20.47/8.03	
5.0 with 80-year decay time	NC	19.84/6.70	20.73/8.52	
5.0 with 300-year decay time	NC	19.83/6.66	20.76/8.49	
	Maximum change in k_{eff} (%Δk_{eff}) unchanneled (31.78 cm exposed fuel/13.65 cm exposed fuel)			
5.0 with 5-year decay time	12.02/0.27	18.66/6.07	19.71/7.78	
5.0 with 80-year decay time	NC	19.10/6.49	19.96/8.24	
5.0 with 300-year decay time	NC	19.06/6.42	20.00/8.20	

Note: NC = not calculated.

Overall, the results indicate that the effects of axial misalignment of intact fuel assemblies increase with increased active fuel exposure beyond the basket neutron absorber envelope, and that displacement towards the canister bottom is inconsequential. For most canister systems, the available displacement distance will be limited because of the presence of assembly end fitting components and fuel spacers. The available displacement distance will be canister design, fuel assembly spacer design, and assembly design dependent.

3.3.2 Shielding

The consequences associated with changes to the intact assembly axial alignment were analyzed assuming that the fuel assemblies could reach either the top or bottom surface of the inner package cavity. Fuel assembly displacement towards the canister cavity top causes an increase in dose rates at the external top surface and at the external radial surface above the neutron shield. Fuel assembly displacement toward the canister cavity bottom causes an increase in dose rates at the external bottom surface and at the external radial surface below the neutron shield. However, for the PWR package radial surface, maximum neutron and gamma dose rate values were only greater by ~15% and 30%, respectively, whereas the BWR package maximum radial neutron and gamma dose rate values did not change relative to the nominal intact fuel configuration. The PWR package maximum neutron and gamma dose rate values were ~40% and 80% greater at the external bottom surface and ~30% and 70% greater at the external top surface, respectively, relative to the nominal intact fuel configuration. The BWR package maximum neutron and gamma dose rate values were ~20% and 55% greater at the external bottom surface and ~15% and 40% greater at the external top surface, relative to the nominal intact fuel configuration. The maximum dose rate increase for the package axial surfaces depends on the free void volume available above or below the fuel assemblies, which varies as a function of fuel assembly length and package design. For the models analyzed, the free void volume was smaller for the BWR fuel than for the PWR fuel because the GE14 fuel assembly is longer than the W 17×17 OFA.

The ratio of the maximum surface dose rate value for the fuel reconfiguration to the maximum surface dose rate value for the nominal intact configuration (the F/I dose rate ratio) is summarized in Table 23 and Table 24 for the evaluated PWR and BWR fuel reconfigurations, respectively, under NCT.

Table 23 – PWR package maximum dose rate change for NCT

Package external surfaces				**Top**			**Side**			**Bottom**		
Case #	**Scenario**	**Fuel relocation region**	**Decay time (years)**	**F/I dose rate ratio[a]**								
				n	**γ**	**Total**	**n**	**γ**	**Total**	**n**	**γ**	**Total**
13	Alignment changes	See Figure B.9 (a)	5	0.80	0.60	0.76	1.15	1.00	0.99	1.35	1.66	1.46
			40	0.80	0.58	0.80	1.14	1.00	1.00	1.34	1.77	1.36
14	Alignment changes	See Figure B.9 (b)	5	1.26	1.59	1.32	1.10	1.29	1.20	0.78	0.59	0.71
			40	1.26	1.68	1.27	1.10	1.01	0.99	0.77	0.57	0.76
2 m from package external surfaces				**Top**			**Side**			**Bottom**		
Case #	**Scenario**	**Fuel relocation region**	**Decay time (years)**	**F/I dose rate ratio[a]**								
				n	**γ**	**Total**	**n**	**γ**	**Total**	**n**	**γ**	**Total**
13	Alignment changes	See Figure B.9 (a)	5	0.79	0.60	0.75	1.01	1.00	1.01	1.30	1.67	1.45
			40	0.80	0.86	0.80	1.01	1.01	1.00	1.29	1.74	1.32
14	Alignment changes	See Figure B.9 (b)	5	1.25	1.61	1.33	1.02	1.00	1.01	0.79	0.59	0.71
			40	1.28	1.57	1.28	1.02	1.00	1.02	0.78	0.57	0.77

[a]Relative error (95% confidence level) less than 5%.

Table 24 – BWR package maximum dose rate change for NCT

Package external surfaces				Top			Side			Bottom		
Case #	Scenario	Fuel relocation region	Decay time (years)	F/I dose rate ratio[a]								
				n	γ	Total	n	γ	Total	n	γ	Total
8	Alignment changes	See Figure B.9 (a)	5	0.88	0.69	0.85	1.01	1.00	1.01	1.16	1.44	1.29
			40	0.89	0.71	0.88	1.01	1.01	1.01	1.17	1.54	1.17
9	Alignment changes	See Figure B.9 (b)	5	1.12	1.42	1.17	1.00	1.00	1.00	0.86	0.71	0.79
			40	1.14	1.39	1.14	1.00	1.01	1.00	0.87	0.72	0.87
2 m from package external surfaces				**Top**			**Side**			**Bottom**		
Case #	**Scenario**	**Fuel relocation region**	**Decay time (years)**	**F/I dose rate ratio[a]**								
				n	**γ**	**Total**	**n**	**γ**	**Total**	**n**	**γ**	**Total**
8	Alignment changes	See Figure B.9 (a)	5	0.88	0.70	0.85	1.01	0.99	1.01	1.13	1.42	1.28
			40	0.88	0.92	0.88	1.01	1.01	1.01	1.18	1.53	1.19
9	Alignment changes	See Figure B.9 (b)	5	1.15	1.41	1.20	1.01	1.00	1.00	0.85	0.72	0.78
			40	1.14	1.08	1.14	0.97	1.02	0.97	0.87	0.75	0.87

[a]Relative error (95% confidence level) less than 5%.

For the analysis under HAC, dose rates at 1 m from the package were calculated with a model using air in place of the outer neutron shield considered in the package models for NCT. The ratio of the maximum surface dose rate value for each fuel reconfiguration analyzed to the maximum dose rate value for the nominal intact configuration (the F/I dose rate ratio) is summarized in Table 25 for the PWR and BWR package models. The maximum neutron and gamma dose rate values on the package top and bottom surfaces increased by ~30% and 70%, respectively.

Table 25 – GBC-32 maximum dose rate change for HAC

1 m from PWR package external surfaces									
				Top	Side	Bottom	Top	Side	Bottom
Case #	Scenario	Fuel relocation region	Decay time (y)	F/I neutron dose rate ratio[a]			F/I gamma dose rate ratio[a]		
13	Alignment changes	See Figure B.9 (a)	5	0.80	0.99	1.30	0.60	1.00	1.66
			40	0.81	0.99	1.29	0.76	0.97	1.73
14	Alignment changes	See Figure B.9 (b)	5	1.25	1.01	0.79	1.57	1.00	0.60
			40	1.26	1.01	0.78	1.30	0.96	0.55
1 m from BWR package external surfaces									
				Top	**Side**	**Bottom**	**Top**	**Side**	**Bottom**
Case #	**Scenario**	**Fuel relocation region**	**Decay time (y)**	**F/I neutron dose rate ratio[a]**			**F/I gamma dose rate ratio[a]**		
8	Alignment changes	See Figure B.9 (a)	5	0.90	1.00	1.16	0.70	0.99	1.41
			40	0.89	1.00	1.16	0.92	0.99	1.35
9	Alignment changes	See Figure B.9 (b)	5	1.09	1.00	0.87	1.41	0.99	0.72
			40	1.06	0.99	0.89	1.10	0.99	0.88

[a]Relative error (95% confidence level) less than 5%.

The effects of assembly alignment change [See Figure B.9 (a)] were also evaluated at 1 m from an individual SNF storage cask in a vertical orientation. The maximum dose rate increase, at 1 m from the cask side surface in a plane through the cask air vent locations, was a factor of ~1.4 for the neutrons and a factor of ~2.7 for gamma rays. The maximum value of the total dose rate increased by a factor of 2.7.

3.3.3 Containment

The containment consequences for this category are the same as for Category 2 (Sect. 3.2.3) because cladding failure is not included in the changes with assembly axial alignment. All cladding failure scenarios are evaluated under Category 1 (Sect. 3.1). Normal, off-normal, and accident conditions of spent fuel storage and normal and accident conditions of transportation that can cause a change in SNF axial alignment can affect the amount of crud that spalls off the cladding. Hence, allowable leakage rate was calculated as a function of the fraction of crud that spalls off cladding to evaluate the effect of varying crud releasable activity (see Appendix C.6). The allowable leakage rate is inversely proportional to the fraction of crud assumed to spall off the cladding. For the 5-year decay time, an increase in the fraction of crud from 0.05 to 1 would cause a decrease in the allowable leakage rate from 6.58×10^{-4} cm^3/s to 3.29×10^{-5} cm^3/s for GBC-32 and from 7.54×10^{-5} cm^3/s to 3.77×10^{-6} cm^3/s for GBC-68. For the 40-year decay time, an increase in the fraction of crud from 0.05 to 1 would cause a decrease in the allowable leakage rate from 6.56×10^{-2} cm^3/s to 3.28×10^{-3} cm^3/s for GBC-32 and from 7.52×10^{-3} cm^3/s to 3.76×10^{-4} cm^3/s for GBC-68.

3.3.4 Thermal

Changes in assembly axial alignment within the basket cells had a minor impact on the component temperatures as provided in Table 26. For the thermal analysis results presented, the case ID naming convention is as described in Sect. 3.1.4.

For the vertical orientation, shifting the assemblies upwards caused an increase in the maximum component temperatures while lowering the minimum component temperatures. Shifting the assemblies upward moves the heat source higher in the canister. This results in less of a “chimney” to drive the circulation within the canister. The recirculating mass flow is 0.498 kg/min when the assemblies are shifted up versus 0.566 kg/min for the nominal intact configuration case. When the assemblies are shifted downward, there is a larger “chimney” to drive the internal recirculating flow, and the peak temperatures are decreased.

For the horizontal orientation, shifting the assemblies had a minor impact on the maximum component temperatures. The maximum component temperatures occur toward the center of the canister. Shifting the assemblies mainly shifts the maximum temperature locations. The minimum cladding temperature was impacted more than the other component temperatures. The minimum cladding temperature is impacted by the heat loss through the ends of the package. By shifting the assemblies such that they become in contact with the ends of the cask/package, the minimum cladding temperature is decreased.

Table 26 – Assembly axial alignment shift results summary

Case ID	Axial shift (cm)	Change in temperature (Δ°C)						
		Max. clad	Min. clad	Max. outer surface	Min. outer surface	Max. neutron absorber	Max. basket SS[b]	Max. neutron shield
V.40.up	+27.27	+8	-10	+2	-2	+8	+9	+3
V.40[a]	0	0	0	0	0	0	0	0
V.40.dn	-8.89	-3	+4	-1	+1	-2	-2	-1
H.40.up	+27.27	+2	-12	+1	-3	+2	+2	+1
V.40[a]	0	0	0	0	0	0	0	0
H.40.dn	-8.89	-1	+5	0	-2	-1	-1	0

[a]Nominal intact fuel configuration.
[b]SS = stainless steel.

4. SUMMARY AND CONCLUSIONS

This report investigates the consequences of fuel configuration changes with regards to SNF storage and transportation systems in four technical disciplines: criticality, shielding (dose rates), containment, and thermal. Three fuel reconfiguration categories were considered: configurations characterized by (1) cladding failure, (2) rod/assembly deformation without cladding failure or (3) changes to assembly axial alignment without cladding failure. The analyses used representative SNF designs and storage cask/ transportation packages, and a range of fuel initial enrichments, discharge burnup values, and decay times. Consequences with respect to the different technical disciplines for the fuel reconfiguration categories were provided relative to the nominal intact configuration in Sect. 3, and detailed descriptions of the analyses performed are provided in Appendices A, B, C, and D. The findings of this research effort are intended to inform the safety evaluation of SNF storage and transportation systems by identifying fuel reconfigurations that would have the most significant impact on safety-significant parameters with respect to the four technical disciplines. However, there was no study or comparison of mechanical properties, finite element analysis stress distribution studies, or physical testing to evaluate the likelihood of each configuration.

In all technical disciplines evaluated, the postuated configurations involving cladding failure exhibited the largest impact on safety-significant parameters. Therefore, it is recommended that these configurations be evaluated further on a cask-specific and assembly-specific basis to identify the impact of changes in analysis assumptions and geometry conditions. Further, future work to evaluate the credibility of these fuel reconfigurations is suggested to fully understand the actual potential impacts on safety when mechanical properties for high-burnup fuel are better understood. A summary of impacts associated with fuel configuration changes for each of the technical disciplines is provided below.

Criticality

A summary of pertinent results for the fuel reconfiguration categories as they apply to criticality safety considerations is provided in Table 27. The results reported are with respect to the following nominal intact configuration cases: (1) PWR fuel at 44.25 GWd/MTU burnup for 5 wt% ^{235}U initial enriched fuel and 5-year decay time for all three categories; and (2) channeled BWR fuel at 5 wt% ^{235}U initial enrichment with 35 GWd/MTU burnup and 5-year decay time for Categories 1 and 3, and for 5 wt% ^{235}U initial enriched fresh fuel for Category 2.

The maximum increase caused by a single failed rod was 0.10% Δk_{eff} for the GBC-32 model and 0.29% Δk_{eff} for the GBC-68 model. The failure of multiple rods increases the reactivity impacts to 1.86% Δk_{eff} for GBC-32 and 2.40% Δk_{eff} for GBC-68. The damaged fuel configurations resulted in significantly higher reactivity increases. Having complete rubblization of the fuel is not physically likely under NCT as prescribed in 10 CFR 71.71, or as a result of impacts from accident loads specified in 10 CFR 71.73. These representations were meant to provide an estimate of the maximum potential increase (upper bound) in k_{eff} available, and to assess the impact of modeling simplifications such as representing the fuel reconfiguration as a homogeneous distribution rather than a heterogeneous distribution. The results indicated that homogeneous representations were non-conservative primarily due to the resonance self-shielding effects of low enriched fuel.

No significant differences were observed in trends between configurations that evaluated fuel at 44.25 GWd/MTU and 70 GWd/MTU.

Table 27 – Fuel reconfiguration results summary pertaining to criticality

Configuration scenario	Case description	Parameter varied	Maximum k_{eff} increase (% Δk_{eff}) (GBC-32/GBC-68)
Category 1: Cladding Failure			
S1(a)—breached spent fuel rods	Multiple rod removal	Multiple missing rod combinations until an upper limit is identified	1.86/2.40
	Combination of multiple rod removal and rubble extended beyond absorber envelope (displaced fuel volume fraction = 0.341)	Number of missing rods and distribution of displaced fuel outside neutron absorber envelope	4.91[b]/NC
S1(b)—damaged SNF	Uniform pellet array[a] (includes SNF distributed outside neutron absorber panel envelope)	The pellet spacing, and thus the debris bed size, was varied to find the largest Δk_{eff}	21.37/34.40[b]
Category 2: Rod/Assembly Deformation			
S2(a)—configurations associated with side drop	Pin pitch contraction	Pin pitch reduced from nominal intact configuration	Not applicable. Nominal intact configuration bounding for this configuration
S2(b)—configurations associated with end drop	Uniform and non-uniform radial and axial pin pitch changes (birdcaging and bottlenecking).	Pitch of all rods radially expanded over different axial lengths until outer pins are in contact with basket cell wall	2.65 to 3.90/ 2.09 to 13.31
Category 3: Changes to Assembly Axial Alignment			
S3—axial displacement of intact fuel	Assembly shift exposing active fuel outside neutron absorber envelope	Length of active fuel above or below the neutron absorber plate	3.64 at 20 cm / 6.29 at 20 cm

Note: NC = not calculated.
[a]Case is bounding but not considered physically likely.
[b]Maximum value from cases evaluated but optimum missing fuel and volume fraction distribution were not determined.

The effect of rod/assembly deformation was modeled with a series of configurations of fuel pin pitch expansions that could result from side or end drop events. For both PWR and BWR fuel, increases in pin pitch cause k_{eff} to increase, and the peak k_{eff} value was not reached before the pitch expansion became restrained by the fuel basket walls. For representations with uniform pin pitch expansion, the maximum increase in k_{eff} for PWR fuel I in the GBC-32 was 2.65%. Configurations where a non-uniform radial pin pitch was created with larger pin pitches in the center of the assembly and smaller pitches along the edges resulted in larger k_{eff} increases relative to the nominal intact configuration. The largest PWR package k_{eff} increase resulting from this non-uniform radial pin pitch expansion was 3.90% Δk_{eff}. For BWR fuel in the GBC-68, the largest increase in k_{eff} for dechanneled fuel was 13.16% Δk_{eff} and 13.31% Δk_{eff} for the uniform pin-pitch expansion and non-uniform pin-pitch expansion cases, respectively. Channeled BWR fuel resulted in an increase of 2.09% Δk_{eff}. The effects of axial non-uniform pin-pitch expansion were also examined for both BWR and PWR fuel, and the reactivity increases observed were consistent with the non-uniform radial pin-pitch expansion results.

The effects of axial alignment changes of intact fuel assemblies increase with increased active fuel exposure beyond the basket neutron absorber envelope. The intact assemblies in both GBC-32 and GBC-68 were displaced axially through a range of distances to determine the reactivity effect of axial alignment changes. Axial alignment shifts toward the canister lid were observed to be the most limiting. Misalignments of 20 cm result in changes of 3.64% Δk_{eff} for PWR fuel and 6.29% Δk_{eff} for BWR fuel. The available displacement distance is canister design, fuel assembly spacer design, and assembly design dependent.

Further investigations should be conducted regarding fuel relocation outside the neutron absorber panel envelope. No credit was taken for volume displacement of guide tubes, other assembly hardware components, or fuel assembly spacers in the models which could significantly reduce the amount of reactivity increase. In addition, sensitivity analyses should also be performed to associate fuel displacement amounts with fuel particle size, hydrogen-to-fuel ratio, and resonance absorption effects for low enriched fuel to better understand the modeling approximations for spent fuel distributed outside the neutron absorber panel region.

Shielding

A summary of pertinent results for the fuel reconfiguration categories as they apply to shielding/dose rate considerations is provided in Table 28. The results reported in the table are with respect to a radiation source term for 5.0 wt% ^{235}U initially enriched fuel at a burnup of 65 GWd/MTU and 40-year decay time. Those results are specific to the generic PWR and BWR shielding analysis models used in this report. Descriptions of the analysis models and evaluations with differences in burnup and decay time are provided in Appendix B. The impact of fuel configuration changes on transportation package/storage cask external dose rates was evaluated by comparing the dose rate values between intact and fuel reconfigurations.

External gamma and neutron dose rate values were evaluated separately because fuel configuration changes have different effects on gamma and neutron radiation dose rates. The overall impact on the external dose rates depends on the individual gamma and neutron dose rate contributions to the total dose rate, which vary with package/cask design, assembly type, burnup, and decay time. The neutron dose rate changes were very similar for the two decay times analyzed (5-year and 40-year decay times) because the neutron spectrum exhibits small variations as a function of decay time within the time interval of 5 to 40 years. Relative to the nominal intact configuration, the impact of fuel configuration changes on the external gamma dose rate was small for short decay times (e.g., 5 years) compared to longer decay times (e.g., 40 years) because of the varying contribution as a function of decay time of the ^{60}Co ($t_{1/2}$ = 5.271 years) activation sources in the assembly top and bottom hardware regions to total dose rate.

Characteristics of the canister internal components such as the heights of assembly hardware regions, fuel axial burnup profile, the lengths of the fuel assembly top and bottom spacers, and the available free volume within the canister cavity, can affect the relative changes in dose rate at the package axial surfaces caused by fuel configuration changes. In this study, the BWR fuel reconfigurations had more pronounced effects on the external dose rates than the PWR fuel reconfigurations. For the intact fuel configuration, assuming the same assembly burnup and decay time, the dose rates at the top and bottom surfaces of the generic BWR package were lower than the dose rates at the corresponding surfaces of the generic PWR package primarily because the BWR assembly used in this study has longer hardware regions and a more pointed axial source profile than the PWR fuel assembly. Relative to the nominal intact configuration,

fuel relocation to the canister bottom or top regions caused a larger change in the dose rate at the outer axial surfaces of the BWR package compared with the PWR package.

Table 28 – Fuel reconfiguration results summary pertaining to shielding

Configuration scenario	Case description	Parameter varied	Relative change in maximum dose rate[a]	
Category 1: Cladding Failure				
S1(a) – breached spent fuel rods	Transportation package; combination of multiple rod failure and source relocation maintained within the active fuel region, distributed to the top end-fitting, or distributed to the bottom end-fitting	Number of missing rods and distribution of displaced fuel particulates at middle of active fuel region	PWR Top: 1.1 Radial: 1.1 Bottom: 1.0	BWR Top: 1.1 Radial: 1.0 Bottom: 1.1
		Number of missing rods and distribution of displaced fuel particulates to top or bottom of assembly	PWR Top: 6.1 Radial: 3.0 Bottom: 2.9	BWR Top: 21.8 Radial: 2.1 Bottom: 4.6
	One meter from a storage cask; multiple rod failure and source relocation distributed to the bottom end-fitting	Source distribution	PWR[b] Radial: 2.9	BWR[b] Radial: 2.7
S1(b) – damaged SNF	Transportation package; homogeneous fuel mixture distribution settled at bottom or uniformly distributed throughout the package cavity	Source distribution	PWR Top: 6.7 Radial: 3.4 Bottom: 4.3	BWR Top: 23.6 Radial: 2.9 Bottom: 6.2
	1 m from a storage cask; homogeneous fuel mixture distribution settled at bottom	Source distribution	PWR[b] Radial: 4.1	BWR[b] Radial: 9.2
	4×2 storage array evaluation at controlled area boundary	Source distribution	PWR 1.8	BWR 2.4
Category 2: Rod/Assembly Deformation				
S2(a) – configurations associated with side drop	Pin pitch contraction with fuel rods collapsed against fuel basket plates	Source distribution within basket cell	PWR Top: 1.4 Radial: 1.1 Bottom: 1.2	BWR Top: 1.5 Radial: 1.1 Bottom: 1.3
S2(b) – configurations associated with end drop	None. This case is bounded by Category 3 representations	None.	NC	
Category 3: Changes to Assembly Axial Alignment				
S3 – axial displacement of intact fuel	Transportation package; assembly shift allowing fuel assemblies to reach top or bottom surface of the canister cavity	Source location	PWR Top: 1.3 Radial: 1.0 Bottom: 1.4	BWR Top: 1.2 Radial: 1.0 Bottom: 1.2
	1 m from a storage cask; assembly shift allowing fuel assemblies to reach bottom surface of the inner cavity	Source location	PWR[b] Radial: 2.7	BWR[b] Radial: 1.2

Note: NC = not calculated.
[a]Relative change in the maximum value of the total dose rate at each package/storage external surface.
[b]Locations that receive radiation streaming through cask air vents.

The conclusions reported for the transportation package under NCT are based on the calculation results for the package external surface. As the results of the calculations show, the effects of fuel configuration changes on dose rates at the external surface of a package are either similar or bounding for the dose rates at the other relevant locations evaluated (i.e., 2 m

from the package as required by 10 CFR 71.47 for NCT and at 1 m from the package external surfaces as specified in 10 CFR 71.51 for HAC).

The effect of multiple fuel rod failures (Scenario S1[a]) on cask external dose rates was analyzed for different percentages of failed fuel rods per assembly with source redistribution to different assembly axial regions, including the active fuel and lower and upper hardware regions. An important parameter associated with the mass density and source strength of the fuel mixture that may collect into the available free space is the particle packing fraction. The shielding analysis used a closely packed mixture with a packing fraction of 0.58 based on powder mechanics for normal settling; with sensitivity calculations performed using a 0.67 packing fraction. The results based on the two packing fraction values were within the statistical error of the Monte Carlo calculations (i.e., 7% at the 95% confidence level).

For the multiple fuel rod failure cases analyzed, the fuel reconfigurations with fuel mixture being relocated into either the assembly bottom or top region caused a significant increase in the dose rate at the respective package outer bottom or top region. For example, the maximum value of the total dose rate at the PWR package bottom surface increased by a factor of 2.7 for the case using 10% of the assembly fuel mixture relocated into the assembly bottom region. A larger percentage (i.e., 25% versus 10% analyzed for the PWR fuel) of fuel mixture distributed to the assembly bottom region increased the maximum value of the total dose rate at the package bottom surface by a factor of 2.9. Hence, the effect of a larger failed fuel percentage was not proportional to the source strength increase because of increased geometric attenuation associated with the larger mass density.

Models with homogenously distributed radiation sources within the inner cavity volume/bottom, simulating damaged fuel conditions (Scenario S1[b]), are bounding for other fuel failure configurations. Note that this configuration produces maximum dose rate increases that are larger than or similar to the analyzed PWR and BWR fuel rod failure cases with 25% and 11%, respectively, of the fuel mixture relocated to different fuel assembly axial locations. However, this type of configuration is not physically likely under normal, off-normal, and accident conditions of spent fuel storage and normal and accident conditions of transportation. This fuel reconfiguration may be used to evaluate the impact of radiation source relocation to the canister wall adjacent regions (i.e., closer to the package external surfaces) due to fuel configuration changes.

Configurations with fuel rod lattice collapse against the fuel basket plates was analyzed for the rod/assembly deformation category. This fuel reconfiguration is considered to be bounding for assembly deformation involving assembly lattice pitch changes with respect to the package radial and axial dose rates because it provides greater radiation source density near the package radial surface and greater neutron axial streaming. For the specific models used in this study, the maximum increase in the total dose rates at the radial surfaces of the PWR and BWR packages increase was ~10%. The collapsed fuel rods cause an increase in dose rates at the package bottom and top surfaces because of neutron streaming. For the specific models used in this study, the maximum axial dose rate increase was ~50%.

The effects of axial alignment shift are dependent on the available volume above or below the fuel assembly and result in increases in the dose rate at the package axial surfaces. For the PWR package model, the maximum values of the total dose rate at the top and bottom surfaces increased by ~ 30% and 40%, respectively; for the BWR package model, the maximum values of the total dose rate at the top and bottom surfaces increased by ~ 20%. The maximum value

of the total dose rate at the cask radial surface did not change relative to the nominal intact configuration.

The dose rate increases at typical lid, vent port, and drain port o-rings, which are used as seals in some transportation packages, were similar to those obtained for the external surfaces of packages under NCT.

Fuel configuration changes within a SNF storage cask can cause significant dose rate changes relative to the nominal intact fuel configuration in the cask outer regions that receive radiation streaming through cask air vents. For example, for the scenario considering homogeneous fuel mixture distribution in the canister cavity bottom, the dose rate increased by a factor of ~4 for the PWR fuel and by a factor of ~9 for the BWR fuel. Away from the air vent locations, the change in radiation dose rate is either small (e.g., 30% increase for damaged fuel configurations) or negligible.

The dose rates at the controlled area boundary were calculated at 100 m from a generic 4×2 storage cask array using two damaged fuel configurations. The results show that the closely packed fuel mixture model reduces the site boundary dose rate by ~70%, whereas the model with the fuel mixture homogeneously distributed within the entire canister cavity increases the site boundary dose rate contribution from the storage casks by a factor of ~2.4, relative to the nominal intact configuration. The dose rate changes are caused by source geometry changes and gamma self-shielding effects associated with the fuel reconfiguration.

Containment

The containment analysis of low-burnup fuel used varying fractions of rods that develop cladding breach (i.e., fuel reconfiguration Category 1) under NCT, from 0.01 to 1, and the release fractions provided in NUREG-1617 [29] for the contributors to the releasable source term. For the high-burnup fuel analysis the parameters important for containment analysis were varied across the following ranges: the fraction of fuel rods assumed to fail was varied from 0.01 to 1; the fraction of crud that spalls off cladding was varied from 0.15 to 1; the fraction of gases was varied from 0.1 to 0.4, the fraction of volatiles was varied from 2×10^{-4} to 2×10^{-3}, and the mass fraction of fuel released as fuel fines was varied from 3×10^{-5} to 3×10^{-4}. For each fuel type, decay time, and fraction of fuel rods assumed to fail, multiple cases were analyzed using different combinations of the values for the containment analysis. Additionally, the impact on the releasable activity of the discharged fuel particulate original location (i.e., non-rim pellet region or the peripheral rim structure) was also evaluated for high-burnup fuel. Fuel reconfiguration categories identified as either Category 2 or Category 3 did not include cladding failure, as all cladding failure configurations were evaluated under Category 1, so the containment analysis varied the fraction of crud that may spall off the cladding. The different parameter combinations from those listed in NUREG-1617 [29] were studied because insufficient data currently exist to establish values for the parameters important to the containment analysis of high-burnup fuel. Total releasable activity, effective A_2 value, allowable radionuclide release rate, and allowable leakage rate were calculated for the representative PWR and BWR transportation packages referred to as GBC-32 and GBC-68, respectively. The W 17×17 OFA and GE14 assemblies with 40 and 65 GWd/MTU burnup values were used in the analysis. The decay times considered were 5, 40, 100, and 300 years.

Relevant observations with respect to the containment analyses are as follows:

- Overall, the results indicated that under NCT, increases in fuel rod failure rates can be off-set by longer decay times. For the GBC-68 cask and low-burnup fuel, an allowable leakage rate of ~2.4×10^{-5} cm^3/s was obtained for the 0.03, 0.4, 0.7, and 1.0 failed fuel fractions at the 5-, 40-, 100-, and 300-year decay times, respectively. For the GBC-32 cask and low-burnup fuel, an allowable leakage rate of ~1×10^{-4} cm^3/s was obtained for the 0.03, 0.10, 0.15, and 0.25 failed fuel fractions at the 5-, 40-, 100-, and 300-year decay times, respectively.

- The allowable leakage rate decreases with increasing failed fuel rod fractions. The decrease is relatively small (e.g., a 15% decrease because of an increase of failed fuel rod fraction from 0.01 to 0.03) if crud has a large contribution to the total releasable activity and is fairly large if the fuel fines dominate the total releasable activity (e.g., a decrease by a factor of 2.5 because of an increase of failed fuel rod fraction from 0.01 to 0.03).

- Crud is an important factor in the calculation of the allowable leakage rate for the time interval 5 to 40 years after fuel discharge from the reactor because of its relatively high contribution to the total releasable activity. Crud had a more pronounced effect on the BWR packages than on the PWR packages because of the larger ^{60}Co activity per fuel rod surface area associated with BWR fuel. As a result, the BWR package allowable leakage rates are smaller (i.e., more restrictive) than the PWR package allowable leakage rates. For GBC-68 with 65 GWd/MTU burnup and 5-year decay time, an increase in the fraction of crud that spalls off the cladding by a factor of two causes a decrease in the allowable leakage rate by a factor of approximately two. However, the GBC-32 and GBC-68 total releasable activities as well as allowable leakage rates were similar for fuel decay times of ≥40 years because the crud contribution becomes negligible at these decay times.

- For each decay time and fraction of failed fuel rods, an increase in the fraction of gaseous species from 0.1 to 0.4 causes a relatively small decrease (up to ~30%) in the allowable release rate for high-burnup fuel.

- An increase in the fraction of volatile source term by one order of magnitude causes a decrease in the allowable leakage rate for high-burnup fuel by a factor of approximately two.

- The allowable leakage rate showed the greatest sensitivity to changes in the mass fraction of fuel released as fuel fines because of cladding breach. Depending on the decay time and crud contribution to the total releasable activity of high-burnup fuel, an increase in the fraction of fuel fines by a factor of 10 can cause a decrease in the allowable leakage rate by a factor of ~1.5 (BWR fuel with 5-year decay time) to 10 (PWR fuel with 40-year decay time).

- Similar to the NCT cases, the HAC allowable leakage rate has the largest sensitivity to the mass fraction of fuel released as fines. For the high-burnup fuel, an increase in the mass fraction of fuel released as fines by a factor of 10 can cause a decrease in the allowable leakage rate by a factor of ~5 to 10 for GBC-32 and by a factor of ~3.5 to 10 for GBC-68 as the decay time increases from 5 to 300 years.

- Allowable radionuclide release rate and leakage rate for high-burnup fuel vary as a function of the pellet regions from which the radioactive material is released. Radioactive material released from the pellet peripheral region produced smaller allowable leakage rates than the radioactive material released from the non-rim region of the fuel pellet. The extent to which the pellet radial region, from which the releasable activity originates, affects the allowable leakage rate depends on the contribution of crud to the total releasable activity. Small effects are observed for GBC-32 with 5-year decay time and small fraction of failed fuel rods (e.g., 0.01), as well as for GBC-68 with 5-year decay time and any fraction of failed fuel rods, as crud has a significant contribution to the total releasable activity for these cases. For the other cases, the allowable leakage rate based on releasable activity from the outer rim structure is approximately half the allowable leakage rate based on releasable activity from the non-rim region. The importance of the pellet region from which the radioactive material is released increases with increasing decay time and failed fuel fraction for NCT.

The currently recommended parameters in NUREG-1617 [29] for containment analysis should be evaluated in the future for their applicability to fuel in long-term dry storage and to high-burnup fuel, and updated if data for these fuels become available.

Thermal

A summary of pertinent results for the fuel reconfiguration categories as they apply to thermal analysis considerations is provided in Table 29 and Table 30 for the vertical and horizontal orientations, respectively. The results reported are with respect to a thermal source term for 5.0 wt % ^{235}U initially enriched W 17×17 OFA fuel at a burnup of 65 GWd/MTU and a 40-year decay time unless identified otherwise. Of the fuel failure categories investigated, Category 1, where cladding failure occurs, has the largest impact on the component temperatures.

Table 29 – Summary of maximum thermal variations for vertical cask

Category	Description	Cases compared	Peak cladding or neutron absorber* temp. variation (Δ°C)
-	Decay time	20 to 60 years	-221
-	Decay time	40 to 60 years	-45
-	No insolation	yes to no insolation	-10
1	Failure of one assembly: only gaseous release	0% to 100% failure	-14
	Failure of one assembly: gaseous release and particle bed	0% to 100% failure, 0.626 packing fraction	-14
	Failure of all assemblies: only gaseous release	0% to 100% failure	-71*
	Failure of all assemblies: gaseous release and particle bed	0% to 100% failure, 0.626 packing fraction	+127*
2	Rod pitch to diameter ratio	1.38 to 1.16	-51
3	Shifting all assemblies	top to bottom	-11

Table 30 – Summary of maximum thermal variations for horizontal cask

Category	Description	Cases compared	Peak cladding or neutron absorber* temp. variation (Δ°C)
-	Decay time	20 to 60 years	-226
-	Decay time	40 to 60 years	-51
-	No insolation	yes to no	-8
1	Failure of one assembly: only gaseous release	0% to 100% failure	+4
	Failure of one assembly: gaseous release and particle bed	0% to 100% failure, 0.313 packing fraction	+3
	Failure of all assemblies: only gaseous release	0% to 100% failure	+42*
	Failure of all assemblies: gaseous release and particle bed	0% to 100% failure, 0.417 packing fraction	+31*
2	Rod pitch to diameter ratio	1.40 to 1.25	-12
3	Shifting all assemblies	top to bottom	+3

For Category 1, for the vertical package orientation where convective heat transport plays a role, the release of fission product gases from the rods into the canister reduced peak internal temperatures and caused an overall flattening of the axial temperature profiles. In contrast, for the horizontal orientations, where the package does not rely on convective heat transfer, the release of fission product gases caused a significant increase in internal temperatures. In all cases, releasing the fuel rod gaseous contents increases the canister internal pressure. Failure of all the assemblies and the formation of a debris bed resulted in a significant increase in the internal component peak temperatures.

For Category 2, packages in the vertical orientation that rely on internal convection for heat transport may be impacted by variations in assembly pitch more than horizontal or vertical package designs that do not rely on internal convection. In general, changes to the assembly pitch had a minor impact on the component temperatures.

For Category 3, where the axial alignment of the assembly was altered, the impact on component temperatures was only minor. Again, vertical packages relying on internal convection for heat transport may be impacted more than horizontal or vertical package designs that do not rely on internal convection.

From 20 to 100 years of decay time, the peak cladding temperature is predicted to decrease by 272°C to 287°C depending on the package orientation. Other internal components also experience temperature reductions on this order. By accounting for insolation, the peak cladding temperature can change by 10°C to 8°C for the 40-year cooled cases. These variations provide a point of comparison as to the impact of fuel configuration changes. Depending on the package design, loading, and time frame for fuel failure, the thermal impacts of fuel failure may only be of secondary importance as compared to the decreased heat load of the fuel. If fuel failure occurs in a package that is already near its design basis (i.e., freshly loaded with decay heat loads near the design basis), the fuel failure could cause the package not to meet the thermal requirements. Conversely, fuel failure in packages loaded much below design basis heat loads may have little consequence on meeting the thermal requirements.

An example of this is illustrated in Figure 33 for the vertical package and Figure 34 for the horizontal package where the peak neutron absorber temperature predicted by all fuel reconfigurations and cases is plotted. For the package loading analyzed, 40-year cooled fuel with 65 GWD/MTU burnup, no fuel reconfiguration resulted in temperatures outside the thermal limits for the neutron absorber. However, a similar package loaded with 25-year cooled fuel, may meet the normal operating condition thermal requirements but may not meet the requirements under fuel reconfiguration scenarios.

In all fuel configurations, the same amount of decay heat must be removed from the package. The fuel reconfigurations redistribute the energy source term within the canister and alter the heat transport paths from the fuel to the canister wall. The possibility for localized energy deposition, or localized isolation from effective heat transfer paths create the concern for localized hot spots and component failure. The current study highly discretized the canister solid material into sections less than 11.8 × 9.8 × 0.75 cm (basket cell wall). This discretization is complemented by modeling every assembly sub-channel. Thus, localized temperature variations of canister structures are resolved to approximately this scale or smaller in this study.

The analysis for Category 1 assumed a 30% release fraction of fission product gases (consistent with NUREG-1536 and NUREG-1617) [2, 29] regardless of whether only the cladding was breached or the entire assembly formed into a particle bed. The release fraction from rubblized fuel, or high-burnup fuel, may be different from that assumed.

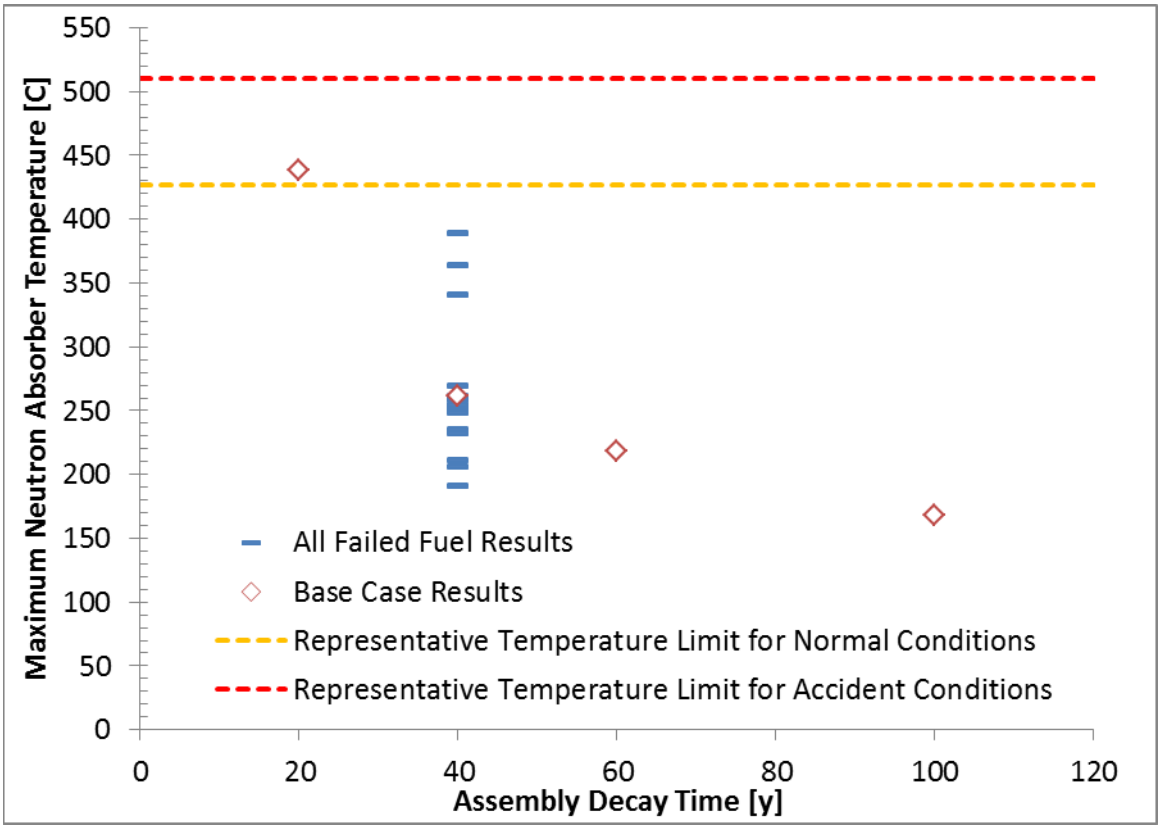

Figure 33 – Peak neutron absorber temperature variation from all fuel reconfigurations—vertical cask

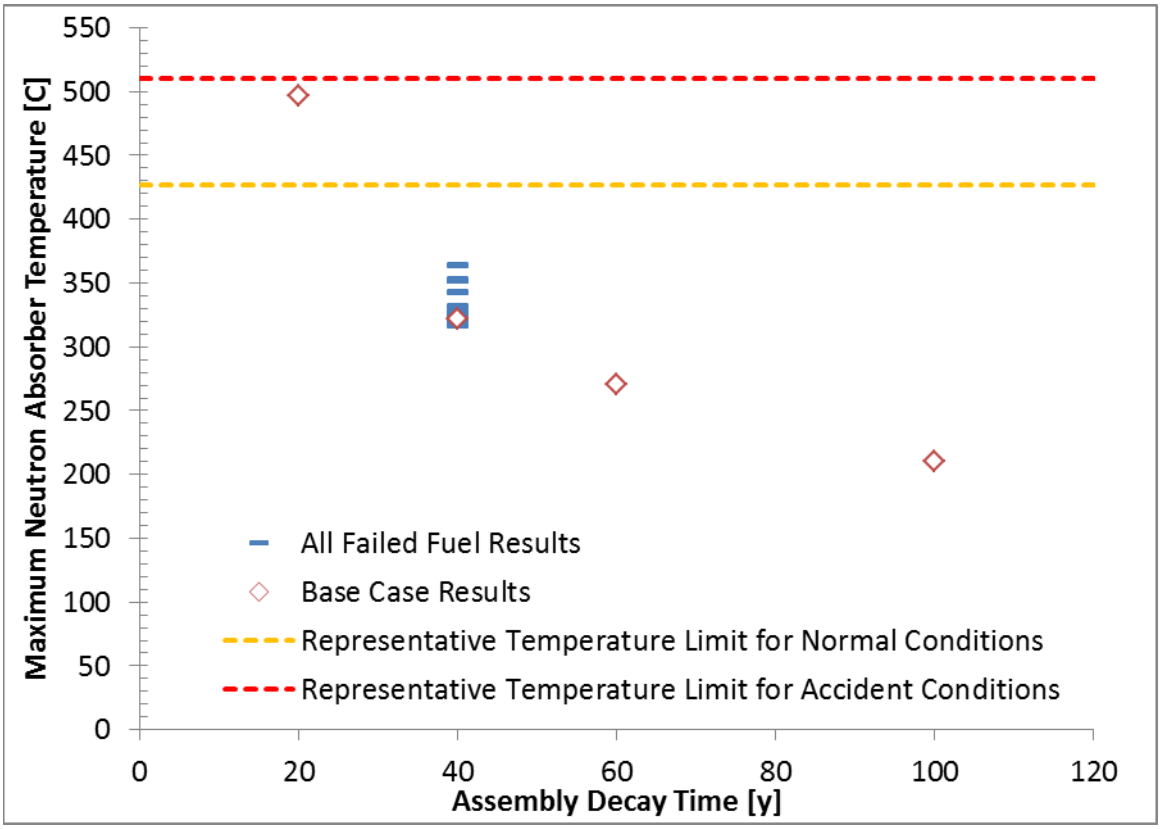

Figure 34 – Peak neutron absorber temperature variation from all fuel reconfigurations—horizontal cask

The fuel failure analysis was performed for only one set of nominal intact boundary conditions (i.e., 100°F still ambient air with insolation). The thermal impact under accident condition boundary conditions was not analyzed as part of this study.

Finally, the change in the package temperature profile from fuel reconfigurations may affect the thermal stresses experienced by the various components. These would need to be resolved and analyzed for structural analysis of the package.

5. REFERENCES

[1] U.S. Nuclear Regulatory Commission, "Interim Staff Guidance -1, Revision 2, Classifying the Condition of Spent Nuclear Fuel for Interim Storage and Transportation Based on Function," Division of Spent Fuel Storage and Transportation, 2007.

[2] U.S. Nuclear Regulatory Commission, "Standard Review Plan for Spent Fuel Dry Storage Systems at a General License Facility, NUREG-1536 Revision 1- Final Report," U.S. Nuclear Regulatory Commission Spent Fuel Project Office, Washington D.C., 2010.

[3] U.S. Nuclear Regulatory Commission, "Interim Staff Guidance - 2, Revision 1, Fuel Retrievability," Division of Spent Fuel Storage and Transportation, 2010.

[4] J. Wagner, "Computational Benchmark for Estimation of Reactivity Margin from Fission Products and Minor Actinides in PWR Burnup Credit, NUREG/CR-6747 (ORNL/TM-

2000/306)," Oak Ridge National Laboratory, Oak Ridge, TN, 2001.

[5] D. Mueller, J. Scaglione, J. Wagner and S. Bowman, "Computational Benchmark for Estimation of Reactivity Margin from Fission Products and Minor Actinides in BWR Burnup Credit, NUREG/CR-7157 (ORNL/TM-2012/96)," U.S. Nuclear Regulatory Commission, Oak Ridge, TN, February 2013.

[6] U.S. Nuclear Regulatory Commission, "Spent Fuel Transporation Risk Assessment, NUREG-2125," U.S. Nuclear Regulatory Commission, Washington D.C., 2014.

[7] EPRI, "Criticality Risks During Transportation of Spent Nuclear Fuel Revision 1, 1016635," Electric Power Research Institute, Palo Alto, California, December 2008.

[8] U.S. Department of Energy, "Gap Analysis to Support Extended Storage of Used Nuclear Fuel. FCRD-USED-2011-000136 Rev. 0.," DOE Office of Nuclear Energy, January 2012.

[9] R. Sindelar, A. Duncan, M. Dupont, P. Lam, M. Louthan Jr and T. Skidmore, "Materials Aging Issues and Aging Management for Extended Storage and Transportation of Spent Nuclear Fuel, NUREG/CR-7116 (SRNL-STI-2011-00005)," U.S. Nuclear Regulatory Commission, Washington D.C., September 2011.

[10] U.S. Nuclear Waste Technical Review Board, "Evaluation of the Technical Basis for Extended Dry Storage and Transportation of Used Nuclear Fuel," U.S. NWTRB, Arlington, Virginia, December 2010.

[11] M. Billone, T. Burtseva and R. Einziger, "Ductile-to-Brittle Transition Temperature forHigh-Burnup Cladding Alloys Exposed to Simulated Drying-Storage Conditions," *Journal of Nuclear Materials,* no. doi: http://dx.doi.org/10.1016/j.jnucmat.2012.10.002, 2012.

[12] J. Rashid and A. Machiels, "Hydride Precipitation in Spent Fuel Cladding During Storage," in *The 10th International Conference on Environmental Remediation and Radioactive Waste Management*, Glasgow, Scotland, September 4-8, 2005.

[13] T. Sanders, K. Seager, Y. Rashid and e. al., "A method for Determining the Spent-Fuel Contribution to Transport Cask Containment Requirements, SAND90-2406, TTC-1019, UC-820," Sandia National Laboratories, Albuquerque, New Mexico, Novemeber 1992.

[14] V. Ballheimer, F. Wille and B. Droste, "Mechanical Safety Analysis For High Burn-Up Spent Fuel Assemblies Under Accident Transport Conditions," in *The 16th International Symposium on the Packaging and Transportation of Radioactive Material*, London UK, 3-8 October 2010.

[15] M. Dallongeville, A. Zeachandirin, P. Purcell and A. Cory, "Description of Fuel Integrity Project Methodology Principles," in *The 16th International Symposium on the Packaging and Transportation of Radioactive Materials*, London, United Kingdom, October 3-8, 2010.

[16] L. Farrington and W. Darby, "An Industry Initiative to Facilitate the Criticality Assessment and Subsequent Licensing of Transport Packages," in *Proceedings of the 15th International Symposium on the Packaging and Transportation of Radioactive Materials*, Miami, Florida, 21-26 October 2007.

[17] EPRI, "Spent-Fuel Transportation Applications-Normal Conditions of Transport, 1015049," Electric Power Research Institute, Palo Alto, California, 2007.

[18] EPRI, "Spent fuel Transportation Applications - Assessment of Cladding Performance: A Synthesis Report, 1015048," Electric Power Research Institute, Palo Alto, California, 2007.

[19] NRC, "ML113120530".

[20] G. Bjorkman, "The Buckling of Fuel Rods in Trasnportation Casks Under Hypothetical Accident Conditions," in *14th International Symposium on the Packaging and Transportation of Radioactive Materials (PATRAM 2004)*, Berlin, Germany, September 20-24, 2004.

[21] DOE, "Yucca Mountain Repository License Application, DOE/RW-0573 Rev. 0," Office of Civilian Radioactive Waste Management, Las Vegas, 2008.

[22] EPRI, "Handbook of Neutron Ansorber Materials for Spent Nuclear Fuel Trasnportation and Storage Applications: 2009 Edition, 1019110," Electric Power Research Institute, Palo Alto, California, 2009.

[23] NRC. [Online]. Available: http://www.nrc.gov/waste/spent-fuel-storage/diagram-typical-dry-cask-system.html. [Accessed 20 June 2013].

[24] NRC. [Online]. Available: http://www.nrc.gov/waste/spent-fuel-storage/diagram-typical-trans-cask-system-2.pdf. [Accessed 20 June 2013].

[25] B. Gogolin, B. Droste and P. Millan, "Drop Tests With the RA-3d Shipping Container for the Transport of Fresh BWR Fuel Assemblies," in *The 13th International Symposium on the Packaging and Transportation of Radioactive Material*, Chicago, Illinois, 3-7 September 2001.

[26] U.S. Nuclear Regulatory Commission, *"NRC Information Notice 2002-09: Potential for top Nozzle Separation and Dropping of a Certain Type of Westinghouse Fuel Assembly", February 13, 2002. ADAMS Accession No. ML020440066.*

[27] R. Brown and J. Richards, Principles of Powder Mechanics, Essays on the Packing and Flow of Powders and Bulk Solids, New York, NY: Pergamon Press, 1970.

[28] NRC, "Standard Review Plan for Transportation Packages for Spent Nuclear Fuel, NUREG-1617," U.S. Nuclear Regulatory Commission Spent Fuel Project Office, Washington, D.C., 2000.

[29] U.S. Nuclear Regulatory Commission, "Standard Review Plan for Transportation Packages for Spent Nuclear Fuel, NUREG-1617," U.S. Nuclear Regulatory Commission Spent Fuel Project Office, Washington, D.C., 2000.

[30] W. Marshall and J. Wagner, "Consequence of Fuel Failure on Criticality Safety of Used Nuclear Fuel, FCRD-UFD-2012-000262 (ORNL/TM-2012/325)," Oak Ridge National Laboratory, Oak Ridge, Tennessee, September 2012.

[31] ORNL, "SCALE: A Comprehensive Modeling and Simulation Suite for Nuclear Safety Analysis and Design, ORNL/TM-2005/39 Version 6.1," Radiation Safety Information Computational Center at Oak Ridge National Laboratory, Oak Ridge, 2011.

[32] ANSI/ANS-6.1.1, "Neutron and Gamma-Ray Flux-to-Dose-Rate Factors," American Nuclear Society, La Grange Park, IL, 1977.

[33] B. Broadhead, "Recommendations for Shielding Evaluations for Transport and Storage Packages, NUREG/CR-6802 (ORNL/TM-2002/31)," U.S. Nuclear Regulatory Commission, Oak Ridge, TN, 2003.

[34] Energy Information Administration, *RW-859 Nuclear Fuel Data, Washington, D.C.(Oct. 2004),* Washington, D.C.: EIA, 2004.

[35] U.S. Department of Energy, "Characteristics of Potential Repository Wastes, DOE/RW-0184-R1, Vol. 1," U.S. Department of Energy, Office of Civilian Radioactive Waste Management, Washington D.C., 1992.

[36] C. Mays, "Summary Report of Commercial Reactor Criticality Data for McGuire Unit 1, B00000000-01717-5705-00063 Rev 01," CRWMS M&O, Las Vegas, Nevada, 1998.

[37] *Fuel Design Data,* Nuclear Engineering International, 2004.

[38] EPRI, "Core Design Operating Data for Cycles 1 and 2 of Quad Cities 1, EPRI-NP-240," Electric Power Research Institute, Palo Alto, California, 1976.

[39] NEA, "Very High Burn-ups in Light Water Reactors, NEA No. 6224," Nuclear Energy

Agency, Organisation for Economic Cooperation and Development, 2006.

[40] B. Anderson, R. Carlson and L. Fisher, "Containment Analysis for Type B Packages Used to Transport Various Contents, NUREG/CR-6487 (UCRL-ID-124822)," U.S. Nuclear Regulatory Commission, Livermore, CA, 1996.

[41] R. C. J. M. A. K. O. a. T. R. Lorenz, "Fission Product Release from Highly Irradiated LWR Fuel, NUREG/CR-0722 (ORNL/NUREG/TM-287/R1)," prepared for the U.S. Nuclear Regulatory Commission by Oak Ridge National Laboratory , Oak Ridge, Tennessee, 1980.

[42] IAEA, "Impact of High Burnup Uranium Oxide and Mixed Uranium-Plutonium Oxide Water Reactor Fuel on Spent Fuel Management, IAEA Nuclear Energy Series No. NF-T-3.8," International Atomic Energy Agency, Vienna, 2011.

[43] IAEA, "Review of Fuel Failures in Water Cooled Reactors, IAEA NUCLEAR ENERGY SERIES No. NF-T-2.1," International Atomic Energy Agency, Vienna, Austria, 2010.

[44] NNL, "The characteristics of LWR fuel at high burnup and their relevance to AGR spent fuel, NNL (10) 10930 Issue 2," National Nuclear Laboratory, 2011.

[45] J. Noirot, L. Desgranges and J. Lamontagne, "Detailed Characterization of High Burn-up Structures in Oxide Fuels," *Journal of Nuclear Materials,* vol. 372, pp. 318-339, 2008.

[46] K. Une, S. Kashibe and A. Takagi, "Fission Gas release Behavior from High Burnup UO2 Fuels under Rapid Heating Conditions," *Journal of Nuclear Science and Technology,* vol. 43, no. 9, pp. 1161-1171, 2006.

[47] Z. Lovasic and R. Einziger, "International Atomic Energy Agency (IAEA) Activity on Technical Influence of High Burnup UOX and MOX Water Reactor Fuel on Spent Fuel Management," in *Proceeding of the Waste Management 2009 Conference*, Phoenix, AZ, March 1-5, 2009.

[48] L. Jernkvist and A. Massih, "Analysis of the effect of UO2 high burnup microstructure on fission gas release, TR-02-010," Quantum Technologies AB, Uppsala, Sweden, 2002.

[49] K. Geelhood, W. Luscher, C. Beyer, D. Senor, M. Cunningham, D. Lanning and H. Adkins, "Predictive Bias and Sensitivity in NRC Fuel Performance Codes, NUREG/CR-7001 (PNNL-17644)," U.S. Nuclear Regulatory Commission, Richland, WA, 2009.

[50] K. Lassman, et al., "Modeling the High Burnup UO2 Structure in LWR Fuel," *Journal of Nuclear Materials,* vol. 226, pp. 1-8, 1995.

[51] American Society for Testing and Materials Standard Method E 321-96 (Reapproved 2005), *"Standard Test Method for Atom Percent Fission in Uranium and Plutonium Fuel (Neodymium-148 Method)",* 2005.

[52] U.S. Nuclear Regulatory Commission, "Standard Review Plan for Spent Fuel Dry Storage Facilities, NUREG-1567," U.S. Nuclear Regulatory Commission Spent Fuel Project Office, Washington, D.C., 2000.

[53] RSICC, "Peripheral Science Routine Collection, COBRA-SFS Cycle 3: Code System for Thermal Hydraulic Analysis of Spent Fuel Cask," November 2003 release.

[54] T. Michener, R. Dodge, D. Rector, C. Enderlin and J. Cuta, "COBRA-SFS: A Thermal-Hydraulic Analysis Code for Spent Fuel Storage and Transportation Casks, PNL-10782," Pacific Northwest Laboratory, Richland, WA, September, 1995.

[55] N. Lombardo, J. Cuta, T. Michener, D. Rector and C. Wheeler, "COBRA-SFS: A Thermal-Hydraulic Analysis Code, Volume III: Validation Assessments, PNL-6049 Vol. III," Pacific Northwest Laboratory, Richland, WA, 1986.

[56] D. Rector, "RADGEN: A Radiation Exchange Factor Generator for Rod Bundles, PNL-6342," Pacific Northwest Laboratory, Richland, WA, 1987.

[57] I. Gauld, S. Bowman and J. Horwedel, "ORIGEN-ARP: Automatic Rapid Processing for Spent Fuel Depletion, Decay, and Source Term Analysis, ORNL/TM-2005/39," Oak Ridge National Laboratory, Oak Ridge, Tennessee, 2009.

[58] U.S. Department of Energy, "Topical Report on Actinide-Only Burnup Credit for PWR Spent Nuclear Fuel Packages, DOE/RW-0472, Rev. 2," Office of Civilian Radioactive Waste Management, Washington D.C., 1998.

[59] F. Incropera and D. DeWitt, Fundamentals of Heat and Mass Transfer, 5th ed., Hoboken, NJ: John Wiley & Sons, Inc., 2002.

[60] L. Siefken, E. Coryell, E. Harvego and J. Hohorst, ""SCDAP/RELAP5/Mod 3.3 Code Manual, MATPRO – A Library of Materials Properties for Light-Water-Reactor Accident Analysis, NUREG/CR-6150, Vol. 4, Rev. 2," U.S. Nuclear Regulatory Commission, Idaho Falls, ID, January 2001.

[61] NIST, "NIST Chemistry WebBook, NIST Standard Reference Database Number 69, Thermophysical Properties of Fluid Systems," National Institute of Standards and Technology, 2011. [Online]. Available: http://webbook.nist.gov/chemistry/fluid. [Accessed 4 March 2013].

[62] E. Tsotsas and H. Martin, "Thermal Conductivity of Packed Beds: A Review," *Chemical Engineering and Processing: Process Intensification,* vol. 22, no. 1, pp. 19-37, July 1987.

[63] EPRI, "Technical Bases for Extended Dry Storage of Spent Nuclear Fuel, 1003416," Electric Power Research Institute, Palo Alto, California, December 2002.

APPENDIX A. CRITICALITY EVALUATIONS FOR FUEL RECONFIGURATIONS

This appendix investigates and quantifies the impacts of changes to calculated k_{eff} values considering the fuel reconfiguration categories evaluated in this report. The term "fuel reconfiguration" refers to any change to the storage and transportation system nominal intact fuel assembly configuration used for the basis of cask certification. For all of the criticality evaluations, the basket structures and neutron poison materials were assumed to remain in the as-loaded condition. Additionally, all evaluations assume that the canister is flooded with water.

A series of cases has been generated for pressurized water reactor (PWR) and boiling water reactor (BWR) storage cask/ transportation package models for several initial enrichment, burnup, and decay time combinations for intact fuel assemblies [30]. This set of cases is used in this report to form a basis of comparison for the various fuel reconfigurations considered. The representative PWR transportation package/cask system is referred to as the generic burnup credit-32 (GBC-32) package/cask, which has typically been used in the past as a GBC benchmark model [4] loaded with Westinghouse (W) 17×17 optimized fuel assembly (OFA) assemblies. The representative GBC-68 BWR cask system [5] was derived from the Holtec HI-STORM 100 multipurpose canister (MPC) 68 cask loaded with representative 10×10 General Electric (GE) 14 BWR fuel assemblies. Note that use of a representative Holtec design in this work is not an endorsement of any design or vendor relative to any others; it was selected so that prior work performed for the Department of Energy Office of Nuclear Energy Fuel Cycle Technologies Used Fuel Disposition Campaign [30] could be leveraged where applicable.

The Scale code system [31] was used to perform the k_{eff} and depletion calculations necessary for these analyses. All calculations used the 238-group neutron data library based on Evaluated Nuclear Data Files, Part B (ENDF/B)-VII.0, distributed with the Scale system.

The KENO V.a and KENO-VI Monte Carlo codes were used for k_{eff} calculations within the appropriate Criticality Safety Analysis Sequence-5 (CSAS5) and CSAS6 sequences. Both codes use Monte Carlo transport to solve the k_{eff} eigenvalue problem. KENO-VI uses a generalized geometry process and is used for the fuel pellet array configuration and some increased fuel rod pitch configurations. KENO V.a has a more restrictive geometry package but is significantly faster because of the simpler geometry treatment. KENO V.a is used for the majority of configurations considered in this analysis. The KENO codes and CSAS sequences are further described and documented in Ref. [31].

For calculations involving irradiated fuel compositions, the isotopic compositions were generated with the Standardized Analysis of Reactivity for Burnup Credit using Scale (STARBUCS) sequence [31]. STARBUCS is a sequence to perform criticality calculations for spent fuel systems employing burnup credit. The STARBUCS sequence uses the Oak Ridge Isotope Generation and Depletion Code–Automatic Rapid Processing (ORIGEN-ARP) methodology to generate depleted fuel compositions and uses the compositions in a KENO model to calculate k_{eff}.

For the PWR cask model criticality evaluations, the initial enrichment and burnup combinations were selected from a representative loading curve such that the calculated k_{eff} was 0.94 after 5-year decay time up to an initial enrichment of 5.0 wt % ^{235}U. For the BWR cask model evaluations, only one initial enrichment was considered, 5.0 wt % ^{235}U. For both cask models, to facilitate evaluations for high-burnup fuel, cases were also developed for a burnup of

70 GWd/MTU. The range of parameters considered for the representative nominal intact configuration cases is provided in Table A.1.

Table A.1 – Range of parameters for criticality nominal intact configurations

Parameter				
PWR system				
Burnup (GWd/MTU)	0	25.5	44.25	70
Initial enrichments (wt % ^{235}U)	Nominal intact k_{eff} [a]/EALF			
1.92	0.940/0.152	NA	NA	NA
3.5	NA	0.940/0.247	NA	NA
5.0	NA	NA	0.940/0.294	0.850/0.311
5.0 with 80-year decay time	NA	NA	0.900/0.297	0.789/0.323
5.0 with 300-year decay time	NA	NA	0.905/0.293	0.795/0.316
BWR system				
Burnup (GWd/MTU)	0	35	70	
Initial enrichment (wt % ^{235}U)	Nominal intact k_{eff} [a]/EALF channeled/EALF unchanneled			
5.0	0.968/0.334/0.312	0.833/0.365/0.340	0.767/0.377/0.351	
5.0 with 80-year decay time	NA	0.824/0.366/0.341	0.753/0.382/0.355	
5.0 with 300-year decay time	NA	0.825/0.364/0.340	0.754/0.379/0.353	

Notes: NA = not applicable; EALF = energy of average lethargy of a neutron causing fission (eV).
[a]Sigma value for k_{eff} calculations was 0.00010.

A.1 CRITICALITY ANALYSIS TO ASSESS IMPACTS OF CATEGORY 1—CLADDING FAILURE

The design basis geometric orientation of the fuel, materials, and neutron energy spectrum are fundamental parameters that must be defined when developing the criticality safety licensing basis. Commercial light water reactor (LWR) fuel assemblies are designed to be under-moderated. The introduction of additional moderator into the assembly lattice can result in a net increase in reactivity depending on location. Fuel rods that suffer cladding failure (i.e., change in design basis geometry) can result in sections of fuel within the lattice being replaced with water, resulting in additional moderator being introduced to the lattice (i.e., change in design basis neutron energy spectrum) and the potential for reactivity increase.

To have an effect on criticality safety performance, the spent nuclear fuel (SNF) rods must be grossly breached such that the geometry and neutron energy spectrum present within the canister are substantially altered from the design basis configuration. To investigate the effects of cladding failure on criticality control performance objectives, cases were developed for two configuration scenarios: (1) breached spent fuel rods where assemblies are partially intact; and (2) damaged fuel where the fuel assembly is represented as a rubble mixture allowing free movement of fuel particles and pellets within a basket cell. Case subclass descriptions are provided in Table A.2 and described in more detail below.

Table A.2 – Cases developed to address Category 1—Cladding Failure

Identifier	Configuration scenario	Subclass description	Parameter varied
S1(a)C1	Breached spent fuel rods	Single fuel rod failure	Individual lattice positions modeled as missing rod
S1(a)C2	Breached spent fuel rods	Multiple fuel rod failure	Multiple missing rod combinations until an upper limit is identified
S1(b)C3	Damaged fuel	Gross assembly failure consisting of homogenized debris	The debris bed size, and thus internal moderation, was varied to find the largest Δk_{eff}
S1(b)C4	Damaged fuel	Gross assembly failure representing debris as discrete lumps	The pellet spacing, and thus the debris bed size, was varied to find the largest Δk_{eff}

A.1.1 Breached Spent Fuel Rods

Two sets of cases were developed for analyses of breached spent fuel rods. The first is an evaluation of lattice position reactivity worth on an individual basis to be used in reducing the combinatorial phase space for multiple rod removal, and the second considers groups of multiple rod removal from the lattice. For these two sets of cases, the displaced fuel was omitted from the model, assuming that it would be sufficiently dispersed from the lattice in a thin, undermoderated heap, resulting in a less reactive system if incorporated into the model. An additional subset of cases was included with the multiple rod removal cases to evaluate the combined effects of rod removal and the distribution of the removed fuel at regions outside the neutron absorber envelope, varying the moderator-to-fuel ratio for the displaced fuel.

S1(a)C1: Single fuel rod failure—A set of cases was developed to evaluate the associated reactivity impact of missing fuel rod segments from each unique lattice position within an assembly. The results of this sensitivity analysis can be used in a combinatorial evaluation to identify a representative bounding lattice configuration with missing fuel rods. Each of the 39 eighth-assembly symmetric rods in the W 17×17 PWR assembly was removed individually to determine its relative worth. Full rod removal is modeled to bound the effects of partial rod removal. The same process was used to evaluate the GE 10×10 BWR fuel assembly; however, half-assembly symmetry was used and resulted in 51 unique fuel lattice locations for evaluation. Cross-sectional lattice arrays showing the symmetry positions for evaluation are presented in Figure A.1 and Figure A.2 for the PWR and BWR assemblies, respectively.

Results showing the change in k_{eff} as a function of position for different initial enrichments, burnups, and decay times for the W 17×17 PWR assembly type in a representative GBC-32 package are provided in Table A.3 through Table A.9. Similar results as a function of position for different initial enrichments, burnups, and decay times for the GE 10×10 BWR assembly type in the GBC-68 cask are provided in Table A.10 through Table A.16

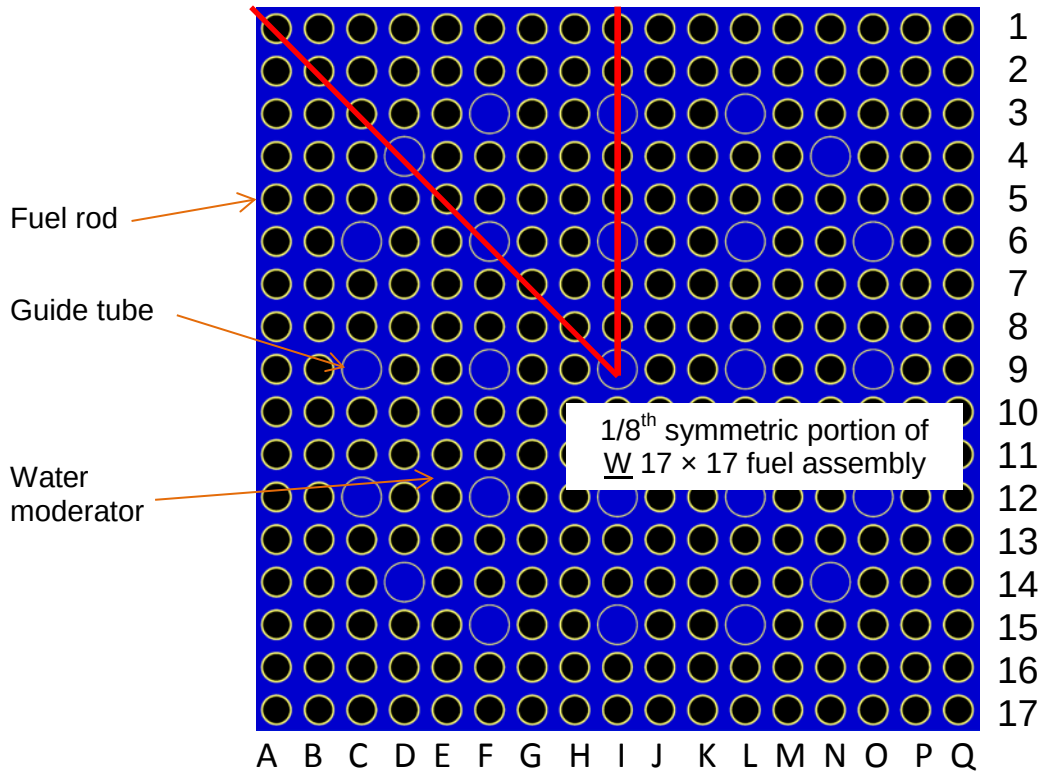

Figure A.1 – Sketch of symmetry, row, and column labels for W 17×17 fuel assembly

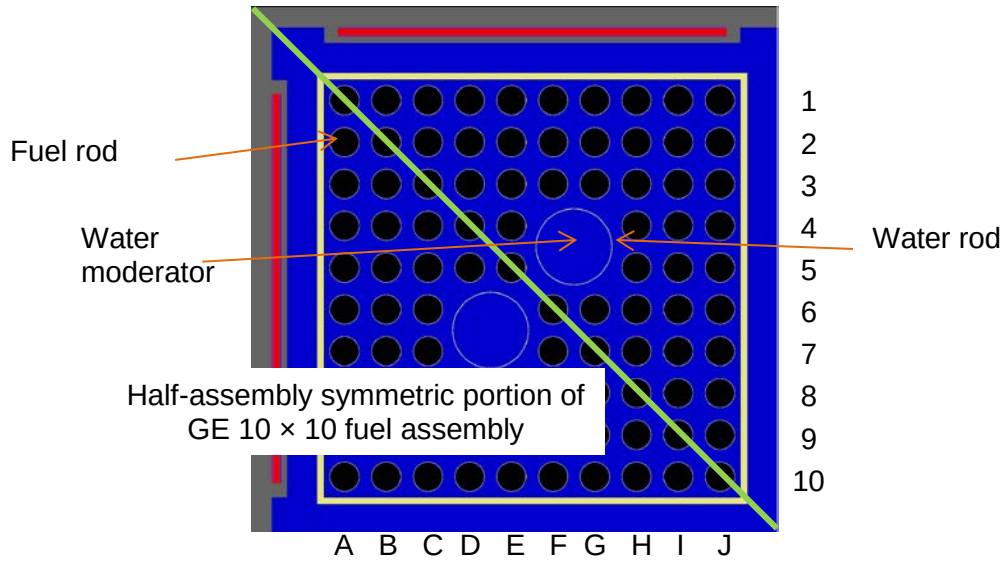

Figure A.2 – Sketch of symmetry, row, and column labels for GE 10×10 fuel assembly

Table A.3 – Change in k_{eff} (%Δk_{eff}) caused by individual removal of each fuel rod in W 17×17 fuel in GBC-32, Fresh fuel, 1.92 w/o ^{235}U (one-sigma uncertainty of all values is 0.014 %Δk_{eff})

	A	B	C	D	E	F	G	H	I
1	-0.14	-0.13	-0.12	-0.10	-0.10	-0.12	-0.14	-0.11	-0.14
2		-0.09	-0.08	-0.06	-0.07	-0.05	-0.07	-0.07	-0.08
3			-0.03	-0.03	-0.04	GT	-0.04	-0.02	GT
4				GT	-0.02	0.00	-0.01	0.00	-0.01
5					0.01	0.00	0.02	0.01	-0.01
6						GT	0.01	0.01	GT
7							0.02	0.02	0.01
8								0.04	0.02
9									IT

Notes: GT = guide tube location; IT = instrument tube location.

Table A.4 – Change in k_{eff} (%Δk_{eff}) caused by individual removal of each fuel rod in W 17×17 fuel in GBC-32, 44.25 GWd/MTU burnup, 5-year decay time (one-sigma uncertainty of all values is 0.014 %Δk_{eff})

	A	B	C	D	E	F	G	H	I
1	-0.15	-0.11	-0.11	-0.09	-0.12	-0.11	-0.08	-0.09	-0.09
2		-0.05	0.02	0.00	0.02	-0.00	0.02	-0.02	-0.00
3			0.04	0.03	0.04	GT	0.05	0.05	GT
4				GT	0.04	0.07	0.08	0.07	0.06
5					0.09	0.07	0.07	0.10	0.07
6						GT	0.08	0.08	GT
7							0.08	0.08	0.09
8								0.09	0.08
9									IT

Notes: GT = guide tube location; IT = instrument tube location.

Table A.5 – Change in k_{eff} (%Δk_{eff}) caused by individual removal of each fuel rod in W 17×17 fuel in GBC-32, 44.25 GWd/MTU burnup, 80-year decay time (one-sigma uncertainty of all values is 0.014 %Δk_{eff})

	A	B	C	D	E	F	G	H	I
1	-0.14	-0.09	-0.07	-0.08	-0.08	-0.09%	-0.08	-0.06	-0.09
2		-0.01	0.00	0.03	0.03	-0.01%	0.01	0.01	0.00
3			0.06	0.04	0.05	GT	0.06	0.04	GT
4				GT	0.05	0.06	0.08	0.07	0.06
5					0.07	0.08	0.08	0.09	0.08
6						GT	0.07	0.08	GT
7							0.09	0.10	0.08
8								0.09	0.08
9									IT

Notes: GT = guide tube location; IT = instrument tube location.

Table A.6 – Change in k_{eff} (%Δk_{eff}) caused by individual removal of each fuel rod in W 17×17 fuel in GBC-32, 44.25 GWd/MTU burnup, 300-year decay time (one-sigma uncertainty of all values is 0.014 %Δk_{eff})

	A	B	C	D	E	F	G	H	I
1	-0.17	-0.12	-0.10	-0.09	-0.10	-0.09	-0.09	-0.08	-0.10
2		-0.01	0.00	0.00	0.02	0.01	0.01	0.01	-0.02
3			0.01	0.04	0.02	GT	0.04	0.05	GT
4				GT	0.06	0.05	0.06	0.06	0.07
5					0.05	0.06	0.09	0.09	0.09
6						GT	0.08	0.08	GT
7							0.10	0.08	0.07
8								0.08	0.08
9									IT

Notes: GT = guide tube location; IT = instrument tube location.

Table A.7 – Change in k_{eff} (%Δk_{eff}) caused by individual removal of each fuel rod in W 17×17 fuel in GBC-32, 70 GWd/MTU burnup, 5-year decay time (one-sigma uncertainty of all values is 0.014 %Δk_{eff})

	A	B	C	D	E	F	G	H	I
1	-0.14	-0.12	-0.11	-0.06	-0.11	-0.11	-0.09	-0.08	-0.10
2		-0.05	-0.01	0.02	-0.01	0.00	0.00	0.00	-0.02
3			0.00	0.03	0.03	GT	0.05	0.03	GT
4				GT	0.05	0.06	0.08	0.06	0.05
5					0.05	0.05	0.07	0.09	0.06
6						GT	0.07	0.07	GT
7							0.07	0.08	0.06
8								0.08	0.08
9									IT

Notes: GT = guide tube location; IT = instrument tube location.

Table A.8 – Change in k_{eff} (%Δk_{eff}) caused by individual removal of each fuel rod in W 17×17 fuel in GBC-32, 70 GWd/MTU burnup, 80-year decay time (one-sigma uncertainty of all values is 0.014 %Δk_{eff})

	A	B	C	D	E	F	G	H	I
1	-0.11	-0.10	-0.08	-0.05	-0.06	-0.07	-0.09	-0.06	-0.08
2		-0.01	0.01	0.02	0.02	0.01	-0.01	0.01	0.02
3			0.02	0.04	0.06	GT	0.05	0.06	GT
4				GT	0.05	0.06	0.07	0.07	0.08
5					0.05	0.08	0.08	0.08	0.08
6						GT	0.06	0.08	GT
7							0.10	0.09	0.09
8								0.08	0.09
9									IT

Notes: GT = guide tube location; IT = instrument tube location.

Table A.9 – Change in k_{eff} (%Δk_{eff}) caused by individual removal of each fuel rod in W 17×17 fuel in GBC-32, 70 GWd/MTU burnup, 300-year decay time (one-sigma uncertainty of all values is 0.014 %Δk_{eff})

	A	B	C	D	E	F	G	H	I
1	-0.12	-0.09	-0.08	-0.08	-0.08	-0.07	-0.08	-0.09	-0.07
2		-0.02	-0.01	0.01	0.03	0.02	0.02	0.02	0.01
3			0.05	0.04	0.02	GT	0.04	0.06	GT
4				GT	0.05	0.06	0.07	0.07	0.06
5					0.08	0.08	0.10	0.09	0.07
6						GT	0.07	0.09	GT
7							0.10	0.08	0.09
8								0.09	0.10
9									IT

Notes: GT = guide tube location; IT = instrument tube location.

Table A.10 – Change in k_{eff} (%Δk_{eff}) caused by individual removal of each fuel rod in GE 10×10 fuel in GBC-68, fresh 5 wt % ^{235}U fuel (one-sigma uncertainty of all values is 0.014 %Δk_{eff})

	A	B	C	D	E	F	G	H	I	J
1	-0.51	-0.21	-0.14	-0.11	-0.10	-0.11	-0.12	-0.15	-0.21	-0.49
2		0.06	0.15	0.18	0.20	0.18	0.17	0.15	0.05	-0.24
3			0.24	0.28	0.25	0.18	0.17	0.21	0.14	-0.16
4				0.26	0.20	WT	WT	0.19	0.16	-0.12
5					0.11	WT	WT	-.19	0.19	-0.12
6						0.11	0.20	0.26	0.19	-0.10
7							0.27	0.29	0.18	-0.13
8								0.23	0.16	-0.14
9									0.08	-0.23
10										-0.50

Note: WT = one quarter of a water tube.

Table A.11 – Change in k_{eff} (%Δk_{eff}) caused by individual removal of each fuel rod in GE 10×10 fuel in GBC-68, 35 GWd/MTU burnup, 5-year decay time (uncertainty of all values is 0.014 %Δk_{eff})

	A	B	C	D	E	F	G	H	I	J
1	-0.43	-0.21	-0.12	-0.07	-0.09	-0.10	-0.11	-0.11	-0.20	-0.41
2		0.06	0.12	0.17	0.19	0.16	0.14	0.12	0.05	-0.20
3			0.23	0.24	0.23	0.18	0.17	0.19	0.12	-0.13
4				0.26	0.17	WT	WT	0.16	0.14	-0.11
5					0.09	WT	WT	0.18	0.16	-0.09
6						0.08	0.19	0.24	0.18	-0.08
7							0.26	0.25	0.15	-0.09
8								0.22	0.16	-0.12
9									0.06	-0.18
10										-0.44

Note: WT = one quarter of a water tube.

Table A.12 – Change in k_{eff} (%Δk_{eff}) caused by individual removal of each fuel rod in GE 10×10 fuel in GBC-68, 35 GWd/MTU burnup, 80-year decay time (one-sigma uncertainty of all values is 0.014 %Δk_{eff})

	A	B	C	D	E	F	G	H	I	J
1	-0.39	-0.17	-0.11	-0.10	-0.07	-0.06	-0.09	-0.12	-0.19	-0.42
2		0.06	0.17	0.16	0.17	0.16	0.15	0.16	0.06	-0.19
3			0.24	0.26	0.24	0.19	0.15	0.21	0.14	-0.11
4				0.27	0.21	WT	WT	0.19	0.15	-0.10
5					0.13	WT	WT	0.17	0.17	-0.07
6						0.09	0.20	0.23	0.19	-0.08
7							0.27	0.26	0.17	-0.07
8								0.23	0.13	-0.11
9									0.07	-0.18
10										-0.40

Note: WT = one quarter of a water tube.

Table A.13 – Change in k_{eff} (%Δk_{eff}) caused by individual removal of each fuel rod in GE 10×10 fuel in GBC-68, 35 GWd/MTU burnup, 300-year decay time (one-sigma uncertainty of all values is 0.014% Δk_{eff})

	A	B	C	D	E	F	G	H	I	J
1	-0.42	-0.17	-0.09	-0.08	-0.05	-0.07	-0.07	-0.10	-0.17	-0.41
2		0.08	0.15	0.15	0.20	0.17	0.16	0.15	0.07	-0.17
3			0.23	0.25	0.25	0.19	0.20	0.21	0.15	-0.13
4				0.28	0.19	WT	WT	0.18	0.17	-0.09
5					0.09	WT	WT	0.19	0.19	-0.06
6						0.13	0.20	0.26	0.18	-0.08
7							0.28	0.26	0.19	-0.09
8								0.25	0.15	-0.10
9									0.08	-0.17
10										-0.44

Note: WT = one quarter of a water tube.

Table A.14 - Change in k_{eff} (%Δk_{eff}) caused by individual removal of each fuel rod in GE 10×10 fuel in GBC-68, 70 GWd/MTU burnup, 5-year decay time (one-sigma uncertainty of all values is 0.014 %Δk_{eff})

	A	B	C	D	E	F	G	H	I	J
1	-0.40	-0.17	-0.11	-0.10	-0.07	-0.07	-0.09	-0.11	-0.18	-0.40
2		0.02	0.12	0.15	0.16	0.13	0.14	0.10	0.04	-0.19
3			0.21	0.26	0.21	0.14	0.14	0.20	0.13	-0.13
4				0.25	0.17	WT	WT	0.15	0.14	-0.10
5					0.09	WT	WT	0.18	0.15	-0.09
6						0.08	0.19	0.22	0.17	-0.07
7							0.25	0.22	0.14	-0.09
8								0.22	0.12	-0.12
9									0.06	-0.15
10										-0.39

Note: WT = one quarter of a water tube.

Table A.15 - Change in k_{eff} (%Δk_{eff}) caused by individual removal of each fuel rod in GE 10×10 fuel in GBC-68, 70 GWd/MTU burnup, 80-year decay time (one-sigma uncertainty of all values is 0.014 %Δk_{eff})

	A	B	C	D	E	F	G	H	I	J
1	-0.37	-0.18	-0.11	-0.09	-0.07	-0.06	-0.08	-0.10	-0.17	-0.37
2		0.04	0.12	0.17	0.16	0.17	0.13	0.12	0.05	-0.15
3			0.21	0.24	0.22	0.17	0.14	0.16	0.11	-0.11
4				0.24	0.19	WT	WT	0.16	0.13	-0.09
5					0.10	WT	WT	0.18	0.14	-0.08
6						0.12	0.18	0.22	0.16	-0.08
7							0.25	0.24	0.15	-0.08
8								0.21	0.12	-0.08
9									0.05	-0.16
10										-0.39

Note: WT = one quarter of a water tube.

Table A.16 - Change in k_{eff} (%Δk_{eff}) caused by individual removal of each fuel rod in GE 10×10 fuel in GBC-68, 70 GWd/MTU burnup, 300-year decay time (one-sigma uncertainty of all values is 0.014 %Δk_{eff})

	A	B	C	D	E	F	G	H	I	J
1	-0.36	-0.16	-0.11	-0.07	-0.07	-0.06	-0.08	-0.09	-0.16	-0.38
2		0.07	0.11	0.18	0.16	0.14	0.15	0.12	0.04	-0.17
3			0.23	0.24	0.23	0.16	0.16	0.21	0.13	-0.11
4				0.25	0.18	WT	WT	0.17	0.14	-0.08
5					0.11	WT	WT	0.18	0.17	-0.08
6						0.10	0.20	0.23	0.17	-0.05
7							0.26	0.23	0.18	-0.07
8								0.22	0.13	-0.10
9									0.07	-0.16
10										-0.38

Note: WT = one quarter of a water tube.

The maximum k_{eff} increase observed for the PWR assembly was 0.10% Δk_{eff} and is associated with rod H5 in the 5.0 wt % ^{235}U initial enrichment, 44.25 GWd/MTU burnup with 5-year decay case. In general, the other cases at different decay times and burnup showed that the lattice position reactivity worths remained nearly constant for different decay times and burnups. It should be noted that several rods across many of the cases have a reactivity worth that is statistically equivalent to the limiting case. Many other rods have a reactivity increase that is less than one standard deviation from 0 and thus have no statistically significant impact on system k_{eff}.

For the BWR fuel assembly, the maximum k_{eff} increase was 0.29% Δk_{eff} and is associated with rod H7 for fresh 5 wt % ^{235}U channeled fuel. Cases have been evaluated investigating how dechanneled BWR fuel assemblies respond to lattice moderator changes and have shown that the k_{eff} increase for channeled fuel assemblies is greater than for unchanneled assemblies [30]. This is likely an artifact of the difference in neutron energy spectrum that occurs from the channel displacing moderator between adjacent fuel regions. The different burnup and decay time sensitivity studies for the BWR fuel also indicate no significant changes in lattice position worth as a function of burnup or decay time.

S1(a)C2: Multiple fuel rod failure—Cases representing multiple fuel rod failures were developed to identify an upper bound on the potential reactivity increase because of the effects of increased moderation resulting from fuel rod segment relocation. A combinatorial evaluation was performed for different groups of fuel rod failure represented. The high worth lattice locations identified in case set S1(a)C1 were used to reduce the sample space of potential combinations to consider from the original lattice orientation. This allowed rod combinations to be selected based on lattice position worth. Multiple rods were removed in symmetric patterns covering different combinations of rods removed until a reactivity peak was identified. For each group of rods removed, various combinations of removal patterns were evaluated.

For the PWR assembly cases, groups of 2, 4, 8, 16, 24, 28, 32, 36, 40, 44, and 48 rods were considered for removal patterns. Results showing the maximum k_{eff} change that was observed from the patterns evaluated for the different enrichment and burnup combinations are provided in Table A.17. The maximum Δk_{eff} value (i.e., a k_{eff} increase of 1.87 $\%\Delta k_{eff}$) for the GBC-32 cask representation occurs for the 5 wt % ^{235}U initial enriched fuel with a burnup of 44.25 GWd/MTU and 300-year decay time when 44 rods have been removed from the lattice configuration. Results for a range of initial enrichment and burnup compositions with 5-year decay time as a function of rods removed are illustrated in Figure A.3, and a cross-sectional view of the corresponding limiting lattice configuration is illustrated in Figure A.4. The higher burnup and longer decay time results indicate that there is no significant increase in reactivity change caused by the different nuclide compositions.

Table A.17 – Multiple rod removal results for W 17×17 OFA in GBC-32

Enrichment (wt % ^{235}U)	Burnup (GWd/MTU)	Number of rods removed	Maximum increase in k_{eff} ($\%\Delta k_{eff}$)
1.92	0	4	0.04
3.5	25.5	36	1.07
5	44.25	44	1.86
44.25	80	44	1.86
44.25	300	44	1.87
70	5	44	1.69
70	80	44	1.62
70	300	44	1.62

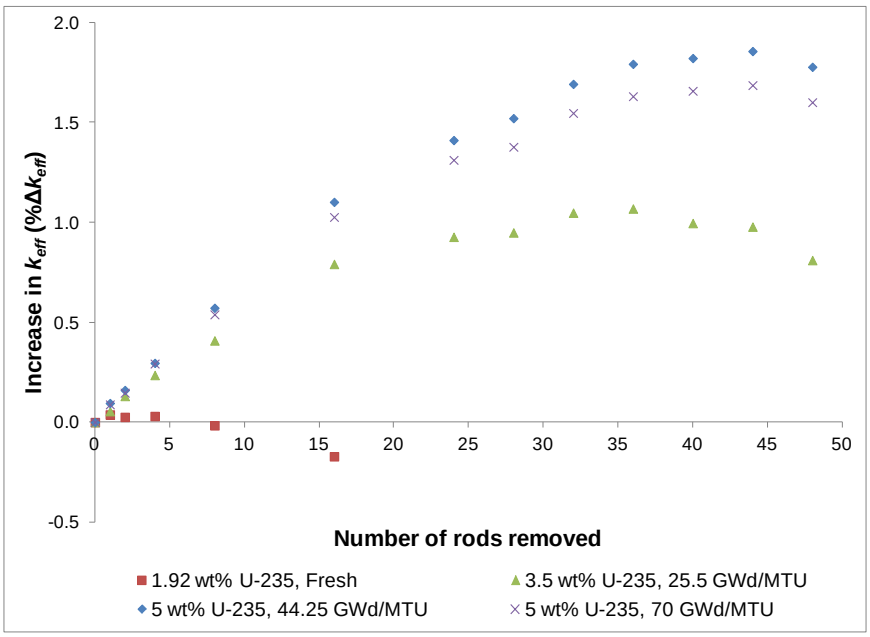

Figure A.3 – Increase in k_{eff} in GBC-32 cask as a function of number of rods removed

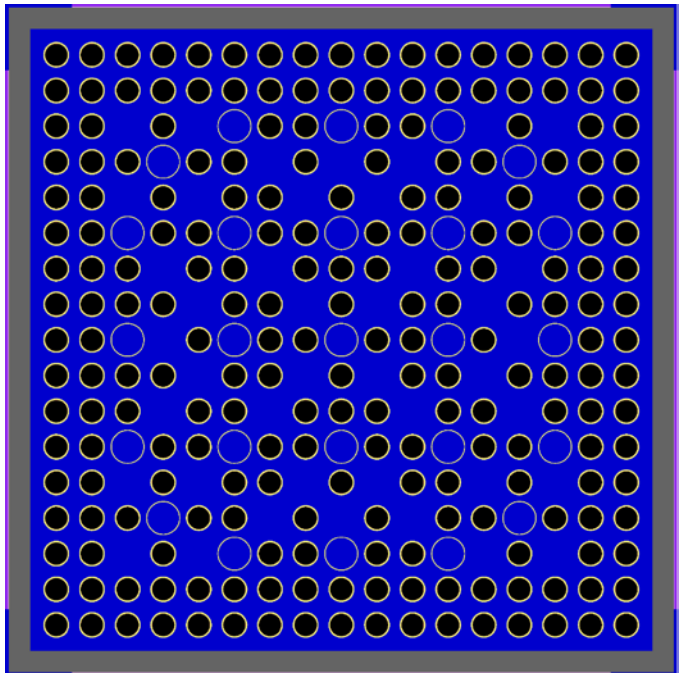

Figure A.4 – Limiting multiple rod removal lattice (44 rods removed)

An additional subset of cases was developed to investigate the combined effects of rod removal and spent fuel displacement in regions outside the neutron absorber envelope. Only the PWR fuel was represented with the 5.0 wt % ^{235}U initial enrichment at 44.25 GWd/MTU burnup and 5-year decay. For these cases, the available void region was modeled with fuel at different volume fractions simulating various sized particles with different bulk densities. The void

displacement of hardware components was omitted from these models. Results are provided in Table A.18 and show that combining the rod removal with displaced fuel distributed at ratios approaching optimum moderation conditions outside the neutron absorber plate envelope yields higher changes in k_{eff} than the displaced fuel configurations alone, which were 1.82, 1.52, and 0.57 $\%\Delta k_{eff}$ for the 40-, 28-, and 8-rod removal cases, respectively.

Table A.18 – Combination rod removal results with heterogeneous distribution of displaced fuel outside neutron absorber plate envelope for GBC-32

# Failed rods	Volume fraction of displaced fuel	Length of void region filled (cm)	Change in k_{eff} ($\%\Delta k_{eff}$)
40	0.524	30	3.89
28	0.341	30	4.91
8	0.146	20	3.55

For the BWR assembly cases, groups of 2, 4, 8, 12, 14, 16, 18, and 20 rods were considered for removal patterns. Results in Table A.19 show the maximum k_{eff} change observed from the patterns evaluated for the different enrichment and burnup combinations presented as a function of rods removed. The maximum Δk_{eff} value (i.e., a k_{eff} increase of 2.42 $\%\Delta k_{eff}$) for the GBC-68 representation occurs for the 5 wt % ^{235}U initial enriched fuel with a burnup of 35 GWd/MTU and 300-year decay time when 18 rods have been removed from the lattice configuration with the channel present. Results for the 35 and 70 GWd/MTU burnup with 5-year decay time compositions and fresh 5 w/o ^{235}U fuel as a function of rods removed are illustrated in Figure A.5, and a cross-sectional view of the corresponding limiting lattice configuration is illustrated in Figure A.6. The results for higher burnups and longer decay times indicate no significant reactivity increases resulting from the use of different nuclide compositions.

Table A.19 – Multiple rod removal results for GE 10×10 fuel in GBC-68

Burnup (GWd/MTU)	Decay time (years)	Channel present	Number of rods removed	Maximum increase in k_{eff} ($\%\Delta k_{eff}$)
0	0	Yes	16	2.24
35	5	Yes	18	2.40
35	80	Yes	18	2.40
35	300	Yes	18	2.42
70	5	Yes	18	2.30
70	80	Yes	20	2.31
70	300	Yes	18	2.32
0	0	No	16	2.11
35	5	No	18	2.30
35	80	No	18	2.31
35	300	No	18	2.29
70	5	No	18	2.20
70	80	No	20	2.18
70	300	No	18	2.20

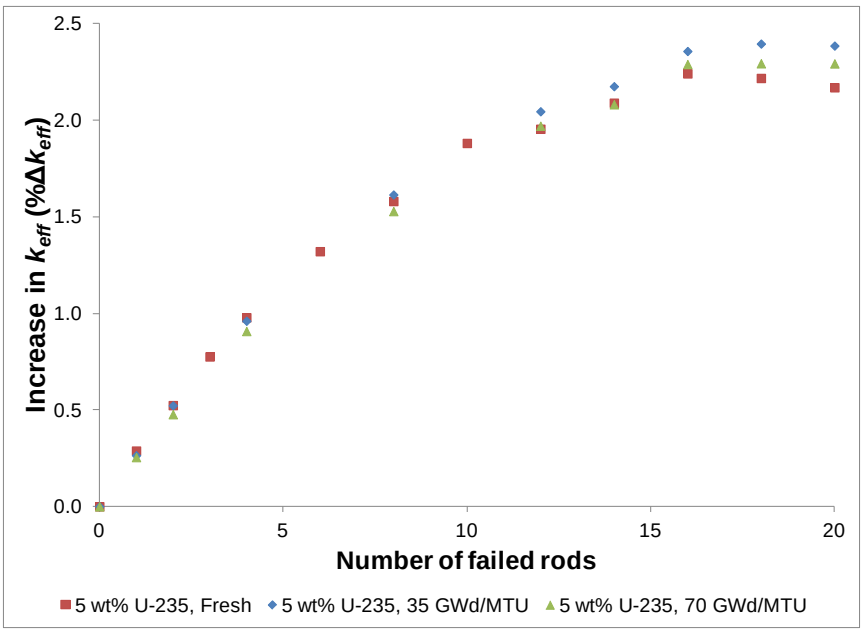

Figure A.5 – Increase in k_{eff} in GBC-68 as a function of number of rods removed

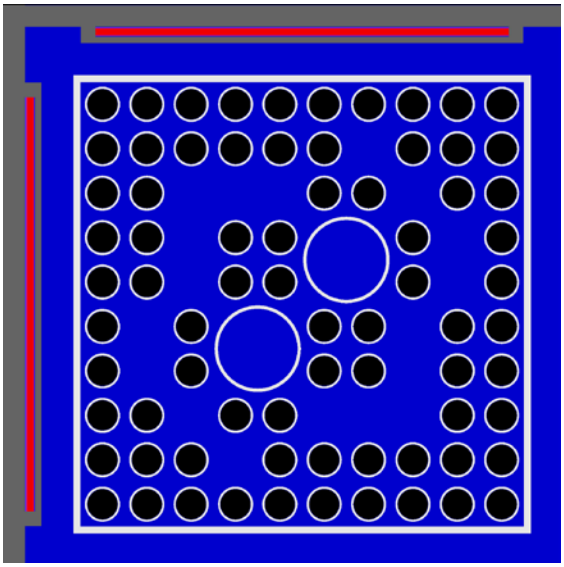

Figure A.6 – Limiting multiple rod removal lattice (18 rods removed)

A.1.2 Damaged Fuel

Two configurations for the physical form of the failed fuel are considered in these analyses: the first is a homogeneous mixture of fuel, cladding materials, and water; and the second is a dodecahedral array of fuel pellets suspended in water. The selected configurations are expected to encompass the range of potential reactivity changes for different rubble configurations. Modeling an ordered array of pellets provides an upper bound of the reactivity of the fuel rubble because low enriched fuel is more reactive lumped when compared with a homogeneous mixture because of resonance self-shielding effects.

S1(b)C3: Homogenized rubble—Extensive cladding failure could lead to a relatively large debris bed composed of fuel pellet fragments of varying sizes as well as assembly hardware pieces distributed throughout the basket cavity region. The height of the debris bed is varied, changing the volume of the debris and the moderation ratio. The modeled heights vary from the entire internal height of the canister to the volume of the fuel and cladding material in the assembly. Cases were developed to evaluate a range of debris concentrations and distributions within the basket cavity. The total fuel mass is conserved in each case. The fuel compositions are represented as stratified to maintain the burnup profile established in the assembly during power operation. A subset of cases was also included to evaluate fractional debris bed heights constrained within the basket absorber panel region. Fuel debris may have limited axial mobility because of the combined effects of hardware (e.g., end fittings and spacers), fuel debris characteristics, and available basket clearances restricting large volumes of fuel from migrating beyond the original axial region of the basket. Additionally, this set of cases provides insight into the possible response of the newer metal matrix composite baskets that have neutron absorber extending the length of the basket.

S1(b)C4: Loose fuel pellets—In the event of extensive cladding failure, representing the debris as discrete lumps may result in a higher k_{eff} value for low enriched fuel than a homogeneous debris because of resonance self-shielding in ^{238}U. To evaluate this condition, a range of uniform, dodecahedral pellet arrays was considered. The pitch of the pellets was varied to change the debris bed heights and moderation ratios. The pellet arrays are represented as stratified to maintain the burnup profile established in the assembly during power operation. The same axial compositions are used in the fuel as in the nominal intact configuration case. For PWR fuel, the pellet pitch varied from approximately 0.742 cm to 0.772 cm corresponding to the height of the nominal intact fuel assembly to the internal height of the canister cavity. For BWR fuel, the pellet pitch varied from approximately 0.771 cm to 0.879 cm, also ranging from the nominal intact assembly height to the internal height of the canister cavity. A subset of cases was also included to evaluate fractional debris bed heights constrained within the basket neutron absorber panel envelope. Fuel debris may have limited axial mobility because of the combined effects of hardware (e.g., end fittings and spacers), fuel debris characteristics, and available basket clearances restricting large volumes of fuel from migrating beyond the original axial region of the basket. Additionally, this set of cases provides insight into the possible response of the newer metal matrix composite baskets that have neutron absorber extending the length of the basket.

The two damaged fuel configurations described above were investigated for PWR and BWR systems. Axial representations of a basket cell are shown in Figure A.7 and Figure A.8 for the homogeneous rubble and ordered pellet array cases, respectively. The results for both configurations with fresh fuel and 5-year decay time conditions are provided in Table A.20 for the maximum increase cases, showing that the k_{eff} increase can be substantial (>20 %Δk_{eff}) depending on how the system is modeled. For the cases evaluated, the 44.25 GWd/MTU burnup case with 5 wt % ^{235}U initial enrichment had the largest change for the GBC-32 cask, and the 35 GWd/MTU with 5 wt % ^{235}U initial enrichment had the largest change for the GBC-68 cask. In both casks, the limiting case occurs when the fissile material is distributed uniformly throughout the basket cell region, extending from the base plate to the lid with the ordered pellet array case being more limiting than the homogeneous rubble case. A floating pellet array of all the fuel is not physically likely, but represents an upper limit for the maximum reactivity increase for damaged fuel. This set of cases demonstrates that homogenous fuel rubble configurations may produce non-conservative results.

The results for fuel compositions with higher burnups and longer decay times for PWR fuel and BWR fuel are provided in Table A.21 and Table A.22, respectively. The results indicate that the reactivity impact of gross assembly failure increases slightly at higher burnups and increases with longer decay time. The additional impacts are small, less than 1.5 %Δk_{eff}, and are less than the margin (i.e., reduction in k_{eff}) provided with the additional burnup and decay time.

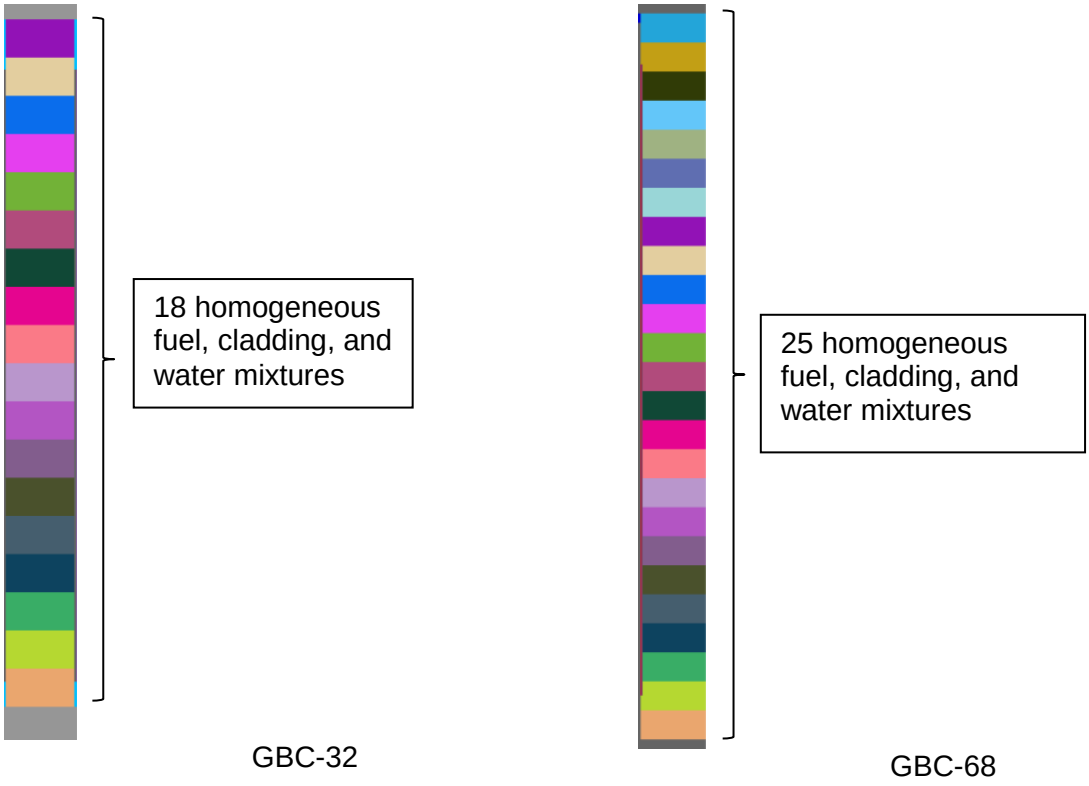

Figure A.7 – Limiting homogeneous rubble configuration for GBC-32 and GBC-68

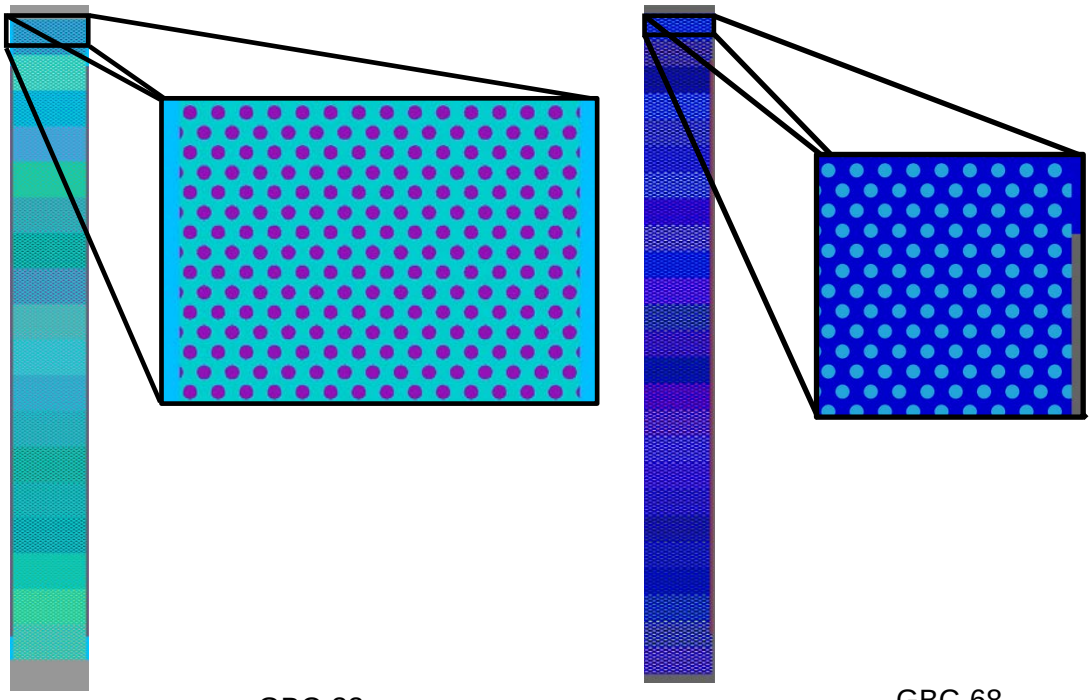

GBC-32 GBC-68

Figure A.8 – Limiting ordered pellet array configuration for GBC-32 and GBC-68

Table A.20 – Increase in k_{eff} because of damaged fuel (fissile material located outside neutron absorber panel envelope)

Cask	Enrichment (wt % ^{235}U)	Burnup (GWd/MTU)	Decay time (years)	Maximum increase in k_{eff} (%Δk_{eff})
GBC-32	**Limiting ordered pellet array**			
	1.92	0	0	11.09
	3.5	25.5	5	20.20
	5.0	44.25	80	22.21
	Homogeneous rubble			
	1.92	0	0	6.66
	3.5	25.5	5	13.95
	5.0	44.25	300	15.34
GBC-68	**Limiting ordered pellet array[a]**			
	5.0	0	0	28.12
	5.0	35	80	34.88
	5.0	70	300	35.63
	Homogeneous rubble[b]			
	5.0	0	0	21.68/22.90
	5.0	35	80	29.12/29.87
	5.0	70	300	29.81/30.40

[a]The BWR pellet array was only represented without the fuel assembly channel.
[b]BWR results are presented with channel / without channel.

Table A.21 – Change in k_{eff} for damaged fuel in GBC-32

Burnup (GWd/MTU)	Decay time (years)	Change in k_{eff} (%Δk_{eff})
Ordered pellet array		
44.25	5	21.37
44.25	80	22.21
44.25	300	22.21
70	5	21.43
70	80	21.63
70	300	21.77
Homogeneous rubble		
44.25	5	14.30
44.25	80	15.29
44.25	300	15.34
70	5	14.20
70	80	14.77
70	300	14.90

Table A.22 – Change in k_{eff} for damaged fuel in GBC-68

Burnup (GWd/MTU)	Decay time (years)	Change in k_{eff} (%Δk_{eff})
Ordered pellet array, channel removed		
35	5	34.40
35	80	34.88
35	300	34.87
70	5	35.22
70	80	35.57
70	300	35.63
Homogeneous rubble, channel included		
35	5	28.58
35	80	29.12
35	300	29.13
70	5	29.31
70	80	29.74
70	300	29.81
Homogeneous rubble, channel removed		
35	5	29.36
35	80	29.87
35	300	29.83
70	5	29.93
70	80	30.33
70	300	30.40

The resulting change in k_{eff} is significantly reduced if the fuel debris is maintained within the neutron absorber panel envelope. The maximum reactivity impact for the ordered array of pellets is reduced from 22.21 %Δk_{eff} to 4.40 %Δk_{eff} for 5 wt % ^{235}U initial enriched fuel with 44.25 GWd/MTU burnup and 80-year decay time in the GBC-32 model. The reduction in the MPC-68 model is from 35.63% Δk_{eff} to 10.81% Δk_{eff} for 5 wt % ^{235}U initial enriched fuel with 70 GWd/MTU burnup and 300-year decay time.

Mixed size, irregular shaped particle packing can vary. To observe the effects of different bulk density changes on system reactivity, a range of homogeneous rubble cases within the neutron absorber panel envelope was evaluated and is provided in Table A.23. The cases resulting in the maximum reactivity increase for GBC-32 are 5.0 wt % ^{235}U initial enrichment, 44.25 GWd/MTU burnup with 5-year decay time isotopic compositions; and for GBC-68 are for 5.0 wt % ^{235}U enriched fresh fuel. Overall, these results show a decrease in reactivity with increased bulk density (i.e., tighter fuel particle packing).

Table A.23 – Change in k_{eff} because of damaged fuel (homogeneous rubble debris within neutron absorber panel envelope)

Fraction of nominal intact assembly height	Change in k_{eff} (%Δk_{eff})		
	GBC-32	GBC-68	
		Channeled	Unchanneled
1.0	-4.64	7.40	9.49
0.9	-7.05	6.65	9.12
0.8	-10.16	5.06	8.10
0.7	-14.36	2.30	6.16
0.6	-20.16	-2.57	2.66
0.5	-28.34	-11.07	-3.62
0.4	-39.10	-25.64	-15.10
0.36 (Fully compressed rubble)	-45.50	-34.23	-31.44[a]

[a]Unchanneled fraction of nominal intact assembly height is 0.32

A.2 CRITICALITY ANALYSIS TO ASSESS IMPACTS OF CATEGORY 2 – ROD/ASSEMBLY DEFORMATION

Fuel assembly distortion, twist, and rod bow are known phenomena present in current spent fuel. Each of these effects can alter the geometry and neutron energy spectrum and hence can affect k_{eff}. This configuration category investigates the impact of pin pitch changes that could result as potential end states associated with side and end impact events which can be exacerbated by grid failure. Side impact events are represented by configurations where the assembly lattice contracts and the fuel assembly is oriented against the basket side. Typical design basis criticality evaluations represent the fuel assembly as centered across the basket cell. The effects of end impact look at both uniform and non-uniform pin pitch expansion. The non-uniform pin-pitch variations expand on the uniform pin-pitch expansion cases to determine if a potential configuration from non-uniform pin-pitch expansion can result in a higher reactivity increase than the uniform pin-pitch expansion cases. Additionally, fuel assembly axial compositions vary with burnup and irradiation history. This set of cases also evaluates the impacts of multiple axial effects that could potentially be present because of lattice pin-pitch changes and varying nodal zone lengths. Case subclass descriptions are provided in Table A.24 and described in more detail below.

Table A.24 – Criticality cases developed to address Category 2—rod/assembly deformation

Case set identifier	Configuration scenario	Subclass description	Parameter varied
S2(a)C1	Configurations associated with side drop	Pin pitch contraction	PWR pin pitch contacted to 95.7% of nominal, cross sectional position of contracted assembly within basket cell
			BWR pitch contracted to 97.4% of nominal, cross sectional position of contracted assembly within basket cell, channel present
S2(b)C1	Configurations associated with end drop	Uniform pin pitch variation	PWR pin pitch of all rods in an assembly expanded up to 104.6% of nominal
			BWR pin pitch of all rods in an assembly expanded up to 102.3% and 121.8% of nominal for channeled and unchanneled models, respectively
S2(b)C2	Configurations associated with end drop	Radial non-uniform pin pitch variation	PWR pin pitch of different radial regions of the assembly expanded up to 116.9% of nominal
			BWR pin pitch of different radial regions of the assembly expanded up to 108.9% and 134% of nominal for channeled and unchanneled fuel, respectively
S2(b)C3	Configurations associated with end drop	Axial non-uniform pin pitch variation (birdcaging and bottlenecking)	PWR pin pitch of different axial regions of the assembly expanded up to 104.6% in expanded regions and contracted to 95.7% of nominal in contracted regions
			BWR pin pitch of different axial regions of the unchanneled assembly expanded up to 121.8% in expanded regions and contracted to 97.4% of nominal in contracted regions

Configuration S2(a)C1: Pin pitch contraction—Side drop events are expected to include configurations where the pin pitch is reduced. The contracted pitch was determined by the size of non-fuel guide, instrument, or water tubes in the various fuel assembly designs that are assumed to maintain nominal dimensions. This resulted in pitch contraction percentages of 95.7% and 97.4% of nominal for the PWR and BWR assemblies, respectively. Because LWR assemblies are under-moderated, pin pitch contraction will result in decreases in k_{eff}. To illustrate the amount of decrease, two subcases for PWR and four for BWR fuel were evaluated. The subcases are based on the fuel assembly being centered within the basket cell or resting against the side of a basket cell, and being channeled versus unchanneled for BWR fuel. Illustrations of the models are show in Figure A.9 and Figure A.10 for PWR fuel and BWR fuel, respectively. Results for the selected cases are shown in Table A.25, where the PWR fuel

corresponds to 5.0 wt % ^{235}U initial enrichment with burnup of 44.25 GWd/MTU and 5-year decay time, and the BWR fuel corresponds to 5.0 wt % ^{235}U enrichment fresh fuel.

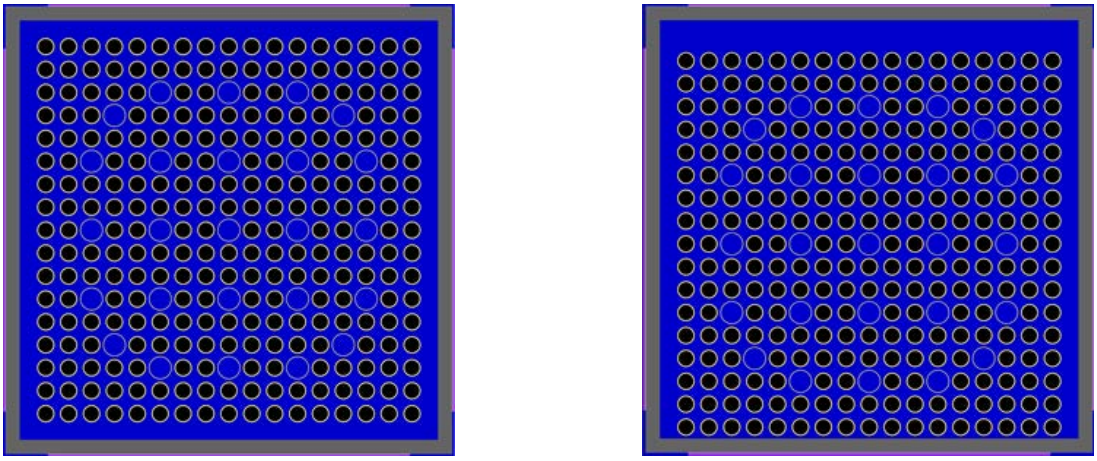

(a) (b)

Figure A.9 – Pin pitch contraction cases in GBC-32

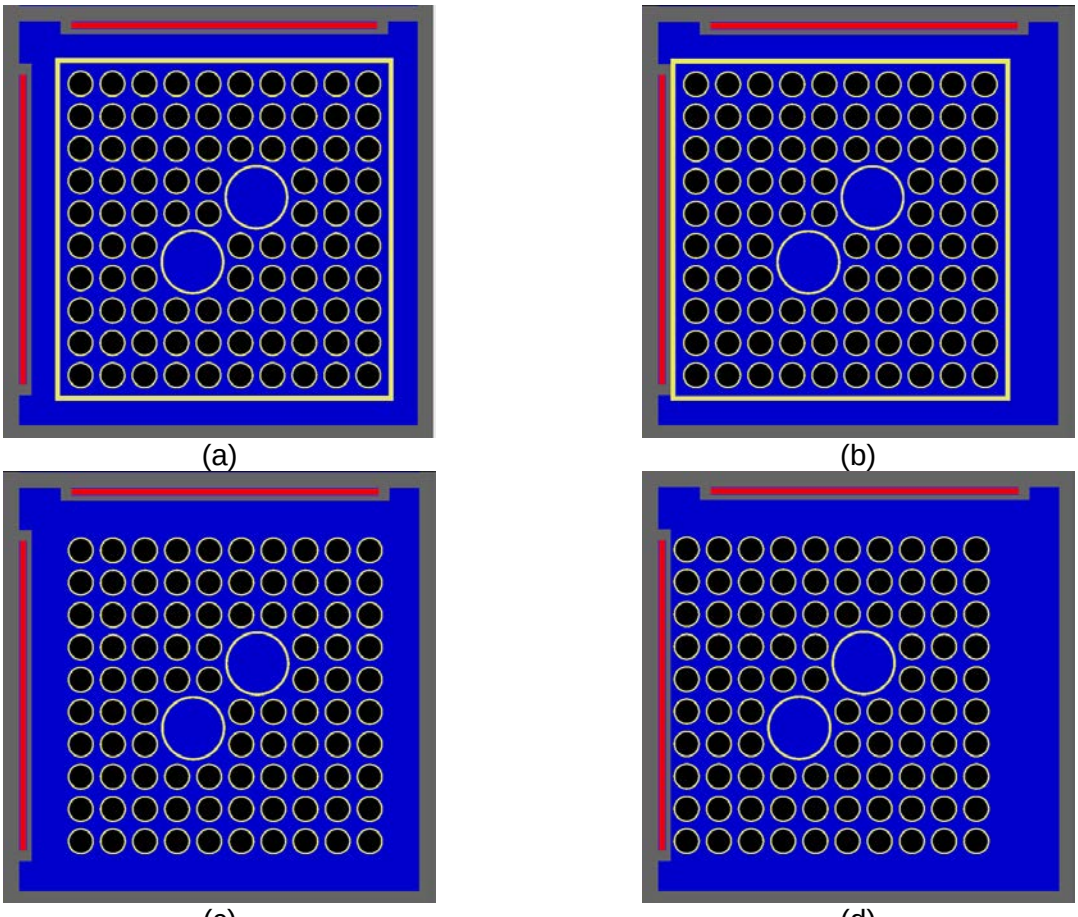

(a) (b)

(c) (d)

Figure A.10 – Pin pitch contraction cases for GBC-68

Table A.25 – Criticality results for pin pitch contraction cases

PWR fuel		
Subcase ID	**Description**	**Change in k_{eff} (%Δk_{eff})**
S2(a)C1	Pitch contraction (95.7% of nominal) with assembly centered within cell (Figure A.9 [a])	-3.63
S2(a)C2	Pitch contraction (95.7% of nominal) with assembly resting against cell (Figure A.9 [b])	-4.05
BWR fuel		
S2(a)C4	Pitch contraction (97.4% of nominal) with assembly centered within cell (Figure A.10 [a])	-2.44
S2(a)C4	Pitch contraction (97.4% of nominal) with assembly resting against cell (Figure A.10 [b])	-3.48
S2(a)C4	Pitch contraction (97.4% of nominal) with unchanneled assembly centered within cell (Figure A.10 [c])	-2.48
S2(a)C4	Pitch contraction (97.4% of nominal) with unchanneled assembly resting against cell (Figure A.10 [d])	-4.42

S2(b)C1: Uniform pin pitch variation—A set of cases was developed to evaluate the associated reactivity impact of uniform pin pitch variations. For this set of cases, the change in pin pitch is applied uniformly, meaning that all pins at all axial heights experience the same changes at the same time. Pin pitches were expanded in several steps from nominal until the outer row of pins was in contact with the storage basket wall (for PWR fuel and dechanneled BWR fuel), representing the maximum amount of pin pitch expansion without a deformed basket structure.

For both GBC-32 and GBC-68 models, the rod/assembly deformation was first modeled with the pin pitch expanded uniformly across the assembly until the outer fuel rod unit cells were coincident with the inner surface of the storage cells. Once the fuel enrichment, burnup, and decay time, which results in the largest increase in reactivity, have been determined, this limiting condition is expanded until the fuel rods are modeled in contact with the storage cell walls. An illustration of the maximum uniform pin pitch configuration for the GBC-32 is shown in Figure A.11.

Two different fuel assembly representations are considered for the GBC-68 cask model—with and without the channel present. For the models where the channel is present, the pin pitch expansion is constrained by the contact of the fuel pins with the assembly channel. For the models with no channel present, the pin pitch is constrained when the outer fuel rods make contact with the neutron absorber wrappers and storage cell walls as shown in Figure A.12.

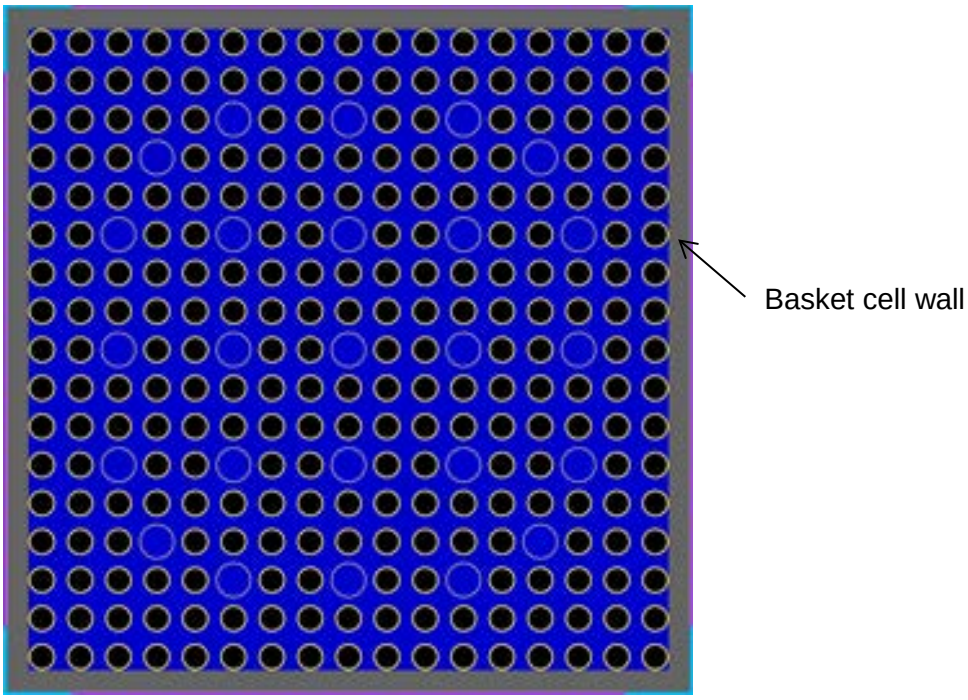

Figure A.11 – Maximum uniform pitch expansion case in GBC-32

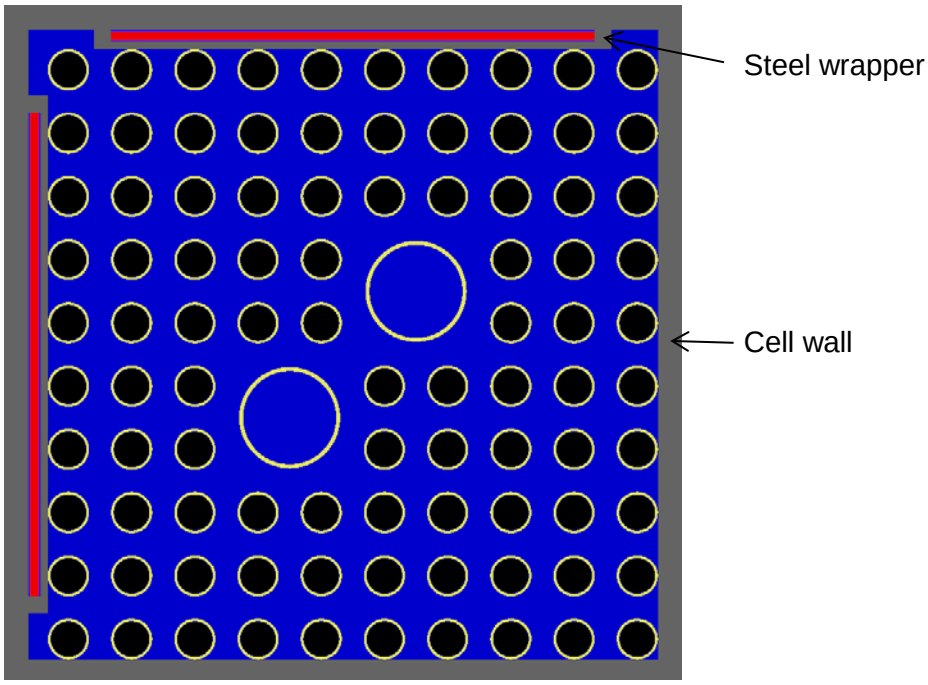

Figure A.12 – Maximum uniform pitch expansion configuration in GBC-68

The results of the uniform pitch expansion cases with the outer unit cell boundary in contact with the storage cell wall are shown in Table A.26 and Table A.27 for GBC-32 and for unchanneled fuel in the GBC-68 models, respectively. For the cases evaluated the 44.25 GWd/MTU burnup

case with 5 wt % ^{235}U initial enrichment and 5-year decay time had the largest change for the GBC-32 system, and the fresh fuel with 5 wt % ^{235}U initial enrichment had the largest change for the GBC-68 system. For both the PWR and BWR fuels, the results indicate that the reactivity impact of uniform pitch expansion is reduced at higher burnups and increased decay times.

Table A.26 – Increase in k_{eff} caused by uniform fuel pin pitch expansion in GBC-32 (pin pitch at 102.7% of nominal, 1.2941 cm)

Burnup (GWd/MTU)	Decay time (years)	Increase in k_{eff} (%Δk_{eff})
1.92	0	0.78
3.5	25.5	1.48
44.25	5	1.69
44.25	80	1.67
44.25	300	1.66
70	5	1.53
70	80	1.44
70	300	1.42

Table A.27 – Increase in k_{eff} caused by uniform fuel pin pitch expansion in GBC-68

Burnup (GWd/MTU)	Decay time (years)	Increase in k_{eff} (%Δk_{eff})
Channel intact, pin pitch 102.3% of nominal, 1.3249 cm		
0	0	2.06
35	5	1.76
35	80	1.76
35	300	1.72
70	5	1.64
70	80	1.55
70	300	1.60
Channel removed, pin pitch 117.5% of nominal, 1.5222 cm		
0	0	12.07
35	5	10.56
35	80	10.45
35	300	10.48
70	5	9.64
70	80	9.40
70	300	9.43

The maximum uniform expansion in the GBC-32 system results in a pitch of 1.3179 cm, which is 104.6% of the nominal pitch. The resulting reactivity increase is 2.65 %Δk_{eff}. The maximum uniform increase for unchanneled BWR fuel is a pitch of 1.5773 cm, which is 121.8% of the nominal pitch. The resulting reactivity increase is 13.22 %Δk_{eff}. For channeled BWR fuel, the maximum pitch is 1.3249 cm, which is 102.3% of the nominal pitch. The results for all burnup and decay time combinations are shown in Table A.27 and show that the maximum reactivity increase is 2.06 %Δk_{eff} for fresh 5 wt % ^{235}U fuel.

S2(b)C2: Radial non-uniform pin pitch variation—Results from the uniform pin pitch expansion cases indicate that the reactivity increase was continuing to rise as the pitch was expanded up to the basket cell wall. This indicates that additional pitch expansion of the inner region of the fuel assembly can result in even higher k_{eff} values. To evaluate this potential further, the limiting cases from the uniform pin pitch expansion cases were modeled with the pin pitch of the rods located in the inner region of the assembly allowed to expand until the outer rows were in contact with each other—at the basket boundary for the PWR fuel and the dechanneled BWR fuel, or at the channel inner boundary for channeled BWR fuel. Each of these configurations results in non-uniform radial pin pitch variations present across the assembly. An example model is shown in Figure A.13. For these models, the pitch in each of the outer rows is constant within the row and is equal to the pitch that caused that row to make contact with the outboard row or the basket wall.

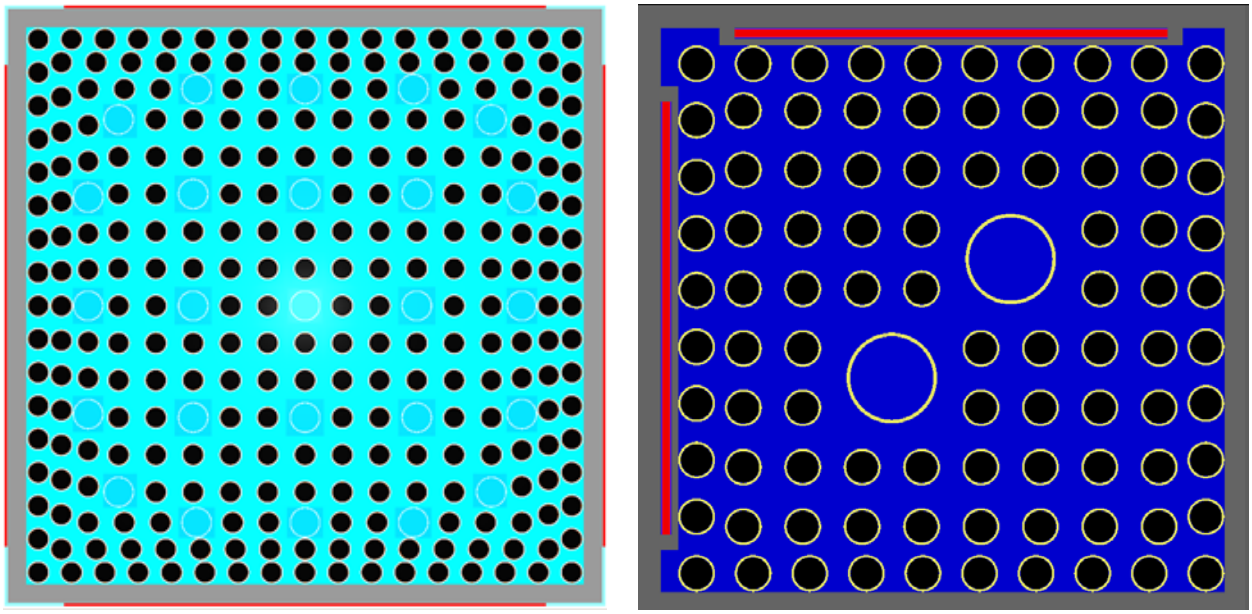

PWR Unchanneled BWR

Figure A.13 – Example configuration for non-uniform radial pitch expansion

The results of the calculations with increasing pitch are shown in Figure A.14, Figure A.15, and Figure A.16 for the GBC-32 model and the GBC-68 model with and without BWR channels, respectively. The results are presented as a function of the pitch of the inner, uniform portion of the assembly (i.e., maximum pin pitch modeled in assembly). The inner region pin pitch expansion was continued until the k_{eff} increase began to diverge. For the GBC-32 results, the first five points show the increase in k_{eff} associated with uniform pitch expansion, with nonuniform expansion beginning when the fuel rod pitch is in excess of 1.32 cm. The GBC-32 maximum k_{eff} increase was 3.90 %Δk_{eff} vs. 2.65 %Δk_{eff} when using a uniform pin pitch expansion. For the GBC-68 results, nonuniform radial expansion causes a reactivity increase for channel constrained pin pitch expansion compared to uniform pin pitch expansion. The maximum increase for radially nonuniform pin pitch expansion is 2.80 %Δk_{eff} compared with 2.09 %Δk_{eff} for uniform radial pin pitch expansion constrained by a nominal size channel. The first point in Figure A.15 shows the impact of uniform pin pitch expansion, and the remaining four points are for non-uniform pin pitch expansion. The results for unchanneled fuel are shown

in Figure A.16; the first six points show the increase in k_{eff} associated with uniform pin pitch expansion, and nonuniform pin pitch expansion begins when the fuel rod pitch is in excess of 1.58 cm. The GBC-68 maximum k_{eff} increase is 13.31 %Δk_{eff} vs. 13.22 %Δk_{eff} when using a uniform pin pitch expansion.

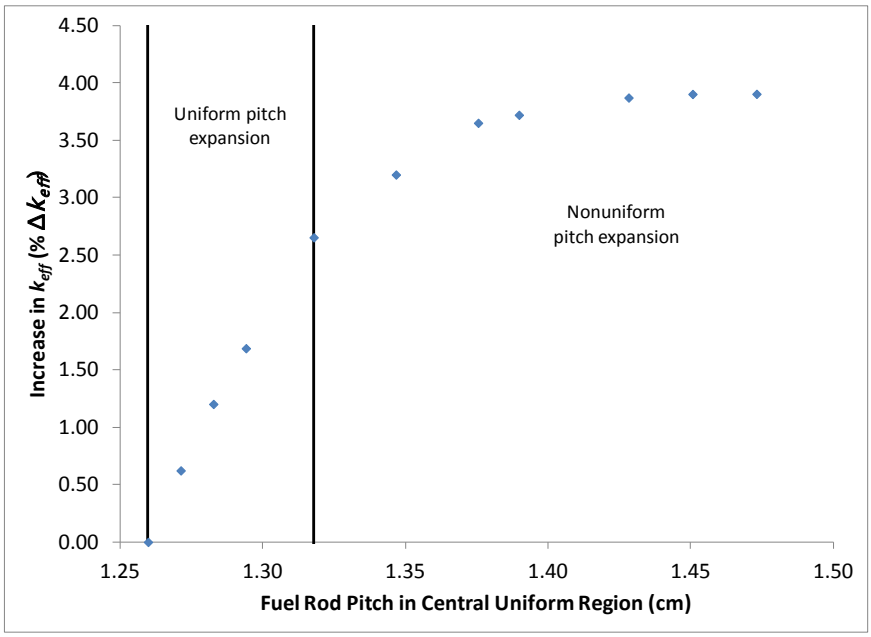

Figure A.14 – Increase in k_{eff} in GBC-32 as a function of fuel rod pitch (5.0 wt % ^{235}U initial enrichment, 44.25 GWd/MTU burnup)

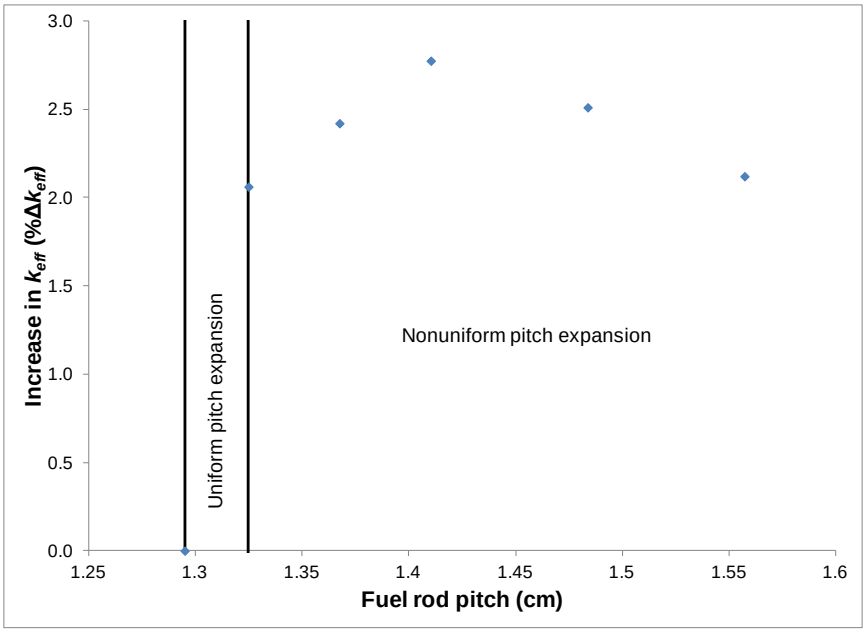

Figure A.15 – Change in k_{eff} in GBC-68 as a function of fuel rod pitch for channeled fuel (5.0 wt % ^{235}U initial enrichment fresh fuel)

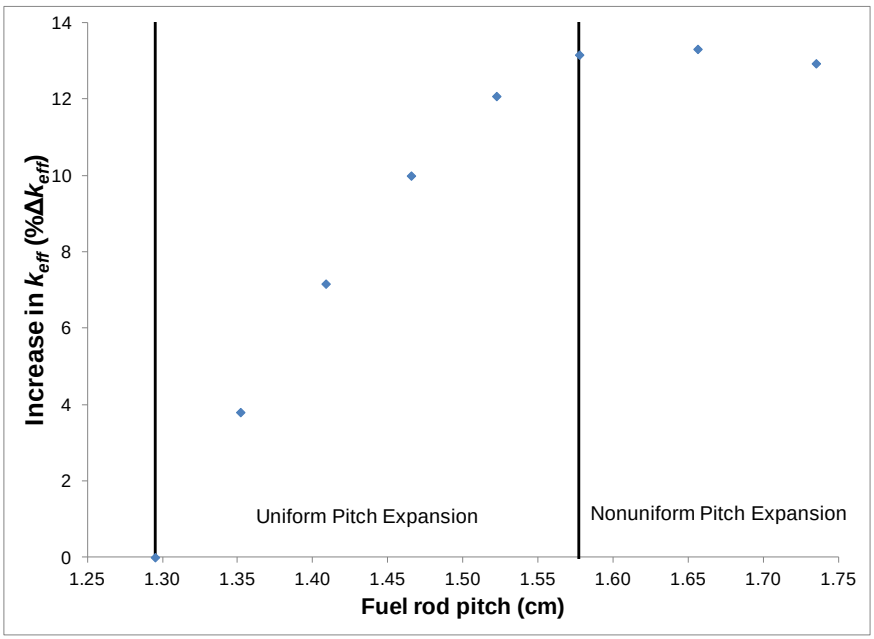

Figure A.16 – Change in k_{eff} in GBC-68 as a function of fuel rod pitch for unchanneled fuel (5.0 wt % ^{235}U initial enrichment fresh fuel)

S2(b)C3: Axial non-uniform pin pitch variation—Cases were developed to evaluate axially non-uniform pin pitch variations to represent the effects of "birdcaging" and/or "bottlenecking" of a fuel assembly. Models were constructed with two different pin pitches at different axial heights. The increased and decreased pitch variations were applied over discrete sections of the fuel rods, not as continuous changes as a function of height. The region of expanded pitch was selected based on the burnup of the assembly, near the top end for fuel irradiated to a burnup of more than 30 GWd/MTU or near the middle for fresh fuel. The length of the expanded zone was varied to evaluate changes in reactivity. The contracted pitch was determined by the size of non-fuel guide, instrument, or water tubes in the various fuel assembly designs which are assumed to maintain nominal dimensions. This resulted in contracted pitches of 95.7% and 97.4% of nominal for the PWR and BWR assemblies, respectively. The contracted pitch zone was also varied in length to evaluate the impacts on reactivity. The expanded pin pitch zones included the pitch required for the fuel rod unit cells to touch the inside of the canister basket walls. Only unchanneled BWR fuel was considered.

The limiting pin pitch expansion case for the GBC-32 model was for the 5 wt % ^{235}U initial enrichment fuel with a burnup of 44.25 GWd/MTU, so the most reactive axial section is near the top of the fuel assembly. The irradiated fuel was represented with 20.32 cm length segments to capture the axial burnup profile, and these segments are used to delineate the pin pitch variation. The size of the contracted pin pitch region was varied from one to four segments, and the expanded pitch section at the top of the assembly ranged from two to eight segments in length in an effort to identify the maximum change in k_{eff} attributable to birdcaging. An example with four segments in the contracted region and four segments in the upper expanded region is shown in Figure A.17. Slight reactivity increases were observed in the cases with four or more fuel segments in the expanded pin pitch zone. Results for the 5 wt % ^{235}U initial enrichment fuel with a burnup of 44.25 GWd/MTU and 5-year decay time are shown in Table A.28. The maximum Δk_{eff} change (i.e., 1.74%) is 0.05 %Δk_{eff} beyond the 1.69 %Δk_{eff} resulting from the

uniform pin pitch expansion configuration. This additional increase in k_{eff} is considered negligible.

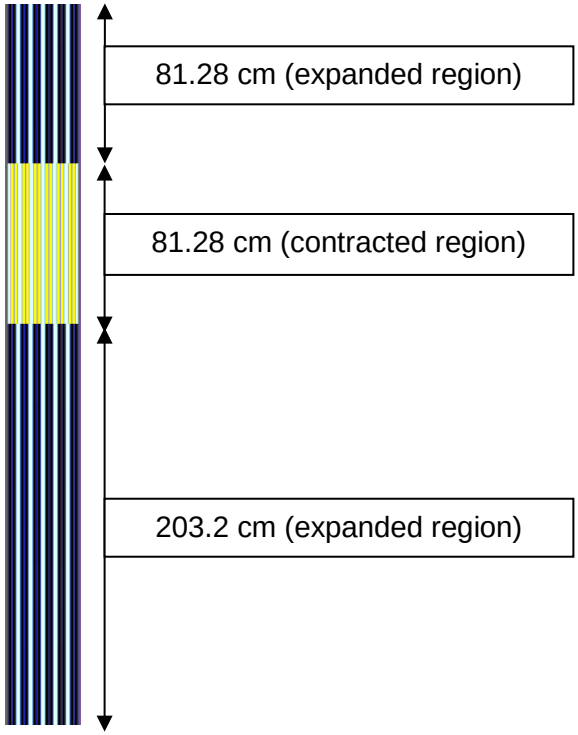

Notes: Fuel in expanded pin pitch segments is shown as black, regardless of isotopic composition.
Fuel in contracted pin pitch segments is shown in yellow, regardless of isotopic composition.
Large gaps between pairs of fuel rods indicate the presence of guide tubes.

Figure A.17 – Assembly model with axially varying pin pitch in GBC-32

Table A.28 – Increase in k_{eff} in GBC-32 for axial nonuniform pin pitch expansion (5.0 wt % ^{235}U initial enrichment, 44.25 GWd/MTU burnup, 5-year decay time)

Top expanded zone length (cm)	Contracted zone length (cm)	Bottom expanded zone length (cm)	Increase in k_{eff} (%Δk_{eff})
40.64	60.96	264.16	1.00
60.96	20.32	284.48	1.58
60.96	40.64	264.16	1.58
60.96	60.96	243.84	1.57
60.96	81.28	223.52	1.58
81.28	20.32	264.16	1.72
81.28	40.64	243.84	1.70
81.28	60.96	223.52	1.70
81.28	81.28	203.2	1.71
101.6	40.64	223.52	1.71
101.6	60.96	203.2	1.71
101.6	81.28	182.88	1.72
121.92	60.96	182.88	1.72
121.92	81.28	162.56	1.73
142.24	60.96	162.56	1.74
142.24	81.28	142.24	1.73
162.56	60.96	142.24	1.72
162.56	81.28	121.92	1.72

The bounding axially non-uniform pitch expansion case was combined with the bounding radially non-uniform pin pitch expansion case to observe the net effect of birdcaging. The resulting k_{eff} increase compared to the nominal intact configuration is 3.89 %Δk_{eff}. This is statistically equivalent to the increase in k_{eff} for the axially uniform, radially nonuniform pin pitch expansion case (i.e., 3.90 %Δk_{eff}). The radial nonuniform pin pitch expansion bounds the potential effects of birdcaging.

The limiting pin pitch expansion case for the GBC-68 cask contains fresh fuel, so the most reactive axial portion of the assembly will be at the center. For that reason, the birdcaging analysis includes two contracted pitch sections, each 30.48 cm in length, symmetrically positioned above and below the mid-plane of the assembly. A range of center section lengths was considered, but no k_{eff} increase was observed in any case containing the contracted pitch sections. Results for the 5 wt % ^{235}U enrichment fresh fuel cases are shown in Table A.29. The effects of birdcaging do not result in any additional k_{eff} increase beyond the 13.22 %Δk_{eff} associated with the uniform pin pitch expansion configuration for fresh fuel in the GBC-68 cask.

Table A.29 – Change in k_{eff} in GBC-68 for axial nonuniform pin pitch expansion (5.0 wt % ^{235}U enriched fresh fuel)

Central expanded zone length (cm)	Contracted zone lengths (cm)	End expanded zone lengths (cm)	Change in k_{eff} (%Δk_{eff})
137.16	60.96	60.96	12.24
198.12	60.96	30.48	12.77
228.60	60.96	15.24	12.91
259.08	60.96	0	13.02

A.3 CRITICALITY ANALYSIS TO ASSESS IMPACTS OF CATEGORY 3 – CHANGES TO ASSEMBLY AXIAL ALIGNMENT

The neutron absorber panels in fuel storage and transportation packages are designed to extend beyond the length of the active fuel region within the fuel assembly, but they typically do not extend the full length of the basket. The primary function of the neutron absorber is to provide sufficient thermal neutron removal along the active fuel length between adjacent assemblies. Changes to the axial alignment of the assembly within the basket cavity can result in adjacent cells with fuel assemblies that do not have absorber panel material between them. Because spent fuel has axially varying fuel compositions, alignment changes above and below the absorber plate region are being evaluated. The upward (toward the lid) misalignment is likely to be of higher importance for SNF criticality evaluations because the reactivity of the assembly is driven by the burnup gradient near the top of the assembly. Case descriptions are provided in Table A.30 and described in more detail below

Table A.30 – Cases developed to address Category 3—changes to assembly axial alignment

Identifier	Configuration scenario	Subclass description	Parameter varied
S3(a)C1	Axial displacement of intact fuel	Not applicable	Length of active fuel above or below absorber region

S3(a)C1: Axial displacement of intact fuel—Cases were developed to evaluate the impact of changes to intact fuel axial alignment. The parameter of interest for criticality safety is the length of fuel that is beyond the neutron absorber panel region of the basket. Because of differences in canister design, fuel spacers, and assembly designs, the amount of space available for the active fuel to potentially be outside the absorber envelope will vary by canister system and site and will affect the extent of the range of movement possible.

The PWR fuel axial displacement models were developed by translating all the fuel assemblies within a canister uniformly up or down to achieve fixed uncovered fuel lengths for evaluation. The GBC-32 basket as described in Ref. [4] has the fuel and basket at the same length. To be more representative of typical storage and transportation package designs, the stainless steel portion of the basket was extended in these models to go from the canister baseplate to 5 cm below the lid. The length of fuel exposed above and below the absorber envelope was varied up to a maximum of 30 cm in 5 cm increments to map the reactivity response as a function of uncovered fuel length. The variation of the k_{eff} change as a function of axial position is shown in Figure A.18 for several fuel initial enrichment and burnup combinations. The assembly displacements in the GBC-32 model are equal to the length of exposed fuel because absorber panels in the GBC-32 model coincide with the active fuel length of the fuel assembly in the nominal alignment. A summary of GBC-32 results for displacements of 20 cm and 30 cm above the neutron absorber panel is shown in Table A.31. These results show that larger reactivity changes can occur for higher burnups and longer decay times. However, the larger reactivity increase is less than the reduction in nominal intact configuration case k_{eff} caused by the additional burnup and decay time. The nominal intact configuration k_{eff} values for each of the sensitivity cases are provided in Table A.1, resulting in margins of 3.5 to 15.1 $\%\Delta k_{eff}$ compared

to the 44.25 GWd/MTU, 5-year decay time case. The largest Δk_{eff} is associated with this moderate burnup, and short decay time point, even though a larger reactivity increase is associated with higher burnups and longer decay times.

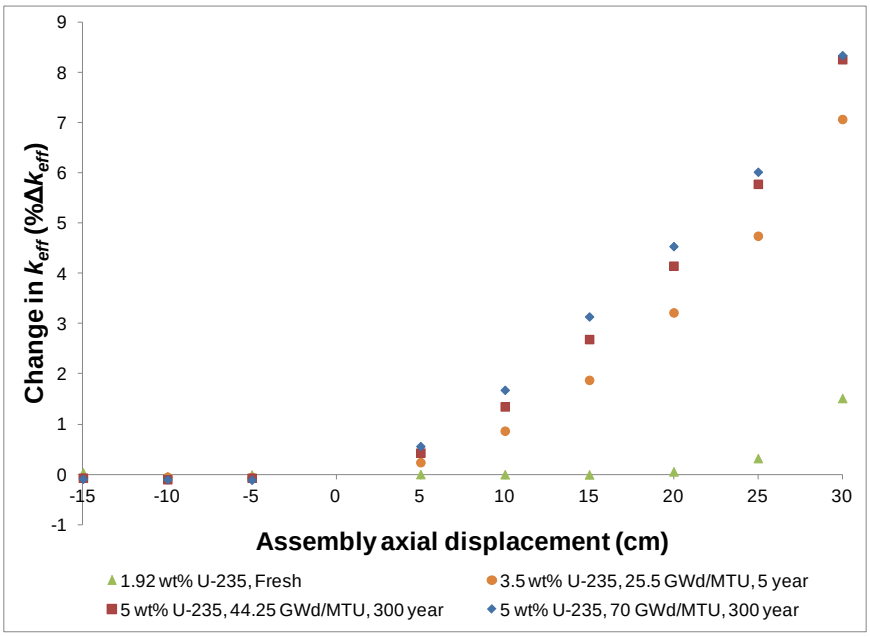

Figure A.18 – Change in k_{eff} in GBC-32 as a function of assembly axial displacement

Table A.31 – Change in k_{eff} for assembly axial displacement in GBC-32 (displacement relative to the neutron absorber panel)

Enrichment (wt % ^{235}U)	Burnup (GWd/MTU)	Decay time (years)	Increase in k_{eff} (%Δk_{eff})	
			30 cm displacement	20 cm displacement
1.92	0	0	1.52	0.06
3.5	25.5	5	7.07	3.22
5	44.25	5	7.69	3.64
5	44.25	80	8.28	4.18
5	44.25	300	8.26	4.15
5	70	5	8.06	4.13
5	70	80	8.28	4.51
5	70	300	8.34	4.54

The BWR fuel axial displacement models were developed translating all the fuel assemblies within a canister uniformly up or down to achieve fixed uncovered fuel lengths for evaluation. Exposed fuel ranges were varied up to a maximum of 31.78 cm above the absorber in 4 cm increments to map the reactivity response as a function of uncovered fuel length. The variation of the k_{eff} change as a function of axial position is shown in Figure A.19. The results for displacements of 13.65 cm and 31.78 cm above the neutron absorber panel are shown in Table A.32 and Table A.33, respectively. The results indicate that the effect of misalignment increases with burnup and is higher at longer decay times. As with the PWR cases, the larger

reactivity increases are less than the reduction in the nominal intact configuration case k_{eff} caused by the additional burnup and decay time. The nominal intact configuration k_{eff} values for each of the sensitivity cases are provided in Table A.1, resulting in margins of 0.75 to 8.0 %Δk_{eff} compared to the 35 GWd/MTU, 5-year decay time case, which is more than 11 %Δk_{eff} less reactive than the 0.95 limit. The largest fuel reconfiguration k_{eff} is associated with this moderate burnup, and short decay time point, even though a larger reactivity increase is associated with higher burnups and longer decay times.

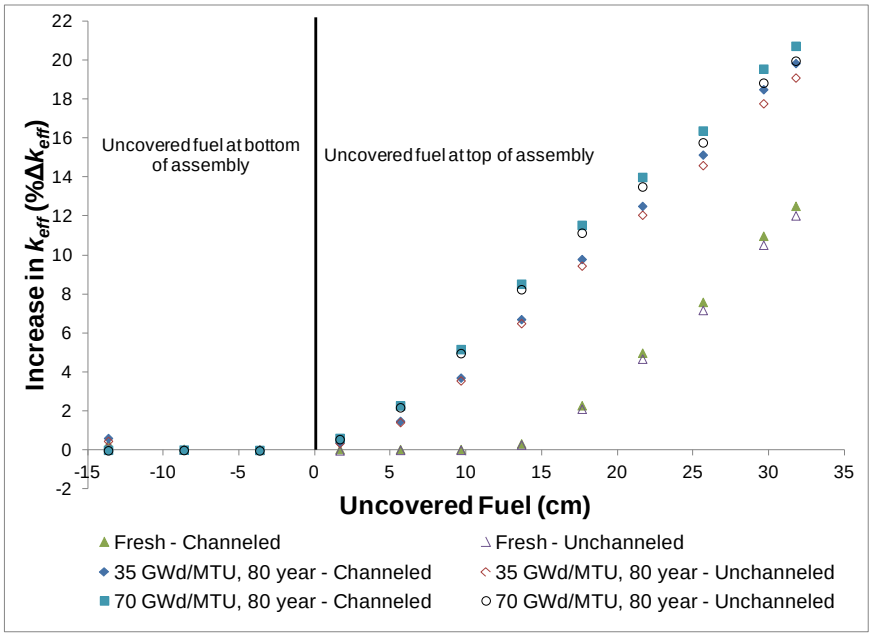

Figure A.19 – Increase in k_{eff} in GBC-68 as a function of assembly axial displacement.

Misalignment toward the bottom of the canister causes a significantly smaller k_{eff} increase because the fuel at the bottom end of the assembly has lower reactivity than that at the top end. The misalignment toward the canister base plate differs for GBC-68 compared to GBC-32 because the GBC-68 model has more distance below the fuel in the nominal intact representation, so larger misalignments are shown.

Table A.32 – Increase in k_{eff} caused by loss of assembly position control in GBC-68, limited displacement of 13.65 cm above absorber

Burnup (GWd/MTU)	Decay time (years)	Increase in k_{eff} (%Δk_{eff})
Channel Intact		
0	0	0.33
35	5	6.29
35	80	6.70
35	300	6.66
70	5	8.03
70	80	8.52
70	300	8.49
Channel Removed		
0	0	0.27
35	5	6.07
35	80	6.49
35	300	6.42
70	5	7.78
70	80	8.24
70	300	8.20

Table A.33 – Increase in k_{eff} for limited assembly axial displacement in GBC-68, displacement of 31.78 cm above absorber

Burnup (GWd/MTU)	Decay time (years)	Increase in k_{eff} (%Δk_{eff})
Channel Intact		
0	0	12.52
35	5	19.40
35	80	19.84
35	300	19.83
70	5	20.47
70	80	20.73
70	300	20.76
Channel Removed		
0	0	12.02
35	5	18.66
35	80	19.10
35	300	19.06
70	5	19.71
70	80	19.96
70	300	20.00

APPENDIX B. SHIELDING EVALUATIONS FOR FUEL RECONFIGURATIONS

B.1 OBJECTIVE

The objective of the shielding analysis is to identify cask external dose rate increases resulting from fuel configuration changes that may affect the ability of transportation packages/storage casks to comply with regulatory dose rate limits. This appendix describes a technical approach for shielding analyses of fuel reconfigurations in transportation packages and storage casks and provides reference values for such analyses. The term "fuel reconfiguration" refers to any change to the storage and transportation system nominal intact fuel assembly configuration used for the basis of cask certification. The analyzed fuel reconfiguration categories are:

(1) cladding failure where fuel fragments and particulates from multiple failed fuel rods can relocate near to and far from fuel cladding breach locations;
(2) rod/assembly deformation; and
(3) changes to assembly axial alignment.

The specific fuel rod failure percentage values used in this study were selected arbitrarily because information about the expected fuel rod failure rate was not available for high-burnup fuel or for fuel in long-term storage.

This study primarily addresses fuel reconfigurations in transportation packages because specific regulatory dose rate limits have been developed for transportation packages under normal conditions of transport (NCT) and hypothetical accident conditions (HAC) (10 CFR 71.47 and 71.51). For storage of spent nuclear fuel (SNF), annual dose limits (i.e., no specific dose rate limits) at the controlled area boundary are specified in 10 CFR 72.104 and 72.106 for normal, off-normal, and accident conditions, respectively. Compliance with 10 CFR 72.104 can be demonstrated only on a site-specific basis because compliance depends on both cask and site characteristics. In this study, a non-site-specific shielding analysis (NUREG-1536) is performed for a generic 4×2 cask array to determine the impact on dose rate at the controlled area boundary for damaged SNF in accordance with 10 CFR 72.106. An analysis of the storage cask surrounding dose rates that contribute to occupational exposure (10 CFR 20.1201 requirements) is also provided in the report. The effects of fuel configuration changes on the neutron and gamma dose rates were determined at 1 m from a generic storage cask.

The consequences of fuel configuration changes were evaluated by comparing external dose rate values between the nominal intact and fuel reconfigurations. This approach helps identify the fuel reconfigurations that yield higher external dose rates than the nominal intact fuel configuration and thus have the potential to exceed the regulatory limits. An advantage of this approach is that the conclusions of the analysis generally can be applied to similar package shielding analysis models because the relative effect of fuel configuration changes on package external dose rates is less sensitive to the specific model parameters used in the analysis than the absolute dose rate values. Package/storage cask external gamma and neutron dose rate values were evaluated separately because fuel configuration changes have different effects on gamma and neutron radiation (e.g., internal high-Z materials have pronounced gamma self-shielding effects), and the overall impact of fuel configuration changes on the external dose rate depends on the individual gamma and neutron dose rate contributions to the total dose rate.

Generic package models for pressurized water reactor (PWR) and boiling water reactor (BWR) SNF, identified as GBC-32 and GBC-68, respectively, were developed for this study and the Westinghouse (W) 17×17 optimized fuel assembly (OFA) and General Electric (GE) 14 10×10 fuel assemblies were selected as representative PWR and BWR fuel assembly types, respectively. The cask models have general shielding characteristics (e.g., thick inner gamma shield and outer neutron shield) similar to real high-capacity SNF transportation packages. The initial enrichment, burnup, and decay time values for the PWR and BWR fuel assemblies were 5 wt % ^{235}U, 65 GWd/MTU, and 5 and 40 years, respectively. The axial variation of the gamma and neutron radiation sources was based on typical PWR and BWR fuel axial burnup profiles.

Applicable codes, guidance, and regulatory criteria related to transportation/storage cask shielding performance were used as the basis for model development and analysis approach. The computer programs and calculation method employed in this analysis are provided in Sect. B.2. The reference transportation and storage cask models as well as representative fuel assembly models for the shielding analysis are described in Sect. B.3. The fuel configurations and specific calculation parameters (e.g., failed fuel fraction) for transportation packages/storage casks evaluated in this analysis are described in Sect. B.4. Shielding analysis results are provided in Section B.5.

B.2 USE OF SOFTWARE

The radiation source terms for the shielding analysis were determined with the depletion and decay capabilities of the Scale 6.1.2 code system [31], including Transport Rigor Implemented with Time-Dependent Operation for Neutronic depletion (TRITON), Oak Ridge Isotope Generation and Depletion Code–Automatic Rapid Processing (ORIGEN-ARP), and Oak Ridge Isotope Generation in Scale (ORIGEN-S). The neutron and gamma radiation source terms were calculated in the group structure of the Scale 27N-19G Evaluated Nuclear Data Files, Part B-VII.0 (ENDF/B-VII.0) shielding library.

The Scale 6.1.2 shielding analysis sequence Monaco with Automated Variance Reduction using Importance Calculations (MAVRIC) [31] and the Scale 27N-19G ENDF/B-VII.0 shielding library were used to perform Monte Carlo transport and dose rate calculations. MAVRIC uses Denovo, a discrete ordinates code [31], to determine particle importance as a function of position and energy and uses Monaco to perform Monte Carlo transport calculations. Radiation transport optimization is accomplished by: (1) sampling more often source particles that have an ability to produce a significant dose rate value outside the source regions, and (2) reducing the variance of particle scores in the spatial region of interest. The MeshView utility in the Scale code system enables visualization of detailed radiation dose maps produced by MAVRIC.

The American National Standards Institute/American Nuclear Society Standard 6.1.1-1977 [32] flux-to-dose-rate conversion factors were used in all dose rate calculations, as recommended in NUREG-1617 [29] and NUREG-1536 [2].

B.3 GENERIC TRANSPORTATION PACKAGE/STORAGE CASK AND REPRESENTATIVE FUEL ASSEMBLY MODELS

The generic models and representative PWR and BWR fuel assemblies described in this section were used in shielding calculations to determine reference dose rate values for failed fuel in transportation packages and storage casks. A transportation package model (see Sect. B.3.1) and a storage cask model (see Sect. B.3.2) were developed because transportation and

storage overpacks are typically different. Descriptions of the representative PWR and BWR intact fuel assembly models are provided in Sect. B.3.3 and B.3.4, respectively. The transportation package and storage cask models have shielding features similar to actual transportation packages and storage casks. Therefore, the trends identified in this analysis for dose rate change because of fuel configuration changes relative to the nominal intact configuration are applicable to actual transportation packages and storage casks. In addition to the overpack shielding design, the geometry and source term characteristics of the canister internal components— such as activation source strength, assembly hardware heights, fuel axial burnup profile, the length of the assembly top and bottom spacers, and the available free volume within the canister cavity—also affect the relative changes in neutron and gamma dose rates caused by fuel configuration changes. That is, variations in these characteristics will cause different changes in the external dose rates because of fuel configuration changes relative to the nominal intact configuration.

B.3.1 Generic Transportation Package Models

The GBC-32 and GBC-68 [4, 5] cask/package models originally were developed for criticality safety analyses of PWR and BWR SNF, respectively, and do not include appropriate shielding features. Simplified SNF transportation package and storage cask models, which are variations of the GBC-32 and GBC-68 original models, were developed for this shielding analysis. The simplified transportation package models include a thick stainless steel (304) cylindrical shell, which serves as a gamma shield, and outer radial and bottom resin neutron shields with the elemental composition described in [33]. Cutaway views of the PWR and BWR package shielding models showing the back half and bottom cask sections are illustrated in Figure B.1 (a) and (b) and Figure B.2 (a) and (b), respectively. As seen in the figures, the radial neutron shield does not extend the entire length of the package radial surface, which is a typical feature of transportation packages. The top, radial, and bottom thicknesses of the stainless steel cylindrical shell are 35, 24.5, and 24.5 cm, respectively; the radial and bottom thicknesses of the neutron shield are 7.5 and 3.5 cm, respectively. The canister inner radius is 87.5 cm for both models. The basket cell inside dimension and cell wall thickness are 22 cm and 0.75 cm, respectively, for the PWR package model and ~15 cm and 0.75 cm, respectively, for the BWR package model. The lower and upper fuel spacers that establish assembly axial position within the basket cell were not explicitly modeled; however, the nominal intact fuel configuration includes void regions in place of the spacers (20 and 10 cm long for the PWR and BWR package models, respectively) above and below the fuel assembly, as seen in the figures. Note that the lengths of the axial void regions are different for the PWR and BWR fuel assemblies because the BWR fuel assembly is longer than the PWR fuel assembly (see Table B.1 and Table B.2). Radial steel fins, pocket trunnions, and small holes that typically cause radiation streaming were not included in the simplified models for the shielding analysis.

The fuel assembly model includes assembly active fuel, plenum, and upper and lower hardware regions, with contents homogenized within the volume delimited by the adjacent basket plates and the region axial height. This simple assembly representation is typically used in shielding analyses because it simplifies the model geometry description, produces slightly conservative results (primarily because of slightly reduced gamma self-shielding of the homogenized fuel contents), and reduces the computer time. The active fuel region was subdivided into axial zones to facilitate the description of the gamma and neutron source axial profiles.

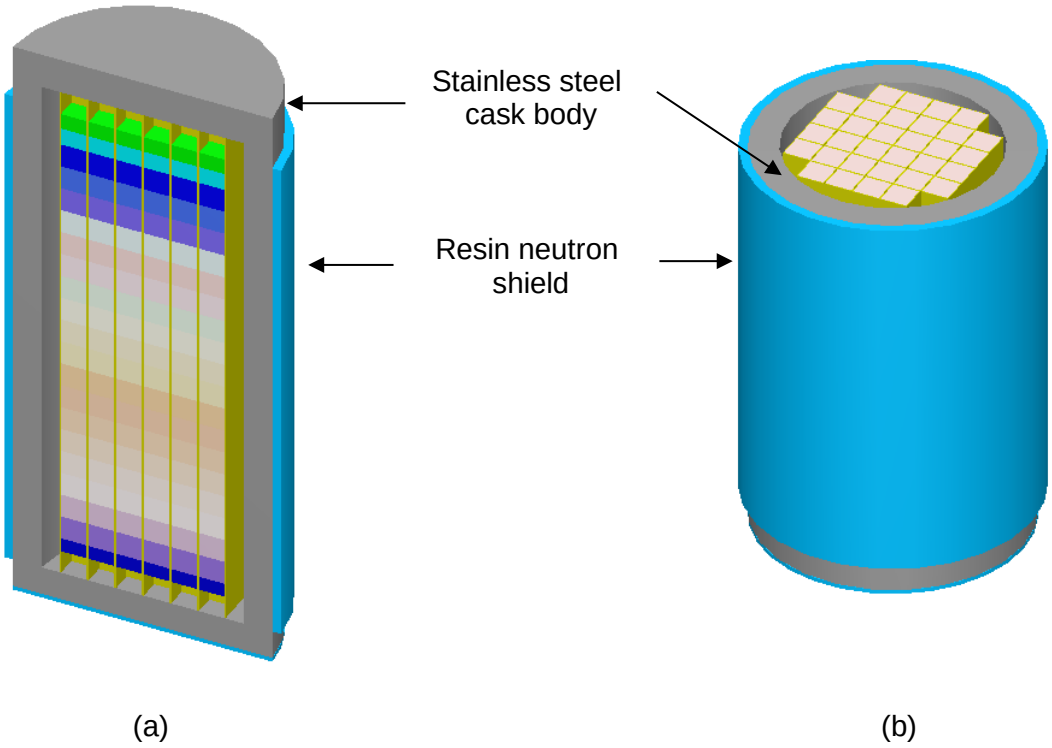

Figure B.1 – Cutaway view of the reference GBC-32 model showing (a) back half and (b) bottom half sections

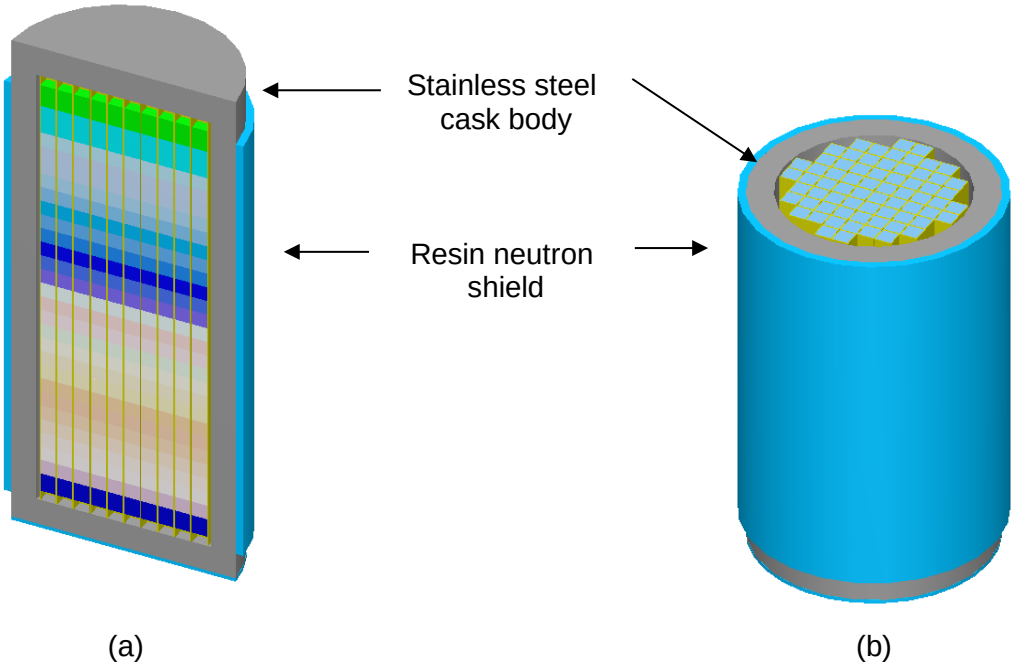

Figure B.2 – Cutaway view of the reference GBC-68 model showing (a) back half (b) bottom half sections

Table B.1 – PWR fuel assembly model description

Assembly axial region	Height (cm)	Stainless steel 304 (kg)	Inconel 718 (kg)	Zircaloy-4 (kg)	UO_2 (kg)	U (kg)	Smear density (g/cm^3)[a]	Free void volume (cm^3)
Upper end fitting	13.44	6.89	0.96	8.58	-	-	1.59	4211.29
Upper fuel plenum and upper end spacer grid	14.66	0.11[b]	0.885	3.27	-	-	0.74	6475.72
Active fuel	365.76	0.00	0.0	113.43[c]	480.191	426.00	3.35	102,136.74[d]
Lower fuel plenum and end fitting	11.95	5.90	0.0	2.72	-	-	1.36	4627.33

[a]Contents homogenized within basket cell volume corresponding to the assembly axial region (22 cm width).
[b]Includes SS304 grid sleeve and SS302 plenum spring.
[c]Includes fuel cladding, guide tubes, instrument tube, and in-core spacers.
[d]Free void volume within basket cell and outside fuel rods, guide tubes, instrument tube, and in-core spacers; total volume for the region is 22×22×365.76 cm^3 = 177,028 cm^3.

Table B.2 – BWR fuel assembly model description

Assembly axial region	Height (cm)	Stainless steel 304 (kg)	Zircaloy-2 (kg)	UO_2 (kg)	U (kg)[a]	Smear density (g/cm^3)[b]	Free void volume (cm^3)
Upper tie and expansion spring	22.29	2.0	1.57	-	-	0.71	4552.74
Upper fuel plenum	28.55	2.32	6.78	-	-	1.41	5136.20
Active fuel	368.91	-	68.88	204.67	180.40	3.28	56,009.03[c]
Lower tie plate	18.76	4.77	1.86	-	-	1.56	3360.93

[a]Ref. [34].
[b]Contents homogenized within basket cell volume corresponding to the assembly axial region (15.0435 cm width).
[c]Free void volume within basket cell and outside fuel rods, water rods, and spacers.

B.3.2 Storage Cask Models

The SNF storage cask model for the analysis of dose rate surrounding a single storage cask is illustrated in Figure B.3. The storage cask model includes a 70 cm thick radial concrete shield and 40 cm thick top and bottom concrete shields, similar to some existing cask designs. The cask model also includes air vents located at cask top and bottom regions. PWR and BWR intact fuel configurations are identical to the GBC-32 and GBC-68 models, respectively. Non-site-specific shielding analysis (NUREG-1536) was performed for a generic 4×2 storage cask array to determine the impact of damaged SNF on the dose rate at the controlled area boundary, which was located 100 m from the cask array. The generic cask array is shown in Figure B.4 along with a cutaway view of the storage cask model with intact PWR fuel. The skyshine calculation model includes the storage cask array, a 60-cm thick concrete storage pad, a 100 cm thick soil layer, and dry air within a 120×120×100 m^3 volume surrounding the cask array. The model for the intact fuel configuration, which is simplified to facilitate skyshine calculations, has radially homogenized fuel contents. However, the cask models for intact PWR and BWR SNF assemblies specify appropriate fuel axial burnup profiles.

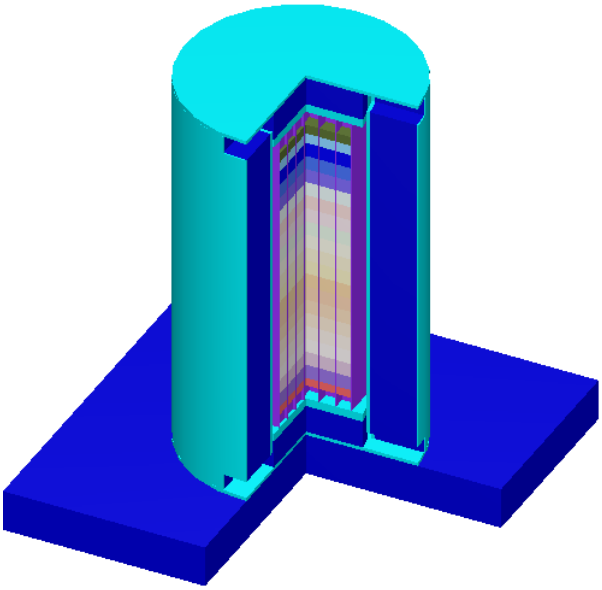

Figure B.3 – Storage cask model with intact fuel assemblies

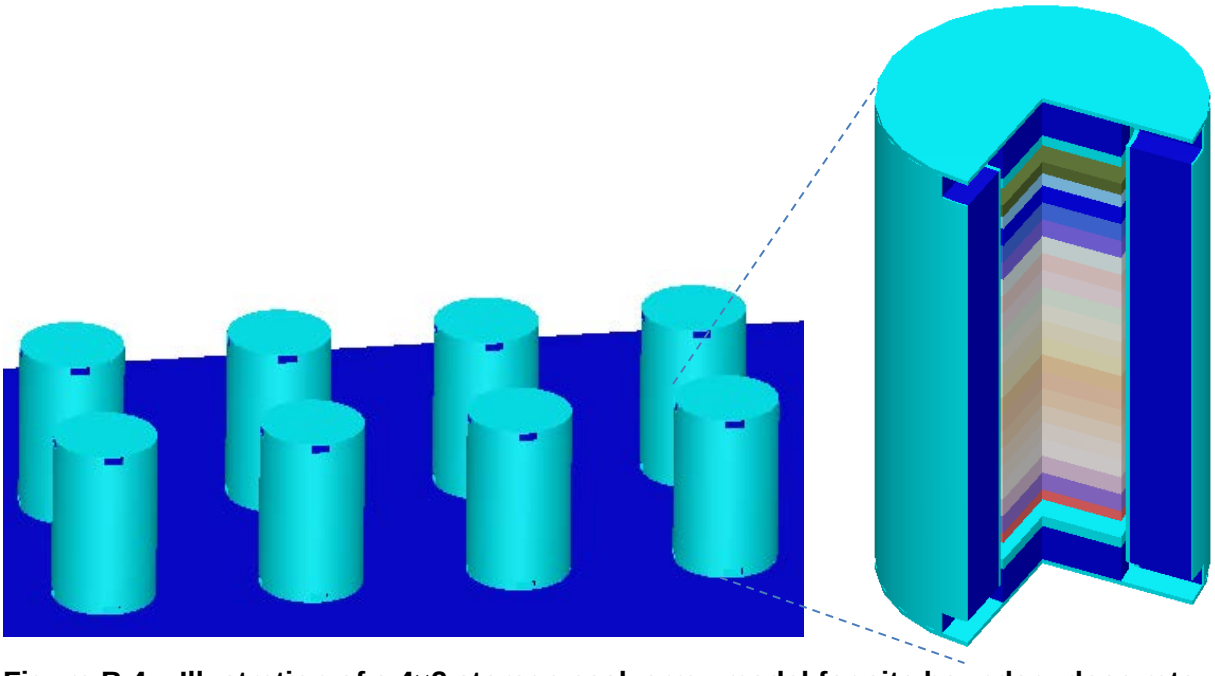

Figure B.4 – Illustration of a 4×2 storage cask array model for site boundary dose rate calculations

B.3.3 Description of Representative PWR Fuel Assembly

The representative PWR fuel assembly for radiation source term and shielding calculations is the W 17×17 OFA with fuel assembly design parameters documented in Refs. [35] and [36]. The fuel assembly model consists of four axial regions: lower end fitting, active fuel, plenum,

and upper end fitting regions. The height, fuel and non-fuel material weights, smear density, and free void volume are provided in Table B.1.

The weights for stainless steel and Inconel assembly parts were used to calculate activation source terms, primarily consisting of ^{60}Co, for assembly hardware and fuel plenum regions. The volume occupied by each hardware component was calculated as the component weight divided by its material mass density. The transversal dimension of a GBC-32 assembly basket cell used in free void volume calculations is 22 cm. The free void volume within the rectangular parallelepiped axially delimited by the assembly axial region height and transversally delimited by the basket cell plates was used in subsequent source intensity spatial distribution and mass density calculations for the different fuel configuration models.

Radiation source terms were determined for the PWR fuel assembly with a 65 GWd/MTU burnup, a 5 wt % ^{235}U initial enrichment, and 5- and 40-year decay times. The axial distributions of gamma and neutron radiation sources in the active fuel region were determined in accordance with the 18-zone assembly burnup profile documented in Ref. [30] for criticality calculations. The gamma radiation source axial profile was based on the direct proportionality between gamma radiation source strength and fuel burnup; the neutron radiation source axial profile was based on the variation of the neutron source strength as the burnup value raised by the power of 4.2 [33]. The profiles thus determined are illustrated in Figure B.5 (a) for the gamma radiation source and Figure B.5 (b) for the neutron radiation source. The active fuel region of the PWR assembly was subdivided into 18 axial zones to facilitate the description of the axial gamma and neutron radiation source distributions.

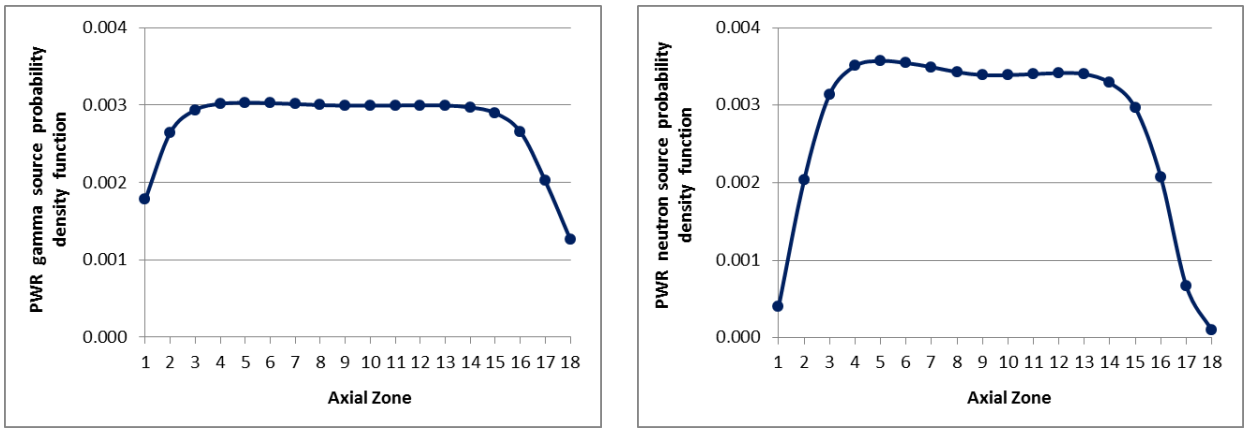

(a) (b)

Figure B.5 – Source intensity distribution as a function of PWR fuel axial zone for (a) gamma radiation source and (b) neutron radiation source

B.3.4 Description of the Representative BWR Fuel Assembly

The representative BWR fuel assembly for radiation source term and shielding calculations is the GE14 fuel assembly type with fuel assembly design parameters documented in Refs. [37] and [31]. The fuel assembly model consists of four axial regions: lower tie plate, active fuel, plenum, upper fuel plenum, and upper tie and expansion spring regions. The height, fuel and non-fuel material weights, smear density, and free void volume values are provided in Table B.2. Fuel assembly hardware weight and material specifications for a Quad Cities 1 reactor 8×8

reload fuel assembly [38] were used to calculate the activation sources for the representative GE14 assembly because this information was not available for the GE14 assembly. The volume occupied by each assembly hardware component was calculated as the component weight divided by its material density. The transversal dimension of a GBC-68 assembly basket cell used in free void volume calculations is ~15 cm. The calculated free void volume within the rectangular parallelepiped axially delimited by the height of each assembly axial region and transversally delimited by the basket cell plates was used in subsequent spatial source distribution and mass density calculations for the different fuel configuration models.

Radiation source terms were determined for the BWR fuel assembly corresponding to 65 GWd/MTU burnup, 5 wt % ^{235}U initial enrichment, and 5- and 40-year decay times. Gamma and neutron sources in the active fuel region have an axial distribution based on the 25-zone assembly burnup profile from LaSalle Unit 1 documented in Ref. [30] for criticality calculations. The gamma radiation source axial profile was developed based on the direct proportionality between the gamma source strength and the burnup value; the neutron radiation source axial profile was developed based on the variation of the neutron source strength as the burnup value raised by the power of 4.2 [33]. The profiles thus determined are illustrated in Figure B.6 (a) for the gamma radiation source and Figure B.6 (b) for the neutron radiation source. In the cask model, the active fuel region of the BWR assembly was subdivided into 25 axial zones to facilitate description of the axial gamma and neutron radiation source distributions. Note that the gamma radiation source axial profile is relatively flat over a large fuel axial region, whereas the neutron radiation source axial profile is significantly pointed in the middle. The axial distribution shape of the BWR neutron radiation source also significantly differs from the axial distribution shape of the PWR neutron radiation source, which is flatter, as seen in Figure B.5.

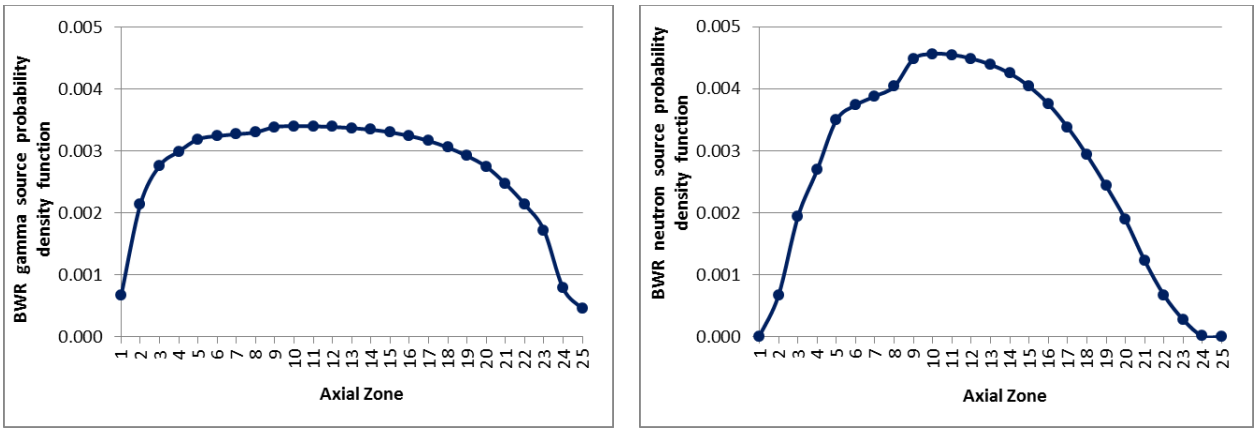

(a) (b)

Figure B.6 – Source intensity distribution as a function of BWR fuel axial zone for (a) gamma radiation source and (b) neutron radiation source

B.4 DESCRIPTION OF FUEL RECONFIGURATION CATEGORY CALCULATION MODELS FOR SHIELDING

The calculation models developed for the fuel reconfiguration categories are described in this section. The configuration categories include cladding failure (see Sect. B.4.1), rod/assembly deformation without cladding failure (see Sect. B.4.2), and changes to assembly axial alignment

without cladding failure (see Sect. B.4.3). A variety of fuel failure effects are addressed in this calculation, including assembly deformation or alignment changes and relocation within different canister cavity regions of fuel mixture from varying percentages of failed fuel rods.

B.4.1 Category 1: Cladding Failure

To investigate the effects of cladding failure on shielding objectives, two configuration scenarios were developed: (1) breached spent fuel rods where assemblies have partially failed and partially intact fuel rods; and (2) damaged fuel representing the maximum degree of fuel configuration change that may occur under cladding failure scenarios.

S1(a)—Breached spent fuel rods

The following configurations were evaluated for the transportation package models:

- Fuel mixture relocated to the middle section of the fuel assembly;
- Fuel mixture relocated to the bottom section of the fuel assembly;
- Fuel mixture relocated to the top section of the fuel assembly.

For the PWR fuel, the evaluated percentages of fuel mixture relocated to different assembly regions are 10% (27 rods/assembly) and 25% (66 rods/assembly). For the BWR fuel, the evaluated percentage of fuel mixture relocated to different assembly regions is 11% (10 rods/assembly). Dose rate calculations were performed for the PWR and BWR package models under both NCT and HAC. The fuel rod failure rate values were arbitrarily selected because this information is not available for commercial high-burnup fuel or for spent fuel in long-term storage. However, the whole range of fuel failure with respect to the amount of fuel mixture (0–100%) that may be displaced to inner cavity regions is analyzed in this report under different consequence categories. The 25% value for PWR SNF was analyzed to determine whether there is a direct proportionality between the amount of relocated fuel mixture and external dose rate (i.e., whether an increase in the displaced fuel mixture quantity from 10% to 25% of the assembly fuel mixture equates to an increase in external dose rate by a factor of 2.5). The effects of a lower percentage of failed fuel, such as single fuel rod failure, were not considered because the change in cask external dose rates is estimated to be comparable to calculation statistical error (i.e., non-discernible effect).

This configuration scenario assumes that the fuel pellets are fractured and that the fuel fragments and particulates can be released from fuel rods that have developed cladding breaches. Pellet fracturing is caused by fuel exposure to thermal gradients early in life. The number of fragments observed for typical fuel varies from 20 to 50 fragments per pellet and more fragmentation has been observed for higher burnup fuel [39]. For this configuration, assembly spacers are assumed intact so that fuel configuration changes cannot occur beyond the assembly location. The fuel material will likely collect beneath its parent rods close to the cladding breach locations (if the package is in the horizontal orientation) or into the assembly lower region (if the package is in the vertical orientation). However, fuel in the horizontal orientation, when subject to transportation vibrations, could relocate axially within the cask from the active fuel region to either bottom or top regions. Furthermore, these fragments and particulates may be spread across the available volume or be packed closely together within a small volume. It is assumed that the most limiting mass packing fraction of the released fuel fragments and particulates that results in the largest source intensity per volume unit is 0.58. This value is based on powder mechanics for particles similar to sand [27]. A mass packing fraction of 0.67 was also used in sensitivity calculations.

Axial locations beyond the normal active fuel location are considered in the analysis because fuel rubble collected into such locations has a greater potential of increasing external top or bottom dose rate because of its proximity to those surfaces. In addition, neutron streaming above or below the radial neutron shield may significantly increase the neutron dose rate on the cask external radial surface. Therefore, fuel relocation beyond the active fuel region is expected to produce significant dose rate increase relative to the nominal intact fuel configuration for the package external upper and lower regions.

Input parameter calculation approach:

Fuel reconfiguration models require input parameters that appropriately describe radiation source and fuel mixture spatial distributions within the package/cask inner cavity. For a realistic dose rate evaluation of fuel reconfigurations, the total source intensity and mass balance must be maintained within the cask. This means that if the source intensity is increased for the assembly region into which fuel material is collected, the source intensity for the active fuel region must be proportionally reduced so that the total source intensity does not change relative to the nominal intact fuel configuration.

Calculation of the radiation source terms and mass density values is described for the 10% fuel failure rate configuration in which fuel material released from 27 PWR failed fuel rods per assembly is collected into the lower assembly region assuming a 0.58 mass packing fraction.

To simplify the radiation source calculation for the fuel reconfiguration, it is assumed that 10% of the total fuel mass per assembly is released into the lower assembly region, i.e., the source intensity of the relocated material is 10% of the total source intensity. The weight of the released fuel material is ~49 kg per assembly, and the minimum volume outside the fuel rods that may be occupied by the released fuel material is ~8227 cm^3, based on the 0.58 packing fraction. The free void volume corresponding to the assembly lower end fitting region in Table B.1 is 4627.3 cm^3, which indicates that up to 56% (i.e., 4627.3/8227×100) of the released fuel mixture can be collected into the assembly lower end fitting region, and the remainder can be collected into the first (bottom) axial zone of the active fuel region. Because of fuel relocation, mass densities, elemental compositions, and radiation source terms for assembly lower end fitting and active fuel axial zones will change relative to the nominal intact assembly configuration. For example, the activation source of the assembly lower end fitting must be combined with 56% of the gamma and neutron source of the released fuel (i.e., 5.6% of the total gamma and neutron source intensities) to determine new source terms for the lower end fitting. The source intensity in the active fuel region will be reduced, relative to the nominal intact fuel intensity, by an amount proportional to the relocated fuel (i.e., 10%). Then 44% of the radiation source of the released fuel (i.e., 4.4% of the total gamma and neutron source intensities) is added to the radiation source of the first active fuel axial zone.

S1(b)—Damaged fuel

The evaluated configurations for the damaged fuel scenario are

- homogenized rubble packed closely together into the bottom of the inner cavity assuming a 0.58 mass packing fraction, as illustrated in Figure B.7 (a) for the transportation package model; and
- homogenized rubble assuming the rubble occupies the whole inner cavity, as illustrated in Figure B.7 (b) for the transportation package model.

Configuration (a) is consistent with a package/storage cask in the vertical orientation. Configuration (b) is consistent with a package/storage cask in the horizontal orientation. A transportation package may have both vertical and horizontal orientations during normal operations. These configurations are bounding for damaged SNF resulting in fuel fragments and particulates being collected into inner cavity regions below or above the assembly spacers or between fuel basket outer plates and the canister radial wall.

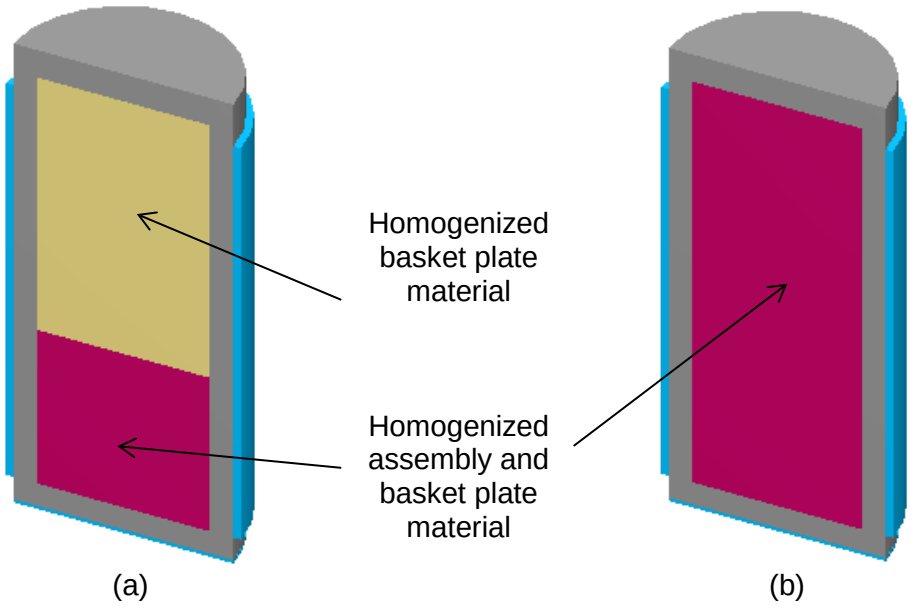

Figure B.7 – Illustration of the transportation package models for damaged SNF configurations with (a) fuel rubble collected into package cavity bottom and (b) fuel rubble homogenized within package cavity

B.4.2 Category 2: Rod/Assembly Deformation

The evaluated configurations consist of intact fuel rods collapsed against the basket plates of a transportation package, as illustrated in Figure B.8 (a) and (b), potentially resulting from a horizontal drop or tip-over. Dose rate calculations were performed for the PWR package model under both NCT and HAC, and for the BWR package model with fuel rods collapsed as shown in Figure B.8 (a) under NCT.

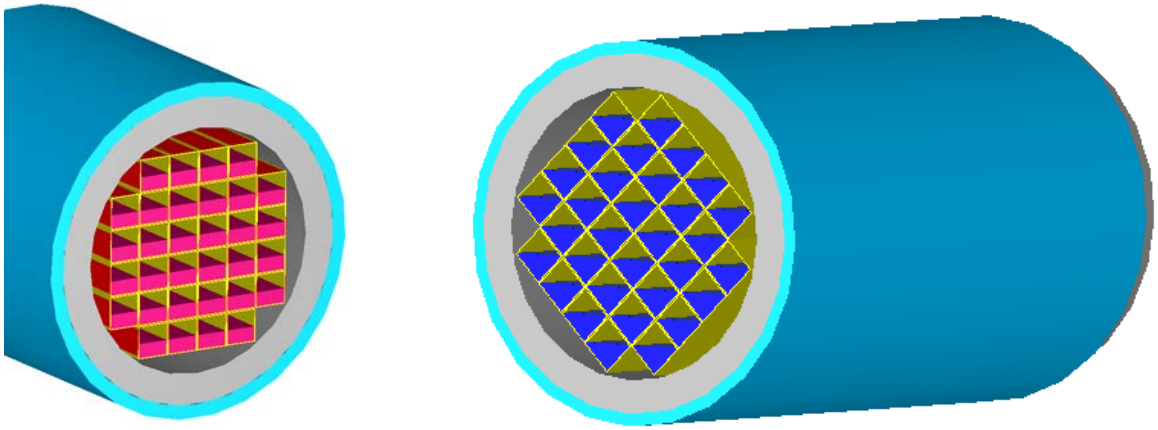

(a) (b)

Figure B.8 – Illustration of the cask model for the collapsed fuel rod configuration

B.4.3 Category 3: Changes to Assembly Axial Alignment

Fuel spacers are typically used to ensure that the fuel assemblies are aligned within a fixed orientation within the storage cask or transportation package. This category evaluates the potential impacts of changes to the original fuel assembly axial alignment, which could result in higher dose rates at the package top and/or bottom external surfaces.

The configurations evaluated for this category are

- intact fuel assemblies axially displaced to the cavity bottom surface, as illustrated for the PWR fuel in Figure B.9 (a); and
- intact fuel assemblies axially displaced to the cavity top surface as illustrated for the PWR fuel in Figure B.9 (b).

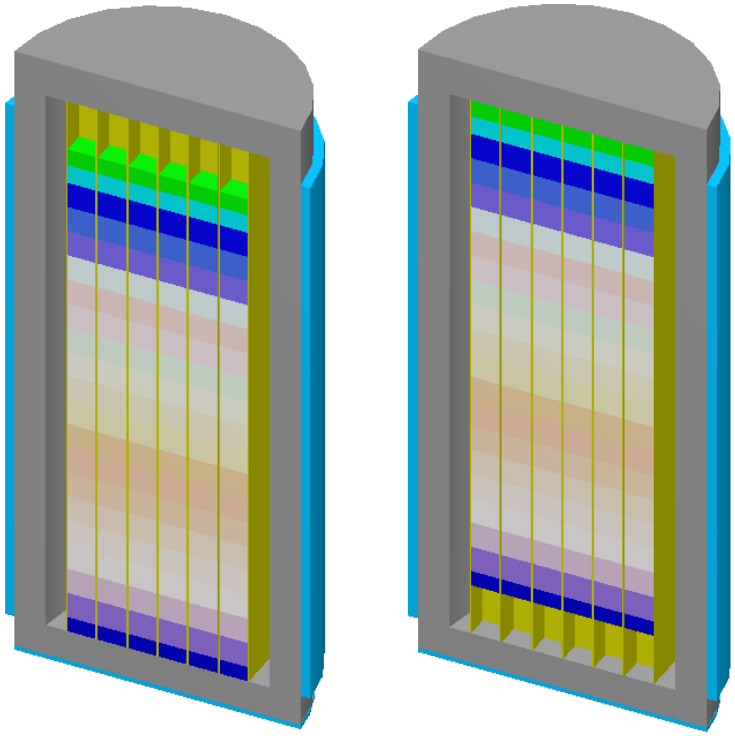

(a) (b)

Figure B.9 – Illustration of the transportation cask models for axial assembly displacement to (a) canister cavity bottom and (b) canister cavity top

Dose rate calculations were performed for the PWR and BWR package models (under both NCT and HAC) and for the PWR and BWR storage cask models.

B.5 SHIELDING ANALYSIS RESULTS

The generic PWR and BWR packages were assumed to be transported by exclusive shipment. For normal conditions of transport, a package transported by exclusive shipment must not exceed the 10 CFR 71.47 dose rate limits for the package outer surfaces (1000 mrem/h), outer surfaces of the conveyance (200 mrem/h), 2 m from the conveyance outer lateral surfaces (10 mrem/h), and any normally occupied space (2 mrem/h). Gamma and neutron dose rates for a package under NCT were calculated for the package top, side, and bottom external surfaces and at 2 m from the conveyance, the lateral surfaces of which were assumed to be located at 30 cm from the package external surfaces. Although the distance between the package outer surfaces and the 2 m locations may vary for the actual transportation packages, the dose rate effects on each surface of interest due to fuel configuration changes relative to the nominal intact fuel configuration are relatively similar at different locations surrounding the package.

For HAC (design basis fire and 30 ft drop), the neutron shield was assumed to be completely lost. The dose rate values for a package under HAC were evaluated at 1 m from the package external surfaces.

The ratio of the maximum surface dose rate for a fuel reconfiguration to the maximum surface dose rate for the intact fuel configuration, which is identified as the failed to intact (F/I)

configuration dose rate ratio, is provided in the tables included in this section. Note that the locations of the maximum dose rate at the package side surface for intact fuel and failed fuel may be different.

The gamma dose rates at the bottom and top surfaces vary significantly as a function of decay time because of the decay of ^{60}Co, which is an activation source in the assembly plenum and lower and upper hardware regions. For the 5-year decay time, the gamma dose rate at the package bottom and top surfaces is high primarily because of the proximity of the ^{60}Co activation source to those surfaces, activation source strength, and energetic gamma rays of 1.25 MeV average energy. The ^{60}Co activation source has negligible contributions to gamma dose rate for the 40-year decay time and beyond ($t_{1/2}$=5.271 years). Therefore, the contribution of the ^{60}Co activation source to the gamma dose rates at the package bottom and top surfaces varies as a function of decay time. A large contribution of the ^{60}Co activation source to the gamma dose rate, as in the case of a 5-year decay time, equates to a relatively small increase of the gamma dose rate because of fuel relocation to assembly hardware regions. A small or negligible contribution of the ^{60}Co activation source to the gamma dose rate, as in the case of a 40-year decay time, equates to a relatively large increase of the gamma dose rate because of fuel relocation to assembly hardware regions. That is, the effects on the gamma dose rates at the package bottom and top surfaces of fuel relocation into the assembly hardware regions are significantly smaller for the 5-year decay time than those for the 40-year decay time.

Beyond 5 years after fuel discharge from the reactor, the F/I neutron dose rate ratio is relatively insensitive to the decay time because neutrons are primarily produced from spontaneous fission and (alpha,n) reaction because of ^{244}Cm ($t_{1/2}$ = 18.1 years) and ^{238}Pu ($t_{1/2}$ = 87.7 years). The F/I gamma dose rate ratio is relatively insensitive to decay times larger than 40 years because the activation source in the assembly plenum and hardware regions is negligible and the fuel gamma dose rate is dominated by ^{137}Cs ($t_{1/2}$ = 30.07 years).

B.5.1 PWR Package Model Assuming Normal Conditions of Transport

The changes (F/I dose rate ratio) relative to the nominal intact fuel configuration of the maximum neutron and gamma dose rates on the PWR package external surfaces and at 2 m from the package are summarized in Table B.3 and Table B.4, respectively. The neutron and gamma dose rate profiles on the PWR package external surfaces and at 2 m from the package are shown in Figure B.10 through Figure B.35 for the 40-year decay time for each fuel reconfiguration case and the nominal intact configuration for comparison.

Table B.3 – PWR package maximum dose rate change for NCT: package external surfaces

				Top	Side	Bottom	Top	Side	Bottom
Case #	Scenario	Fuel relocation region [a]	Decay time (years)	F/I neutron dose rate ratio [b]			F/I gamma dose rate ratio [b]		
1	10% fuel rod failure	Assembly active fuel	5	1.09	1.01	1.04	1.01	1.02	1.00
			40	1.09	1.01	1.03	1.00	1.01	1.00
2	10% fuel rod failure	Assembly lower end fitting	5	1.06	1.62	2.52	1.00	0.99	1.34
			40	1.06	1.59	2.53	1.00	0.98	5.17
3	10% fuel rod failure	Assembly plenum	5	3.96	2.37	1.03	0.98	0.99	1.01
			40	3.96	2.38	1.02	3.35	0.99	0.99
4	10% fuel rod failure	Assembly upper end fitting	5	4.98	2.75	1.05	0.93	0.99	1.01
			40	4.99	2.77	1.02	11.55	0.99	1.00
5	25% fuel rod failure	Assembly active fuel	5	1.12	1.06	1.00	1.00	1.12	1.00
			40	1.13	1.06	1.00	1.00	1.10	0.96
6	25% fuel rod failure	Assembly lower end fitting	5	1.05	1.76	2.76	1.00	0.98	1.33
			40	1.05	1.76	2.76	1.00	0.97	5.16
7	25% fuel rod failure	Assembly plenum	5	4.59	2.79	1.00	0.97	0.95	0.99
			40	4.58	2.80	0.99	3.34	0.96	0.96
8	25% fuel rod failure	Assembly upper end fitting	5	6.16	3.50	1.00	0.93	0.95	1.00
			40	6.13	3.51	0.99	11.59	0.96	0.95
9	Damaged	Canister cavity bottom	5	0.32	2.57	4.18	0.001	1.19	1.72
			40	0.32	2.59	4.13	0.02	1.21	8.37
10	Damaged	Entire canister cavity	5	6.69	3.89	3.04	0.84	1.10	1.43
			40	6.67	3.89	3.05	14.10	1.24	7.30
11	Assembly deformation	See Figure B.8 (a)	5	1.36	1.13	1.22	0.96	1.11	0.93
			40	1.36	1.14	1.19	0.87	1.10	0.64
12	Assembly deformation	See Figure B.8 (b)	5	1.27	1.03	1.17	0.99	0.93	0.96
			40	1.16	1.04	1.16	0.89	0.96	0.80
13	Alignment changes	See Figure B.9 (a)	5	0.80	1.15	1.35	0.60	1.00	1.66
			40	0.80	1.14	1.34	0.58	1.00	1.77
14	Alignment changes	See Figure B.9 (b)	5	1.26	1.10	0.78	1.59	1.29	0.59
			40	1.26	1.10	0.77	1.68	1.01	0.57

[a] Farthest region for fuel relocation identified. Fuel mixture may extend into adjacent assembly axial regions, as described further in this section.

[b] Relative error (95% confidence level) less than 5% for all values except for the value for case #9, gamma dose rate on top surface, the relative error is 15%.

Table B.4 – PWR package maximum dose rate change for NCT: 2 m from the package surfaces

				Top	Side	Bottom	Top	Side	Bottom
Case #	**Scenario**	**Fuel relocation region [a]**	**Decay time (years)**	**F/I neutron dose rate ratio [b]**			**F/I gamma dose rate ratio [b]**		
1	10% fuel rod failure	Assembly active fuel	5	1.07	1.02	1.02	1.01	1.00	1.00
			40	1.08	1.02	1.02	1.00	1.00	0.99
2	10% fuel rod failure	Assembly lower end fitting	5	1.04	1.02	2.29	1.01	0.99	1.33
			40	1.06	1.06	2.23	1.02	1.01	4.82
3	10% fuel rod failure	Assembly plenum	5	3.48	1.02	1.04	0.99	0.98	1.01
			40	3.36	1.07	1.00	1.26	1.01	0.98
4	10% fuel rod failure	Assembly upper end fitting	5	4.27	1.01	1.04	0.94	0.99	1.01
			40	4.19	1.08	1.00	2.85	1.01	0.98
5	25% fuel rod failure	Assembly active fuel	5	1.11	1.04	0.99	1.00	1.04	0.99
			40	1.11	1.02	0.98	0.99	1.00	0.96
6	25% fuel rod failure	Assembly lower end fitting	5	1.04	0.99	2.51	1.00	0.96	1.34
			40	1.05	1.03	2.39	0.96	1.00	4.76
7	25% fuel rod failure	Assembly plenum	5	4.08	1.06	0.99	0.98	0.95	0.99
			40	4.00	1.09	0.96	1.28	1.01	0.96
8	25% fuel rod failure	Assembly upper end fitting	5	5.27	1.25	0.99	0.95	0.95	0.99
			40	5.13	1.15	0.97	2.88	1.01	0.95
9	Damaged	Canister cavity bottom	5	0.30	1.02	4.01	0.03	1.07	2.17
			40	0.29	0.94	3.95	0.26	0.94	10.56
10	Damaged	Entire canister cavity	5	5.94	1.28	2.90	1.04	1.11	1.78
			40	5.79	1.24	2.80	5.02	1.32	9.11
11	Assembly deformation	See Figure B.8 (a)	5	1.31	1.15	1.19	0.98	1.10	0.93
			40	1.32	1.17	1.17	1.04	1.09	0.73
12	Assembly deformation	See Figure B.8 (b)	5	1.22	1.04	1.15	1.00	0.94	0.95
			40	1.12	1.04	1.11	0.96	0.96	0.77
13	Alignment changes	See Figure B.9 (a)	5	0.79	1.01	1.30	0.60	1.00	1.67
			40	0.80	1.01	1.29	0.86	1.01	1.74
14	Alignment changes	See Figure B.9 (b)	5	1.25	1.02	0.79	1.61	1.00	0.59
			40	1.28	1.02	0.78	1.57	1.00	0.57

[a] Farthest region for fuel relocation identified. Fuel mixture may extend into adjacent assembly axial regions, as described further in this section.

[b] Relative error (95% confidence level) less than 7% for all values except for the value for case #9, gamma dose rate on top surface, the relative error is 15%.

Cases 1 to 4 evaluate the impact of 27 failed fuel rods per assembly (~10% failure rate) distributed to different axial locations. Discussions of the results are as follows:

Case 1. The redistributed fuel mixture is located at 285.5 to 326 cm relative to the package bottom surface. This location corresponds to assembly axial fuel zones 12 and 13. The fuel relocation caused ~9% increase in the maximum neutron dose rate on the top surface of the package. The gamma dose rate change relative to the nominal intact configuration was negligible for all surfaces and decay times evaluated. The neutron and gamma dose rate profiles along the PWR package outer surfaces and at the 2 m locations are shown in Figure B.10 and Figure B.11, respectively, for the 40-year decay time.

Case 2. The redistributed fuel mixture is located at 50 to 82.3 cm relative to the package bottom surface. This location corresponds to the assembly lower end fitting and bottom axial fuel zone. The maximum neutron dose rate at the package bottom surface was ~2.5 times as large as that of the nominal intact configuration. For the 40-year decay time, the maximum gamma dose rate on the package bottom surface increased by a factor of ~5. Similar effects were obtained for the maximum neutron and gamma dose rates at 2 m from the package surfaces. The neutron and gamma dose rate profiles along the PWR package outer surfaces and at the 2 m locations are shown in Figure B.12 and Figure B.13, respectively, for the 40-year decay time. This case was also analyzed for a mass packing fraction of 0.67. The neutron and gamma dose rate values based on the 0.67 mass package fraction were within the statistical errors (i.e., 7% at the 95% confidence level) of the values based on the 0.58 mass package fraction.

Case 3. The redistributed fuel mixture is located at 407.4 to 442.4 cm relative to the package bottom surface. This location corresponds to the assembly top axial fuel and plenum zones. The maximum neutron dose rates on the package top and side surfaces were ~4 and ~2.5 times, respectively, as large as the corresponding dose rates for the nominal intact configuration. At 2 m from the package top surface, the maximum neutron dose rate increased by a factor of ~3.5. The gamma dose rate increase relative to the nominal intact configuration was negligible for the 5-year decay time. For the 40-year decay time, the maximum gamma dose rate at the package top surface increased by a factor of ~3.5. The neutron and gamma dose rate profiles along the PWR package outer surfaces and the 2 m locations are shown in Figure B.14 and Figure B.15, respectively, for the 40-year decay time.

Case 4. The redistributed fuel mixture is located at 427.7 to 455.8 cm relative to the package bottom surface. This location corresponds to the assembly top axial fuel and plenum zones. The maximum neutron dose rates on the package top and side surfaces were ~5 and ~3 times, respectively, as large as the corresponding dose rates for the nominal intact configuration. At 2 m from the package top surface, the maximum neutron dose rate increased by a factor of ~4.5. The gamma dose rate increase relative to the nominal intact configuration was negligible for the 5-year decay time. For the 40-year decay time, the maximum gamma dose rate at the package top surface increased by a factor of ~12. At 2 m from the package top surface, the maximum gamma dose rate increased by a factor of ~3. The neutron and gamma dose rate profiles along the PWR package outer surfaces and the 2 m locations are shown in Figure B.16 and Figure B.17, respectively, for the 40-year decay time.

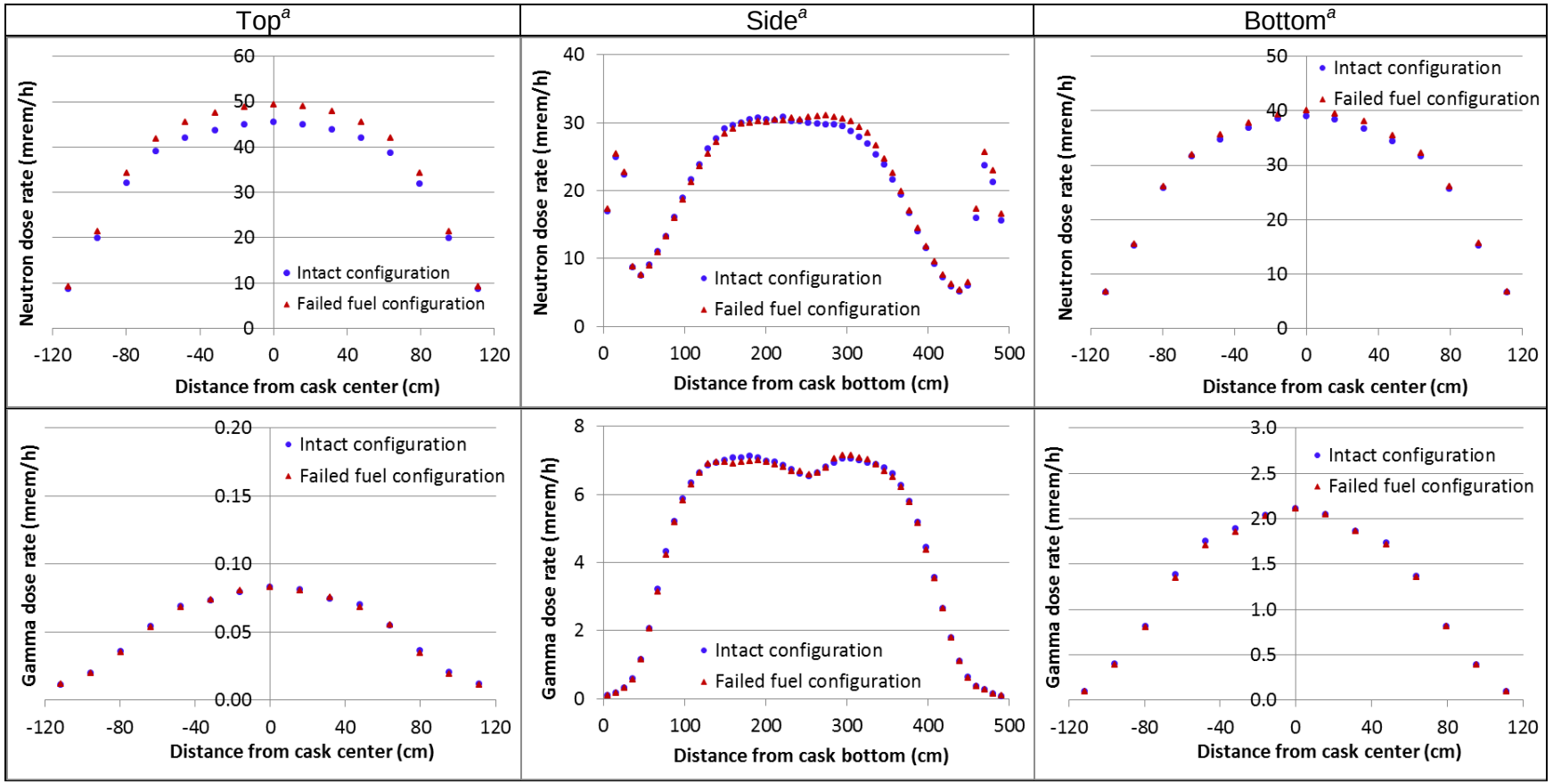

[a]PWR assemblies of 65 GWd/MTU burnup and 40-year decay time.

Figure B.10 – Dose rate comparison between the intact fuel configuration and the fuel reconfiguration assuming 10% of the fuel mixture collected into the free void volume of two axial fuel zones—PWR package outer surfaces, NCT (Case 1)

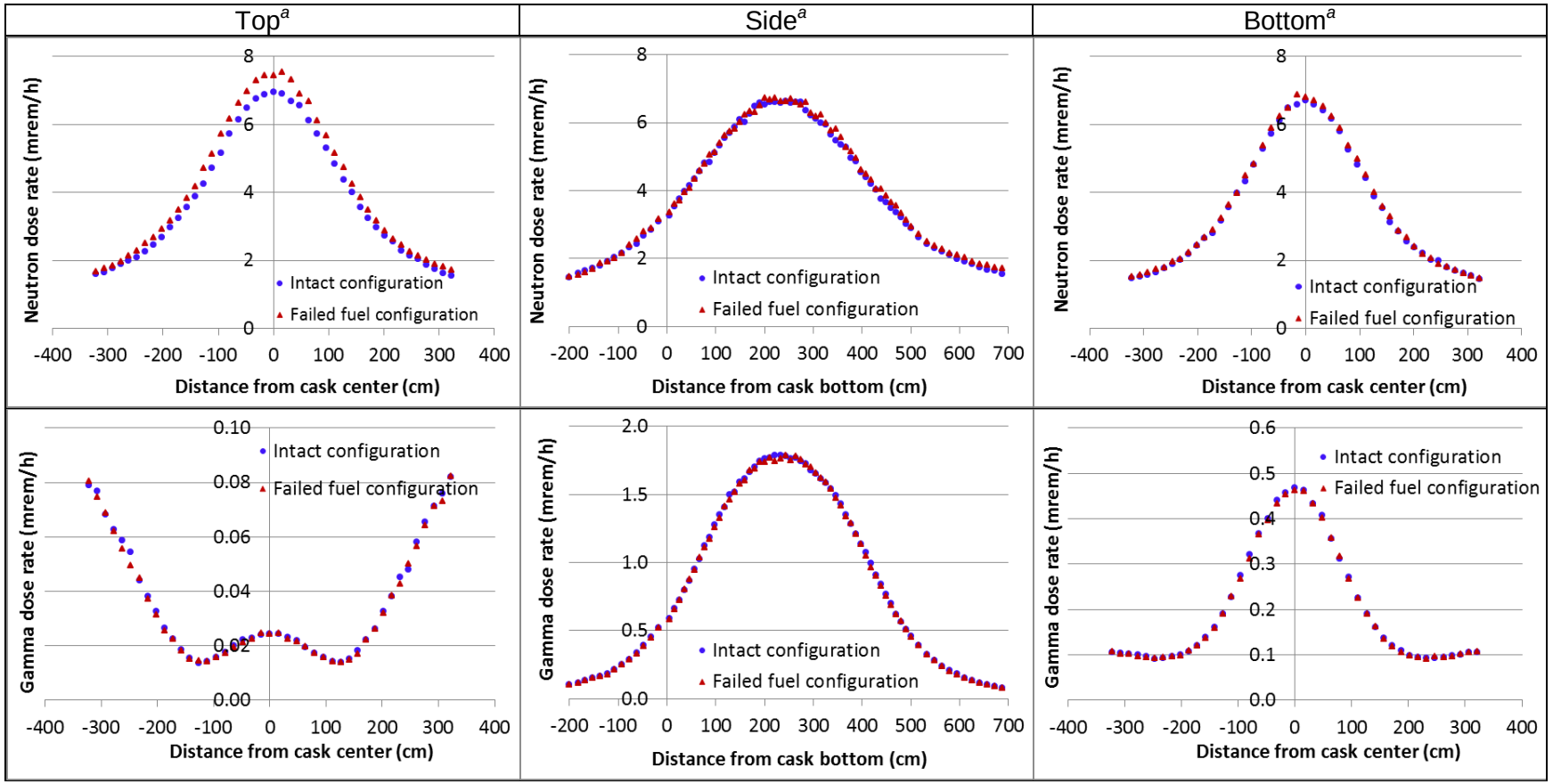

[a]PWR assemblies of 65 GWd/MTU burnup and 40-year decay time.

Figure B.11 – Dose rate comparison between the intact fuel configuration and the fuel reconfiguration assuming 10% of the fuel mixture collected into the free void volume of two axial fuel zones—2 m locations, PWR package NCT (Case 1)

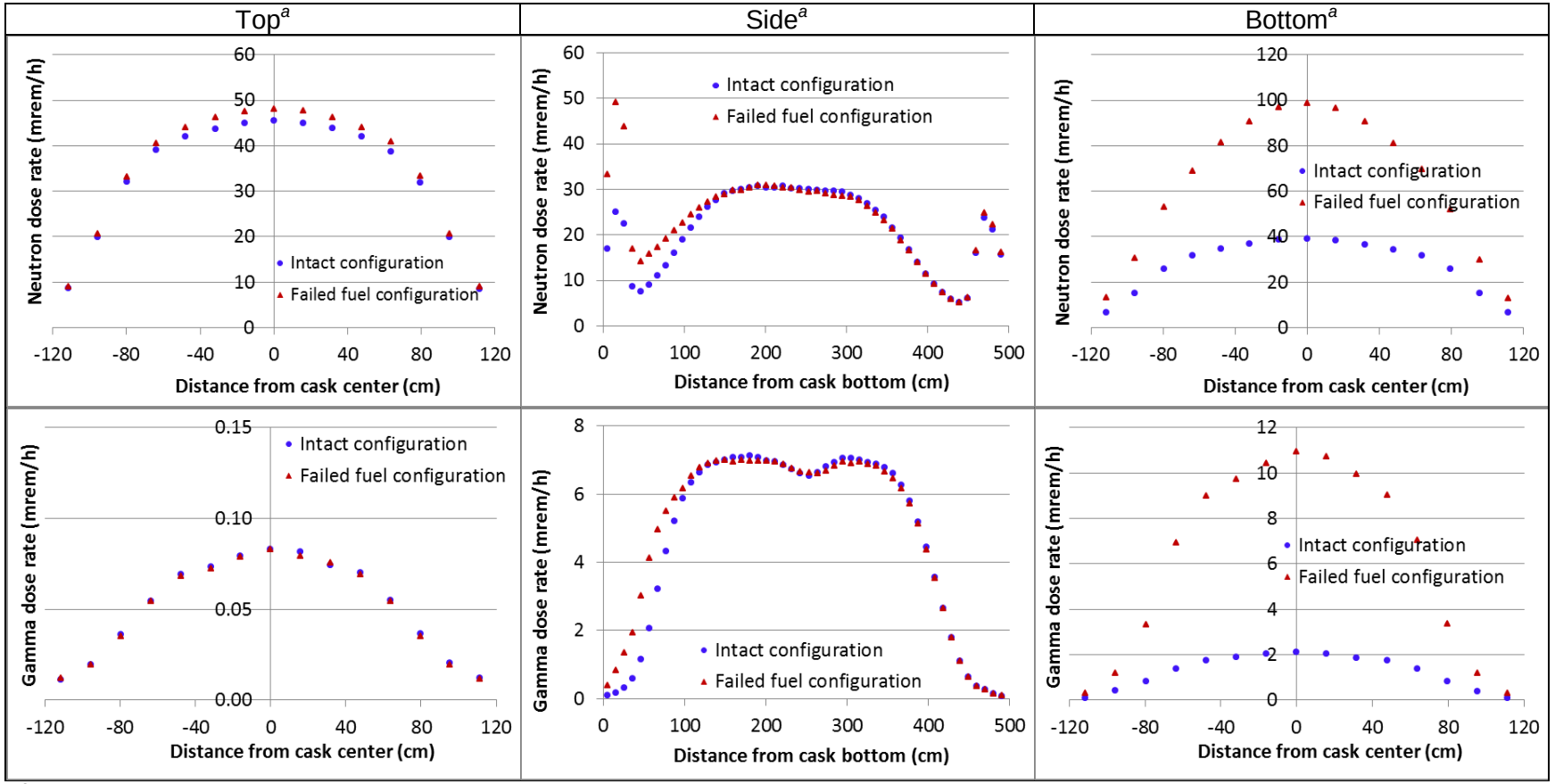

[a]PWR assemblies of 65 GWd/MTU burnup and 40-year decay time.

Figure B.12 – Dose rate comparison between the intact fuel configuration and the fuel reconfiguration assuming 10% of the fuel mixture collected into assembly lower end fitting region—PWR package outer surfaces, NCT (Case 2)

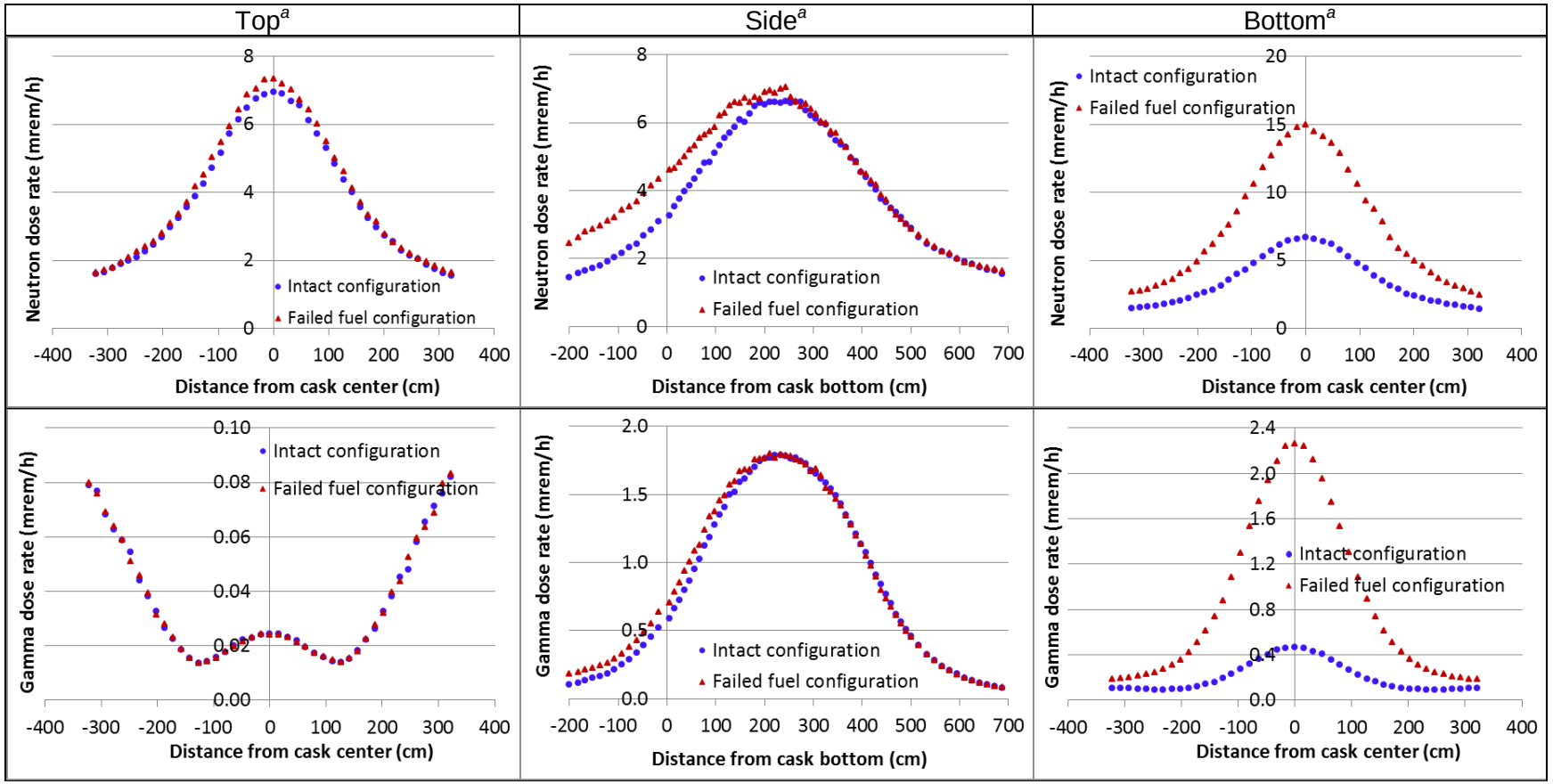

[a]PWR assemblies of 65 GWd/MTU burnup and 40-year decay time.

Figure B.13 – Dose rate comparison between the intact fuel configuration and the fuel reconfiguration assuming 10% of the fuel mixture collected into assembly lower end fitting region—2 m locations, PWR package NCT (Case 2)

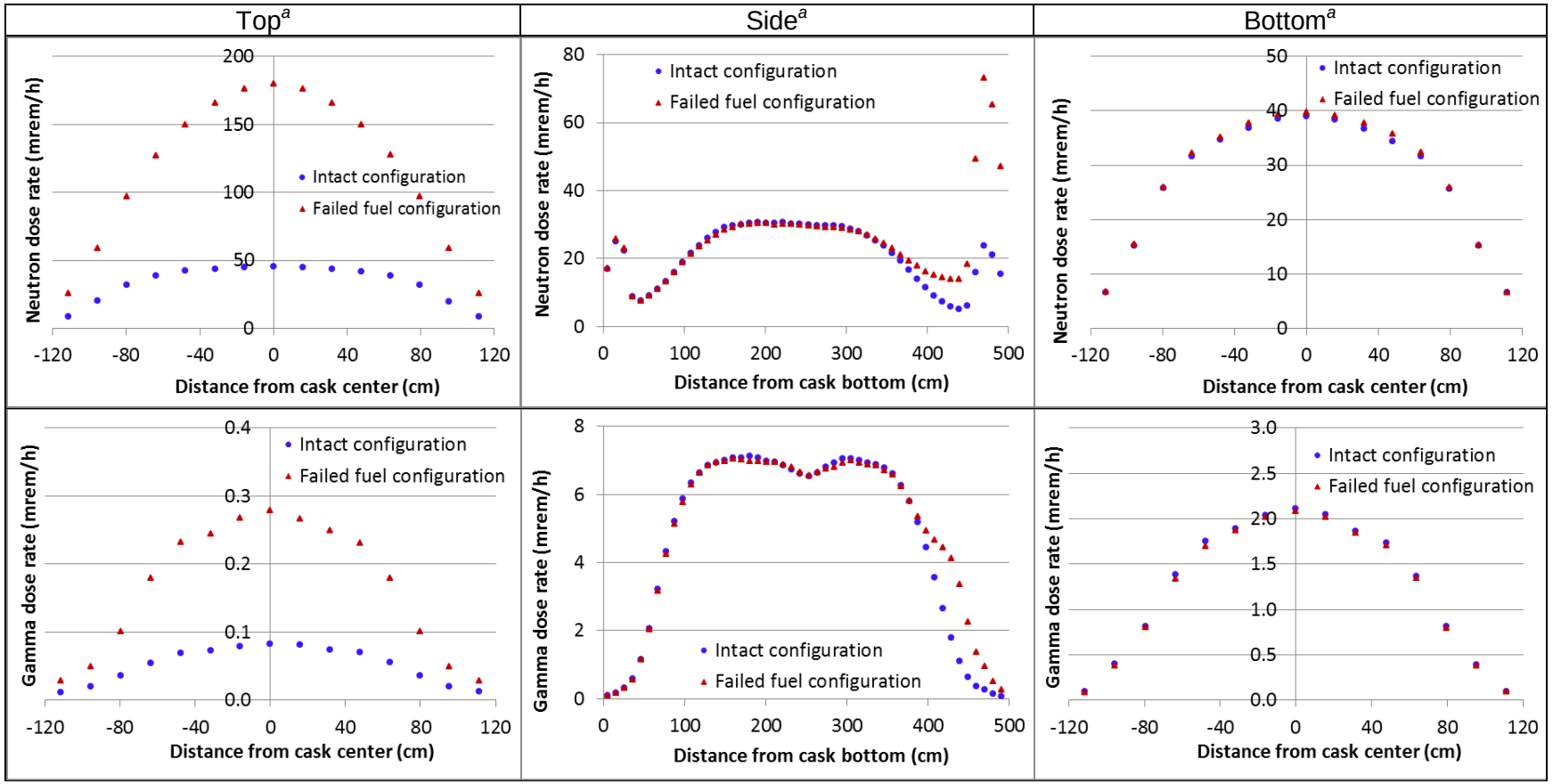

[a]PWR assemblies of 65 GWd/MTU burnup and 40-year decay time.

Figure B.14 – Dose rate comparison between the intact fuel configuration and the fuel reconfiguration assuming 10% of the fuel mixture collected into the top axial fuel and plenum regions—PWR package outer surfaces, NCT (Case 3)

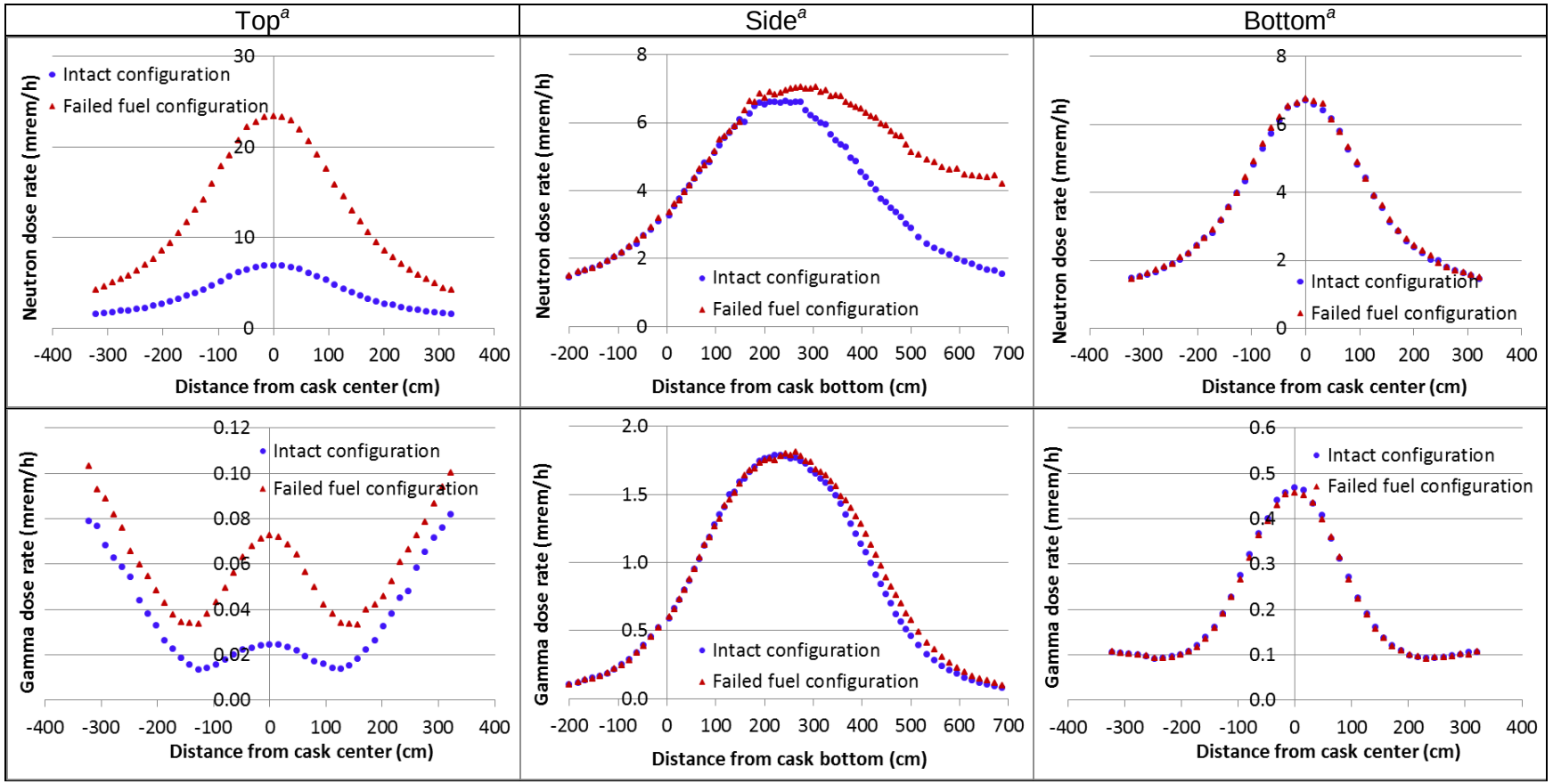

[a]PWR assemblies of 65 GWd/MTU burnup and 40-year decay time.

Figure B.15 - Dose rate comparison between the intact configuration and the fuel reconfiguration assuming 10% of the fuel mixture collected into the top axial fuel and plenum regions—2 m locations, PWR package NCT (Case 3)

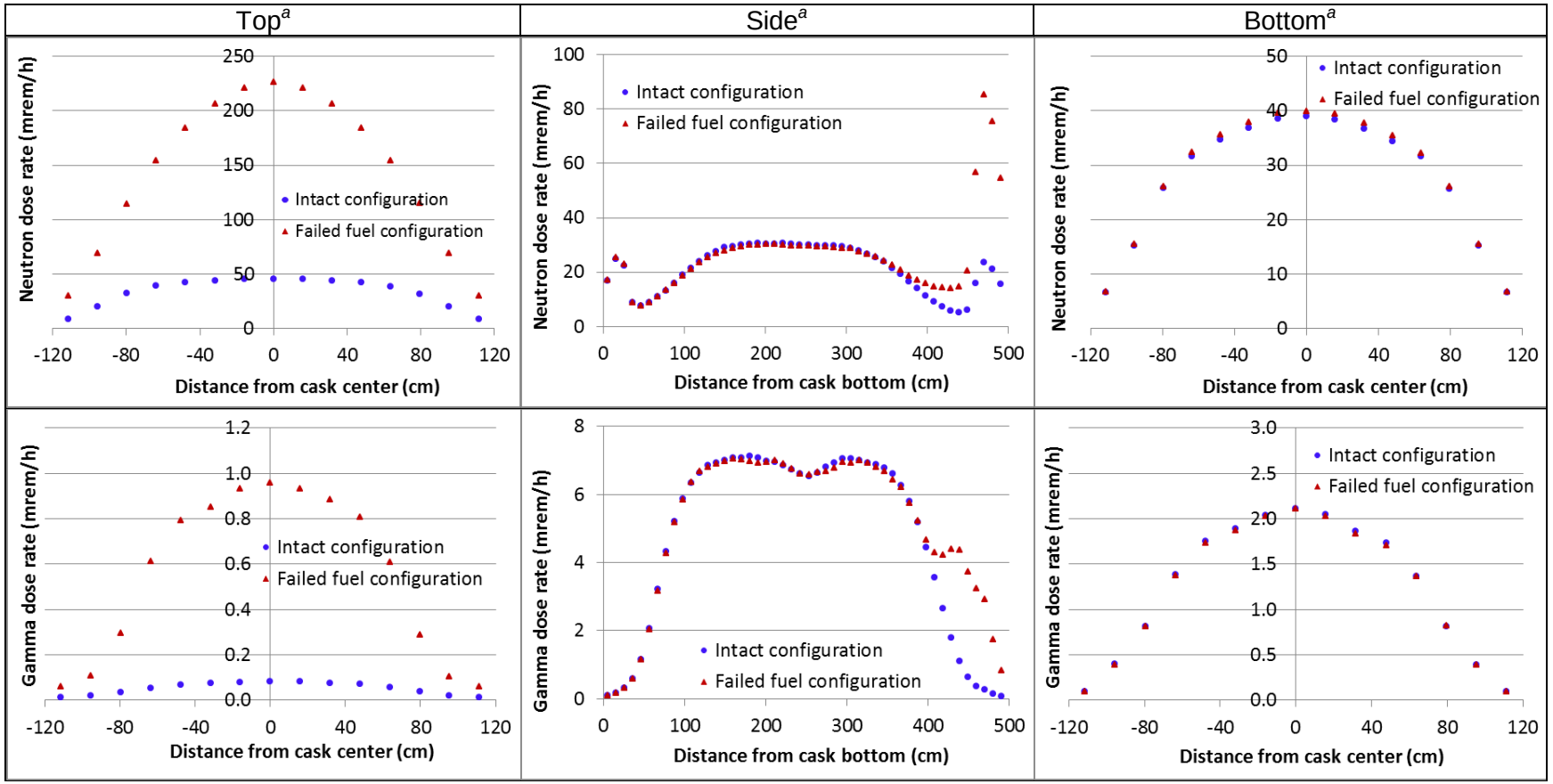

[a]PWR assemblies of 65 GWd/MTU burnup and 40-year decay time.

Figure B.16 – Dose rate comparison between the intact fuel configuration and the fuel reconfiguration assuming 10% of the fuel mixture collected into assembly plenum and upper end fitting regions—PWR package outer surfaces, NCT(Case 4)

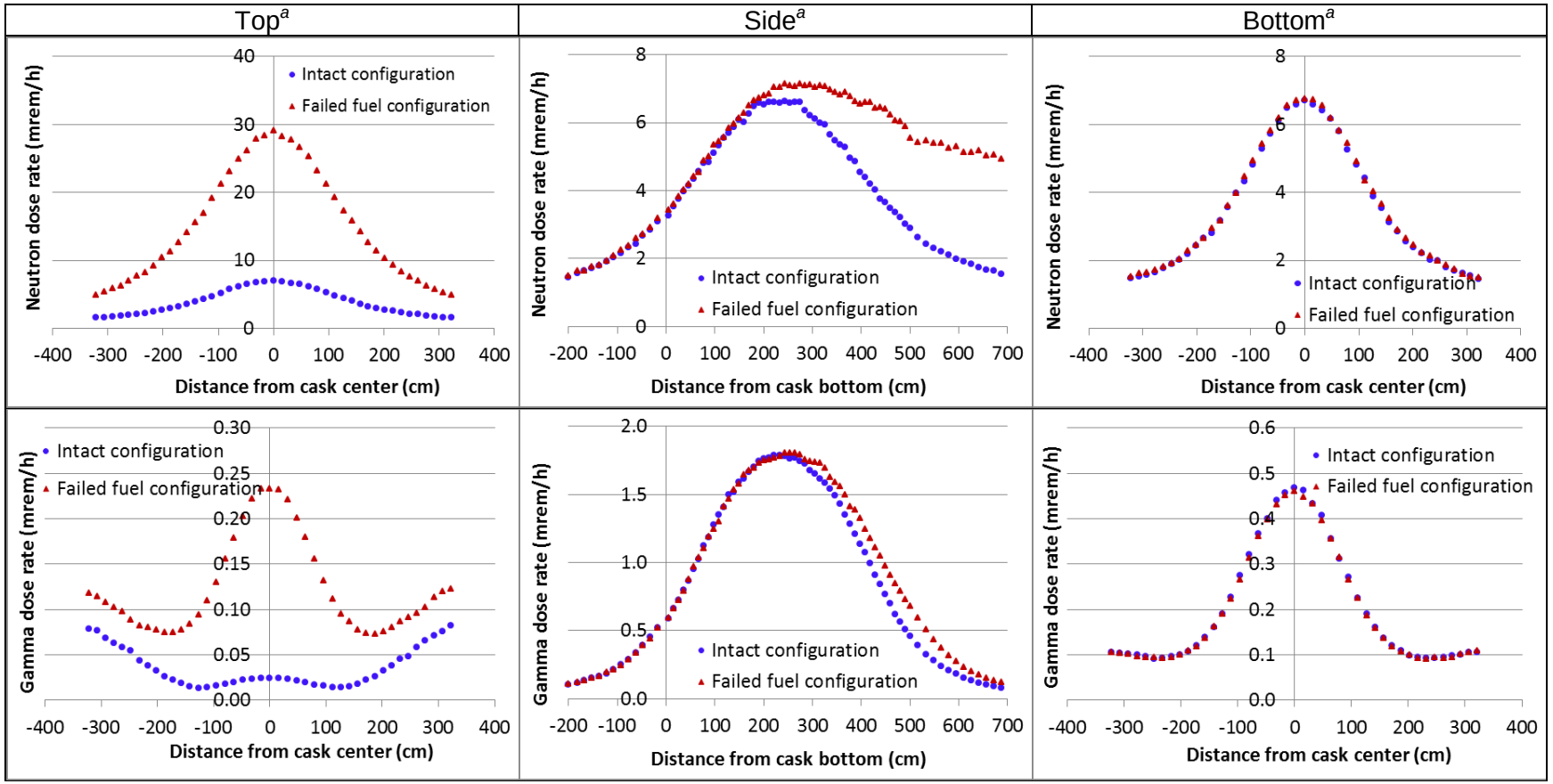

[a]PWR assemblies of 65 GWd/MTU burnup and 40-year decay time.

Figure B.17 – Dose rate comparison between the intact fuel configuration and the fuel reconfiguration assuming 10% of the fuel mixture collected into assembly plenum and upper end fitting regions—2 m locations, PWR package NCT (Case 4)

Cases 5 to 8 evaluate the impact of 66 failed fuel rods per assembly (~25% failure rate) distributed to different axial locations. Discussions of the results are as follows:

Case 5. The redistributed fuel mixture is located at 244.8 to 326 cm relative to the package bottom surface. This location corresponds to the assembly axial fuel zones 10 through 13. This fuel reconfiguration caused ~6% and ~12% increases in the maximum neutron dose rates on the side and top surfaces of the package, respectively, and ~12% increase in the maximum gamma dose rate on the side surface of the package, relative to the nominal intact configuration. Similar effects were obtained at 2 m from the package surfaces. The neutron and gamma dose rate profiles along the PWR package outer surfaces and the 2 m locations are shown in Figure B.18 and Figure B.19, respectively, for the 40-year decay time.

Case 6. The redistributed fuel mixture is located at 50 to 122.9 cm relative to the package bottom surface. This location corresponds to the assembly lower end fitting and axial fuel zones 1 through 3. The maximum neutron dose rate at the package bottom surface was ~3 times as large as that of the nominal intact configuration. The maximum gamma dose rate increase on the package bottom surface was ~30% for the 5-year decay time. For the 40-year decay time, the maximum gamma dose rate on the package bottom surface increased by a factor of ~5. Similar increases were obtained for the maximum neutron and gamma dose rates at 2 m from the package surfaces. The neutron and gamma dose rate profiles along the PWR package outer surfaces and the 2 m locations are shown in Figure B.20 and Figure B.21, respectively, for the 40-year decay time.

Case 7. The redistributed fuel mixture is located at 366.8 to 442.4 cm relative to the package bottom surface. This location corresponds to the axial fuel zones 16 through 18 and to the plenum region. The maximum neutron dose rate values for the package top and side surfaces were ~4.6 and ~2.8 times, respectively, as large as those of the nominal intact configuration. At 2 m from the package top surface, the maximum neutron dose rate increased by a factor of ~4.1. Gamma dose rate increase relative to the nominal intact configuration was negligible for the 5-year decay time. For the 40-year decay time, the maximum gamma dose rate at the package top surface increased by a factor of ~3.5. The neutron and gamma dose rate profiles along the PWR package outer surfaces and the 2 m locations are shown in Figure B.22 and Figure B.23, respectively, for the 40-year decay time.

Case 8. The redistributed fuel mixture is located at 387 to 455.8 cm relative to the package bottom surface. This location corresponds to the assembly axial fuel zones 17 and 18, plenum region, and upper end fitting. The maximum neutron dose rate values for the package top and side surfaces were ~6 and ~3.5 times, respectively, as large as those of the nominal intact configuration. At 2 m from the package top surface, maximum neutron dose rate increased by a factor of ~5. Gamma dose rate increase relative to the nominal intact configuration was negligible for the 5-year decay time. For the 40-year decay time, the maximum gamma dose rate at the package top surface increased by a factor of ~12. At 2 m from the package top surface, the maximum gamma dose rate increased by a factor of ~3. The neutron and gamma dose rate profiles along the PWR package outer surfaces and the 2 m locations are shown in Figure B.24 and Figure B.25, respectively, for the 40-year decay time.

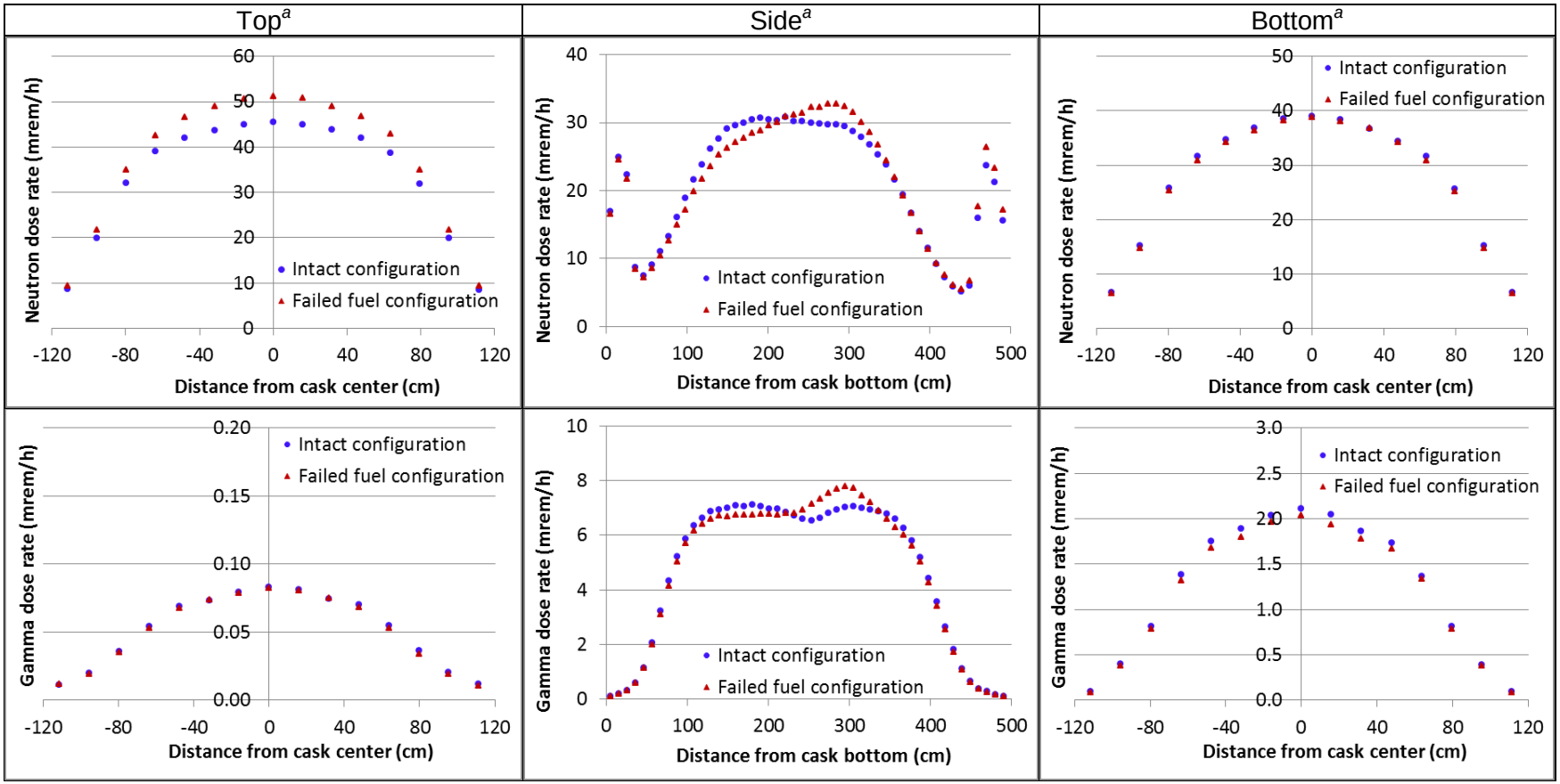

[a]PWR assemblies of 65 GWd/MTU burnup and 40-year decay time.

Figure B.18 – Dose rate comparison between the intact fuel configuration and the fuel reconfiguration assuming 25% of the fuel mixture collected into the free void volume of four axial fuel zones—PWR package outer surfaces, NCT (Case 5)

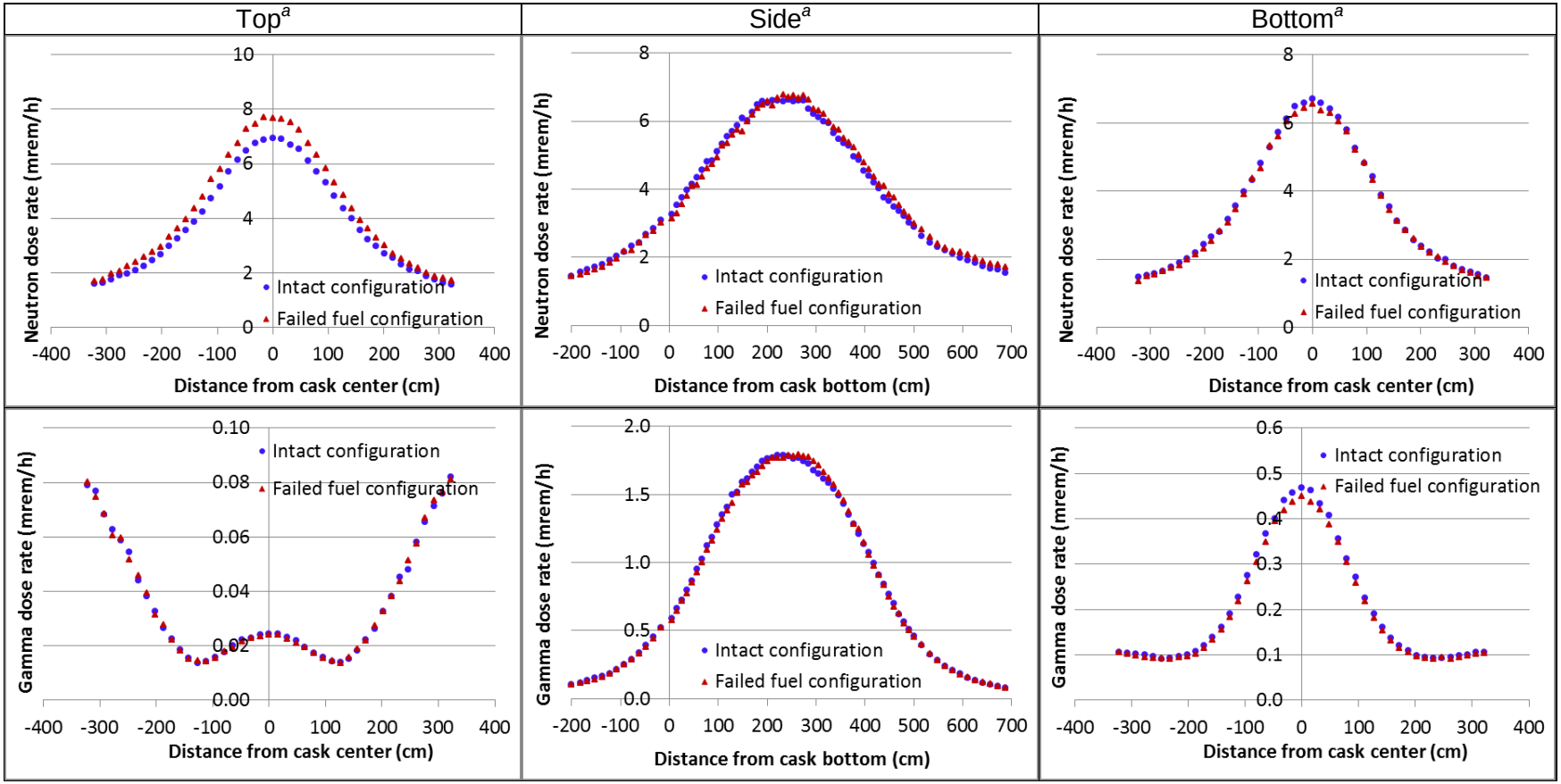

[a]PWR assemblies of 65 GWd/MTU burnup and 40-year decay time.

Figure B.19 – Dose rate comparison between the intact fuel configuration and the fuel reconfiguration assuming 25% of the fuel mixture collected into the free void volume of four axial fuel zones—2 m locations, PWR package NCT (Case 5)

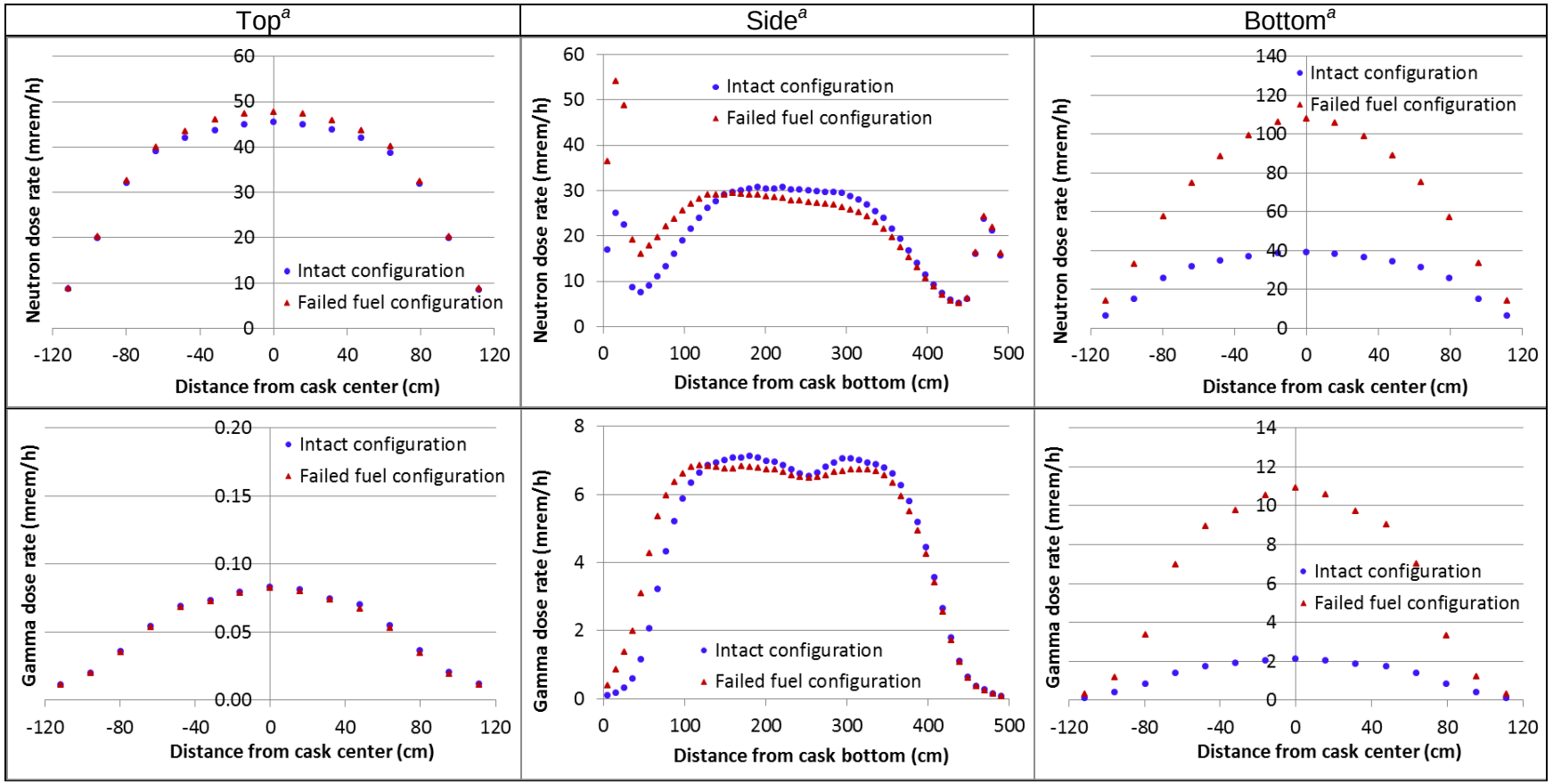

[a]PWR assemblies of 65 GWd/MTU burnup and 40-year decay time.

Figure B.20 – Dose rate comparison between the intact fuel configuration and the fuel reconfiguration assuming 25% of the fuel mixture collected into assembly bottom region—PWR package outer surfaces, NCT (Case 6)

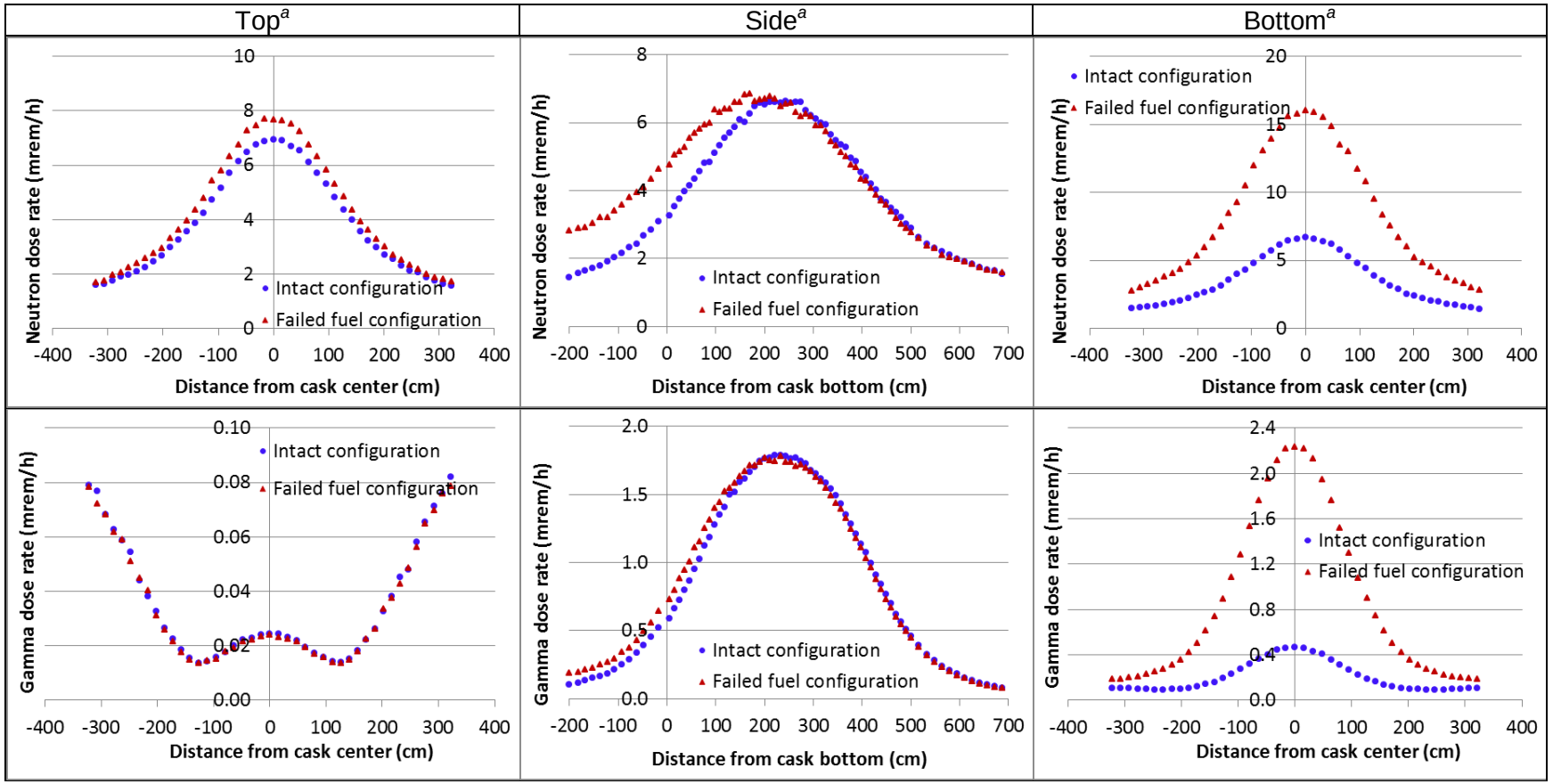

[a]PWR assemblies of 65 GWd/MTU burnup and 40-year decay time.

Figure B.21 – Dose rate comparison between the intact fuel configuration and the fuel reconfiguration assuming 25% of the fuel mixture collected into assembly bottom region—2 m locations, PWR package NCT (Case 6)

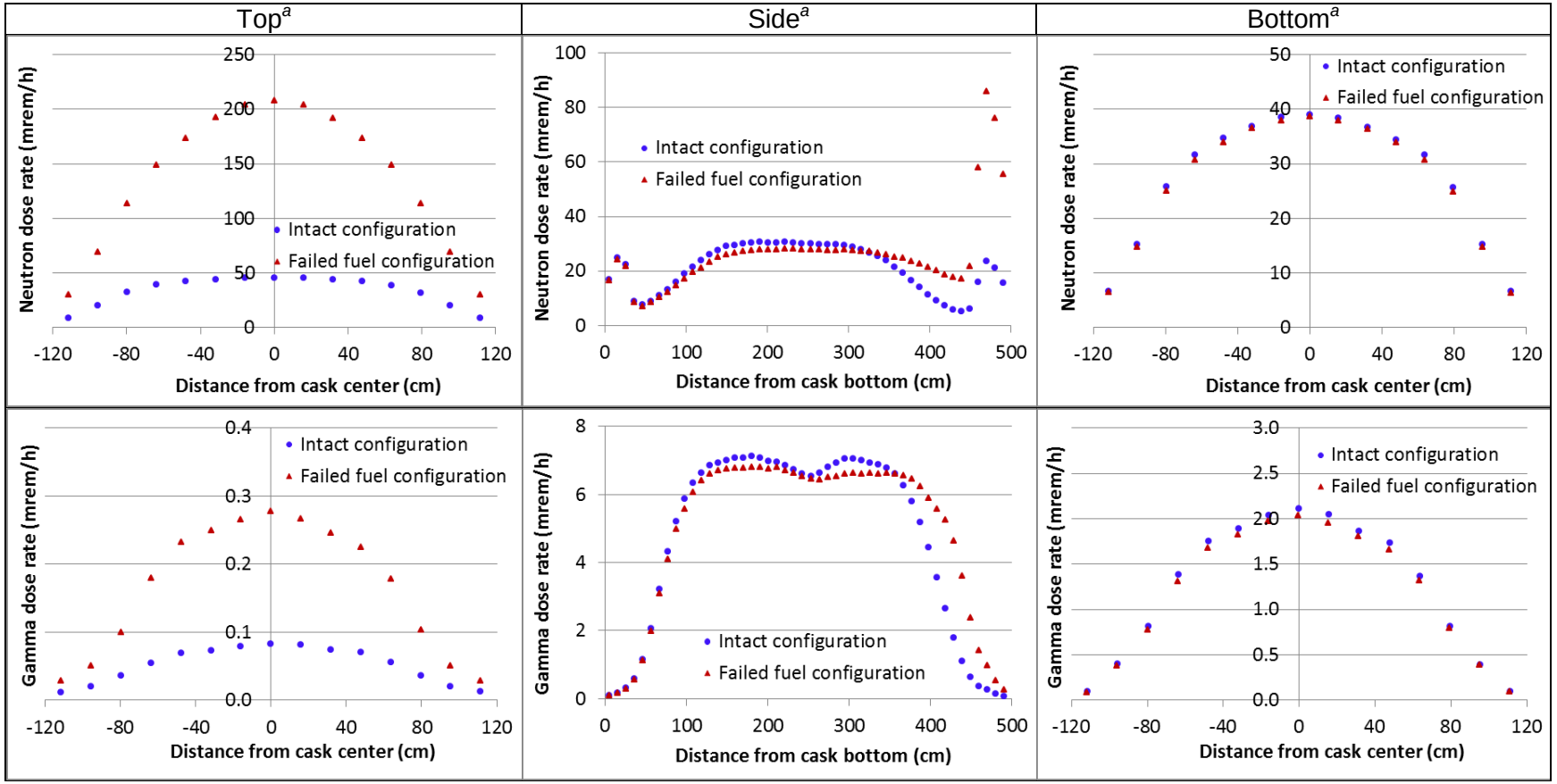

[a]PWR assemblies of 65 GWd/MTU burnup and 40-year decay time.

Figure B.22 – Dose rate comparison between the intact fuel configuration and the fuel reconfiguration assuming 25% of the fuel mixture collected into top axial fuel and plenum regions—PWR package outer surfaces, NCT (Case 7)

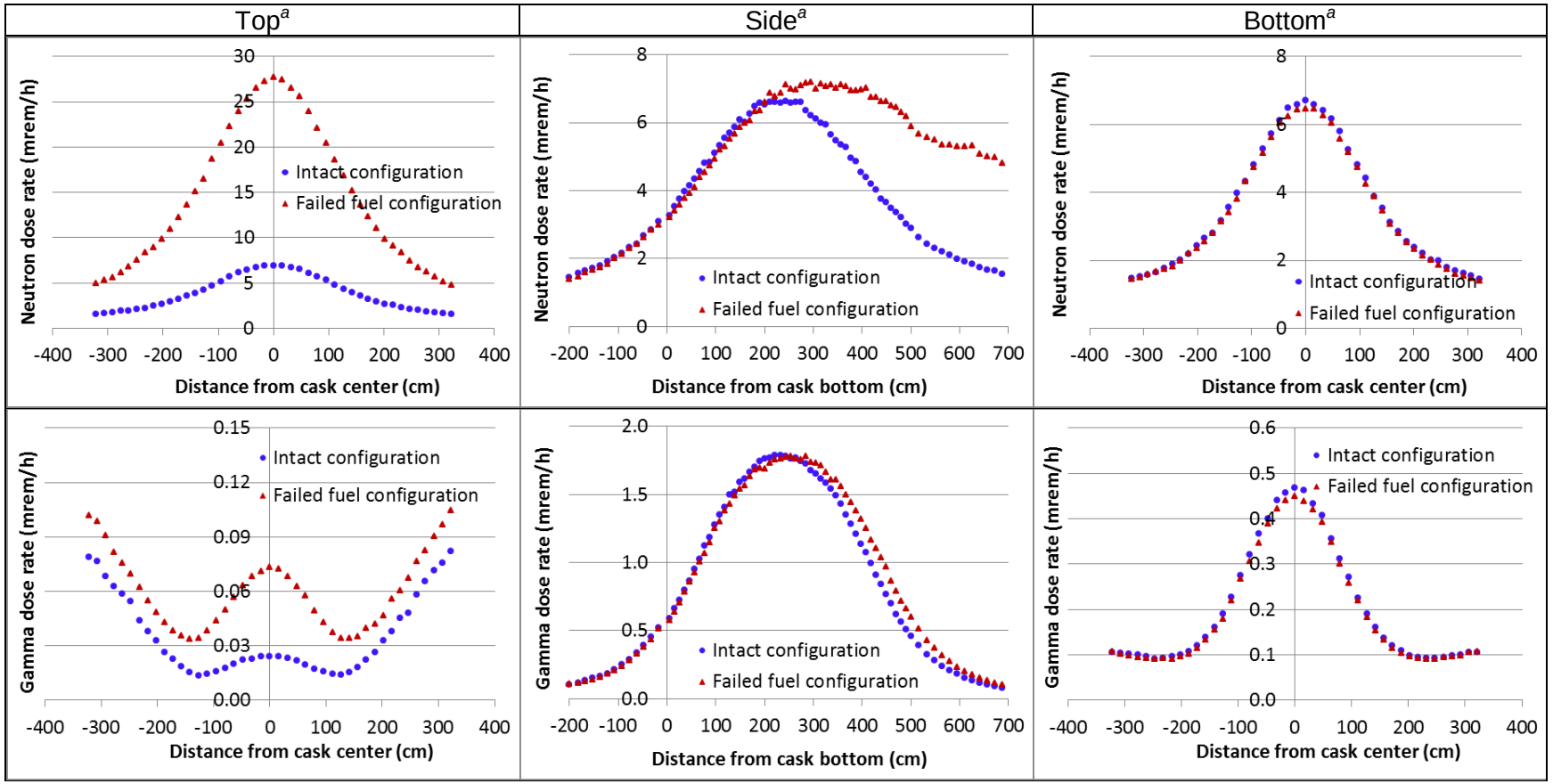

[a]PWR assemblies of 65 GWd/MTU burnup and 40-year decay time.

Figure B.23 – Dose rate comparison between the intact fuel configuration and the fuel reconfiguration assuming 25% of the fuel mixture collected into top axial fuel and plenum regions—2 m locations, PWR package NCT (Case 7)

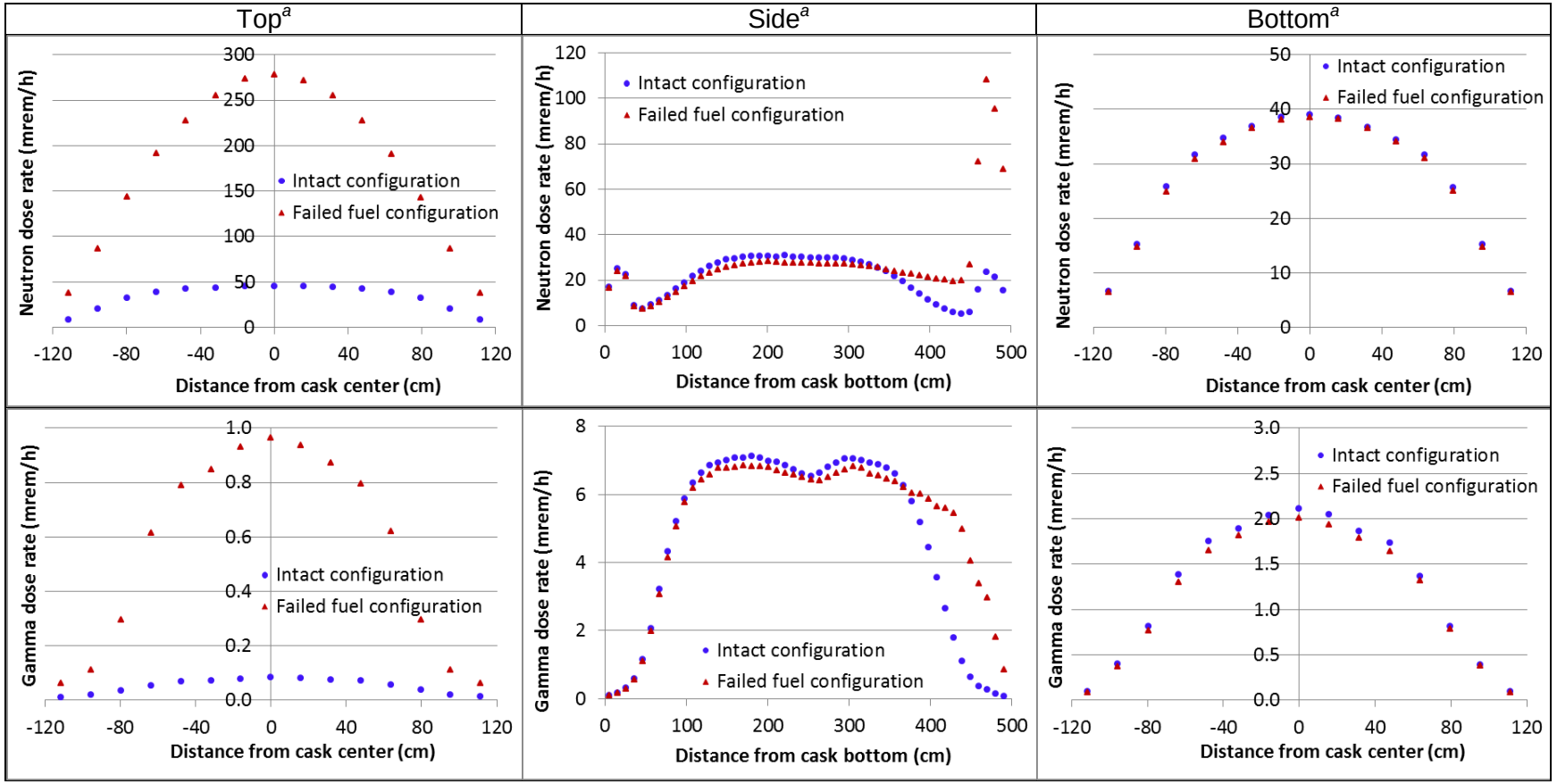

[a]PWR assemblies of 65 GWd/MTU burnup and 40-year decay time.

Figure B.24 – Dose rate comparison between the intact fuel configuration and the fuel reconfiguration assuming 25% of the fuel mixture collected into top axial fuel, plenum, and upper end fitting regions—PWR package outer surfaces, NCT (Case 8)

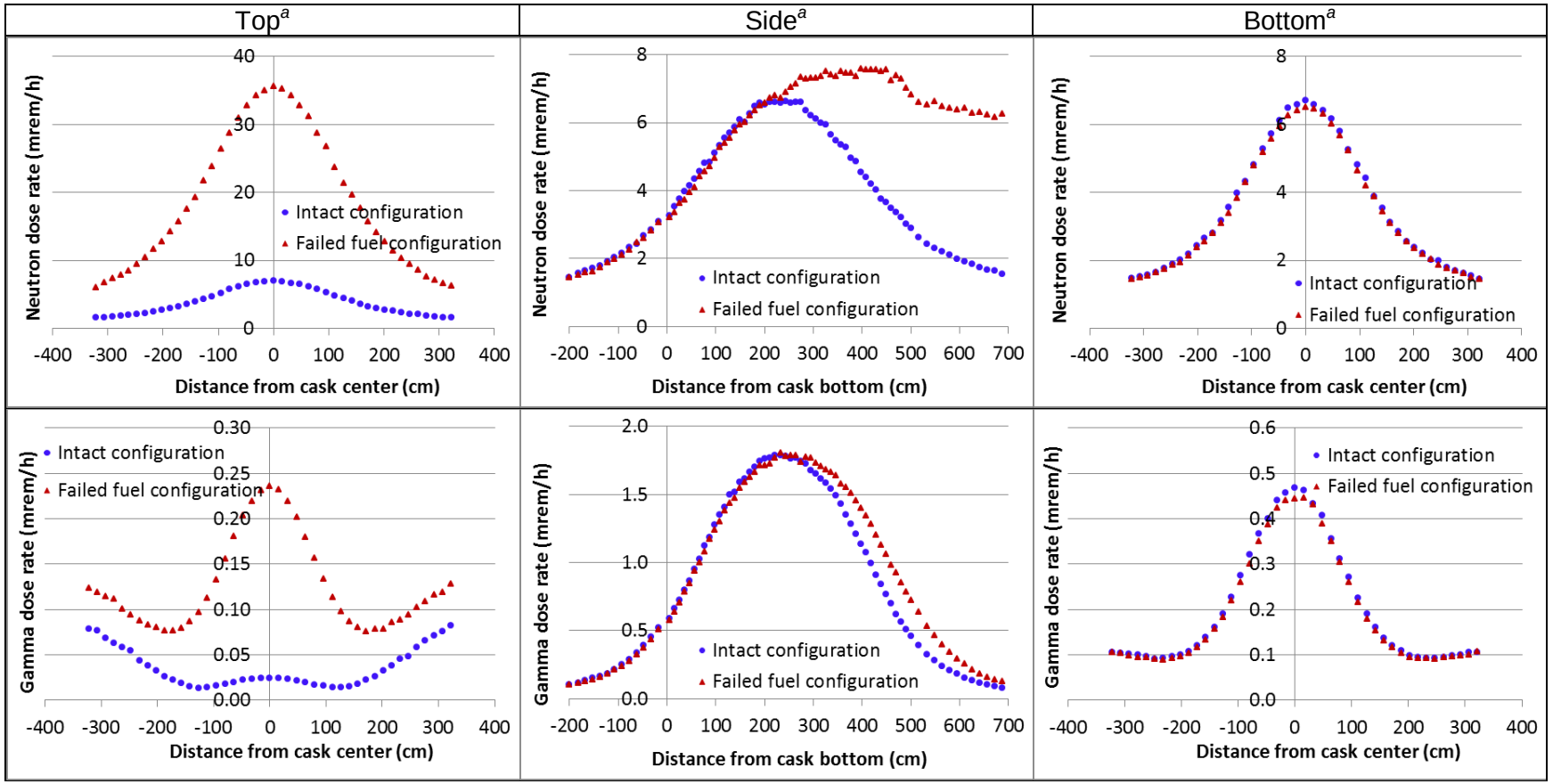

[a]PWR assemblies of 65 GWd/MTU burnup and 40-year decay time.

Figure B.25 – Dose rate comparison between the intact fuel configuration and the fuel reconfiguration assuming 25% of the fuel mixture collected into top axial fuel, plenum, and upper end fitting regions—2 m locations, PWR package NCT (Case 8)

Cases 9 and 10 evaluate the impact of extensive cladding failure representative of damaged fuel, where the fuel mixture is represented as collecting into the internal regions adjacent to the canister wall such as the space between the outer basket plates and canister wall. Discussions of the results are as follows:

Case 9. For this case, the stainless steel basket plate materials and fuel rubble from the damaged fuel rods are homogenously distributed within the canister bottom region as shown in Figure B.8 (a). The height and mass density of the homogenous mixture were based on a mass packing fraction of 0.58 for the fuel rubble. The maximum neutron dose rate values for the bottom outer region of the package were ~4 times as large as those of the nominal intact configuration, and the maximum neutron dose rate at the package side surface increased by a factor of ~3. For the 40-year decay time, the maximum gamma dose rate at the package bottom surface increased by a factor of ~8, and the maximum gamma dose rate at 2 m from the package bottom surface increased by a factor of ~11.The neutron and gamma dose rate profiles along the PWR package outer surfaces and the 2 m locations are shown in Figure B.26 and Figure B.27, respectively, for the 40-year decay time. This case was also analyzed for a mass packing fraction of 0.67. The neutron and gamma dose rate values based on a 0.67 mass packing fraction were within the statistical errors (i.e., 7% at the 95% confidence level) of the results based on the 0.58 mass packing fraction.

Case 10. This case represents fuel rubble from the damaged fuel rods as homogeneously distributed within the canister cavity as shown in Figure B.8 (b). This case is a bounding representation of extensive fuel damage that may cause the fuel mixture to collect into internal regions adjacent to the canister wall. The fuel mixture representation corresponds to a 0.22 mass packing fraction. The neutron and gamma dose rates significantly increased outside the package. Compared to the nominal intact configuration, the maximum neutron dose rate values were ~7, 4, and 3 times as large for the package top, radial, and bottom surfaces, respectively and ~6, 1.5, and 3 times as large at 2 m from the package top, radial, and bottom surfaces, respectively. For the 40-year decay time, the maximum gamma dose rates at the package top surface, the package bottom surface, the 2 m top locations, and the 2 m bottom locations were ~14, 7, 5, and 9 respectively, as large as those of the nominal intact configuration. The neutron and gamma dose rate profiles along the PWR package outer surfaces and the 2 m locations are shown in Figure B.28 and Figure B.29, respectively, for the 40-year decay time.

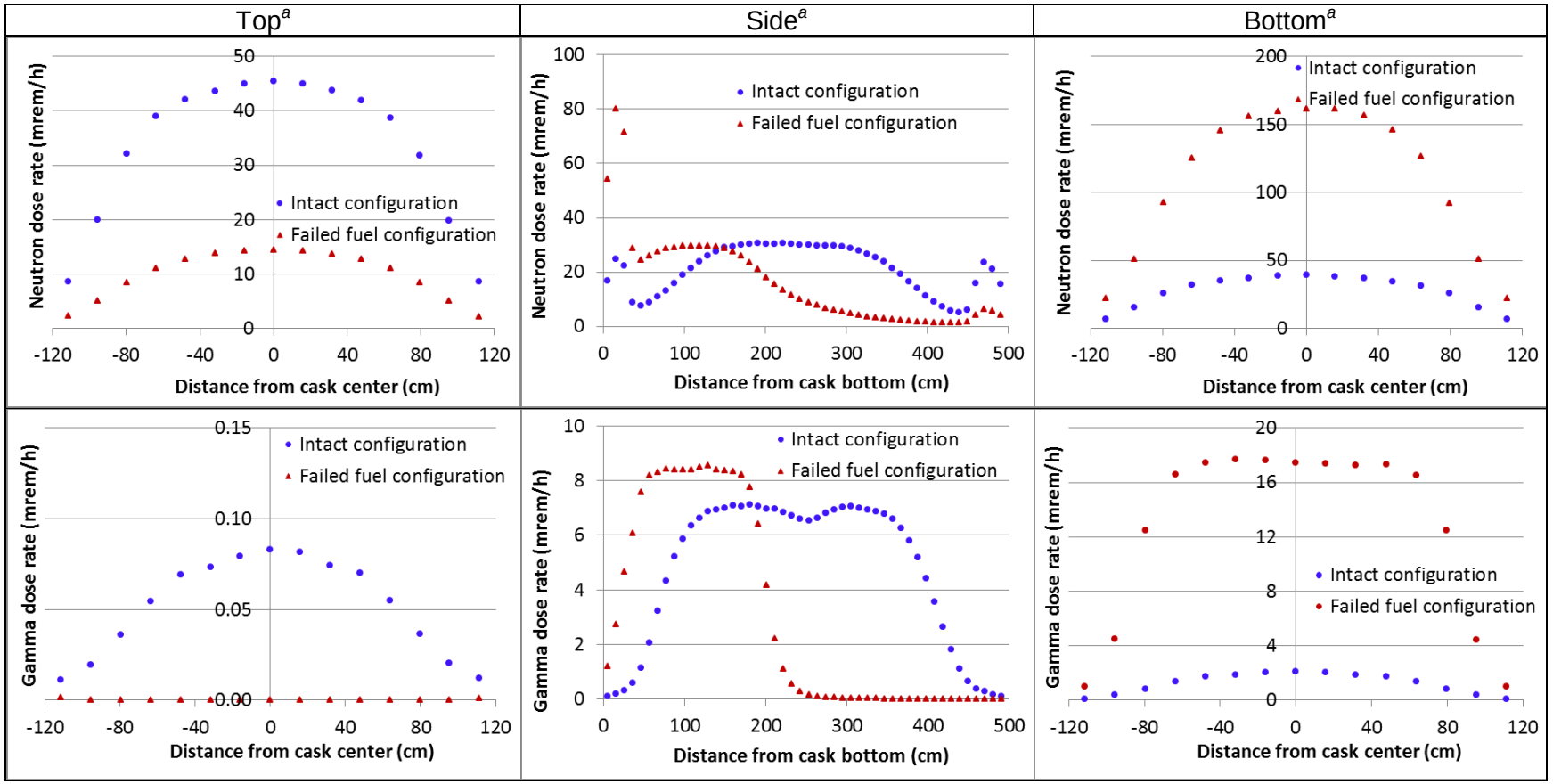

[a]PWR assemblies of 65 GWd/MTU burnup and 40-year decay time.

Figure B.26 – Comparison between dose rate values for the intact fuel configuration and the damaged SNF configuration with fuel rubble collected into canister cavity bottom—PWR package outer surfaces, NCT (Case 9)

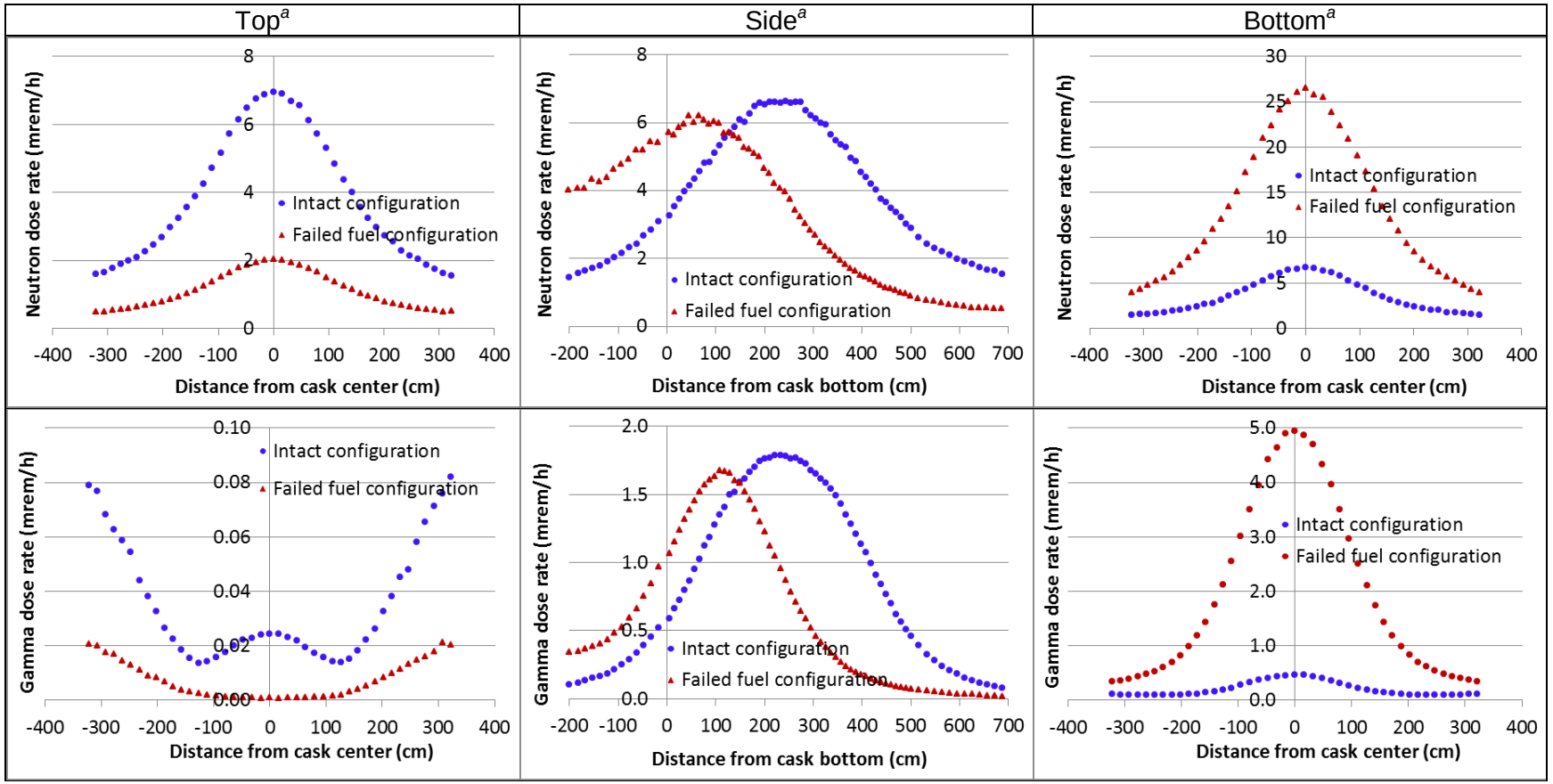

[a]PWR assemblies of 65 GWd/MTU burnup and 40-year decay time.

Figure B.27 – Comparison between dose rate values for the intact fuel configuration and the damaged SNF configuration with fuel rubble collected into canister cavity bottom—2 m locations, PWR package NCT (Case 9)

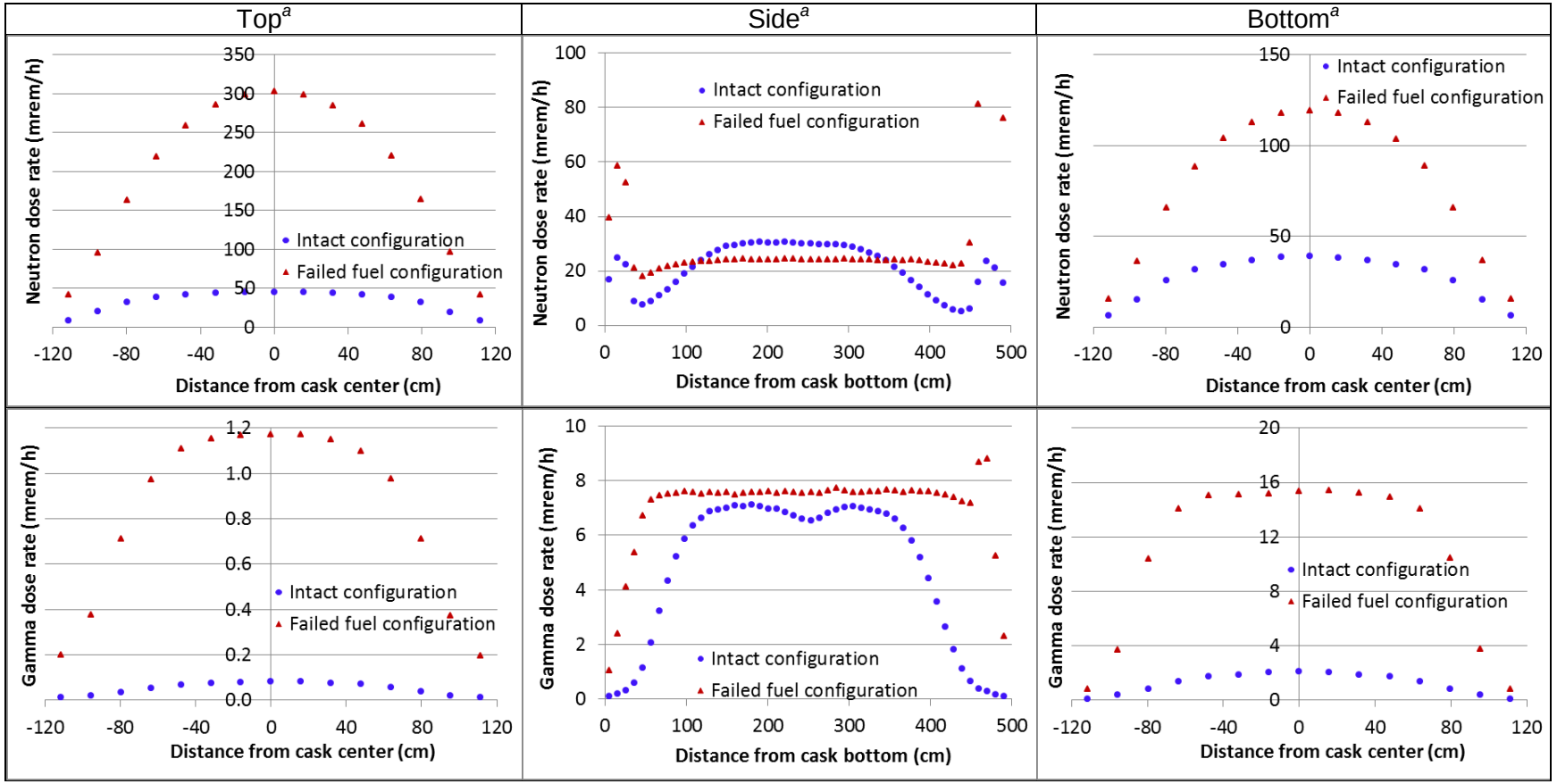

[a]PWR assemblies of 65 GWd/MTU burnup and 40-year decay time.

Figure B.28 – Comparison between dose rate values for the intact fuel configuration and the damaged SNF configuration with fuel rubble homogeneously distributed within canister cavity—PWR package outer surfaces, NCT (Case 10)

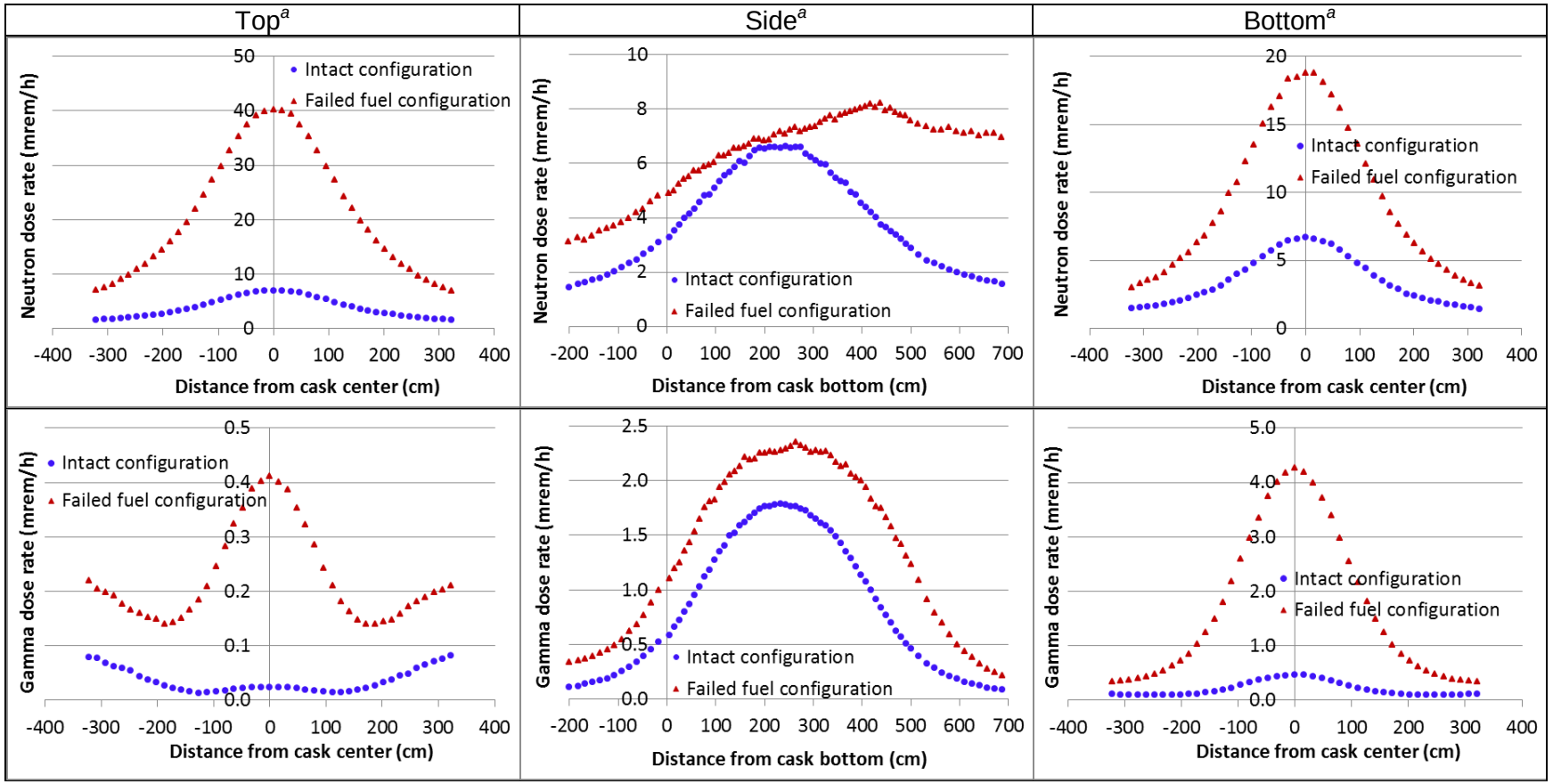

[a]PWR assemblies of 65 GWd/MTU burnup and 40-year decay time.

Figure B.29 – Comparison between dose rate values for the intact fuel configuration and the damaged SNF configuration with fuel rubble homogeneously distributed within canister cavity—2 m locations, PWR package NCT (Case 10)

Cases 11 and 12 evaluate the impact of fuel rods collapsed against the basket plates of a transportation package representative of rod/assembly deformation, and Cases 13 and 14 evaluate the impacts of fuel axial displacement. Discussions of the results are as follows:

Case 11. All the PWR assembly fuel rods in the package are represented as collapsed against the basket plates as depicted in Figure B.9 (a). The maximum neutron dose rates on the top, radial, and bottom surfaces increased by ~40%, 15%, and 20%, respectively, relative to the nominal intact configuration. A relatively small increase (~10%) of the maximum gamma dose rate was obtained for the radial surfaces. The neutron and gamma dose rate profiles along the PWR package outer surfaces and the 2 m locations are shown in Figure B.30 and Figure B.31, respectively, for the 40-year decay time.

Case 12. All the PWR assembly fuel rods in the package are represented as collapsed against the basket plates as depicted in Figure B.9 (b). The maximum neutron dose rates on the top and bottom surfaces increased by ~30% and 20%, respectively, relative to the nominal intact configuration. The neutron and gamma dose rate profiles along the PWR package outer surfaces and the 2 m locations are shown in Figure B.32 and Figure B.33, respectively, for the 40-year decay time.

Case 13. All the PWR fuel assemblies in the package are displaced toward the canister bottom, as depicted in Figure B.7 (a). Relative to the nominal intact configuration, the maximum neutron dose rate value for the package radial surface increased by ~15%; the maximum neutron and gamma dose rate values for the bottom region increased by ~35% and 70%, respectively. The neutron and gamma dose rate profiles along the PWR package outer surfaces and the 2 m locations are shown in Figure B.34 and Figure B.35, respectively, for the 40-year decay time.

Case 14. All the PWR fuel assemblies in the package are displaced toward the canister cavity top, as depicted in Figure B.7 (b). Relative to the nominal intact configuration, the maximum neutron dose rate values for the top and radial surfaces increased by ~30% and 10%, respectively. The maximum gamma dose rate values for the top surfaces increased by ~70%. The maximum gamma dose rate on the package radial surface was ~30% higher than that of the nominal intact configuration for the 5-year decay time. The neutron and gamma dose rate profiles along the PWR package outer surfaces and the 2 m locations are shown in Figure B.36 and Figure B.37, respectively, for the 40-year decay time.

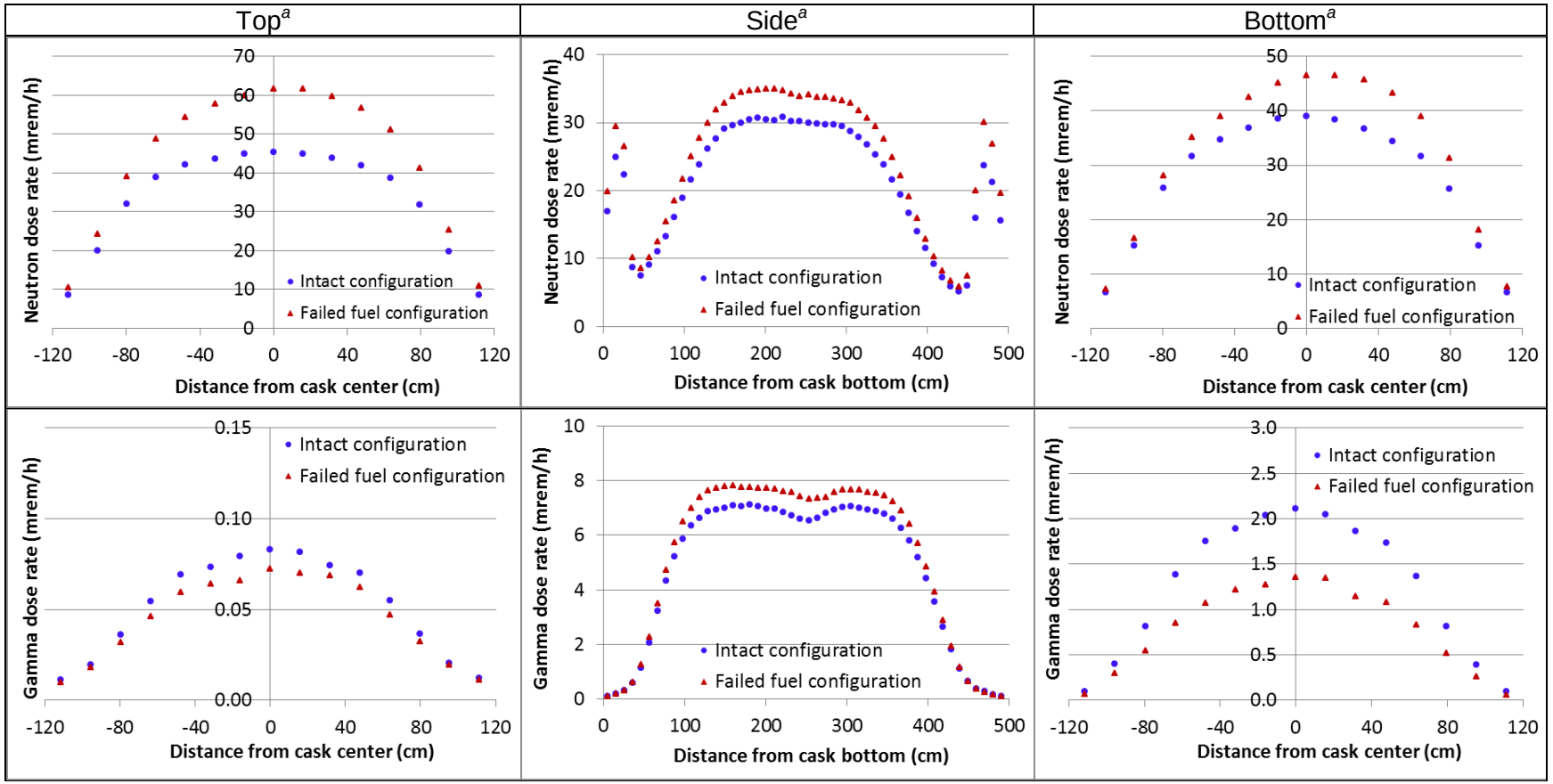

[a]PWR assemblies of 65 GWd/MTU burnup and 40-year decay time.

Figure B.30 – Comparison between dose rate values for the intact fuel configuration and the configuration assuming all fuel rods collapsed against the basket plates—PWR package outer surfaces, NCT (Case 11)

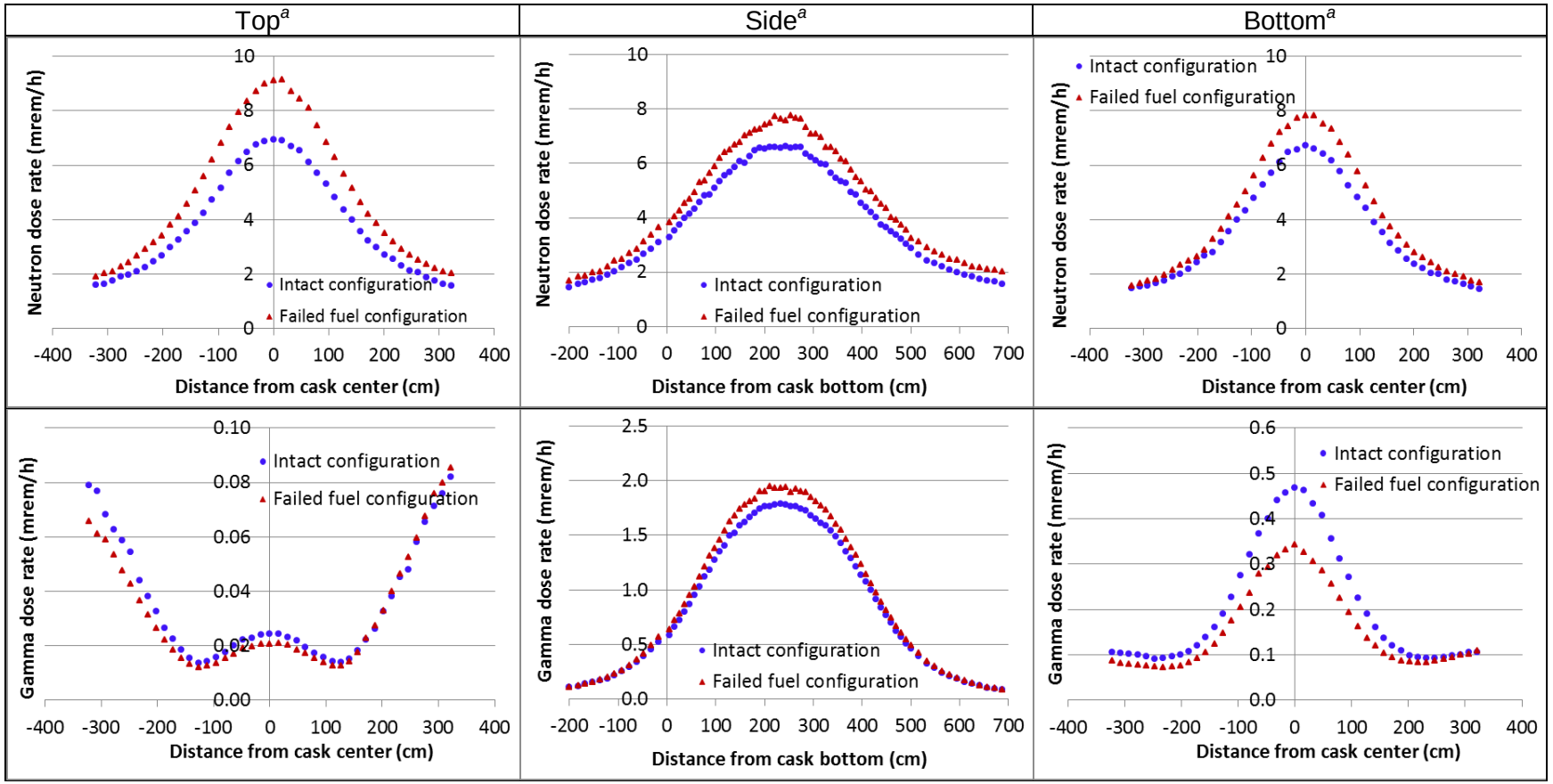

[a]PWR assemblies of 65 GWd/MTU burnup and 40-year decay time.

Figure B.31 – Comparison between dose rate values for the intact fuel configuration and the configuration assuming all fuel rods collapsed against the basket plates—2 m locations, PWR package NCT (Case 11)

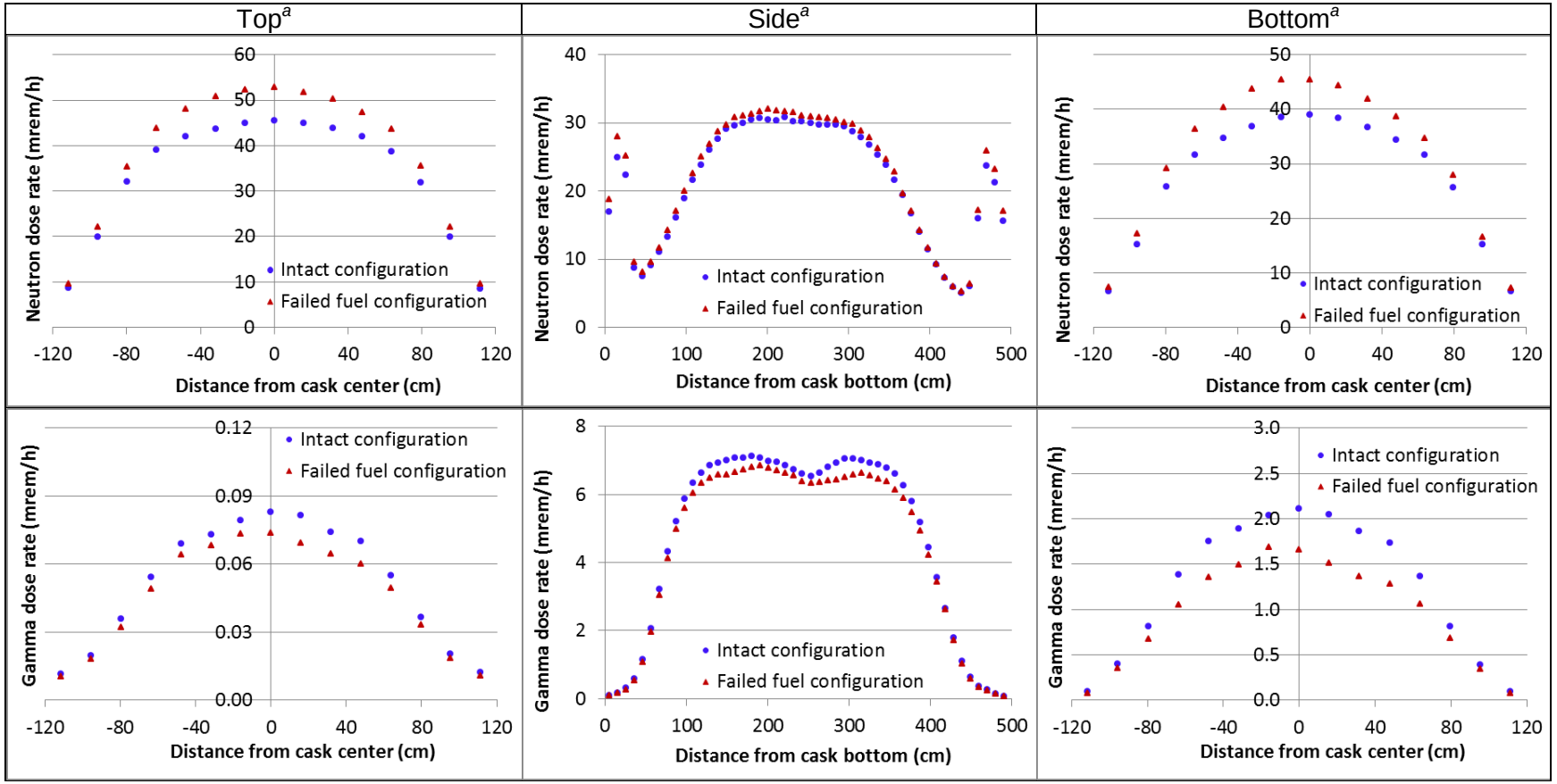

[a]PWR assemblies of 65 GWd/MTU burnup and 40-year decay time.

Figure B.32 – Comparison between dose rate values for the intact fuel configuration and the configuration assuming all fuel rods collapsed against the basket plates—PWR package outer surfaces, NCT (Case 12)

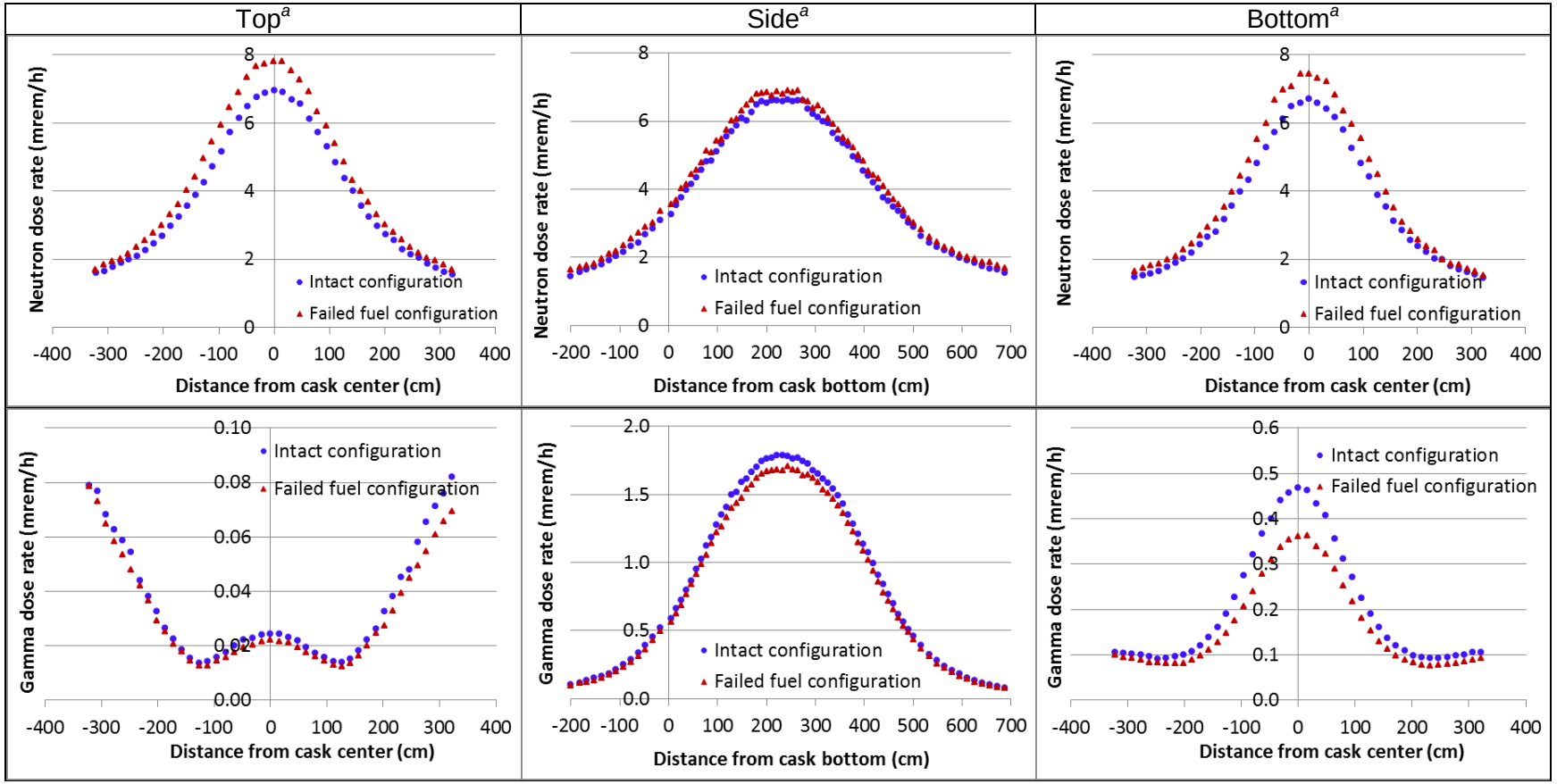

[a]PWR assemblies of 65 GWd/MTU burnup and 40-year decay time.

Figure B.33 – Comparison between dose rate values for the intact fuel configuration and the configuration assuming all fuel rods collapsed against the basket plates—2 m locations, PWR package NCT (Case 12)

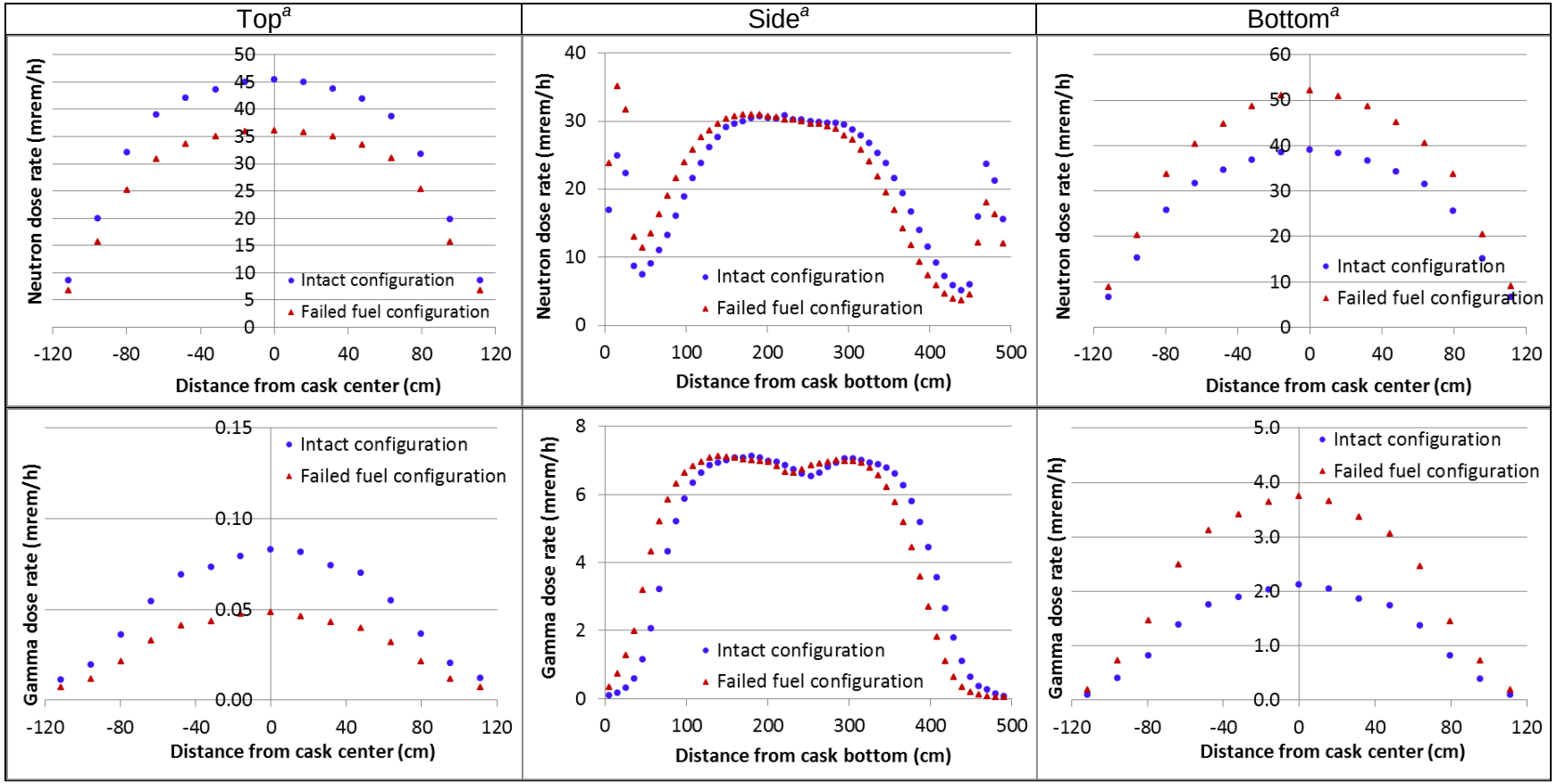

[a]PWR assemblies of 65 GWd/MTU burnup and 40-year decay time.

Figure B.34 – Comparison between dose rate values for the intact fuel configuration and the configuration assuming displacement of the fuel assemblies to canister cavity bottom—PWR package outer surfaces, NCT (Case 13)

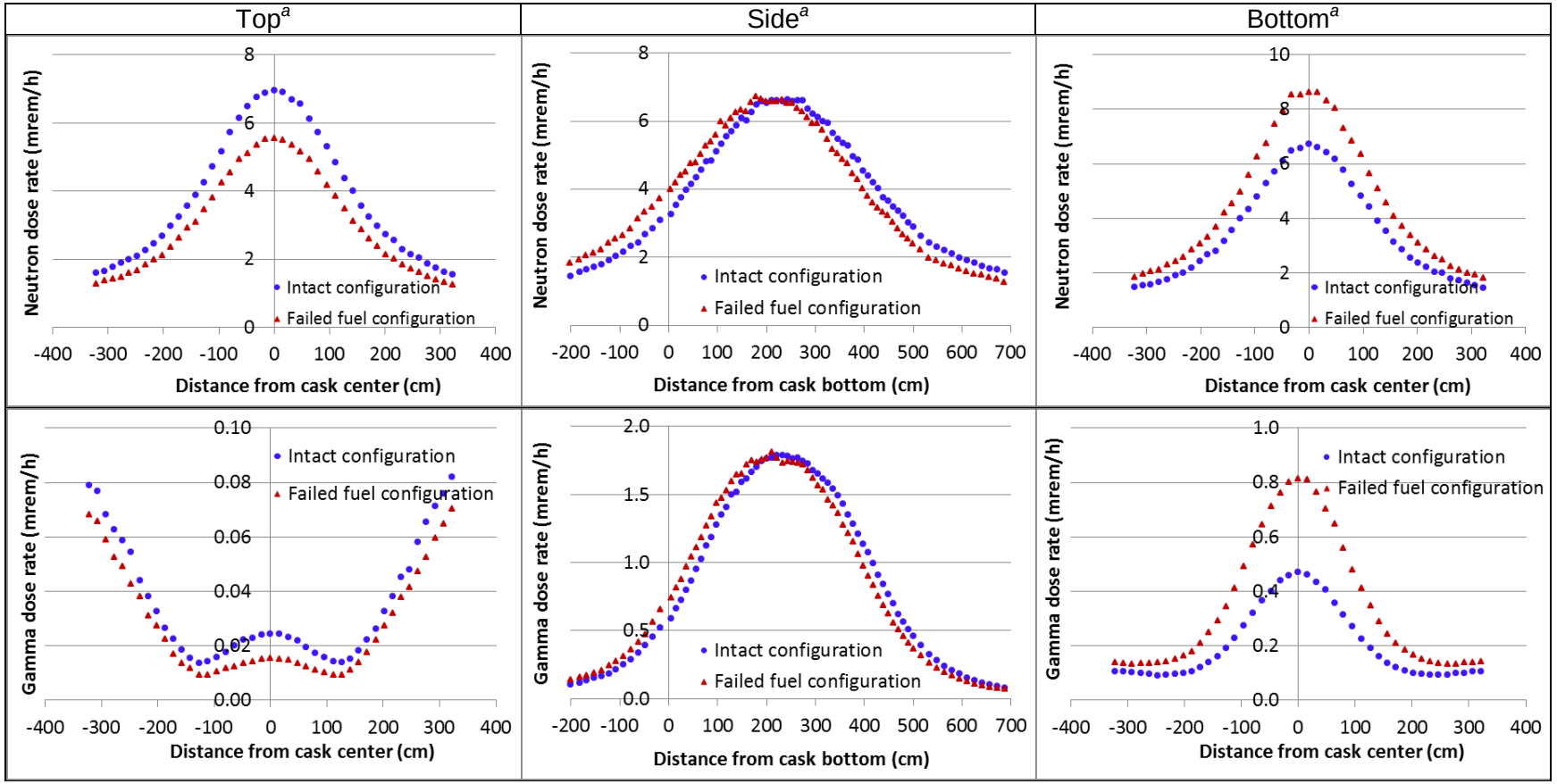

[a]PWR assemblies of 65 GWd/MTU burnup and 40-year decay time.

Figure B.35 – Comparison between dose rate values for the intact fuel configuration and the configuration assuming displacement of the fuel assemblies to canister cavity bottom—2 m locations, PWR package NCT (Case 13)

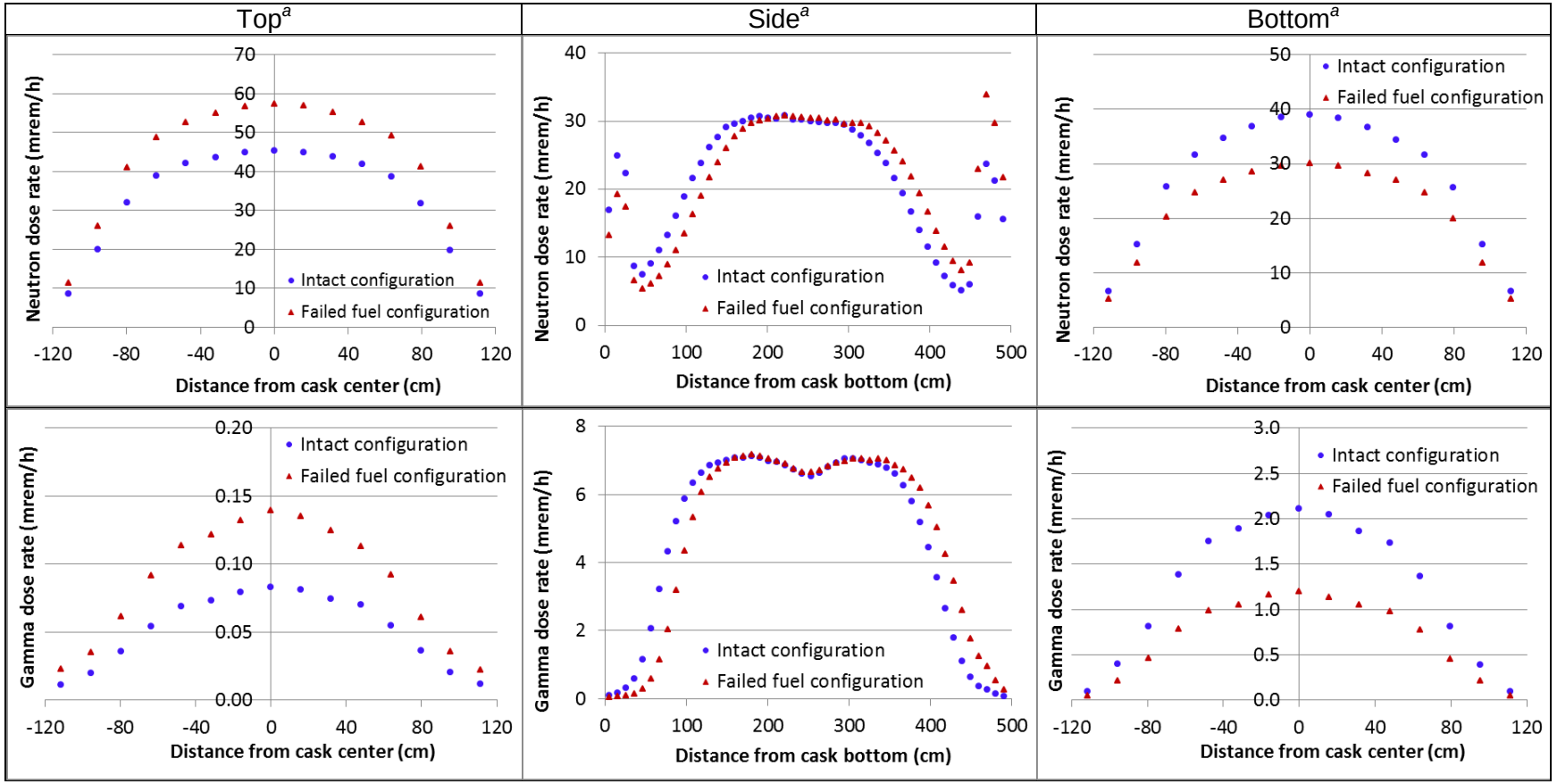

[a]PWR assemblies of 65 GWd/MTU burnup and 40-year decay time.

Figure B.36 – Comparison between dose rate values for the intact fuel configuration and the configuration assuming displacement of the fuel assemblies to canister cavity top—PWR package outer surfaces, NCT (Case 14)

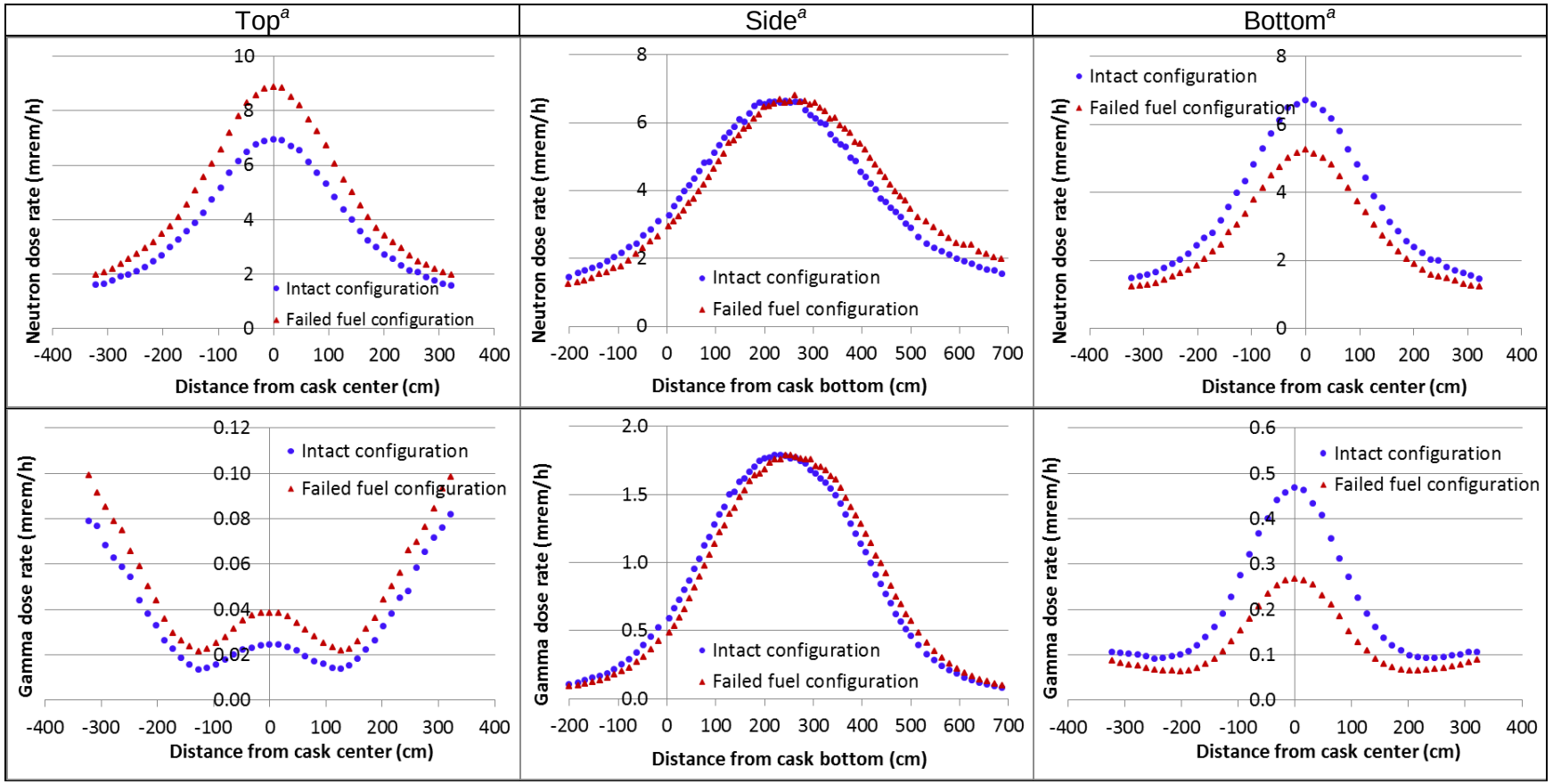

[a]PWR assemblies of 65 GWd/MTU burnup and 40-year decay time.

Figure B.37 – Comparison between dose rate values for the intact fuel configuration and the configuration assuming displacement of the fuel assemblies to canister cavity top—2 m locations, PWR package NCT (Case 14)

B.5.2 PWR Package Assuming Hypothetical Accident Conditions

For the transportation package HAC calculations, the neutron shield considered in the PWR package model for NCT was replaced with air. The ratio of the maximum surface dose rate value for each fuel reconfiguration analyzed to the maximum dose rate value for the nominal intact configuration, which is identified as F/I dose rate ratio, is summarized in Table B.5. For illustrative purposes, the radial and axial dose rate values are shown in Figure B.38 for the fuel reconfiguration assuming 10% fuel failure rate with the fuel mixture redistributed into the assembly bottom region. The values in the graphs correspond to a 40-year decay time.

The radial dose rate change relative to the nominal intact configuration was negligible for the majority of the fuel reconfigurations analyzed. The maximum increase in the radial neutron and gamma dose rates was approximately 20%. However, the neutron and gamma dose rates significantly increased at the top and bottom surfaces relative to the nominal intact configuration for most fuel reconfigurations. Relative to the nominal intact configuration, fuel damage represented with fuel rubble homogeneously distributed within the canister cavity yielded the greatest increase in the neutron dose rate at the top surface, by a factor of ~6, and fuel damage represented with fuel rubble collected into the canister cavity bottom yielded the greatest increase in the neutron dose rate at the bottom surface, by a factor of ~4. For the 5-year decay time, the maximum F/I gamma dose rate ratio values on the top and bottom surfaces were ~1.6 for assembly displacement to the canister cavity top and ~2.2 for damaged fuel represented with fuel rubble redistributed into the canister cavity bottom based on a mass packing fraction of 0.58. For the 40-year decay time, the maximum F/I gamma dose rate ratio values on the top and bottom surfaces were ~6 and 10, for damaged fuel represented with fuel rubble homogeneously distributed within the canister cavity and damaged fuel represented with fuel rubble into the canister cavity bottom, respectively.

Table B.5 – PWR package maximum dose rate change for hypothetical accident conditions

				Top	Side	Bottom	Top	Side	Bottom
Case #	**Scenario**	**Fuel relocation region[a]**	**Decay time (years)**	**F/I neutron dose rate ratio[b]**			**F/I gamma dose rate ratio[b]**		
1	10% fuel rod failure	Assembly active fuel	5	1.07	1.01	1.02	1.00	1.00	1.00
			40	1.07	1.02	1.02	0.98	0.97	0.96
2	10% fuel rod failure	Assembly lower end fitting	5	1.04	1.02	2.14	0.99	1.00	1.33
			40	1.05	1.02	2.19	1.00	0.97	4.89
3	10% fuel rod failure	Assembly plenum	5	3.35	1.02	1.03	0.98	1.00	1.01
			40	3.36	1.00	1.02	1.28	0.97	0.95
4	10% fuel rod failure	Assembly upper end fitting	5	4.12	0.99	1.13	0.93	0.97	1.01
			40	4.17	1.01	1.09	3.31	0.96	0.95
5	25% fuel rod failure	Assembly active fuel	5	1.10	1.01	0.99	0.99	1.02	0.98
			40	1.10	1.01	1.16	1.04	0.99	0.94
6	25% fuel rod failure	Assembly lower end fitting	5	1.03	1.00	2.42	1.00	0.96	1.35
			40	1.03	0.99	2.37	1.01	0.94	4.88
7	25% fuel rod failure	Assembly plenum	5	3.92	0.99	0.99	0.98	0.97	0.99
			40	3.99	0.98	0.98	2.02	1.08	1.05
8	25% fuel rod failure	Assembly upper end fitting	5	5.05	0.99	1.00	0.93	0.96	0.99
			40	5.12	0.98	0.98	4.74	1.09	1.05
9	Damaged	Canister cavity bottom	5	0.29	0.78	3.79	0.02	0.99	2.23
			40	0.29	0.80	3.82	0.26	1.05	10.19
10	Damaged	Entire canister cavity	5	5.80	0.96	2.73	1.06	1.14	1.83
			40	5.90	0.93	2.69	5.43	1.17	8.66
11	Assembly deformation	See Figure B.8 (a)	5	1.31	1.12	1.19	0.99	1.09	0.93
			40	1.30	1.13	1.17	1.04	1.06	0.66
12	Assembly deformation	See Figure B.8 (b)	5	1.13	1.04	1.13	1.00	0.94	0.95
			40	1.13	0.95	1.14	0.91	0.90	0.74
13	Alignment changes	See Figure B.9 (a)	5	0.80	0.99	1.30	0.60	1.00	1.66
			40	0.81	0.99	1.29	0.76	0.97	1.73
14	Alignment changes	See Figure B.9 (b)	5	1.25	1.01	0.79	1.57	1.00	0.60
			40	1.26	1.01	0.78	1.30	0.96	0.55

[a]See Sect. B.5.1 for case description.
[b]Relative error (at the 95% confidence level) less than 5% for all values except for the maximum gamma dose rate change for case #9, top surface, the relative error of which is 20%.

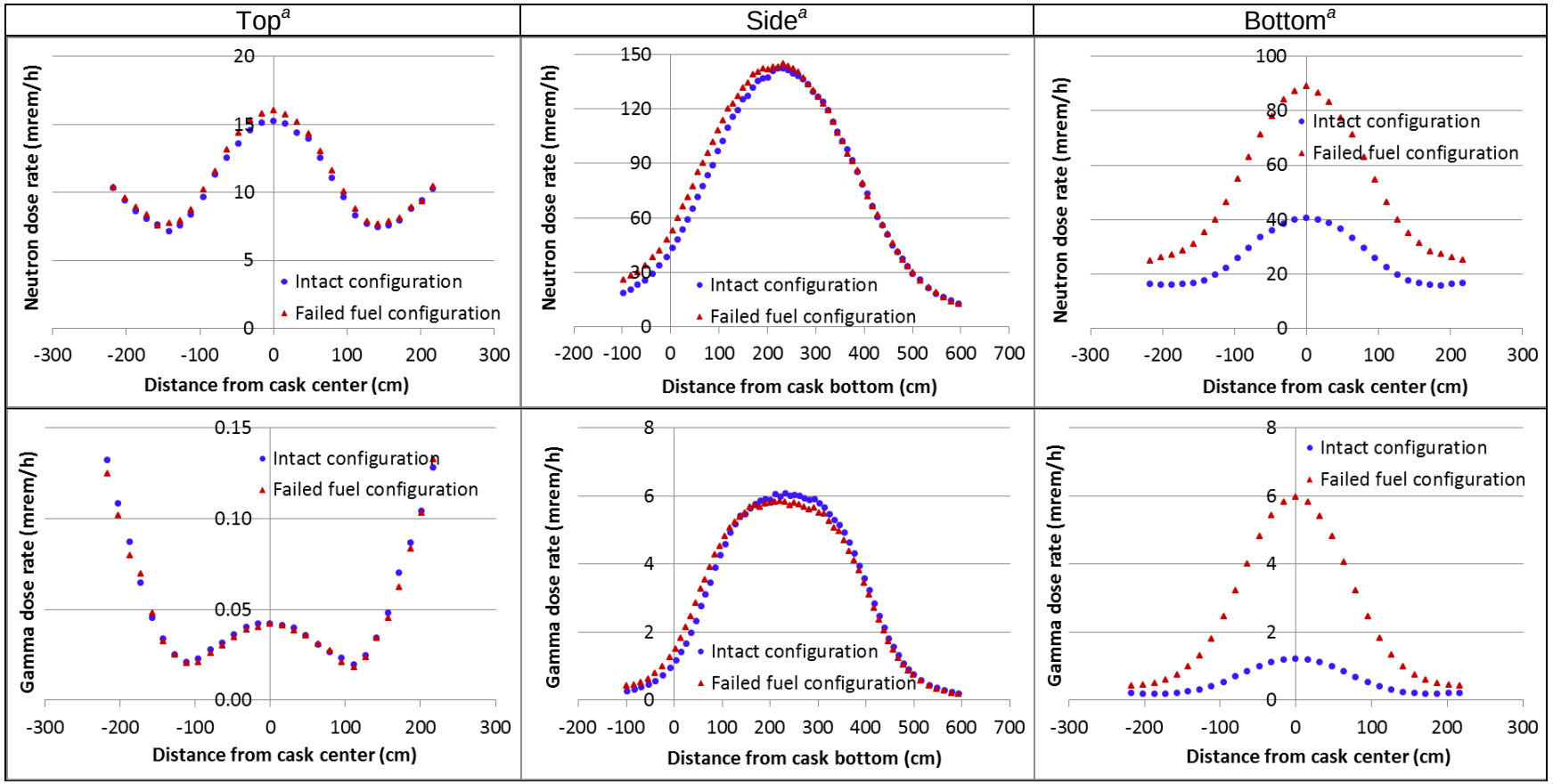

[a]BWR assemblies of 65 GWd/MTU burnup and 40-year decay time.

Figure B.38 – Dose rate comparison between the intact fuel configuration and the fuel reconfiguration assuming 10% of the fuel mixture collected into assembly bottom region—1 m from package outer surfaces, HAC

B-51

B.5.3 BWR Package Assuming Normal Conditions of Transport

The changes (F/I dose rate ratio) relative to the nominal intact fuel configuration of the maximum neutron and gamma dose rates on the BWR package external surfaces and at 2 m from the package are summarized in Table B.6 and Table B.7, respectively. The neutron and gamma dose rate profiles on the BWR package external surfaces and at 2 m from the package are shown in Figure B.39 through Figure B.56 for the 40-year decay time for each fuel reconfiguration and the nominal intact configuration for comparison.

Table B.6 – BWR package maximum dose rate change for NCT: package external surfaces

				Top	Side	Bottom	Top	Side	Bottom
Case #	**Scenario**	**Fuel relocation region[a]**	**Decay time (years)**	**F/I neutron dose rate ratio[b]**			**F/I gamma dose rate ratio[b]**		
1	11% fuel rod failure	Assembly active fuel	5	1.13	1.02	1.06	0.98	1.02	0.99
			40	1.14	1.03	1.07	1.01	1.01	0.97
2	11% fuel rod failure	Assembly lower tie plate and nosepiece	5	1.14	1.43	4.37	1.02	0.97	1.21
			40	1.14	1.42	4.44	1.00	0.97	24.39
3	11% fuel rod failure	Assembly plenum	5	12.74	1.78	1.05	1.40	0.96	0.99
			40	12.98	1.75	1.08	13.67	0.98	0.97
4	11% fuel rod failure	Assembly upper tie plate and handle	5	21.78	2.42	1.06	3.22	0.96	1.01
			40	21.77	2.41	1.07	84.60	0.99	0.98
5	Damaged	Canister cavity bottom	5	0.60	1.84	5.99	0.003	1.35	1.17
			40	0.61	1.81	6.04	0.15	1.40	32.19
6	Damaged	Entire canister cavity	5	23.48	3.27	4.31	2.90	0.98	0.94
			40	23.52	3.26	4.37	84.18	1.11	26.71
7	Assembly deformation	See Figure B.8 (a)	5	1.48	1.07	1.26	1.01	1.08	1.00
			40	1.49	1.06	1.27	1.01	1.07	0.89
8	Alignment changes	See Figure B.9 (a)	5	0.88	1.01	1.16	0.69	1.00	1.44
			40	0.89	1.01	1.17	0.71	1.01	1.54
9	Alignment changes	See Figure B.9 (b)	5	1.12	1.00	0.86	1.42	1.00	0.71
			40	1.14	1.00	0.87	1.39	1.01	0.72

[a] Farthest region for fuel relocation identified. Fuel mixture may extend into adjacent assembly axial regions, as described further in this section.
[b] Relative error (at the 95% confidence level) less than 5% for all values except for the maximum gamma dose rate change for case #5, top surface, the relative error is 20%.

Table B.7 – BWR package maximum dose rate change for NCT: 2 m from package surfaces

				Top	Side	Bottom	Top	Side	Bottom
Case #	**Scenario**	**Fuel relocation region[a]**	**Decay time (years)**	**F/I neutron dose rate ratio[b]**			**F/I gamma dose rate ratio[b]**		
1	11% fuel rod failure	Assembly active fuel	5	1.11	1.04	1.04	0.99	0.98	0.99
			40	1.11	0.98	1.03	0.98	1.00	0.99
2	11% fuel rod failure	Assembly lower tie plate and nosepiece	5	1.12	1.04	3.78	1.00	0.96	1.19
			40	1.09	1.05	3.79	1.01	1.00	19.79
3	11% fuel rod failure	Assembly plenum	5	10.62	1.03	1.04	1.44	0.96	0.99
			40	10.15	1.07	1.05	1.37	0.99	1.00
4	11% fuel rod failure	Assembly upper tie plate and handle	5	17.12	1.02	1.02	3.21	0.97	1.00
			40	16.24	1.04	1.05	4.94	0.99	1.01
5	Damaged	Canister cavity bottom	5	0.53	2.19	5.62	0.12	1.29	1.34
			40	0.52	2.01	5.57	0.46	1.24	32.09
6	Damaged	Entire canister cavity	5	25.23	1.23	3.93	3.28	0.98	1.07
			40	18.88	1.11	3.89	6.07	1.18	26.50
7	Assembly deformation	See Figure B.8 (a)	5	1.41	1.06	1.20	1.00	1.05	1.00
			40	1.37	1.04	1.19	0.96	1.05	0.89
8	Alignment changes	See Figure B.9 (a)	5	0.88	1.01	1.13	0.70	0.99	1.42
			40	0.88	1.01	1.18	0.92	1.01	1.53
9	Alignment changes	See Figure B.9 (b)	5	1.15	1.01	0.85	1.41	1.00	0.72
			40	1.14	0.97	0.87	1.08	1.02	0.75

[a]Farthest region for fuel relocation identified. Fuel mixture may extend into adjacent assembly axial regions, as described further in this section.
[b]Relative error (at the 95% confidence level) less than 7% for all values except for the maximum gamma dose rate change for case #5, top surface, the relative error is 20%.

Cases 1 to 4 evaluate the impact of 10 failed fuel rods per assembly (~11% failure rate) distributed to different axial locations. Discussions of the results are as follows:

Case 1. The redistributed fuel mixture is located from 221.1 to 260.6 cm relative to the package bottom surface. This location corresponds to the axial fuel zones 12 and 13. This fuel reconfiguration caused ~15% increase in the maximum neutron dose rate on the top surface of the package. The gamma dose rate change relative to the nominal intact configuration was negligible for all surfaces and decay times evaluated. The neutron and gamma dose rate profiles along the BWR package outer surfaces and the 2 m locations are shown in Figure B.39 and Figure B.40, respectively, for the 40-year decay time.

Case 2. The redistributed fuel mixture is located from 40 to 73.5 cm relative to the package bottom surface. This location corresponds to the assembly lower region. Relative to the nominal intact configuration, the maximum neutron dose rate at the package bottom surface increased by a factor of ~4.5. For the 40-year decay time, the maximum gamma dose rate at the package bottom surface was ~24.5 times as large as that of the nominal intact configuration. Similar effects were obtained for the maximum neutron and gamma dose rate at 2 m from the package surfaces. The neutron and gamma dose rate profiles along the BWR package outer surfaces and the 2 m locations are shown in Figure B.41 and Figure B.42, respectively, for the 40-year decay time.

Case 3. The redistributed fuel mixture is located from 427.7 to 456.2 cm relative to the package bottom surface. This location corresponds to the assembly plenum region. The maximum neutron dose rates on package top and radial surfaces were ~13 and ~2 times, respectively, as large as those of the nominal intact configuration. At 2 m from the package top surface, the maximum neutron dose rate increased by a factor of ~11. The gamma dose rate increase relative to the nominal intact configuration was small (e.g., 40% in the top outer region of the package) for the 5-year decay time. For the 40-year decay time, the maximum gamma dose rate at the package top surface increased by a factor of ~14. The neutron and gamma dose rate profiles along the BWR package outer surfaces and the 2 m locations are shown in Figure B.43 and Figure B.44, respectively, for the 40-year decay time.

Case 4. The redistributed fuel mixture is located from 456.2 to 478.5 cm relative to the package bottom surface. This location corresponds to the assembly upper tie plate and handle region. The maximum neutron dose rates on the package top and radial surfaces were ~22 and ~3 times, respectively, as large as those of the nominal intact configuration. At 2 m from the package top surface, the maximum neutron dose rate increased by a factor of ~17 relative to the nominal intact configuration. The maximum gamma dose rate increased relative to the nominal intact configuration by a factor of ~3 for the 5-year decay time. For the 40-year decay time, the maximum gamma dose rate at the package top surface increased by a factor of ~85. At 2 m from the package top surface, the maximum gamma dose rate increased by a factor of ~5. The neutron and gamma dose rate profiles along the BWR package outer surfaces and the 2 m locations are shown in Figure B.45 and Figure B.46, respectively, for the 40-year decay time.

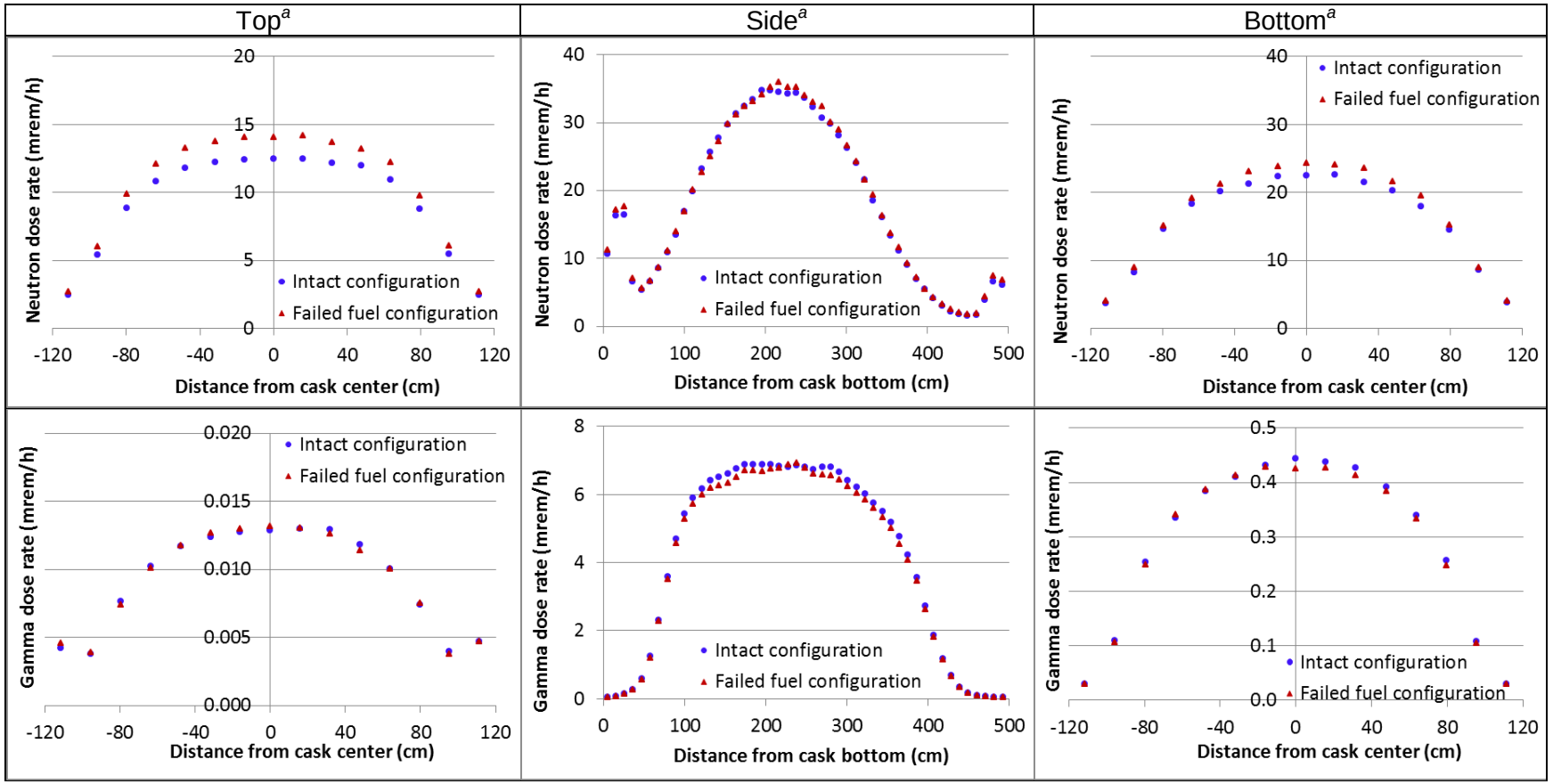

[a]BWR assemblies of 65 GWd/MTU burnup and 40-year decay time.

Figure B.39 – Dose rate comparison between the intact fuel configuration and the fuel reconfiguration assuming 11% of the fuel mixture collected into the free void volume of two axial fuel zones—BWR package outer surfaces, NCT (Case 1)

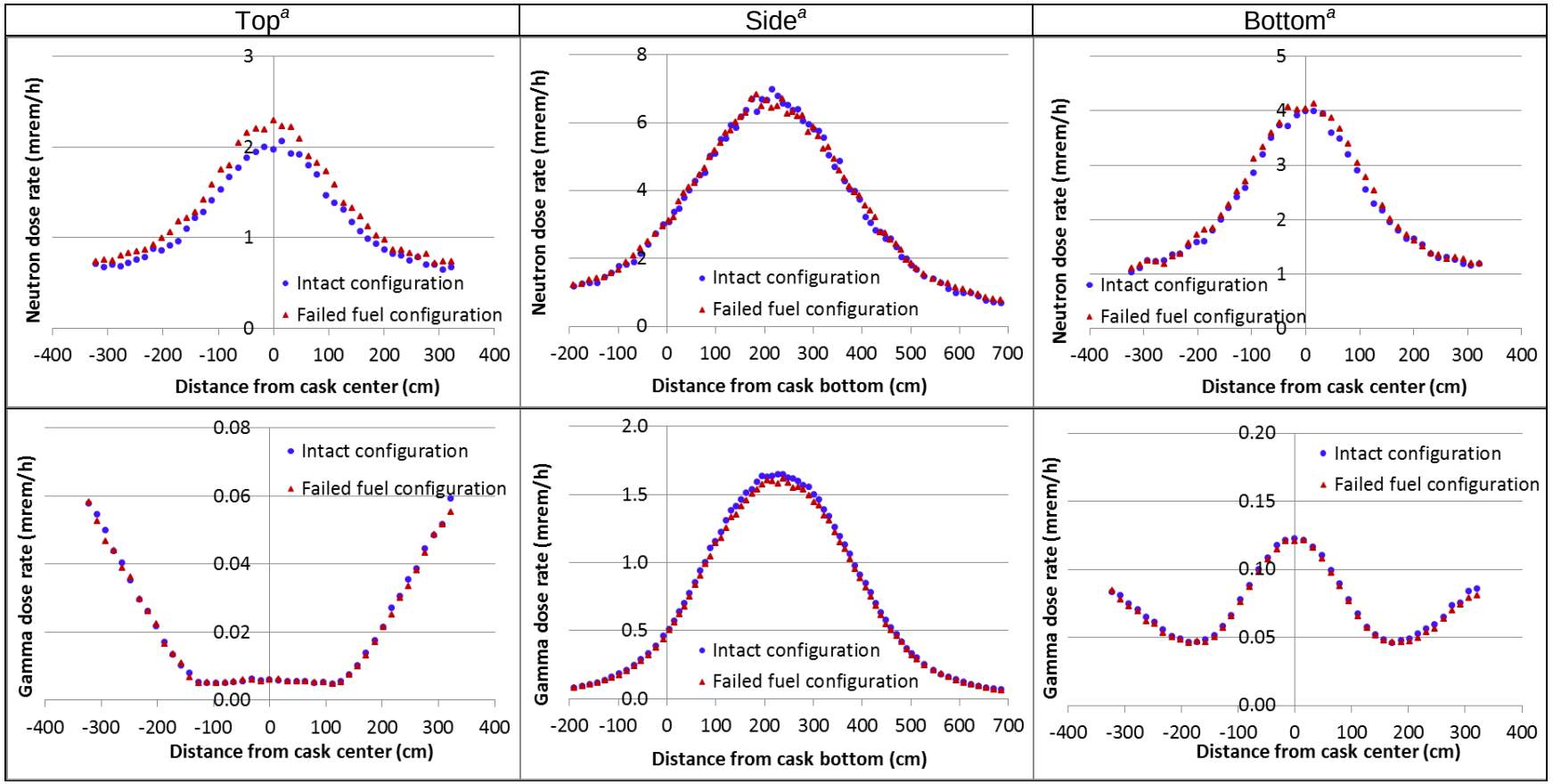

[a]BWR assemblies of 65 GWd/MTU burnup and 40-year decay time.

Figure B.40 – Dose rate comparison between the intact fuel configuration and the fuel reconfiguration assuming 11% of the fuel mixture collected into the free void volume of two axial fuel zones—2 m locations, BWR package NCT (Case 1)

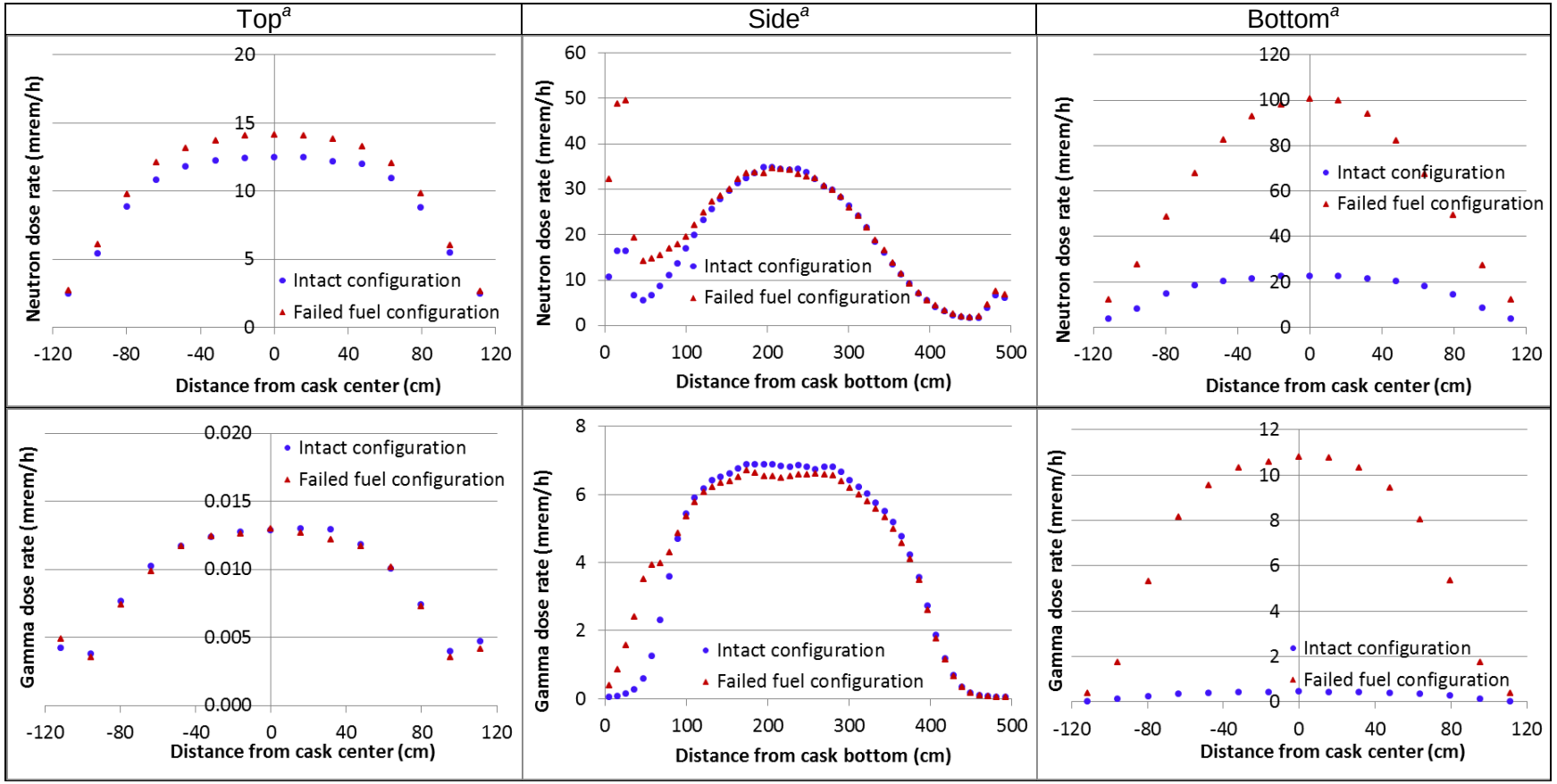

[a]BWR assemblies of 65 GWd/MTU burnup and 40-year decay time.

Figure B.41 – Dose rate comparison between the intact fuel configuration and the fuel reconfiguration assuming 11% of the fuel mixture collected into assembly lower region—BWR package outer surfaces, NCT (Case 2)

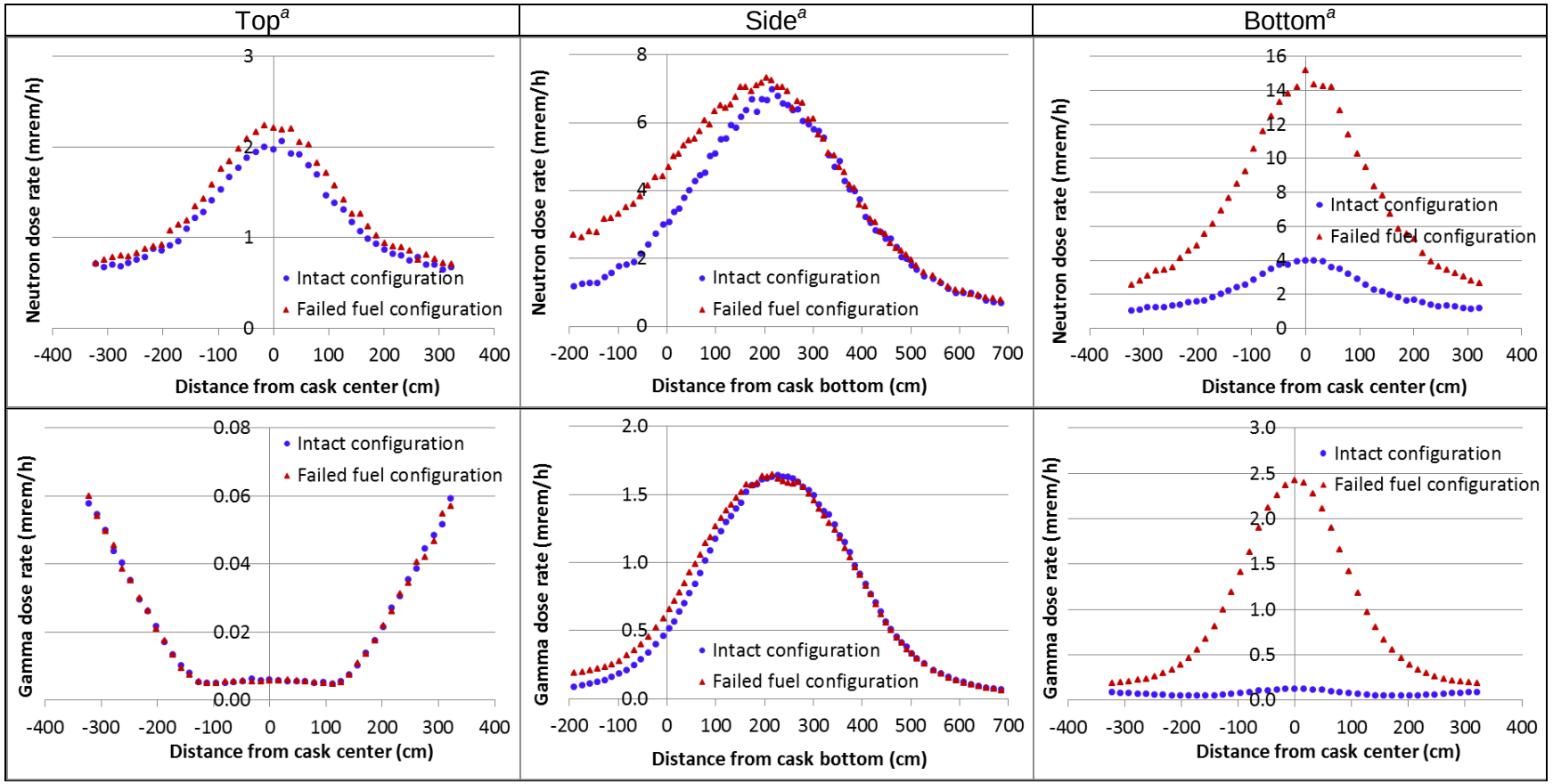

[a]BWR assemblies of 65 GWd/MTU burnup and 40-year decay time.

Figure B.42 – Dose rate comparison between the intact fuel configuration and the fuel reconfiguration assuming 11% of the fuel mixture collected into assembly lower region—2 m locations, BWR package NCT (Case 2)

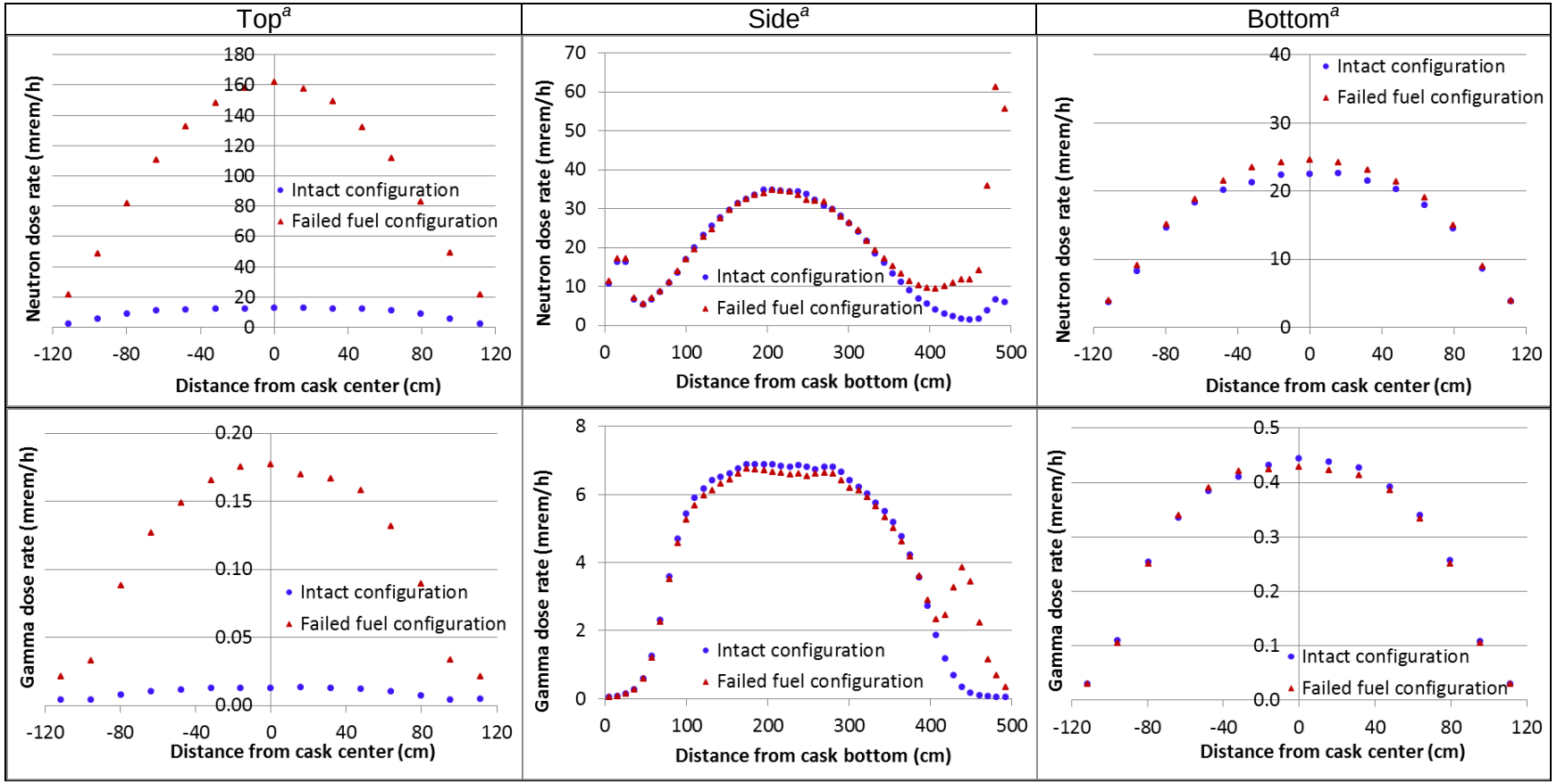

[a]BWR assemblies of 65 GWd/MTU burnup and 40-year decay time.

Figure B.43 – Dose rate comparison between the intact fuel configuration and the fuel reconfiguration assuming 11% of the fuel mixture collected into assembly plenum region—BWR package outer surfaces, NCT (Case 3)

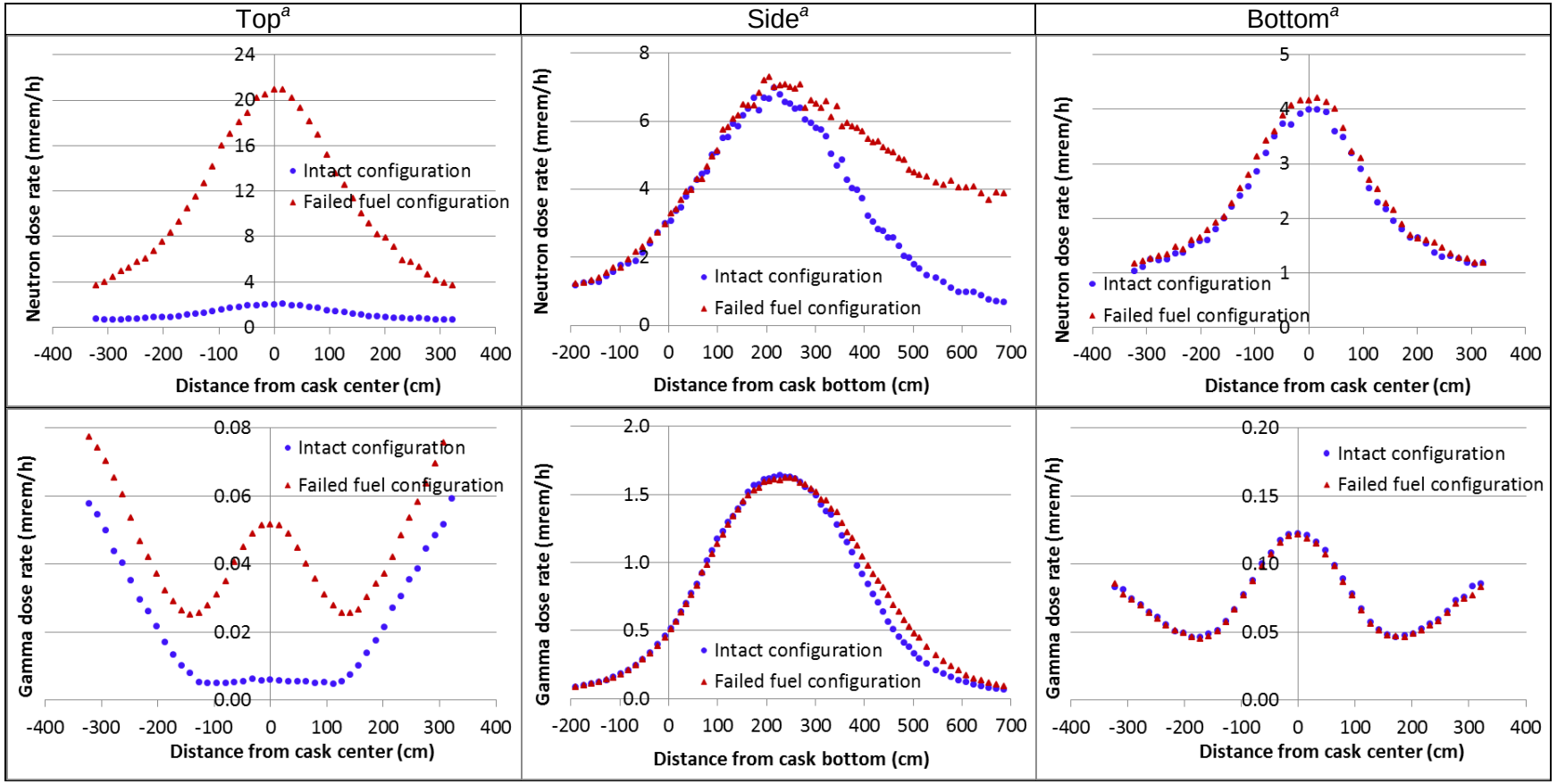

[a]BWR assemblies of 65 GWd/MTU burnup and 40-year decay time.

Figure B.44 – Dose rate comparison between the intact fuel configuration and the fuel reconfiguration assuming 11% of the fuel mixture collected into assembly plenum region—2 m locations, BWR package NCT (Case 3)

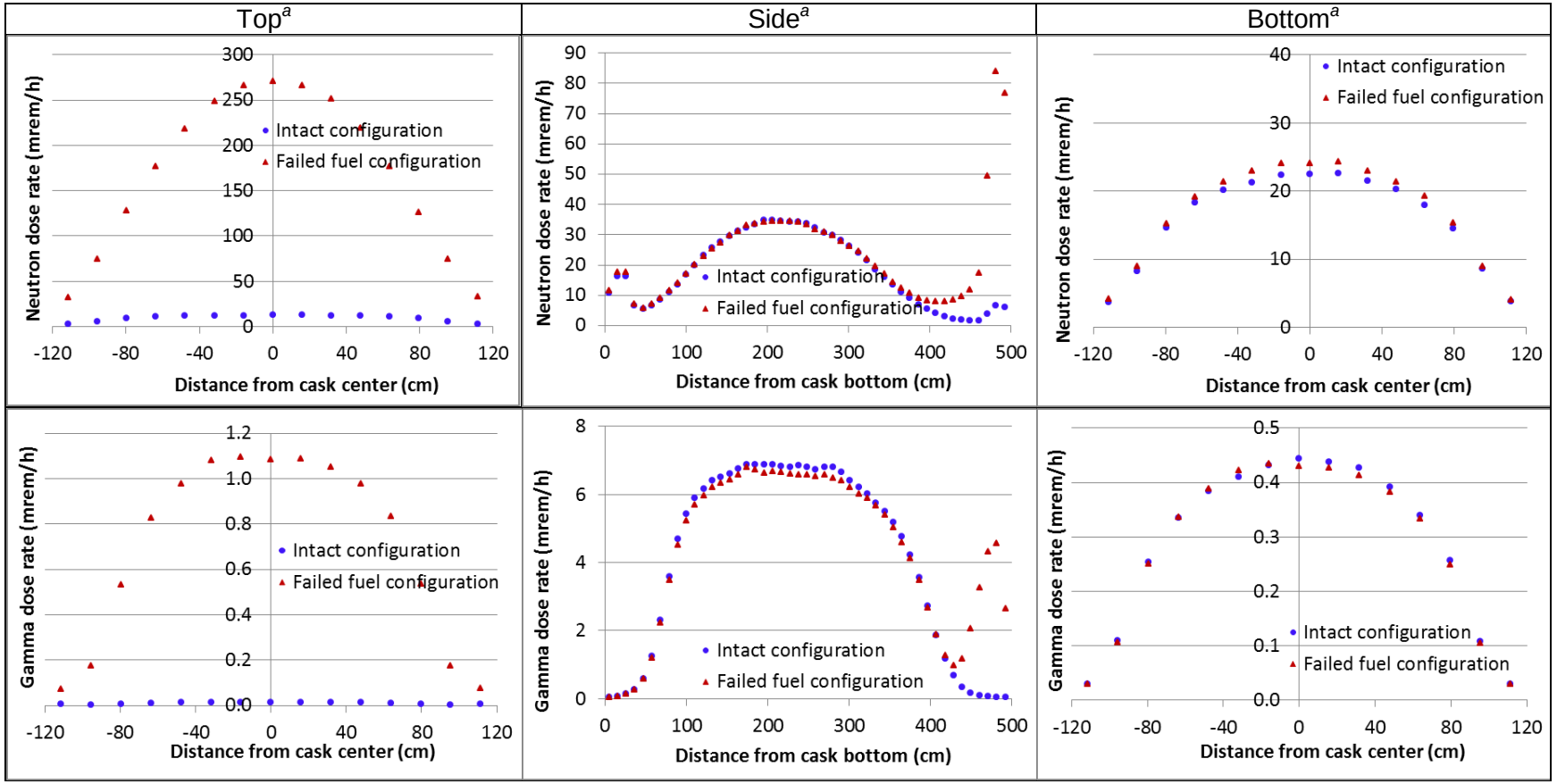

[a]BWR assemblies of 65 GWd/MTU burnup and 40-year decay time.

Figure B.45 – Dose rate comparison between the intact fuel configuration and the fuel reconfiguration assuming 11% of the fuel mixture collected into assembly top region—BWR package outer surfaces, NCT (Case 4)

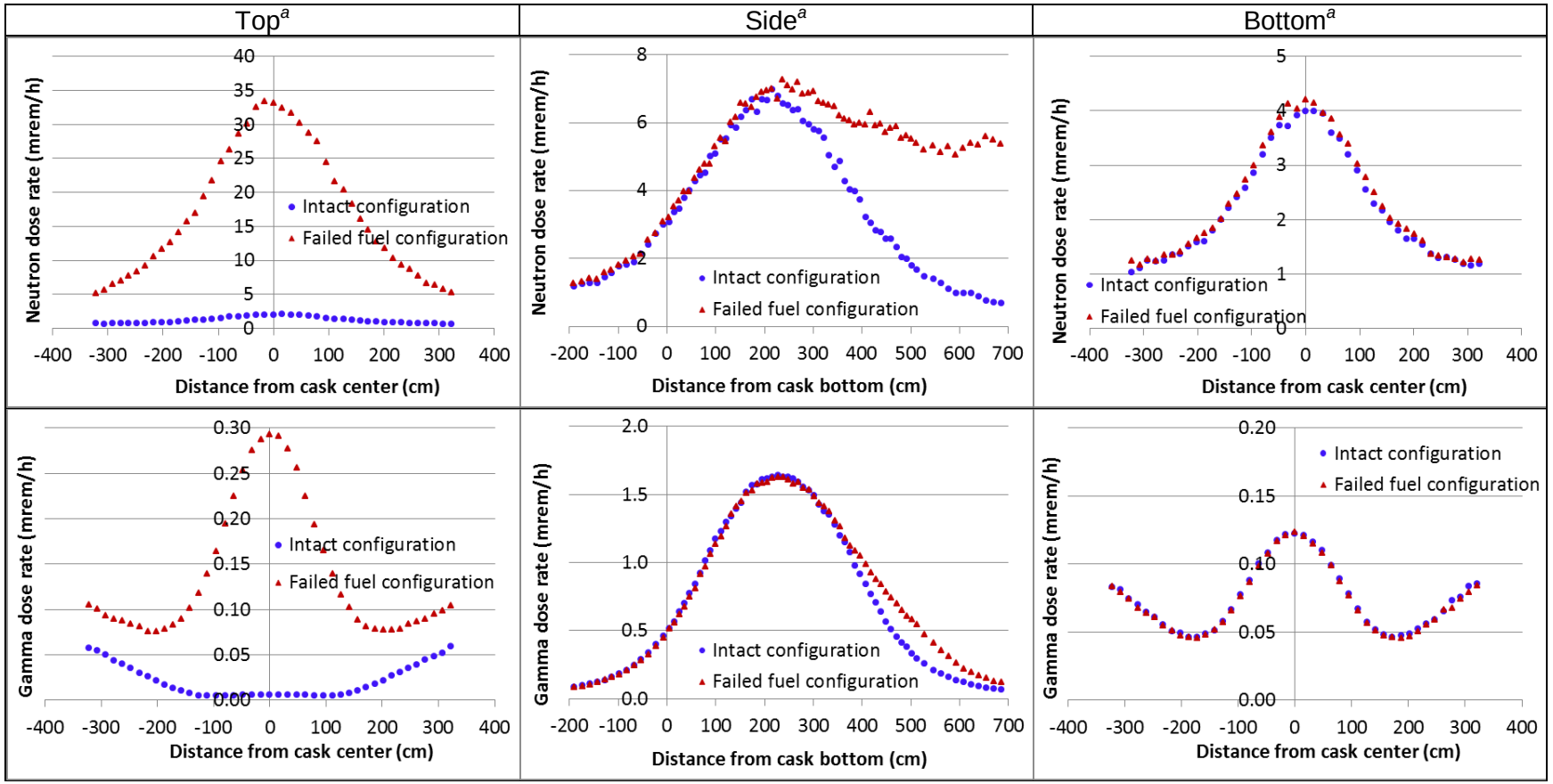

[a]BWR assemblies of 65 GWd/MTU burnup and 40-year decay time.

Figure B.46 – Dose rate comparison between the intact fuel configuration and the fuel reconfiguration assuming 11% of the fuel mixture collected into assembly top region—2 m locations, BWR package NCT (Case 4)

Cases 5 and 6 evaluate the impact of extensive cladding failure representative of damaged fuel, where the fuel mixture is represented as collecting into the internal regions adjacent to the canister wall such as the space between the outer basket plates and canister wall. Discussions of the results are as follows:

Case 5. This case represents fuel rubble from the damaged fuel rods being axially located from 30 to 212 cm relative to the package bottom surface, as shown in Figure B.7 (a). The maximum neutron dose rate values for the bottom outer region of the package were ~6 times as large as those of the nominal intact configuration. The maximum neutron dose rate at the package radial surface increased by a factor of ~2. For the 40-year decay time, the maximum gamma dose rate values for the bottom outer region of the package increased by a factor of ~32. The maximum gamma dose rate values for the outer radial region of the package were higher by ~40% than those of the nominal intact configuration. The neutron and gamma dose rate profiles along the BWR package outer surfaces and the 2 m locations are shown in Figure B.47 and Figure B.48, respectively, for the 40-year decay time.

Case 6. This case represents fuel rubble from the damaged fuel rods as homogeneously distributed within the canister cavity, as shown in Figure B.7 (b). This case is a bounding representation of extensive fuel damage that may cause the fuel mixture to collect into internal regions adjacent to the canister wall. The fuel mixture representation corresponds to a 0.23 mass packing fraction. The neutron and gamma dose rates significantly increased outside the package. Compared to the nominal intact configuration, the maximum neutron dose rate values were ~24, 3.5, and 4.5 times as large for the package top, radial, and bottom surfaces, respectively, and ~25, 1.5, and 4 times as large at 2 m from the package top, radial, and bottom surfaces, respectively. For the 40-year decay time, the maximum gamma dose rate at the package top surface, package bottom surface, the 2 m top locations, and the 2 m bottom locations were ~84, 27, 6 and 27 respectively, as large as those of the nominal intact configuration. For the 5-year decay time, the maximum gamma dose rate values for the top outer region of the package increased by a factor of ~3. The neutron and gamma dose rate profiles along the BWR package outer surfaces and the 2 m locations are shown in Figure B.49 and Figure B.50, respectively, for the 40-year decay time.

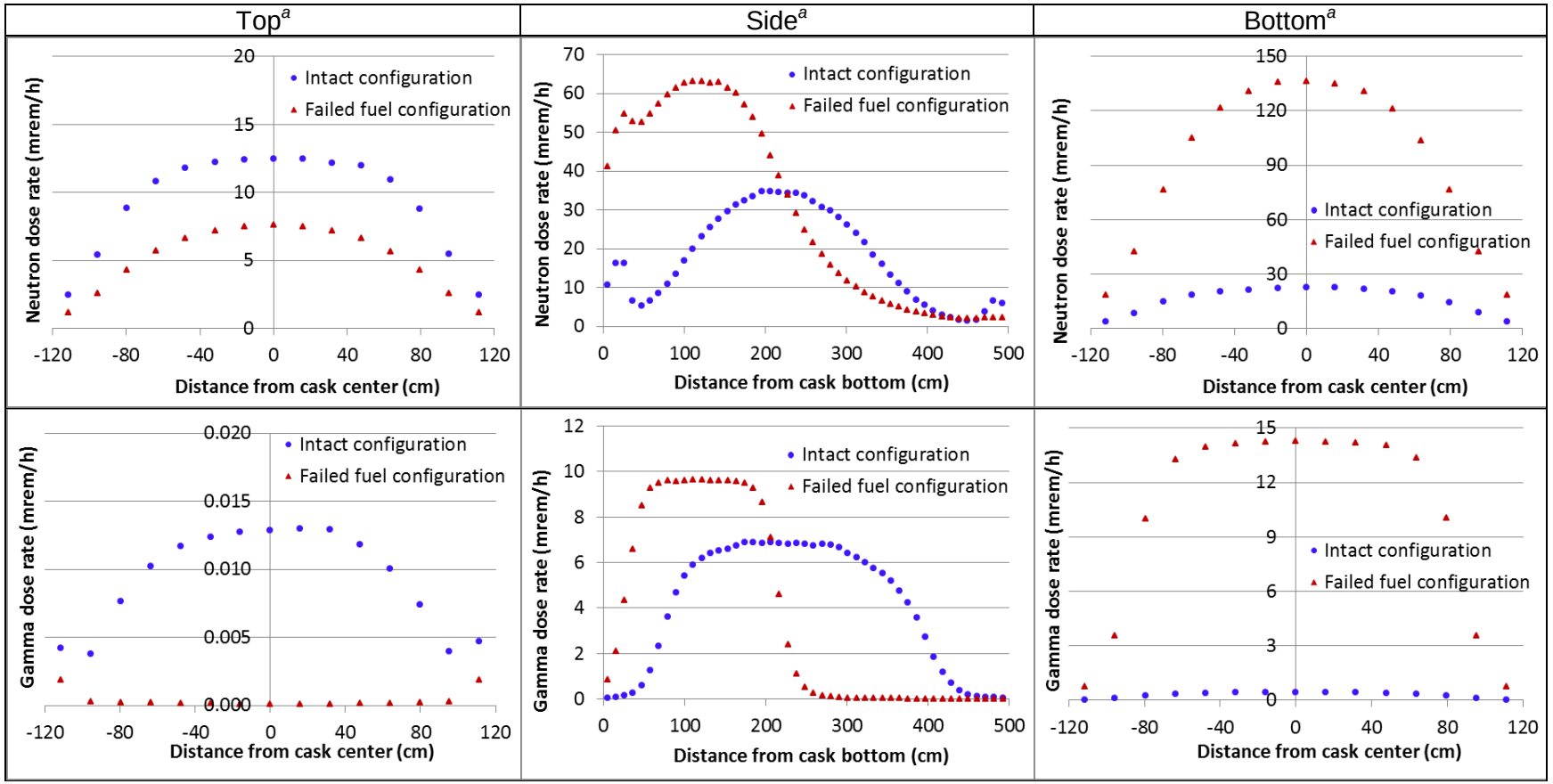

[a]BWR assemblies of 65 GWd/MTU burnup and 40-year decay time.

Figure B.47 – Comparison between package dose rate values for the intact fuel configuration and the damaged SNF configuration with fuel rubble collected into canister cavity bottom—BWR package outer surfaces, NCT (Case 5)

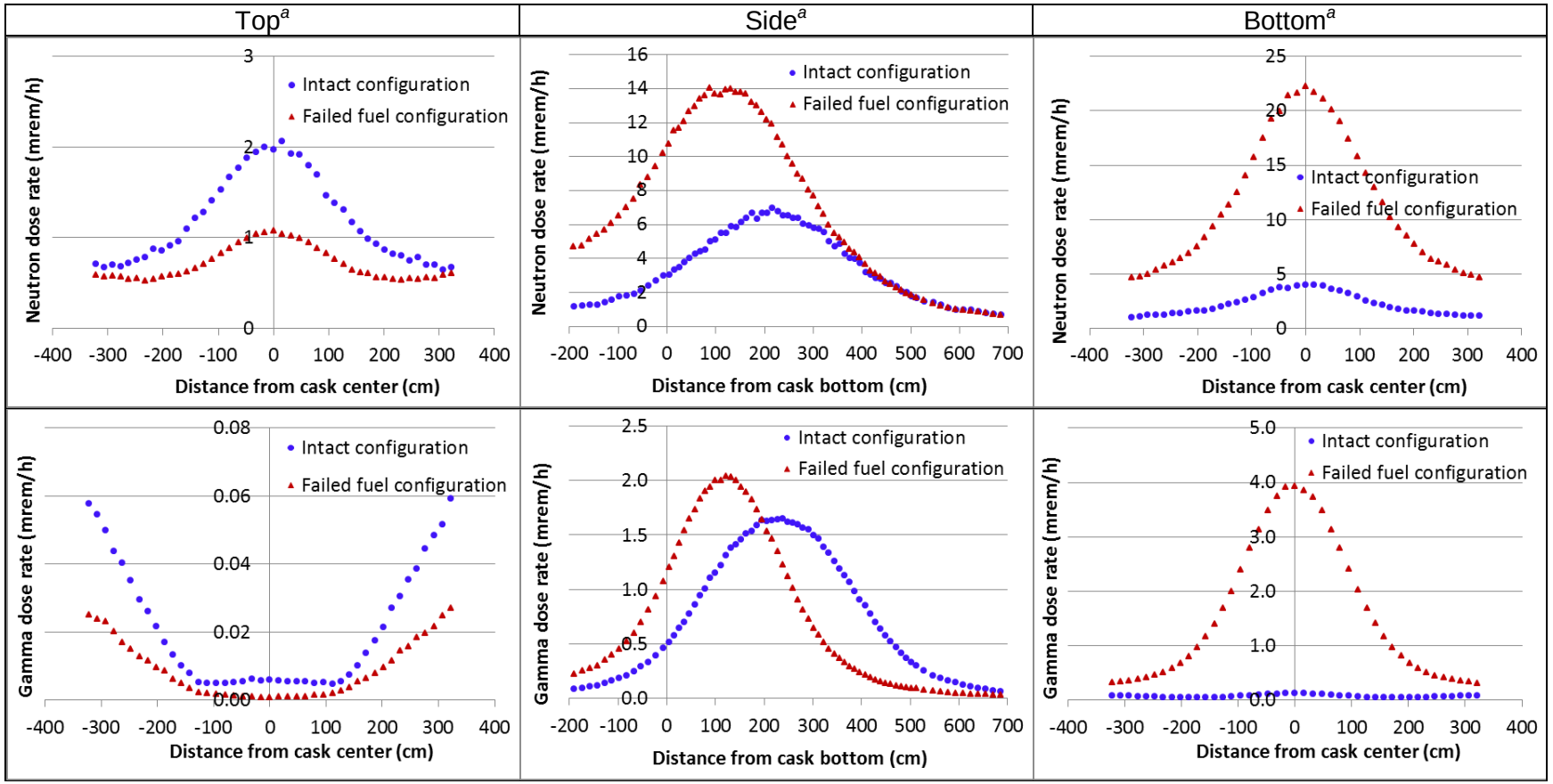

[a]BWR assemblies of 65 GWd/MTU burnup and 40-year decay time.

Figure B.48 – Comparison between package dose rate values for the intact fuel configuration and the damaged SNF configuration with fuel rubble collected into canister cavity bottom—2 m locations, BWR package NCT (Case 5)

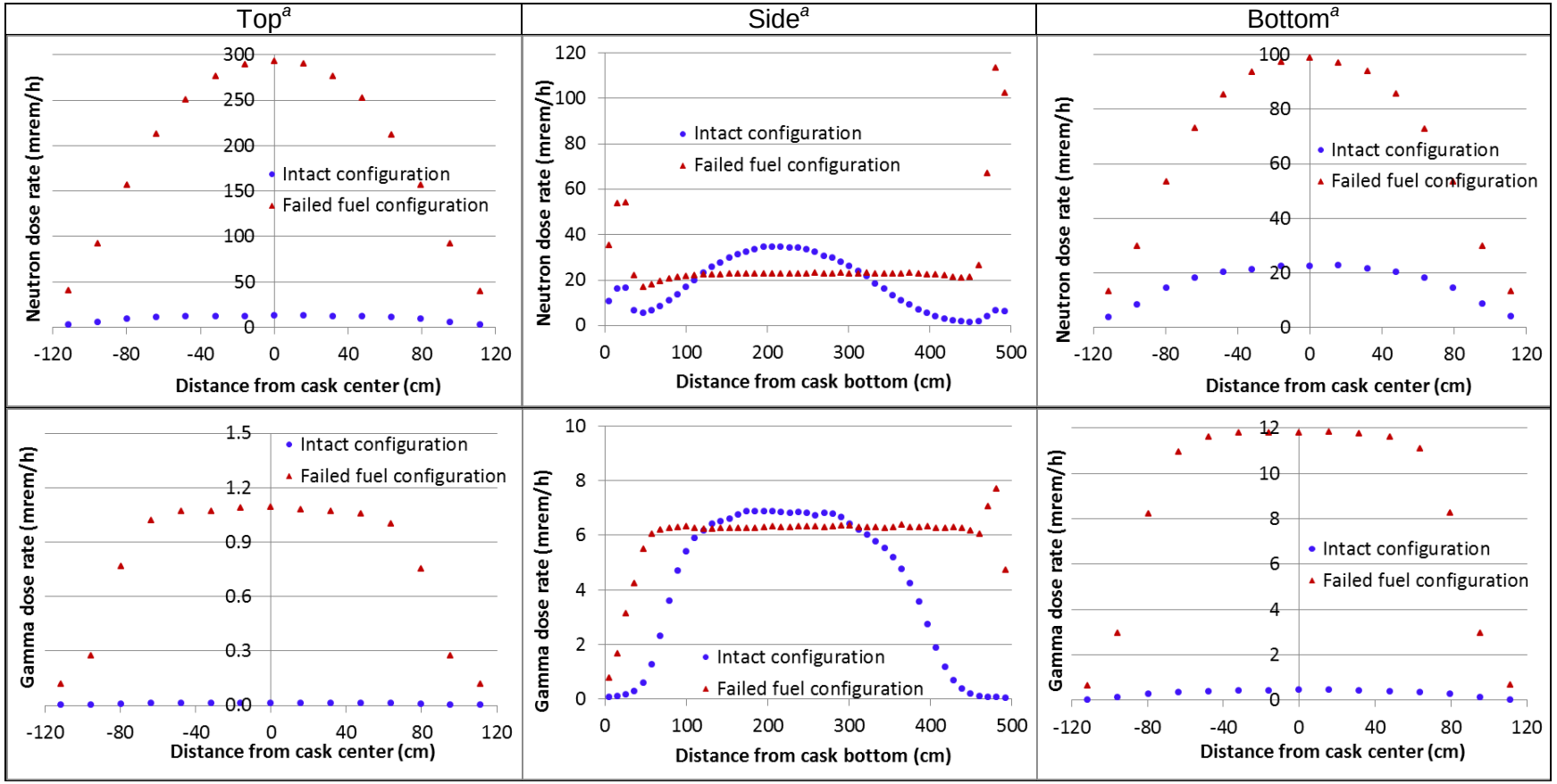

[a]BWR assemblies of 65 GWd/MTU burnup and 40-year decay time.

Figure B.49 – Comparison between package dose rate values for the intact fuel configuration and the damaged SNF configuration with fuel rubble homogeneously distributed within canister cavity—BWR package outer surfaces, NCT (Case 6)

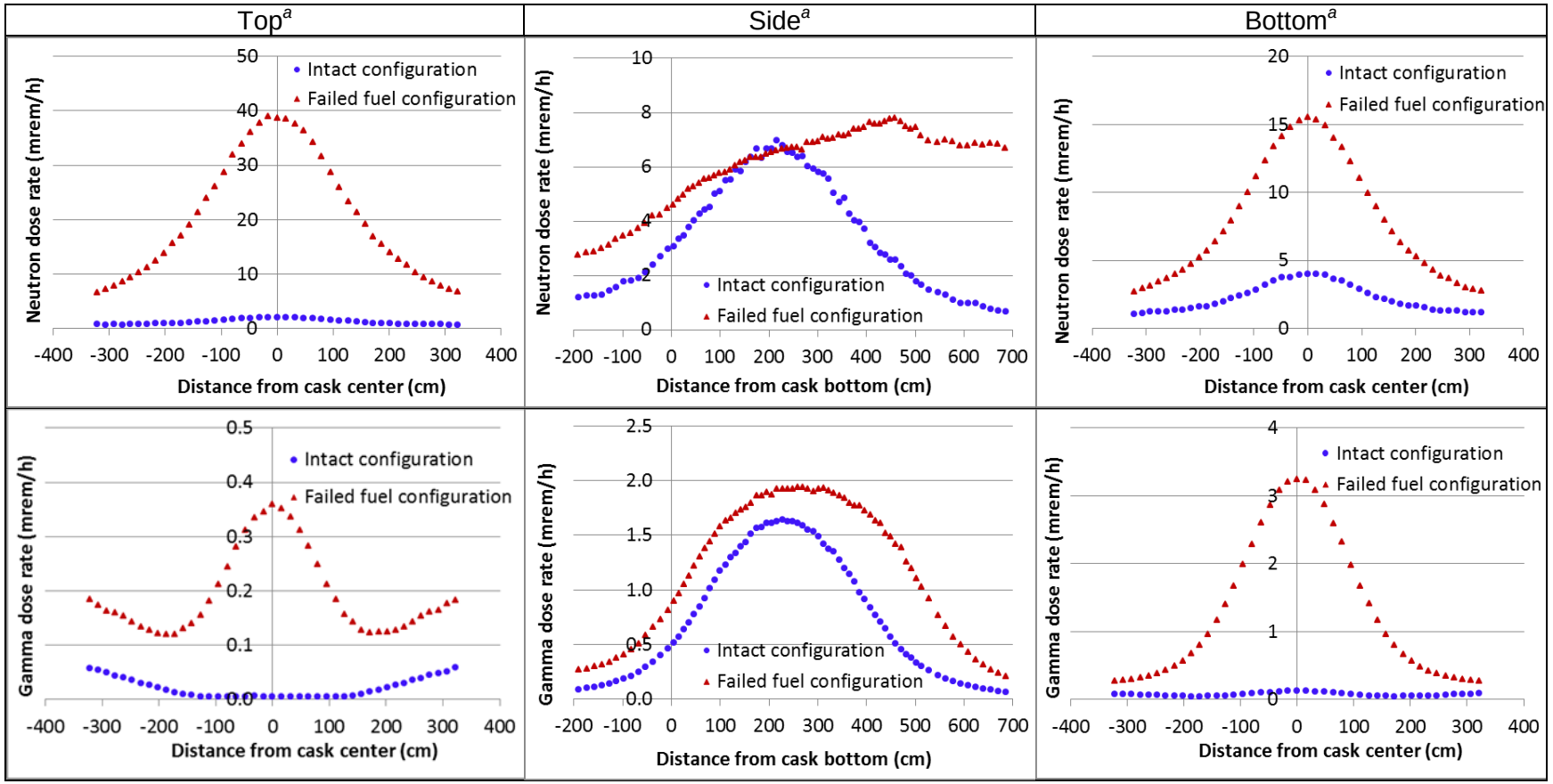

[a]BWR assemblies of 65 GWd/MTU burnup and 40-year decay time.

Figure B.50 – Comparison between package dose rate values for the intact fuel configuration and the damaged SNF configuration with fuel rubble homogeneously distributed within canister cavity—2 m locations, BWR package NCT (Case 6)

Case 7 evaluates the impact of fuel rods collapsed against the basket plates of a transportation package representative of rod/assembly deformation, and Cases 8 and 9 evaluate the impacts of fuel axial displacement. Discussions of the results are as follows:

Case 7. All the BWR assembly fuel rods in the package are represented as collapsed against the basket plates as depicted in Figure B.8 (a) for the PWR fuel. The maximum neutron dose rate increase of ~10%, 50%, and 30% relative to the nominal intact configuration was obtained for the radial, top, and bottom surfaces, respectively. A relatively small increase of 10% in the maximum gamma dose rate was obtained for the package outer radial region. The neutron and gamma dose rate profiles along the BWR package outer surfaces and the 2 m locations are shown in Figure B.51 and Figure B.52, respectively, for the 40-year decay time.

Case 8. All the BWR fuel assemblies in the package are displaced toward the canister bottom, as shown in Figure B.9 (a) for the PWR fuel. The maximum neutron and gamma dose rate values for the package bottom surface increased by ~20% and 50%, respectively, relative to the nominal intact configuration. Similar increase percentages were obtained for the 2 m bottom locations. The neutron and gamma dose rate profiles along the BWR package outer surfaces and the 2 m locations are shown in Figure B.53 and Figure B.54, respectively, for the 40-year decay time.

Case 9. All the BWR fuel assemblies in the package are displaced toward the canister top, as shown in Figure B.9 (b) for the PWR fuel. The maximum neutron dose rate values for the top outer region of the top increased by ~15% relative to the nominal intact configuration. The maximum gamma dose rate on the package top surface was ~40% higher than that of the nominal intact configuration for the 5- and 40-year decay times. Similar gamma dose rate increase percentage was obtained for the 2 m top locations and 5-year decay time. The neutron and gamma dose rate profiles along the BWR package outer surfaces and the 2 m locations are shown in Figure B.55 and Figure B.56, respectively, for the 40-year decay time.

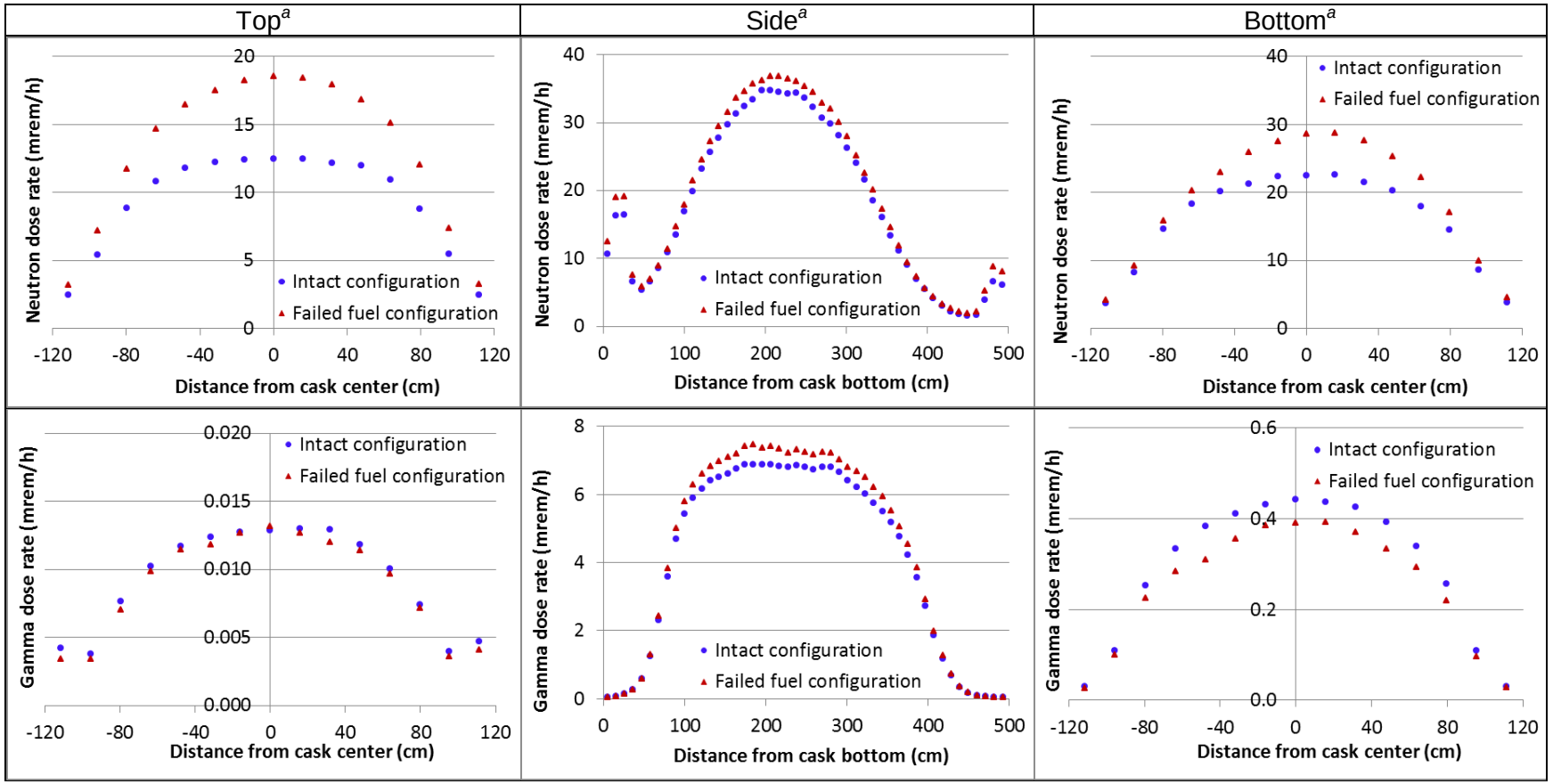

[a]BWR assemblies of 65 GWd/MTU burnup and 40-year decay time.

Figure B.51 – Comparison between package dose rate values for the intact fuel configuration and the configuration assuming all fuel rods collapsed against the basket plates—BWR package outer surfaces, NCT (Case 7)

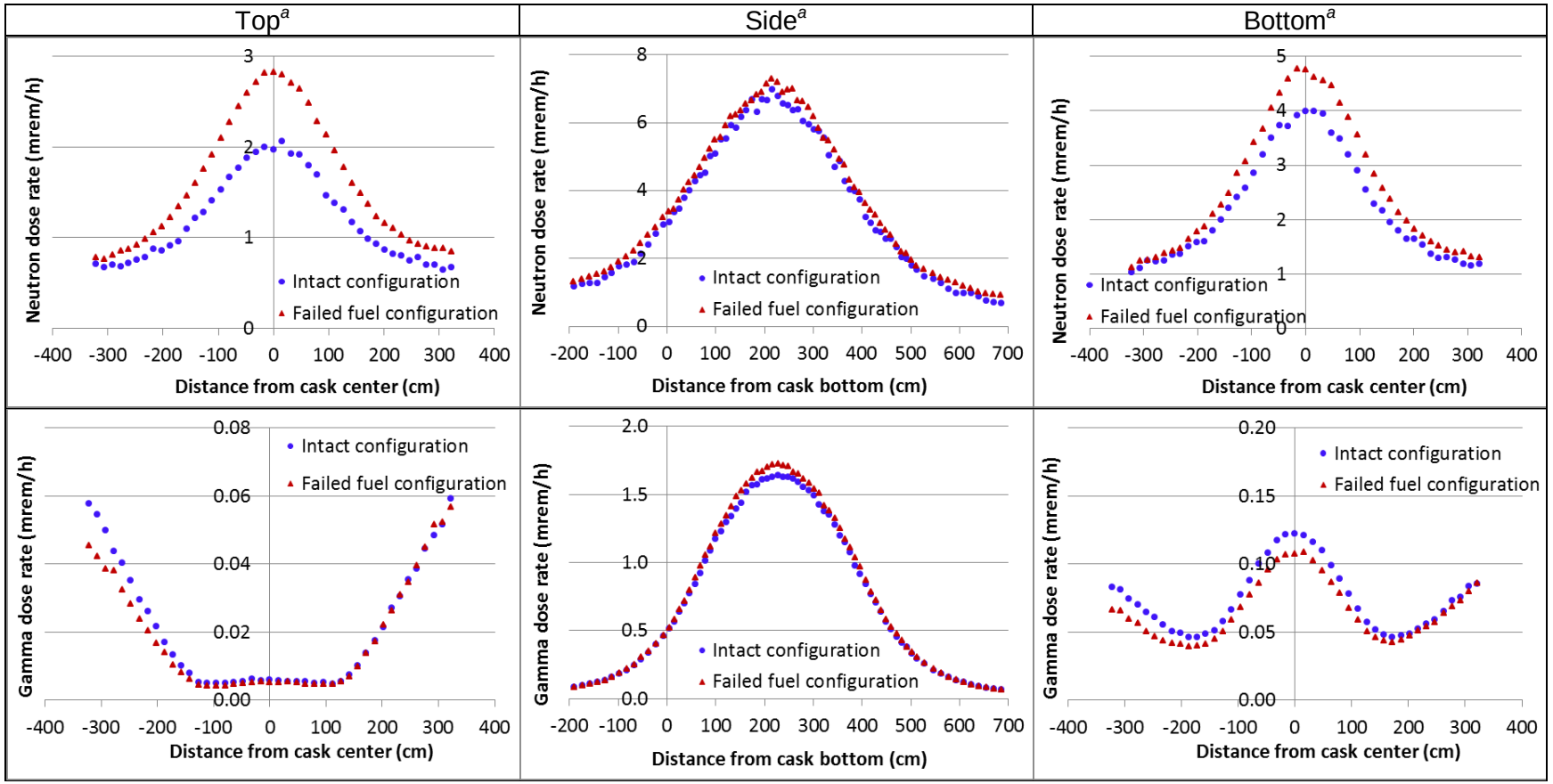

[a]BWR assemblies of 65 GWd/MTU burnup and 40-year decay time.

Figure B.52 – Comparison between package dose rate values for the intact fuel configuration and the configuration assuming all fuel rods collapsed against the basket plates—2 m locations, BWR package NCT (Case 7)

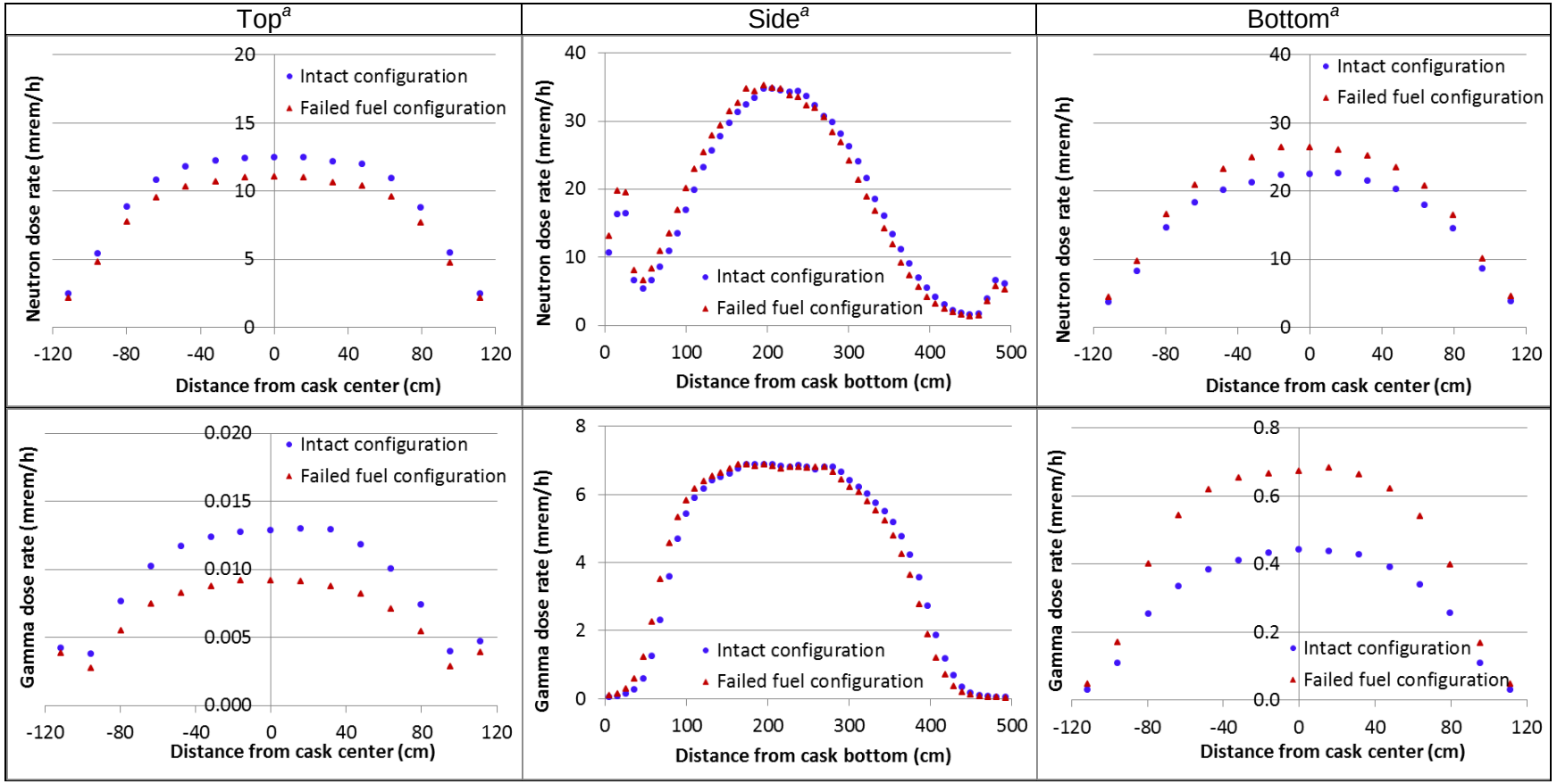

[a]BWR assemblies of 65 GWd/MTU burnup and 40-year decay time.

Figure B.53 – Comparison between package dose rate values for the intact fuel configuration and the configuration assuming displacement of the fuel assemblies to canister cavity bottom—BWR package outer surfaces, NCT (Case 8)

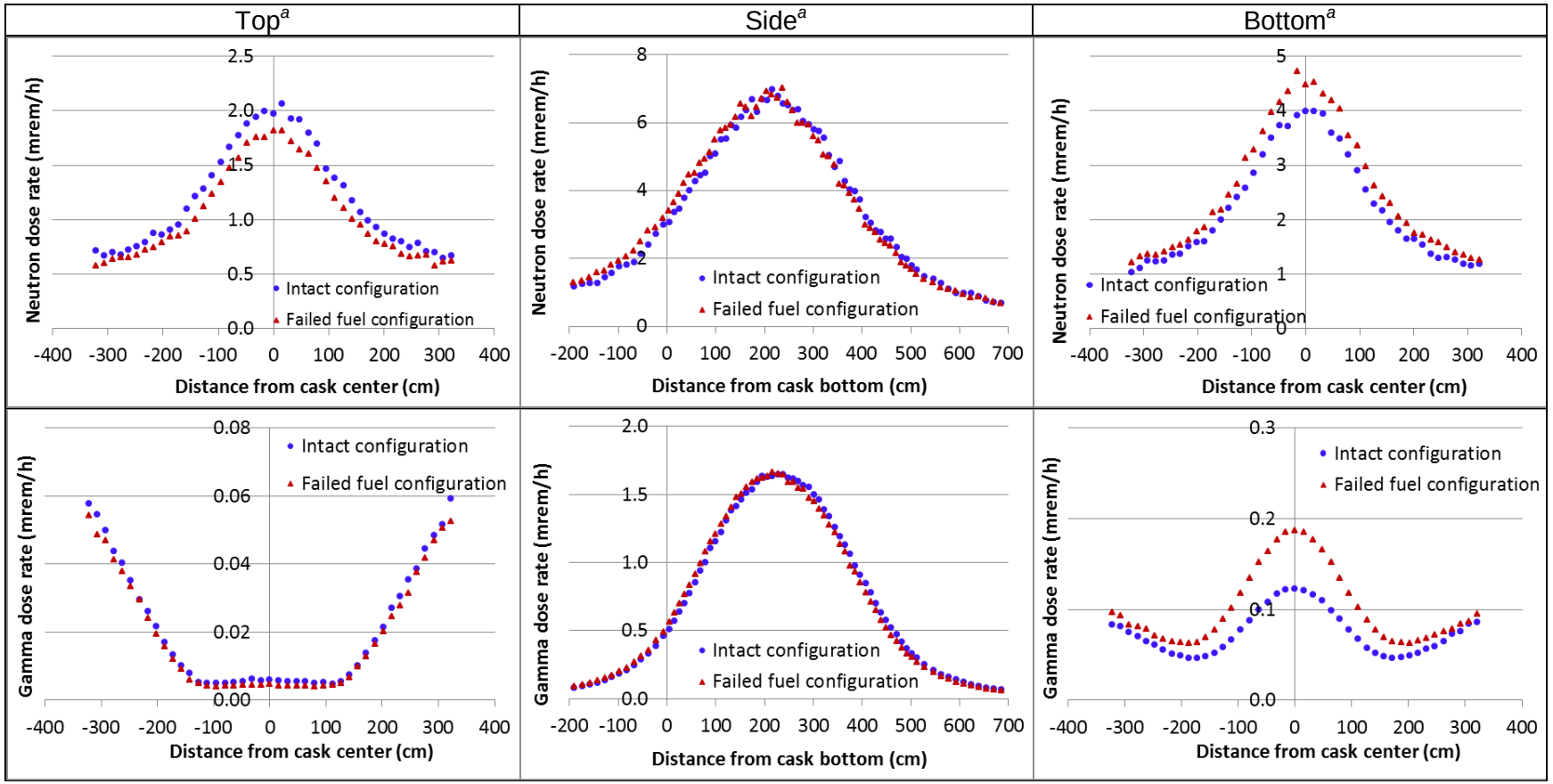

[a]BWR assemblies of 65 GWd/MTU burnup and 40-year decay time.

Figure B.54 – Comparison between package dose rate values for the intact fuel configuration and the configuration assuming displacement of the fuel assemblies to canister cavity bottom—2 m locations, BWR package NCT (Case 8)

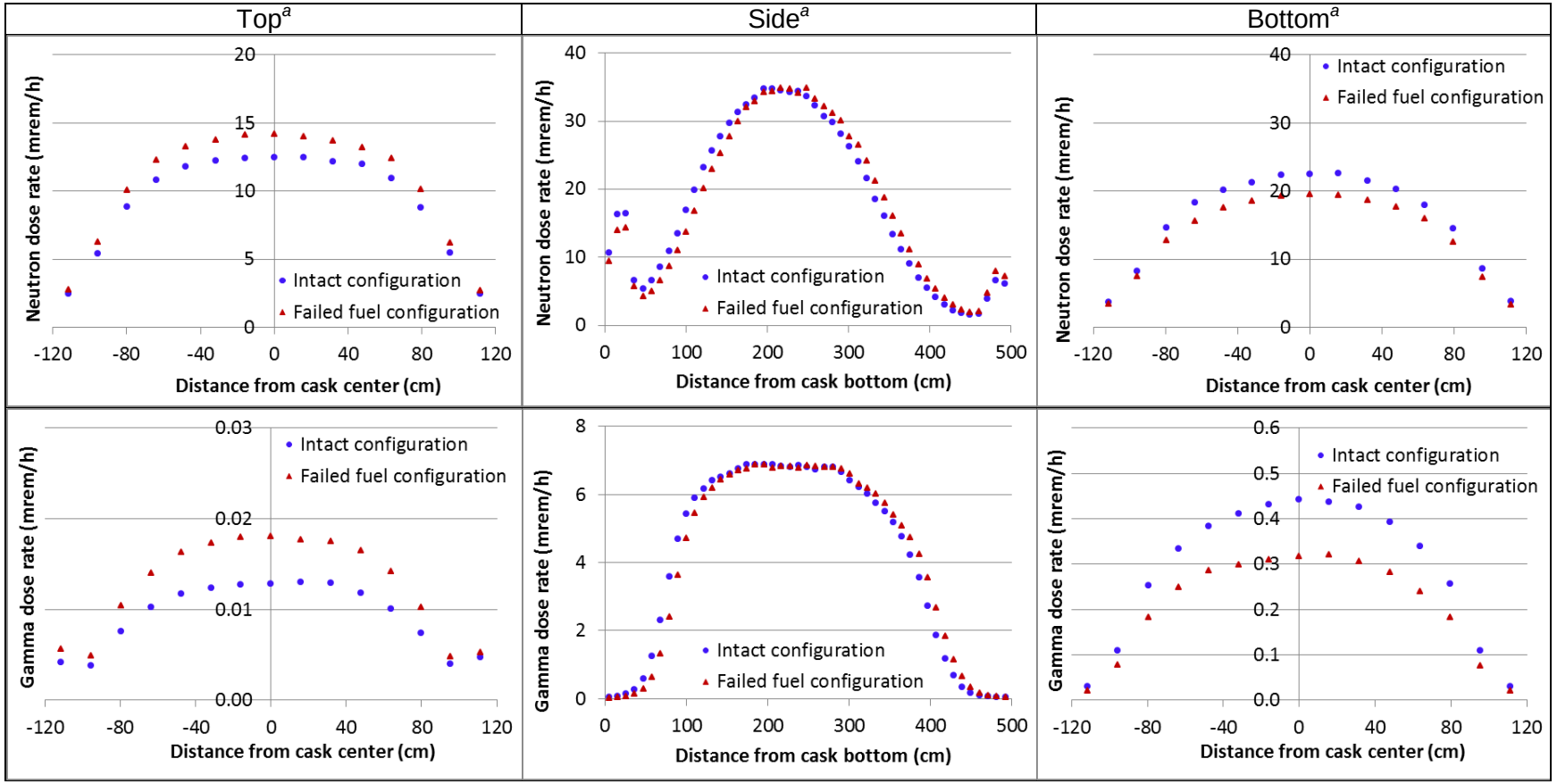

[a]BWR assemblies of 65 GWd/MTU burnup and 40-year decay time.

Figure B.55 – Comparison between package dose rate values for the intact fuel configuration and the configuration assuming displacement of the fuel assemblies to canister cavity top—BWR package outer surfaces, NCT (Case 9)

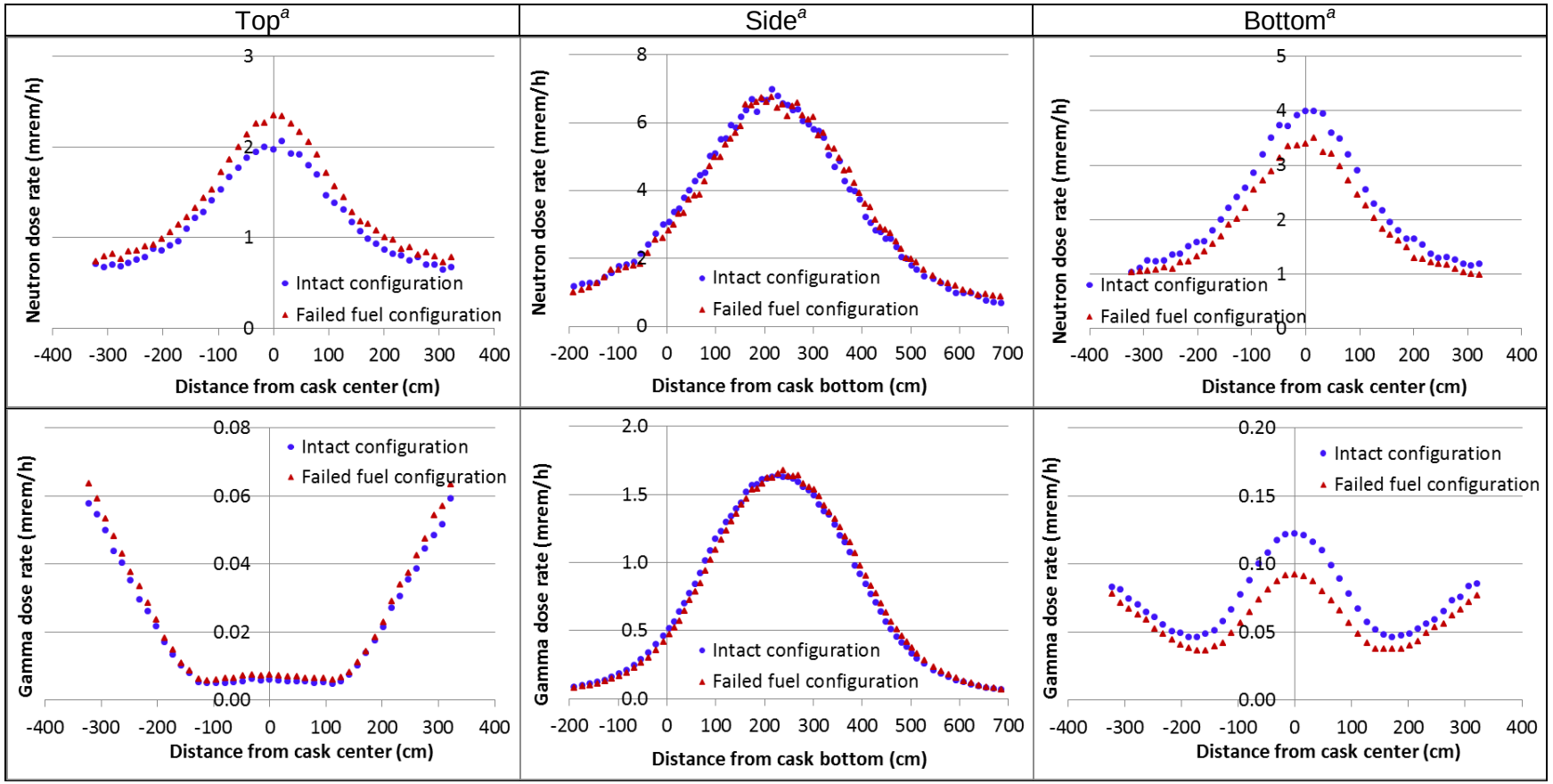

[a]BWR assemblies of 65 GWd/MTU burnup and 40-year decay time.

Figure B.56 – Comparison between package dose rate values for the intact fuel configuration and the configuration assuming displacement of the fuel assemblies to canister cavity top—2 m locations, BWR package NCT (Case 9)

B.5.4 BWR Package Assuming Hypothetical Accident Conditions

For the transportation package under HAC, the neutron shield considered in the BWR package model for NCT was replaced with air. The ratio of the maximum surface dose rate value for each fuel reconfiguration analyzed to the maximum surface dose rate value for the nominal intact configuration, which is identified as F/I dose rate ratio, is summarized in Table B.8.

Table B.8 – BWR package maximum dose rate change for hypothetical accident conditions

				Top	Side	Bottom	Top	Side	Bottom
Case #	**Scenario**	**Fuel relocation region[a]**	**Decay time (years)**	**F/I neutron dose rate ratio[b]**			**F/I gamma dose rate ratio[b]**		
1	11% fuel rod failure	Assembly active fuel	5	1.04	1.04	1.08	1.01	0.98	0.99
			40	0.99	1.02	1.06	0.99	0.98	0.96
2	11% fuel rod failure	Assembly lower tie plate and nosepiece	5	1.04	1.01	3.57	1.00	0.96	1.21
			40	1.01	1.00	3.65	1.01	0.97	16.99
3	11% fuel rod failure	Assembly plenum	5	6.86	1.04	1.04	1.42	0.97	1.00
			40	6.72	1.01	1.07	1.58	0.98	0.98
4	11% fuel rod failure	Assembly upper tie plate and handle	5	11.36	1.00	1.06	3.18	0.97	1.00
			40	11.06	1.00	1.05	6.49	0.97	0.94
5	Damaged	Canister cavity bottom	5	0.43	0.77	5.26	0.06	1.02	1.37
			40	0.44	0.77	5.33	0.33	1.03	26.24
6	Damaged	Entire canister cavity	5	12.84	0.83	3.69	3.28	0.99	1.09
			40	12.74	0.83	3.68	7.39	1.05	21.69
7	Assembly deformation	See Figure B.8 (a)	5	1.07	1.03	1.20	1.00	1.06	1.00
			40	1.03	1.03	1.21	1.00	1.04	1.02
8	Alignment changes	See Figure B.9 (a)	5	0.90	1.00	1.16	0.70	0.99	1.41
			40	0.89	1.00	1.16	0.92	0.99	1.35
9	Alignment changes	See Figure B.9 (b)	5	1.09	1.00	0.87	1.41	0.99	0.72
			40	1.06	0.99	0.89	1.10	0.99	0.88

[a]See Sect. B.5.3 for case description.
[b]Relative error (at the 95% confidence level) less than 5% for all values except for the maximum gamma dose rate change for case #9, top surface, the relative error is 20%.

The radial dose rate change relative to the nominal intact configuration was within statistical error, i.e., negligible. However, the neutron and gamma dose rates significantly increased at the top and bottom surfaces relative to the nominal intact configuration for most fuel reconfigurations. Relative to the nominal intact configuration, fuel damage represented with fuel rubble homogeneously distributed within the canister cavity yielded the greatest increase in the neutron dose rate at the top surface, by a factor of ~13, and fuel damage represented with fuel rubble collected into the canister cavity bottom yielded the greatest increase in the neutron dose rate at the bottom surface, by a factor of ~5.5. For the 5-year decay time, the maximum increase in axial gamma dose rate relative to the nominal intact configuration was by a factor of ~1.4 for assembly displacement to the package cavity top and bottom. For the 40-year decay time, the maximum F/I gamma dose rate ratio values on the top and bottom surfaces were ~7.5

and 26, for damaged fuel represented with fuel rubble homogeneously distributed within the canister cavity and damaged fuel represented with fuel rubble into the canister cavity bottom, respectively.

B.5.5 Individual Storage Cask

Dose rates were calculated at 1 m from a concrete storage cask containing either PWR or BWR fuel assemblies of 65 GWd/MTU burnup and either 5- or 40-year decay time. The scenarios analyzed include: cladding breach (fuel mixture from 10% fuel assembly rods collected into the available free volume within assembly lower hardware region), fuel damage (fuel rubble collected into the canister cavity bottom), and changes to assembly axial alignment (fuel assembly displaced to the canister cavity bottom). The changes (F/I dose rate ratio) relative to the nominal intact fuel configuration of the maximum neutron and gamma dose rates at 1 m from a concrete storage cask are summarized in Table B.9 and Table B.10 for PWR and BWR fuel assemblies, respectively. Figure B.57 shows the effects of 10% fuel rod failure with the fuel mixture redistributed into the assembly lower region on the PWR neutron and gamma dose rate profiles for the 40-year decay time. Fuel configuration changes cause significant dose rate increases relative to the nominal intact fuel configuration in the cask outer regions that face air vent locations. Away from air vent locations, the change in radiation dose rate is either small (e.g., 30% for damaged fuel configurations) or negligible.

Table B.9 – Maximum dose rate change at 1 m from a PWR storage cask

				Top[a]	Side[a]	Side[b]	Top[a]	Side[a]	Side[b]
Case #	**Scenario**	**Fuel relocation region**	**Decay time (years)**	**F/I neutron dose rate ratio[c]**			**F/I gamma dose rate ratio**		
2	10% fuel rod failure	Assembly lower end fitting	5	1.09	1.68	1.05	0.70	1.87	1.00
			40				0.90	2.91	1.04
9	Damaged	Canister cavity bottom	5	0.22	2.73	0.97	0.07	4.17	1.20
			40				0.18	4.09	0.77
11	Alignment changes	See Figure B.9 (a)	5	0.87	1.35	1.02	1.09	2.02	1.00
			40				0.80	2.73	0.95

[a]Facing air vent locations; relative error (at the 95% confidence level) is 10% for the radial surface and 20% for the top surface.
[b]Away from air vent locations; relative error (at the 95% confidence level) is 5%.
[c]F/I neutron dose rate ratio values are very similar for the 5- and 40-year decay times.

Table B.10 – Maximum dose rate change at 1 m from a BWR storage cask

				Top[a]	Side[a]	Side[b]	Top[a]	Side[a]	Side[b]
Case #	**Scenario**	**Fuel relocation region**	**Decay time (years)**	**F/I neutron dose rate ratio[c]**			**F/I gamma dose rate ratio**		
2	11% fuel rod failure	Assembly lower tie plate and nosepiece	5	1.02	2.16	1.05	0.56	1.78	0.97
			40				0.82	2.73	1.00
5	Damaged	Canister cavity bottom	5	0.22	3.23	0.92	0.15	5.58	1.09
			40				0.40	9.58	1.31
7	Alignment changes	See Figure B.9 (a)	5	0.77	1.19	0.99	0.54	1.28	1.01
			40				0.73	1.13	0.99

[a]Facing air vent locations; relative error (at the 95% confidence level) is 10% for the radial surface and 20% for the top surface.
[b]Away from air vent locations; relative error (at the 95% confidence level) is 6%.
[c]F/I neutron dose rate ratio values are very similar for the 5- and 40-year decay times.

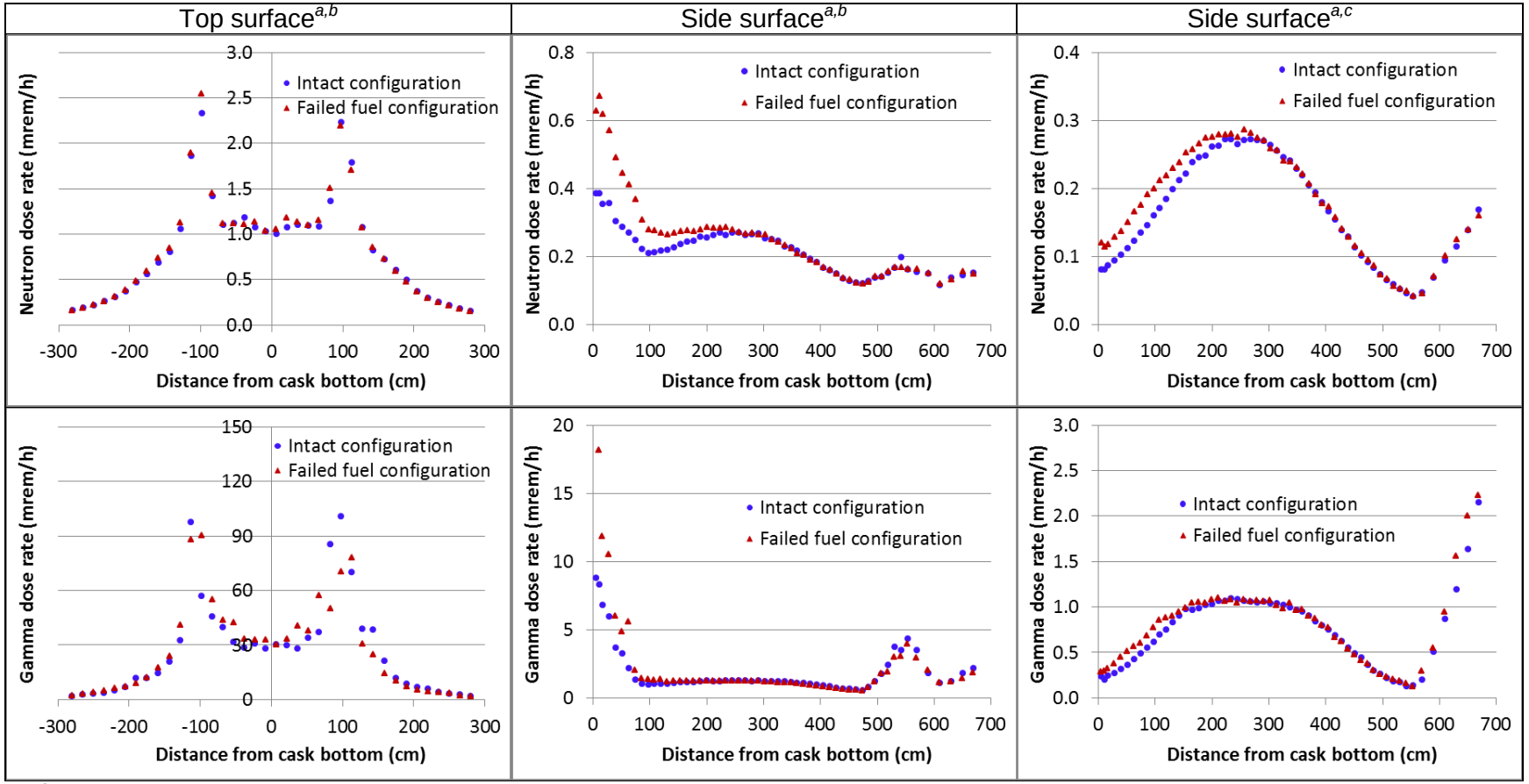

[a]PWR assemblies of 65 GWd/MTU burnup and 40-year decay time.
[b]Dose rate profiles in a vertical plane through air vent locations.
[c]Dose rate profiles in a vertical plane not through air vent locations.

Figure B.57 – Neutron and gamma dose rate profiles at 1 m from a PWR storage cask assuming 10% fuel mixture collected into assembly lower region

B.5.6 Generic Storage Cask Array

A site boundary dose rate comparison was performed based on a 4×2 array of storage casks using intact and damaged SNF conditions. The site boundary was assumed to be 100 m from the cask array (10 CFR 72.106[b]). The model for the cask array and cask internal configuration of the nominal intact configuration for the PWR fuel is illustrated in Figure B.4. A similar model was used for the BWR fuel, except the active fuel region was subdivided into 25 axial regions to facilitate the description of the BWR gamma and neutron radiation source axial profiles. The impact of changes in fuel configuration was evaluated for the damaged SNF case with fuel rubble collected into the canister cavity bottom based on a 0.58 mass packing fraction (see Sect. B.4.1), and for the case with fuel rubble homogeneously distributed within the canister cavity.

Table B.11 presents the ratio of site boundary dose rate for the cask array with failed fuel to the site boundary dose rate for the cask array with intact fuel for the PWR and BWR fuel, which is identified as F/I dose rate ratio. The results showed that closely packed fuel rubble reduces the site boundary dose rate by ~80% for gamma radiation and ~40 % for neutron radiation, whereas fuel rubble dispersed within the entire canister cavity increases the site boundary dose rate ~2.4 times for gamma radiation and ~2.7 times for neutron radiation relative to the nominal intact fuel configuration. The dose rate changes are caused by source geometry changes and gamma self-shielding effects associated with the different configurations.

Table B.11 - Site boundary dose rate change because of fuel configuration changes

Case description	F/I gamma dose rate ratio[a]	F/I neutron dose rate ratio[a]
PWR fuel rubble collected into canister cavity bottom	0.22 ± 0.03	0.58 ± 0.07
BWR fuel rubble collected into canister cavity bottom	0.30 ± 0.01	0.65 ± 0.01
PWR fuel rubble homogeneously distributed within canister cavity	1.75 ± 0.12	2.20 ± 0.08
BWR fuel rubble homogeneously distributed within canister cavity	2.41 ± 0.05	2.74 ± 0.04

[a]F/I dose rate ratio ± 2 sigma statistical error.

B.5.7 O-ring Locations

Lid, vent port, and drain port o-rings may be installed at cask top and bottom regions. O-rings serve as seals that provide primary containment. Fuel configuration changes may increase radiation dose rate and temperature at the o-ring locations, affecting the safety of the package. The F/I ratio values were calculated at typical vent and drain port o-ring locations within the package top lid and lower region, respectively, and are applicable to both NCT and HAC. The F/I ratio values for the PWR and BWR packages are provided in Table B.12 and Table B.13, respectively.

Table B.12. PWR package dose rate change at o-ring locations

				Top	Bottom	Top	Bottom
Case #	**Scenario**	**Fuel relocation region[a]**	**Decay time (years)**	**F/I neutron dose rate ratio[b,c]**		**F/I gamma dose rate ratio[c]**	
1	10% fuel rod failure	Assembly active fuel	5	1.07	1.02	1.02	1.01
			40			0.98	1.00
2	10% fuel rod failure	Assembly lower end fitting	5	1.05	1.97	1.02	1.23
			40			1.00	4.33
3	10% fuel rod failure	Assembly plenum	5	3.29	1.02	1.02	1.00
			40			3.30	0.99
4	10% fuel rod failure	Assembly upper end fitting	5	3.96	0.99	0.97	1.00
			40			11.23	1.00
5	25% fuel rod failure	Assembly active fuel	5	1.10	0.99	1.01	0.98
			40			0.98	0.98
6	25% fuel rod failure	Assembly lower end fitting	5	1.03	1.90	1.01	1.24
			40			0.99	4.45
7	25% fuel rod failure	Assembly plenum	5	3.85	0.98	1.00	0.98
			40			3.31	0.98
8	25% fuel rod failure	Assembly upper end fitting	5	4.92	0.98	0.94	1.00
			40			11.29	0.97
9	Damaged	Canister cavity bottom	5	0.29	2.83	0.0002	3.16
			40			0.0001	15.06
10	Damaged	Entire canister cavity	5	5.68	2.33	1.25	2.66
			40			17.93	13.27
11	Assembly deformation	See Figure B.8 (a)	5	1.26	1.19	1.01	1.01
			40			0.95	1.02
12	Assembly deformation	See Figure B.8 (b)	5	1.20	1.13	1.00	0.93
			40			0.90	0.91
13	Alignment changes	See Figure B.9 (a)	5	0.80	1.40	0.61	1.86
			40			1.68	0.31
14	Alignment changes	See Figure B.9 (b)	5	1.26	0.77	1.68	0.37
			40			0.60	4.10

[a]See Sect. B.5.1 for case description.
[b]F/I neutron dose rate ratio values are very similar for the 5- and 40-year decay times.
[c]Relative error (95% confidence level) less than 5% for all values except for the value for case #9, gamma dose rate on top surface, the relative error is 15%.

Table B.13. BWR package dose rate change at o-ring locations

				Top	Bottom	Top	Bottom
Case #	**Scenario**	**Fuel relocation region[a]**	**Decay time (years)**	**F/I neutron dose rate ratio[b,c]**		**F/I gamma dose rate ratio[c]**	
1	10% fuel rod failure	Assembly active fuel	5	1.12	1.05	1.01	1.00
			40			0.99	0.99
2	10% fuel rod failure	Assembly lower tie plate and nosepiece	5	1.11	2.99	1.00	1.20
			40			0.97	11.07
3	10% fuel rod failure	Assembly plenum	5	10.15	1.04	1.39	1.00
			40			12.44	0.98
4	10% fuel rod failure	Assembly upper tie plate and handle	5	16.26	1.05	3.30	1.05
			40			80.84	0.99
5	Damaged	Canister cavity bottom	5	0.52	3.32	0.0004	2.22
			40			0.02	30.71
6	Damaged	Entire canister cavity	5	19.46	3.27	3.64	1.60
			40			97.73	22.31
7	Assembly deformation	See Figure B.8 (a)	5	1.34	1.19	1.00	1.01
			40			0.96	1.01
8	Alignment changes	See Figure B.9 (a)	5	0.88	1.20	0.69	1.55
			40			0.73	2.05
9	Alignment changes	See Figure B.9 (b)	5	1.13	0.85	1.44	0.57
			40			1.40	0.57

[a]See Sect. B.5.3 for case description.
[b]F/I neutron dose rate ratio values are very similar for the 5- and 40-year decay times.
[c]Relative error (95% confidence level) less than 5% for all values except for the value for case #9, gamma dose rate on top surface, the relative error is 15%.

APPENDIX C. CONTAINMENT EVALUATIONS FOR FUEL RECONFIGURATIONS

Containment is associated with the capability of a transportation package system to retain the radioactive material during transport within the limits established in 10 CFR 71.51 for normal conditions of transport (NCT) and hypothetical accident conditions (HAC). Current regulatory recommendations for the fractions of failed fuel rods and radioactive material release for use in the containment analysis of transportation systems have been based on data available for low-burnup fuel.

High-burnup fuel may have different characteristics than low-burnup fuel with respect to crud thickness, cladding oxide thickness and hydride content, radionuclide inventory and distribution, heat load, fuel grain size, fuel fragmentation, and fission gas release to the rod plenum. High-burnup fuel cladding properties such as reduced ductility because of hydriding and increased stiffness because of binding of the fuel to the cladding are of concern for the handling of high-burnup fuel after in-reactor irradiation. This study provides a brief review of the phenomena associated with high-burnup fuel that are relevant to the containment analysis. Evaluation of the applicability of the current regulatory recommendations to high-burnup fuel and long-term dry storage is necessary. However, determination of fuel failure rate and radionuclide release fractions for high-burnup fuel is outside the scope of this report.

Releasable activity, allowable radionuclide release rate, and allowable leakage rate for the generic pressurized water reactor (PWR) and boiling water reactor (BWR) transportation packages referred to as generic burnup credit-32 (GBC-32) and GBC-68, respectively, were calculated with the formulas presented in Sect. C.2. The fuel assemblies selected for analysis were representative of the Westinghouse (W) 17×17 optimized fuel assembly (OFA) and General Electric (GE) 14 assemblies with 40 and 65 GWd/MTU burnup values. For low-burnup (e.g., 40 GWd/MTU) fuel in long-term dry storage, releasable activities of gas, volatile, and fine species were calculated as a function of decay time and fraction of fuel rods that develop breach based on NUREG-1617, Table 4-1 [28] recommended release fractions for gases (0.3), volatiles (2×10^{-4}), and fuel fines (3×10^{-5}) (see Table C.1). For high-burnup fuel (e.g., 65 GWd/MTU), a sensitivity analysis is provided. Parameters important to the containment of failed fuel (i.e., the release fractions and failed fuel fraction) were varied, and their impact on the allowable leakage rate was evaluated. The impact on the allowable leakage rate of the discharged radioactive material original location (i.e., non-rim pellet region or the rim structure) was also evaluated.

Table C.1 – Release fractions for the contributors to the releasable PWR and BWR source terms

	NCT	HAC
Fraction of fuel rods that develop cladding breaches	0.03	1.0
Fraction of gases released due to a cladding breach, f_G[a]	0.3	0.3
Fraction of volatiles released due to a cladding breach, f_V[a]	2×10^{-4}	2×10^{-4}
Mass fraction of fuel released as fines due to cladding breach, f_F	3×10^{-5}	3×10^{-5}
Fraction of crud that spalls off cladding, f_C[b]	0.15	1.0

[a] In accordance with NUREG/CR-6487 [40], gas species include ^{3}H, ^{129}I, ^{81}Kr, ^{85}Kr, and ^{127}Xe; volatile species include ^{134}Cs, ^{135}Cs, ^{137}Cs, ^{103}Ru, ^{106}Ru, ^{89}Sr, and ^{90}Sr.

[b] The source of radioactivity in crud is ^{60}Co on fuel rods. At the time of discharge from the reactor, the crud surface activity, S_C, is estimated to be 140 μCi/cm^2 for PWRs and 1254 μCi/cm^2 for BWRs. Total ^{60}Co activity is this estimate times the total surface area of all rods in the cask. Decay of ^{60}Co to determine activity at the minimum time before loading is acceptable.

Currently applicable regulatory requirements and guidance used in the containment analysis are provided in Sect. C.1. The computer codes used to calculate the radiation source terms and mathematical formulas for calculating the quantities relevant to containment analyses are described in Sect. C.2. The parameters that were considered in this study are described in Sect. C.3. The calculation results for low-burnup and high-burnup fuel assemblies that develop rod breaches (Category 1) are provided in Sections C.4 and C.5, respectively. The calculation results for fuel assembly deformation (Categories 2 and 3) are provided in Section C.6.

C.1 CURRENTLY APPLICABLE REGULATORY REQUIREMENTS AND GUIDANCE

The regulatory activity limits for NCT and HAC are specified in terms of A_2 quantities, as defined in 10 CFR Part 71.51 and Part 71–Appendix A. Following are the requirements for a spent fuel package:

1. Loss or dispersal of radioactive contents should not exceed 10^{-6} A_2 per hour under NCT.
2. Krypton-85 should not exceed 10 A_2 in 1 week under HAC.
3. Other radioactive material should not exceed a total amount A_2 in 1 week under HAC.

Current regulatory guidance for the fractions of failed fuel rods and radioactive material release to be used in the containment analysis of transportation systems are provided in NUREG-1617 [29], and are summarized in Table C.1. A fraction of 0.03 is recommended for fuel rods that develop cladding breach under NCT. This fraction has been used in NUREG/CR-6487 [40] as a reasonable bounding value based on in-reactor and out-of-reactor cladding breach frequencies for fuel rods as of Dec. 31, 1986. The fraction of fuel rods assumed to fail as a result of HAC is 1 (i.e., 100% of the fuel rods). The release fractions for the gaseous, volatile, and fuel fine species have been justified in Ref. [13] based on the fuel test series described in NUREG/CR-0722 [41] that had the objective to investigate fission products released in steam and dry air in the temperature range 500°C to 1200°C. The release fractions are typically used for low-burnup fuel because the maximum burnup of the fuel experimentally analyzed was ~30 GWd/MTU. The release fractions are also applicable to an inert atmosphere (i.e., not chemically reducing atmosphere as in the case of air ingress into the cask that would cause fuel oxidation and significant increases in the releases of fission product nuclides) [41]. The fuel tests demonstrated that burst release of the volatile species is significantly higher than release by diffusion. However, the diffusional release of cesium radionuclides is important for a rod break or other cladding failure that exposes a large amount of fuel directly to the cask environment [41].

Although the gap inventories of fission product nuclides appear to be identical, the release fractions of the radionuclides categorized as gaseous and volatile species are significantly different because of their different physico-chemical properties (e.g., boiling temperatures of elemental iodine and cesium are ~184°C and 678°C, respectively).

C.2 USE OF SOFTWARE AND APPLICABLE FORMULAS

The radionuclide activities of the W 17×17 OFA and GE14 assemblies were calculated with the depletion and decay capabilities of the Scale 6.1.1 code system [31], including Transport Rigor Implemented with Time-Dependent Operation for Neutronic depletion (TRITON) and Oak Ridge Isotope Generation in Scale (ORIGEN-S). The Scale 238-group Evaluated Nuclear Data Files, Part B-VII.0 (ENDF/B-VII.0) nuclear data library was used in the TRITON depletion calculations.

Analysis results are provided for releasable source term, the effective A_2 value for the total source term, allowable radionuclide release rate, and allowable leakage rate at operating conditions for the GBC-32 and GBC-68 casks described in the shielding analysis section. The calculation methodology described in NUREG/CR-6487 and the containment acceptance criteria provided in 10 CFR Part 71 were used in this study. Releasable activity for each individual contributor to the releasable source terms was calculated as:

$$RA_C = f_C N_A A_C \ ; \tag{C.1}$$

$$RA_G = f_{FFR} f_G N_A A_G \ ; \tag{C.2}$$

$$RA_V = f_{FFR} f_V N_A A_V \ ; \tag{C.3}$$

$$RA_F = f_{FFR} f_F N_A A_F \ ; \tag{C.4}$$

where

RA_C = releasable activity (Ci) as a result of crud spallation;
RA_G = releasable activity (Ci) from gases as a result of cladding breach;
RA_V = releasable activity (Ci) from volatile radionuclides as a result of cladding breach;
RA_F = releasable activity (Ci) from fuel fines as a result of cladding breach;
N_A = number of assemblies in the cask;
A_C = crud activity (Ci/assembly);
A_G = activity (Ci/assembly) of gaseous species;
A_V = activity (Ci/assembly) of volatile species;
A_F = activity of fuel fines (Ci/assembly);
f_{FFR} = fraction of fuel rods that develop cladding breach;

f_G, f_V, f_F, and f_C are the fractions for individual contributors to the releasable source term (i.e., gases, volatiles, fuel fines, and crud, respectively, provided in Table C.1).

Crud primarily consists of ^{60}Co with a half-life of ~5.3 years. Surface activity at the time of fuel discharge, which has been estimated to be 140 μCi/cm^2 for PWRs and 1254 μCi/cm^2 for BWRs (see Table C.1), was used to calculate crud releasable activity.

Total releasable activity was calculated as the sum of RA_C, RA_G, RA_V, and RA_F.

The effective A_2 value for each individual contributor that consists of a mixture of radionuclides was calculated in accordance with 10 CFR 71, Appendix A:

$$A_{2,mixture} = \frac{1}{\sum_{n=1}^{N} \frac{f_n}{A_{2,n}}} \ , \tag{C.5}$$

where

$A_{2,mixture}$ = the A_2 value (Ci) for each individual contributor to the releasable source term (i.e., gases, volatiles, and fuel fines);

f_n = the fraction of activity of radionuclide *n* in the mixture for each individual contributor to the releasable source term;

$A_{2,n}$ = the A_2 value (Ci) for radionuclide *n*, which is provided in 10 CFR71, Appendix A.

Allowable radionuclide release rates for NCT and HAC were determined using the containment requirements in 10 CFR 71.51(1) and 71.51(2), respectively. For NCT, "there would be no loss or dispersal of radioactive contents—as demonstrated to a sensitivity of 10^{-6} A_2 per hour" (10 CFR 71.51[1]). For HAC, "there would be no escape of krypton-85 exceeding 10 A_2 in 1 week, no escape of other radioactive material exceeding a total amount A_2 in 1 week" (10 CFR 71.51[2]). Hence, allowable radioactivity release rate for NCT, RR_N (Ci/s), is $RR_N \leq A_2 \times 2.78 \times 10^{-10}$. Allowable radioactivity release rate for HAC, RR_A (Ci/s), is $RR_A \leq A_2 \times 1.65 \times 10^{-6}$; and the bounding value release rate for HAC is 4.46×10^{-3}Ci/s (i.e., 10 times the A_2 value for ^{85}Kr).

Allowable leakage rate, in cm^3/s, at operating conditions was calculated as: $LR_N = RR_N/C_N$ and $LR_A = RR_A/C_A$, for NCT and for HAC, respectively, where C_N and C_A are the total source term activity concentration, in Ci/cm^3, for NCT and for HAC, respectively [40]. The free void volumes for the GBC-32 and GBC-68 cask models described in Appendix B were 7.06×10^6 cm^3 and 5.68×10^6 cm^3, respectively.

C.3 DESCRIPTION OF FUEL RECONFIGURATION CATEGORY CALCULATION MODELS FOR CONTAINMENT

The containment analysis includes selected values for the fraction of fuel rods that may develop cladding breach. Currently, the applicability of the release fractions described in NUREG-1617 to long-term storage and for high-burnup fuel is uncertain. In this respect, additional variations on the parameters important for containment analysis are included making this is a parametric analysis.

C.3.1 Category 1: Cladding Failure

Configurations evaluated:

a) Fuel assembly parameters:
   - 40 GWd/MTU burnup
     - 3 wt % ^{235}U initial enrichment
     - 5-, 40-, 100-, and 300-year decay times
   - 65 GWd/MTU burnup
     - 5 wt % ^{235}U initial enrichment
     - 5-, 40-, 100-, and 300-year decay times

b) For the 40 GWd/MTU assembly burnup, the fraction of rods that develop cladding breach was varied from 0.01 to 1. The release fractions for gases, volatiles, and fuel fines from Table 4-1 in NUREG-1617, [28], are assumed to be applicable to long-term dry storage.

c) For the 65 GWd/MTU assembly burnup, the following parameters were varied: the fraction of rods that develop cladding breach (0.01, 0.03, 0.10, and 1); and the

release fractions for crud (0.15, 0.3, 0.5, and 1), gases (0.1, 0.3, and 0.4), volatiles (2×10^{-4}, 1×10^{-3}, and 2×10^{-3}), and fuel fines (3×10^{-5}, 1.5×10^{-4}, and 3×10^{-4}). In addition, the impact on the releasable activity of the radioactive material original location (i.e., inner pellet region or the rim structure) was evaluated.

C.3.2 Category 2: Rod/Assembly Deformation

Rod/assembly deformation is assumed not to cause cladding breach. Crud is assumed to be released as a result of rod/assembly deformation. The allowable leakage rate was calculated as a function of the fraction of crud (0.05 to 1) that spalls off cladding for the 5- and 40-year decay times. The releasable activity for this category is independent of assembly burnup.

C.3.3 Category 3: Changes to Intact Assembly Axial Alignment

Axial displacement of an intact assembly is assumed not to cause cladding breach. Crud is assumed to be released as a result of assembly axial displacement. The allowable leakage rate was calculated as a function of the fraction of crud (0.05 to 1) that spalls off cladding for the 5- and 40-year decay times. The releasable activity for this category is independent of assembly burnup.

C.4 LOW-BURNUP FUEL

A containment analysis for fuel rods that develop cladding failure for NCT was performed for the PWR GBC-32 and BWR GBC-68 transportation package models containing low-burnup (e.g., 40 GWd/MTU) fuel assemblies. The total releasable activity, source term effective A_2 values, allowable radionuclide release rates, and allowable leakage rates calculated as a function of fraction or rods that develop cladding breach and fuel decay time are provided in Table C.2 and Table C.3 for the GBC-32 and GBC-68 packages, respectively. The fraction of fuel rods that develop cladding breach under NCT was varied from 0.01 to 1. The value typically used for the fraction of fuel rods assumed to fail in NCT containment analyses, as recommended in NUREG-1617 [28], is 0.03. Releasable activity for gas, volatile, and fine species was calculated as a function of decay time and fraction of fuel rods that develop breach assuming currently recommended release fractions for gases (0.3), volatiles (2×10^{-4}), and fines (3×10^{-5}) (see Table C.1).

For the GBC-32 cask, the allowable leakage rate value based on the 0.03 fuel rod failure rate was ~1.0×10^{-4} cm^3/s for a 5-year decay time. An equivalent allowable leakage rate value was obtained for PWR fuel rod failure rates of ~0.10, 0.15, and 0.25, for 40-, 100-, and 300-year decay times, respectively.

For the GBC-68 cask, the allowable leakage rate value based on the 0.03 fuel rod failure rate was ~2.4×10^{-5} cm^3/s for a 5-year decay time. An equivalent allowable leakage rate value was obtained for the BWR fuel rod failure rates of ~0.4, 0.7, and 1.0 for 40-, 100-, and 300-year decay times, respectively. With a more restrictive allowable leakage rate, the GBC-68 cask can accommodate greater fuel rod failure rates than the GBC-32. Crud contribution to GBC-68 releasable activity is significantly higher than that of the GBC-32 cask for low decay times and a small fraction of failed fuel rods. As a result, the GBC-68 cask allowable leakage rates are smaller (i.e., more restrictive) than the GBC-32 cask allowable leakage rates for low decay times. However, the GBC-32 and GBC-68 total releasable activity and allowable leakage rates were similar for fuel decay times of 40, 100, and 300 years because the crud contribution effect becomes negligible at these decay times.

Table C.2 – GBC-32 source term, allowable release rate, and allowable leakage rate: 40 GWd/MTU

	5-year decay time				40-year decay time			
Failed fuel fraction	Releasable activity (Ci)[a]	Effective A_2 value (Ci)	Allowable release rate (Ci/s)	Allowable leakage rate (cm^3/s)	Releasable activity (Ci)[a]	Effective A_2 value (Ci)	Allowable release rate (Ci/s)	Allowable leakage rate (cm^3/s)
0.01	4.97E+02	3.99E+01	1.11E-08	1.57E-04	4.54E+01	2.49E+01	6.93E-09	1.08E-03
0.02	8.97E+02	5.62E+01	1.56E-08	1.23E-04	8.97E+01	2.53E+01	7.03E-09	5.53E-04
0.03	1.30E+03	6.66E+01	1.85E-08	1.01E-04	1.34E+02	2.54E+01	7.07E-09	3.72E-04
0.04	1.70E+03	7.38E+01	2.05E-08	8.52E-05	1.79E+02	2.55E+01	7.09E-09	2.80E-04
0.06	2.50E+03	8.32E+01	2.31E-08	6.53E-05	2.67E+02	2.55E+01	7.10E-09	1.87E-04
0.08	3.30E+03	8.90E+01	2.47E-08	5.29E-05	3.56E+02	2.56E+01	7.11E-09	1.41E-04
0.10	4.10E+03	9.30E+01	2.58E-08	4.45E-05	4.45E+02	2.56E+01	7.12E-09	1.13E-04
0.15	6.10E+03	9.89E+01	2.75E-08	3.18E-05	6.67E+02	2.56E+01	7.12E-09	7.53E-05
0.20	8.10E+03	1.02E+02	2.84E-08	2.47E-05	8.89E+02	2.56E+01	7.13E-09	5.65E-05
0.25	1.01E+04	1.04E+02	2.90E-08	2.02E-05	1.11E+03	2.56E+01	7.13E-09	4.53E-05
0.30	1.21E+04	1.06E+02	2.94E-08	1.71E-05	1.33E+03	2.57E+01	7.13E-09	3.77E-05
0.35	1.41E+04	1.07E+02	2.97E-08	1.49E-05	1.55E+03	2.57E+01	7.13E-09	3.23E-05
0.40	1.61E+04	1.08E+02	2.99E-08	1.31E-05	1.78E+03	2.57E+01	7.13E-09	2.83E-05
0.50	2.01E+04	1.09E+02	3.03E-08	1.06E-05	2.22E+03	2.57E+01	7.13E-09	2.27E-05
0.60	2.41E+04	1.10E+02	3.05E-08	8.92E-06	2.66E+03	2.57E+01	7.13E-09	1.89E-05
0.70	2.81E+04	1.10E+02	3.07E-08	7.69E-06	3.11E+03	2.57E+01	7.13E-09	1.62E-05
0.80	3.21E+04	1.11E+02	3.08E-08	6.76E-06	3.55E+03	2.57E+01	7.14E-09	1.42E-05
0.90	3.61E+04	1.11E+02	3.09E-08	6.03E-06	4.00E+03	2.57E+01	7.14E-09	1.26E-05
1.00	4.01E+04	1.11E+02	3.09E-08	5.44E-06	4.44E+03	2.57E+01	7.14E-09	1.13E-05
	100-year decay time				300-year decay time			
Failed fuel fraction	Releasable activity (Ci)[a]	Effective A_2 value (Ci)	Allowable release rate (Ci/s)	Allowable leakage rate (cm^3/s)	Releasable activity (Ci)[a]	Effective A_2 value (Ci)	Allowable release rate (Ci/s)	Allowable leakage rate (cm^3/s)
0.01	1.56E+00	1.31E+00	3.65E-10	1.65E-03	2.72E-02	3.72E-02	1.04E-11	2.68E-03
0.02	3.12E+00	1.31E+00	3.65E-10	8.27E-04	5.45E-02	3.72E-02	1.04E-11	1.34E-03
0.03	4.67E+00	1.31E+00	3.65E-10	5.51E-04	8.17E-02	3.72E-02	1.04E-11	8.93E-04
0.04	6.23E+00	1.31E+00	3.65E-10	4.13E-04	1.09E-01	3.72E-02	1.04E-11	6.70E-04
0.06	9.35E+00	1.31E+00	3.65E-10	2.76E-04	1.63E-01	3.72E-02	1.04E-11	4.47E-04
0.08	1.25E+01	1.31E+00	3.65E-10	2.07E-04	2.18E-01	3.72E-02	1.04E-11	3.35E-04
0.10	1.56E+01	1.31E+00	3.65E-10	1.65E-04	2.72E-01	3.72E-02	1.04E-11	2.68E-04
0.15	2.34E+01	1.31E+00	3.65E-10	1.10E-04	4.08E-01	3.72E-02	1.04E-11	1.79E-04
0.20	3.12E+01	1.31E+00	3.65E-10	8.27E-05	5.45E-01	3.72E-02	1.04E-11	1.34E-04
0.25	3.89E+01	1.31E+00	3.65E-10	6.62E-05	6.81E-01	3.72E-02	1.04E-11	1.07E-04
0.30	4.67E+01	1.31E+00	3.65E-10	5.51E-05	8.17E-01	3.72E-02	1.04E-11	8.93E-05
0.35	5.45E+01	1.31E+00	3.65E-10	4.73E-05	9.53E-01	3.72E-02	1.04E-11	7.66E-05
0.40	6.23E+01	1.31E+00	3.65E-10	4.13E-05	1.09E+00	3.72E-02	1.04E-11	6.70E-05
0.50	7.79E+01	1.31E+00	3.65E-10	3.31E-05	1.36E+00	3.72E-02	1.04E-11	5.36E-05
0.60	9.35E+01	1.31E+00	3.65E-10	2.76E-05	1.63E+00	3.72E-02	1.04E-11	4.47E-05
0.70	1.09E+02	1.31E+00	3.65E-10	2.36E-05	1.91E+00	3.72E-02	1.04E-11	3.83E-05
0.80	1.25E+02	1.31E+00	3.65E-10	2.07E-05	2.18E+00	3.72E-02	1.04E-11	3.35E-05
0.90	1.40E+02	1.31E+00	3.65E-10	1.84E-05	2.45E+00	3.72E-02	1.04E-11	2.98E-05
1.00	1.56E+02	1.31E+00	3.65E-10	1.65E-05	2.72E+00	3.72E-02	1.04E-11	2.68E-05

[a]Total releasable activity of crud and fuel fission gas, volatile, and fine species.

Table C.3 – GBC-68 source term, allowable release rate, and allowable leakage rate: 40 GWd/MTU

	5-year decay time				40-year decay time			
Failed fuel fraction	Releasable activity (Ci)[a]	Effective A_2 value (Ci)	Allowable release rate (Ci/s)	Allowable leakage rate (cm^3/s)	Releasable activity (Ci)[a]	Effective A_2 value (Ci)	Allowable release rate (Ci/s)	Allowable leakage rate (cm^3/s)
0.01	1.04E+03	1.58E+01	4.39E-09	2.67E-05	4.70E+01	2.17E+01	6.03E-09	8.14E-04
0.02	1.40E+03	2.03E+01	5.64E-09	2.55E-05	8.73E+01	2.35E+01	6.54E-09	4.76E-04
0.03	1.77E+03	2.44E+01	6.78E-09	2.44E-05	1.27E+02	2.43E+01	6.75E-09	3.36E-04
0.04	2.13E+03	2.82E+01	7.83E-09	2.34E-05	1.68E+02	2.47E+01	6.87E-09	2.60E-04
0.06	2.86E+03	3.48E+01	9.68E-09	2.15E-05	2.48E+02	2.51E+01	6.99E-09	1.79E-04
0.08	3.58E+03	4.05E+01	1.13E-08	2.00E-05	3.29E+02	2.54E+01	7.06E-09	1.36E-04
0.10	4.31E+03	4.55E+01	1.26E-08	1.86E-05	4.09E+02	2.55E+01	7.10E-09	1.10E-04
0.15	6.12E+03	5.53E+01	1.54E-08	1.59E-05	6.10E+02	2.57E+01	7.15E-09	7.44E-05
0.20	7.94E+03	6.26E+01	1.74E-08	1.39E-05	8.11E+02	2.58E+01	7.18E-09	5.62E-05
0.25	9.75E+03	6.83E+01	1.90E-08	1.24E-05	1.01E+03	2.59E+01	7.19E-09	4.51E-05
0.30	1.16E+04	7.29E+01	2.03E-08	1.11E-05	1.21E+03	2.59E+01	7.21E-09	3.77E-05
0.35	1.34E+04	7.66E+01	2.13E-08	1.01E-05	1.41E+03	2.59E+01	7.21E-09	3.24E-05
0.40	1.52E+04	7.97E+01	2.22E-08	9.26E-06	1.62E+03	2.60E+01	7.22E-09	2.84E-05
0.50	1.88E+04	8.46E+01	2.35E-08	7.93E-06	2.02E+03	2.60E+01	7.23E-09	2.27E-05
0.60	2.25E+04	8.82E+01	2.45E-08	6.94E-06	2.42E+03	2.60E+01	7.23E-09	1.90E-05
0.70	2.61E+04	9.11E+01	2.53E-08	6.16E-06	2.82E+03	2.60E+01	7.24E-09	1.63E-05
0.80	2.97E+04	9.33E+01	2.59E-08	5.55E-06	3.23E+03	2.60E+01	7.24E-09	1.43E-05
0.90	3.33E+04	9.52E+01	2.65E-08	5.04E-06	3.63E+03	2.61E+01	7.24E-09	1.27E-05
1.00	3.70E+04	9.67E+01	2.69E-08	4.62E-06	4.03E+03	2.61E+01	7.25E-09	1.14E-05
	100-year decay time				300-year decay time			
Failed fuel fraction	Releasable activity (Ci)[a]	Effective A_2 value (Ci)	Allowable release rate (Ci/s)	Allowable leakage rate (cm^3/s)	Releasable activity (Ci)[a]	Effective A_2 value (Ci)	Allowable release rate (Ci/s)	Allowable leakage rate (cm^3/s)
0.01	1.41E+00	1.36E+00	3.77E-10	1.70E-03	2.39E-02	3.76E-02	1.05E-11	2.78E-03
0.02	2.82E+00	1.36E+00	3.77E-10	8.49E-04	4.78E-02	3.76E-02	1.05E-11	1.39E-03
0.03	4.23E+00	1.36E+00	3.77E-10	5.66E-04	7.17E-02	3.76E-02	1.05E-11	9.26E-04
0.04	5.63E+00	1.36E+00	3.77E-10	4.25E-04	9.56E-02	3.76E-02	1.05E-11	6.95E-04
0.06	8.45E+00	1.36E+00	3.77E-10	2.83E-04	1.43E-01	3.76E-02	1.05E-11	4.63E-04
0.08	1.13E+01	1.36E+00	3.77E-10	2.12E-04	1.91E-01	3.76E-02	1.05E-11	3.47E-04
0.10	1.41E+01	1.36E+00	3.77E-10	1.70E-04	2.39E-01	3.76E-02	1.05E-11	2.78E-04
0.15	2.11E+01	1.36E+00	3.77E-10	1.13E-04	3.59E-01	3.76E-02	1.05E-11	1.85E-04
0.20	2.82E+01	1.36E+00	3.77E-10	8.49E-05	4.78E-01	3.76E-02	1.05E-11	1.39E-04
0.25	3.52E+01	1.36E+00	3.77E-10	6.79E-05	5.98E-01	3.76E-02	1.05E-11	1.11E-04
0.30	4.23E+01	1.36E+00	3.77E-10	5.66E-05	7.17E-01	3.76E-02	1.05E-11	9.26E-05
0.35	4.93E+01	1.36E+00	3.77E-10	4.85E-05	8.37E-01	3.76E-02	1.05E-11	7.94E-05
0.40	5.63E+01	1.36E+00	3.77E-10	4.25E-05	9.56E-01	3.76E-02	1.05E-11	6.95E-05
0.50	7.04E+01	1.36E+00	3.77E-10	3.40E-05	1.20E+00	3.76E-02	1.05E-11	5.56E-05
0.60	8.45E+01	1.36E+00	3.77E-10	2.83E-05	1.43E+00	3.76E-02	1.05E-11	4.63E-05
0.70	9.86E+01	1.36E+00	3.77E-10	2.43E-05	1.67E+00	3.76E-02	1.05E-11	3.97E-05
0.80	1.13E+02	1.36E+00	3.77E-10	2.12E-05	1.91E+00	3.76E-02	1.05E-11	3.47E-05
0.90	1.27E+02	1.36E+00	3.77E-10	1.89E-05	2.15E+00	3.76E-02	1.05E-11	3.09E-05
1.00	1.41E+02	1.36E+00	3.77E-10	1.70E-05	2.39E+00	3.76E-02	1.05E-11	2.78E-05

[a]Total releasable activity of crud and fuel fission gas, volatile, and fine species.

C.5 HIGH-BURNUP FUEL

Physical phenomena relevant to the containment analysis of high-burnup fuel are described in Sect. C.5.1. A description of the high-burnup depletion calculation models for the W 17×17 OFA and GE14 assemblies is provided in Sect. C.5.2 and the Scale 6.1.1-calculated radionuclide activities are provided in Sect. C.5.3. The containment analysis for high-burnup fuel is provided in Sect. C.5.4.

C.5.1 Physical Phenomena Relevant to Containment Analysis of High-Burnup Fuel

A limited review of publicly available documents addressing the properties of high-burnup fuel assemblies relevant to spent fuel management was performed for this study. Major differences between high- and low-burnup light water reactor fuels concern radiation source term, pressure of fission gas in the fuel cladding gap, cladding mechanical properties, and the fuel rim-effect associated only with high-burnup fuel. These characteristics affect the mechanisms by which the fuel can breach and the amount of fuel that can be released from failed fuel rods. Hence, the fuel rod failure rate for NCT as well as radionuclide release fractions based on low-burnup studies may need to be reevaluated for their applicability to high- burnup fuel, which is outside the scope of this report. Major high-burnup fuel physical characteristics relevant to containment analysis are summarized below.

The mechanical properties of high-burnup fuel cladding can be adversely affected by embrittling factors such as in-reactor irradiation damage, oxidation, and circumferential hydriding (i.e. uptake of hydrogen from corrosion in the coolant). The cladding of discharged high-burnup PWR fuel contains an oxide coating up to 100 microns and between 50 and 700 parts per million by weight (wppm) hydrogen, depending on the zirconium alloy composition; in comparison, the cladding of low-burnup PWR fuel has less than 100 wppm hydrogen. The cladding of high-burnup BWR fuel contains a thin uniform oxide layer with nodular corrosion of larger extent and lower hydrogen concentrations than the high-burnup PWR fuel [42]. Fission gas released from the fuel matrix to the fuel cladding gap is significantly larger in high-burnup fuel rods compared to the low-burnup fuel rods [43]. Excessive hoop stress because of higher internal pressurization and thinner cladding may cause cladding to be more susceptible to failure. In addition, the formation of radial hydrides can result in reduced ductility and tensile strength of the cladding [11].

The properties of high-burnup fuel pellets are more heterogeneous than for low-burnup fuel. Higher burnup (>55 GWd/MTU) and in-reactor fuel temperatures below ~1100˚C cause a restructuring of the UO_2 matrix in the pellet outer region [39, 44]. The resulting microstructure is usually referred to as a high-burnup rim structure. The rim structure is characterized by sub-micron grains, which are depleted of fission gas, and much higher closed porosity (15 to 20%) than the bulk material (6%), which contains fission gas at high pressures [42]. The inside of the closed porosity tends to be lined with many submicron-sized fuel particulates in the 10–200 nm range. Hence, fission gas and fuel particles in the respirable range would be released when the fission gas bubbles in the rim structure burst.

High-burnup fuel pellets exhibit greater fragmentation than low-burnup fuel pellets. Pellet fracturing is caused by fuel exposure to thermal gradients early in life. The number of fragments observed for typical fuel varies from 20 to 50 fragments per pellet; more fragmentation has been observed for higher burnup fuel [39]. Cracks observed in the rim structure are caused by strong pellet-cladding bonding—because of inter-penetration between the rim structure and the

zirconia formed at the cladding inner surface after closure of the pellet-to-cladding gap—and by the differential thermal expansion of the pellet and cladding during the cooling phases [45]. Microcracks in the rim structure also may be caused by overpressurization within the intergranular fission gas bubbles coupled with sudden relief of pellet cladding mechanical interaction restraints by cladding [46]. Greater fuel pellet fragmentation causes a greater amount of fuel particulates to be released from high-burnup failed fuel rods.

Fuel fragmentation and fission gas release are correlated. The larger quantity of fission gas released to the fuel rod free-void volume increases fission gas pressure, which increases the risk of cladding breach. The fission gas bubbles formed in the central portion of a fuel pellet become interlinked with continued irradiation releasing the fission gas and volatile products to the fuel cladding gap. Fission gas release from the pellet to the fuel cladding gap increases with increasing fuel burnup (e.g., from 5 to 25% for burnup increases of 20 to 100 GWd/MTU burnup) [47]. Fission gas release from the rim structure has been evaluated to be generally low [45]. However, significantly more fission gas may be released under rapid heating conditions such as transient and off-normal irradiation conditions, as demonstrated by rapid heating tests, or because of the occurrence of microcracks upon the sudden relief of pellet cladding mechanical interaction restraints by cladding. Under certain heating conditions, such as those used in rapid or slow heating tests to very high temperatures (e.g., 1500-1800˚C), fission gas release fraction from high-burnup fuel (with burnup greater than 60 GWd/MTU) may exceed the 0.3 value currently used in the containment analyses. Rapid heating tests that simulate transient and off-normal irradiation conditions have measured fission gas release fractions up to ~46% for a 74 GWd/MTU burnup fuel specimen [46].

The average amount of crud for high-burnup fuel assemblies has been estimated to be similar to that observed on lower burnup fuel assemblies [42].

C.5.2 Depletion Calculation Models

Neutron capture is more pronounced in the fuel pellet outer region. As a result, the power production at the center of a fuel rod is slightly less than that at the surface. As fuel burnup increases, the distributions of fissile material, fission rate, and fission products in irradiated fuel develop peaks at the pellet surface [48, 49]. A mathematical model, shown in Eq. (C.6), has been developed for the rim structure width as a function of pellet burnup based on best available data obtained by optical microscopy [42]. The rim width as a function of pellet burnup is illustrated in Figure C.1. Based on Eq. (C.6), the width of the rim structure corresponding to an assembly average burnup value of 65 GWd/MTU is approximately 150 microns.

$$w = 1.439e^{-6} \times burnup^{4.427}, \qquad \text{(C.6)}$$

where

w = the rim width where the grains are fully transformed (microns), and
$burnup$ = the pellet-average burnup in GWd/MTU.

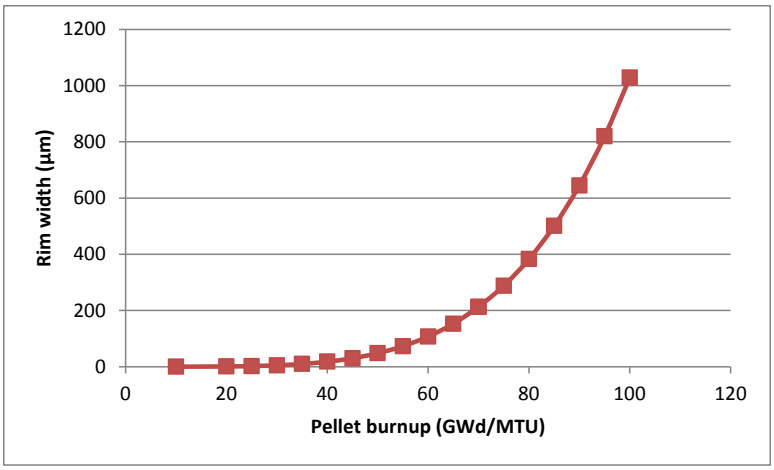

Figure C.1 – Rim width as a function of pellet burnup

The TRITON 2-D depletion calculation models for the W 17×17 OFA and GE14 assembly with a 5 wt % ^{235}U initial enrichment and 65 GWd/MTU assembly average burnup are illustrated in Figure C.2 and Figure C.3, respectively. In these models, the UO_2 fuel pellet consists of 14 concentric rings, five of which are in the pellet rim structure. The simulated assembly operating conditions include:

- four 12-month irradiation cycles with a 30 day down time period between the cycles,
- cycle-specific power values varying from 60 to 37 MW/MTU from cycle 1 to cycle 4, and
- fuel temperature variation as a function of pellet radial region and irradiation time.

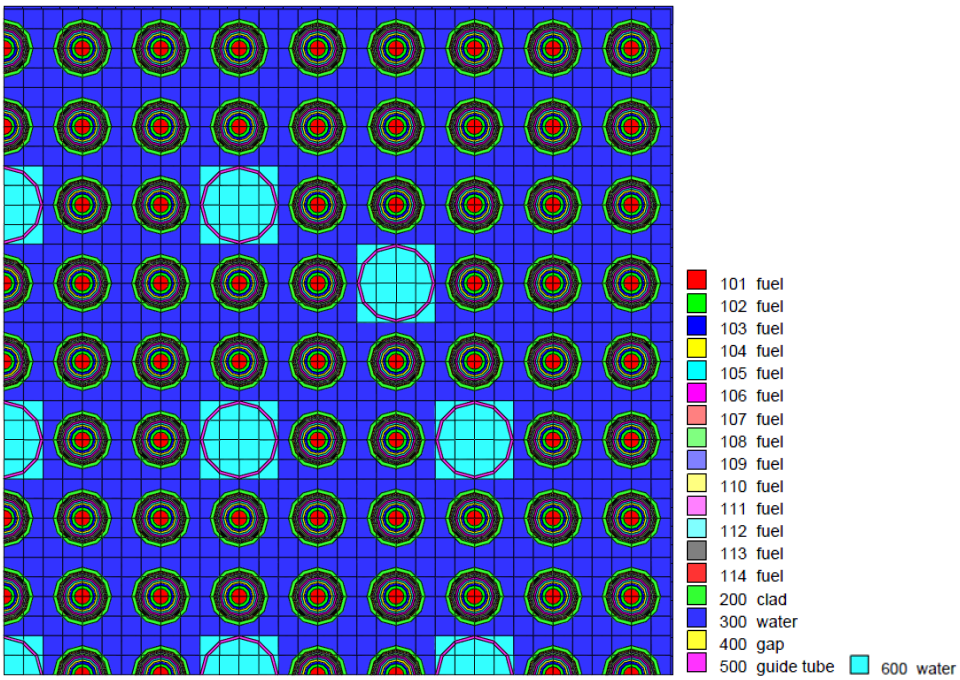

Figure C.2 – Illustration of the TRITON 2-D model for the PWR high-burnup assembly

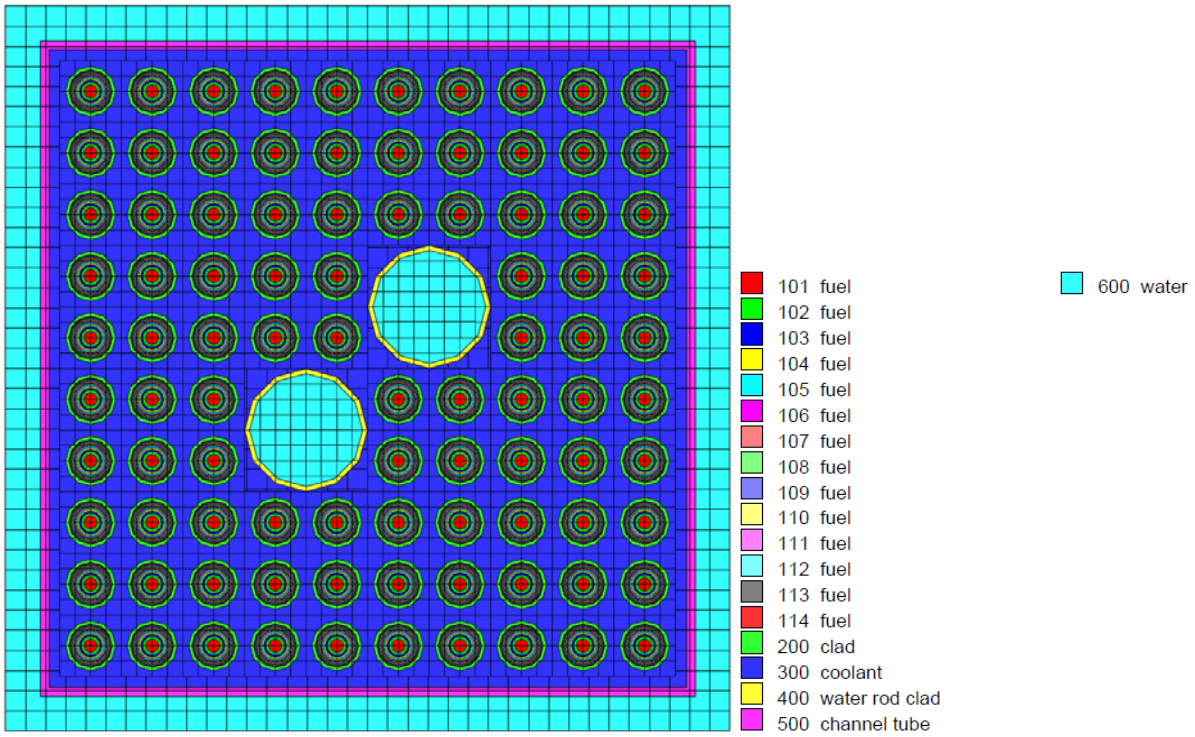

Figure C.3 – Illustration of the TRITON 2-D model for the BWR high-burnup assembly

C.5.3 Radionuclide Inventory

Within the rim structure, there is a pronounced pellet radial burnup increase near the pellet outer radius [50], as illustrated by the calculated ^{148}Nd concentration variation as a function of pellet radial location for the W 17×17 OFA (Figure C.4). The isotope ^{148}Nd is a burnup monitor used as a standard test method for atom fission in ASTM E 321 [51]. Pellet radial burnup variation results in significant variation in local nuclide concentrations primarily near the pellet periphery.

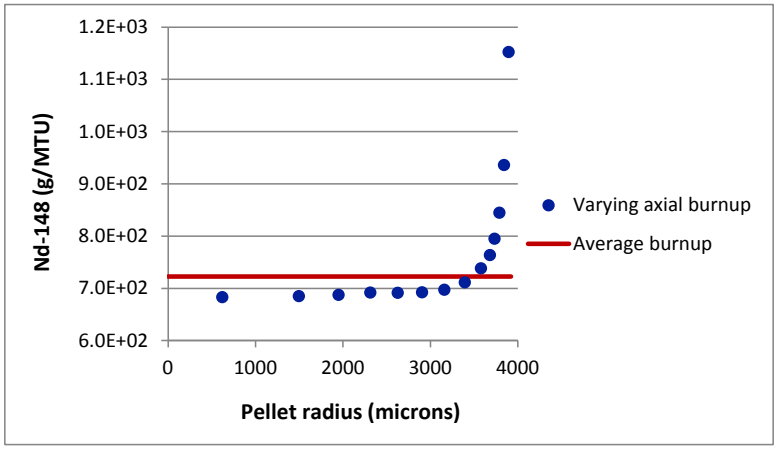

Figure C.4 – Variation of ^{148}Nd concentration as a function of pellet radial location

The calculated radionuclide activity values, in Ci per assembly, for W 17×17 OFA and GE14 fuel assemblies with a 65 GWd/MTU assembly average burnup value are tabulated in Table C.4 and Table C.5, respectively, as a function of fuel decay time. The radionuclide activity values are separately shown for the crud, radioactive gas species, radioactive volatile species, and fuel fines. Crud was assumed to consist of ^{60}Co and the total ^{60}Co activity was calculated as the surface activity times the total surface area of all rods in the cask. The average amount of crud formation on the fuel pin surface for high-burnup fuel assemblies was estimated with currently recommended ^{60}Co surface activities of 140 μCi/cm^2 for PWRs and 1254 μCi/cm^2 for BWRs [28] at the time of discharge from the reactor.

Radionuclide activity, in Ci per unit heavy metal mass (e.g., one metric ton uranium, or 1 MTU), is approximately constant in the pellet inner region (rings 1 through 8 of the pellet model) and then varies as a function of pellet radius because of varying pellet radial burnup. This variation is illustrated by the values provided in Table C.6 and Table C.7 for the W 17×17 OFA and the decay times of 5 and 300 years, respectively. The tables present the ratio of radionuclide activity in a pellet radial region (in Ci per MTU), to pellet radionuclide activity (in Ci per MTU). As can be seen in the table, radionuclide activity per unit heavy metal mass in the pellet periphery region is significantly greater than the pellet-averaged radionuclide activity for the majority of radionuclides (e.g., ~3.5 times as much for ^{252}Cf). Similar values were obtained for the GE14 assembly with 65 GWd/MTU burnup.

Table C.4 – Radionuclide activities (Ci/assembly) for W 17×17 OFA with 65 GWd/MTU burnup

Nuclide/ decay time	5 years	40 years	100 years	300 years
Crud (^{60}Co) activity (Ci/assembly)				
	2.01E+01	2.02E-01	7.55E-05	0.00E+00
Total fuel activity (Ci/assembly)				
	4.00E+05	1.30E+05	3.26E+04	3.25E+03
Gas species (Ci/assembly)				
^{3}H	2.95E+02	4.11E+01	1.41E+00	1.82E-05
^{129}I	2.30E-02	2.30E-02	2.30E-02	2.30E-02
^{81}Kr	4.38E-07	4.38E-07	4.38E-07	4.38E-07
^{85}Kr	6.21E+03	6.51E+02	1.36E+01	3.44E-05
^{127}Xe	1.02E-19	0.00E+00	0.00E+00	0.00E+00
Total	6.51E+03	6.92E+02	1.50E+01	2.30E-02
Volatile species (Ci/assembly)				
^{134}Cs	2.20E+04	1.74E-01	3.12E-10	0.00E+00
^{135}Cs	3.42E-01	3.42E-01	3.42E-01	3.42E-01
^{137}Cs	7.55E+04	3.37E+04	8.45E+03	8.40E+01
^{103}Ru	1.18E-11	0.00E+00	0.00E+00	0.00E+00
^{106}Ru	6.30E+03	3.14E-07	6.86E-25	0.00E+00
^{89}Sr	2.74E-08	0.00E+00	0.00E+00	0.00E+00
^{90}Sr	5.00E+04	2.15E+04	5.07E+03	4.11E+01
Total	1.54E+05	5.52E+04	1.35E+04	1.25E+02
Fuel fines[a] (Ci/assembly)				
^{225}Ac	3.82E-07	5.60E-07	1.24E-06	7.85E-06
^{227}Ac	2.78E-06	1.23E-05	2.23E-05	4.91E-05
^{241}Am	8.87E+02	2.63E+03	2.76E+03	2.02E+03
^{242m}Am	4.75E+00	4.00E+00	2.98E+00	1.11E+00
^{242}Am	4.72E+00	3.98E+00	2.96E+00	1.11E+00
^{243}Am	3.09E+01	3.08E+01	3.07E+01	3.01E+01
^{137m}Ba	7.13E+04	3.18E+04	7.97E+03	7.93E+01
^{247}Bk	1.49E-11	1.47E-11	1.42E-11	1.29E-11
^{144}Ce	2.82E+03	8.76E-11	0.00E+00	0.00E+00
^{248}Cf	3.95E-09	1.14E-20	0.00E+00	0.00E+00
^{249}Cf	8.86E-05	8.34E-05	7.40E-05	4.99E-05
^{250}Cf	7.67E-04	1.20E-04	4.99E-06	1.31E-10
^{251}Cf	6.84E-06	6.65E-06	6.35E-06	5.44E-06
^{252}Cf	3.97E-04	4.12E-08	6.10E-15	0.00E+00
^{242}Cm	8.21E+00	3.29E+00	2.45E+00	9.16E-01
^{243}Cm	1.89E+01	8.20E+00	1.97E+00	1.68E-02
^{244}Cm	5.03E+03	1.32E+03	1.32E+02	6.23E-02
^{245}Cm	1.13E+00	1.12E+00	1.12E+00	1.10E+00
^{246}Cm	3.21E-01	3.20E-01	3.17E-01	3.08E-01
^{247}Cm	1.57E-06	1.57E-06	1.57E-06	1.57E-06
^{248}Cm	6.04E-06	6.04E-06	6.04E-06	6.04E-06
^{154}Eu	3.85E+03	2.29E+02	1.81E+00	1.78E-07
^{155}Eu	1.51E+03	9.15E+00	1.45E-03	3.11E-16
^{93m}Nb	4.17E-01	1.18E+00	1.38E+00	1.39E+00
^{236}Np	2.98E-06	2.98E-06	2.98E-06	2.97E-06
^{237}Np	2.95E-01	3.18E-01	3.72E-01	5.25E-01
^{239}Np	3.09E+01	3.08E+01	3.07E+01	3.01E+01
^{231}Pa	1.43E-05	1.89E-05	2.68E-05	5.33E-05

Table C.4 (continued)

Nuclide/ decay time	5 years	40 years	100 years	300 years
^{233}Pa	2.95E-01	3.18E-01	3.72E-01	5.25E-01
^{147}Pm	2.02E+04	1.94E+00	2.53E-07	2.82E-30
^{210}Po	8.89E-08	8.34E-07	9.24E-06	1.63E-04
^{144}Pr	2.82E+03	8.76E-11	0.00E+00	0.00E+00
^{236}Pu	3.02E-01	6.25E-05	3.72E-07	3.72E-07
^{238}Pu	3.65E+03	2.77E+03	1.72E+03	3.56E+02
^{239}Pu	1.77E+02	1.76E+02	1.76E+02	1.75E+02
^{240}Pu	3.43E+02	3.52E+02	3.53E+02	3.46E+02
^{241}Pu	6.88E+04	1.26E+04	6.87E+02	1.14E+00
^{242}Pu	2.05E+00	2.05E+00	2.05E+00	2.05E+00
^{244}Pu	5.73E-07	5.73E-07	5.73E-07	5.73E-07
^{223}Ra	2.78E-06	1.24E-05	2.23E-05	4.91E-05
^{224}Ra	4.50E-02	5.17E-02	2.83E-02	3.78E-03
^{225}Ra	3.82E-07	5.60E-07	1.24E-06	7.85E-06
^{226}Ra	9.79E-08	2.49E-06	1.72E-05	2.06E-04
^{228}Ra	2.05E-10	6.11E-10	1.19E-09	3.23E-09
^{106}Rh	6.30E+03	3.14E-07	6.86E-25	0.00E+00
^{222}Rn	9.79E-08	2.49E-06	1.72E-05	2.06E-04
^{125}Sb	1.54E+03	2.33E-01	6.58E-08	9.81E-30
^{151}Sm	1.85E+02	1.41E+02	8.88E+01	1.90E+01
^{121m}Sn	1.13E+01	7.24E+00	3.40E+00	2.73E-01
^{99}Tc	1.07E+01	1.07E+01	1.06E+01	1.06E+01
^{125m}Te	3.77E+02	5.72E-02	1.62E-08	0.00E+00
^{227}Th	2.75E-06	1.22E-05	2.20E-05	4.84E-05
^{228}Th	4.50E-02	5.17E-02	2.83E-02	3.78E-03
^{229}Th	3.82E-07	5.60E-07	1.24E-06	7.85E-06
^{230}Th	4.69E-05	2.87E-04	8.93E-04	3.79E-03
^{231}Th	6.25E-03	6.26E-03	6.27E-03	6.30E-03
^{232}U	5.84E-02	5.03E-02	2.75E-02	3.68E-03
^{233}U	3.11E-05	7.75E-05	1.68E-04	5.61E-04
^{234}U	5.82E-01	8.98E-01	1.27E+00	1.76E+00
^{236}U	1.96E-01	1.96E-01	1.97E-01	1.99E-01
^{90}Y	5.00E+04	2.15E+04	5.07E+03	4.11E+01
^{93}Zr	1.43E+00	1.43E+00	1.43E+00	1.43E+00
Total	2.40E+05	7.36E+04	1.91E+04	3.12E+03

[a]Nuclides with individual activity greater than 10^{-4} times total assembly activity and nuclides with A_2 (Ci) values less than 1; ^{240}Cm, ^{210m}Bi, ^{254}Cf, ^{148}Gd, and ^{230}U are not shown because these nuclides have zero or negligible activities.

Table C.5 – Radionuclide activities (Ci/assembly) for the GE14 assembly with 65 GWd/MTU burnup

Nuclide/ decay time	5 years	40 years	100 years	300 years
Crud (^{60}Co) activity (Ci/assembly)				
	6.65E+01	6.67E-01	2.50E-04	0.00
Total fuel activity (Ci/assembly)				
	1.70E+05	5.49E+04	1.38E+04	1.38E+03
Gas species (Ci/assembly)				
^{3}H	1.25E+02	1.74E+01	5.95E-01	7.71E-06
^{129}I	9.74E-03	9.74E-03	9.74E-03	9.74E-03
^{81}Kr	2.13E-07	2.13E-07	2.12E-07	2.12E-07
^{85}Kr	2.63E+03	2.76E+02	5.77E+00	1.46E-05
^{127}Xe	5.40E-20	0.00E+00	0.00E+00	0.00E+00
Total	2.76E+03	2.93E+02	6.38E+00	9.76E-03
Volatile species (Ci/assembly)				
^{134}Cs	9.58E+03	7.57E-02	1.36E-10	0.00E+00
^{135}Cs	1.50E-01	1.50E-01	1.50E-01	1.50E-01
^{137}Cs	3.20E+04	1.43E+04	3.58E+03	3.56E+01
^{103}Ru	5.01E-12	0.00E+00	0.00E+00	0.00E+00
^{106}Ru	2.65E+03	1.32E-07	2.89E-25	0.00E+00
^{89}Sr	1.16E-08	0.00E+00	0.00E+00	0.00E+00
^{90}Sr	2.12E+04	9.11E+03	2.15E+03	1.74E+01
Total	6.54E+04	2.34E+04	5.73E+03	5.31E+01
Fuel Fines[a] (Ci/assembly)				
^{225}Ac	1.85E-07	2.59E-07	5.43E-07	3.27E-06
^{227}Ac	1.23E-06	5.41E-06	9.70E-06	2.11E-05
^{241}Am	3.69E+02	1.09E+03	1.15E+03	8.40E+02
^{242m}Am	2.05E+00	1.72E+00	1.28E+00	4.80E-01
^{242}Am	2.04E+00	1.71E+00	1.28E+00	4.77E-01
^{243}Am	1.26E+01	1.25E+01	1.24E+01	1.22E+01
^{137m}Ba	3.02E+04	1.35E+04	3.38E+03	3.36E+01
^{247}Bk	1.17E-11	1.15E-11	1.12E-11	1.01E-11
^{144}Ce	1.20E+03	3.71E-11	0.00E+00	0.00E+00
^{248}Cf	3.20E-09	9.23E-21	0.00E+00	0.00E+00
^{249}Cf	6.48E-05	6.10E-05	5.42E-05	3.65E-05
^{250}Cf	5.30E-04	8.29E-05	3.45E-06	9.10E-11
^{251}Cf	5.12E-06	4.98E-06	4.76E-06	4.08E-06
^{252}Cf	2.89E-04	3.00E-08	4.44E-15	0.00E+00
^{242}Cm	3.42E+00	1.42E+00	1.06E+00	3.95E-01
^{243}Cm	8.51E+00	3.69E+00	8.85E-01	7.55E-03
^{244}Cm	2.26E+03	5.90E+02	5.93E+01	2.79E-02
^{245}Cm	5.83E-01	5.81E-01	5.78E-01	5.69E-01
^{246}Cm	1.65E-01	1.64E-01	1.62E-01	1.58E-01
^{247}Cm	9.34E-07	9.34E-07	9.34E-07	9.34E-07
^{248}Cm	3.76E-06	3.76E-06	3.76E-06	3.76E-06
^{154}Eu	1.74E+03	1.03E+02	8.15E-01	8.02E-08
^{155}Eu	6.41E+02	3.89E+00	6.16E-04	1.32E-16
^{93m}Nb	1.76E-01	4.98E-01	5.83E-01	5.90E-01
^{236}Np	1.38E-06	1.37E-06	1.37E-06	1.37E-06
^{237}Np	1.21E-01	1.30E-01	1.53E-01	2.17E-01
^{239}Np	1.26E+01	1.25E+01	1.24E+01	1.22E+01
^{231}Pa	6.29E-06	8.26E-06	1.16E-05	2.29E-05

Table C.5 (continued)

Nuclide/ decay time	5 years	40 years	100 years	300 years
^{233}Pa	1.21E-01	1.30E-01	1.53E-01	2.17E-01
^{147}Pm	8.71E+03	8.39E-01	1.09E-07	1.22E-30
^{210}Po	4.24E-08	3.48E-07	3.90E-06	6.98E-05
^{144}Pr	1.20E+03	3.71E-11	0.00E+00	0.00E+00
^{236}Pu	1.35E-01	2.79E-05	1.72E-07	1.72E-07
^{238}Pu	1.62E+03	1.23E+03	7.64E+02	1.58E+02
^{239}Pu	7.85E+01	7.85E+01	7.84E+01	7.80E+01
^{240}Pu	1.59E+02	1.63E+02	1.63E+02	1.60E+02
^{241}Pu	2.86E+04	5.24E+03	2.86E+02	5.87E-01
^{242}Pu	7.85E-01	7.85E-01	7.85E-01	7.85E-01
^{244}Pu	2.62E-07	2.62E-07	2.62E-07	2.62E-07
^{223}Ra	1.23E-06	5.42E-06	9.70E-06	2.11E-05
^{224}Ra	2.01E-02	2.31E-02	1.26E-02	1.69E-03
^{225}Ra	1.85E-07	2.59E-07	5.43E-07	3.27E-06
^{226}Ra	3.94E-08	1.04E-06	7.27E-06	8.85E-05
^{228}Ra	8.53E-11	2.60E-10	5.15E-10	1.41E-09
^{106}Rh	2.65E+03	1.32E-07	2.89E-25	0.00E+00
^{222}Rn	3.94E-08	1.04E-06	7.27E-06	8.85E-05
^{125}Sb	6.58E+02	9.96E-02	2.82E-08	4.20E-30
^{151}Sm	8.42E+01	6.43E+01	4.05E+01	8.68E+00
^{121m}Sn	4.84E+00	3.12E+00	1.46E+00	1.18E-01
^{99}Tc	4.52E+00	4.52E+00	4.52E+00	4.52E+00
^{125m}Te	1.62E+02	2.45E-02	6.93E-09	0.00E+00
^{227}Th	1.21E-06	5.34E-06	9.57E-06	2.08E-05
^{228}Th	2.01E-02	2.31E-02	1.26E-02	1.69E-03
^{229}Th	1.85E-07	2.59E-07	5.43E-07	3.27E-06
^{230}Th	1.91E-05	1.21E-04	3.81E-04	1.64E-03
^{231}Th	2.66E-03	2.66E-03	2.66E-03	2.68E-03
^{232}U	2.61E-02	2.25E-02	1.23E-02	1.64E-03
^{233}U	1.34E-05	3.24E-05	6.93E-05	2.31E-04
^{234}U	2.43E-01	3.83E-01	5.48E-01	7.65E-01
^{236}U	8.57E-02	8.59E-02	8.62E-02	8.72E-02
^{90}Y	2.12E+04	9.12E+03	2.15E+03	1.74E+01
^{93}Zr	6.05E-01	6.05E-01	6.05E-01	6.05E-01
Total	1.02E+05	3.12E+04	8.11E+03	1.33E+03

[a]Nuclides with individual activity greater than 10^{-4} times total assembly activity and nuclides with A_2 (Ci) values less than 1; ^{240}Cm, ^{210m}Bi, ^{254}Cf, ^{148}Gd, and ^{230}U are not shown because these nuclides have zero or negligible activities.

Table C.6 – Pellet radial region radionuclide activity (Ci/MTU) relative to average pellet radionuclide activity (Ci/MTU) for a 5-year decay time

Pellet ring number	1-8	9	10	11	12	13	14
Volume fraction	0.8	0.0682	0.0264	0.0264	0.0264	0.0264	0.0264
Gas species							
^{3}H	0.95	1.02	1.07	1.12	1.20	1.36	1.72
^{129}I	0.94	1.02	1.07	1.13	1.23	1.41	1.84
^{81}Kr	0.94	1.05	1.10	1.16	1.26	1.43	1.85
^{85}Kr	0.98	1.02	1.04	1.06	1.10	1.17	1.33
^{127}Xe	0.94	1.04	1.09	1.15	1.25	1.43	1.85
Total	0.97	1.02	1.04	1.06	1.10	1.18	1.35
Volatile species							
^{134}Cs	0.95	1.06	1.10	1.14	1.21	1.33	1.62
^{135}Cs	0.97	0.99	1.03	1.07	1.14	1.26	1.56
^{137}Cs	0.96	1.02	1.06	1.10	1.18	1.31	1.62
^{103}Ru	0.93	1.03	1.10	1.17	1.30	1.53	2.09
^{106}Ru	0.91	1.04	1.11	1.20	1.35	1.62	2.27
^{89}Sr	0.97	1.00	1.03	1.07	1.14	1.26	1.56
^{90}Sr	0.98	1.02	1.03	1.06	1.09	1.15	1.30
Total	0.96	1.03	1.06	1.10	1.16	1.27	1.54
Fuel fines							
^{225}Ac	1.00	1.01	1.01	1.02	1.02	1.02	1.03
^{227}Ac	1.01	0.97	0.97	0.97	0.97	0.96	0.96
^{241}Am	0.90	1.04	1.12	1.23	1.40	1.71	2.45
^{242m}Am	0.91	1.02	1.10	1.20	1.37	1.68	2.42
^{242}Am	0.91	1.02	1.10	1.20	1.37	1.68	2.42
^{243}Am	0.88	1.08	1.18	1.30	1.49	1.85	2.69
^{137m}Ba	0.96	1.02	1.06	1.10	1.18	1.31	1.62
^{247}Bk	0.84	1.16	1.28	1.43	1.65	2.06	3.06
^{144}Ce	0.96	1.01	1.05	1.10	1.18	1.32	1.67
^{249}Cf	0.84	1.16	1.29	1.43	1.66	2.07	3.07
^{250}Cf	0.83	1.18	1.31	1.46	1.69	2.12	3.14
^{251}Cf	0.83	1.18	1.31	1.45	1.68	2.10	3.11
^{252}Cf	0.81	1.21	1.35	1.51	1.76	2.20	3.27
^{254}Cf	0.79	1.26	1.42	1.59	1.85	2.33	3.48
^{242}Cm	0.90	1.03	1.12	1.23	1.41	1.73	2.50
^{243}Cm	0.89	1.06	1.16	1.27	1.46	1.80	2.61
^{244}Cm	0.87	1.10	1.20	1.33	1.53	1.90	2.78
^{245}Cm	0.87	1.09	1.20	1.32	1.52	1.89	2.77
^{246}Cm	0.85	1.13	1.25	1.38	1.60	1.99	2.93
^{247}Cm	0.85	1.14	1.26	1.39	1.61	2.00	2.96
^{248}Cm	0.84	1.17	1.29	1.44	1.67	2.08	3.08
^{154}Eu	0.95	1.02	1.06	1.12	1.21	1.37	1.77
^{155}Eu	0.94	1.03	1.08	1.13	1.23	1.41	1.82
^{93m}Nb	0.97	1.02	1.04	1.07	1.12	1.20	1.40
^{236}Np	1.01	0.97	0.97	0.97	0.97	0.97	0.97
^{237}Np	0.99	1.03	1.04	1.05	1.05	1.06	1.07
^{239}Np	0.88	1.08	1.18	1.30	1.49	1.85	2.69
^{231}Pa	1.01	0.98	0.97	0.97	0.97	0.97	0.96
^{233}Pa	0.99	1.03	1.04	1.05	1.05	1.06	1.07
^{147}Pm	0.96	0.99	1.02	1.07	1.15	1.29	1.65
^{210}Po	1.00	0.99	0.99	0.98	0.98	0.99	0.99

Table C.6 (continued)

Pellet ring number	1-8	9	10	11	12	13	14
Volume fraction	0.8	0.0682	0.0264	0.0264	0.0264	0.0264	0.0264
^{144}Pr	0.96	1.01	1.05	1.10	1.18	1.32	1.67
^{236}Pu	0.99	1.01	1.02	1.02	1.03	1.03	1.04
^{238}Pu	0.97	1.04	1.07	1.09	1.13	1.19	1.33
^{239}Pu	0.92	1.00	1.07	1.16	1.30	1.57	2.20
^{240}Pu	0.97	0.91	0.96	1.02	1.13	1.34	1.82
^{241}Pu	0.90	1.04	1.13	1.23	1.40	1.71	2.46
^{242}Pu	0.88	1.07	1.17	1.29	1.48	1.83	2.65
^{244}Pu	0.87	1.10	1.20	1.33	1.53	1.90	2.79
^{223}Ra	1.01	0.97	0.97	0.97	0.97	0.96	0.96
^{224}Ra	1.00	1.01	1.01	1.02	1.02	1.03	1.04
^{225}Ra	1.00	1.01	1.01	1.02	1.02	1.02	1.03
^{226}Ra	1.01	0.98	0.97	0.97	0.97	0.97	0.97
^{228}Ra	1.00	1.01	1.01	1.01	1.02	1.02	1.02
^{106}Rh	0.91	1.04	1.11	1.20	1.35	1.62	2.27
^{222}Rn	1.01	0.98	0.97	0.97	0.97	0.97	0.97
^{125}Sb	0.94	1.02	1.07	1.13	1.23	1.42	1.86
^{151}Sm	0.95	1.01	1.05	1.11	1.21	1.39	1.81
^{121m}Sn	0.95	1.02	1.06	1.12	1.21	1.39	1.80
^{99}Tc	0.96	1.01	1.04	1.09	1.16	1.29	1.60
^{125m}Te	0.94	1.02	1.07	1.13	1.23	1.42	1.86
^{227}Th	1.01	0.97	0.97	0.97	0.97	0.96	0.96
^{228}Th	1.00	1.01	1.01	1.02	1.02	1.03	1.04
^{229}Th	1.00	1.01	1.01	1.02	1.02	1.02	1.03
^{230}Th	1.01	0.97	0.97	0.97	0.97	0.97	0.97
^{231}Th	1.03	0.91	0.90	0.89	0.89	0.88	0.87
^{232}U	1.00	1.01	1.01	1.02	1.02	1.03	1.04
^{233}U	1.01	0.97	0.96	0.96	0.96	0.96	0.96
^{234}U	1.00	0.98	0.98	0.98	0.98	0.98	1.00
^{236}U	1.00	1.00	1.00	1.00	1.00	1.00	1.00
^{90}Y	0.98	1.02	1.03	1.06	1.09	1.15	1.30
^{93}Zr	0.97	1.02	1.04	1.07	1.12	1.21	1.42
Total	0.94	1.02	1.07	1.13	1.23	1.41	1.84

Table C.7 - Pellet radial region radionuclide activity (Ci/MTU) relative to average pellet radionuclide activity (Ci/MTU) for a 300-year decay time

Pellet ring number	1-8	9	10	11	12	13	14
Volume fraction	0.8	0.0682	0.0264	0.0264	0.0264	0.0264	0.0264
Gas species							
^{3}H	0.95	1.02	1.07	1.12	1.20	1.36	1.72
^{129}I	0.94	1.02	1.07	1.13	1.23	1.41	1.84
^{81}Kr	0.94	1.05	1.10	1.16	1.26	1.43	1.85
^{85}Kr	0.98	1.02	1.04	1.06	1.10	1.17	1.33
Total	0.94	1.02	1.07	1.13	1.23	1.41	1.84
Volatile species							
^{135}Cs	0.97	0.99	1.03	1.07	1.14	1.26	1.56
^{137}Cs	0.96	1.02	1.06	1.10	1.18	1.31	1.62
^{90}Sr	0.98	1.02	1.03	1.06	1.09	1.15	1.30
Total	0.96	1.02	1.05	1.09	1.15	1.26	1.52
Fuel fines							
^{225}Ac	0.98	1.02	1.04	1.07	1.10	1.16	1.30
^{227}Ac	1.02	0.93	0.92	0.92	0.91	0.91	0.90
^{241}Am	0.90	1.04	1.12	1.23	1.40	1.71	2.45
^{242m}Am	0.91	1.02	1.10	1.20	1.37	1.68	2.42
^{242}Am	0.91	1.02	1.10	1.20	1.37	1.68	2.42
^{243}Am	0.88	1.08	1.18	1.30	1.49	1.85	2.69
^{137m}Ba	0.96	1.02	1.06	1.10	1.18	1.31	1.62
^{247}Bk	0.84	1.16	1.28	1.43	1.65	2.06	3.06
^{249}Cf	0.84	1.16	1.29	1.43	1.66	2.07	3.07
^{250}Cf	0.83	1.18	1.31	1.46	1.70	2.12	3.14
^{251}Cf	0.83	1.18	1.31	1.45	1.68	2.10	3.11
^{242}Cm	0.91	1.02	1.10	1.20	1.37	1.68	2.42
^{243}Cm	0.89	1.06	1.16	1.27	1.46	1.80	2.61
^{244}Cm	0.87	1.09	1.20	1.33	1.53	1.89	2.78
^{245}Cm	0.87	1.09	1.20	1.32	1.52	1.89	2.77
^{246}Cm	0.85	1.13	1.25	1.38	1.60	1.99	2.93
^{247}Cm	0.85	1.14	1.26	1.39	1.61	2.00	2.96
^{248}Cm	0.84	1.17	1.29	1.44	1.67	2.08	3.07
^{154}Eu	0.95	1.02	1.06	1.12	1.21	1.38	1.77
^{155}Eu	0.94	1.03	1.08	1.14	1.23	1.41	1.82
^{93m}Nb	0.97	1.02	1.04	1.07	1.12	1.21	1.42
^{236}Np	1.01	0.97	0.97	0.97	0.97	0.97	0.97
^{237}Np	0.95	1.04	1.08	1.13	1.21	1.35	1.68
^{239}Np	0.88	1.08	1.18	1.30	1.49	1.85	2.69
^{231}Pa	1.02	0.93	0.92	0.92	0.91	0.90	0.90
^{233}Pa	0.95	1.04	1.08	1.13	1.21	1.35	1.68
^{147}Pm	0.96	0.99	1.02	1.07	1.15	1.29	1.65
^{210}Po	0.99	1.01	1.02	1.03	1.05	1.08	1.16
^{236}Pu	1.01	0.97	0.97	0.97	0.97	0.97	0.97
^{238}Pu	0.97	1.04	1.07	1.09	1.13	1.19	1.33
^{239}Pu	0.92	1.00	1.07	1.16	1.30	1.57	2.20
^{240}Pu	0.96	0.92	0.97	1.03	1.15	1.36	1.85
^{241}Pu	0.87	1.09	1.20	1.32	1.52	1.88	2.76
^{242}Pu	0.88	1.07	1.17	1.29	1.48	1.83	2.65
^{244}Pu	0.87	1.10	1.20	1.33	1.53	1.90	2.79
^{223}Ra	1.02	0.93	0.92	0.92	0.91	0.91	0.90

Table C.7 (continued)

Pellet ring number	1-8	9	10	11	12	13	14
Volume fraction	0.8	0.0682	0.0264	0.0264	0.0264	0.0264	0.0264
^{224}Ra	0.99	1.01	1.01	1.02	1.02	1.03	1.04
^{225}Ra	0.98	1.02	1.04	1.07	1.10	1.16	1.30
^{226}Ra	0.99	1.01	1.02	1.03	1.05	1.09	1.16
^{228}Ra	1.00	1.00	1.00	1.00	1.00	1.00	1.00
^{222}Rn	0.99	1.01	1.02	1.03	1.05	1.09	1.16
^{125}Sb	0.94	1.02	1.07	1.13	1.23	1.42	1.86
^{151}Sm	0.95	1.01	1.05	1.11	1.21	1.39	1.81
^{121m}Sn	0.95	1.02	1.06	1.12	1.21	1.39	1.80
^{99}Tc	0.96	1.01	1.04	1.09	1.16	1.29	1.60
^{227}Th	1.02	0.93	0.92	0.92	0.91	0.91	0.90
^{228}Th	0.99	1.01	1.01	1.02	1.02	1.03	1.04
^{229}Th	0.98	1.02	1.04	1.07	1.10	1.16	1.30
^{230}Th	0.98	1.01	1.03	1.04	1.06	1.10	1.19
^{231}Th	1.03	0.92	0.90	0.90	0.89	0.89	0.88
^{232}U	0.99	1.01	1.01	1.02	1.02	1.03	1.04
^{233}U	0.97	1.03	1.06	1.09	1.14	1.23	1.44
^{234}U	0.98	1.02	1.04	1.05	1.08	1.12	1.22
^{236}U	1.00	1.00	1.00	1.00	1.00	1.00	1.01
^{90}Y	0.98	1.02	1.03	1.06	1.09	1.15	1.30
^{93}Zr	0.97	1.02	1.04	1.07	1.12	1.21	1.42
Total	0.92	1.02	1.09	1.18	1.32	1.59	2.20

C.5.4 Containment Analysis

A sensitivity analysis was performed in this study because the range of parameters important for the containment analysis of high-burnup fuel (i.e., the release fractions and breached spent fuel rod fraction) has not been established yet for normal and accident conditions of transport.

Normal Conditions of Transport

The allowable leakage rate for NCT was calculated as a function of decay time (5, 40, 100, and 300 years), pellet radial region from which the releasable radioactive material originates (non-rim region and rim structure corresponding to ring No. 14 in the calculation model previously described in Sect.C.5.2), and fraction of fuel rods assumed to fail (0.01, 0.03, 0.10, and 1) using the following release fractions:

- crud: 0.15, 0.3, 0.5, and 1;
- gaseous species: 0.1, 0.3, and 0.4;
- volatile species: 2×10^{-4}, 1×10^{-3}, and 2×10^{-3}; and
- fuel fines: 3×10^{-5}, 1.5×10^{-4}, and 3×10^{-4}.

where, the underlined values are the release fractions typically used for low-burnup fuel (see Table C.1).

Using these release fractions, 15 different cases were developed for each decay time, pellet radial region, and fraction of fuel rods assumed to develop cladding breaches. Case 1 is the

nominal intact configuration that uses the release fractions typically used for low-burnup fuel. For cases 2 through 10, the varying parameters were changed one at a time. Cases 2 through 4 use varying fraction of crud that spalls off cladding; cases 5 and 6 use a varying fraction of gases released due to a cladding breach; cases 7 and 8 use a varying fraction of volatiles released due to a cladding breach; and cases 9 and 10 use a varying mass fraction of fuel released as fuel fines due to a cladding breach. For cases 11 through 15, multiple varying parameters were changed simultaneously because fuel fragmentation and fission gas release are expected to be correlated. The NCT allowable release rates are summarized in Table C.8 and Table C.9 for the GBC-32 and GBC-68, respectively. The free void volumes of the GBC-32 and GBC-68 used in the calculations were 7.05E+06 cm^3 and 5.68E+06 cm^3, respectively. The graphs in Figure C.5 and Figure C.6 illustrate the effects of varying release fractions on the GBC-32 and GBC-68 allowable leakage rates, respectively. For each decay time, the effects of each parameter relevant to failed fuel containment are further analyzed.

Decay time

Decay time has a significant impact on the releasable activity and allowable leakage rate primarily because of the decay of ^{60}Co ($t_{1/2}$ = 5.271 years), which is the source of radioactivity in crud, and ^{85}Kr ($t_{1/2}$ = 10.76 years), which dominates the gaseous species. The allowable leakage rate increases with increasing decay time.

Fuel pellet radial region

The extent to which the pellet radial region from which the releasable activity originates affects the allowable leakage rate depends on the contribution of the crud to the total releasable activity. Small effects are observed for GBC-32, the 5-year decay time, and small fraction of breached spent fuel rods (e.g., 0.01), as well as for GBC-68, the 5-year decay time, and any fraction of breached spent fuel rods, as crud has a significant contribution to the total releasable activity for these cases. For the other cases, the allowable leakage rate based on releasable activity from the outer rim structure is approximately half the allowable leakage rate based on releasable activity from the non-rim region.

Fraction of fuel rods that develop cladding breaches

Allowable leakage rate decreases with increasing fraction of breached spent fuel rods. The decrease is relatively small (e.g., a 15% decrease because of an increase in spent fuel rod breach fraction from 0.01 to 0.03) if crud has a large contribution to the total releasable activity (e.g., cases 1 through 4) and is fairly large if the fuel fines dominate the total releasable activity (e.g. a decrease by a factor of 2.5 because of an increase of failed fuel rod fraction from 0.01 to 0.03).

Fraction of crud that spalls off cladding

Crud is an important factor in the calculation of the allowable leakage rate for the time interval 5 to 40 years after fuel discharge from the reactor because of its relatively high contribution to the total releasable activity. Crud has a more pronounced effect on the BWR packages than on the PWR packages because of the larger ^{60}Co activity per fuel rod surface area associated with the BWR fuel. As a result, the BWR package allowable leakage rates are smaller (i.e., more restrictive) than the PWR package allowable leakage rates. For GBC-68 and the 5-year decay time, an increase in the fraction of crud that spalls off the cladding by a factor of two would cause a decrease in the allowable leakage rate by a factor of approximately two.

Table C.8 – GBC-32 allowable leakage rate for NCT

5-year decay time												
					Non-rim pellet region				Rim pellet region			
					Fraction of breached fuel rods				Fraction of breached fuel rods			
					0.01	0.03	0.10	1.00	0.01	0.03	0.10	1.00
Case#	f_G[a]	f_V[b]	f_F[c]	f_C[d]	Allowable leakage rate (cm^3/s)				Allowable leakage rate (cm^3/s)			
1	0.3	2.0E-4	3.0E-5	0.15	1.3E-04	7.3E-05	2.9E-05	3.3E-06	1.0E-04	4.8E-05	1.7E-05	1.8E-06
2	0.3	2.0E-4	3.0E-5	0.3	8.2E-05	5.5E-05	2.5E-05	3.2E-06	6.8E-05	3.9E-05	1.6E-05	1.8E-06
3	0.3	2.0E-4	3.0E-5	0.5	5.5E-05	4.1E-05	2.2E-05	3.1E-06	4.8E-05	3.2E-05	1.4E-05	1.8E-06
4	0.3	2.0E-4	3.0E-5	1.0	3.0E-05	2.5E-05	1.6E-05	3.0E-06	2.8E-05	2.1E-05	1.2E-05	1.7E-06
5	0.1	2.0E-4	3.0E-5	0.15	1.5E-04	8.8E-05	3.6E-05	4.3E-06	1.1E-04	5.6E-05	2.0E-05	2.2E-06
6	0.4	2.0E-4	3.0E-5	0.15	1.3E-04	6.8E-05	2.6E-05	2.9E-06	9.5E-05	4.4E-05	1.6E-05	1.7E-06
7	0.3	1.0E-3	3.0E-5	0.15	1.1E-04	5.4E-05	1.9E-05	2.1E-06	7.9E-05	3.5E-05	1.2E-05	1.2E-06
8	0.3	2.0E-3	3.0E-5	0.15	8.8E-05	4.0E-05	1.4E-05	1.5E-06	6.3E-05	2.6E-05	8.4E-06	8.7E-07
9	0.3	2.0E-4	1.5E-4	0.15	7.3E-05	3.2E-05	1.1E-05	1.1E-06	4.3E-05	1.6E-05	5.2E-06	5.3E-07
10	0.3	2.0E-4	3.0E-4	0.15	4.7E-05	1.8E-05	5.9E-06	6.0E-07	2.5E-05	9.1E-06	2.8E-06	2.8E-07
11	0.3	2.0E-3	3.0E-4	0.15	4.0E-05	1.5E-05	4.8E-06	4.9E-07	2.2E-05	7.8E-06	2.4E-06	2.4E-07
12	0.1	2.0E-3	3.0E-4	0.15	4.1E-05	1.6E-05	5.0E-06	5.1E-07	2.2E-05	8.0E-06	2.5E-06	2.5E-07
13	0.4	2.0E-3	3.0E-4	0.15	4.0E-05	1.5E-05	4.7E-06	4.8E-07	2.2E-05	7.7E-06	2.4E-06	2.4E-07
14	0.4	2.0E-3	3.0E-4	0.5	2.8E-05	1.3E-05	4.5E-06	4.8E-07	1.8E-05	7.1E-06	2.3E-06	2.4E-07
15	0.4	2.0E-3	3.0E-4	1.0	2.0E-05	1.1E-05	4.2E-06	4.8E-07	1.4E-05	6.4E-06	2.2E-06	2.4E-07
40-year decay time												
					Non-rim pellet region				Rim pellet region			
					Fraction of breached fuel rods				Fraction of breached fuel rods			
					0.01	0.03	0.10	1.00	0.01	0.03	0.10	1.00
Case#	f_G[a]	f_V[b]	f_F[c]	f_C[d]	Allowable leakage rate (cm^3/s)				Allowable leakage rate (cm^3/s)			
1	0.3	2.0E-4	3.0E-5	0.15	6.8E-04	2.3E-04	7.0E-05	7.0E-06	3.4E-04	1.2E-04	3.5E-05	3.5E-06
2	0.3	2.0E-4	3.0E-5	0.3	6.6E-04	2.3E-04	6.9E-05	7.0E-06	3.4E-04	1.1E-04	3.5E-05	3.5E-06
3	0.3	2.0E-4	3.0E-5	0.5	6.3E-04	2.2E-04	6.9E-05	7.0E-06	3.3E-04	1.1E-04	3.5E-05	3.5E-06
4	0.3	2.0E-4	3.0E-5	1.0	5.8E-04	2.2E-04	6.8E-05	7.0E-06	3.1E-04	1.1E-04	3.4E-05	3.5E-06
5	0.1	2.0E-4	3.0E-5	0.15	7.1E-04	2.4E-04	7.4E-05	7.4E-06	3.6E-04	1.2E-04	3.6E-05	3.6E-06
6	0.4	2.0E-4	3.0E-5	0.15	6.6E-04	2.2E-04	6.8E-05	6.8E-06	3.4E-04	1.1E-04	3.4E-05	3.4E-06
7	0.3	1.0E-3	3.0E-5	0.15	4.8E-04	1.6E-04	4.9E-05	4.9E-06	2.6E-04	8.8E-05	2.7E-05	2.7E-06
8	0.3	2.0E-3	3.0E-5	0.15	3.5E-04	1.2E-04	3.6E-05	3.6E-06	2.0E-04	6.8E-05	2.0E-05	2.1E-06
9	0.3	2.0E-4	1.5E-4	0.15	1.6E-04	5.5E-05	1.6E-05	1.6E-06	7.8E-05	2.6E-05	7.8E-06	7.8E-07
10	0.3	2.0E-4	3.0E-4	0.15	8.4E-05	2.8E-05	8.4E-06	8.4E-07	4.0E-05	1.3E-05	4.0E-06	4.0E-07
11	0.3	2.0E-3	3.0E-4	0.15	7.5E-05	2.5E-05	7.5E-06	7.5E-07	3.7E-05	1.2E-05	3.7E-06	3.7E-07
12	0.1	2.0E-3	3.0E-4	0.15	7.6E-05	2.5E-05	7.6E-06	7.6E-07	3.7E-05	1.2E-05	3.7E-06	3.7E-07
13	0.4	2.0E-3	3.0E-4	0.15	7.5E-05	2.5E-05	7.5E-06	7.5E-07	3.7E-05	1.2E-05	3.7E-06	3.7E-07
14	0.4	2.0E-3	3.0E-4	0.5	7.4E-05	2.5E-05	7.5E-06	7.5E-07	3.6E-05	1.2E-05	3.7E-06	3.7E-07
15	0.4	2.0E-3	3.0E-4	1.0	7.3E-05	2.5E-05	7.5E-06	7.5E-07	3.6E-05	1.2E-05	3.7E-06	3.7E-07

Table C.8 (continued)

100-year decay time												
					Non-rim pellet region				Rim pellet region			
					Fraction of breached fuel rods				Fraction of breached fuel rods			
					0.01	0.03	0.10	1.00	0.01	0.03	0.10	1.00
Case#	f_G[a]	f_V[b]	f_F[c]	f_C[d]	Allowable leakage rate (cm^3/s)				Allowable leakage rate (cm^3/s)			
1	0.3	2.0E-4	3.0E-5	0.15	1.1E-03	3.7E-04	1.1E-04	1.1E-05	5.1E-04	1.7E-04	5.1E-05	5.1E-06
2	0.3	2.0E-4	3.0E-5	0.3	1.1E-03	3.7E-04	1.1E-04	1.1E-05	5.1E-04	1.7E-04	5.1E-05	5.1E-06
3	0.3	2.0E-4	3.0E-5	0.5	1.1E-03	3.7E-04	1.1E-04	1.1E-05	5.1E-04	1.7E-04	5.1E-05	5.1E-06
4	0.3	2.0E-4	3.0E-5	1.0	1.1E-03	3.7E-04	1.1E-04	1.1E-05	5.1E-04	1.7E-04	5.1E-05	5.1E-06
5	0.1	2.0E-4	3.0E-5	0.15	1.1E-03	3.7E-04	1.1E-04	1.1E-05	5.1E-04	1.7E-04	5.1E-05	5.1E-06
6	0.4	2.0E-4	3.0E-5	0.15	1.1E-03	3.7E-04	1.1E-04	1.1E-05	5.1E-04	1.7E-04	5.1E-05	5.1E-06
7	0.3	1.0E-3	3.0E-5	0.15	9.5E-04	3.2E-04	9.5E-05	9.5E-06	4.6E-04	1.5E-04	4.6E-05	4.6E-06
8	0.3	2.0E-3	3.0E-5	0.15	8.1E-04	2.7E-04	8.1E-05	8.1E-06	4.1E-04	1.4E-04	4.1E-05	4.1E-06
9	0.3	2.0E-4	1.5E-4	0.15	2.3E-04	7.6E-05	2.3E-05	2.3E-06	1.1E-04	3.5E-05	1.1E-05	1.1E-06
10	0.3	2.0E-4	3.0E-4	0.15	1.1E-04	3.8E-05	1.1E-05	1.1E-06	5.3E-05	1.8E-05	5.3E-06	5.3E-07
11	0.3	2.0E-3	3.0E-4	0.15	1.1E-04	3.7E-05	1.1E-05	1.1E-06	5.1E-05	1.7E-05	5.1E-06	5.1E-07
12	0.1	2.0E-3	3.0E-4	0.15	1.1E-04	3.7E-05	1.1E-05	1.1E-06	5.1E-05	1.7E-05	5.1E-06	5.1E-07
13	0.4	2.0E-3	3.0E-4	0.15	1.1E-04	3.7E-05	1.1E-05	1.1E-06	5.1E-05	1.7E-05	5.1E-06	5.1E-07
14	0.4	2.0E-3	3.0E-4	0.5	1.1E-04	3.7E-05	1.1E-05	1.1E-06	5.1E-05	1.7E-05	5.1E-06	5.1E-07
15	0.4	2.0E-3	3.0E-4	1.0	1.1E-04	3.7E-05	1.1E-05	1.1E-06	5.1E-05	1.7E-05	5.1E-06	5.1E-07
300-year decay time												
					Non-rim pellet region				Rim pellet region			
					Fraction of breached fuel rods				Fraction of breached fuel rods			
					0.01	0.03	0.10	1.00	0.01	0.03	0.10	1.00
Case#	f_G[a]	f_V[b]	f_F[c]	f_C[d]	Allowable leakage rate (cm^3/s)				Allowable leakage rate (cm^3/s)			
1	0.3	2.0E-4	3.0E-5	0.15	2.1E-03	6.8E-04	2.1E-04	2.1E-05	8.4E-04	2.8E-04	8.4E-05	8.4E-06
2	0.3	2.0E-4	3.0E-5	0.3	2.1E-03	6.8E-04	2.1E-04	2.1E-05	8.4E-04	2.8E-04	8.4E-05	8.4E-06
3	0.3	2.0E-4	3.0E-5	0.5	2.1E-03	6.8E-04	2.1E-04	2.1E-05	8.4E-04	2.8E-04	8.4E-05	8.4E-06
4	0.3	2.0E-4	3.0E-5	1.0	2.1E-03	6.8E-04	2.1E-04	2.1E-05	8.4E-04	2.8E-04	8.4E-05	8.4E-06
5	0.1	2.0E-4	3.0E-5	0.15	2.1E-03	6.8E-04	2.1E-04	2.1E-05	8.4E-04	2.8E-04	8.4E-05	8.4E-06
6	0.4	2.0E-4	3.0E-5	0.15	2.1E-03	6.8E-04	2.1E-04	2.1E-05	8.4E-04	2.8E-04	8.4E-05	8.4E-06
7	0.3	1.0E-3	3.0E-5	0.15	2.0E-03	6.8E-04	2.0E-04	2.0E-05	8.4E-04	2.8E-04	8.4E-05	8.4E-06
8	0.3	2.0E-3	3.0E-5	0.15	2.0E-03	6.8E-04	2.0E-04	2.0E-05	8.4E-04	2.8E-04	8.4E-05	8.4E-06
9	0.3	2.0E-4	1.5E-4	0.15	4.1E-04	1.4E-04	4.1E-05	4.1E-06	1.7E-04	5.6E-05	1.7E-05	1.7E-06
10	0.3	2.0E-4	3.0E-4	0.15	2.1E-04	6.8E-05	2.1E-05	2.1E-06	8.4E-05	2.8E-05	8.4E-06	8.4E-07
11	0.3	2.0E-3	3.0E-4	0.15	2.1E-04	6.8E-05	2.1E-05	2.1E-06	8.4E-05	2.8E-05	8.4E-06	8.4E-07
12	0.1	2.0E-3	3.0E-4	0.15	2.1E-04	6.8E-05	2.1E-05	2.1E-06	8.4E-05	2.8E-05	8.4E-06	8.4E-07
13	0.4	2.0E-3	3.0E-4	0.15	2.1E-04	6.8E-05	2.1E-05	2.1E-06	8.4E-05	2.8E-05	8.4E-06	8.4E-07
14	0.4	2.0E-3	3.0E-4	0.5	2.1E-04	6.8E-05	2.1E-05	2.1E-06	8.4E-05	2.8E-05	8.4E-06	8.4E-07
15	0.4	2.0E-3	3.0E-4	1.0	2.1E-04	6.8E-05	2.1E-05	2.1E-06	8.4E-05	2.8E-05	8.4E-06	8.4E-07

[a]Fraction of gases released due to a cladding breach
[b]Fraction of volatiles released due to a cladding breach
[c]Mass fraction of fuel released as fines due to a cladding breach
[d]Fraction of crud that spalls off cladding.

Table C.9 – GBC-68 allowable leakage rate for NCT

5-year decay time												
					Non-rim pellet region				Rim pellet region			
					Fraction of breached fuel rods				Fraction of breached fuel rods			
					0.01	0.03	0.10	1.00	0.01	0.03	0.10	1.00
Case#	f_G[a]	f_V[b]	f_F[c]	f_C[d]	Allowable leakage rate (cm^3/s)				Allowable leakage rate (cm^3/s)			
1	0.3	2.0E-4	3.0E-5	0.15	2.3E-05	2.0E-05	1.3E-05	2.6E-06	2.2E-05	1.8E-05	1.0E-05	1.6E-06
2	0.3	2.0E-4	3.0E-5	0.3	1.2E-05	1.1E-05	8.7E-06	2.3E-06	1.2E-05	1.0E-05	7.3E-06	1.5E-06
3	0.3	2.0E-4	3.0E-5	0.5	7.3E-06	7.0E-06	6.0E-06	2.1E-06	7.2E-06	6.7E-06	5.3E-06	1.4E-06
4	0.3	2.0E-4	3.0E-5	1.0	3.7E-06	3.6E-06	3.3E-06	1.6E-06	3.7E-06	3.5E-06	3.1E-06	1.2E-06
5	0.1	2.0E-4	3.0E-5	0.15	2.4E-05	2.1E-05	1.5E-05	3.3E-06	2.2E-05	1.9E-05	1.2E-05	2.0E-06
6	0.4	2.0E-4	3.0E-5	0.15	2.3E-05	1.9E-05	1.3E-05	2.3E-06	2.2E-05	1.7E-05	9.7E-06	1.5E-06
7	0.3	1.0E-3	3.0E-5	0.15	2.2E-05	1.8E-05	1.1E-05	1.7E-06	2.1E-05	1.5E-05	8.0E-06	1.1E-06
8	0.3	2.0E-3	3.0E-5	0.15	2.1E-05	1.6E-05	8.6E-06	1.2E-06	1.9E-05	1.3E-05	6.3E-06	8.1E-07
9	0.3	2.0E-4	1.5E-4	0.15	2.0E-05	1.4E-05	6.9E-06	9.1E-07	1.7E-05	1.0E-05	4.3E-06	5.0E-07
10	0.3	2.0E-4	3.0E-4	0.15	1.7E-05	1.0E-05	4.3E-06	5.0E-07	1.3E-05	6.7E-06	2.5E-06	2.7E-07
11	0.3	2.0E-3	3.0E-4	0.15	1.6E-05	9.0E-06	3.6E-06	4.2E-07	1.2E-05	5.9E-06	2.1E-06	2.3E-07
12	0.1	2.0E-3	3.0E-4	0.15	1.6E-05	9.3E-06	3.7E-06	4.3E-07	1.2E-05	6.0E-06	2.2E-06	2.4E-07
13	0.4	2.0E-3	3.0E-4	0.15	1.6E-05	8.9E-06	3.6E-06	4.1E-07	1.2E-05	5.9E-06	2.1E-06	2.3E-07
14	0.4	2.0E-3	3.0E-4	0.5	6.4E-06	4.9E-06	2.7E-06	3.9E-07	5.7E-06	3.8E-06	1.8E-06	2.2E-07
15	0.4	2.0E-3	3.0E-4	1.0	3.5E-06	3.0E-06	2.0E-06	3.7E-07	3.2E-06	2.5E-06	1.4E-06	2.2E-07
40-year decay time												
					Non-rim pellet region				Rim pellet region			
					Fraction of breached fuel rods				Fraction of breached fuel rods			
					0.01	0.03	0.10	1.00	0.01	0.03	0.10	1.00
Case#	f_G[a]	f_V[b]	f_F[c]	f_C[d]	Allowable leakage rate (cm^3/s)				Allowable leakage rate (cm^3/s)			
1	0.3	2.0E-4	3.0E-5	0.15	4.9E-04	1.9E-04	5.9E-05	6.0E-06	3.0E-04	1.1E-04	3.3E-05	3.4E-06
2	0.3	2.0E-4	3.0E-5	0.3	4.1E-04	1.7E-04	5.8E-05	6.0E-06	2.7E-04	1.0E-04	3.3E-05	3.4E-06
3	0.3	2.0E-4	3.0E-5	0.5	3.4E-04	1.6E-04	5.6E-05	6.0E-06	2.3E-04	9.8E-05	3.2E-05	3.4E-06
4	0.3	2.0E-4	3.0E-5	1.0	2.3E-04	1.3E-04	5.2E-05	6.0E-06	1.8E-04	8.7E-05	3.1E-05	3.4E-06
5	0.1	2.0E-4	3.0E-5	0.15	5.1E-04	2.0E-04	6.2E-05	6.4E-06	3.1E-04	1.1E-04	3.5E-05	3.5E-06
6	0.4	2.0E-4	3.0E-5	0.15	4.8E-04	1.8E-04	5.8E-05	5.9E-06	2.9E-04	1.1E-04	3.3E-05	3.3E-06
7	0.3	1.0E-3	3.0E-5	0.15	3.7E-04	1.4E-04	4.2E-05	4.3E-06	2.3E-04	8.3E-05	2.5E-05	2.6E-06
8	0.3	2.0E-3	3.0E-5	0.15	2.8E-04	1.0E-04	3.1E-05	3.2E-06	1.8E-04	6.4E-05	2.0E-05	2.0E-06
9	0.3	2.0E-4	1.5E-4	0.15	1.3E-04	4.6E-05	1.4E-05	1.4E-06	7.4E-05	2.5E-05	7.6E-06	7.6E-07
10	0.3	2.0E-4	3.0E-4	0.15	7.0E-05	2.4E-05	7.2E-06	7.2E-07	3.8E-05	1.3E-05	3.9E-06	3.9E-07
11	0.3	2.0E-3	3.0E-4	0.15	6.3E-05	2.2E-05	6.5E-06	6.5E-07	3.5E-05	1.2E-05	3.6E-06	3.6E-07
12	0.1	2.0E-3	3.0E-4	0.15	6.4E-05	2.2E-05	6.5E-06	6.5E-07	3.5E-05	1.2E-05	3.6E-06	3.6E-07
13	0.4	2.0E-3	3.0E-4	0.15	6.3E-05	2.1E-05	6.5E-06	6.5E-07	3.5E-05	1.2E-05	3.6E-06	3.6E-07
14	0.4	2.0E-3	3.0E-4	0.5	6.0E-05	2.1E-05	6.4E-06	6.5E-07	3.4E-05	1.2E-05	3.5E-06	3.6E-07
15	0.4	2.0E-3	3.0E-4	1.0	5.5E-05	2.0E-05	6.4E-06	6.5E-07	3.3E-05	1.2E-05	3.5E-06	3.6E-07

Table C.9 (continued)

100-year decay time												
					Non-rim pellet region				Rim pellet region			
					Fraction of breached fuel rods				Fraction of breached fuel rods			
					0.01	0.03	0.10	1.00	0.01	0.03	0.10	1.00
Case#	f_G[a]	f_V[b]	f_F[c]	f_C[d]	Allowable leakage rate (cm^3/s)				Allowable leakage rate (cm^3/s)			
1	0.3	2.0E-4	3.0E-5	0.15	9.6E-04	3.2E-04	9.6E-05	9.6E-06	5.1E-04	1.7E-04	5.1E-05	5.1E-06
2	0.3	2.0E-4	3.0E-5	0.3	9.6E-04	3.2E-04	9.6E-05	9.6E-06	5.1E-04	1.7E-04	5.1E-05	5.1E-06
3	0.3	2.0E-4	3.0E-5	0.5	9.6E-04	3.2E-04	9.6E-05	9.6E-06	5.1E-04	1.7E-04	5.1E-05	5.1E-06
4	0.3	2.0E-4	3.0E-5	1.0	9.6E-04	3.2E-04	9.6E-05	9.6E-06	5.1E-04	1.7E-04	5.1E-05	5.1E-06
5	0.1	2.0E-4	3.0E-5	0.15	9.6E-04	3.2E-04	9.6E-05	9.6E-06	5.1E-04	1.7E-04	5.1E-05	5.1E-06
6	0.4	2.0E-4	3.0E-5	0.15	9.6E-04	3.2E-04	9.6E-05	9.6E-06	5.1E-04	1.7E-04	5.1E-05	5.1E-06
7	0.3	1.0E-3	3.0E-5	0.15	8.3E-04	2.8E-04	8.3E-05	8.3E-06	4.5E-04	1.5E-04	4.5E-05	4.5E-06
8	0.3	2.0E-3	3.0E-5	0.15	7.1E-04	2.4E-04	7.1E-05	7.1E-06	4.0E-04	1.3E-04	4.0E-05	4.0E-06
9	0.3	2.0E-4	1.5E-4	0.15	2.0E-04	6.6E-05	2.0E-05	2.0E-06	1.0E-04	3.5E-05	1.0E-05	1.0E-06
10	0.3	2.0E-4	3.0E-4	0.15	1.0E-04	3.3E-05	1.0E-05	1.0E-06	5.2E-05	1.7E-05	5.2E-06	5.2E-07
11	0.3	2.0E-3	3.0E-4	0.15	9.6E-05	3.2E-05	9.6E-06	9.6E-07	5.1E-05	1.7E-05	5.1E-06	5.1E-07
12	0.1	2.0E-3	3.0E-4	0.15	9.6E-05	3.2E-05	9.6E-06	9.6E-07	5.1E-05	1.7E-05	5.1E-06	5.1E-07
13	0.4	2.0E-3	3.0E-4	0.15	9.6E-05	3.2E-05	9.6E-06	9.6E-07	5.1E-05	1.7E-05	5.1E-06	5.1E-07
14	0.4	2.0E-3	3.0E-4	0.5	9.6E-05	3.2E-05	9.6E-06	9.6E-07	5.1E-05	1.7E-05	5.1E-06	5.1E-07
15	0.4	2.0E-3	3.0E-4	1.0	9.6E-05	3.2E-05	9.6E-06	9.6E-07	5.1E-05	1.7E-05	5.1E-06	5.1E-07
300-year decay time												
					Non-rim pellet region				Rim pellet region			
					Fraction of breached fuel rods				Fraction of breached fuel rods			
					0.01	0.03	0.10	1.00	0.01	0.03	0.10	1.00
Case#	f_G[a]	f_V[b]	f_F[c]	f_C[d]	Allowable leakage rate (cm^3/s)				Allowable leakage rate (cm^3/s)			
1	0.3	2.0E-4	3.0E-5	0.15	1.8E-03	5.9E-04	1.8E-04	1.8E-05	8.5E-04	2.8E-04	8.5E-05	8.5E-06
2	0.3	2.0E-4	3.0E-5	0.3	1.8E-03	5.9E-04	1.8E-04	1.8E-05	8.5E-04	2.8E-04	8.5E-05	8.5E-06
3	0.3	2.0E-4	3.0E-5	0.5	1.8E-03	5.9E-04	1.8E-04	1.8E-05	8.5E-04	2.8E-04	8.5E-05	8.5E-06
4	0.3	2.0E-4	3.0E-5	1.0	1.8E-03	5.9E-04	1.8E-04	1.8E-05	8.5E-04	2.8E-04	8.5E-05	8.5E-06
5	0.1	2.0E-4	3.0E-5	0.15	1.8E-03	5.9E-04	1.8E-04	1.8E-05	8.5E-04	2.8E-04	8.5E-05	8.5E-06
6	0.4	2.0E-4	3.0E-5	0.15	1.8E-03	5.9E-04	1.8E-04	1.8E-05	8.5E-04	2.8E-04	8.5E-05	8.5E-06
7	0.3	1.0E-3	3.0E-5	0.15	1.8E-03	5.9E-04	1.8E-04	1.8E-05	8.4E-04	2.8E-04	8.4E-05	8.4E-06
8	0.3	2.0E-3	3.0E-5	0.15	1.8E-03	5.9E-04	1.8E-04	1.8E-05	8.4E-04	2.8E-04	8.4E-05	8.4E-06
9	0.3	2.0E-4	1.5E-4	0.15	3.6E-04	1.2E-04	3.6E-05	3.6E-06	1.7E-04	5.6E-05	1.7E-05	1.7E-06
10	0.3	2.0E-4	3.0E-4	0.15	1.8E-04	5.9E-05	1.8E-05	1.8E-06	8.5E-05	2.8E-05	8.5E-06	8.5E-07
11	0.3	2.0E-3	3.0E-4	0.15	1.8E-04	5.9E-05	1.8E-05	1.8E-06	8.5E-05	2.8E-05	8.5E-06	8.5E-07
12	0.1	2.0E-3	3.0E-4	0.15	1.8E-04	5.9E-05	1.8E-05	1.8E-06	8.5E-05	2.8E-05	8.5E-06	8.5E-07
13	0.4	2.0E-3	3.0E-4	0.15	1.8E-04	5.9E-05	1.8E-05	1.8E-06	8.5E-05	2.8E-05	8.5E-06	8.5E-07
14	0.4	2.0E-3	3.0E-4	0.5	1.8E-04	5.9E-05	1.8E-05	1.8E-06	8.5E-05	2.8E-05	8.5E-06	8.5E-07
15	0.4	2.0E-3	3.0E-4	1.0	1.8E-04	5.9E-05	1.8E-05	1.8E-06	8.5E-05	2.8E-05	8.5E-06	8.5E-07

[a]Fraction of gases released due to a cladding breach.
[b]Fraction of volatiles released due to a cladding breach.
[c]Mass fraction of fuel released as fines due to a cladding breach.
[d]Fraction of crud that spalls off cladding.

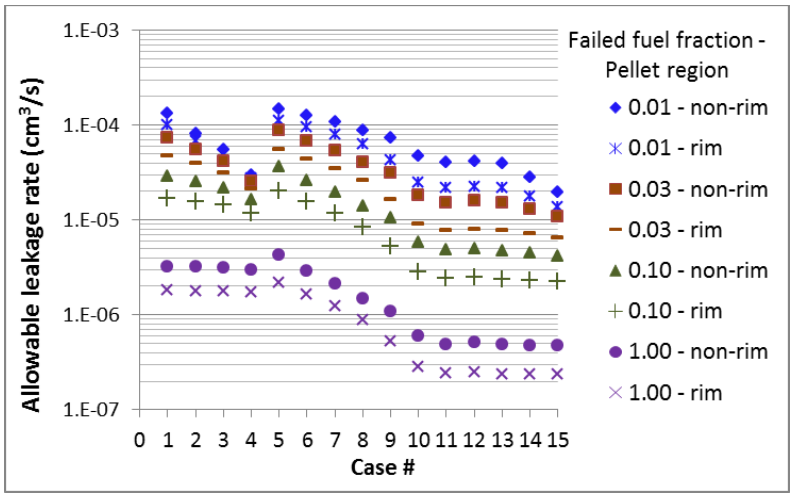

(a)

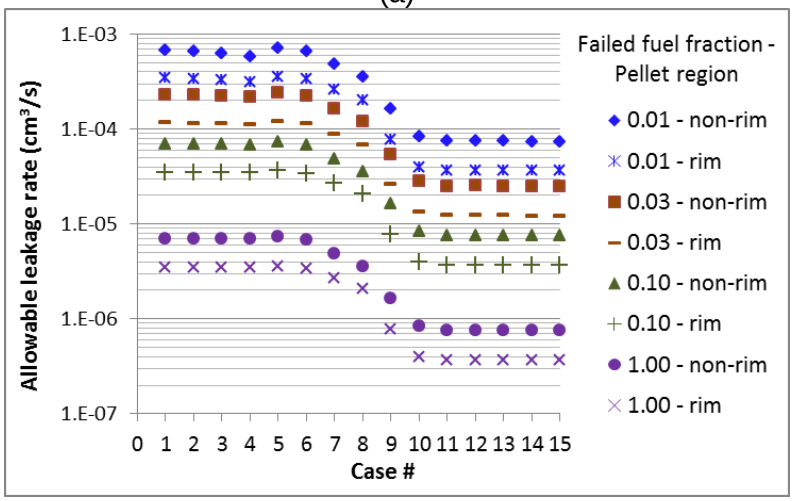

(b)

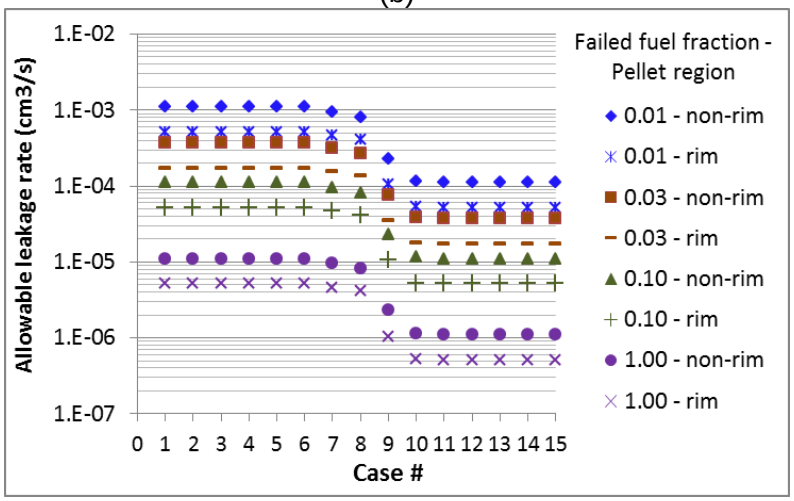

(c)

Figure C.5 – Illustration of the effects of varying release fractions on GBC-32 NCT allowable leakage rate at: (a) 5, (b) 40, and (c) 100 years after fuel discharge from the reactor

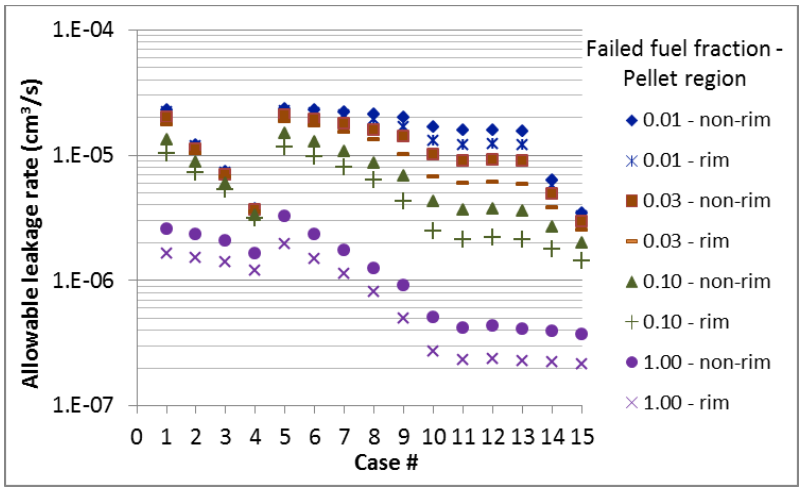

(a)

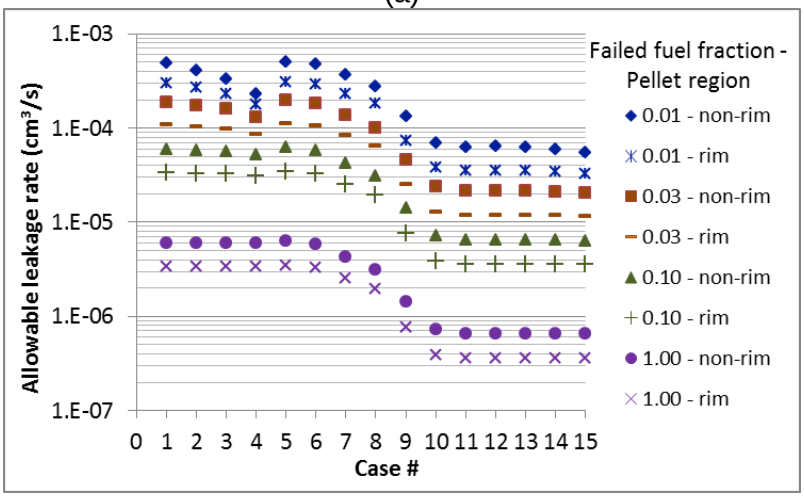

(b)

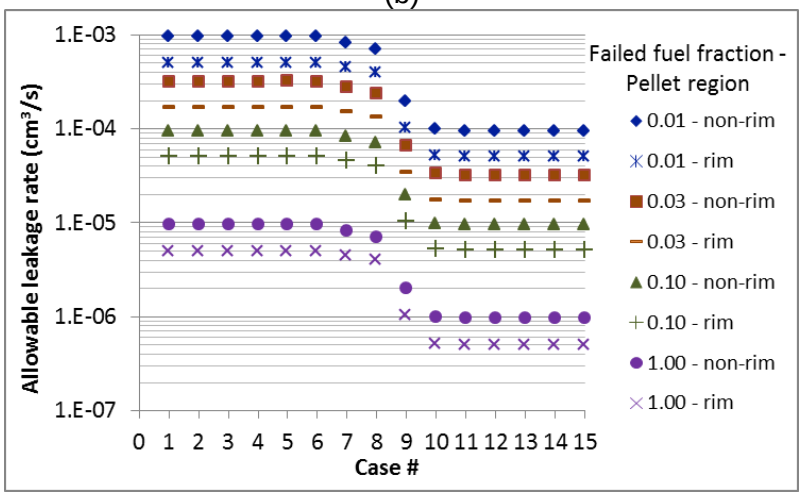

(c)

Figure C.6 – Illustration of the effects of varying release fractions on GBC-68 NCT allowable leakage rate at: (a) 5, (b) 40, and (c) 100 years after fuel discharge from the reactor

Fraction of gases released due to cladding breach

For each decay time and fraction of breached spent fuel rods, an increase in the fraction of gaseous species from 0.1 to 0.4 would cause a relatively small decrease (up to ~30%) in the allowable release rate.

Fraction of volatiles released due to cladding breach

The volatile source term is dominated by ^{137}Cs ($T_{1/2}$ = 30.07 years) and ^{90}Sr ($T_{1/2}$ = 28.78 years). An increase in the fraction of volatile source term by one order of magnitude would cause a maximum decrease in the allowable leakage rate by a factor of approximately two (see Table C.9, 40-year decay time, cases 1 and 8).

Fraction of fuel fines released due to cladding breach

Allowable leakage rate exhibits the greatest sensitivity to changes in the mass fraction of fuel released as fuel fines due to cladding breach. Depending on the crud contribution to the total releasable activity, an increase in the fraction of fuel fines by a factor of 10 would cause a decrease in the allowable leakage rate by a factor of ~1.5 to 10.

Hypothetical Accident Conditions

The allowable leakage rate for HAC was calculated as a function of decay time (5, 40, 100, and 300 years), and pellet radial region from which the fission products and fuel fines originate (non-rim region and rim structure corresponding to ring No. 14 in the calculation model previously described in Sect. C.5.2) assuming a breached fuel rod fraction of 1 and the following release fractions:

- crud: 1.0;
- gaseous species: 0.3 and 0.4;
- volatile species: 2×10^{-4}, and 2×10^{-3}; and
- fuel fines: 3×10^{-5} and 3×10^{-4}.

where the underlined values are the release fractions typically used for HAC of low-burnup fuel.

The calculated allowable release rates for HAC are summarized in Table C.10 for both generic casks. Similar to the NCT results, the HAC allowable leakage rate has the largest sensitivity to the mass fraction of fuel released as fines. Depending on the decay time, an increase in the mass fraction of fuel released as fuel fines by a factor of 10 would cause a decrease in the allowable leakage rate by a factor of ~5 to 10 for the PWR fuel and by a factor of ~3.5 to 10 for the BWR fuel.

Table C.10 – GBC-32 and GBC-68 allowable leakage rate for HAC

GBC-32											
Decay time (years)				5		40		100		300	
Pellet region				Non-rim	Rim	Non-rim	Rim	Non-rim	Rim	Non-rim	Rim
Case#	f_G[a]	f_V[b]	f_F[c]	Allowable leakage rate (cm^3/s)							
1	0.3	2.0E-4	3.0E-5	1.78E-02	1.03E-02	4.14E-02	2.07E-02	6.56E-02	3.05E-02	1.22E-01	5.00E-02
2	0.4	2.0E-4	3.0E-5	1.60E-02	9.43E-03	4.03E-02	2.03E-02	6.56E-02	3.05E-02	1.22E-01	5.00E-02
3	0.3	2.0E-3	3.0E-5	8.42E-03	5.08E-03	2.13E-02	1.22E-02	4.82E-02	2.44E-02	1.21E-01	4.98E-02
4	0.3	2.0E-4	3.0E-4	3.52E-03	1.67E-03	4.98E-03	2.35E-03	6.82E-03	3.13E-03	1.22E-02	5.00E-03
5	0.4	2.0E-3	3.0E-4	2.83E-03	1.41E-03	4.46E-03	2.17E-03	6.58E-03	3.05E-03	1.22E-02	5.00E-03
GBC-68											
Decay time (years)				5		40		100		300	
Pellet region				Non-rim	Rim	Non-rim	Rim	Non-rim	Rim	Non-rim	Rim
Case#	f_G[a]	f_V[b]	f_F[c]	Allowable leakage rate (cm^3/s)							
1	0.3	2.0E-4	3.0E-5	9.67E-03	7.07E-03	3.53E-02	1.99E-02	5.69E-02	3.00E-02	1.06E-01	5.02E-02
2	0.4	2.0E-4	3.0E-5	9.06E-03	6.65E-03	3.44E-02	1.95E-02	5.69E-02	3.00E-02	1.06E-01	5.02E-02
3	0.3	2.0E-3	3.0E-5	5.74E-03	4.09E-03	1.86E-02	1.17E-02	4.21E-02	2.39E-02	1.05E-01	5.00E-02
4	0.3	2.0E-4	3.0E-4	2.69E-03	1.51E-03	4.28E-03	2.29E-03	5.91E-03	3.09E-03	1.06E-02	5.02E-03
5	0.4	2.0E-3	3.0E-4	2.23E-03	1.29E-03	3.85E-03	2.11E-03	5.70E-03	3.01E-03	1.06E-02	5.02E-03

[a]Fraction of gases released due to a cladding breach.
[b]Fraction of volatiles released due to a cladding breach.
[c]Mass fraction of fuel released as fines due to a cladding breach.

C.6 CONFIGURATION CATEGORIES 2 AND 3

Crud was assumed to be released as a consequence of normal, off-normal, and accident conditions of spent fuel storage, and normal and accident conditions of transportation that do not cause cladding breach (i.e., Category 2—rod/assembly deformation; and Category 3—changes to assembly axial alignment). The GBC-32 and GBC-68 NCT allowable leakage rate as a function of the fraction of crud that spalls off cladding and decay time is provided in Table C.11. The allowable leakage rate is inversely proportional to the fraction of crud assumed to spall off the cladding. Hence, allowable leakage rate was calculated as a function of the fraction of crud that spalls off the cladding to evaluate the effect of varying the crud releasable activity (see Appendix C.6). For the 5-year decay time, an increase in the fraction of crud from 0.05 to 1 would cause a decrease in the allowable leakage rate from 6.58×10^{-4} cm^3/s to 3.29×10^{-5} cm^3/s for the GBC-32 package and from 7.54×10^{-5} cm^3/s to 3.77×10^{-6} cm^3/s for the GBC-68 package. For the 40-year decay time, an increase in the fraction of crud from 0.05 to 1 would cause a decrease in the allowable leakage rate from 6.56×10^{-2} cm^3/s to 3.28×10^{-3} cm^3/s for the GBC-32 package and from 7.52×10^{-3} cm^3/s to 3.76×10^{-4} cm^3/s for the GBC-68 package.

Table C.11 – Allowable leakage rate for rod/assembly deformation and changes to axial alignment categories

GBC-32								
	5-year decay time				40-year decay time			
Fraction of crud released	Releasable activity (Ci)	Effective A_2 value (Ci)	Allowable release rate (Ci/s)	Allowable leakage rate (cm^3/s)	Releasable activity (Ci)	Effective A_2 value (Ci)	Allowable release rate (Ci/s)	Allowable leakage rate (cm^3/s)
0.05	3.22E+01	1.08E+01	3.00E-09	6.58E-04	3.23E-01	1.08E+01	3.00E-09	6.56E-02
0.1	6.44E+01	1.08E+01	3.00E-09	3.29E-04	6.46E-01	1.08E+01	3.00E-09	3.28E-02
0.15	9.66E+01	1.08E+01	3.00E-09	2.19E-04	9.68E-01	1.08E+01	3.00E-09	2.19E-02
0.2	1.29E+02	1.08E+01	3.00E-09	1.64E-04	1.29E+00	1.08E+01	3.00E-09	1.64E-02
0.3	1.93E+02	1.08E+01	3.00E-09	1.10E-04	1.94E+00	1.08E+01	3.00E-09	1.09E-02
0.4	2.58E+02	1.08E+01	3.00E-09	8.22E-05	2.58E+00	1.08E+01	3.00E-09	8.20E-03
0.5	3.22E+02	1.08E+01	3.00E-09	6.58E-05	3.23E+00	1.08E+01	3.00E-09	6.56E-03
0.6	3.86E+02	1.08E+01	3.00E-09	5.48E-05	3.87E+00	1.08E+01	3.00E-09	5.47E-03
0.7	4.51E+02	1.08E+01	3.00E-09	4.70E-05	4.52E+00	1.08E+01	3.00E-09	4.68E-03
0.8	5.15E+02	1.08E+01	3.00E-09	4.11E-05	5.16E+00	1.08E+01	3.00E-09	4.10E-03
0.9	5.80E+02	1.08E+01	3.00E-09	3.65E-05	5.81E+00	1.08E+01	3.00E-09	3.64E-03
1	6.44E+02	1.08E+01	3.00E-09	3.29E-05	6.46E+00	1.08E+01	3.00E-09	3.28E-03
GBC-68								
	5-year decay time				40-year decay time			
Fraction of crud released	Releasable activity (Ci)	Effective A_2 value (Ci)	Allowable release rate (Ci/s)	Allowable leakage rate (cm^3/s)	Releasable activity (Ci)	Effective A_2 value (Ci)	Allowable release rate (Ci/s)	Allowable leakage rate (cm^3/s)
0.05	2.26E+02	1.08E+01	3.00E-09	7.54E-05	2.27E+00	1.08E+01	3.00E-09	7.52E-03
0.1	4.52E+02	1.08E+01	3.00E-09	3.77E-05	4.54E+00	1.08E+01	3.00E-09	3.76E-03
0.15	6.79E+02	1.08E+01	3.00E-09	2.51E-05	6.80E+00	1.08E+01	3.00E-09	2.51E-03
0.2	9.05E+02	1.08E+01	3.00E-09	1.88E-05	9.07E+00	1.08E+01	3.00E-09	1.88E-03
0.3	1.36E+03	1.08E+01	3.00E-09	1.26E-05	1.36E+01	1.08E+01	3.00E-09	1.25E-03
0.4	1.81E+03	1.08E+01	3.00E-09	9.42E-06	1.81E+01	1.08E+01	3.00E-09	9.40E-04
0.5	2.26E+03	1.08E+01	3.00E-09	7.54E-06	2.27E+01	1.08E+01	3.00E-09	7.52E-04
0.6	2.71E+03	1.08E+01	3.00E-09	6.28E-06	2.72E+01	1.08E+01	3.00E-09	6.27E-04
0.7	3.17E+03	1.08E+01	3.00E-09	5.39E-06	3.17E+01	1.08E+01	3.00E-09	5.37E-04
0.8	3.62E+03	1.08E+01	3.00E-09	4.71E-06	3.63E+01	1.08E+01	3.00E-09	4.70E-04
0.9	4.07E+03	1.08E+01	3.00E-09	4.19E-06	4.08E+01	1.08E+01	3.00E-09	4.18E-04
1	4.52E+03	1.08E+01	3.00E-09	3.77E-06	4.54E+01	1.08E+01	3.00E-09	3.76E-04

APPENDIX D. THERMAL EVALUATIONS FOR FUEL RECONFIGURATION CATEGORIES

D.1 THERMAL ANALYSES

The objective of the thermal analysis was to identify cask temperature variations resulting from fuel configuration changes that can affect the ability of transportation packages and storage casks to comply with regulatory thermal limits. This appendix describes a technical approach for thermal analyses of fuel reconfigurations in transportation packages and storage casks and provides reference values for such analyses. The term "fuel reconfiguration" refers to any change to the storage and transportation system nominal intact fuel assembly configuration used for the basis of cask certification. The analyzed fuel reconfiguration categories are: (1) cladding failure where fuel fragments and particulates from multiple spent nuclear fuel (SNF) rods can relocate near to and far from fuel cladding breach locations; (2) rod/assembly deformation; and (3) changes to assembly axial alignment.

D.1.1 Applicable Codes, Guidance, Regulatory Criteria

During normal and off-normal conditions of storage and accident conditions, the cask must reject the decay heat to the environment without exceeding the operational temperature ranges of the components important to safety.

To maintain fuel rod integrity for normal conditions of storage the fuel must be maintained at a sufficiently low temperature to preclude fuel rod cladding deterioration. To ensure fuel rod integrity, the maximum allowable cladding temperature under normal conditions of storage and short-term loading operations is 400°C (752°F) for zirconium-based alloys and stainless steel cladding [52]. The maximum cladding temperature under off-normal and accident conditions must remain below 570°C (1,058°F) for zirconium-based alloys and stainless steel cladding [52]. In addition, all components important to safety (confinement, shielding, criticality, and heat removal) must remain within their individual material temperature limits.

It is important to note that the thermal characteristics and response of the cask are also integral to the cask structural requirements. The thermal characteristics can affect the failure limits of components (yield strength, creep, and fatigue) and the mechanical loading of components (thermally induced stresses and system pressure).

In transportation, the accessible surfaces of the cask must have temperatures at or below 85°C (185°F) for an exclusive use shipment (10 CFR 71.43 [g]).

D.2 USE OF SOFTWARE

The thermal analysis used the Coolant Boiling in Rod Arrays—Spent Fuel Storage (COBRA-SFS) cycle 3 and the RADGEN cycle 3 computer codes [53]. COBRA-SFS has been validated and used extensively to analyze SNF storage casks and transportation packages [54], [55]. The software was developed by Pacific Northwest National Laboratory (PNNL) and tailored specifically for transportation package/storage cask analysis. The code includes convection, conduction and thermal radiation heat transfer and can accommodate a range of environmental boundary conditions, fuel assemblies and transportation package/storage cask designs. View factor information for the assemblies, which is required by COBRA-SFS, is generated using the

RADGEN code. The RADGEN code determines thermal radiation view factors analytically for each pin in an assembly as well as other cavity view factors [56].

Both the COBRA-SFS cycle 3 and RADGEN cycle 3 computer codes will be used “as-is”. Code modifications were not included within the work scope. Any code deficiencies or limitations found during the conduct of this work are reported and discussed.

D.3 GENERIC CASK AND REPRESENTATIVE FUEL ASSEMBLY DESCRIPTIONS

The gernic burnup credit-32 (GBC-32) package for SNF was previously developed as a computational benchmark problem for reactivity and burnup credit analysis [4]. A variant of the GBC-32 package suitable for thermal analysis, the GBC-32T, was developed and used in this study. Many aspects of the original GBC-32 package are retained; however, the GBC-32T package system model contains some modifications and additional details necessary for thermal analysis.

The GBC-32T package system is composed of the following:

- Spent fuel canister – contains up to 32 pressurized water reactor (PWR) spent fuel assemblies; placed inside the transportation overpack for off-site transportation or a storage cask for on-site dry storage
- Rail Transportation Package – package for rail transportation consisting of the spent fuel canister, the transportation overpack, and associated impact limiters

The GBC-32T system is intended for testing thermal analysis methodologies and for the general impact of system and modeling variations. While the GBC-32T system shares similarities to other transportation package/storage cask systems, it was not designed to meet manufacturing, vendor, or regulatory requirements for such physical systems. Because thermal performance is intimately coupled with structural design, analyses with this system should not be interpreted as defining performance limits for actual canisters at design-basis decay heat loadings.

The spent fuel canister is comprised of a steel cylinder with an internal basket that can contain up to 32 PWR assemblies. The spent fuel canister is placed inside the transportation overpack for rail transportation. Two orientation cases are considered; horizontal geometry and vertical. Horizontal orientation corresponds to the configuration for transportation by rail, and the rail transportation package includes impact limiters. Vertical orientation of the rail transportation package is assumed for the package on a concrete pad awaiting loading onto a rail car, before placement of impact limiters.

Illustrations of the GBC-32T system are given in Figure D.1 to Figure D.5. The material specifications and system dimensions are given in Table D.1 and Table D.2, respectively.

D.3.1 Canister

The GBC-32T canister holds a basket with space for up to 32 PWR assemblies. The basket is constructed with stainless steel walls with neutron absorber plates sandwiched in between, as shown in Figure D.5. The neutron absorber plates are a composite with an outer layer of aluminum that sandwiches a BORAL® panel. The neutron absorber plate was represented as extending from the top to the bottom of the basket. Stainless steel support pieces connect the basket to the canister wall as shown in Figure D.4. These support pieces are welded to both

structures. They extend from the top of the basket to 5.08 cm (2 in.) above the bottom of the basket. The bottom of the basket sits on the bottom of the canister. Rectangular openings through the bottom of the basket walls measure 5.08 cm (2 in.) high by 19.69 cm (7.752 in.) wide. The canister is evacuated and backfilled with helium at 2 atm abs at a reference temperature of 21°C (70°F). At an average gas temperature of 177°C (350°F), the canister would be at 3.06 atm abs.

D.3.2 Assemblies

The canister is fully loaded with 32 Westinghouse (W) 17×17 optimized fuel assembly (OFA) SNF assemblies. The assembly contains 264 fueled rods with an active fuel length of 144 in. All assemblies are assumed to be radially centered within their respective basket cells. This is because of a limitation of the current version of the RADGEN code. The assemblies sit upon bottom fuel spacers which are 8.89 cm (3.5 in.) tall and made of stainless steel. Top fuel spacers are present above the fuel assemblies to prevent axial shifting of the assemblies during transport. The length of the spacers varies based on the assembly length and canister design. For the W 17×17 OFA assembly, the top spacer length used is 27.27 cm (10.735 in.).

D.3.3 Rail Transportation Package

The canister resides inside a transportation package. The gas in between the canister and package is helium at 2 atm (at 21°C). At an average gas temperature of 93°C (200°F), the canister would be at 2.49 atm abs. The transportation package walls include a 25.4 cm (10 in) thick inner wall made of stainless steel. Outside of the stainless steel wall is a neutron shield consisting of resin epoxy placed inside 36 can-like structures of carbon steel that are uniformly spaced around the package, as shown in Figure D.3. The neutron shield starts 30.48 cm (12 in) above the bottom of the package and ends 30.48 cm (12 in.) below the top of the package, for a total 457.5 cm (180.125 in.) axial length. The top lid and package base (bottom) are made of stainless steel and are 7 and 11 in. thick, respectively. The impact limiters are made of foamed aluminum with a bulk thermal conductivity of 4.68 W m^{-1} K^{-1}. The impact limiters are 50.8 cm (20 in.) thick in both the axial and radial direction. The impact limiters cover the first 30.48 cm (12 in.) of the transportation package in the axial direction, as shown in Figure D.6.

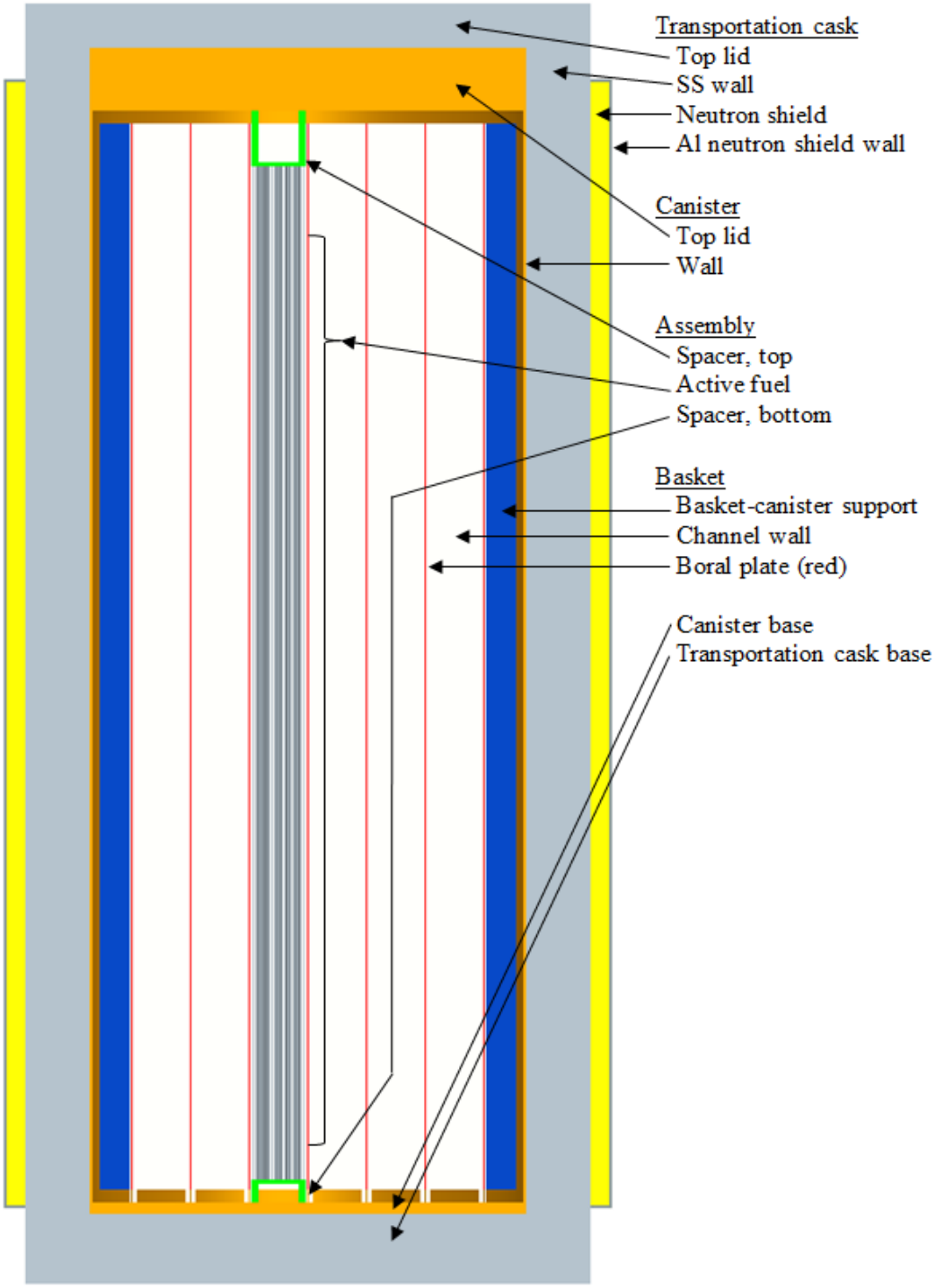

Figure D.1 – Package component identification

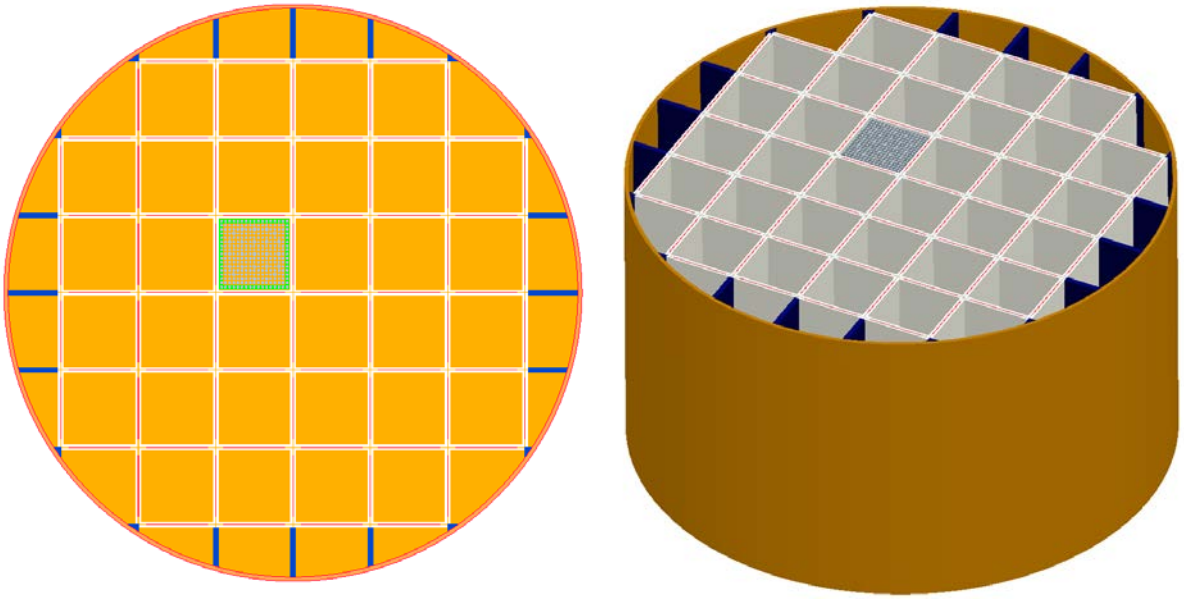

Figure D.2 – Illustration of canister and basket

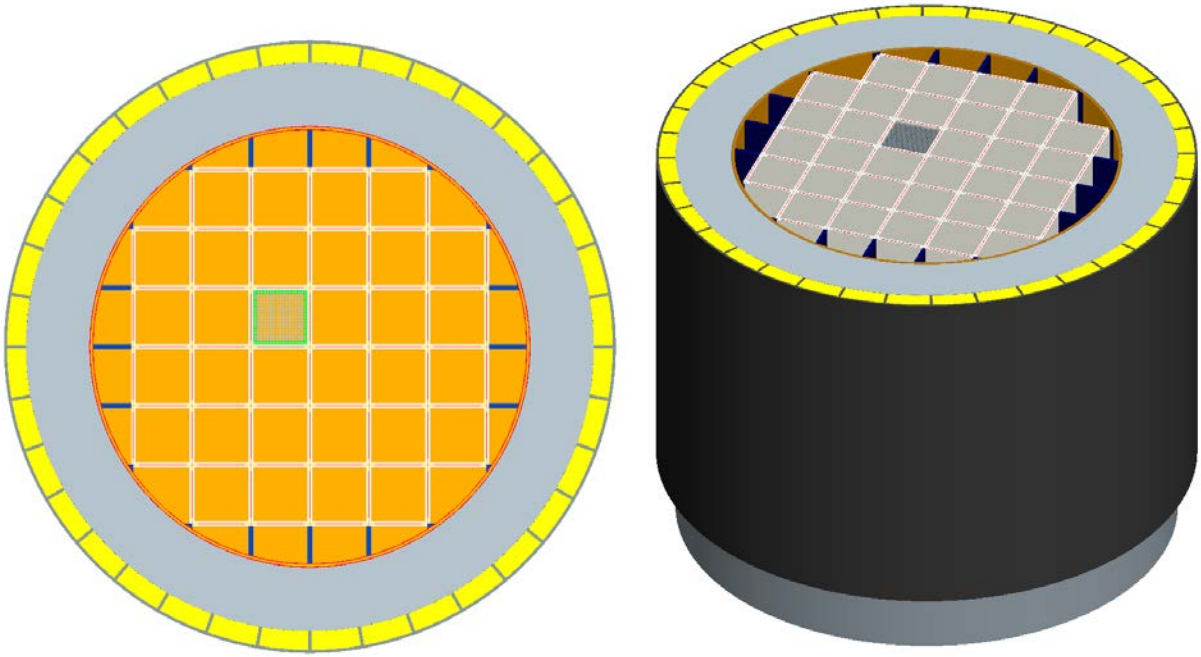

Figure D.3 – Illustration of canister and basket within transportation package

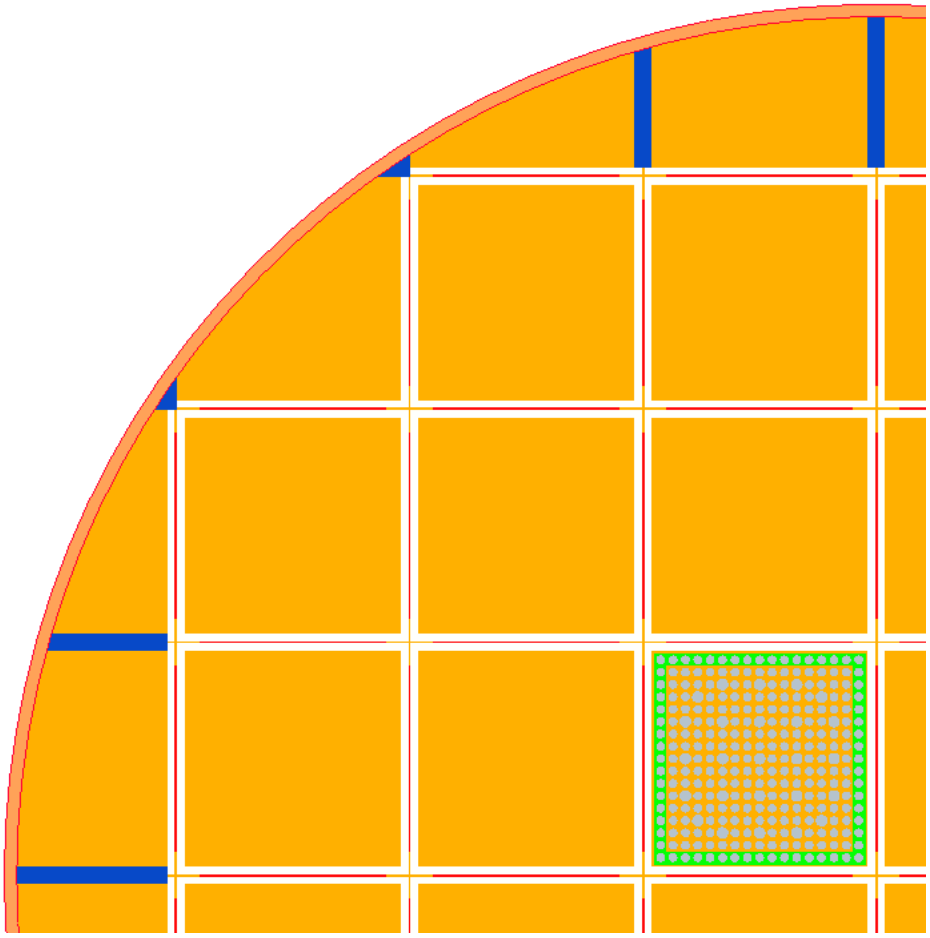

Figure D.4 – Illustration of one-quarter of basket with single assembly

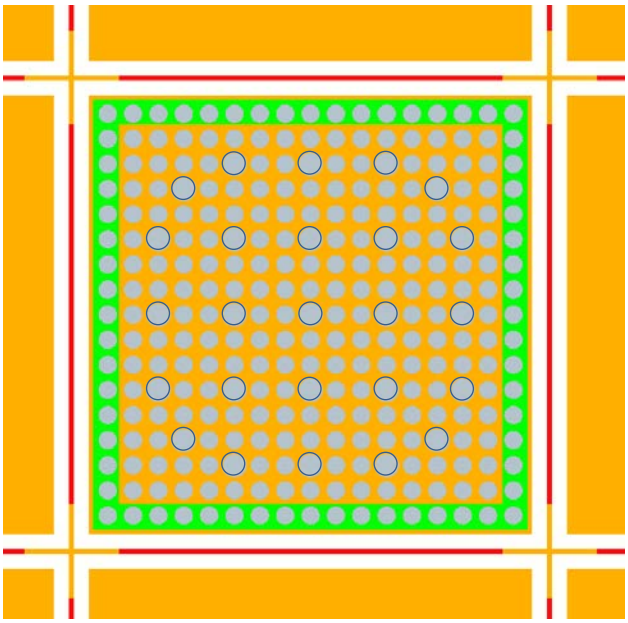

Figure D.5 – Illustration of basket cell with assembly

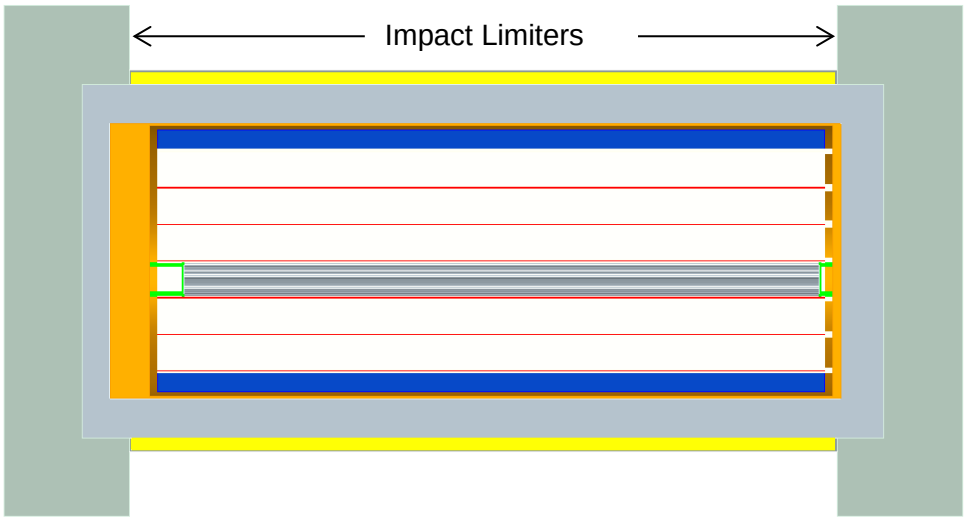

Figure D.6 – Illustration of transportation package in horizontal orientation

Table D.1 – Package material summary

Part	Material
Transportation package outer wall	Carbon steel (1010)
Transportation package neutron shield	Epoxy resin
Transportation package inner wall	Stainless steel 304
Transportation package lid and base	Stainless steel 304
Transportation package impact limiters	Al foam, closed cell
Canister	Stainless steel 304
Basket walls	Stainless steel 304
Basket supports	Stainless steel 304
Basket neutron absorber	BORAL® plates—Composite B_4C & Al
Assembly spacers	Stainless steel 304
Assembly rod cladding	Zicaloy-4
Canister void space	Helium—2 atm (at 21°C)
Transportation package void space	Helium—2 atm (at 21°C)

Table D.2 – GBC-32T package dimensions for thermal analysis

Parameter	cm	in.
Fuel Assembly (W 17x17 OFA)		
Active fuel length	365.76	144.00
Bottom hardware length	15.00	5.9055
Top hardware length	25.04	9.8595
Total assembly length	405.80	159.765
Pin pitch	1.26	0.4960
Clad outside diameter	0.914	0.3600
Guide/thimble tube outside diameter	1.2040	0.4740
Fuel Spacer		
Total height—top	27.27	10.735
Material thickness—top	1.27	0.50
Total height—bottom	8.89	3.50
Material thickness—bottom	1.27	0.50
Basket		
Total basket length	436.88	172.00
Basket length between openings	431.80	170.00
Gap between basket and canister top	5.08	2.00
Length of opening at bottom of basket	5.08	2.00
Width of opening at bottom of basket	19.69	7.752
Neutron absorber plate length	431.80	170.00
Basket cell inside width	22.00	8.6614
Basket wall material thickness	0.750	0.2953
Neutron absorber plate total thickness	0.257	0.1010
Neutron absorber plate width	19.05	7.50
Basket to canister wall support thickness	1.76	0.6916
Basket to canister wall support length	431.80	170.00
Canister		
Total cavity length	441.96	174.00
Total exterior length	472.44	186.00
Top lid thickness	25.4	10.00
Base thickness	5.08	2.00
Outer shell thickness	1.27	0.50
Outer shell inside diameter	175.00	68.8976
Outer shell outside diameter	177.54	69.8976
Transportation Package		
Total cavity length	472.76	186.125
Total outside height	518.48	204.125
Top lid thickness	17.78	7.00
Base thickness	27.94	11.00
Total outside shell thickness	34.29	13.50
Stainless steel inner shell thickness	25.40	10.00
Neutron shield shell thickness	7.62	3.00
Carbon steel outer shell thickness	1.27	0.50
Cavity inside diameter	178.18	70.1476
Outer shell outside diameter	246.76	97.1476

D.4 NOMINAL THERMAL MODELING SETUP WITH THE COBRA-SFS CODE

Thermal models of the GBC-32T were developed for the COBRA-SFS cycle 3 code. Two orientations, vertical and horizontal, were modeled and are described in Sect. D.4.1. Using COBRA-SFS convention, the package is divided axially in three zones: top plenum, bottom plenum, and the assembly zone, as illustrated in Figure D.7. In the horizontal orientation, the impact limiters are included in the top and bottom plenum. The COBRA-SFS modeling of each zone is discussed in Sect. D.4.2 and D.4.3.

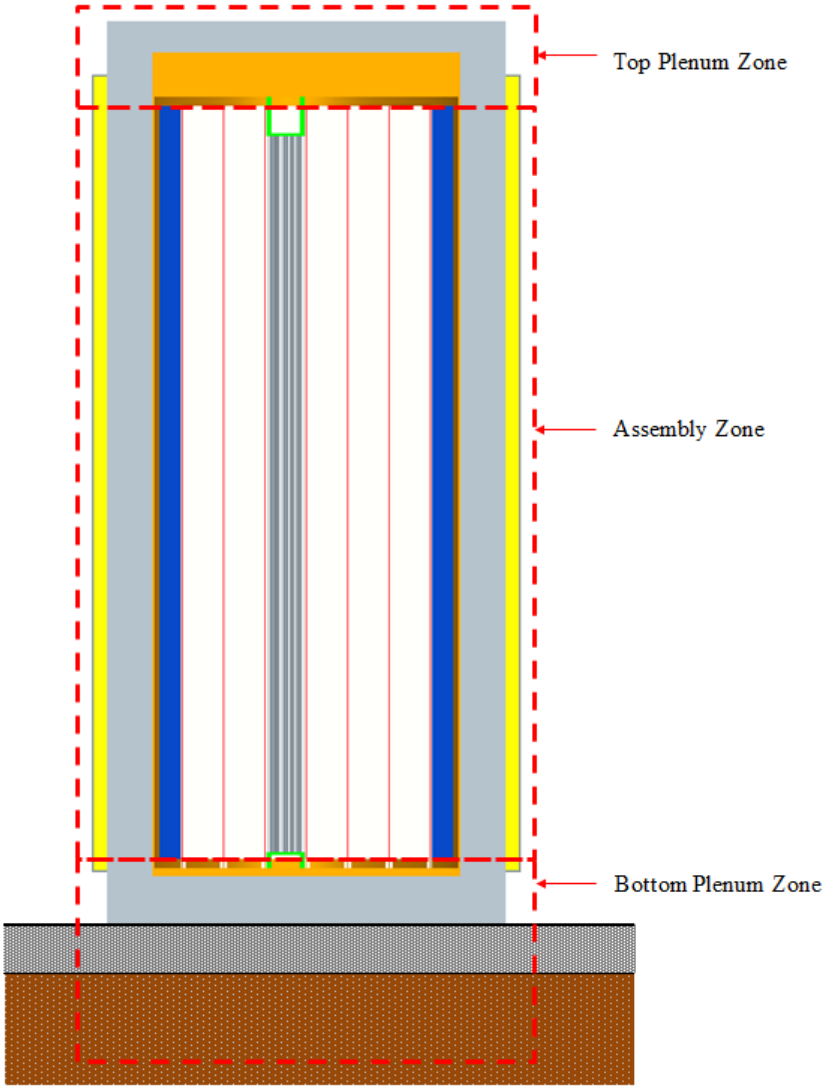

Figure D.7 – Illustration of COBRA-SFS modeling zones

D.4.1 Package Orientation Cases

D.4.1.1 Case 1—Rail Transportation Package in Vertical Configuration on Pad

The vertical configuration represents the transportation package waiting to be placed onto the rail transportation car or after being removed from the rail transportation car and placed back on the ground. In general, long term storage casks are vented, allowing air—t he ultimate heat sink—to cool the internal canister. The transportation package, in contrast to long-term storage casks, does not allow the ultimate heat sink to contact the internal canister and contains additional layers of material between the canister and ultimate heat sink. Therefore, the transportation package in a vertical configuration would be hotter than a vertical storage cask and represents the bounding case for vertical orientations. For this reason, the vertical orientation of the transportation package, as illustrated in Figure D.8, was selected for analysis.

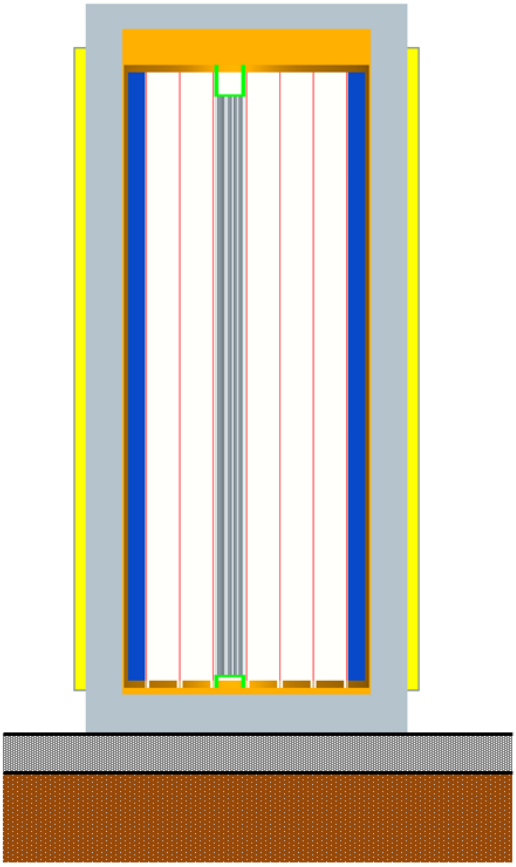

Figure D.8 – Illustration of transportation package in vertical orientation

The assemblies are centered radially within each basket cell. The canister is centered radially within the transportation package and rests on the bottom plate of the transportation package. The transportation package rests on a 25.4 cm (10 in.) thick concrete slab. Under the concrete slab is earth.

D.4.1.2 Case 2—Rail Transportation Package in Horizontal Configuration

The horizontal configuration represents the package during transportation. The assemblies are centered radially within each basket cell. The canister is centered horizontally and rests on the lower surface of the transportation package inner shell. Impact limiters are placed on the ends of the transportation package, as illustrated in Figure D.6.

D.4.2 Assembly Zone

D.4.2.1 Flow Channel and Solid Material Discretization

The GBC-32T was divided into 52 “assemblies” and 516 solid conduction nodes. The full package was modeled, and no symmetry was assumed. Illustrations of the discretization are provided in Figure D.9 to Figure D.11.

Of the 52 assemblies, 32 model fuel assemblies as detailed rod-and-subchannel arrays, and the remaining 20 model the open flow channel regions between the fuel basket and the canister. All 289 rods and 324 flow subchannels between rods were modeled for each of the 32 fuel assemblies. Each assembly contains 25 guide/thimble/instrument tubes.

The basket walls consist of 304 solid conduction nodes of stainless steel 304, and 152 nodes are used to represent the neutron absorber plates between the basket walls. Each of the 20 basket-to-canister supports is modeled with a node. The canister is divided into eight sections circumferentially and two sections radially, resulting in 16 nodes. Finally, the transportation package is divided into eight sections circumferentially and five sections radially (three across the stainless steel wall, one across the neutron shielding material, and one across the carbon steel outer wall), resulting in 40 nodes.

As illustrated in Figure D.7 for the vertical orientation, the assembly zone extends from the top of the cutout at the bottom of the basket (5.08 cm [2 in.] up from the canister base) to the top of the basket for a total of 4.318 m (170 in.). The assembly zone is divided into 44 uniformly spaced sections.

In the COBRA-SFS model, the fuel rods, guide/thimble tubes and instrument tube are modeled with the appropriate diameters and spacing. However, as discussed in Sect. D.4.2.5, the radiation view factors for the bundle assume all rods are of the same diameter. Future code enhancements of RADGEN could eliminate this modeling artifact.

Three modeling simplifications are employed in the assembly zone of the model. First, the fuel rods are modeled as extending from the bottom to the top of the assembly zone. This extends the axial length of the rods by approximately 48 cm (18.9 in.), relative to their actual overall length of 388.9 cm (153.1 in.). Second, the grid spacers are not explicitly modeled, and therefore their effect on heat transport is not modeled. This is a minor conservatism in the model, because the grid spacers do not substantially affect heat transfer within the assembly. The effect of the grid spacers on momentum transport in the helium gas, however, is not neglected. This is modeled with form loss coefficients appropriate to the hydrodynamic losses associated with the particular grid design. Finally, the small cruciform shaped channels formed between the neutron absorber panels of neighboring basket cells, as shown in Figure D.5, are not modeled as flow channels. However, the thermal radiation and conductive heat transfer from one basket wall, across the cruciform gap, to the neighboring basket wall are included in the

model. The gas volume in the cruciform gaps is included in the canister free volume when determining gas mixture properties.

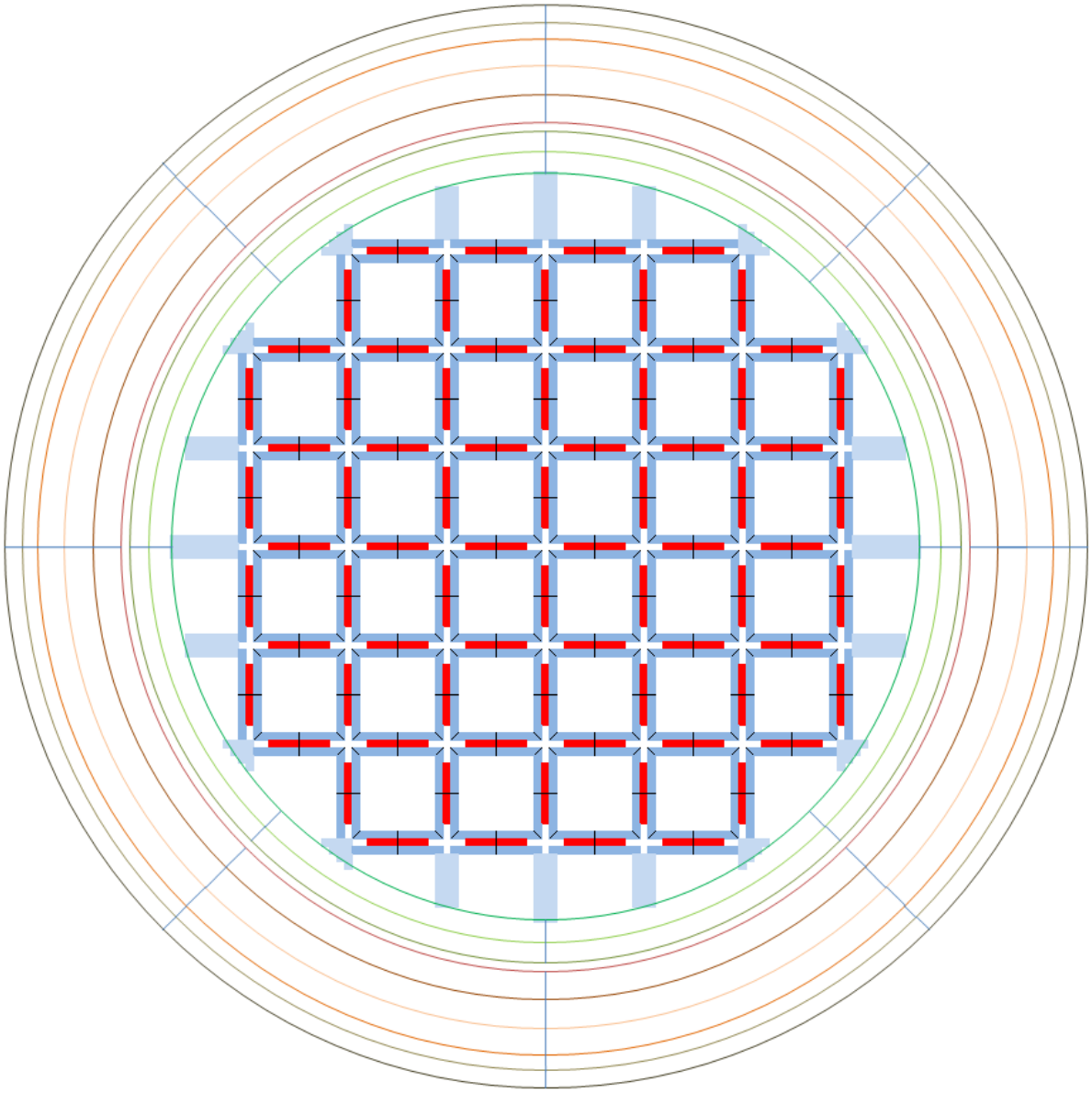

Figure D.9 – Nodalization illustration of package (not to scale)

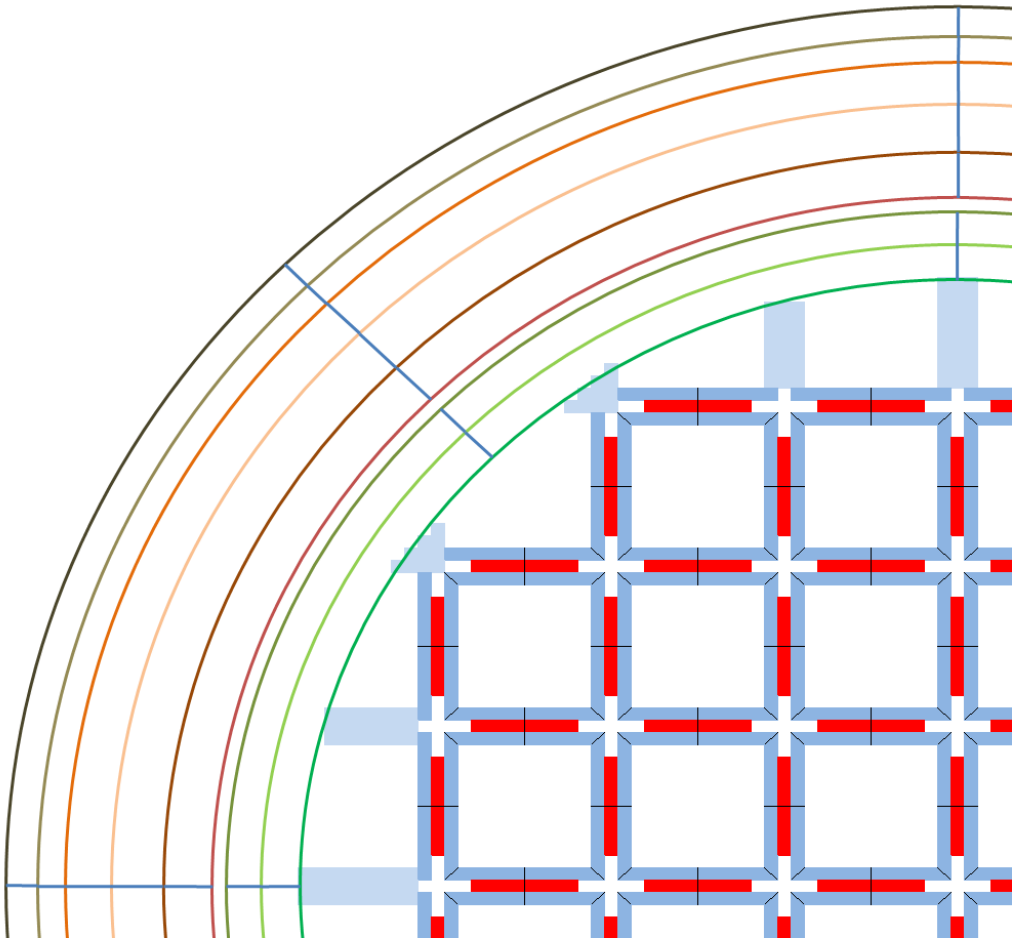

Figure D.10 – Nodalization illustration of one-quarter of package (not to scale)

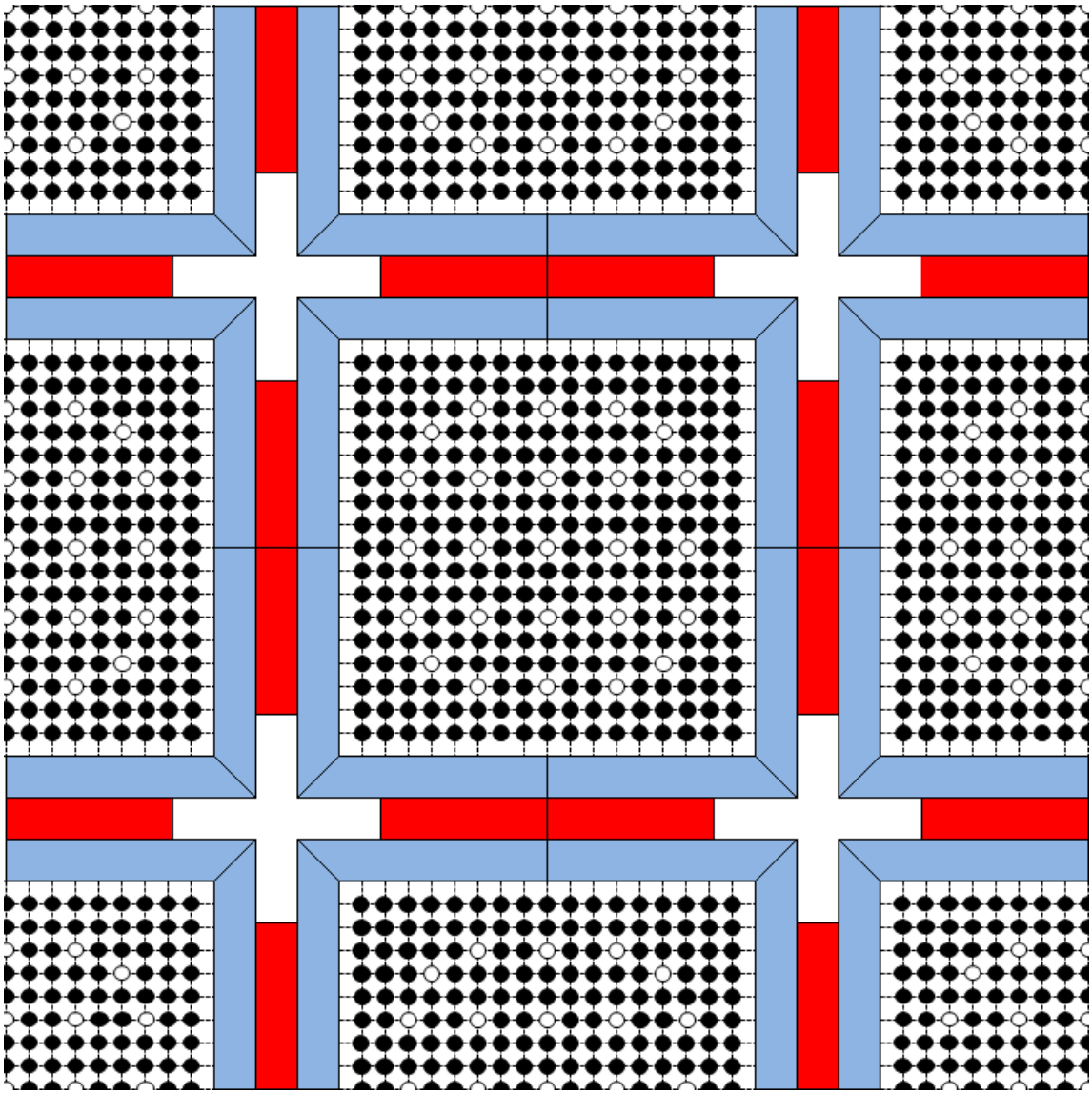

Figure D.11 – Nodalization illustration of a basket cell with assembly subchannels (not to scale)

D.4.2.2 Gap Thermal Resistances

Thermal resistances were included between certain solid nodes to account for gas gaps between surfaces. Table D.3 and

Table D.4 summarize the assumed gap widths and the fill gas thermal conductivity for the vertical and horizontal package orientations, respectively. For the horizontal configuration, the gaps between the canister and package varied along the circumference. Figure D.12 illustrates the positions of the gaps, A through D, specified in Table D.3 and

Table D.4

Table D.3 – Assumed gap thermal resistances, vertical orientation

Location	Gap width		Gas Thermal Conductivity	
	(cm)	(in.)	(W/m K)	(Btu/h ft °F)
Basket SS wall— Neutron Absorber Plate	0.0254	0.01	0.2155 (He, 3.06 atm. 204°C)	0.1245 (He, 3.06 atm. 400°F)
Outer Canister Shell— Inner Package Wall (A–D)	0.3175	0.125	0.1793 (He, 2.49 atm. 93.3°C)	0.1036 (He, 2.49 atm. 200°F)
Package Outer SS Shell— Package Inner Neutron Shield	0.0254	0.01	0.0267 (He, 1.00 atm. 38.8°C)	0.0154 (He, 1.00 atm. 100°F)

Note: SS = stainless steel.

Table D.4 – Assumed gap thermal resistances horizontal orientation

Location	Gap width		Gas thermal conductivity	
	(cm)	(in.)	(W/m K)	(Btu/h ft °F)
Basket SS wall— Neutron Absorber Plate	0.0254	0.01	0.2155 (He, 3.06 atm. 204°C)	0.1245 (He, 3.06 atm. 400°F)
Outer Canister Shell— Inner Package Wall Top Solid Nodes (A)	0.5556	0.2188	0.1793 (He, 2.49 atm. 93.3°C)	0.1036 (He, 2.49 atm. 200°F)
Outer Canister Shell— Inner Package Wall Side Upper Solid Nodes (B)	0.3969	0.1563	0.1793 (He, 2.49 atm. 93.3°C)	0.1036 (He, 2.49 atm. 200°F)
Outer Canister Shell— Inner Package Wall Side Lower Solid Nodes (C)	0.2381	0.0938	0.1793 (He, 2.49 atm. 93.3°C)	0.1036 (He, 2.49 atm. 200°F)
Outer Canister Shell— Inner Package Wall Bottom Solid Nodes (D)	0.0794	0.0313	0.1793 (He, 2.49 atm. 93.3°C)	0.1036 (He, 2.49 atm. 200°F)
Package Outer SS Shell— Package Inner Neutron Shield	0.0254	0.01	0.0267 (He, 1.00 atm. 38.8°C)	0.0154 (He, 1.00 atm. 100°F)

Note: SS = stainless steel.

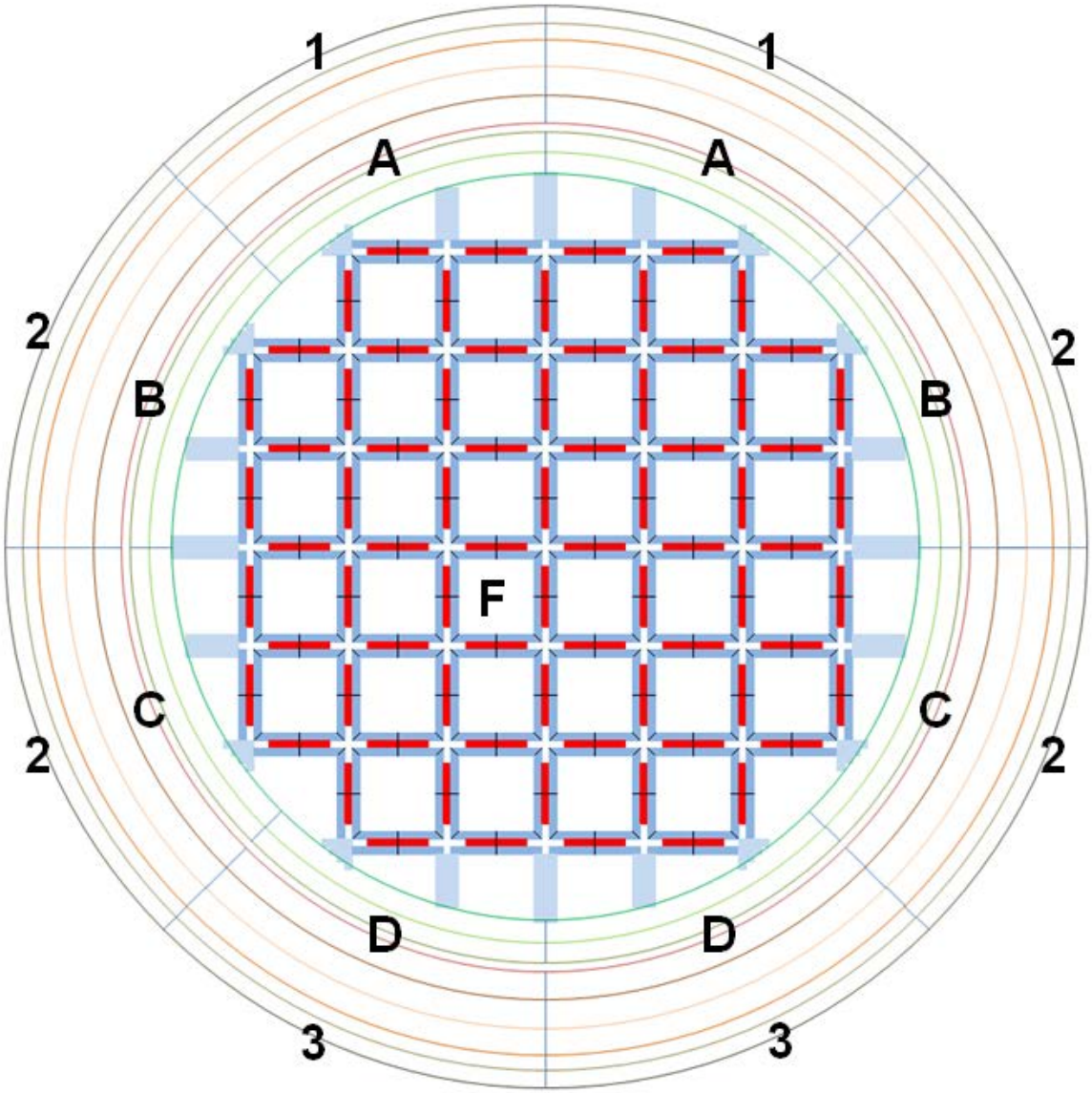

Figure D.12 – Canister-package gap, outer wall, and failed assembly location identification

D.4.2.3 Assembly Decay Heat, Profile, and Nuclide Inventory

The package is uniformly loaded with 32 W 17×17 OFA assemblies assumed to have an average burnup of 65 GWd/MTU. There are 264 fueled rods, 24 locations that are guide/thimble tubes and one instrument tube, as shown in Figure D.5. Each assembly has the same total decay heat, decay heat axial power profile, and radioisotope inventory.

The total decay heat per assembly is given in Table D.5 for various decay times and shown in Figure D.13. The assembly decay heat and radioisotope inventory were calculated using Oak Ridge Isotope Generation and Depletion Code–Automatic Rapid Processing (ORIGEN-ARP) [57] assuming a PWR assembly with the following characteristics:

- 0.426 MTU,
- 65 GWd/MTU burnup, and
- 5 wt % ^{235}U initial enrichment.

Table D.5 - Assembly total decay heat as a function of decay time

Decay time (years)	Decay heat (W/assembly)
5	1800.
20	870.5
40	445.5
60	344.0
100	233.2

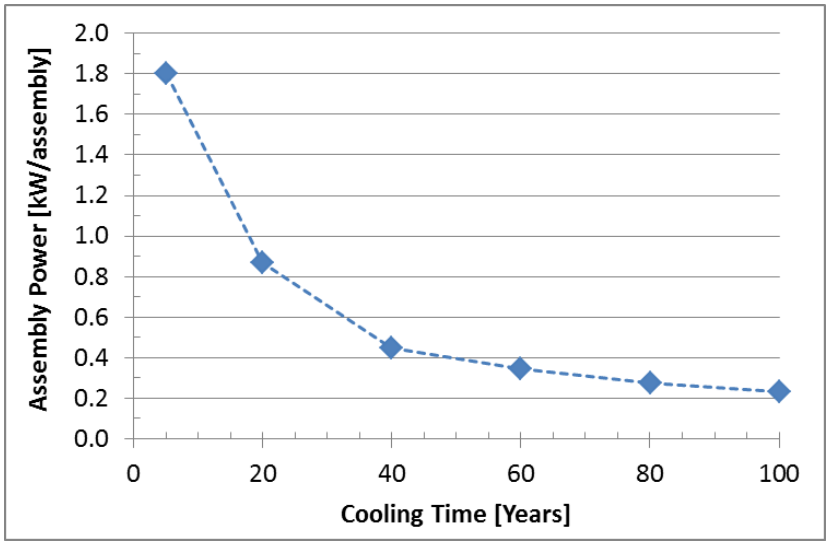

Figure D.13 – Assembly total decay heat as a function of decay time

All assemblies have the axial decay heat profile given in Table D.6. The axial profile is derived from profiles representative of PWR fuel with >30 GWd/MTU burnup [58]. The profile power peaking factors are linearly interpolated within the COBRA-SFS code between points in the input table. The inventory of fission gas products in the assembly is given in Table D.7.

Table D.6 – Assembly axial decay heat profile

Normalized height with respect to active fuel length	Normalized height with respect to assembly zone	Power profile
-	0.000	0.000
0.000	0.044	0.000
0.028	0.067	0.652
0.083	0.114	0.967
0.139	0.161	1.074
0.194	0.208	1.103
0.250	0.255	1.108
0.306	0.302	1.106
0.361	0.349	1.102
0.417	0.397	1.097
0.472	0.444	1.094
0.528	0.491	1.094
0.583	0.538	1.095
0.639	0.585	1.096
0.694	0.632	1.095
0.750	0.679	1.086
0.806	0.726	1.059
0.861	0.773	0.971
0.917	0.820	0.738
0.972	0.867	0.462
1.000	0.891	0.000
-	1.000	0.000

Note: The first column is the power profile, with respect to the active fuel length from DOE-RW-0472 [58]. In the second column the axial power profile was shifted and re-normalized to correctly position the profile within the assembly channels.

Table D.7 – Assembly inventory of fission product gases and volatile species

Decay time (years)	Fission product gases (moles/assembly)				Volatile fission products (moles/assembly)		
	Xe	Kr	He	H	Cs	I	Ru
5	33.54	3.27	1.05	0.013	15.18	1.32	19.03
20	33.54	3.16	1.33	0.008	13.20	1.32	19.01
40	33.54	3.11	1.64	0.005	11.54	1.32	19.01
60	33.54	3.09	1.90	0.004	10.49	1.32	19.01
100	33.54	3.09	2.35	0.003	9.41	1.32	19.01

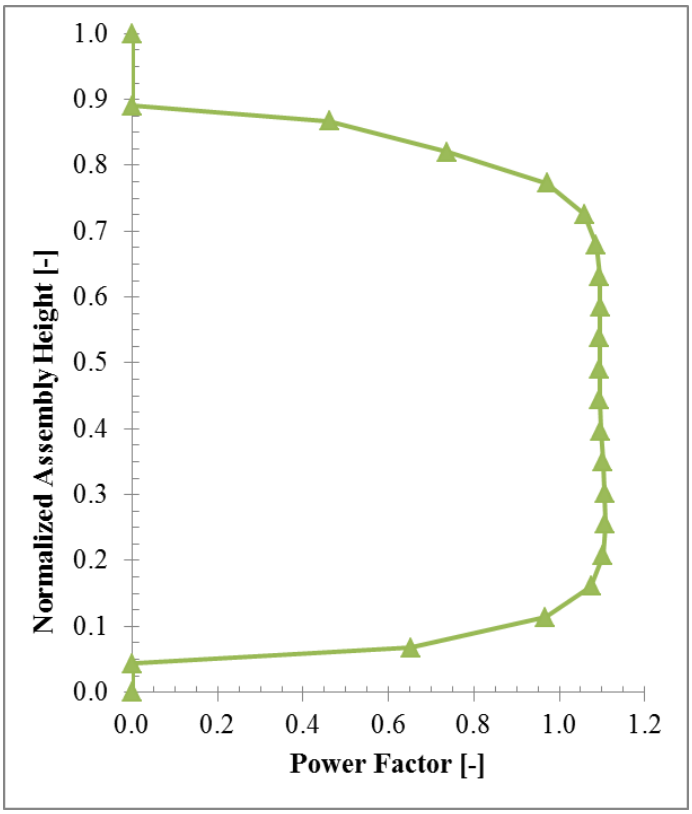

Figure D.14 – Power profile with respect to assembly zone height

D.4.2.4 Flow Pressure Loss Modeling

The pressure loss experienced by the flow is determined as the summation of the frictional losses and any form losses, as shown in Eq. (D.1).

$$\Delta P = \Delta P_{friction} + \Delta P_{form} \tag{D.1}$$

The flow pressure losses because of obstructions or other local effects (form losses), across the assembly zone, are prescribed to the model. These losses are specified as loss coefficients, Cd, as shown in Eq. (D.2).

$$\Delta P_{form} = C_d \frac{1}{2} \rho V^2 \quad . \tag{D.2}$$

where

ρ = the fluid density, and
V = the fluid velocity.

Table D.8 summarizes the position and value of the loss coefficients for the fueled assembly locations. The top and bottom of the channel have a loss coefficient of 0.5 to account for the 90 degree turn in the flow. The bottom of the assembly has a loss coefficient of 0.4 representative of flow contraction from a large plenum into a small channel. The top of the assembly has a loss coefficient of 1.0 representative of flow expansion from a small channel to a large plenum. Finally, the losses across the eight spacer grids are modeled using a flow loss coefficient of 2.0,

which is typical of vaned mixing grids. The empty flow channels around the periphery of the basket include only the top (0.5) and bottom (0.5) loss coefficients.

Table D.8 – Modeled drag coefficients for assemblies

Position from bottom				
(cm)	(in.)	Location	x/L	Cd
431.8	170.00	Top Channel	1.00	0.50
409.6	161.27	Top Assembly.	0.95	1.00
364.5	143.51	Grid	0.84	2.00
319.4	125.76	Grid	0.74	2.00
274.3	108.01	Grid	0.64	2.00
229.3	90.26	Grid	0.53	2.00
184.2	72.51	Grid	0.43	2.00
139.1	54.76	Grid	0.32	2.00
94.0	37.00	Grid	0.22	2.00
48.9	19.25	Grid	0.11	2.00
3.8	1.50	Bottom Assembly	0.01	0.40
0.0	0.00	Bottom Channel	0.00	0.50

Notes: x/L = normalized length of assembly zone;
Cd = loss coefficient.

The pressure loss because of frictional losses across the assembly zone is calculated based on Eq. (D.3). The frictional pressure loss coefficient , *f*, is modeled as the maximum of either the predicted laminar or turbulent frictional pressure loss coefficients, as shown in Eq. (D.4), that is calculated by the code.

$$\Delta P_{friction} = \frac{f L}{D} \frac{1}{2} \rho V^2 \tag{D.3}$$

$$f = \max\left(0.1 \cdot Re^{-0.3} , 96 \cdot Re^{-1.0}\right) \tag{D.4}$$

where

L = the axial segment length,
D = the characteristic channel diameter, and
f = the frictional pressure loss coefficient
Re = the local Reynolds number in the flow channels

D.4.2.5 Radiation View Factors

The RADGEN code was used to determine gray body radiation view factors within the fuel rod assembly and between the basket walls and the fuel assembly. The view factors generated by RADGEN are provided as input to COBRA-SFS, and are used in the energy equation solution to calculate rod-to-rod, rod-to-wall, and wall-to-wall radiation heat transfer based on local surface temperatures of the rods and walls at each axial level in the assembly zone.

Black body radiation view factors were determined for the 16 open channels around the periphery of the basket that did not contain fuel assemblies. The RADGEN code was used to determine the black body view factors through entering the geometry information and specifying the emissivity as 1.0. These black body view factors are included in the COBRA-SFS input, and the COBRA-SFS code internally converts the black body view factors into gray body view

factors, based on the specified surface emissivity values defined for the nodes representing the surfaces enclosing the flow channel.

D.4.2.6 Internal Convective Heat Transfer

The heat transfer between the fluid flow channels and the rods or wall surface nodes is modeled with a user-specified heat transfer coefficient correlation, expressed as a Nusselt number, Nu. The transition between laminar and turbulent flow conditions is captured automatically in the code by the convention of selecting the local maximum of the user-specified laminar and turbulent flow correlations. For this geometry, the Dittus-Boelter correlation is specified for internal, fully developed, turbulent flow; and for laminar flow, a constant Nusselt number of 3.66 is specified, as shown in Eq. (D.5). The value of 3.66 is based on validation of the COBRA-SFS code against experimental data obtained from numerous full-scale tests of SNF casks loaded with spent fuel.

$$Nu=\max\left(0.023\cdot Re^{0.8}Pr^{0.4}\ ,\ 3.66\right) \tag{D.5}$$

where

Pr = Prandtl number

D.4.2.7 Package Outer Surface Thermal Boundary Condition

The ambient still air temperature is assumed to be 38°C (100°F).

For the vertical package orientation, the convective thermal boundary condition on the vertical sides of the package is based on natural convection along a vertical flat plate [59] and is shown in Eq. (D.6), where Ra_L is the Rayleigh number. The region of applicability for Eq. (D.6) is for $Ra_L < 10^9$. The convective thermal boundary condition on the horizontal top of the package is based on natural convection from a horizontal, upward facing heated plate [59], as shown in Eq. (D.7). The region of applicability for Eq. (D.7) is for Ra_L between 10^7 and 10^{11}.

$$Nu=0.10\cdot Ra_L^{0.333}\ , \tag{D.6}$$

$$Nu=0.15\cdot Ra_L^{0.333}\ . \tag{D.7}$$

For the horizontal cask orientation, the convective thermal boundary condition on the curved outer walls of the cask was approximated as follows. The top two solid nodes, labeled as “1” in Figure D.12, were approximated as horizontal upward-facing flat plates. The boundary condition for these two solid nodes was modeled based on natural circulation using Eq. (D.7). The four solid nodes on the side of the package, labeled as “2” in Figure D.12, were approximated as vertical plates. The boundary condition for these four solid nodes was modeled based on natural circulation using Eq. (D.6). Finally, the bottom two slabs, labeled as “3” in Figure D.12, were approximated as horizontal downward-facing flat plates. The boundary condition for these two solid nodes was modeled based on natural circulation using Eq. (D.8), and is applicable for Ra_L between 10^5 and 10^{10} [59]. The convective thermal boundary condition on the vertical ends of the impact limiters of the package is based on natural convection along a vertical flat plate and is shown in Eq. (D.6).

$$Nu=0.27\cdot Ra_L^{0.25} \quad . \qquad (D.8)$$

Insolation was applied to the external surfaces of the package. For the vertical orientation case, the imposed heat load is 387 W/m^2 (123 Btu/h-ft^2) on the top lid of the transportation package and 97 W/m^2 (30.7 Btu/h-ft^2) on the transportation package side walls. For the horizontal orientation case, the imposed heat load is 194 W/m^2 (61.5 Btu/h-ft^2) on the curved horizontal surfaces of the package, and 97 W/m^2 (30.7 Btu/h-ft^2) on the vertical outer faces of the ends of the impact limiters. The total insolation for the vertical package was 5.12 kW and 8.15 kW for the horizontal configuration.

Heat rejection via thermal radiation was included for the outer surfaces of the package. For thermal radiation to ambient, the outer surface of the package is assumed to have an emissivity of 0.80.

D.4.3 Upper and Lower Plenum

The 32 fueled assemblies and 16 periphery flow channels are connected at the top and bottom via upper and lower plenums. The upper and lower plenums allow for fluid exchange between assemblies and also include modeling the heat loss paths through the top and bottom of the package. The fluid space in the upper and lower plenum is modeled as completely mixed with a single fluid temperature.

D.4.3.1 Vertical Orientation Plenum Modeling

For the package in the vertical orientation, the upper plenum (see Table D.9) was divided into nine axial sections to represent the layers of the canister and package lids. The first section of the upper plenum represents the helium gas region above the basket connected to all assembly zone channels. The second region accounts for axial heat conduction from the canister walls to canister lid. The 10 in. thick canister lid is represented with two nodes (Regions 3 and 4), and Region 5 represents the gap between the top of the canister lid and the inner surface of the package lid. Both conduction and thermal radiation are modeled across this gap. Three nodes (Regions 6 through 8) are used to represent conduction through the package lid. Region 9 represents the surface of the package lid and is connected to the appropriate boundary type to represent free convection and thermal radiation to the environment from this horizontal surface.

Table D.9 – Upper plenum axial sections, vertical orientation

Region	Section	length (cm)	length (in.)
1	conduction through helium gas	5.08	2.00
2	conduction through canister walls to canister lid	9.982	3.93
3	conduction through canister lid (1/2)	12.7	5.00
4	conduction through canister lid (1/2)	12.7	5.00
5	conduction through Nitrogen gap	0.318	0.125
6	conduction through package lid (1/3)	5.918	2.33
7	conduction through package lid (1/3)	5.918	2.33
8	conduction through package lid (1/3)	5.918	2.33
9	convection off the top horizontal surface	-	-

Similarly, the lower plenum (see Table D.10) was divided into 10 sections. The first section represents the helium gas region beneath the basket that connects to all assembly zone channels. Region 2 represents paths for conduction from the basket and canister wall nodes to the canister base. The effective length for this heat transfer path is from the center of the first axial node of the basket slabs in the assembly zone. Regions 3 and 4 represent conduction through the 2 in. thick canister base, and Regions 5 through 7 represent conduction through the package base. Regions 8 and 9 represent conduction through the concrete pad, and Region 10 models heat transfer through the underlying soil to the earth sink temperature. This is modeled with a typical representative value of 4.4°C (40°F). Because of the extreme weight of the entire package, contact conductance between adjacent components of the base is assumed to be nearly perfect, and thermal resistance because of contact gaps is not included in this model.

Table D.10 – Lower plenum axial sections, vertical orientation

Region	Section	length (cm)	length (in.)
1	conduction through helium gas	5.08	2.00
2	conduction through basket and canister walls to canister base	9.982	3.93
3	conduction through canister base (1/2)	2.54	1.00
4	conduction through canister base (1/2)	2.54	1.00
5	conduction through package base (1/3)	9.322	3.67
6	conduction through package base (1/3)	9.322	3.67
7	conduction through package base(1/3)	9.322	3.67
8	conduction through concrete pad (1/2)	12.7	5.00
9	conduction through concrete pad (1/2)	12.7	5.00
10	conduction through earth	182.88	72

D.4.3.2 Horizontal Orientation Plenum Modeling

As similar to the vertical orientation, the upper and lower plenum of the package in the horizontal orientation were each divided into 11 axial sections to represent the layers of the canister, package, and impact limiters (see Table D.11 and Table D.12). The first section represents the helium gas region between the basket and the canister ends. The second region accounts for axial heat conduction from the canister walls and the basket in the lower plenum to

the canister lid. The canister lid is represented with two nodes (Regions 3 and 4), and Region 5 represents the gap between the canister lid or base and the inner surface of the package lid or base. Both conduction and thermal radiation are modeled across this gap. Three nodes (Regions 6 through 8) are used to represent conduction through the ends of the package. Two nodes (Regions 9 and 10) represent conduction across the impact limiters placed on the ends of the package. Finally, Region 11 represents the surface of the impact limiter and is connected to the appropriate boundary type to represent free convection and thermal radiation to the environment from this vertical surface.

Table D.11 – Upper plenum axial sections, horizontal orientation

Region	Section	length (cm)	length (in.)
1	conduction through helium gas	5.08	2.00
2	conduction through canister walls to canister lid	9.982	3.93
3	conduction through canister lid (1/2)	12.7	5.00
4	conduction through canister lid (1/2)	12.7	5.00
5	conduction through Nitrogen gap	0.159	0.0625
6	conduction through package lid (1/3)	5.918	2.33
7	conduction through package lid (1/3)	5.918	2.33
8	conduction through package lid (1/3)	5.918	2.33
9	conduction through impact limiter (1/2)	25.4	10.00
10	conduction through impact limiter (1/2)	25.4	10.00
11	convection off the vertical surface	-	-

Table D.12 – Lower plenum axial sections, horizontal orientation

Region	Section	length (cm)	length (in.)
1	conduction through helium gas	5.08	2.00
2	conduction through basket to canister base	9.982	3.93
3	conduction through canister base (1/2)	2.54	1.00
4	conduction through canister base (1/2)	2.54	1.00
5	conduction through Nitrogen gap	0.159	0.0625
6	conduction through package base (1/3)	9.322	3.67
7	conduction through package base (1/3)	9.322	3.67
8	conduction through package base(1/3)	9.322	3.67
9	conduction through impact limiter (1/2)	25.4	10.00
10	conduction through impact limiter (1/2)	25.4	10.00
11	convection off the vertical surface	-	-

D.4.4 Material Properties

The modeled solid material properties are provided in Table D.13. The zircaloy emissivity is for that of highly oxided cladding. The helium properties are provided in Table D.14. Additional material properties related to fuel configuration changes are discussed in their respective sections.

To determine the effective thermal conductivity of the neutron shield, the shield was divided into two radial sections. The outer section is a 0.5 in. thick carbon steel wall on the outside of the

package. The inner section is 3 in. thick and consists of 36 periodic regions of carbon steel and resin epoxy, as shown in Figure D.3. A single, effective, thermal conductivity was used to model the inner section. The effective thermal conductivity of the region was determined, using Eq. (D.9), to be 2.05 Btu h^{-1} ft^{-1} °F^{-1}.

$$k_{eff} = \frac{k_{Al} \cdot n_{sections} \cdot t_{Al} \cdot \ln\frac{r_o}{r_i}}{2 \cdot \pi \cdot L_{path}} + \frac{k_{re} \cdot n_{sections} \cdot t_{re} \cdot \ln\frac{r_o}{r_i}}{2 \cdot \pi \cdot L_{path}} , \quad \text{(D.9)}$$

where:

r_o = Outer radius of material
r_i = Inner radius of material
L_{path} = Radial thickness of material
$n_{sections}$ = Number of repeating sections of carbon steel and resin epoxy
t_{Al} = Width of carbon steel
t_{re} = Width of resin epoxy
k_{re} = Thermal conductivity of resin epoxy
k_{Al} = Thermal conductivity of carbon steel
k_{eff} = Effective thermal conductivity

Table D.13 – Modeled solid material properties

Material	Thermal conductivity (Btu/h ft °F)	Emissivity
Stainless Steel 304	5.901468+0.004870*T(R)	0.36
BORAL®	61.033037-0.011262*T(R)	-
Carbon Steel 1010	28.89	0.8
Neutron Shield	0.289	-
Effective Neutron Shield	2.05	-
Concrete	1.068	-
Earth	0.347	-
Foamed Al Impact Limiters	2.70	0.8
Zircaloy	8.83	0.8
Uranium Dioxide	3.47	-

Table D.14 – Helium gas properties

Temp. (°F)	Enthalpy (Btu/lbm)	Thermal conductivity (Btu/h ft °F)	Specific heat (Btu/lbm °F)	Specific volume (ft^3/lbm)	Viscosity (lbm/ft h)
0	573.2	0.0807	1.24	27.45	0.0432
50	635.3	0.0867	1.24	30.43	0.0464
100	697.3	0.0925	1.24	33.41	0.0494
150	759.4	0.0981	1.24	36.39	0.0524
200	821.4	0.1036	1.24	39.37	0.0553
300	945.5	0.1143	1.24	45.34	0.0610
400	1069.7	0.1245	1.24	51.30	0.0665
500	1193.8	0.1344	1.24	57.26	0.0718
600	1317.9	0.1440	1.24	63.22	0.0769
700	1442.0	0.1533	1.24	69.18	0.0819
800	1566.1	0.1624	1.24	75.14	0.0868
900	1690.2	0.1713	1.24	81.10	0.0916
1000	1814.3	0.1800	1.24	87.07	0.0963
1500	2434.9	0.2212	1.24	116.87	0.1186
2000	3055.5	0.2593	1.24	146.68	0.1393

D.4.5 Computational Setup

The COBRA-SFS convergence criteria were set to 0.0003 for the total energy error and 0.0001 for the fluid enthalpy error. All simulations were performed as steady state calculations.

D.5 DESCRIPTION OF THE FAILED FUEL CATEGORIES AND CALCULATION MODELS

D.5.1 Category 1: Cladding Failure

D.5.1.1 Breached Spent Fuel Rods

This cladding failure scenario investigates the impact of the release of backfill and fission product gases into the canister gas space from the fuel rods. The rods are assumed to breach in such a manner that the cladding remains in its nominal geometry (i.e., the ruptured cladding does not block flow paths).

The assumed amount of gases released by the ruptured rods is 100 percent of the initial fill gas and 30 percent of the fission product gases generated within the fuel rods during operation (consistent with NUREG-1536 [2]). The impact of He, Xe, and Kr is included in the determination of the package gas phase mixture thermo-physical properties. Volatile radionuclides, such as Cs, I, and Ru are not included in determination of the mixture thermophysical properties. The gas is assumed to be homogeneously mixed within the canister.

The source term from the ruptured rods, with respect to decay heat, is modeled as remaining inside the rods. Although Xe, Kr, and radionuclides such as Cs may be released into the canister gas space, the decay heat source term is modeled as remaining inside the rods. COBRA-SFS does not contain the capability of radionuclide tracking/deposition or the capability for the gas phase to have volumetric heat generation. Also, these nuclides contribute a small

percentage of the overall decay heat. Modeling all of the decay heat as staying within the fuel rods is conservative with respect to the peak cladding temperature prediction.

In the vertical package orientation, cases with 0%, 3.125%, 10%, 50%, and 100% of the total fuel rods developing breaches were investigated. The case with 3.125% of the fuel rods developing breaches coincides with the number of fuel rods in one assembly.

Gas Inventory

The free space of the canister is estimated to be 6.30 m^3. To backfill the canister to 2 atm at 21°C requires 521 mol of helium.

The as-manufactured free space of each fuel rod is estimated to be 16.0×10^{-6} m^3. The initial helium backfill pressure is assumed to be 350 psig standard temperature and pressure. It follows that the total initial helium backfill of the fuel rods is approximately 4.67 mol per assembly or 149 mol per 32 assemblies.

The amount of fission product gases within each assembly was previously provided in Table D.7. Table D.15 summarizes the total canister gas inventory and the gas mixture in the canister free space for various fractions of rod breach.

Table D.15 – Total inventory and canister gas mixture for various rod failure fractions

Species	Total inventory (mol)	Canister gas mixture (mol) for rod failure fraction]				
		0.0	**0.03125**	**0.10**	**0.50**	**1.00**
He	722.4	521	526.1	537.5	603.4	685.7
Xe	1073.2	0	10.1	321.2	161.0	322.0
Kr	99.4	0	0.9	3.0	14.9	29.8
Total	1895.1	521	537.1	572.7	779.3	1037.5

Gas Mixture Properties

The initial canister pressure at 177°C (350°F) was previously given as 3.06 atm. For a given rod failure fraction, the canister average pressure, at 177°C (350°F), was determined using the ideal gas law. At a constant volume and temperature, the change in pressure caused by a change in the number of moles of gas can be determined using the ideal gas law, as shown in Eq. (D.10), where P is the absolute pressure, n is the number of moles of gas, and the subscripts 1 and 2 indicate the initial and final states, respectively.

$$P_2 = P_1 \frac{n_2}{n_1} . \qquad \text{(D.10)}$$

The free volume of the canister was determined by summing the initial canister free volume and the free volume added by the ruptured fuel rods. The average canister gas density was then determined by summing the masses of the individual species and dividing by the free volume. At the pressure, P_2, determined by Eq. (D.10), this canister average gas density would occur at 177°C (350°F).

The canister was then assumed to be at the pressure, P_2, determined by Eq. (D.11). The density of the gas mixture at various temperatures at this pressure was then determined by using the ideal gas law shown in Eq. (D.11), where T_1 is 450 K (177°C or 350°F), T_2 is the temperature at which the density, ρ_2, is to be determined, and ρ_1 is the canister average density.

$$\rho_2=\rho_1 \frac{T_1}{T_2} . \tag{D.11}$$

The thermal conductivity of the gas mixture was determined using Eqs. (D.12) through (D.14) [60].

$$k_{mix}= \sum_i^n \left(\frac{k_i x_i}{x_i+\sum_{j=1}^{n}(1-\delta_{ij})\varphi_{ij}x_j} \right) , \tag{D.12}$$

where

$$\varphi_{ij}=\theta_{ij}\left(1+2.41 \frac{(M_i-M_j)(M_i-0.142M_j)}{(M_i+M_j)^2} \right) , \tag{D.13}$$

and

$$\theta_{ij}=\frac{\left[1+\left(\frac{k_i}{k_j}\right)^{1/2}\left(\frac{M_i}{M_j}\right)^{1/4} \right]^2}{2^{3/2}\left(1+\frac{M_i}{M_j}\right)^{1/2}} , \tag{D.14}$$

where

- δ = Kronecker Delta (equals 1 for i=j, 0 otherwise)
- n = Number of components in mixture
- M = Molecular weight
- x = Mole fraction
- k = Thermal conductivity
- φ = Parameter defined by Eq. (D.13)
- θ = Parameter defined by Eq. (D.14)
- μ = Viscosity

The viscosity of the gas mixture was determined using Eqs. (D.15) and (D.16) [60].

$$\mu_{mix}= \sum_i^n \left(\frac{k_i \mu_j}{\sum_{j=1}^{n}(1-\delta_{ij})\varphi_{ij}x_j} \right), \tag{D.15}$$

and

$$\theta_{ij}=\frac{\left[1+\left(\frac{\mu_i}{\mu_j}\right)^{1/2}\left(\frac{M_j}{M_i}\right)^{1/4} \right]^2}{2^{3/2}\left(1+\frac{M_i}{M_j}\right)^{1/2}} . \tag{D.16}$$

The specific heat and enthalpy are also required as input for a COBRA-SFS model. The specific heat was determined by weight averaging the individual species specific heats. The enthalpy, as a function of temperature, was then determined using the gas mixture specific heat and using 0 K as the reference point.

The properties for the individual gas species were obtained from the National Institute of Standards and Technology database for a temperature range of 17.8°C to 426.7°C [61].

The density, viscosity, and thermal conductivity of the gas mixtures were evaluated as functions of temperature from 17.8°C to 426.7°C (0°F to 800°F). Table D.16 summarizes the evaluated canister gas mixture properties. When implementing the gas mixture properties into the COBRA-SFS models, an additional point at 906.7°C (1600°F) was included and was derived by linear extrapolation from the 426.7°C data point.

Table D.16 – Evaluated gas mixture properties for various fractions of fuel rods that develop cladding breaches

Failed rod fraction	**(-)**	**0.00**	**0.03125**	**0.10**	**0.50**	**1.00**
Free volume	[m^3]	6.299	6.303	6.308	6.313	6.316
Mole fraction He	(-)	1.000	0.980	0.939	0.774	0.661
Mole fraction Xe	(-)	0.000	0.019	0.056	0.207	0.310
Mole fraction Kr	(-)	0.000	0.002	0.005	0.019	0.029
Average canister pressure (at 350°F)	(atm)	3.06	3.16	3.36	4.58	6.09
Specific heat	(kJ/kg K)	5.28	3.18	1.80	0.67	0.46
Density[a] ($kg\ m^{-3}$)	Temp. (°C)					
	-17.8	0.583	0.979	1.850	6.861	13.008
	37.8	0.479	0.804	1.519	5.635	10.684
	93.3	0.406	0.683	1.289	4.781	9.064
	148.9	0.353	0.593	1.119	4.152	7.871
	204.4	0.312	0.524	0.989	3.669	6.955
	260.0	0.279	0.469	0.886	3.287	6.231
	315.6	0.253	0.425	0.802	2.976	5.643
	371.1	0.231	0.388	0.733	2.720	5.156
	426.7	0.213	0.357	0.675	2.504	4.747
Thermal conductivity ($W\ m^{-1}\ K^{-1}$)	Temp. (°C)					
	-17.8	0.140	0.128	0.109	0.063	0.045
	37.8	0.160	0.147	0.125	0.073	0.053
	93.3	0.179	0.165	0.141	0.083	0.060
	148.9	0.198	0.182	0.156	0.092	0.067
	204.4	0.215	0.199	0.171	0.102	0.074
	260.0	0.233	0.215	0.185	0.110	0.081
	315.6	0.249	0.230	0.199	0.119	0.087
	371.1	0.265	0.245	0.212	0.127	0.093
	426.7	0.281	0.260	0.225	0.135	0.099
Viscosity (Pa s)	Temp. (°C)					
	-17.8	1.79E-05	1.94E-05	2.12E-05	2.27E-05	2.24E-05
	37.8	2.04E-05	2.23E-05	2.46E-05	2.68E-05	2.65E-05
	93.3	2.29E-05	2.51E-05	2.79E-05	3.07E-05	3.06E-05
	148.9	2.52E-05	2.78E-05	3.11E-05	3.45E-05	3.45E-05
	204.4	2.75E-05	3.04E-05	3.41E-05	3.82E-05	3.83E-05
	260.0	2.97E-05	3.30E-05	3.71E-05	4.18E-05	4.19E-05
	315.6	3.18E-05	3.54E-05	4.00E-05	4.52E-05	4.55E-05
	371.1	3.39E-05	3.78E-05	4.27E-05	4.86E-05	4.89E-05
	426.7	3.59E-05	4.01E-05	4.55E-05	5.18E-05	5.22E-05

[a] At average canister pressure.

D.5.1.2 Damaged SNF

This cladding failure scenario investigates the impact of redistribution of SNF within the canister.

For the vertical package orientation, two configurations were investigated. First, a single assembly near the center of the basket, and indicated by “F” in Figure D.12, is assumed to have cladding failure to the extent to allow free movement of fuel particles and pellets within a basket cell. The whole assembly is assumed to form a debris bed that slumps and stays within the basket cell. A gas space is formed within the basket cell above the debris. A few cases are simulated assuming a range of debris bed porosities (debris bed heights). The second configuration is based on the same assumptions as the first configuration except all the assemblies are assumed to have clad failure.

Two configurations were also investigated for the evaluation of gross assembly failure with the package in a horizontal orientation. The first configuration assumes a single assembly fails, forms a debris bed, and slumps within a basket cell. The debris bed slumps downward onto the lower face of the basket cell wall, leaving a gas space above the debris bed. The second configuration is similar to the first configuration except all the assemblies are assumed to fail.

To model the material of a damaged fuel assembly, the assembly is represented as a block of homogeneous material within the basket cell. The material comprising each assembly is assumed to stay within its respective basket cell within the assembly zone of the model (see Figure D.7) and does not spill out into the plenum regions. The free space within the basket cell that is not occupied by the assembly material is also modeled as blocks of homogeneous material with the properties of the canister gas phase. The discretization of these blocks of material (solid conduction nodes) is illustrated in Figure D.15 for the vertical and Figure D.16 for the horizontal case. The entire assembly zone, including the basket cell and reconfigured material, is divided into 44 sections in the axial direction (i.e., 9.81 cm sections). In the radial cross section of the basket cell, the material is divided into a uniform 4×4 grid (i.e., 5.5×5.5 cm sections).

The entire assembly, including the fuel, cladding, and spacer grids, was assumed to fail. The mass of each component was based on Table B.1. As the shape of the particulate debris is unknown, the packing fraction was varied from 0.612 to 0.313 to simulate a range of possible bed porosities. A packing fraction of 0.612 is near the limit for randomly packed spheres of the same size and results in half of the basket channel being filled with debris. At a packing fraction of 0.313, the debris completely fills the basket channel.

Heat transfer via thermal conduction was modeled between adjacent solid nodes representing the debris, gas space, and basket walls. No contact resistance was modeled between the debris and the basket cell walls. Thermal radiation across the gas space was not included in the model. Any possible convective heat transfer within the gas space above the debris was not modeled. In addition, no gas flow through the debris was modeled. Not modeling these heat transfer paths is conservative and results in higher debris bed temperature predictions.

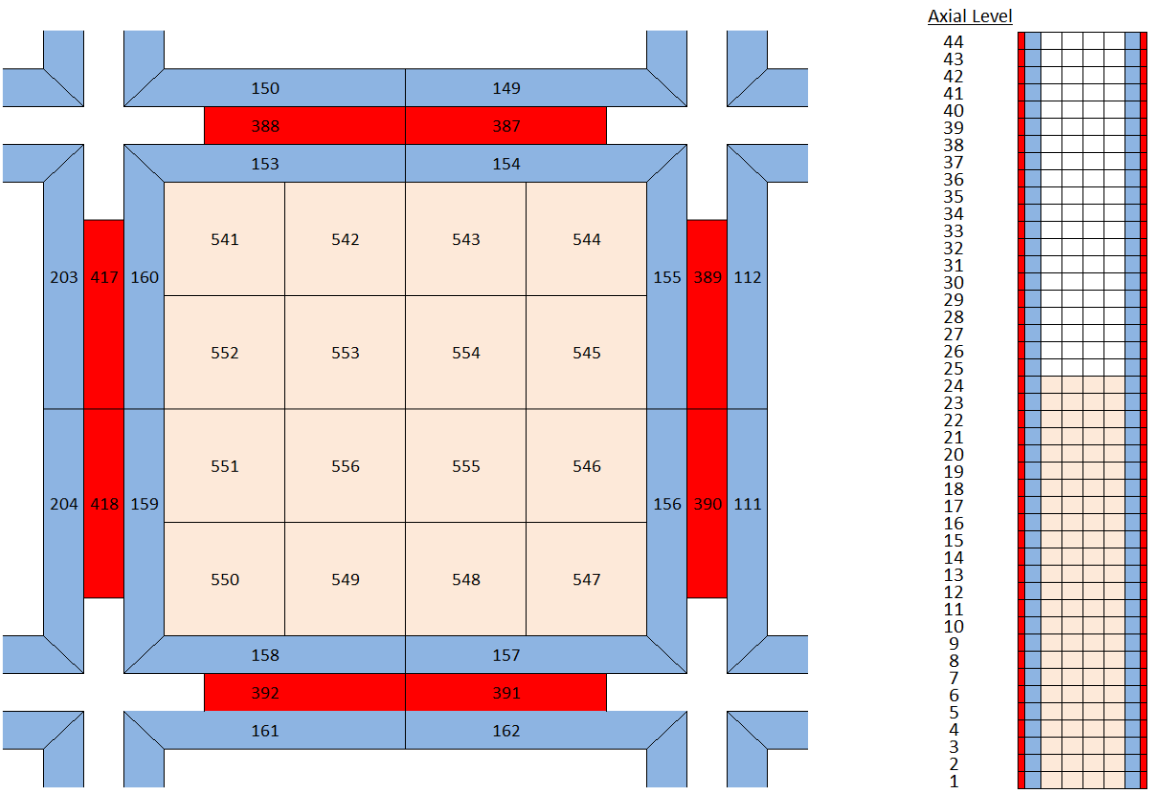

Figure D.15 – Illustration of failed fuel basket cell nodalization for vertical package orientation

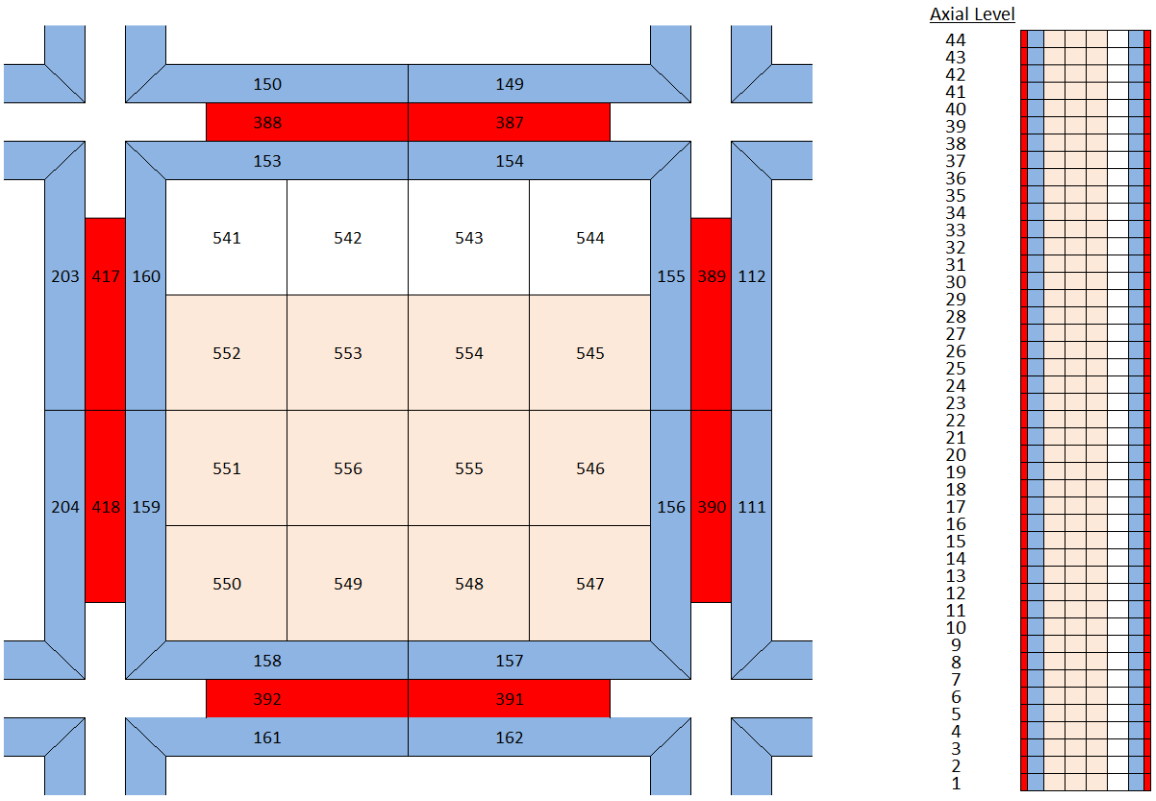

Figure D.16 – Illustration of failed fuel basket cell nodalization for horizontal package orientation

The thermal conductivity of the particle bed, k_{bed}, was determined using the method developed by Zehner and Bauer as described by Tsotsas and Martin [62]. The method used assumes stagnant gas within the debris bed and does not account for thermal radiation heat transfer within the bed. The method uses a deformation parameter, β, which allows for the extension of the model to beds of non-spherical particles. The deformation parameter is only a function of the bed porosity, α, a measureable quantity. For the current simulations, the bed porosity, which is one minus the packing fraction, is specified. The method has been successfully applied to a wide range of dispersed systems and conditions [62]. The average thermal conductivity of the solid debris, k_d, was determined by volume weighting the individual components from Table B.1 using the thermal conductivity values given in Table D.13. The gas thermal conductivity, kg, was taken as that of the canister gas space at 204°C (400°F).

$$k_{bed}=k_g\left\{1-\sqrt{1-\alpha}+\sqrt{1-\alpha}\left(\frac{2}{N}\right)\left[\frac{\beta}{N^2}\frac{k_d-k_g}{k_d}ln\left(\frac{k_d}{\beta\cdot k_g}\right)-\frac{\beta+1}{2}-\frac{\beta-1}{N}\right]\right\}, \qquad \text{(D.17)}$$

where: $\beta=\left(\frac{1-\alpha}{\alpha}\right)^{10/9}$ and $N=1-\frac{\beta\cdot k_g}{k_d}$.

The gas space above and within the debris bed is assumed to have the same composition and material properties as that computed in Sect. D.5.1.1 to account for fuel failure of either 3.125% (for the single-assembly failure configuration) or 100% of the rods (for failure of all assemblies). For the gas space above and within the debris bed, the material properties are not specified as

a function of temperature and instead are provided for an assumed temperature of 204°C (400°F).

The decay heat, from the originally intact assembly, is applied uniformly, both axially and radially, to the debris bed. This assumes the decay heat source term relocates with the bulk material and stays within the basket cell. In reality, some species may volatilize or become suspended, transport to another location within the canister and possibly deposit onto other surfaces. This also assumes the debris becomes homogeneous (i.e., well mixed) with respect to the decay heat. In reality, there is a possibility that the debris may become stratified with heavier or smaller debris sinking with larger and lighter debris on top.

D.5.2 Category 2: Rod/Assembly Deformation

This fuel reconfiguration category investigates the impact of changes to the assembly lattice pitch.

Five cases were analyzed including the expansion and contraction of the lattice pitch. The assembly pitch is assumed to change uniformly throughout the rod array cross-section and along the length of the assembly. In all cases, the entrance and exit pressure losses and the pressure losses because of spacer grids are assumed to remain unchanged. Also, the rods are assumed to remain intact without gaseous leakage into the canister space, as all cladding failure scenarios are evaluated under Category 1.

The nominal pitch of the W 17×17 OFA assembly is 1.26 cm (0.496 in.), with a pitch-to-diameter ratio of 1.38. In the case of the vertical orientation, assuming the assembly is centered within the GBC-32T basket cell; this leaves a 1.013 cm (0.399 in.) gap around the periphery between the outer fuel rods and the basket wall. Currently, RADGEN, the code used to generate the rod-to-rod and rod-to-wall thermal radiation view factors, is limited to pitch-to-diameter ratios of less than $\sqrt{2}$. Therefore, the largest pitch considered was 1.28 cm (0.50 in., a pitch-to-diameter ratio of 1.4). The smallest pitch considered was 1.06 cm (0.42 in.) where the fuel rods and guide/thimble tubes are nearly in contact. Finally, intermediate pitches of 1.143 cm (0.45 in.) and 1.234 cm (0.486 in.) were also considered to provide additional resolution of the trends.

D.5.3 Category 3: Changes to Intact Assembly Axial Alignment

This fuel reconfiguration category investigates the impact of changes to axial position of the fuel assembly within the basket.

Two cases were analyzed in which the end fittings that support the assembly within the canister were assumed to fail or deform, allowing the assemblies to shift upward or downward within their respective basket cells. For the first case, the assembly is relocated 27.27 cm (10.735 in.) toward the canister lid. For the second case, the assembly is relocated 8.89 cm (3.5 in.) toward the canister base. In both cases, the rods are assumed to remain in the nominal intact geometry without gaseous leakage into the canister space, as all cladding failure scenarios are evaluated under Category 1.

An assumption and a modeling simplification were employed to model these cases. First, no heat conduction was modeled from contact between the fuel rods and the canister base or lid. This is a conservative assumption limiting the axial heat removal from the fuel rods. Second, the flow loss coefficient for the assembly inlet (or outlet), which is shifted into the plenum region,

was added to the basket entrance (or exit) flow loss coefficient for the assemblies. This simplification was made because of the lack of detailed geometric information as to how the spacers would fail or how the assemblies would relocate into the plenums. This simplification only affects the vertical cask orientation cases because the horizontal cask orientation cases have very limited internal flow.

D.6 THERMAL ANALYSIS RESULTS

D.6.1 Discussion of Comparison Methodology

Two simulations were selected to represent the nominal intact configuration—one for the vertical package orientation and one for the horizontal package orientation as described in Sect. D.4. The decay time selected was 40 years. All the simulations were performed under the nominal boundary conditions described in Sect. D.4.2 (38˚C [100°F]) in still ambient air with insolation).

The thermal impacts of fuel configuration changes were evaluated by comparing predicted component temperatures between the nominal intact configuration and the fuel reconfiguration. This approach helps identify the fuel reconfiguration scenarios that yield the largest temperature changes in the package components.

An alternative approach would be to compare predicted package thermal response to regulatory limits. This approach, evaluating the margin to the regulatory limits, would require many simulations for multiple boundary conditions/scenarios (i.e., hot storage, cold storage, transportation, accident conditions). Comparing the margins to the regulatory limits would also be strongly coupled to the decay heat load of the package (decay time) and the particular materials and package design. Ultimately such comparisons may be required for real-world systems and may be informed by the results of the current study.

Specific component responses were selected to quantify the impacts of fuel configuration changes. The maximum cladding temperature is reported for its importance for fission product retention and maintaining assembly integrity. The minimum cladding temperature is also reported as it relates to phenomena that may occur at low temperature such as embrittlement. The maximum outer surface temperature is reported for its regulatory importance in transportation systems. The maximum neutron absorber, basket, and neutron shield temperatures are presented as they are important to the safety function of the package.

Finally, as noted previously, the thermal response of the package is integral to the structural performance. This report does not discuss phenomena coupled with the structural performance such as thermal gradients, which cause thermal stresses, and thermal expansion/contraction, which can cause mechanical stresses and geometry alterations.

D.6.2 Nominal Intact Configuration Results

The predicted package temperatures within the assembly zone (see Figure D.7) are summarized in Table D.17. As noted previously, this package design was not thoroughly designed to meet all regulatory requirements for such real-world systems. The cladding, neutron absorber, basket stainless steel, and neutron shield materials are within the temperature limits generally applicable for such materials. The maximum package outer surface temperatures are greater than 85˚C; however, the 85˚C regulation refers to shaded conditions, whereas the

current simulations include insolation. A personnel barrier could be included in the design to meet this regulation for transportation packages.

Table D.17 – Thermal nominal intact configuration results summary

Case ID	Decay time (years)	Total decay heat (kW)	Temperature (˚C)						
			Max. clad	Min. clad	Max. outer surface	Min. outer surface	Max. neutron absorber	Max. basket SS	Max. neutron shield
V.40	40	14.26	267	104	90	73	262	262	95
H.40	40	14.26	326	97	103	78	322	322	108

Temperature profiles, at a number of positions within the package are illustrated in Figure D.17 for the vertical package orientation case and in Figure D.18 for the horizontal package orientation case.

The vertical package orientation case has considerable convection (approx. 0.57 kg/min recirculating flow) in contrast to the horizontal package orientation case. This produces top peaked temperature profiles for the vertical package, while the horizontal package is center peaked. The convective flow, the lower total insolation, and the absence of the large impact limiters result in the vertical package orientation case generally having lower predicted temperatures than the horizontal case.

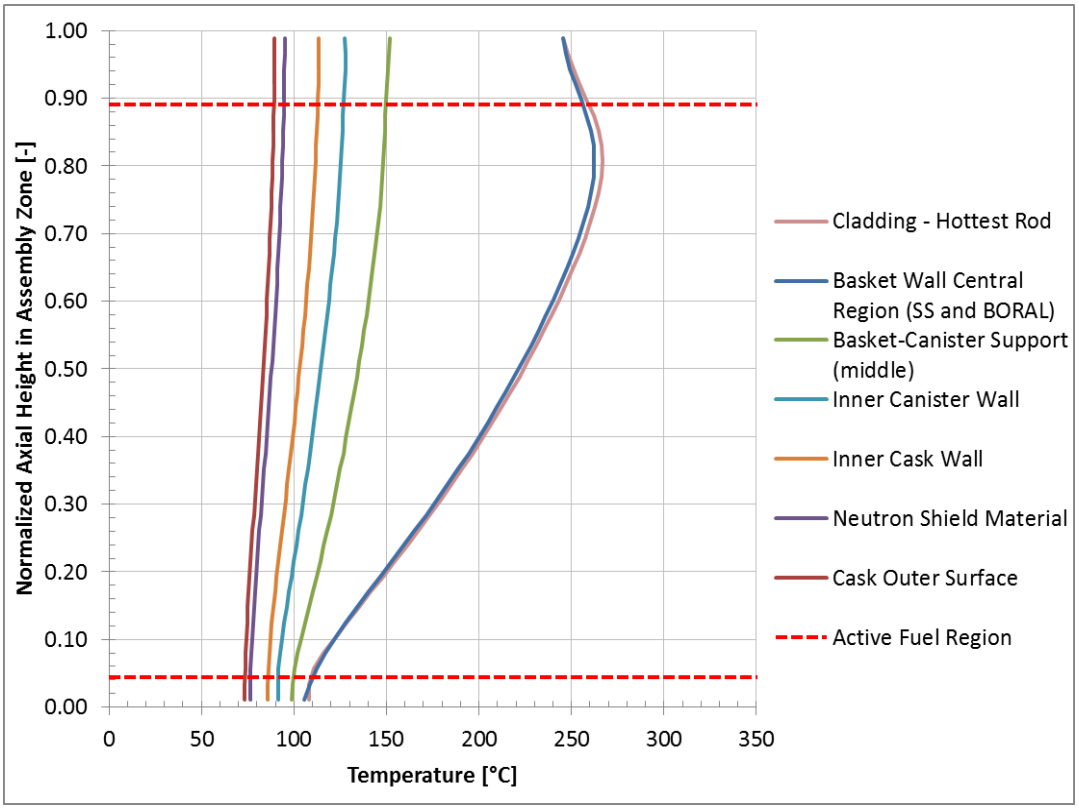

Figure D.17 – Structure temperatures—vertical orientation

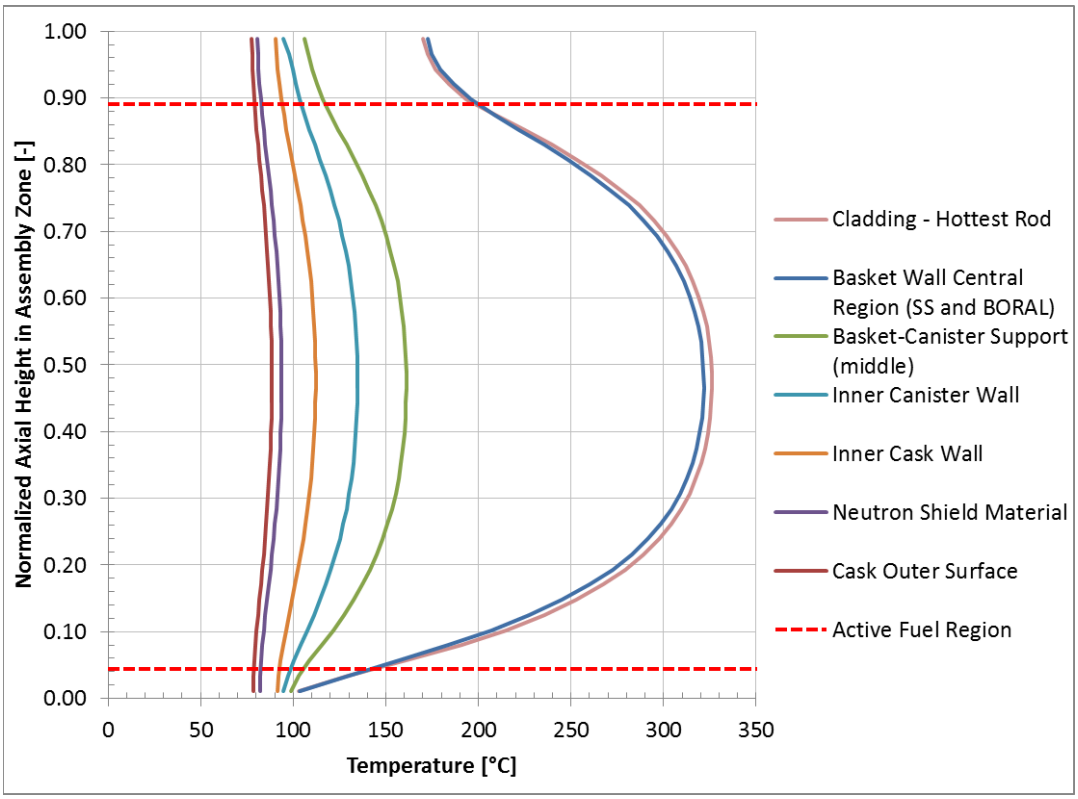

Figure D.18 – Structure temperatures— horizontal orientation

The nominal intact configuration models were used to investigate the package thermal response as a function of fuel decay times. Decay times less than 20 years were not simulated. The particular package design being investigated is not suitable for such high heat loads. A non-uniform loading pattern with cooler assemblies is one possible way to incorporate higher decay heat load assemblies. However, such mixed loading configurations were not investigated as part of this study. The results are summarized in Table D.18. As shown in Table D.17, the results are provided as the change in temperature from their respective nominal intact configuration case (i.e., +176 for the maximum cladding temperature for the V.20 case indicates the predicted maximum cladding temperature is 176˚C greater than that of the nominal intact configuration case, V.40). The change in component temperature is nearly linear with respect to the total package decay heat. An additional set of simulations was performed to investigate the impact of the solar insolation on the package. The results shown in Table D.19 indicate that removing the insolation heat load lowered the maximum component temperatures approximately 8˚C to 15˚C. These simulations with varying decay times as well as the cases of no insolation were conducted to provide perspective for the results from the fuel reconfiguration investigation.

Table D.18 – Thermal results vs. decay time

Case ID	Decay time (years)	Total decay heat (kW)	Change in temperature (Δ°C)						
			Max. clad	Min. clad	Max. outer surface	Min. outer surface	Max. neutron absorber	Max. basket SS[b]	Max. neutron shield
V.20	20	27.86	+176	+44	+27	+19	+176	+176	+32
V.40[a]	40	14.26	0	0	0	0	0	0	0
V.60	60	11.01	-45	-12	-8	-5	-44	-44	-9
V.100	100	7.46	-96	-26	-18	-10	-94	-94	-20
H.20	20	27.86	+175	+35	+33	+15	+175	+175	+37
H.40[a]	40	14.26	0	0	0	0	0	0	0
H.60	60	11.01	-51	-9	-9	-5	-51	-51	-10
H.100	100	7.46	-112	-20	-19	-10	-112	-112	-21

[a]Nominal intact configuration.
[b]SS = stainless steel.

Table D.19 – Thermal results vs. insolation heat load

Case ID	Insolation (kW)	Change in temperature (Δ°C)						
		Max. clad	Min. clad	Max. outer surface	Min. outer surface	Max. neutron absorber	Max. basket SS[b]	Max. neutron shield
V.40[a]	5.12	0	0	0	0	0	0	0
V.40.no	0.0	-10	-7	-8	-7	-9	-9	-8
H.40[a]	8.15	0	0	0	0	0	0	0
H.40.no	0.0	-8	-10	-14	-13	-9	-9	-15

[a]Nominal intact configuration.
[b]SS = stainless steel.

D.6.3 Particle Bed Modeling Sensitivities

As the damaged fuel assembly configuration may deviate from that assumed for the analyses, additional simulations were performed to help understand the impact of the modeled effective bed thermal conductivity and the decay heat axial power profile in the particle bed.

The effective thermal conductivity of the particle bed was calculated using the methodology discussed in Sect. D.5.1.2. This methodology assumed the contents of the bed were broken into pieces much smaller than the model nodalization size (2.17 cm [0.85 in.]) for the bed and homogeneously mixed. If pieces of the assembly remained largely intact, such as the spacer grids or fragments of the cladding, they would provide non-interrupted heat conduction paths augmenting the effective axial and/or radial bed thermal conductivity. Conversely, the fuel thermal conductivity, one component of the particle bed effective thermal conductivity, decreases with burnup because of void formation and fission products. The impact of voids on thermal conductivity is accounted for in the model through the packing fraction. If the thermal conductivity of the fuel is reduced to zero in the model, the predicted bed effective thermal conductivity is decreased by 17%, 13% and 10% for bed packing fractions of 63%, 42%, and 31%, respectively. Finally, different assembly types may contain different volumes of fuel, cladding, spacer grids, and free space that can affect the effective bed thermal conductivity.

To investigate the impact of the particle bed thermal conductivity, four additional cases were simulated where the effective particle bed thermal conductivity was increased or decreased by 25% or 50%. The cases assume all of the fuel assemblies are damaged and configured into particle beds with packing fractions of 62.6%, filling half of the height of the basket. The transportation package is assumed to be in the vertical orientation. The results are presented as the change in structure temperatures with respect to the nominal intact fuel configuration case.

Variations in the particle bed effective thermal conductivity did affect the peak basket stainless steel and neutron absorber temperatures (see Table D.20).

Table D.20 – Thermal results vs. particle bed effective thermal conductivity

Case ID	Debris packing fraction	Change in temperature (Δ°C)						
		Max. intact clad	Min. intact clad	Max. outer surface	Min. outer surface	Max. neutron absorber	Max. basket SS[c]	Max. neutron shield
V.40[a]	NA	0	0	0	0	0	0	0
V.40.100pr.626pf.+50%	0.626	NA	NA	-3	+7	+99	+99	-2
V.40.100pr.626pf.+25%	0.626	NA	NA	-3	+7	+112	+112	-2
V.40.100pr.626pf[b]	0.626	NA	NA	-3	+7	+127	+128	-2
V.40.100pr.626pf.-25%	0.626	NA	NA	-3	+7	+146	+147	-2
V.40.100pr.626pf.-50%	0.626	NA	NA	-3	+7	+169	+169	-2

[a]Nominal intact configuration.
[b]100% damaged fuel, nominal bed thermal conductivity.
[c]SS = stainless steel.

A uniform axial decay heat profile was applied to the particle bed. Depending on how the fragments of a failed fuel assembly settle within the basket, the decay heat power profile in the debris may be top or bottom skewed. To investigate the impact of the particle bed decay heat profile, two additional cases were simulated where the decay heat in the bed was either top or bottom peaked. For the top peaked profile case, the relative power profile linearly varied from 0.75 at the bottom of the bed to 1.25 at the top of the bed. For the bottom peaked profile case, the relative power profile linearly varied from 1.25 at the bottom of the bed to 0.75 at the top of the bed. The cases assume all of the fuel assemblies are damaged and reconfigured into particle beds with packing fractions of 62.6%, filling half of the height of the basket. The transportation package is assumed to be in the vertical orientation.

The decay heat axial power profile had a relatively minor impact on the peak basket temperatures. The impact of the axial power distribution did not propagate to the outer package structures (see Table D.21).

Table D.21 – Thermal results vs. particle bed axial power profile

Case ID	Debris packing fraction	Change in temperature (∆°C)						
		Max. intact clad	Min. intact clad	Max. outer surface	Min. outer surface	Max. neutron absorber	Max. basket SS[c]	Max. neutron shield
V.40[a]	NA	0	0	0	0	0	0	0
V.40.100pr.626pf.TopPeak	0.626	NA	NA	-3	+7	+138	+139	-3
V.40.100pr.626pf[b]	0.626	NA	NA	-3	+7	+127	+128	-2
V.40.100pr.626pf.BotPeak	0.626	NA	NA	-2	+7	+126	+126	-2

[a]Nominal intact configuration.
[b]Uniform axial power profile.
[c]SS = stainless steel.

D.6.4 Seal Temperature

The integrity of the canister seal under various scenarios of fuel configuration changes is a combined structural–thermal–materials problem and is seal design dependent. However, the conditions at the seal location are important in understanding the containment performance of the system.

The modeled GBC-32 storage/transport system is generic and does not have a seal design. The canister seal would be located toward the top edge of the canister. The COBRA-SFS model of the GBC-32 modeled the upper and lower regions of the package in a 1-D fashion as described in Sect. D.4.3. Thus, the simulation results provide an average temperature for the lid and other upper and lower plenum structures. Table D.22 provides the 1-D temperature results for the inner layer of the canister lid and base for the various scenarios investigated. However, a detailed thermal–structural simulation may be warranted for various fuel failure scenarios to understand the seal integrity for a particular design.

Table D.22 – Summary of canister lid and base temperature changes because of fuel configuration changes

Case ID	Rod Pitch to Diam. Ratio	Rods Ruptured (%)	Rods Damaged (%)	Packing Fraction (%)	Assem. Axial Shifting (cm)	Change in Lid Temp. (Δ°C)	Change in Base Temp. (Δ°C)
V.40[a]	1.38	0	0	NA	0	0	0
V.40.3.125pr	1.38	3.125	0	NA	0	+1	+3
V.40.10pr	1.38	10.0	0	NA	0	-3	+10
V.40.50pr	1.38	50.0	0	NA	0	-11	+21
V.40.100pr	1.38	100.0	0	NA	0	-15	+28
V.40.3.125pr.313pf	1.38	3.125	3.125	31.3	0	-1	+3
V.40.3.125pr.320pf	1.38	3.125	3.125	32.0	0	-1	+3
V.40.3.125pr.417pf	1.38	3.125	3.125	41.7	0	-1	+4
V.40.3.125pr.574pf	1.38	3.125	3.125	57.4	0	-1	+4
V.40.3.125pr.626pf	1.38	3.125	3.125	62.6	0	-1	+4
V.40.100pr.313pf	1.38	100.0	100.0	31.3	0	-18	+65
V.40.100pr.417pf	1.38	100.0	100.0	41.7	0	-19	+75
V.40.100pr.626pf	1.38	100.0	100.0	62.6	0	-19	+96
V.40.116pdr	1.16	0	0	NA	0	-2	+12
V.40.125pdr	1.25	0	0	NA	0	0	+6
V.40.135pdr	1.35	0	0	NA	0	0	0
V.40.140pdr	1.40	0	0	NA	0	0	0
V.40.up	1.38	0	0	NA	+27.27	3	-10
V.40.dn	1.38	0	0	NA	-8.89	-1	+4
H.40[a]	1.38	0	0	NA	0	0	0
H.40.3.125pr	1.38	3.125	0	NA	0	0	0
H.40.10pr	1.38	10.0	0	NA	0	0	+1
H.40.50pr	1.38	50.0	0	NA	0	0	+2
H.40.100pr	1.38	100.0	0	NA	0	0	+3
H.40.3.125pr.313pf	1.38	3.125	3.125	31.3	0	0	+1
H.40.3.125pr.417pf	1.38	3.125	3.125	41.7	0	0	+1
H.40.3.125pr.626pf	1.38	3.125	3.125	62.6	0	0	+1
H.40.100pr.313pf	1.38	100.0	100.0	31.3	0	+2	+13
H.40.100pr.417pf	1.38	100.0	100.0	41.7	0	+2	+13
H.40.100pr.626pf	1.38	100.0	100.0	62.6	0	+2	+13
H.40.116pdr	1.16	0	0	NA	0	0	0
H.40.125pdr	1.25	0	0	NA	0	0	0
H.40.135pdr	1.35	0	0	NA	0	0	0
H.40.140pdr	1.40	0	0	NA	0	0	0
H.40.up	1.38	0	0	NA	+27.27	+1	-11
H.40.dn	1.38	0	0	NA	-8.89	0	+5

Note: NA = not applicable.
[a]Nominal intact configuration.